

**Characterizing transformation processes of
environmental contaminants by multi-element
isotope analysis – proving concepts and developing
methods**

Dissertation

der Mathematisch-Naturwissenschaftlichen Fakultät
der Eberhard Karls Universität Tübingen
zur Erlangung des Grades eines
Doktors der Naturwissenschaften
(Dr. rer. nat.)

vorgelegt von
Frau Langping Wu
aus Gansu/China

Tübingen
2018

Gedruckt mit Genehmigung der Mathematisch-Naturwissenschaftlichen Fakultät der
Eberhard Karls Universität Tübingen.

Tag der mündlichen Qualifikation:	18.09.2018
Dekan:	Prof. Dr. Wolfgang Rosenstiel
1. Berichterstatter:	Prof. Dr. Stefan B. Haderlein
2. Berichterstatter:	PD Dr. habil. Hans H. Richnow

Table of Contents

Acknowledgements	1
Abbreviations and symbols	2
Summary	4
Zusammenfassung.....	5
List of publications in the thesis.....	6
Personal contribution.....	8
1. General introduction	11
1.1 Stable isotope fractionation as a tool for analysis organic contaminants	11
1.2. Stable isotope effects and quantification of isotope fractionation.....	12
1.3. Analytical challenges of stable hydrogen and chlorine isotope analysis	14
1.4. CSIA application for characterizing transformation mechanisms and evaluating <i>in situ</i> degradation	16
1.5. Target compounds and their main degradation pathways in the environment	18
1.5.1. Organophosphorus compounds (OPs)	18
1.5.2. Substituted chlorobenzenes.....	20
1.5.3. Phthalate esters (PAEs)	21
1.5.4. Hexachlorocyclohexanes (HCHs).....	22
2. Objectives	25
3. Results and discussion.....	26
3.1. Validation of GC–IRMS techniques for $\delta^{13}\text{C}$ and $\delta^2\text{H}$ CSIA of OPs	26
3.2. Effects of sample preparation on CSIA of HCHs for food web studies.....	29
3.3. CSIA for characterizing chemical and biological transformation of organic compounds	32
3.3.1. Isotope fractionation of OPs during hydrolysis.....	32
3.3.2. Isotope fractionation of OPs during radical oxidation.....	34
3.3.3. Isotope fractionation of substituted chlorobenzenes during photodegradation	36
3.3.4. Isotope fractionation of phthalate esters during abiotic and biotic degradation	39

3.3.5. Enantiomer and carbon isotope fractionation of α -HCH.....	42
3.4. Field application of CSIA for charactering natural attenuation of parathion by hydrolysis	46
4. Conclusion and outlook	51
5. References	59
6. Appendix	73
6.1. Compound specific isotope analysis of organophosphorus pesticides	73
6.2. Validation of GC-IRMS techniques for $\delta^{13}\text{C}$ and $\delta^2\text{H}$ CSIA of organophosphorus compounds and their potential for studying the mode of hydrolysis in the environment	88
6.3. Characterizing chemical transformation of organophosphorus compounds by ^{13}C and ^2H stable isotope analysis	110
6.4. Aqueous photodegradation of substituted chlorobenzenes: Kinetics, carbon isotope fractionation, and reaction mechanisms	132
6.5. Carbon and hydrogen isotope fractionation of phthalate esters during degradation by sulfate and hydroxyl radicals	157
6.6. Development of extraction and clean-up methods for multi- element compound specific isotope analysis of hexachlorocyclohexanes for isotope forensic and food web studies	173
6.7. Carbon and hydrogen isotope analysis of parathion for characterizing natural attenuation by hydrolysis at a contaminated site.....	190
6.8. Carbon and hydrogen stable isotope analysis for characterizing the chemical degradation of tributyl phosphate.....	209
6.9. Enantiomer and carbon isotope fractionation of α -hexachlorocyclohexane by <i>Sphingobium indicum</i> strain B90A and corresponding enzymes	229
6.10. Carbon and hydrogen isotope fractionation during abiotic hydrolysis and aerobic biodegradation of phthalate esters.....	260
Curriculum Vitae.....	278

The presented studies were conducted in the Department of Isotope Biogeochemistry at the Helmholtz Centre for Environmental Research-UFZ in Leipzig. The experimental work was performed in the time period between March 2014 and December 2017 under the supervision of Dr. habil. Hans-Hermann Richnow.

Acknowledgements

I'm deeply grateful to my PhD advisor Dr. Hans-Hermann Richnow for the opportunity to learn from his experience and to work on a number of fruitful and fascinating research topics. He had always time for my problems and questions. He could squeeze time to shape my skills in the lab even when he was extremely busy. He guided me to develop and follow my own ideas and taught me how to handle complicated scientific questions with countless constructive discussions. I'm especially grateful for the patience, support and appreciation I have received from him. I appreciate his trust to give me many opportunities for representing the group at various conferences and at laboratories of collaborators, as well as for involving me in supervision of internships and guest scientists. He paid attention on the training for my future perspectives. He always found ways to motivate me when I was frustrated with work. I could always rely on his help and guidance. I would also like to thank Prof. Dr. Stefan B. Haderlein for accepting and evaluating the presented thesis as my University supervisor.

I would like to express my gratitude to Prof. Dr. Hartmut Herrmann, Dr. Carsten Vogt, Dr. Steffen Kümmel, Dr. Julian Renpenning and Yaqing Liu for their close co-operation, for sharing ideas and fruitful discussions which led to joint findings. I appreciate the instrumental supports from Dr. Matthias Gehre and Ursula Günther in the Lab. I am grateful to all project collaborators and co-authors for their outstanding cooperation. I would also like to thank our very motivated master students Anke Reese, Sonya Moses, Barbora Chladkova, Juliane Chaud, Marine Desnoyers and Kamile Vonzodaite for their commitments and contributions to this thesis.

Finally, I'd like to thank all colleagues from the Department of Isotope Biogeochemistry for the pleasant working environment over the past four years. Most importantly I want to thank my family for their love, trust and unlimited support throughout my life.

Abbreviations and symbols

AKIE	apparent kinetic isotope effect
CMB	chloromethyl benzene
Cr/HTC	chromium based high temperature conversion
CSIA	compound-specific stable isotope analysis
DBP	dibutyl phthalate
DCB	dichlorobenzene
DEP	diethyl phthalate
DMP	dimethyl phthalate
DNAPL	dense non-aqueous phase liquid
E	element
EIE	equilibrium isotope effects
EP	ethyl parathion
ESIA	enantioselective stable isotope analysis
GC	gas chromatography
GC-IRMS	gas chromatograph-isotope ratio mass spectrometer
GC-MC-ICPMS	gas chromatography coupled with multiple-collector inductively coupled plasma mass spectrometry
HCHs	hexachlorocyclohexanes
HTC	high temperature conversion
ISCO	<i>in situ</i> chemical oxidation
KIE	kinetic isotope effect
MP	methyl parathion
NCB	nitrochlorobenzene
OPs	organophosphorus compounds
PAEs	phthalate esters
PS	persulfate

SKIE	secondary kinetic isotope effect
SMOC	standard mean ocean chloride
TBA	<i>tert</i> -butyl alcohol
TBP	tributyl phosphate
TCEP	tris(2-chloroethyl) phosphate
TDCPP	tris(1,3-dichloro-2-propyl)phosphate
VPDB	Vienna Pee Dee Belemnite
VSMOW	Vienna Standard Mean Ocean Water
α -HCH	α -hexachlorocyclohexane
β -HCH	β -hexachlorocyclohexane
γ -HCH	γ -hexachlorocyclohexane
δ -HCH	δ -hexachlorocyclohexane
k	reaction rate constant
R	isotope ratio
δ	isotope composition (‰)
ϵ	isotope enrichment factor
Λ	slope derived from regression of a dual element isotope plot
σ^+	Hammett substituent constant

Summary

Compound-specific stable isotope analysis (CSIA) is increasingly applied in fundamental research, environmental sciences and forensic studies. The analysis of stable isotopes may largely improve the evaluation of sources, transformation processes and sinks of organic compounds in the environment. To extend the CSIA application to new compounds and to improve the evaluation of organic pollutants transformation in the environment, this thesis focused on providing insights into the transformation of ubiquitous organic pollutants including pesticides (organophosphorus compounds (OPs), hexachlorocyclohexanes (HCHs)), plasticizers (phthalate esters (PAEs)) and substituted chlorobenzenes.

Firstly, analytical challenges associated with the reproducibility and trueness of hydrogen isotope analysis of heteroatom-bearing OPs was overcome by applying the chromium based high temperature conversion system. Secondly, sample preparation procedures for extraction and clean-up of HCHs from various matrixes including water, soil, plants, milk, fish oil and pork liver were evaluated for conservation of isotopic values. The carbon, hydrogen and chlorine isotope fractionation observed in HCHs extracted from contaminated soil, plants and pork liver highlighted the potential of multi-element CSIA for investigating the transformation of persistent contaminants in food webs.

The main focus of this thesis was to characterize the fundamental (bio)chemical processes of relevant organic pollutants using CSIA. To determine factors governing isotope fractionation and to characterize fundamental processes at the molecular level, the stable isotope fractionation patterns associated with (1) hydrolysis at various pH, (2) oxidation by sulfate and hydroxyl radicals, (3) biodegradation by whole cells and (4) enzymatic transformation of selected compounds were obtained under controlled laboratory conditions. The results demonstrated that CSIA has a diagnostic value for characterizing transformation mechanisms of the tested compounds. Finally, the natural attenuation of OPs by hydrolysis at a contaminated site was investigated using carbon and hydrogen isotope analysis, which delineated the potential of CSIA for field applications.

Zusammenfassung

Die Komponenten-spezifische Analyse stabiler Isotope (engl. CSIA) wird zunehmend in der Grundlagenforschung, den Umweltwissenschaften und in der Forensik eingesetzt. Die Analyse der isotopischen Zusammensetzung besitzt dabei ein großes Potential Quellen, Transformationsprozesse und Senken organischer Verbindungen in der Natur zu bewerten. Zur Ausweitung der Isotopenanalyse auf neue Verbindungsklassen wurden im Rahmen dieser Arbeit Studien mit organischen Modellverbindungen durchgeführt. Dabei wurden neben den als Pestizid verwendeten Organophosphaten (OPs) sowie Hexachlorozyklohexan (HCH), die als Weichmacher genutzten Phthalsäure-Ester (PAEs) und chlorierte Benzole untersucht.

Es wurden Methoden für die Multiisotopenanalyse für OPs und HCHs entwickelt. Insbesondere wurde die Analyse der Wasserstoffisotopensignaturen heteroatomhaltiger organischer Verbindungen weiterentwickelt und validiert, wobei die Chrom-unterstützte Hochtemperaturpyrolyse verwendet wurde. Isotopenfraktionierungsfreie Techniken für die Extraktion und Aufreinigung von HCHs aus unterschiedlichen Matrices wurden entwickelt und für die Multiisotopenanalyse der HCHs (^2H , ^{13}C , ^{37}Cl) aus Böden, Pflanzen, tierischen Produkten sowie Organen (z. B. Leber) eingesetzt. Die Ergebnisse dieser Versuche demonstrieren das Potential von CSIA für die Analyse von Transformationen persistenter Chemikalien innerhalb von Nahrungsketten.

Isotopenfraktionierungsmuster wurden genutzt um Transformationsreaktionen wie (1) die Hydrolyse bei verschiedenen pH Werten, (2) die Oxidation durch Sulfat- und Hydroxylradikale, (3) den biologischen Abbau sowie (4) enzymatische Reaktionen zu untersuchen. Labor-Referenzexperimente wurden mit Modellkomponenten durchgeführt und die erhaltenen isotopenspezifischen Faktoren wurden zur Charakterisierung der fundamentalen Prinzipien dieser biogeochemischen Transformationsprozesse auf molekularer Ebene genutzt. Der natürliche Abbau der OPs durch chemische Hydrolyse wurde anhand der im Labor bestimmten ^{13}C und ^2H Fraktionierungsfaktoren an einem kontaminierten Standort überprüft und validiert, wodurch das Potential von CSIA zur Feldanwendung aufgezeigt wurde.

List of publications in the thesis

a) Accepted papers

1. **Wu, L.**; Yao, J.; Trebse, P.; Zhang, N.; Richnow, H. H., Compound specific isotope analysis of organophosphorus pesticides. *Chemosphere* 2014, 111, 458-63. (Wu et al. 2014)
2. **Wu, L.**; Kümmel, S.; Richnow, H. H., Validation of GC-IRMS techniques for $\delta^{13}\text{C}$ and $\delta^2\text{H}$ CSIA of organophosphorus compounds and their potential for studying the mode of hydrolysis in the environment. *Anal. Bioanal. Chem.* 2017, 409, (10), 2581-2590. (Wu et al. 2017)
3. **Wu, L.**; Chladkova, B.; Lechtenfeld, O. J.; Lian, S.; Schindelka, J.; Herrmann, H.; Richnow, H. H., Characterizing chemical transformation of organophosphorus compounds by ^{13}C and ^2H stable isotope analysis. *Sci. Total. Environ.* 2018, 615, 20-28. (Wu et al. 2018a)
4. Passeport, E.; Zhang, N.; **Wu, L.**; Herrmann, H.; Sherwood Lollar, B.; Richnow, H. H., Aqueous photodegradation of substituted chlorobenzenes: Kinetics, carbon isotope fractionation, and reaction mechanisms. *Water Res.* 2018, 135, 95-103. (Passeport et al. 2018)
5. Zhang, D.; **Wu, L.**; Yao, J.; Herrmann, H.; Richnow, H. H., Carbon and hydrogen isotope fractionation of phthalate esters during degradation by sulfate and hydroxyl radicals. *Chem. Eng. J.* 2018, 347, 111-118. (Zhang et al. 2018a)
6. **Wu, L.**; Verma, D.; Bondgaard, M.; Melvej, A.; Vogt, C.; Subudhi, S.; Richnow, H. H., Carbon and hydrogen isotope analysis of parathion for charactering natural attenuation by hydrolysis at a contaminated site. *Water Res.* 2018, 143, 145-154. (Wu et al. 2018c)
7. Liu, J.; **Wu, L.**; Kümmel, S.; Yao, J.; Schaefer, T.; Herrmann, H.; Richnow, H. H., Carbon and hydrogen stable isotope analysis for characterizing the chemical degradation of tributyl phosphite. *Chemosphere* 2018, 212, 133-142. (Liu et al. 2018a)

b) Submitted manuscripts

8. **Wu, L.**; Moses, S.; Liu, Y.; Renpenning, J.; Richnow, H. H., Development of extraction and clean-up methods for multi-element compound specific isotope analysis of hexachlorocyclohexanes for isotope forensic and food web studies. *Anal. Chem.* 2018. (Wu et al. 2018b)
9. Liu, Y.; **Wu, L.**; Kohli, P.; Kumar, R.; Stryhanyuk, H.; Nijenhuis, I.; Lal, R.; Richnow, H. H., Enantiomer and carbon isotope fractionation of α -hexachlorocyclohexane by *Sphingobium indicum* strain B90A and corresponding enzymes. *Environ. Sci. Technol.* 2018. (Liu et al. 2018b)
10. Zhang, D.; **Wu, L.**; Yao, J.; Vogt, C.; Richnow, H. H., Carbon and hydrogen isotope fractionation during abiotic hydrolysis and aerobic biodegradation of phthalate esters. *Environ. Sci. Technol.* **2018**. (Zhang et al. 2018b)

Personal contribution

The significance of the personal contribution is described as below:

Publication 1: The concept of this study was developed by P. Trebse and H. H. Richnow. L. Wu performed the major work on laboratory experiments, isotope measurement, data evaluation and manuscript writing. P. Trebse gave the scientific advices on hydrolysis and photolysis of OPs. N. Zhang supported the carbon isotope measurement in the laboratory. H. H. Richnow gave the major scientific advices on CSIA. All authors were involved in the manuscript correction.

Publication 2: The concept of this study was developed by L. Wu and H. H. Richnow. L. Wu performed the major work on laboratory experiments, isotope measurement, data evaluation and manuscript writing. S. Kümmel supported the isotope measurement in the laboratory. H. H. Richnow gave the major scientific advices during the entire study. All authors were involved in the manuscript correction.

Publication 3: The concept of this study was developed by L. Wu and H. H. Richnow. L. Wu performed the major work on laboratory experiments, isotope measurement, data evaluation and manuscript writing. B. Chladkova provided the kinetic data of Fenton reaction of TCEP. S. Lian provided partially the kinetic data of hydrolysis of MP. O. J. Lechtenfeld supported the analysis of transformation products in the laboratory. J. Schindelka and H. Herrmann gave scientific advices on photochemistry mechanisms. H. H. Richnow gave the major scientific advices during the entire study. All authors were involved in the manuscript correction.

Publication 4: L. Wu conducted the indirect photolysis experiments of 3-CMB, 4-CMB, 4-NCB and the direct photolysis experiment of 4-NCB. L. Wu was involved in isotope measurement, discussion on data interpretation of Hammett plot and AKIE data. The concept of this study was developed by E. Passeport, N. Zhang and H. H. Richnow. H. Herrmann gave scientific advices on photochemistry mechanisms. B. Sherwood-Lollar and H. H. Richnow gave scientific advices on CSIA. E. Passeport performed the major work on experiment conduction, data evaluation and manuscript writing. All authors were involved in the manuscript correction.

Publication 5: The concept of this study was developed by D. Zhang, L. Wu and H. H. Richnow. L. Wu was also involved in the discussion on data interpretation, reaction mechanisms and manuscript writing. D. Zhang performed the major work on experiment conduction, data evaluation and manuscript writing. H. Herrmann gave scientific advices on radical reaction mechanisms. H. H. Richnow gave the major scientific advices during the entire study. All authors were involved in the manuscript correction.

Publication 6: The concept of this study was developed by L. Wu and H. H. Richnow. L. Wu performed the major work on field sampling, laboratory experiments, isotope measurement, data evaluation and manuscript writing. D. Verma conducted the biodegradation experiments of parathion. M. Bondgaard and A. Melvej organized the field sampling and provided the field site information. C. Vogt and S. Subudhi gave scientific advices on biodegradation experiments in the UFZ and TERI laboratory. H. H. Richnow gave the major scientific advices during the entire study. All authors were involved in the manuscript correction.

Publication 7: L. Wu and J. Liu are the equally contributing first authors. The concept of this study was developed by J. Liu, L. Wu and H. H. Richnow. L. Wu was involved in the discussion on data interpretation, evaluating reaction mechanisms and manuscript writing. J. Liu and L. Wu contributed equally to writing of the manuscript. J. Liu conducted the major experiment and data evaluation as well as partially manuscript writing. S. Kümmel supported the isotope analysis in the laboratory. T. Schaefer calculated the radical contributions in the reaction system. H. Herrmann gave scientific advices on photochemistry mechanisms. H. H. Richnow gave major scientific advices during the entire study. All authors were involved in the manuscript correction.

Publication 8: The concept of this study was developed by L. Wu and H. H. Richnow. L. Wu developed the extraction and clean-up protocols, and performed the major work on laboratory experiments, isotope measurement, data evaluation and manuscript writing. S. Moses provided the extraction recovery data from plants, fish oil, milk and liver. Y. Liu provided the extraction recovery data from water and soil. J. Renpenning supported the Cl isotope measurement in the laboratory. H. H. Richnow gave the major scientific advices during the entire study. All authors were involved in the manuscript correction.

Publication 9: The concept of this study was developed by H. H. Richnow and P. Lal. L. Wu was involved in the discussion on data interpretation, development of the mathematic model for enantiomer fractionation quantification and manuscript writing. Y. Liu performed the major work on experiment conduction, data evaluation and manuscript writing. P. Kohli and R. Kumar were involved in the purification of LinA enzyme. H. Stryhanyuk was involved in the development of the mathematic model for the quantification of the enantiomer fractionation. I. Nijenhuis gave scientific advices on experiments using crude extracts and resting cells. H. H. Richnow gave the major scientific advices during the entire study. All authors were involved in the manuscript correction.

Publication 10: The concept of this study was developed by D. Zhang, L. Wu and H. H. Richnow. L. Wu was also involved in the discussion on data interpretation, reaction mechanisms and manuscript writing. D. Zhang performed the major work on experiment conduction, data evaluation and manuscript writing. C. Vogt gave scientific advices on aerobic biodegradation. H. H. Richnow gave the major scientific advices during the entire study. All authors were involved in the manuscript correction.

1. General introduction

1.1 Stable isotope fractionation as a tool for analysis organic contaminants

The benefits of the massive usage of manmade organic chemicals in modern society come at the cost of their widespread occurrence in the environment. The occurrence of organic contaminants represents threats to human, animal, and environmental health. Therefore, it becomes a worldwide issue with increasing concerns. Knowledge of transformation mechanisms and factors governing transformation processes is an essential prerequisite for the understanding and assessment of the fate of organic contaminants in the environment. Current approaches to characterize the transformation of organic contaminants in nature either are based on the detection of parent compound disappearance, detection of transformation products, or rely on the evidence of an intrinsic transformation potential in a given environment. However, many of the existing methods suffer from their limitations (Fenner et al. 2013), for instance, when transformation products are unknown, their detection becomes more challenging or even impossible for suspect or non-target analysis. The stable isotope composition provides clues that can be used to identify sources, transformation reactions, and sinks of organic compounds in the environment (Meckenstock et al. 2004). The stability of chemical bonds of isotopologues depends on the mass of the substituent. Thus higher activation energy is needed to cleave a bond formed by heavy isotopologues leading to kinetic isotope fractionation in (bio)chemical processes (Bigeleisen and Wolfsberg 1958, Wolfsberg et al. 2010). Gas or liquid chromatography (GC, LC) coupled to isotope ratio mass spectrometry (IRMS) via an online conversion enables the precise measurement of stable isotopes at natural abundance (such as $^{13}\text{C}/^{12}\text{C}$, $^{15}\text{N}/^{14}\text{N}$, $^2\text{H}/^1\text{H}$, $^{37}\text{Cl}/^{35}\text{Cl}$) within organic molecules. The coupling of GC or LC to IRMS makes it possible to analyse isotope ratios of individual compounds in complex mixtures and is known as compound-specific stable isotope analysis (CSIA). Due to its highly reaction-specific isotope fractionation patterns, CSIA has the potential to provide insights into contaminant reaction mechanisms without the need to identify transformation products (Hunkeler et al. 2008). Therefore, the importance of CSIA is increasing in fundamental

research, environmental sciences, and forensic studies (Elsner 2010, Elsner and Imfeld 2016, Nijenhuis and Richnow 2016, Vogt et al. 2016).

1.2. Stable isotope effects and quantification of isotope fractionation

The theoretical background and definitions of isotope effects in (bio)chemical reactions have been summarized elsewhere (Swiderek and Paneth 2013, Wolfsberg et al. 2010). Stable Isotope effects can be caused by equilibrium and kinetic processes of (bio)chemical and physical procedures. Equilibrium isotope effect (EIE) comes from considering equilibrium constants for isotopologues (molecules differing only in the isotopic composition), which is connected with any physical process or chemical reaction that reached an equilibrium. For instance, EIE could be relevant in reactions in which a substrate binds to the binding pocket of an enzyme (Swiderek and Paneth 2013). Broadly speaking, EIE is usually much smaller than kinetic isotope effect (KIE). The KIE is based on the difference in kinetic rates during, for example, irreversible chemical bond change reactions (cleavage or formation) of isotopologues, reflecting the relative stability of bonds formed by the heavy vs. light stable isotopes of an element (E) (Wolfsberg et al. 2010). The KIE characterize the rate limitation associated with the activation energies needed to reach the transition stage and thus yield information on the mode of bond cleavage. A secondary kinetic isotope effect (SKIE) occurs when isotopologues substituted bonds are close to a reactive bond but not directly involved in the bond breaking reaction (Westaway 2006). Usually, SKIE tends to be much smaller than primary kinetic isotope effects which are directly involved in bond changes. Nevertheless, large SKIE is possible for hydrogen isotope fractionation due to the large mass difference of ^2H and ^1H (Franke et al. 2017). The apparent kinetic isotope effect (AKIE) is the observed KIE of an experimental reaction and is considered to contain information of the isotope sensitive mode of bond cleavage and rate limitations prior bond cleavage (Northrop 1981). The theoretical KIE can be calculated by pure quantum chemical calculation and may be compared with observed AKIE to obtain information about occurring isotope effects (Wolfsberg et al. 2010).

Stable isotope composition of an element is conventionally expressed as the deviation of a sample from an international standard in parts per thousand (‰) and are given in

the δ notation ($\delta^{13}\text{C}$, $\delta^2\text{H}$ and $\delta^{37}\text{Cl}$) as shown in Eq. (1). R indicates the isotope ratio of $^{13}\text{C}/^{12}\text{C}$, $^2\text{H}/^1\text{H}$ or $^{37}\text{Cl}/^{35}\text{Cl}$. International standards for C, H and Cl are Vienna Pee Dee Belemnite (VPDB) (Coplen 2011, Coplen et al. 2006), Vienna Standard Mean Ocean Water (VSMOW) (Schimmelmann et al. 2016) and Standard Mean Ocean Chloride (SMOC) (Bernstein et al. 2011, Brand et al. 2014), respectively.

$$\delta E_{\text{sample}} = \frac{R_{\text{sample}}}{R_{\text{standard}}} - 1 \quad (1)$$

The isotope enrichment factor (ϵ) can be determined from the logarithmic form of the Rayleigh equation as in Eq. (2) (Meckenstock et al. 2004). δE_t and δE_0 are the isotopic signatures of the compound for the element E at a given time t and at the beginning of the reaction; while C_t/C_0 is the fraction of the remaining compound.

$$\ln\left(\frac{\delta E_t + 1}{\delta E_0 + 1}\right) = \epsilon \times \ln\left(\frac{C_t}{C_0}\right) \quad (2)$$

An extended Rayleigh-type equation was derived by Van Breukelen to improve the quantification of isotopic fractionation expressed during substrate consumption via competing pathways (Van Breukelen 2007). If a substrate is degraded via two pathways and the degradation reaction follows the first-order kinetics, the rate ratio of two competing degradation pathways (F) can be calculated from the observed isotope enrichment factor (ϵ_A) and the isotope enrichment factors associated with the two pathways ϵ_1 and ϵ_2 , as shown in Eq. (3). F indicates contribution of pathway 1 to the observed isotope fractionation ϵ_A . Note that Eq. (3) is applicable only for two competing pathways (Van Breukelen 2007).

$$F = \frac{\epsilon_A - \epsilon_2}{\epsilon_1 - \epsilon_2} \quad (3)$$

The enrichment factors represent isotope effects for the whole molecule. To characterize the isotope effect at the reactive position for a given compound, the AKIE value is calculated using Eq. (4) (Elsner et al. 2005). For a given postulated reaction mechanism, n is the number of E atoms in the molecule, x is the number of E atoms at reactive positions, and z is the number of E atoms at reactive positions with equal reactivity.

$$AKIE = 1 / \left(\frac{z \cdot n \cdot \varepsilon}{x \cdot 1000} + 1 \right) \quad (4)$$

To overcome the bias related to single-element isotope analyses, the use of two-element isotope analysis has been developed for identifying reaction mechanisms (Kuder et al. 2005, Zwank et al. 2005). If both elements are equally influenced by rate limitations in the rate-limiting step (known as the slowest step determining the overall kinetic rate) of a reaction, the effect on the KIE cancels (Fischer et al. 2008). Hence, the combination of two elements (eg. $\delta^{13}\text{C}$ vs. $\delta^2\text{H}$ values) is a useful way for more accurate assessment of the reaction mechanisms for many organic contaminants. The slope of the linear regression of simultaneously measured $\delta^2\text{H}$ versus $\delta^{13}\text{C}$ is known as the lambda value (Λ) which is calculated using Eq. (5) (Fischer et al. 2008). Accordingly, Λ values can be regarded as fingerprints of distinct reactions, providing useful and reproducible parameters for elucidating specific reaction pathways (Elsner et al. 2005).

$$\Lambda = \frac{\Delta \delta^2\text{H}}{\Delta \delta^{13}\text{C}} = \frac{\delta^2\text{H}_t - \delta^2\text{H}_0}{\delta^{13}\text{C}_t - \delta^{13}\text{C}_0} \approx \frac{\varepsilon_{\text{H}}}{\varepsilon_{\text{C}}} \quad (5)$$

The extent of *in situ* degradation (D%) in the field can be estimated for individual compounds using the isotope shifts between the source and the residual non-degraded fraction of the reacting compound using the Eq. (6) which is derived from the rearrangement of the logarithmic form of the Rayleigh equation (Eq. (2)). C_t is the concentration at a given reaction time t or on a flow path downgradient a source; C_0 is the concentration at the beginning of a reaction or in a source area; δ_t and δ_0 are the corresponding isotope ratios of the reacting compound; ε is the isotope enrichment factor for a degradation process, obtained from reference experiments under laboratory conditions using the Rayleigh equation (Eq. (2)).

$$D (\%) = \left(1 - \frac{C_t}{C_0} \right) \times 100 = \left[1 - \left(\frac{\delta_t + 1}{\delta_0 + 1} \right)^{\frac{1}{\varepsilon}} \right] \times 100 \quad (6)$$

1.3. Analytical challenges of stable hydrogen and chlorine isotope analysis

Current challenges in CSIA of organic contaminants in environmental science have been recently summarized elsewhere (Elsner and Imfeld 2016, Elsner et al. 2012, Nijenhuis et al. 2016, Nijenhuis and Richnow 2016, Schmidt et al. 2004, Vogt et al.

2016). CSIA has greatly facilitated assessment of sources and transformation processes of organic pollutants. However, most laboratories specialized in the usage of GC-IRMS focus on carbon isotope measurements. Until recently, the feasibility of multi-element CSIA was limited by the low availability of a robust methodology for precise isotope analysis (except ^{13}C) of heteroatom-bearing organic compounds (Nijenhuis et al. 2016). The extension of CSIA methods to additional elements (H, Cl, S, O, etc.) is therefore needed to improve environmental monitoring schemes of organic pollutants.

The high-temperature conversion (HTC) technique is a widely used method for H isotopic analysis of water and many organic materials (Sofer and Schiefelbein 1986, Tobias and Brenna 1997). However, it becomes more challenging for N-, Cl-, and S-containing organics due to the formation of H-containing byproducts such as HCN, HCl and H_2S . This incomplete conversion of organically bound H to molecular H_2 can finally lead to inaccurate $\delta^2\text{H}$ values. To overcome these limitations, many efforts have been made (Chartrand et al. 2007, Vetter et al. 2006). Gehre and colleagues (Gehre et al. 2015) developed a concept using a pyrolysis unit filled with chromium in an elemental analyzer and coupled to an IRMS. Due to a quantitative scavenging of the heteroatoms by the chromium, a complete conversion of the organically bound H to molecular H_2 was obtained. Moreover, Renpenning and colleagues (Renpenning et al. 2015b) successfully demonstrated the principle feasibility of the chromium-based high-temperature conversion (Cr/HTC) concept for CSIA in a GC-IRMS system. These findings imply that conventional HTC units for CSIA need critical evaluation as H-containing byproducts may be formed, preventing the accurate determination of hydrogen isotope compositions.

Chlorinated compounds are one of the priority environmental contaminants. Stable Cl isotope analysis of organic compounds is potentially applicable in various fields such as forensics and environmental analytics to investigate the fate of these substances. However, the wider use of this technique is still hampered by the limited applicability of available techniques. Several innovative solutions for GC coupling based on different strategies have been developed: (1) GC-MC-ICPMS method (Van Acker et al. 2006): Cl isotope composition is determined online using gas chromatography coupled with

multiple-collector inductively coupled plasma mass spectrometry (GC-MC-ICPMS). This method is very precise ($1\sigma=0.06\text{‰}$) and universally applicable, but it suffers from high interference of ArH^+ ions from the inductively coupled plasma. (2) GC-HTCMS method (Hitzfeld et al. 2011): an online HTC converts organic Cl into gaseous HCl under H_2 gas flow. It successfully converts organic Cl online to a Cl-containing gas. However, so far analysis was only realized on a quadrupole MS instrument with an IRMS, and with a precision better than $1\sigma=0.5\text{--}1\text{‰}$. This method suffers from the stability of the ceramic tube used for HTC operating at high temperatures (Renpenning et al. 2015a). (3) non-conversion method: the GC effluent is transferred directly to a high-precision IRMS (Shouakar-Stash et al. 2006) or a quadrupole MS (Aeppli et al. 2010, Jin et al. 2011, Sakaguchi-Soder et al. 2007). This method is only applicable to masses of target compounds for which a dedicated cup is configured in the IRMS detector. Therefore, molecularly identical reference components with defined isotope compositions and an anchor for scaling the chlorine isotope compositions are needed. Until recently, the isobaric interference of the ^{36}ArH dimer with ^{37}Cl was minimized by employing dry plasma conditions using GC-MC-ICPMS methods (Horst et al. 2017). The MC-ICPMS is operating in low resolution mode ($m/\Delta m = 300$) using a super dry plasma, which reduces interferences from protonation. The transfer line connecting GC and ICP was modified further in order to extend the range of analytes towards semi-volatile organic substances with boiling points of up to 350 °C (Renpenning et al. 2018). Thus, the modified method now allows the development of compound-specific stable chlorine isotope analysis concepts for virtually all GC-compatible organics with versatility, high accuracy, and sensitivity.

1.4. CSIA application for characterizing transformation mechanisms and evaluating *in situ* degradation

Previous studies have shown the potential use of stable isotope fractionation for characterizing transformation mechanisms of organic compounds. CAIS approach can reveal the rate-limiting step in reaction mechanisms such as the mode of chemical bond cleavage (Northrop 1981). It is well known that changes in single element isotope ratios (e.g. $\delta^{13}\text{C}$) tend to become smaller with larger molecular size due to isotope dilution

effects (Elsner et al. 2005, Meckenstock et al. 2004). Moreover, single element isotope ratios are possibly influenced by masking of isotope fractionation which makes the identification of degradation pathways by single-element isotope analysis more difficult (Renpenning et al. 2015c). Multi-element isotope analysis offers an opportunity to circumvent the problem. In the last decades, several studies showed the potential of multi-element CSIA ($\delta^{13}\text{C}$, $\delta^2\text{H}$, $\delta^{37}\text{Cl}$, $\delta^{15}\text{N}$ etc.) to explore different transformation processes (Badin et al. 2014, Kuder et al. 2013, Penning et al. 2010, Zhang et al. 2016a, Zhang et al. 2015).

CSIA opens the door to assess the field-based degradation reactions. CSIA enables the detection of *in situ* biodegradation of organic contaminants (Elsner 2010, Thullner et al. 2012). It has been applied to estimate the extent of *in situ* biodegradation of a specific compound based on changes in isotope ratios of field samples if the isotope enrichment factor of that compound is determined in laboratory experiments based on the Rayleigh equation (Bashir et al. 2015, Hofstetter et al. 2008, Liu et al. 2017, Thullner et al. 2012). For a better interpretation of the field data applying CSIA, isotope enrichment factors from laboratory experiments on enzymatic transformation and abiotic transformation (such as hydrolysis and photodegradation) are necessary to understand transformation mechanisms.

So far, CSIA has been used for investigation of traditional contaminant classes including BTEX, chlorinated aliphatic and aromatic hydrocarbons and others (Mak et al. 2006, Nijenhuis and Richnow 2016, Rosell et al. 2012, Vogt et al. 2016, Zhang et al. 2015). In addition, it has been proposed as a useful approach for characterizing degradation processes of micropollutants such as pesticides at field scale (Elsner and Imfeld 2016). However, only a few field studies applied CSIA to assess microbial degradation of different pesticides or herbicides (Bashir et al. 2015, Liu et al. 2017, Milosevic et al. 2013). Nevertheless, the application of CSIA for characterizing degradation processes of organophosphorus compounds has not been reported prior this dissertation.

CSIA is mostly applied to study the fate of organic pollutants in groundwater (Fischer et al. 2006, Mundle et al. 2012, Pooley et al. 2009, Thullner et al. 2012, Van Keer et al. 2012, Wiegert et al. 2012). Its application to other environmental compartments such as

sediments (Passeport et al. 2016) and surface waters is limited. In natural environments such as lakes and rivers, and in water treatment plants where UV/H₂O₂ advanced oxidation processes are applied, organic compounds can be eliminated via direct photolysis and indirect photolysis induced by reactive species such as OH radicals (HO[•]) (Boreen et al. 2003, Wols and Hofman-Caris 2012). HO[•] are naturally generated in all surface water environments by the photolysis of dissolved organic (Vaughan and Blough 1998) and inorganic compounds (Zafiriou 1974). Therefore, there is a great potential to evaluate the attenuation of contaminants with HO[•] in various aquatic systems using CSIA, which could be a promising tool for water quality monitoring and assessment.

1.5. Target compounds and their main degradation pathways in the environment

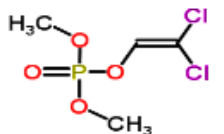
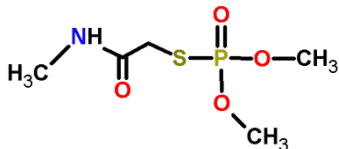
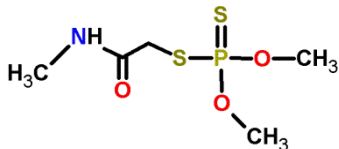
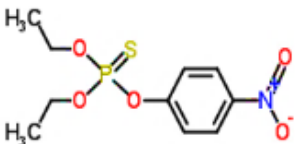
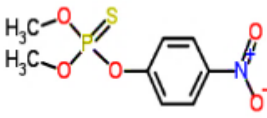

1.5.1. Organophosphorus compounds (OPs)

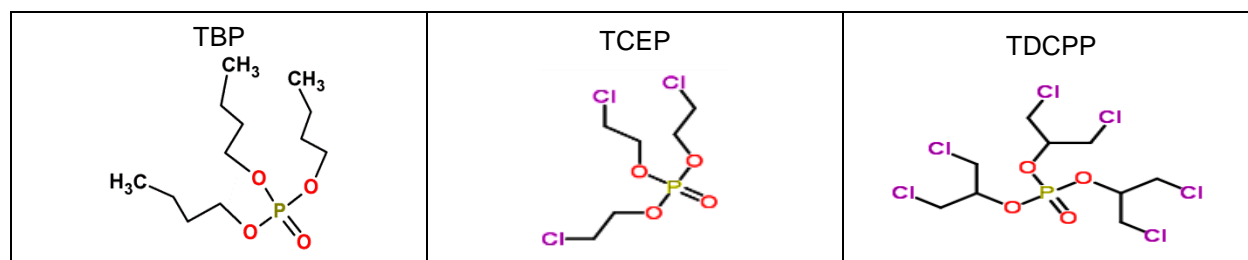
Organophosphorus compounds (OPs) are often used as pesticides, warfare agents, flame retardants, plasticizers, or flotation agents (Delfino et al. 2009). Today the consumption of OPs ranks in second position of the total global pesticide usage (Fenner et al. 2013). The OPs discussed in the present thesis are esters of phosphoric acids, thiophosphoric acids and dithiophosphoric acids, forming a wide variety of phosphates, phosphorothioates, or phosphorodithioates (Table 1), each of them has different reactivities towards hydrolysis, oxidation and biodegradation (Pehkonen and Zhang 2002, Singh and Walker 2006). Many OP derivatives are associated with acute toxicity by inhibiting acetylcholinesterase (AChE) in the nervous system (Pope 1999). Hence, they are used as pesticides for control of insects and other higher organisms (Colovic et al. 2013). OP pesticides are less persistent in the environment when compared with organochlorine pesticides and thus have been widely used on a global scale. The continuous and excessive use of OPs has led to severe environmental pollutions.

Hydrolysis is stated to be one major pathway controlling the fate of OPs in the environment. Hydrolysis of OPs proceeds by a bimolecular nucleophilic substitution mechanism (S_N2 mechanism), where H₂O and OH⁻ act as nucleophiles (Pehkonen and Zhang 2002). The ester bonds of OPs can be hydrolyzed under acidic and alkaline

conditions by two different pathways, however, the relative contribution of each hydrolysis pathway is pH-dependent (Pehkonen and Zhang 2002). Photodegradation and chemical oxidation are other important degradation processes. Several studies investigated the reaction mechanisms of OPs during photodegradation, in which simultaneously proceeding pathways including oxidation of P=S to P=O, elimination of nitro group, re-methylation and oxidation of the alkyl substituent were proposed (Araújo et al. 2007, Durand et al. 1994, Kanmoni et al. 2012, Sakellarides et al. 2003, Santos et al. 2005, Wu and Linden 2008). Photosensitizer-promoted indirect photolysis is considered to be a naturally occurring degradation process, which could be an important factor governing the fate of organic contaminants in the environment. Microbial degradation of OPs by most of the bacteria is catalyzed by a structurally similar enzyme called organophosphate hydrolase or phosphotriesterase (Singh and Walker 2006). In previous studies, several species of bacteria have been isolated and were shown to be able to degrade parathion via co-metabolic and bio-mineralization modes, including *Flavobacterium sp.* (Sethunathan and Yoshida 1973), *Bacillus sp.* (Nelson 1982, Nelson et al. 1982), *Pseudomonas sp.* (Siddaramappa et al. 1973), *Arthrobacter sp.* (Nelson 1982). The proposed first step of biodegradation mechanisms of parathion include three pathways: (A) hydrolysis of the phosphotriester bond to form *p*-nitrophenol (P-O bond cleavage), which is the major pathway; (B) reduction of the nitro group acting as electron acceptor to form amino parathion (N-O bond cleavage); (C) oxidation of the sulfur group of parathion to form paraoxon (P=S bond cleavage).

Table 1: Chemical structure of the target compounds of organophosphorus compounds (OPs).

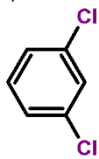
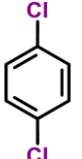
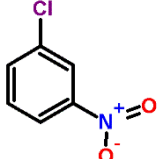
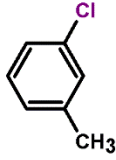
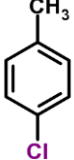
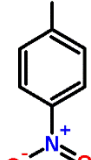
<p>dichlorvos</p> 	<p>omethoate</p> 	<p>dimethoate</p> 
<p>parathion</p> 	<p>methyl parathion</p> 	<p>chlorpyrifos</p> 



1.5.2. Substituted chlorobenzenes

Substituted chlorobenzenes are the basic chemical structures of many environmental contaminants such as the herbicides 2,4-D and dichlorprop, drugs and personal care products like triclosan and diclofenac. Isomers of dichlorobenzene (DCB), chloromethylbenzene (CMB), and nitrochlorobenzene (NCB) (Table 2) are the simplest forms of substituted chlorobenzenes. They are widely distributed in surface waters (Schwarzbauer and Ricking 2010) in the low ng L^{-1} or $\mu\text{g L}^{-1}$ range (Bester et al. 1998, Lekkas et al. 2004, Trova et al. 1991), due to their use as chemical intermediates in the production of dyes, solvents, pesticides, and pharmaceuticals. They have all been listed as substances which belong to List I of European Council Directive 76/464/EEC (European Commission 1982) due to their known or suspected toxicity to aquatic organisms and mutagenic and carcinogenic potentials (Calamari et al. 1983, OECD 2005, Shimizu et al. 1983, Weisburger et al. 1978). Characterizing transfer and transformation processes of substituted chlorobenzenes in surface waters is therefore essential for developing effective remediation strategies and, thus, to protect human and aquatic life. In natural environments such as lakes and rivers, and in water treatment plants where UV/H₂O₂ advanced oxidation processes are used, organic compounds can be eliminated via direct photolysis and indirect photolysis induced by the formation of reactive species such as HO[•] (Boreen et al. 2003, Wols and Hofman-Caris 2012). The reaction mechanisms governing the direct and indirect photodegradation of substituted chlorobenzenes are not well understood yet. In addition, the magnitude of isotope fractionation during photodegradation reactions, and the extent to which it can contribute to deciphering reaction pathways have not been the subject of many studies.

Table 2: Chemical structure of the target compounds of substituted chlorobenzenes.

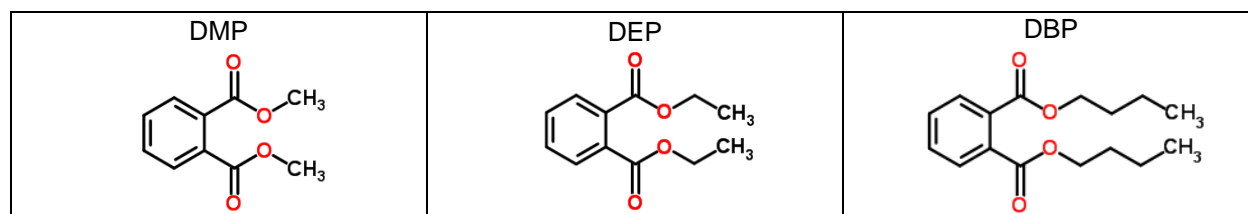
<p>1,3-DCB</p> 	<p>1,4-DCB</p> 	<p>3-NCB</p> 
<p>3-CMB</p> 	<p>4-CMB</p> 	<p>4-NCB</p> 

1.5.3. Phthalate esters (PAEs)

Phthalate esters (PAEs) are widely used as plasticizers and additives in numerous products, including polymers such as polyvinylchloride (PVC) and plastic toys, cosmetics, medical devices, and detergents (Staples et al. 1997). PAEs are not linked by covalent bonds within the product matrix; therefore, they can leach out from the matrix by lipophilic solvents or diffusion and spread into the environment (Sun et al. 2015, Vamsee-Krishna and Phale 2008). Consequently, the broad usage of PAEs have resulted in rising concerns due to the potential hepatotoxic, teratogenic and carcinogenic effects (Tang et al. 2016). Dimethyl phthalate (DMP), diethyl phthalate (DEP) and dibutyl phthalate (DBP) (Table 3) have been listed as priority pollutants by the US EPA. Biodegradation plays an important role for PAEs removal in various environments. The de-esterification of phthalate diesters to phthalate monoesters is considered to be the primary biodegradation pathway under aerobic and anoxic conditions (Gao and Wen 2016, Shelton et al. 1984). A well-known model organism for aerobic biodegradation of PAEs is *Rhodococcus opacus* strain DSM 43250 (Engelhardt and Wallnöfer 1978, Engelhardt et al. 1975). Even though the hydrolysis rates of PAEs are reported to be rather slow, with half-lives of more than 100 days (Staples et al. 1997), hydrolysis is expected to be an relevant abiotic degradation mechanism and even dominant abiotic process under certain environmental conditions, such as lower landfill layers due to high temperatures (Huang et al. 2013). It is well noted that PAEs

undergo two hydrolytic steps: they are initially converted to the corresponding monoester releasing one alcohol moiety via hydrolysis of the ester group, and followed by the hydrolysis of the monoester to phthalic acid and a second alcohol moiety (Staples et al. 1997). Hydrogen peroxide (H₂O₂) and persulfate (PS) are the most commonly used oxidants in *in situ* chemical oxidation (ISCO) (Devi et al. 2016, Tsitonaki et al. 2010). UV/H₂O₂ has been proven as an efficient activation method to produce HO[•] and has been used to degrade several organic compounds such as PAEs, BPA, dyes, benzene and PAHs (Gmurek et al. 2017, Xu et al. 2009, Xu et al. 2007). Over the last few years, sulfate radicals (SO₄^{•-}) generated by persulfate were suggested as an alternative to HO[•] due to its long lifetime and high redox potential. SO₄^{•-} has the ability to oxidize a variety of compounds, including PAEs, BTEX, PCBs, PAHs and others (Tsitonaki et al. 2010, Zhang et al. 2016b). It has been well demonstrated that the formation of SO₄^{•-} and HO[•] is pH dependent in the persulfate based ISCO system (Devi et al. 2016, Liang and Su 2009, Romero et al. 2010), however, it is still not clear how to quantify their relative contributions.

Table 3: Chemical structure of the target compounds of phthalate esters (PAEs).

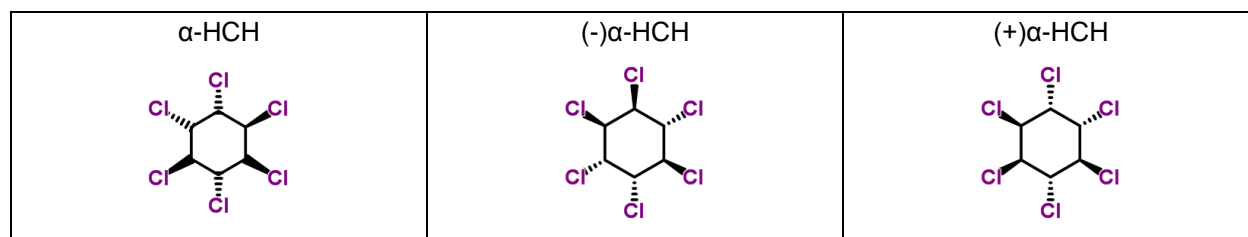


1.5.4. Hexachlorocyclohexanes (HCHs)

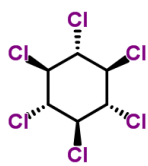
Hexachlorocyclohexane isomers (HCHs) (Table 4) are commercially manufactured by the reaction between benzene and chlorine in the presence of UV light. Except for γ -HCH which was one of the most extensively used organochlorine pesticides, all other isomers do not possess any specific insecticidal property. The production of γ -HCH generates up to 90% (weight) of HCHs containing waste. Huge amounts of HCHs waste were often deposited in uncontrolled manners, resulting in a serious environmental pollution worldwide (Li 1999, Vijgen 2006). HCHs are considered as persistent organic pollutants due to their relative long-life time in the environment. Because of their low

water solubility, HCHs tend to accumulate in the soil and enter the food web through plant uptake from the roots and air (Calvelo Pereira et al. 2006, Trapp 2015). HCHs can be transported over long distances by geochemical processes like global distillation (Simonich and Hites 1995). Thus, HCHs residues were found in elevated concentration in Arctic and Antarctic animals at the end of the food chain (Carlsson et al. 2014, Lana et al. 2014, Wiberg et al. 2000, Yasunaga et al. 2015). To date, the only study using CSIA to investigate reactive bioaccumulation of contaminants was reported by Holmstrand and colleagues (Holmstrand et al. 2007), where dichlorodiphenyltrichloroethane (DDT) was extracted from 16 kg of seal blubber by continuous partitioning using a Wallenberg perforator. This approach is limited by the availability of large amounts of sample material, as well as of appropriate laboratory equipment. Thus, methods for extraction and clean-up of HCHs from various biota matrixes, as well as routine laboratory preparation methods are needed to be developed for exploitation of isotope fractionation concepts for long range transports and food webs studies. The combination of enantiomer and isotope fractionation holds promising potential for the characterization and quantification of biodegradation processes, which has already been applied for evaluating chiral compounds such as phenoxy acid herbicides in the field (Milosevic et al. 2013). Recently, CSIA and enantioselective stable isotope analysis (ESIA) have been proposed as tools to monitor transformation of α -HCH in a complex groundwater system (Liu et al. 2017). Nevertheless, the application of the combined isotope and enantiomer fractionation analysis for evaluating contaminants degradation has challenged environmental scientists for almost a decade (Jammer et al. 2015), as a theoretical foundation for models which describe the molecular mechanisms governing isotope and enantiomer fractionation processes are still lacking.

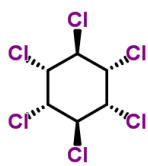
Table 4: Chemical structure of the target compounds of hexachlorocyclohexanes (HCHs).



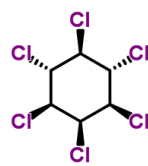
β -HCH



γ -HCH



δ -HCH



2. Objectives

The aim of the thesis was to extend multi-element CSIA methods to new compounds (OP pesticides, flame retardants) and to characterize fundamental processes such as hydrolysis, photodegradation and enzymatic transformation using isotope fractionation concepts. Therefore, the specific objectives of this PhD study were the following:

- (1) To validate analytical methods for $\delta^{13}\text{C}$ and $\delta^2\text{H}$ analysis of eight OPs as model compounds for phosphates, phosphorothioates or phosphorodithioates for multi-element CSIA and to explore method detection limits (section 3.1).
- (2) To develop methods for HCHs enrichment and clean-up from environmental and particularly from biological samples for stable carbon, hydrogen and chlorine isotope analysis in order to explore the potential of multi-element CSIA as tool for assessing transformation reactions in food web studies (section 3.2).
- (3) To characterize fundamental processes such as hydrolysis, radical oxidation, photodegradation and enzymatic transformation of target compounds using isotope fractionation concepts and to provide insights into the reaction mechanisms (section 3.3). Specific transformation processes include the hydrolysis and radical oxidation of OPs (section 3.3.1 and 3.3.2), the direct and indirect photodegradation of CH_3 -, Cl -, and NO_2 - substituted chlorobenzenes in aqueous solution (section 3.3.3), the radical oxidation, hydrolysis and aerobic biodegradation of three PAEs (section 3.3.4), and the aerobic biodegradation and the LinA-catalyzed enzymatic transformation of α -HCH (section 3.3.5).
- (4) To investigate natural attenuation of parathion by hydrolysis at a contaminated site using CSIA (section 3.4).

The ultimate goal was to understand the transformation of organic pollutants in the environment by applying CSIA. It was expected that the isotope fractionation patterns characterizing fundamental (bio)chemical processes of model compounds can be obtained from laboratory experiments under controlled conditions. This knowledge could be then applied for extending CSIA field application in complex environments. Particular process understanding is needed for tackling new issues such as transformation of persistent contaminants in food webs or degradation in engineered systems.

3. Results and discussion

3.1. Validation of GC–IRMS techniques for $\delta^{13}\text{C}$ and $\delta^2\text{H}$ CSIA of OPs

The feasibility of multi-element CSIA was limited by missing robust analytical methods for precise hydrogen isotope analysis of heteroatom-bearing organic compounds. This study aimed to compare the HTC and Cr/HTC conversion units to explore the limitations of hydrogen isotope analysis of OPs which are complex heteroatom-bearing compounds and may contain N, S, O and Cl in one molecule besides C and H. Some OPs are thermally labile and can disintegrate in the injector system, which may complicate analysis. The first aim was to develop analytical methods for $\delta^{13}\text{C}$ and $\delta^2\text{H}$ analysis of eight OPs (Fig. 1) used as model compounds for phosphates, phosphorothioates or phosphorodithioates for multi-element CSIA and to explore detection limits. The second aim was the comparison of HTC and Cr/HTC for complex heteroatomic compounds in order to validate the reliability of these methods using OPs as model substrates.

Decomposition of OPs in the GC injector

Many OPs including parathion, dimethoate and omethoate are thermally unstable and decompose at relatively low temperatures. For example, parathion decomposes above 200 °C (ICSC 2004) and omethoate starts to decompose at about 135 °C (HSDB 2004). The disintegration of thermally labile OPs in the hot injector was investigated and the measures to reduce such thermal disintegration were taken. The following suggestions can be applied to get more reliable isotope analysis especially regarding $\delta^2\text{H}$ analysis for OPs: 1) lower the injector temperature; 2) avoid high amounts of sample injected into the GC; 3) use glass liner without glass wool; 4) deactivate the liner with N,O-Bis(trimethylsilyl)trifluoroacetamide (BSTFA). The GC injector temperature was optimized for each tested compound, which is 180 °C for omethoate, dimethoate, methyl parathion (MP) and parathion (EP), 195 °C for dichlorvos and tris(2-chloroethyl) phosphate (TCEP), 220 °C for chlorpyrifos and 260 °C for tris(1,3-dichloro-2-propyl)phosphate (TDCPP).

Dependency of isotope compositions on the concentration of OPs (Linearity ranges)

Linearity ranges of $\delta^{13}\text{C}$ were obtained for both chlorinated and non-chlorinated OPs (Fig. 1 (Wu et al. 2014) and Fig. 1 (Wu et al. 2017)). The $\delta^2\text{H}$ values via GC-Cr/HTC-IRMS are independent of the injected amount of hydrogen within 42 - 120 Vs area signal for eight tested OPs. The significant variety of the lower limits for precise CSIA could be caused by the compound-specific transformation efficiency of different OPs in the Cr/HTC reactor. In contrast, linearity ranges for $\delta^2\text{H}$ via GC-HTC-IRMS were only obtained for non-chlorinated OPs (Fig. 1). Nonlinearity of $\delta^2\text{H}$ for analyzed chlorinated compounds may be due to the conversion process and byproduct formation via GC-HTC-IRMS (Fig. 1). Mass spectrometric analysis of byproduct formation indicated that the formation of HCl was a significantly isotope fractionating process leading to inaccurate $\delta^2\text{H}$ analysis in HTC. Nevertheless, in case of non-chlorinated OPs, byproduct formation of HCN, H_2S or PH_3 in HTC was observed. However, it did not affect the dynamic range of reproducible isotope values above the limit of detection. Good linearity for non-chlorinated OPs was obtained via conventional HTC, which indicates that H-containing byproducts might not be associated with isotope fractionation or the fractionation during thermal decomposition is minor and stable. No H-containing byproducts were found in the Cr/HTC conversion process by using ion trap mass spectrometry analysis (Fig. 2 (Wu et al. 2017)). The mean $\delta^2\text{H}$ value of parathion obtained via HTC ($-115 \pm 3\text{‰}$) differs from that obtained via Cr/HTC ($-138 \pm 4\text{‰}$), which is mostly probably due to the typical peak shape of parathion via HTC, which usually shows peak fronting and peak tailing in the chromatogram. The accuracy of GC-IRMS was validated in comparison to EA-IRMS (Fig. 3 (Wu et al. 2017)). The developed method allows an accurate and precise isotope analysis of OPs. Cr/HTC is a promising approach for hydrogen isotope analysis of heteroatom-bearing organic compounds, such as OPs. However, if no Cr/HTC is available, ^2H isotope fractionation processes can be reproducibly analyzed by conventional HTC for non-chlorinated OPs if a good linearity can be achieved.

Effect of evaporation processes on the isotope composition

Compound-specific stable isotope analyses of carbon, hydrogen and chlorine are several orders or magnitude less sensitive than modern GC or HPLC analysis, and thus

samples usually need to be concentrated to enrich sufficient material prior to their analysis via GC-IRMS systems. The effects of solvent evaporation on the isotope composition of analyte were evaluated. Evaporation is a distillation process which in principle can lead to isotope fractionation. Therefore, an evaporation experiment was conducted and the isotopic composition of the target OPs was determined before and after the evaporation procedure. After reducing the solvent volume from 100 mL to 0.5 mL, the observed shifts of $\delta^{13}\text{C}$ and $\delta^2\text{H}$ for tested OPs are negligible.

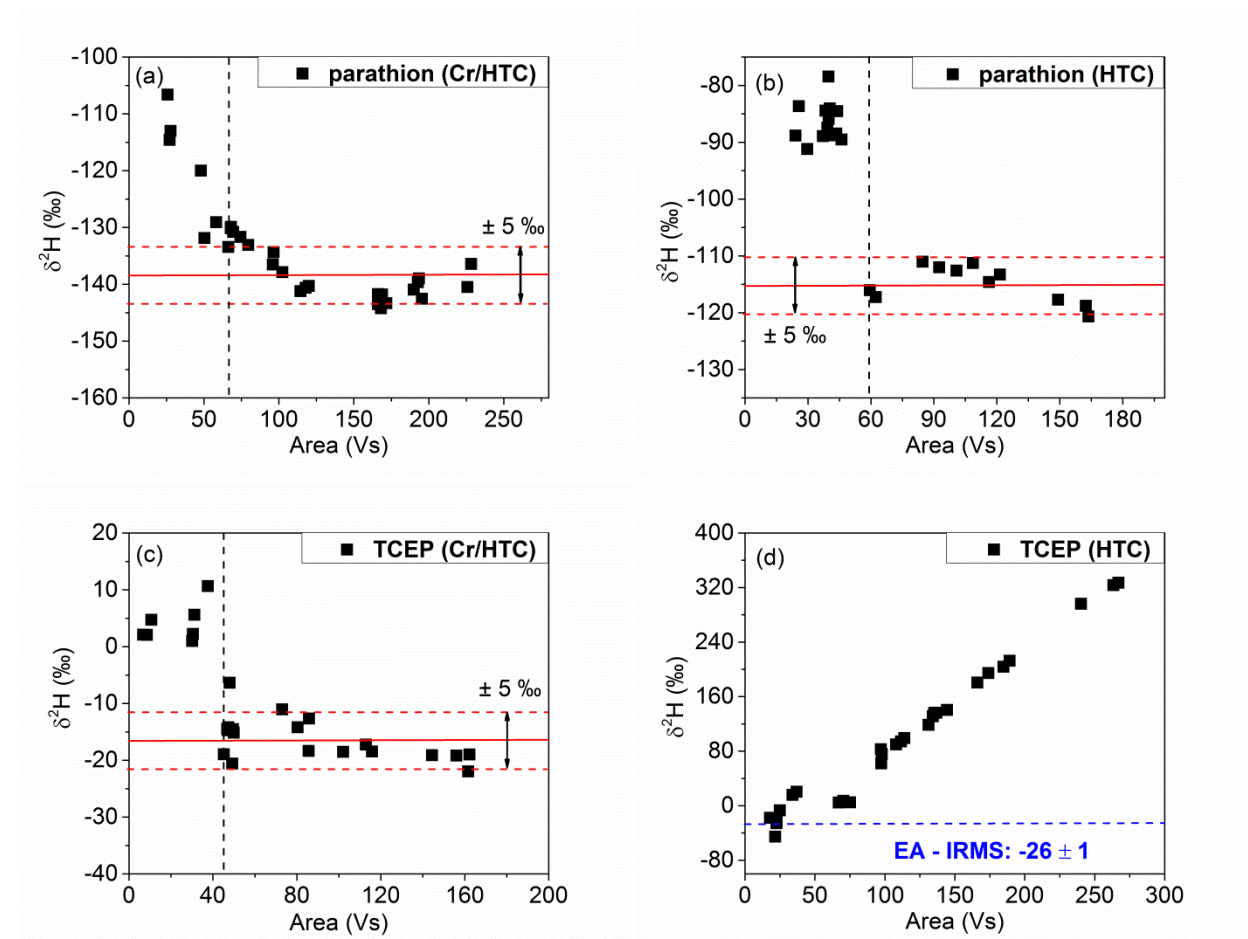


Fig. 1: Linearity analysis of $\delta^2\text{H}$ values of parathion and TCEP to correlate isotope composition to the signal intensity. The linearity of $\delta^2\text{H}$ measurements were assessed with GC-Cr/HTC-IRMS (a, c) and GC-HTC-IRMS (b, d). Black dotted lines indicate the lower limits of precise CSIA; red dotted lines indicate the analytical uncertainty for hydrogen isotope analysis; solid lines represent the mean values of all measurements within the linearity ranges.

3.2. Effects of sample preparation on CSIA of HCHs for food web studies

One of the main bottlenecks for CSIA is the moderate analytical sensitivity and high purity required for a good chromatographic baseline separation which is necessary for the accurate isotope analysis. The high detection limit of CSIA makes the investigation of contaminants in food webs challenging, since large amounts of sample material are required to enable isolation of sufficient compound quantities. Extraction is a process of phase partitioning which in principle is associated with isotope effects, and the isotope effects can become significant if it accumulated during phase partitioning (Kopinke et al. 2005). Moreover, the high lipophilicity of HCHs makes the separation from lipids highly challenging. Thus, methods for extraction, separation and clean-up of HCHs from biological matrices, as well as routine laboratory preparation methods are needed for the implementation of CSIA. The main objective of this study is to develop methods for HCHs extraction and clean-up from environmental and particularly from biological samples including water, soil, plant, milk, fish oil and pork liver for stable carbon, hydrogen and chlorine isotope analysis.

HCHs extraction protocols and efficiencies from different matrixes

A central step of enrichment strategies is evaporation of the solvent for concentrating target components. Insignificant isotope effects associated with solvent evaporation were observed by Ivdra et al (Ivdra et al. 2017). Column chromatography packed with Florisil slurry and pre-eluted by hexane gives almost complete recovery of HCHs. Florisil was selected in the present study due to its potential to retain lipids and high polar materials, as well as its capability of effecting clean-up of nonpolar pesticide residues from food samples (Koc and Karakus 2011). Plants were first freeze-dried in order to minimize the losses in comparison to air-drying, as HCHs are relatively volatile hydrophobic compounds. Lipids have relative lower solubility in acetonitrile compared to hexane. Therefore, acetonitrile was applied to remove large amounts of lipids from fish oil which was selected to represent samples extremely enriched in lipids. Hexane was applied to remove water and hydrophilic substances in the first extraction step from the milk which is the representative sample containing not only lipids but also a large amount of water. Moreover, fresh pork liver was chosen as a representative sample

containing high amounts of fat and protein. Liver sample was homogenized using a food blender before solvent extraction. Co-extracted lipids from fish oil, milk and liver were removed by acidic hydrolysis using 95% concentrated H_2SO_4 , and then followed by a saponification process using 0.5 M NaOH solution. The majority of hydrolyzed carboxylic acids were deprotonated and polar hydrolysis products were dissolved in the water phase, so that HCHs could be extracted with hexane. Obtaining a clear phase separation in each step is essential to improve the HCHs recoveries. The overall HCHs recoveries were 86 - 95% from water and soil, 36 - 66% from plants, and 16 - 44% from fish oil, milk and liver, respectively.

Effects of sample treatment on stable isotope composition

Considering the typical analytical uncertainty of $\pm 0.5\text{‰}$ for $\delta^{13}\text{C}$, $\pm 5\text{‰}$ for $\delta^2\text{H}$ and $\pm 0.2\text{‰}$ for $\delta^{37}\text{Cl}$, the slight shifts of isotope compositions before and after HCHs extraction from different matrices were found to be lower than the analytical uncertainty and hence within acceptable ranges (Table 2 (Wu et al. 2018b)). Conclusively, negligible stable isotope fractionation could be observed after extraction and separation of HCHs from biological samples. Among the procedures applied in the present study, HCHs transformation processes could occur during the saponification step, since HCHs can be hydrolyzed under alkaline conditions (Zhang et al. 2014). However, the observed slight shifts of isotope compositions indicated that the isotope fractionation occurring during the short time period of the saponification process was negligible. Despite the lower extraction recoveries achieved above, the main contribution of the presented study is to prove that it is possible to extract and purify HCHs from complicated matrices by using the modified methods, and most importantly the isotopic composition is not changed by the method procedures. Therefore, it can be applied to investigate the reactive transformation of HCHs in food webs.

Matrix effects on the $\delta^{37}\text{Cl}$ analysis

The bottle neck for $\delta^{13}\text{C}$ and $\delta^2\text{H}$ analysis is the clean-up step to obtain analytes containing fractions that allow base line separation from other organic compounds. In contrast, the analysis of $\delta^{37}\text{Cl}$ requires base line separation of only Cl-containing

analytes. In order to evaluate potential interference of the Cl-free matrix on $\delta^{37}\text{Cl}$ values, HCHs and different amounts of diesel were dissolved in hexane. The GC-MS chromatography indicated that HCHs peaks overlapped with matrices (Figure S1 (Wu et al. 2018b)). However, when the same samples were injected into the GC-MC-ICPMS, a clear base line separation could be achieved (Figure S2 (Wu et al. 2018b)). No significant changes in $\delta^{37}\text{Cl}$ were observed. The large carbon and hydrogen background from the diesel component do not cause interferences during determination of chlorine isotope ratios. Conclusively, Cl-free matrices are not likely to affect the performance of the $\delta^{37}\text{Cl}$ analysis when using GC-MC-ICPMS.

Environmental applications

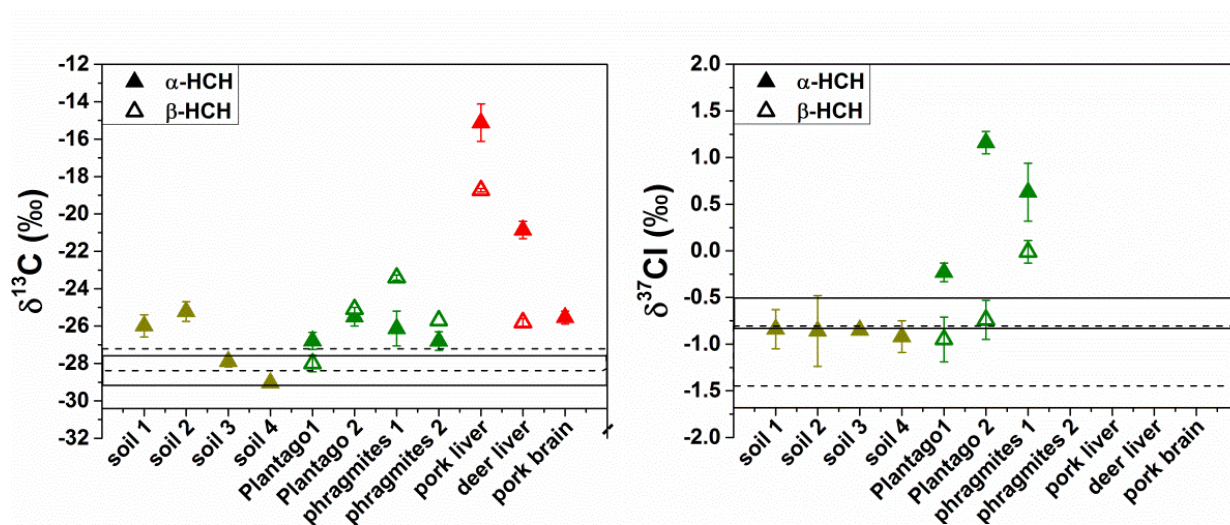


Fig. 2: $\delta^{13}\text{C}$ and $\delta^{37}\text{Cl}$ values of α -HCH (solid triangles) and β -HCH (open triangles) from contaminated soil, plants, animal liver and brain. The HCHs extracted from contaminated soil, plants and livers are indicated by brown, green and red color, respectively. Solid lines indicate the isotope composition variation of α -HCH muck; dotted lines indicate the isotope composition variation of β -HCH muck.

The $\delta^{13}\text{C}$ and $\delta^{37}\text{Cl}$ of HCHs from various contaminated samples from Bitterfeld/Wolfen (Germany) were analyzed in order to validate the potential of CSIA for food web studies (Fig. 2). HCH muck, which is composed of gray to white crystals, contains more than 90% (weight) of HCHs and is considered to represent the original source and hence the initial isotopic composition of HCH waste material in Bitterfeld (Liu et al. 2017). Compared to the HCH muck, the shifts of $\delta^{13}\text{C}$ and $\delta^{37}\text{Cl}$ in contaminated plants indicated that uptake

of HCHs in plants were associated with isotope fractionation, suggesting biodegradation in the rhizosphere or in the plants. In addition, strong carbon isotope enrichment of HCHs in the liver (up to 14.1‰ for α -HCH and 9.7‰ for β -HCH) suggests that there is active degradation probably by liver enzymes and only a residual fraction was accumulated in the liver after intensive metabolism. Based on the Rayleigh approach, significant isotope enrichment combined with specific ϵ can be applied to quantify the reactive transport of HCHs from soil to plant, and to higher organisms. The isotope enrichment may illustrate the degradation taking place during this process. Correlation of ^{13}C , ^2H and ^{37}Cl isotope fractionation (Multi-element CSIA) may be used to identify the bond cleavage reactions of degradation processes of halogenated contaminants in future studies (Franke et al. 2017, Kuder et al. 2013, Renpenning et al. 2014).

3.3. CSIA for characterizing chemical and biological transformation of organic compounds

3.3.1. Isotope fractionation of OPs during hydrolysis

Hydrolysis is considered to be an important chemical transformation reaction of OPs in the environment. Dimethoate, EP, MP and tributyl phosphate (TBP) were selected as model compounds to study different modes of hydrolysis by CSIA. The main objective was to investigate the ^{13}C and ^2H isotope fractionation patterns associated with hydrolysis of OPs.

Table 5: Summary of the reaction rate constants (κ), isotope enrichment factors (ϵ), and 95% confidence intervals (CI 95%) upon hydrolysis of OPs at different pH.

reaction	T (°C)	pH	K ($\times 10^{-5} \text{ s}^{-1}$)	$\epsilon_{\text{C}} \pm 95\% \text{CI}$ (‰)	$\epsilon_{\text{H}} \pm 95\% \text{CI}$ (‰)
dichlorvos	22	10	n.c.	-0.2 ± 0.1	n.c.
dimethoate	22	10	n.c.	-1.0 ± 0.1	n.c.
dimethoate	60	7	0.57	-8.3 ± 0.3	n.d.
dimethoate	30	9	0.35	-1.4 ± 0.1	-10 ± 3
dimethoate	4	12	121.31	-0.4 ± 0.1	-10 ± 5
MP	60	2	0.78	-10.0 ± 0.7	n.d.
MP	60	5	1.00	-10.5 ± 1.1	n.d.
MP	60	7	1.36	-9.9 ± 0.7	n.d.
MP	60	9	1.53	-6.5 ± 0.4	n.d.

MP	20	12	5.58	n.d.	n.d.
EP	60	2	0.25	-6.9 ± 0.8	n.d.
EP	60	5	0.28	-6.7 ± 0.4	n.d.
EP	60	7	0.31	-6.0 ± 0.2	n.d.
EP	60	9	0.42	-3.5 ± 0.4	n.d.
EP	20	12	0.64	n.d.	n.d.
EP	30	12	2.19	n.d.	n.d.
EP	40	12	7.92	n.d.	n.d.
TBP	80	2	0.06	-3.8 ± 0.3	n.d.
TBP	80	7	0.05	-4.6 ± 0.5	n.d.
TBP	80	9	0.11	-2.8 ± 0.1	n.d.
TBP	35	12	0.03	n.d.	n.d.

n.d. = "not determined"; n.c. = "not conducted".

The hydrolysis of EP is a homogeneous reaction following pseudo-first-order kinetics. Significant ^{13}C isotope fractionation was observed at lower pH, corresponding to $\epsilon_{\text{C}} = -6.9 \pm 0.8\text{‰}$ at pH 2, $-6.7 \pm 0.4\text{‰}$ at pH 5 and $-6.0 \pm 0.2\text{‰}$ at pH 7 (Table 5). Smaller but still significant ^{13}C isotope fractionation corresponding to $\epsilon_{\text{C}} = -3.5 \pm 0.4\text{‰}$ for EP was observed during hydrolysis at pH 9. However, no ^{13}C isotope fractionation was observed for EP hydrolysis at pH 12. The reduction of ϵ_{C} by almost half at pH 9 compared to neutral conditions suggests two pathways of hydrolysis. According to the calculation using the extended Rayleigh-type equation derived by Van Breukelen (Van Breukelen 2007), EP hydrolysis at pH 9 has a contribution of 51 - 58% compared to the reaction pathway under acidic condition. Furthermore, no significant changes in hydrogen isotope ratios of EP were observed during hydrolysis at any pH, indicating no H bond cleavage is involved during the rate limiting step of the hydrolysis. Similar ^{13}C and ^2H isotope fractionation patterns were observed for the other tested OPs, the isotope enrichment factors are summarized in Table 5.

In summary, two general hydrolysis pathways of OPs, including phosphates, phosphorothioates and phosphorodithioates, can be proposed (Fig. 3): one is P-O (or P-S) bond cleavage by nucleophilic attack at the P atom, resulting in no ^{13}C and no ^2H isotope fractionation; another one is C-O bond cleavage by nucleophilic attack at the C atom, resulting in a significant ^{13}C but no ^2H isotope fractionation. Therefore, ^{13}C isotope fractionation can be used to distinguish different hydrolysis pathways of OPs.

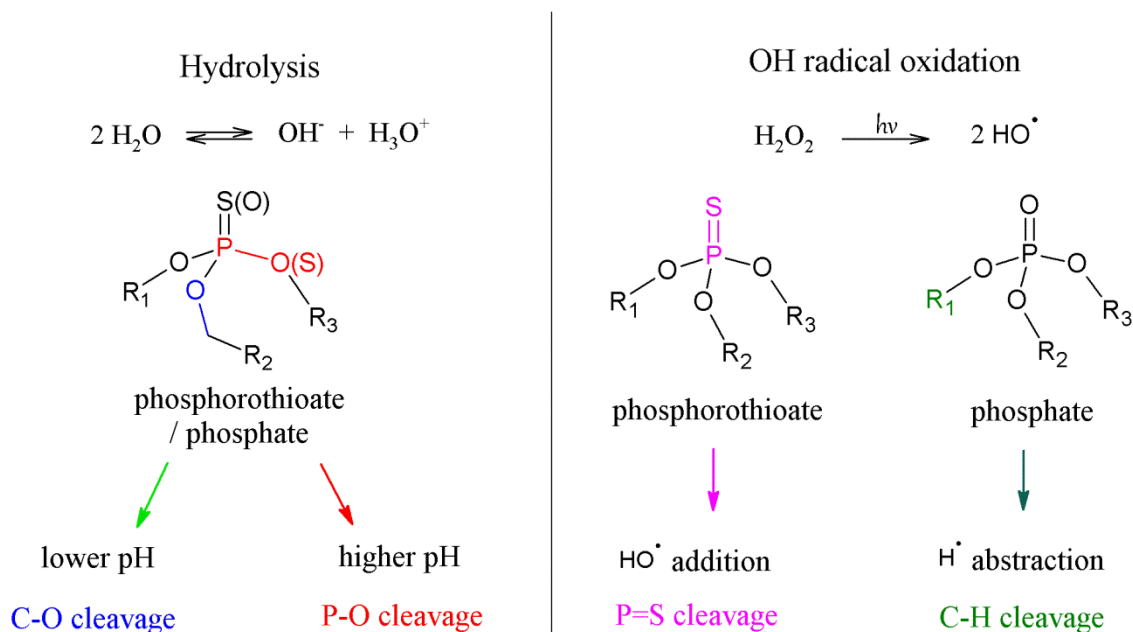


Fig. 3: Proposed transformation mechanisms of OPs during hydrolysis at different pH and HO[•] oxidation. R₁ and R₂ are predominantly aryl or alkyl group. R₃ can be diverse and may belong to a wide range of aliphatic, aromatic or heterocyclic groups.

3.3.2. Isotope fractionation of OPs during radical oxidation

The main objective of this study was to evaluate the ¹³C and ²H isotope fractionation patterns associated with radical oxidation of OPs. HO[•] oxidation of EP (model of phosphorothioates) by indirect photolysis (UV/H₂O₂) was investigated to compare isotope fractionation patterns with those obtained from hydrolysis. HO[•] oxidation of TCEP (model of phosphate) by Fenton reaction and indirect photolysis (UV/H₂O₂) was performed to understand the isotope fractionation associated with an H-abstraction step. Moreover, the isotope fractionation patterns of TBP by SO₄^{•-} and HO[•] oxidation, generated by potassium peroxydisulfate (KPS) and UV/H₂O₂, were also examined in order to investigate the contribution of different radicals.

Isotope effects and insight into reaction mechanisms of EP and TCEP by HO[•] oxidation

The obtained ε values are summarized in Table 6. The ¹³C isotope fractionation of EP associated with HO[•] reaction induced by UV/H₂O₂ photolysis was low but still could be quantified by the Rayleigh model, which corresponded to a ε_C of -0.8 ± 0.1‰. No

detectable ^2H isotope fractionation was observed. The ^{13}C and ^2H isotope fractionation of TCEP in the UV/ H_2O_2 system yielded a ϵ_{C} of $-1.4 \pm 0.1\text{‰}$, and a ϵ_{H} of $-56 \pm 3\text{‰}$. The ^2H and ^{13}C isotope fractionation are linearly correlated yielding a dual isotope enrichment factor (Λ) of 43 ± 5 . The Fenton reaction of TCEP yielded an ϵ_{C} of $-1.0 \pm 0.2\text{‰}$ and an ϵ_{H} of $-34 \pm 5\text{‰}$, which corresponded to a Λ factor of 35 ± 5 . These results suggest that the major reaction mechanisms of OPs during HO^\bullet reaction are related to their chemical structures as illustrated in Fig. 3: (1) In case of a phosphorothioate structure (e.g. EP), the P=S bond is oxidized to form a P=O bond in the rate determining step yielding very low or no ^{13}C and ^2H isotope fractionation. This is in contrast to (2) C-H bond breaking during the H abstraction step in case of alkyl-substituted phosphate structure (e.g. TCEP). In addition, the photodegradation products of EP and TCEP were characterized to confirm proposed OP transformation pathways using transformation product patterns. These two major chemical structure-dependent reaction mechanisms of OPs can be distinguished by applying the ^{13}C and ^2H isotope fractionation approach diagnostically.

Table 6: Summary of the reaction rate constants (κ), isotope enrichment factors (ϵ), and 95% confidence intervals (CI 95%) for radical oxidation of OPs at different pH.

Reaction	T (°C)	pH	K ($\times 10^{-5} \text{ s}^{-1}$)	Major radicals	$\epsilon_{\text{C}} \pm 95\% \text{CI}$ (‰)	$\epsilon_{\text{H}} \pm 95\% \text{CI}$ (‰)
EP_UV/ H_2O_2	25	7	4.6	HO^\bullet	-0.8 ± 0.1	n.d. ^a
TCEP_UV/ H_2O_2	20	7	7.9	HO^\bullet	-1.4 ± 0.1	-56 ± 3
TCEP_Fenton	25	3	35.8	HO^\bullet	-1.0 ± 0.2	-34 ± 5
^b TBP_UV/ H_2O_2 _1	20	7	474.2	HO^\bullet	-0.8 ± 0.1	-14 ± 1
^c TBP_UV/ H_2O_2 _2	15	7	27.9	HO^\bullet	-0.6 ± 0.3	-13 ± 3
^c TBP_UV/ H_2O_2 _3	15	7	6.8	HO^\bullet	-0.6 ± 0.2	-17 ± 7
^d TBP_UV/ H_2O_2 _ave.				HO^\bullet	-0.7 ± 0.1	-15 ± 2
TBP_pH7/KPS	35	7	10.4	$\text{SO}_4^{\bullet-}$	-0.9 ± 0.1	-16 ± 2
TBP_pH9/KPS	35	9	8.8	$\text{HO}^\bullet, \text{SO}_4^{\bullet-}$	-0.8 ± 0.1	-20 ± 2
TBP_pH12/KPS	35	12	5.5	HO^\bullet	-0.5 ± 0.1	-11 ± 1
^e TBP_radical_oxidation_ave.				$\text{HO}^\bullet, \text{SO}_4^{\bullet-}$	-0.7 ± 0.1	-16 ± 3

a: "n.d." = not determined;

b: the distance between the photo-reactor and light source was 13 cm;

c: the distance between the photo-reactor and light source was 22 cm;

d: average ϵ values for UV/ H_2O_2 , which were calculated from the three individual UV/ H_2O_2 experiments;

e: average ϵ values for radical oxidation of TBP, which were calculated from all individual radical oxidation experiments except pH 12/KPS.

Isotope effects and the contribution of HO^\bullet and $\text{SO}_4^{\bullet-}$ to TBP degradation

During the radical reaction of TBP, a C-H bond is cleaved at the sub-terminal position of the alkane side chain in the transition state, leading to ^2H and ^{13}C isotope fractionation. The ^2H and ^{13}C isotope fractionation observed in experiments showed that this pathway took place during the radical oxidation of TBP by HO^\bullet and $\text{SO}_4^{\bullet-}$. The obtained enrichment factors from pH7/KPS ($\text{SO}_4^{\bullet-}$ dominating) and pH9/KPS ($\text{SO}_4^{\bullet-}$ and HO^\bullet co-existing) were nearly identical with the ones from UV/ H_2O_2 (pure HO^\bullet) (Table 6). The slightly smaller ϵ_{C} of $-0.5 \pm 0.1\text{‰}$ and ϵ_{H} of $-11 \pm 1\text{‰}$ at pH12/KPS (HO^\bullet dominating) is due to the effect of alkaline hydrolysis of TBP at pH 12. Considering 35% of TBP degradation was contributed by alkaline hydrolysis at pH12/KPS (Fig. S2 (Liu et al. 2018a)), the ϵ associated with the HO^\bullet oxidation process was estimated to be $-0.8 \pm 0.2\text{‰}$ for carbon and $-17 \pm 2\text{‰}$ for hydrogen using Eq. (3), which were identical with the ones obtained from radical oxidation of TBP under different conditions (Table 6). The average values of $\epsilon_{\text{C}} = -0.7 \pm 0.1\text{‰}$, $\epsilon_{\text{H}} = -16 \pm 3\text{‰}$, and $\Lambda = 20 \pm 4$ calculated from all individual radical oxidation experiments suggest that $\text{SO}_4^{\bullet-}$ and HO^\bullet oxidation processes of TBP cannot not be distinguished if the analytical uncertainty of the isotope enrichment factors is considered. The results suggest that both reaction processes had similar mechanisms of attacking carbon atoms and cleaving C-H bonds. However, P-O bond splitting cannot be characterized via the ^2H and ^{13}C isotope fractionation of TBP in this study. Therefore, the assessment ^2H and ^{13}C isotope fractionation cannot provide direct evidence to evaluate the process of P-O bond cleavage.

3.3.3. Isotope fractionation of substituted chlorobenzenes during photodegradation

Substituted chlorobenzenes are the basic substructure of many surface water contaminants. In this study, the isotope fractionation and reaction mechanisms involved during direct and indirect photodegradation of CH_3 -, Cl-, and NO_2 - substituted chlorobenzenes in aqueous solution were investigated in lab experiments. The objectives were: 1) to estimate the extent of direct and indirect photolysis using HO^\bullet for substituted chlorobenzenes in aqueous solution; 2) to quantify stable ^{13}C isotope fractionation during photodegradation; 3) to characterize the mode of bond cleavage related to electron configuration of the substrate using the Hammett concept .

Photolysis and carbon isotope fractionation

In general, direct photolysis through UV light absorption (for wavelength $\lambda \geq 280$ nm) did not significantly affect concentrations and isotope values ($\pm 0.5\text{‰}$) of most studied compounds. Only 4-NCB showed slow but isotopically fractionating direct photolysis. This is due to the potential of 4-NCB to partially absorb light at wavelengths higher than the cut-off filter at 280 nm, with a maximum absorbance at 281 nm. The 4-NCB direct photolysis was associated with a first-order degradation rate constant of $0.0043 \pm 0.0003 \text{ h}^{-1}$ ($R^2 = 0.97$) and an enrichment factor of $-5.1 \pm 0.4 \text{‰}$ ($R^2 = 0.96$) over the reduction of 34% of the initial compound. During indirect photodegradation using UV/H₂O₂-generated HO[•], the pseudo first-order reaction rate constants increased in the order of the NO₂- < Cl- < CH₃- substituted chlorobenzenes. The most pronounced ϵ_C was observed for nitrochlorobenzenes (up to $-4.8 \pm 0.5\text{‰}$), whereas the least significant was for chlorotoluenes ($\leq -1.0 \pm 0.1\text{‰}$).

Hammett plot and insight into reaction mechanisms

A Hammett plot was constructed using the pseudo first-order rate constants with respect to the aromatic compound (k_X) obtained from the indirect photodegradation experiments for each substituted chlorobenzene. The linear relationship between $\log(k_X/k_H)$ vs. σ^+ showed a good fit, and displayed a negative Hammett ρ value of -2.1 (Fig. 4), suggesting that the reaction rates increase due to presence of electron-donating groups (CH₃), and decrease due to the presence of electron-withdrawing groups (Cl, NO₂). This is in line with the observed lower half-life of CMBs compared to DCBs and NCBs. It is well established that the attack of HO[•] on aromatic compounds proceeds via a mechanism analogous to electrophilic aromatic substitution (Anbar et al. 1966). For such reactions, electron-withdrawing groups increase the energy barrier for the addition of an electrophile to the aromatic ring. This is due to a combination of transition state destabilization and ground state stabilization, and results in a decreasing reaction rate.

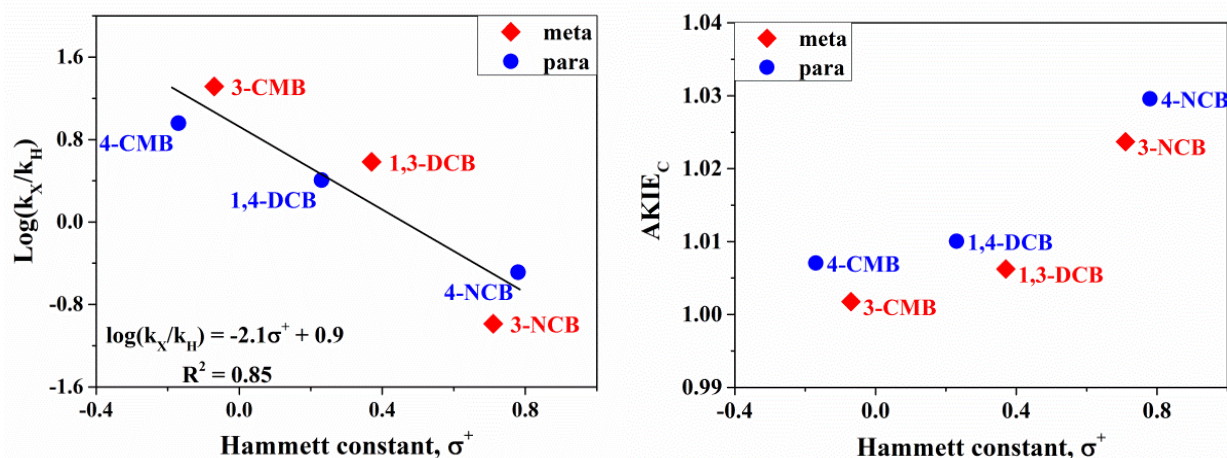


Fig. 4: Hammett plot (left) and the relationship between AKIE_C values and substituents' Hammett constants (right). The Hammett plot presents the logarithm of the ratio of the pseudo first-order rate constants for the reaction between HO^\bullet and the non-substituted chlorobenzene (k_H , chlorobenzene), and the X-substituted chlorobenzenes (k_X , X = Cl, CH_3 , and NO_2). The Hammett constant, σ^+ , is the substituent constant obtained from Hansch et al. (1991).

Isotope effects and Insight into reaction mechanisms

AKIE_C were calculated to characterize the isotope effect of the cleavage of the chemical bond at the reactive positions. The absolute magnitude of the ϵ_C and the AKIE_C values for the *meta*-substituted chlorobenzenes were always lower than those of their *para*-substituted counterparts (Table S2 (Passeport et al. 2018)). The AKIE_C values increased with increasing Hammett substituent constants σ^+ (Fig. 4). As the substituents became more electron-withdrawing, the activation energy barrier increased, leading to slower reaction rates, and the transition state changed to a more symmetrical or less reactant-like structure, resulting in larger AKIE_C . Based on these kinetics and isotope results, the proposed dominant reaction pathway for the studied compounds involves the initial formation of a C–O bond at one of the unsubstituted carbon atoms on the benzene ring during the rate-determining step, followed by the release of a hydrogen atom.

In summary, the kinetics and stable ^{13}C isotope studies provided two lines of evidence that the reaction of HO^\bullet with substituted chlorobenzenes proceeds primarily via OH aromatic substitution, involving first the rate-determining C–O bond formation, followed

by H release. The substituents on the chlorobenzene structure affected both reactivity and stable ^{13}C isotope fractionation. While the ^{13}C isotope enrichment factors obtained in this study were small, they will likely be sufficient to identify indirect photodegradation of the NCB and potentially the DCB isomers provided that at least 40% of the NCBs and 70 – 87% of the DCBs are degraded via reaction with HO^\bullet . In order to conclusively assess the diagnostic capabilities of CSIA for monitoring the photodegradation of substituted chlorobenzenes, further research should be conducted to analyze the ^2H isotope fractionation as a further indicator for bond cleavage reactions.

3.3.4. Isotope fractionation of phthalate esters during abiotic and biotic degradation

PAEs have drawn increasing attention due to their wide utilization as plasticizers and additives in the manufacturing of plastic and personal care products (Ventrice et al. 2013). The main aims of this study were (1) to investigate the potential of ^{13}C and ^2H isotope fractionations for characterizing different radical oxidation processes, hydrolysis and aerobic biodegradation of three PAEs, and (2) to get insights into the reaction mechanisms of PAEs by using the AKIE. Three PAEs (DMP, DEP and DBP) with different lengths of alkyl side chain were selected for investigation. The hypothesis is that multi-element isotope fractionation pattern allows characterizing reaction mechanisms at the aromatic rings and the side chains.

Isotope fractionation of PAEs during radical oxidation

The radical species discussed here include $\text{SO}_4^{\bullet-}$ induced by heat-activated PS and HO^\bullet induced by UV/ H_2O_2 . The chemical oxidation processes of three PAEs followed a pseudo-first order kinetic in all experiments. ϵ_{C} values decreased with increasing length of the alkyl side chain, which is likely related to isotope dilution effect by carbon atoms in non-reactive positions during intrinsic isotope fractionation. ϵ_{H} values obtained in UV/ H_2O_2 reactions were smaller than those from PS oxidation. The obtained ϵ_{H} values do not show a consistent trend of isotope dilution effects during PS oxidation, which is probably due to the to changing contributions of different pathways responsible for the decomposition of PAEs with different alkyl side chain lengths, as suggested in a

previous study on HO[•]-initiated photochemical transformation of four PAEs (Gao et al. 2015).

The correlations of ²H and ¹³C isotope fractionation of three PAEs from different reactions were compared in a dual isotope plot (Fig. 5, DEP as example). The difference between dual isotope fractionation patterns of UV/H₂O₂ and PS oxidation at pH 2 and pH 7 could be due to different dominating radical species. Previous studies have demonstrated that SO₄^{•-} and HO[•] were possibly present in persulfate oxidation systems (Anipsitakis and Dionysiou 2004, Han et al. 2015, Li et al. 2016, Liang and Su 2009, Xie et al. 2015). *tert*-Butyl alcohol (TBA) is considered as an efficient scavenger of HO[•], as it reacts much slower with SO₄^{•-} compared to the high reactivity of TBA/HO[•] systems (Li et al. 2016). Similar ε_H and Λ values were obtained from PS oxidation with DEP at pH 2 and 7 after the addition of TBA (Fig. 5). The Λ values of the DEP quenching experiment are almost identical to that of PS oxidation at pH 2 (Λ = 26 ± 3), suggesting that SO₄^{•-} is the dominant radical at pH 2, while SO₄^{•-} and HO[•] both contribute to the degradation at pH 7 yielding a smaller Λ value of 15 ± 3. A contribution of 21 - 63% by HO[•] was calculated from the ²H and ¹³C isotope enrichment using the extended Rayleigh-type equation (Van Breukelen 2007).

Isotope fractionation of PAEs during hydrolysis and aerobic biodegradation

In this study, the changes of carbon and hydrogen isotope signatures of three PAEs were systematically investigated during (1) abiotic hydrolysis over the pH range of 2, 7 and 10, and (2) aerobic biodegradation by *Rhodococcus opacus* strain DSM 43250. Significant ¹³C isotope fractionation was detected under all investigated reactions. ²H isotope fractionation was observed and is hypothesized to be a secondary hydrogen isotope effect (Table 2 (Zhang et al. 2018b)). Dual stable isotope values determined from abiotic hydrolysis and aerobic degradation showed similar magnitudes for DMP and DEP, indicating that abiotic and enzymatically catalyzed hydrolytic processes proceed similarly. The ¹³C and ²H isotope fractionation pattern of the persulfate oxidation of DMP, DEP and DBP could be clearly separated from chemical and biological hydrolysis (Fig. 5, DBP as example). Although the ²H isotope fractionation is low, the fractionation pattern allows identifying hydrolysis mechanisms. The secondary

isotope effect still allows classification of neutral, alkaline and biologically induced hydrolysis. Oxidation by $\text{SO}_4^{\cdot-}$ and HO^\bullet can be different in any case from each other. This systematic investigation shows the prospects and limitations of ^2H and ^{13}C isotope fractionation analysis for diagnostically applying Λ values in laboratory and possibly in field studies.

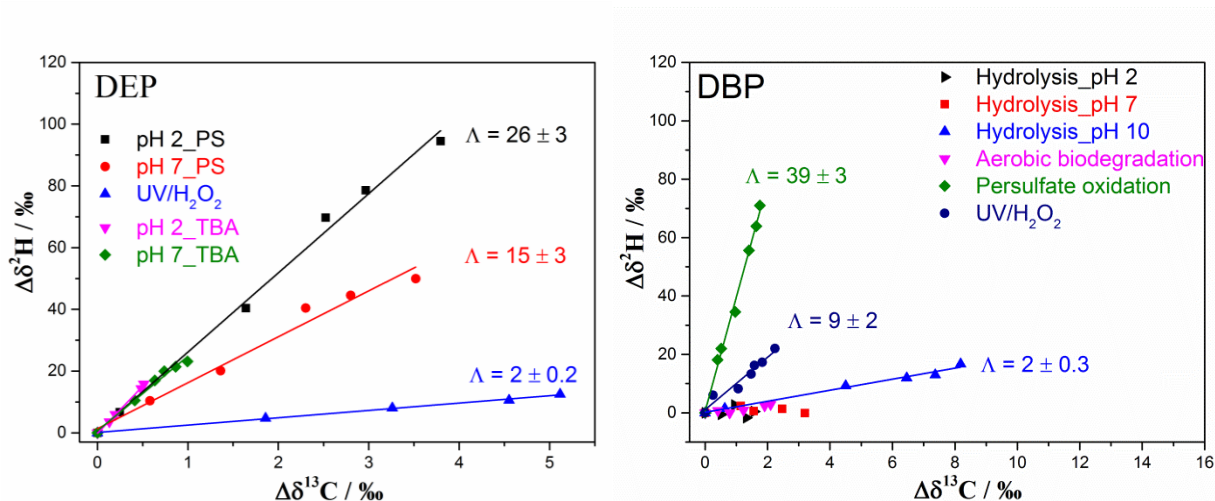


Fig. 5: Dual ^2H - ^{13}C isotope plots of DEP during chemical oxidation reactions (left) and dual ^2H - ^{13}C isotope plots of DBP during abiotic hydrolysis, aerobic biodegradation and chemical oxidation reactions (right).

AKIE and reaction mechanisms of PAEs

Based on identified transformation product of diethyl 3-hydroxyphthalate, HO^\bullet addition to the aromatic ring of DEP is assumed to be the main reaction mechanism in the UV/H₂O₂ experiment, which is consistent with Gauss computational results on HO^\bullet -initiated degradation of PAEs in a previous study (Gao et al. 2015). Experimentally determined KIE values for reactions involving oxidation of C-H bonds are generally in the range of 1.01-1.03 for carbon and 2-8 for hydrogen (Elsner et al. 2005). The calculated $\text{AKIE}_\text{C} = 1.028$ for DEP in UV/H₂O₂ experiment falls in the typical range. However, AKIE_H of DEP in UV/H₂O₂ experiment was found to be 1.11 which was lower than the values reported for the same type of chemical reactions. The reason is likely associated with a sp^2 to sp^3 hybridization change at the reacting carbon in aromatic ring as reported elsewhere (Zhang et al. 2016a). $\text{AKIE}_\text{C} = 1.017$ and $\text{AKIE}_\text{H} = 2.41$ obtained from $\text{SO}_4^{\cdot-}$ dominated reactions of DEP are both in accordance with the general KIE

ranges for C-H bond oxidation, it supports the hypothesis of C-H bond cleavage but cannot be used to predict degradation mechanisms at the side chain or aromatic ring of DEP with SO_4^{2-} . More information on intermediate products may be needed to further elucidate the reaction mechanisms. For possible hydrolytic mechanisms under aerobic and abiotic conditions, an acyl group transfer reaction of esters leads to a primary carbonyl-C kinetic isotope effect. H-bonding to the adjacent carbon atom is assumed to affect the vibration of the C-O bond and H-bonding to both α - and β -carbon can contribute to a secondary AKIE_H (Wolfsberg et al. 2010). The calculated AKIE_C for the proposed hydrolytic pathway (C-O bond cleavage) falls within the previous experimentally determined KIE range of 1.03-1.09 for typical nucleophilic substitution ($\text{S}_\text{N}2$ type) reactions involving C-O bond cleavage (Elsner et al. 2005), with the exception of lower AKIE_C values for DBP hydrolysis at pH 2 and aerobic biodegradation (Table 2 (Zhang et al. 2018b)). The slightly different AKIE_C of DBP obtained during hydrolysis at pH 2 and pH 10 is likely related to a transition state from reactant-like to tetrahedral intermediate-like structure. Abiotic and biotic hydrolysis of PAEs demonstrate similar AKIE_C and Λ values due to the C-O bond cleavage, thus indicating the potential of dual isotope analysis to characterize hydrolytic processes of PAEs in the environment.

3.3.5. Enantiomer and carbon isotope fractionation of α -HCH

The genes responsible for HCH degradation, known as *lin* genes, are generally present in aerobic HCH degrading *Sphingomonads*. The corresponding LinA enzyme catalyzes the initial step of dehydrochlorination. It has been reported that the linA enzymes are under continuous selection pressure and thus exist in several variants (Böltner et al. 2005, Macwan et al. 2012, Mohn et al. 2006, Sharma et al. 2011, Shrivastava et al. 2017). There are two copies of linA enzymes, linA1 and linA2, which differ by 10% in their amino acid sequence, and preferentially degrade (+) α -HCH and (-) α -HCH enantiomers, respectively (Suar et al. 2004, Verma et al. 2014). Aerobic biodegradation experiments were carried out with (1) resting cells and (2) crude cell extracts of *Sphingobium indicum* strain B90A in parallel and (3) isolated LinA1 and LinA2 proteins,

to investigate the underlying mechanisms leading to ^{13}C isotope and enantiomer fractionation of α -HCH.

Correlation of isotope and enantiomer fractionation

The isotope fractionation of (+) α - and (-) α -HCH, along with the enantiomer fractionation were quantified to describe the degradation processes at different cell integrities (Table 7). The average ϵ_{C} obtained from parallel experiments for (+) α - and (-) α -HCH degradation were $-6.3 \pm 0.1\text{‰}$ and $-2.3 \pm 0.03\text{‰}$ by resting cells and $-7.7 \pm 0.4\text{‰}$ and $-3.4 \pm 0.02\text{‰}$ by crude cell extract, respectively. Purified LinA1 and LinA2 enzymes gave an ϵ_{C} of $-11.1 \pm 0.3\text{‰}$ for (+) α -HCH and $-3.8 \pm 0.2\text{‰}$ for (-) α -HCH, respectively. The absolute values of enantiomer fractionation factors (ϵ_{e}) varied between $0.54 \pm 0.14 \%$ and $2.70 \pm 0.50 \%$ from resting cells to purified enzymes.

Isotope fractionation is determined by bond cleavage/formation in the first irreversible reaction step and can be modified due to rate limitation of preceding steps in a complex biochemical reaction. For the degradation of α -HCH, LinA dehydrochlorinates the substrates most likely via an E2 elimination mechanism (Okai et al. 2010), which is probably identical for both enantiomers (Manna et al. 2015). As suggested by QM/MM modeling studies (Manna et al. 2015), the rate limitation might be a result of binding within the enzyme pocket. In addition, preceding reaction steps such as transport in the cell, binding to the enzyme can modify the KIE of the bond cleavage reaction (Nijenhuis et al. 2005), resulting in different carbon enrichment factors (Table 7). The kinetics of binding of α -HCH enantiomers to the individual enzymes might lead to rate limitation which would explain the observed different enantiomer fractionation factors (Table 7). Enantiomer fractionation can be influenced by two factors: (1) binding of substrate to the enzyme with respect to the stereo chemical position in the enzyme pocket which can lead to different reaction ratios (Reetz 2011); (2) the reactivity of two individual enzymes with specificity towards enantiomers as observed in the enzyme assays with LinA1 and LinA2. In this case, the enantiomer degradation should be rationalized as individual substances which are controlled by the expression and activity of individual enzymes within the machinery of the cell (Muller et al. 2001).

Table 7: Summary of carbon isotope enrichment factors (ϵ_c) and enantiomer fractionation factors (ϵ_e) of (-) α -HCH and (+) α -HCH, and related kinetic constants κ in different sets of degradation experiments by strain B90A.

		Kinetic constant			Isotope fractionation		Enantiomer fractionation	
		bulk	(-) α -HCH	(+) α -HCH	(-) α -HCH	(+) α -HCH	ϵ_e (M)	ϵ_e (C)
		κ (h ⁻¹)	κ^- (h ⁻¹)	κ^+ (h ⁻¹)	ϵ_c^- (‰)	ϵ_c^+ (‰)	(%)	(%)
Resting cell	a	0.61±0.06	0.81±0.12	0.49±0.03	n.s.	-6.4±0.7	-0.54±0.14	-0.52
	b	0.47±0.05	0.76±0.09	0.30±0.03	n.s.	-6.2±1.2	-0.97±0.12	-0.96
	c	0.21±0.03	0.35±0.02	0.12±0.02	-2.3±0.4	-6.1±1.1	-1.07±0.20	-1.11
	d	0.10±0.01	0.15±0.02	0.06±0.01	-2.3±0.3	n.a.	-0.82±0.07	-0.81
	Average value				-2.3±0.03	-6.3±0.1		
Crude extract	e	0.38±0.10	0.58±0.13	0.30±0.07	n.s.	-7.4±0.7	-0.71±0.19	-0.73
	f	0.24±0.04	0.45±0.06	0.12±0.02	n.s.	-8.0±1.3	-1.35±0.13	-1.38
	g	0.13±0.02	0.19±0.02	0.04±0.01	-3.4±0.5	n.a.	-1.13±0.17	-1.12
	h	0.11±0.02	0.18±0.04	0.05±0.01	-3.4±0.6	n.a.	-1.25±0.22	-1.27
	Average value				-3.4±0.02	-7.7±0.4		
LinA2	i	0.23±0.06	0.65±0.10	n.a.	-3.7±0.6	n.a.	-2.70±0.50	-2.79
	j	0.23±0.11	0.54±0.28	n.a.	-4.0±1.0	n.a.	-2.28±0.19	-2.37
	k	0.11±0.02	0.27±0.05		-3.6±0.5	n.a.	-2.42±0.20	-2.46
	Average value				-3.8±0.2			
LinA1	l	0.12±0.02	n.a.	0.28±0.02	n.a.	-11.3±2.0	2.13±0.52	2.23
	m	0.05±0.01	n.a.	0.13±0.02	n.a.	-10.9±1.5	2.37±0.48	2.40
	Average value					-11.1±0.3		

n.a.: not assessed; n.s.: no significant; ϵ_e (M): obtained by modeling; ϵ_e (C): obtained by calculation.

Effect of mass transport on isotope and enantiomer fractionation

The ϵ_c^+ values obtained from resting cells and crude extract with the same degradation rate showed that mass transfer across the outer and cytoplasmic membranes may reduce the isotope fractionation (Table 7). Significant higher ϵ_c^+ values were obtained in the purified enzyme (LinA1) experiments. The difference of ϵ_c^+ between crude extract and enzyme indicates that cell material such as vesicles or membrane remnants may affect the transport of substrate leading to lower isotope fractionation. Statistically similar ϵ_c^- values were obtained comparing pure enzyme and crude extract experiments, indicating that mass transfer is not limited and that bond cleavage of the reaction governs the observed isotope enrichment. Overall, the uptake and passage through the cell wall led to rate limitation reducing the ϵ_c for both enantiomers, indicating that uptake affects the isotope fractionation of individual enantiomers in a similar way. Moreover,

uptake of substrate into the cell often reduce isotope fractionation and a similar effect has been observed with a non-enantiomeric substance as well (Renpenning et al. 2015c). The mass transport into cells and within the cells has different effects on the isotope fractionation of (+) α - and (-) α -HCH. However, as enantiomer fractionation only depends on the difference of the degradation rate of (-) and (+) α -HCH, mass transfer will only affect the enantiomer fractionation in the case that mass transfer is the rate limiting step of the reaction.

Effect of the degradation rate on isotope and enantiomer fractionation

Significant ϵ_c^- in the resting cell experiments was only observed when the κ^- was lower than 0.35 h^{-1} , the κ^- higher than 0.76 h^{-1} lead to the masking of isotope fractionation (Table 7). The same observation was made in the crude extract experiments, demonstrating that the isotope fractionation at higher κ^- does not characterize the bond cleavage because it is not the rate determining step of the reaction. When the κ^+ value of resting cell experiments fall below 0.5 h^{-1} , significant but nearly identical ϵ_c^+ were observed in parallel experiments (Table 7), indicating that the bond cleavage was the main rate limiting step of the reaction. The same results were observed in the crude extract experiments. The ϵ_e values indicated preferential degradation of (-) α -HCH over (+) α -HCH in all resting cell and crude extract degradation experiments (Table 7). The significant variability of ϵ_e indicates that the enantiomer fractionation depends on reaction rates and the amount of each individual enzyme. Comparison of resting cell with crude extract suggested that uptake of α -HCH into cells reduced the enantiomer fractionation to some extent. Nevertheless, the chemical passage through the membrane should not affect the enantiomer ratio as diffusion is identical for enantiomers. Therefore, the degradation kinetic of individual enantiomer governs the enantiomer fractionation of α -HCH. If varying enantiomer fractionation over time is observed, it is an indicator of multiple enzymes involved in the degradation.

In summary, the isotope fractionation of individual enantiomers is governed by the mechanisms of bond cleavage. Nevertheless, the binding within the enzyme and the transition state of bond cleavage may not be chemically identical and therefore result in

different isotope enrichment factors. One may hypothesize that the kinetic of binding to enzymes leads to the rate limitation and thus modifies the observed ϵ_c , as the chemical bond cleavage is probably not much different in a chemical sense. Future studies on modeling the KIE during enzymatic transformation of α -HCH by QC/QM approaches are needed to gain deeper insights into enzyme mechanisms. This study validates that enantiomer fractionation and isotope fractionation are two independent processes and that both are affected by the degradation rate and mass transport. Therefore the quantification of the fate of chiral compounds in the environment by combination of isotope and enantiomer fractionation needs to be done with caution.

3.4. Field application of CSIA for charactering natural attenuation of parathion by hydrolysis

Parathion was one of the most widely applied organophosphorus insecticides in agriculture in the past decades, and was primarily used as an insecticide on fruit, cotton, wheat, vegetables, and nut crops (FAO 1990). Due to its toxicity, parathion has been banned or restricted in many countries; however, stockpiles and waste from previous manufacturing and former landfill sites often contain parathion (LRSB 2014, Nielsen et al. 2014) forming serious point source contaminations which require management strategies. Thus, it is crucial to have a proper understanding of the fate of parathion for risk assessment at landfill sites and for groundwater quality protection and management. CSIA has not been applied yet in field studies to assess the *in situ* degradation of OPs. In order to fill this research gap, parathion was selected as a model compound of OPs and its natural attenuation by hydrolysis at a contaminated site was investigated using ^{13}C and ^2H isotope analysis. Groyne 42 is situated at Harboøre Tongue in Denmark facing the North Sea. Waste chemicals were disposed at the site between 1950 and 1960. The area is heavily contaminated by approximately 100 tons of primarily OPs (NorthPestClean 2014). The background information of this site has been described elsewhere (Bondgaard et al. 2012, Hvidberg et al. 2008). Because of the demonstration experiments, the site contained discrete areas which were treated areas with sodium hydroxide (pH 13) and untreated areas with neutral to acidic conditions (pH 2-7).

Hydrogeochemical conditions and isotope analysis of parathion from field samples

Concentrations of dissolved oxygen were always below 0.1 mg L^{-1} , indicating almost anoxic conditions. The pH ranged from 3.2 to 6.5 in the untreated area, the acidic conditions were likely due to acid chemical waste deposition. In the treated area, the pH ranged from 6.9 to 12.4, demonstrating the effectiveness of the remediation measure. Samples from well TC3-9-3 in the treated area were strongly acidic (pH 2.2), indicating that this well is very close to the core of acid waste deposition and mixing of alkaline solutions with DNAPL did not result in alkaline conditions. Most of the parathion concentrations (0.76 to 155.33 mg L^{-1}) in the treated area are above its solubility of 10.4 mg L^{-1} in water at $8 \text{ }^\circ\text{C}$ (the average temperature of ground water in Denmark). This is due to the location of the treated area close to the contamination hotspot where free organic phases of a mixture of OPs, intermediate products, reactants and solvents are present. The large variations of pH values and parathion concentrations in both areas illustrate rather heterogenic biogeochemical conditions at the investigated site.

The average value of all isotope analyses of source samples was taken as source signature of parathion, resulting in $-22.9 \pm 0.8 \text{ }‰$ for $\delta^{13}\text{C}$ ($n = 10$) and $-212 \pm 15 \text{ }‰$ for $\delta^2\text{H}$ ($n = 12$). Compared to the source signature of parathion, $\delta^{13}\text{C}$ enrichment from $0.8 \text{ }‰$ to $4.9 \text{ }‰$ was obtained from the wells in the untreated area (Fig. 6), indicating *in situ* acidic and neutral hydrolysis was taking place. The $\delta^{13}\text{C}$ values in the treated area were almost identical with the source signature (Fig. 6) showing that no ^{13}C isotope fractionation of parathion occurs under strong alkaline conditions, which is in agreement with the results of laboratory hydrolysis experiments (Wu et al. 2018a). $\delta^{13}\text{C}$ enrichments of $2.8 \text{ }‰$ and $2.1 \text{ }‰$ were observed in samples from wells TC3-6-3 and TC3-7-2, respectively, which are characterized by strongly alkaline pH values (11.7 - 12.4). This result might be explained by mixing of alkaline water and plumes during sampling. Mixing during sampling needs to be taken into account for interpreting the isotope composition and leads to an underestimation of degradation reactions (Kopinke et al. 2005). The ^{13}C isotope fractionation is an indication that the hydrolysis may have taken place under acidic, neutral or slight alkaline conditions. However, the $\delta^2\text{H}$ values obtained in both areas were all overlapping with the source signature (Fig. 6) because the hydrolysis of parathion is not associated with a detectable ^2H isotope fractionation effect, independent of the pH value.

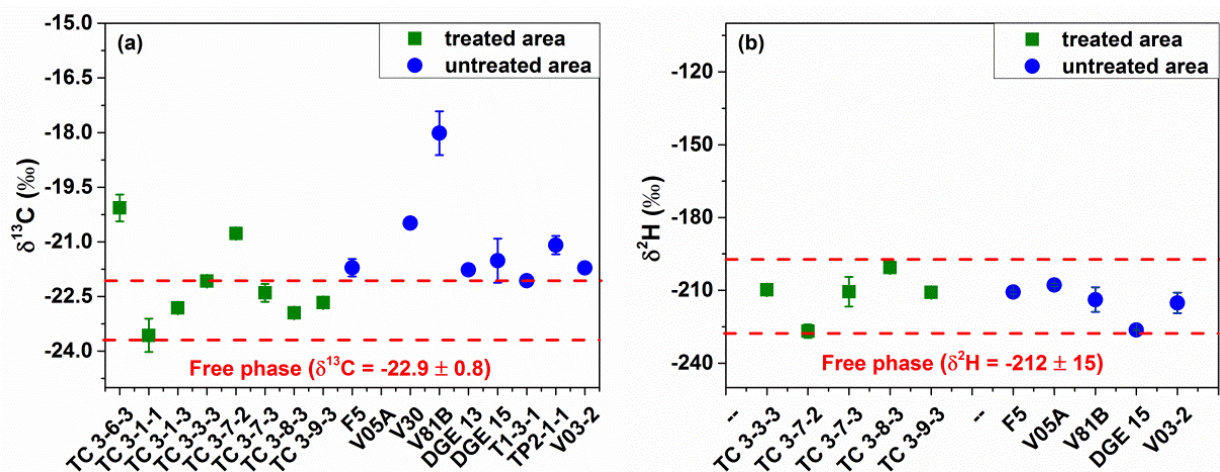


Fig. 6: Carbon and hydrogen isotope ratios of parathion obtained from the ground water from the “Groyne 42” field site. Green squares indicate the samples from the treated area; blue circles indicate the samples from untreated area; Red dotted lines indicate the carbon and hydrogen source signatures of parathion.

Isotopic profiles of parathion during hydrolysis and biodegradation

Chemical oxidation of parathion occurs via oxidation of the P=S bond to a P=O bond by an HO^\bullet in the first rate-determining irreversible step; the reaction is not linked to detectable ^2H or ^{13}C isotope fractionation. In contrast, the hydrolysis of parathion results in no detectable ^2H isotope fractionation but significant ^{13}C isotope fractionation, corresponding to isotope enrichment factors of $\epsilon_{\text{C}} = -6.9 \pm 0.8$ ‰ at pH 2, -6.7 ± 0.4 ‰ at pH 5, -6.0 ± 0.2 ‰ at pH 7, -3.5 ± 0.4 ‰ at pH 9, and insignificant ^{13}C isotope fractionation at pH 12. The reduction of the ^{13}C isotope fractionation factor at pH 9 suggests that two hydrolysis pathways take place simultaneously. Parathion is hydrolyzed completely by the P-O bond cleavage pathway at pH values above 10, as shown experimentally (Wanamaker et al. 2013). Therefore, ^{13}C isotope fractionation can be expected and used to characterize parathion hydrolysis at $\text{pH} < 10$.

Isotopic profiles of parathion during biodegradation were investigated under laboratory cultivation using two isolated aerobic strains and one anaerobic strain, however, the reaction using the three tested strains was not associated with ^{13}C and ^2H isotope fractionation. The biodegradation mechanisms of parathion using several microbial strains affiliated to the genera *Flavobacterium*, *Bacillus*, *Pseudomonas* or *Arthrobacter* have been proposed previously (Singh and Walker 2006), which are summarized in Fig.

7: (A) hydrolysis of the phosphotriester bond to form *p*-nitrophenol (P-O bond cleavage); (B) reduction of the nitro group acting as electron acceptor to form amino parathion (N-O bond cleavage); (C) oxidation of the sulfur group of parathion to form paraoxon (P=S bond cleavage). No carbon and hydrogen bond breaking is involved in the first rate determining step of all three pathways, thus, no significant ^{13}C and ^2H isotope fractionation is expected to be associated with the biodegradation of parathion. However, only a limited number of studies exist on aerobic and anaerobic parathion degradation, it cannot be fully excluded that microorganisms could attack parathion by oxidizing a carbon entity leading to ^{13}C and ^2H isotope fractionation.

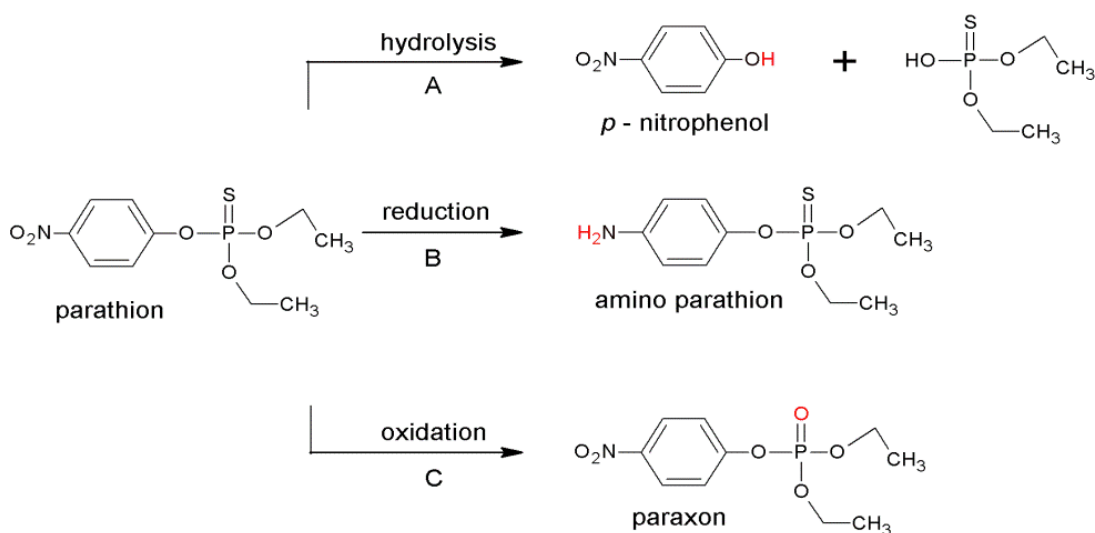


Fig. 7: Different pathways of parathion first step degradation by microorganisms (modified from Sing & Walker 2006), including hydrolysis of the phosphotriester bond (A), reduction of the nitro group (B) and oxidation of the sulfur group (C).

Quantitative assessment of *in situ* hydrolysis at the investigated field site

It is unlikely that significant ^{13}C and ^2H isotope fractionation is associated with the biodegradation of parathion, and no ^{13}C isotope fractionation can be expected during the hydrolysis of parathion at pH > 10. Hence, the ^{13}C isotope enrichment obtained in parathion at the Groyne 42 site can be contributed exclusively to hydrolysis at pH < 10. The estimation using Eq. (6) revealed the evidence that up to 8.6 % natural attenuation of parathion was contributed by hydrolysis under neutral and acidic conditions and resulted in up to 16 % of removal was contributed by hydrolysis under slightly alkaline conditions when considering the mixed hydrolysis pathways. A half-life time of 1521

days at the average ground water temperature in Denmark (8 °C) can be roughly predicted according to the Arrhenius plot describing the correlation of temperature and the rate constants of parathion hydrolysis at pH < 7.8. Thus, the relative low temperature at the Groyne 42 field site would lead to long retention times of parathion in the untreated area.

Muff and colleagues suggested that the hydrolysis reactions are limited by the rate of hydrolysis rather than NAPL dissolution (Muff et al. 2016). The results of present study contradict to some extent with this assumption and support that mixing is a major factor limiting the *in situ* degradation. Firstly, the indication for neutral and acidic hydrolysis was found even in the treated areas where someone would expect prevailing alkaline conditions. Secondly, the high parathion concentrations are clearly above the water solubility and this suggests that phases are present which are obviously not accessible to hydrolysis. Thirdly, in spite of long half-life time, the high concentrations suggest that phases not accessible to hydrolysis still provide a source of contamination leaching into the ground water. Thus, the kinetic of hydrolytic transformation is expected to be controlled by mixing of alkaline water in the subsurface, and mixing in porous media is slow. Similar assumptions could be made for neutral and acidic hydrolysis. Mixing of alkaline solutions with DNAPL seems to be a challenge for all *in situ* measures. Heterogenic reaction conditions could be expected as suggested by the ¹³C isotope enrichment of parathion even at places with high pH pointing to a predominance of neutral or acidic hydrolysis.

4. Conclusion and outlook

The results of this study clearly demonstrate the great prospects for characterizing transformation processes of targeted organic components using CSIA.

The CSIA approach has been successfully extended to the compound class of OPs. Accurate and precise $\delta^{13}\text{C}$ and $\delta^2\text{H}$ analysis of OPs could be obtained using the developed methods. The Cr/HTC system can be a promising approach for routine ^2H isotope analysis of heteroatom-bearing organic compounds. The systematic study on ^2H and ^{13}C isotope fractionation patterns shows the potential of CSIA for investigating chemical transformation of OPs. The obtained knowledge has been applied for quantification of the hydrolysis of parathion at a contaminated field site. Therefore, the isotope fractionation approach might be used in the future to assess and monitor the hydrolysis of OPs in aquatic environments under typical environmental conditions (pH 3 - 10). Results from the Hammett relationship, the stable carbon isotope analysis and degradation product analysis provide evidences that the reaction of OH^\bullet with substituted chlorobenzenes proceeds primarily via aromatic ring addition and is followed by H release. The substituents on aromatic ring affect both reactivity and stable carbon isotope fractionation due to the electron-donating or electron-withdrawing nature of the substituents affecting the reaction rate. As the substituents became more electron-withdrawing, the activation energy barrier increased, leading to slower reaction rates, and the transition state changed to a more symmetrical or less reactant-like structure, resulting in larger apparent kinetic isotope effects. Further research should be conducted to analyze the hydrogen isotope fractionation as another indicator for bond cleavage reactions of substituted chlorobenzenes. Additionally, dual isotope analysis has diagnostic value for characterizing reaction mechanisms of PAEs. CSIA provides a novel approach to estimate the relative contribution of radicals ($\text{SO}_4^{\bullet-}$ and HO^\bullet) to the overall reaction. The obtained isotope fractionation patterns are of fundamental importance to evaluate *in situ* chemical oxidation processes for the removal of PAEs. This study is an important step forward in understanding degradation mechanisms of organic compounds with $\text{SO}_4^{\bullet-}$ and HO^\bullet radicals in the aqueous phase.

However, my studies also demonstrate the limitations of CSIA with regard to characterizing the transformation mechanisms of OPs. For instance, possible radical oxidation reactions cannot be analyzed by ^2H and ^{13}C isotope fractionation when the degradation process is initiated with a desulfurization step (P=S bond cleavage) in the first irreversible reaction of phosphorothioates and phosphorodithioates (Fig. 3). ^{13}C and ^2H isotope fractionation is unlikely to characterize aerobic and anaerobic parathion biodegradation involving P=S, P-O or N-O bond cleavage (Fig. 7). Additionally, hydrolysis pathways of OPs involving P-O and C-O bond cleavage cannot be characterized by ^2H isotope fractionation (Fig. 3). Interestingly, significant ^2H isotope fractionation was observed in our preliminary experiments of parathion degradation using biogas slurry under anaerobic condition, resulting in a ϵ_{H} of $-40 \pm 6 \text{ ‰}$ using fresh slurry and ϵ_{H} of $-61 \pm 4 \text{ ‰}$ using cell-free slurry, respectively (unpublished data). This indicates that the enzymatic transformation of OPs may occur via a different mechanism which could be characterized by ^2H isotope fractionation. The preliminary data suggests that unknown pathways cleaving a C-H bond are at work in biogas plants which remained to be discovered. In addition a yet uncharacterized pathway could be characterized by ^2H isotope fractionation for the assessment of OPs degradation in biogas reactors or in waste water treatment plants. For further exploring the diagnostic potential of tracing reaction mechanisms of OPs in the environment using isotope fractionation concepts, more systematic studies on microbial degradation are needed in the future and the associated ^2H and ^{13}C isotope fractionation patterns need to be compared with those of chemical transformation of OPs.

^{13}C isotope fractionation of $\alpha\text{-HCH}$ enantiomers can potentially be used to quantify the degradation in field studies. The LinA1 and LinA2 enzymes have shown to exhibit a highly selective degrading potential using only one enantiomer almost exclusively. Therefore, the degradation can only be quantified robustly by enantiomer specific isotope analysis. Attempts for using the Rayleigh equation for modeling both enantiomer and isotope fractionation need to be critically assessed, as the basic Rayleigh concept holds no validation for quantifying enantiomer fractionation. This study represents the first step towards developing a better understanding of isotope and enantiomer fractionation and will aid in field site evaluation. For instance, enantiomer fractionation

may provide additional information reflecting degradation conditions. Additionally, a method for extraction and purification of HCHs for the analysis of stable isotope composition in various environmental compartments was developed and evaluated. All steps of sample preparation have been shown to be free of isotope fractionation concerning the typical uncertainty of the $\delta^{13}\text{C}$, $\delta^2\text{H}$ and $\delta^{37}\text{Cl}$ analysis. Due to the high detection limit of IRMS, improvements in the sensitivity of GC-IRMS and in the efficiency of HCHs enrichment are needed in the future for reducing the sample sizes and lowering matrix interferences. In the preliminary field study using CSIA, the isotope enrichment of HCHs observed in contaminated soil, plants and animal liver provided evidence that degradation took place. This led to the hypothesis that isotope fractionation of HCHs can be used to assess biodegradation in food webs, whereas the isotope enrichment in the residual fraction reflects the metabolism in the higher organisms. Thus, isotope combined with enantiomer fractionation may be used as a biomarker for the contamination load in the diet of the organism at a specific position of the food chain. The work as presented herein is, the first step towards new investigations on tracing the reactive transport processes of organic contaminants in a complex environment and food webs.

In order to overcome the limited diagnostic potential of ^2H and ^{13}C isotope fractionation, compound-specific oxygen isotope analysis ($\delta^{18}\text{O}$) may hold great potential for investigating the transformation processes of OPs, since O is involved in the first irreversible reaction steps of hydrolysis and biodegradation. Hitzfeld and colleagues evaluated the performance of different HTC reactors for $\delta^{18}\text{O}$ analysis via GC-HTC-IRMS system (Hitzfeld et al. 2017). It is shown that physical and chemical properties of a given reactor design impact high temperature conversion processes, and thus the accuracy of $\delta^{18}\text{O}$ analysis was prevented by non-quantitative HTC and significant CO_2 byproduct formation. For instance, the reported variation of $\delta^{18}\text{O}$ precision ranges from less than 0.5 ‰ to more than 2‰ for various sugars (Lehmann et al. 2016, Zech and Glaser 2009, Zech et al. 2013). Therefore, it may be necessary to standardize the precision for $\delta^{18}\text{O}$ analysis, or to develop new concepts for HTC method for further investigation of ^{18}O -CSIA.

Compound-specific sulfur isotope analysis ($\delta^{34}\text{S}$ and/or $\delta^{33}\text{S}$) might be a very promising subject of future research, which could offer the opportunity for characterizing the P=S bond cleavage during radical oxidation and biodegradation of phosphorothioates such as parathion, and for characterizing the P-S bond cleavage during alkaline hydrolysis of phosphorodithioates such as dimethoate. The recent achievement on accurate and sensitive $\delta^{34}\text{S}$ ($^{34}\text{S}/^{32}\text{S}$) analysis of volatile organic substances using GC-MC-ICPMS method makes the ^{34}S -CSIA possible to be developed in the future (Said-Ahmad et al. 2017). The $\delta^{34}\text{S}$ analytical methods could be adapted to OPs inspired by of the recent development of $\delta^{37}\text{Cl}$ analysis by operating in low resolution mode ($m/\Delta m = 300$) using a super dry plasma to reduce interferences from protonation (Horst et al. 2017), as well as by installing a transfer line connecting GC and ICP to extend the range of analytes towards semi-volatile organic substances (Renpenning et al. 2018). The isotope analysis at low mass resolution is expected to allow an increase of the sensitivity for isotope analysis and therefore gives new options to develop selective and sensitive methods for CSIA. Potentially, the sulfur isotope fractionation can be further investigated as a new indicator for sulfur bond cleavage reactions of OPs. This may open prospect for exploring the diagnostic potential of multi-element isotope analysis in transformation process studies but also for forensic approaches. For example, isotope analysis of $\delta^{18}\text{O}$, $\delta^{34}\text{S}$ and $\delta^{37}\text{Cl}$ is needed to exploit the potential of multi-element isotope fingerprinting for identification of sources and providing a database of isotope compositions of OPs, which might improve the tracing of origin, transport pathways and degradation of OPs in the environment. To verify the applicability of this approach for source identification of OPs, I have selected chlorpyrifos, one of the most applied OP pesticides, as a starting point for investigation. The preliminary results of $\delta^{13}\text{C}$, $\delta^2\text{H}$ and $\delta^{15}\text{N}$ analysis indicated the potential of multi-element isotope analysis as tool for distinguishing chlorpyrifos from different countries (Fig. 8). More information is expected to be obtained by the analysis of $\delta^{18}\text{O}$, $\delta^{34}\text{S}$ and $\delta^{37}\text{Cl}$ in the next step, as the multi-element isotope ratios might reflect synthetic pathways and/or usage of different raw materials, as well as possible isotope fractionation during the synthesis reactions (Gilevska et al. 2015).

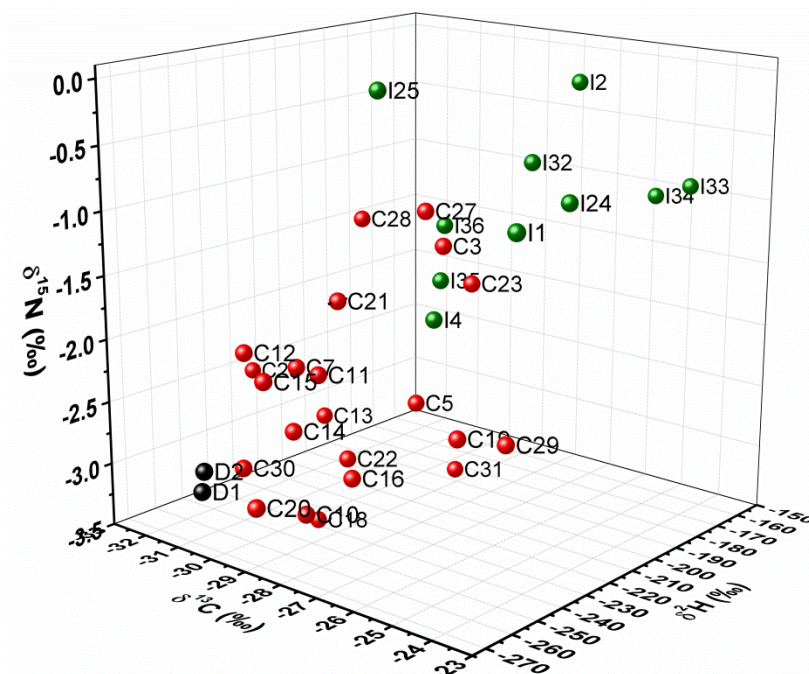


Fig. 8: Variability of $\delta^{13}\text{C}$, $\delta^2\text{H}$ and $\delta^{15}\text{N}$ values of commercial chlorpyrifos from different manufacturers in different countries including India (green balls), China (red balls) and Germany (black balls) (Wu and colleagues, unpublished data)

As shown for halogenated ethenes, multi-element CSIA employing ^{13}C , ^2H and ^{37}Cl isotope fractionation is promising to characterize the degradation reactions (Franke et al. 2017, Kuder et al. 2013, Renpenning et al. 2014). The recent development of analytical technics using GC-Cr/HTC-IRMS for $\delta^2\text{H}$ analysis and GC-MC-ICPMS for $\delta^{37}\text{Cl}$ is feasible for HCH and has potential to provide insights into transformation mechanisms of HCHs in depth by applying multi-element CSIA. In addition, HCHs contain different isomers. Multi-element isotope analysis of HCH isomers may provide quantitative structure–activity relationship (QSAR) with respect to the relationship between HCH isomers with axial and planar Cl and the associated isotope fractionation during dehalogenation reactions. In a preliminary approach, initiative has been taken to study the ^{13}C , ^2H and ^{37}Cl isotope fractionation of γ -HCH and β -HCH during alkaline hydrolysis, Fe reduction and enzymatic transformation using LinA. The preliminary results showed that similar ϵ_{C} and ϵ_{Cl} were obtained from the alkaline hydrolysis of γ -HCH and β -HCH. However, even though the similar dehydrochlorination mechanism is proposed, significantly different ϵ_{H} values were observed with -162 ± 26 ‰ for γ -HCH

and with $-27 \pm 8 \text{ ‰}$ for β -HCH, respectively (Wu and colleagues, unpublished data). The reason could be due to the different planar and axial positions of C-H and C-Cl bonds in the molecules of γ -HCH and β -HCH. This short example may indicate that for better characterizing bond cleavage reactions of HCHs, multi-element isotope fractionation patterns including ^{13}C , ^2H and ^{37}Cl are needed and could be to be the next steps for an investigation of bond cleavage mechanisms.

HCHs are one of the prominent persistent organic pollutants in the environment. Due to their low water solubility and persistence in the environment, HCHs tend to be accumulated in the soil and will be taken up into plants from the roots and air, and eventually be accumulated in food and wild animals. Thus, for sustainable management of contaminated lands and health risks assessment, it is necessary to trace the fate of HCHs in the food webs. In this thesis, the carbon isotope enrichment of HCHs observed in the contaminated soil and plants (Fig. 2) gives indication that isotope fractionation concepts could be used to assess their transformation in food webs. Especially, the strong carbon isotope enrichment of HCHs in the contaminated pork and deer livers (Fig. 2) leads to the hypothesis that isotope fractionation of HCHs may reflect the metabolism in higher organisms. Future research interests can be focused on the degradation assessment of HCHs at a land scape scale. As an example for the investigation of the HCHs fate on a land scape level, preliminary data has been acquired from a HCHs dumpsite in Lucknow, India (Fig. 9). The $\delta^{13}\text{C}$ values and enantiomeric fraction (EF) of were applied as tools to elucidate the transformation of α -HCH and the selective uptake processes of α -HCH enantiomers in soil, plant, animal milk and dung. The preliminary results of the $\delta^{13}\text{C}$ signature of α -HCH showed that degradation processes were associated with the uptake into plants, implying degradation in the rhizosphere potentially attenuating the load of HCHs (Fig. 9). The isotope enrichment of α -HCH in dung samples indicated that degradation of HCHs may take place in the digestive track of cows and buffalo during metabolism potentially in the anaerobic rumens. This digestive passage of HCHs is probably undergoing the similar transformation processes as in the anaerobic digestion of contaminated biomass during biogas production (Lian et al. 2018). However, further investigations are necessary for confirmation. The significant carbon isotope enrichment of α -HCH in the contaminated milk samples (Fig. 9) is in

agreement with the significant isotope enrichment in liver samples (Fig. 2), which raises the hypothesis that the HCHs residuals in milk undergo the liver passage as well and that the metabolization of HCHs in higher organisms is more significant isotope fractionating processes comparing to HCHs transformation governed by microbial community. Additionally, the preliminary analysis on EF of α -HCH implied that (+) α -HCH was preferentially degraded in milk, in contrast, (-) α -HCH was preferentially transformed in other contaminated compartments (Fig. 9). It is well known that linA2 enzyme preferentially catalyzes (-) α -HCH transformation and is expressed in almost all identified microbes which are capable for HCHs degradation. My hypothesis is that Cytochromes P450 presented in liver could be the key factor governing the metabolization of HCHs in higher organisms, and that the corresponding P450 enzyme preferentially catalyzes (+) α -HCH transformation. Further reference experiments of HCHs transformation using P450 enzyme need to be conducted in the laboratory for proving of these hypotheses.

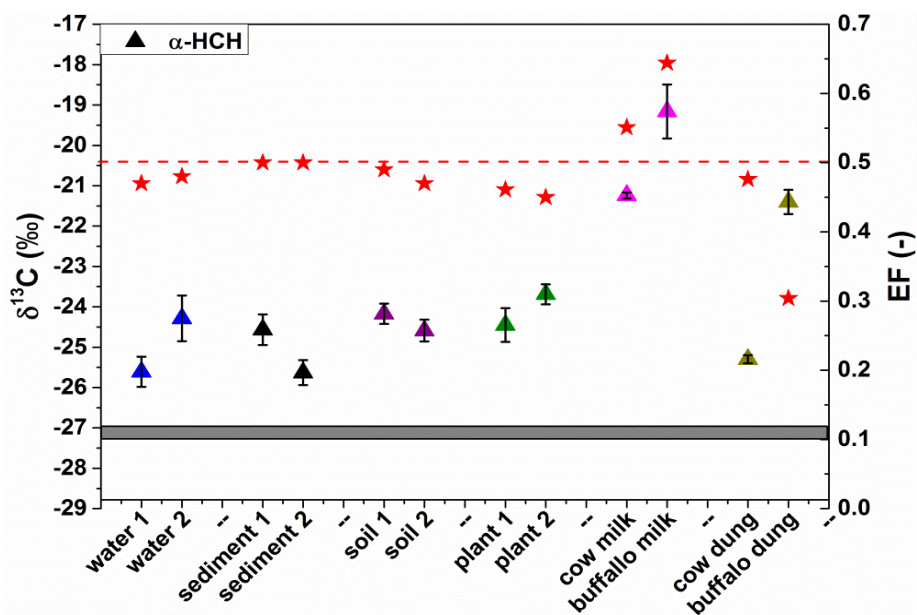


Fig. 9: $\delta^{13}\text{C}$ values (solid triangles) and enantiomeric fraction (EF) (red stars) of α -HCH extracted from water, sediment, soil, plants, animal milk and dung from contaminated site in Lucknow, India. The color of triangles indicates different sample matrixes. The solid bar indicates the isotope composition variation of α -HCH sources. The red dashed line indicates the EF = 0.5 for racemic α -HCH from the production (Wu and colleagues, unpublished data).

Many of the modern pesticides and pharmaceuticals contain enantiomers. The preliminary investigation described above illustrates the potential of enantiomeric fraction and stable isotope fractionation for characterization of transformation processes by microbes even in digestive tracks of higher organisms. The analysis of transformation of organic chemicals in higher organisms offers new perspective for evaluation of chemicals fates, which could be interesting for the regulation of pesticides and pharmaceuticals.

5. References

- Aeppli, C., Holmstrand, H., Andersson, P. and Gustafsson, O. (2010) Direct Compound-Specific Stable Chlorine Isotope Analysis of Organic Compounds with Quadrupole GC/MS Using Standard Isotope Bracketing. *Anal. Chem.* 82(1), 420-426.
- Anbar, M., Meyerstein, D. and Neta, P. (1966) The reactivity of aromatic compounds toward hydroxyl radicals hydroxyl radicals. *J. Phys. Chem.* 8(70), 2660-2662.
- Anipsitakis, G.P. and Dionysiou, D.D. (2004) Radical generation by the interaction of transition metals with common oxidants. *Environ. Sci. Technol.* 38(13), 3705-3712.
- Araújo, T.M., Campos, M.N.N. and Canela, M.C. (2007) Studying the photochemical fate of methyl parathion in natural waters under tropical conditions. *Int. J. Environ. An. Ch.* 87(13-14), 937-947.
- Badin, A., Buttet, G., Maillard, J., Holliger, C. and Hunkeler, D. (2014) Multiple dual C-Cl isotope patterns associated with reductive dechlorination of tetrachloroethene. *Environ. Sci. Technol.* 48(16), 9179-9186.
- Bashir, S., Hitzfeld, K.L., Gehre, M., Richnow, H.H. and Fischer, A. (2015) Evaluating degradation of hexachlorocyclohexane (HCH) isomers within a contaminated aquifer using compound-specific stable carbon isotope analysis (CSIA). *Water Res.* 71, 187-196.
- Bernstein, A., Shouakar-Stash, O., Ebert, K., Laskov, C., Hunkeler, D., Jeannotat, S., Sakaguchi-Soder, K., Laaks, J., Jochmann, M.A., Cretnik, S., Jager, J., Haderlein, S.B., Schmidt, T.C., Aravena, R. and Elsner, M. (2011) Compound-Specific Chlorine Isotope Analysis: A Comparison of Gas Chromatography/Isotope Ratio Mass Spectrometry and Gas Chromatography/Quadrupole Mass Spectrometry Methods in an Interlaboratory Study. *Anal. Chem.* 83(20), 7624-7634.
- Bester, K., Gatermann, R., Huhnerfuss, H., Lange, W. and Theobald, N. (1998) Results of non target screening of lipophilic organic pollutants in the German Bight. IV: Identification and quantification of chloronitrobenzenes and dichloronitrobenzenes. *Environ. Pollut.* 102(2-3), 163-169.
- Bigeleisen, J. and Wolfsberg, M. (1958) Theoretical and experimental aspects of isotope effects in chemical kinetics. *Adv. Chem. Phys.* 1, 15-76.
- Böltner, D., Moreno- Morillas, S. and Ramos, J.L. (2005) 16S rDNA phylogeny and distribution of lin genes in novel hexachlorocyclohexane- degrading *Sphingomonas* strains. *Environ. Microbiol.* 7(9), 1329-1338.
- Bondgaard, M., Hvidberg, B. and Ramsay, L. (2012) Remediation of pesticide contamination by in situ alkaline hydrolysis - a new soil remediation technology, Monterey, California.

- Boreen, A.L., Arnold, W.A. and McNeill, K. (2003) Photodegradation of pharmaceuticals in the aquatic environment: A review. *Aquat. Sci.* 65(4), 320-341.
- Brand, W.A., Coplen, T.B., Vogl, J., Rosner, M. and Prohaska, T. (2014) Assessment of international reference materials for isotope-ratio analysis (IUPAC Technical Report). *Pure Appl. Chem.* 86(3), 425-467.
- Calamari, D., Galassi, S., Setti, F. and Vighi, M. (1983) Toxicity of selected chlorobenzenes to aquatic organisms. *Chemosphere* 12(2), 253-262.
- Calvelo Pereira, R., Camps-Arbestain, M., Rodriguez Garrido, B., Macias, F. and Monterroso, C. (2006) Behaviour of alpha-, beta-, gamma-, and delta-hexachlorocyclohexane in the soil-plant system of a contaminated site. *Environ. Pollut.* 144(1), 210-217.
- Carlsson, P., Warner, N.A., Hallanger, I.G., Herzke, D. and Kallenborn, R. (2014) Spatial and temporal distribution of chiral pesticides in *Calanus* spp. from three Arctic fjords. *Environ. Pollut.* 192, 154-161.
- Chartrand, M.M.G., Hirschorn, S.K., Lacrampe-Couloume, G. and Sherwood Lollar, B. (2007) Compound-specific hydrogen isotope analysis of 1,2-dichloroethane: potential for delineating source and fate of chlorinated hydrocarbon contaminants in groundwater. *Rapid Commun. Mass. Sp.* 21(12), 1841-1847.
- Colovic, M.B., Krstic, D.Z., Lazarevic-Pasti, T.D., Bondzic, A.M. and Vasic, V.M. (2013) Acetylcholinesterase inhibitors: pharmacology and toxicology. *Curr. Neuropharmacol.* 11(3), 315-335.
- Coplen, T.B. (2011) Guidelines and recommended terms for expression of stable-isotope-ratio and gas-ratio measurement results. *Rapid Commun. Mass. Sp.* 25(17), 2538-2560.
- Coplen, T.B., Brand, W.A., Gehre, M., Groning, M., Meijer, H.A.J., Toman, B. and Verkouteren, R.M. (2006) After two decades a second anchor for the VPDB delta C-13 scale. *Rapid Commun. Mass. Sp.* 20(21), 3165-3166.
- Delfino, R.T., Ribeiro, T.S. and Figueroa-Villar, J.D. (2009) Organophosphorus Compounds as Chemical Warfare Agents: a Review. *J. Brazil. Chem. Soc.* 20(3), 407-428.
- Devi, P., Das, U. and Dalai, A.K. (2016) In-situ chemical oxidation: Principle and applications of peroxide and persulfate treatments in wastewater systems. *Sci. Total. Environ.* 571, 643-657.
- Durand, G., Abad, J.L., Sanchezbaeza, F., Messeguer, A. and Barcelo, D. (1994) Unequivocal identification of compounds formed in the photodegradation of fenitrothion in water-methanol and proposal of selected transformation pathways. *J. Agr. Food Chem.* 42(3), 814-821.
- Elsner, M. (2010) Stable isotope fractionation to investigate natural transformation mechanisms of organic contaminants: principles, prospects and limitations. *J. Environ. Monit.* 12(11), 2005-2031.

- Elsner, M. and Imfeld, G. (2016) Compound-specific isotope analysis (CSIA) of micropollutants in the environment - current developments and future challenges. *Curr. Opin. Biotechnol.* 41, 60-72.
- Elsner, M., Jochmann, M.A., Hofstetter, T.B., Hunkeler, D., Bernstein, A., Schmidt, T.C. and Schimmelmann, A. (2012) Current challenges in compound-specific stable isotope analysis of environmental organic contaminants. *Anal. Bioanal. Chem.* 403(9), 2471-2491.
- Elsner, M., Zwank, L., Hunkeler, D. and Schwarzenbach, R.P. (2005) A New Concept Linking Observable Stable Isotope Fractionation to Transformation Pathways of Organic Pollutants. *Environ. Sci. Technol.* 18(39), 6896–6916.
- Engelhardt, G. and Wallnöfer, P.R. (1978) Metabolism of di-and mono-n-butyl phthalate by soil bacteria. *Appl. Environ. Microb.* 35(2), 243-246.
- Engelhardt, G., Wallnöfer, P.R. and Hutzinger, O. (1975) The microbial metabolism of Di-n-Butyl phthalate and related dialkyl phthalates. *Bull. Environ. Contam. Toxicol.* 13(3), 342-347.
- European Commission (1982) Official Journal of the European Communities C176, Communication from the Commission to the Council on dangerous substances which might be included in List I of Council Directive 76/464/EEC, 14 July 1982, Volume 25, p. 14.
- FAO (1990) Parathion (58), Food and Agriculture Organization of the United Nations.
- Fenner, K., Canonica, S., Wackett, L.P. and Elsner, M. (2013) Evaluating pesticide degradation in the environment: blind spots and emerging opportunities. *Science* 341(6147), 752-758.
- Fischer, A., Bauer, J., Meckenstock, R.U., Stichler, W., Griebler, C., Maloszewski, P., Kastner, M. and Richnow, H.H. (2006) A multitracer test proving the reliability of Rayleigh equation-based approach for assessing biodegradation in a BTEX contaminated aquifer. *Environ. Sci. Technol.* 40(13), 4245-4252.
- Fischer, A., Herklotz, I., Herrmann, S., Thullner, M., Weelink, S.A.B., Stams, A.J.M., Schlomann, M., Richnow, H.H. and Vogt, C. (2008) Combined carbon and hydrogen isotope fractionation investigations for elucidating benzene biodegradation pathways. *Environ. Sci. Technol.* 42(12), 4356-4363.
- Franke, S., Lihl, C., Renpenning, J., Elsner, M. and Nijenhuis, I. (2017) Triple-element compound-specific stable isotope analysis of 1,2-dichloroethane for characterization of the underlying dehalogenation reaction in two *Dehalococcoides mccartyi* strains. *Fems Microbiol. Ecol.* 93(12), 1-9.
- Gao, D.W. and Wen, Z.D. (2016) Phthalate esters in the environment: A critical review of their occurrence, biodegradation, and removal during wastewater treatment processes. *Sci. Total. Environ.* 541, 986-1001.

- Gao, Y., An, T., Ji, Y., Li, G. and Zhao, C. (2015) Eco-toxicity and human estrogenic exposure risks from OH-initiated photochemical transformation of four phthalates in water: A computational study. *Environ. Pollut.* 206, 510-517.
- Gehre, M., Renpenning, J., Gilevska, T., Qi, H., Coplen, T.B., Meijer, H.A., Brand, W.A. and Schimmelmann, A. (2015) On-line hydrogen-isotope measurements of organic samples using elemental chromium: an extension for high temperature elemental-analyzer techniques. *Anal. Chem.* 87(10), 5198-5205.
- Gilevska, T., Gehre, M. and Richnow, H.H. (2015) Multidimensional isotope analysis of carbon, hydrogen and oxygen as tool for identification of the origin of ibuprofen. *J Pharm. Biomed. Anal.* 115, 410-417.
- Gmurek, M., Olak-Kucharczyk, M. and Ledakowicz, S. (2017) Photochemical decomposition of endocrine disrupting compounds - A review. *Chem. Eng. J.* 310, 437-456.
- Han, D.H., Wan, J.Q., Ma, Y.W., Wang, Y., Li, Y., Li, D.Y. and Guan, Z.Y. (2015) New insights into the role of organic chelating agents in Fe(II) activated persulfate processes. *Chem. Eng. J.* 269, 425-433.
- Hansch, C., Leo, A. and Taft, R.W. (1991) A survey of Hammett substituent constants and resonance and field parameters. *Chem. Rev.* 91(2), 165-195.
- Hitzfeld, K.L., Gehre, M. and Richnow, H.H. (2011) A novel online approach to the determination of isotopic ratios for organically bound chlorine, bromine and sulphur. *Rapid Commun. Mass. Sp.* 25(20), 3114-3122.
- Hitzfeld, K.L., Gehre, M. and Richnow, H.H. (2017) Evaluation of the performance of high temperature conversion reactors for compound-specific oxygen stable isotope analysis. *Isot. Environ. Healt. S.* 53(2), 116-133.
- Hofstetter, T.B., Schwarzenbach, R.P. and Bernasconi, S.M. (2008) Assessing transformation processes of organic compounds using stable isotope fractionation. *Environ. Sci. Technol.* 42(21), 7737-7743.
- Holmstrand, H., Mandalakis, M., Zencak, Z., Andersson, P. and Gustafsson, O. (2007) First compound-specific chlorine-isotope analysis of environmentally-bioaccumulated organochlorines indicates a degradation-relatable kinetic isotope effect for DDT. *Chemosphere* 69(10), 1533-1539.
- Horst, A., Renpenning, J., Richnow, H.H. and Gehre, M. (2017) Compound Specific Stable Chlorine Isotopic Analysis of Volatile Aliphatic Compounds Using Gas Chromatography Hyphenated with Multiple Collector Inductively Coupled Plasma Mass Spectrometry. *Anal. Chem.* 89(17), 9131-9138.
- HSDB (2004) HSDB: omethoate U.S. National Library of Medicine, <http://toxnet.nlm.nih.gov/cgi-bin/sis/search2/r?dbs+hsdb:@term+@rn+@rel+1113-1102-1116>.

- Huang, J.Y., Nkrumah, P.N., Li, Y. and Appiah-Sefah, G. (2013) Chemical behavior of phthalates under abiotic conditions in landfills. *Rev. Environ. Contam. T.* 224, 39-52.
- Hunkeler, D., Meckenstock, R.U., Sherwood Lollar, B., Schmidt, T.C. and Wilson, J.T. (2008) A guide for assessing biodegradation and source identification of organic ground water contaminants using Compound Specific Isotope Analysis (CSIA), p. 67, United States Environmental Protection Agency, Ada, OK.
- Hvidberg, B., Ramsay, L., Kirkegaard, C., Elkjær, L., Jorgensen, C., Oberender, A. and Kiilerich, O. (2008) Remediation technologies for a large pesticide-contaminated site: enclosure, alkaline hydrolysis and bioventing.
- ICSC (2004) ICSC: 0006 - Parathion. <http://www.inchem.org/documents/icsc/icsc/eics0006.htm>.
- Ivdrá, N., Fischer, A., Herrero-Martin, S., Giunta, T., Bonifacie, M. and Richnow, H.H. (2017) Carbon, Hydrogen and Chlorine Stable Isotope Fingerprinting for Forensic Investigations of Hexachlorocyclohexanes. *Environ. Sci. Technol.* 51(1), 446-454.
- Jammer, S., Rizkov, D., Gelman, F. and Lev, O. (2015) Quantitative structure-activity relationship correlation between molecular structure and the Rayleigh enantiomeric enrichment factor. *Environ. Sci.: Processes Impacts* 17(8), 1370-1376.
- Jin, B.A., Laskov, C., Rolle, M. and Haderlein, S.B. (2011) Chlorine Isotope Analysis of Organic Contaminants Using GC-qMS: Method Optimization and Comparison of Different Evaluation Schemes. *Environ. Sci. Technol.* 45(12), 5279-5286.
- Kanmoni, V.G.G., Daniel, S. and Raj, G.A.G. (2012) Photocatalytic degradation of chlorpyrifos in aqueous suspensions using nanocrystals of ZnO and TiO₂. *React. Kinet. Mechan. Catal.* 106(2), 325-339.
- Koc, F. and Karakus, E. (2011) Determination of Organochlorinated Pesticide Residues By Gas Chromatography - Mass Spectrometry after Elution in A Florisil Column. *Kafkas Universitesi Veteriner Fakultesi Dergisi* 17(1), 65-70.
- Kopinke, F.D., Georgi, A., Voskamp, M. and Richnow, H.H. (2005) Carbon isotope fractionation of organic contaminants due to retardation on humic substances: Implications for natural attenuation studies in aquifers. *Environ. Sci. Technol.* 39(16), 6052-6062.
- Kuder, T., van Breukelen, B.M., Vanderford, M. and Philp, P. (2013) 3D-CSIA: Carbon, Chlorine, and Hydrogen Isotope Fractionation in Transformation of TCE to Ethene by a Dehalococcoides Culture. *Environ. Sci. Technol.* 47(17), 9668-9677.
- Kuder, T., Wilson, J.T., Kaiser, P., Kolhatkar, R., Philp, P. and Allen, J. (2005) Enrichment of stable carbon and hydrogen isotopes during anaerobic biodegradation of MTBE: Microcosm and field evidence. *Environ. Sci. Technol.* 39(1), 213-220.

- Lana, N.B., Berton, P., Covaci, A., Ciocco, N.F., Barrera-Oro, E., Atencio, A. and Altamirano, J.C. (2014) Fingerprint of persistent organic pollutants in tissues of Antarctic notothenioid fish. *Sci. Total. Environ.* 499, 89-98.
- Lehmann, M.M., Fischer, M., Bles, J., Zech, M., Siegwolf, R.T.W. and Saurer, M. (2016) A novel methylation derivatization method for O-18 analysis of individual carbohydrates by gas chromatography/pyrolysis-isotope ratio mass spectrometry. *Rapid Commun. Mass. Sp.* 30(1), 221-229.
- Lekkas, T., Kolokythas, G., Nikolaou, A., Kostopoulou, M., Kotrikla, A., Gatidou, G., Thomaidis, N.S., Golfinopoulos, S., Makri, C., Babos, D., Vagi, M., Stasinakis, A., Petsas, A. and Lekkas, D.F. (2004) Evaluation of the pollution of the surface waters of Greece from the priority compounds of List II, 76/464/EEC Directive, and other toxic compounds. *Environ. Int.* 30(8), 995-1007.
- Li, H., Wan, J., Ma, Y. and Wang, Y. (2016) Reaction pathway and oxidation mechanisms of dibutyl phthalate by persulfate activated with zero-valent iron. *Sci. Total. Environ.* 562, 889-897.
- Li, Y.F. (1999) Global technical hexachlorocyclohexane usage and its contamination consequences in the environment: from 1948 to 1997. *Sci. Total. Environ.* 232(3), 121-158.
- Lian, S., Nikolausz, M., Nijenhuis, I., Francisco Leite, A. and Richnow, H.H. (2018) Biotransformation and inhibition effects of hexachlorocyclohexanes during biogas production from contaminated biomass characterized by isotope fractionation concepts. *Bioresour. Technol.* 250, 683-690.
- Liang, C.J. and Su, H.-W. (2009) Identification of sulfate and hydroxyl radicals in thermally activated persulfate. *Ind. Eng. Chem. Res.* 48(11), 5558-5562.
- Liu, J., Wu, L., Yao, J., Schaefer, T., Herrmann, H. and Richnow, H.H. (2018a) Carbon and hydrogen stable isotope analysis for characterizing the chemical degradation of tributyl phosphate. *Chemosphere.* 212, 133-142.
- Liu, Y., Bashir, S., Stollberg, R., Trabitzsch, R., Weiss, H., Paschke, H., Nijenhuis, I. and Richnow, H.H. (2017) Compound specific and enantioselective stable isotope analysis as tools to monitor transformation of hexachlorocyclohexane (HCH) in a complex aquifer system. *Environ. Sci. Technol.* 51(16), 8909-8916.
- Liu, Y., Wu, L., Kohli, P., Kumar, R., Stryhanyuk, H., Nijenhuis, I., Lal, R. and Richnow, H.H. (2018b) Enantiomer and carbon isotope fractionation of α -hexachlorocyclohexane by *Sphingobium indicum* strain B90A and corresponding enzymes. *Environ. Sci. Technol.*
- LRSB, L. (2014) Pilot experiments on the remediation technology in situ alkaline hydrolysis at Groyne 42, Final report, NorthPestClean, Kongens Lyngby, Denmark.
- Macwan, A.S., Kukshal, V., Srivastava, N., Javed, S., Kumar, A. and Ramachandran, R. (2012) Crystal structure of the hexachlorocyclohexane dehydrochlorinase (LinA-

- type2): mutational analysis, thermostability and enantioselectivity. *PLoS One* 7(11), e50373.
- Mak, K.S., Griebler, C., Meckenstock, R.U., Liedl, R. and Peter, A. (2006) Combined application of conservative transport modelling and compound-specific carbon isotope analyses to assess in situ attenuation of benzene, toluene, and o-xylene. *J. Contam. Hydrol.* 88(3-4), 306-320.
- Manna, R.N., Zinovjev, K., Tunon, I. and Dybala-Defratyka, A. (2015) Dehydrochlorination of Hexachlorocyclohexanes Catalyzed by the LinA Dehydrohalogenase. A QM/MM Study. *J. Phys. Chem. B* 119(49), 15100-15109.
- Meckenstock, R.U., Morasch, B., Griebler, C. and Richnow, H.H. (2004) Stable isotope fractionation analysis as a tool to monitor biodegradation in contaminated aquifers. *J. Contam. Hydrol.* 75(3-4), 215-255.
- Milosevic, N., Qiu, S., Elsner, M., Einsiedl, F., Maier, M.P., Bensch, H.K., Albrechtsen, H.J. and Bjerg, P.L. (2013) Combined isotope and enantiomer analysis to assess the fate of phenoxy acids in a heterogeneous geologic setting at an old landfill. *Water Res.* 47(2), 637-649.
- Mohn, W.W., Mertens, B., Neufeld, J.D., Verstraete, W. and de Lorenzo, V. (2006) Distribution and phylogeny of hexachlorocyclohexane-degrading bacteria in soils from Spain. *Environ. Microbiol.* 8(1), 60-68.
- Muff, J., MacKinnon, L., Durant, N.D., Bennedsen, L.F., Ruge, K., Bondgaard, M. and Pennell, K. (2016) The influence of cosolvent and heat on the solubility and reactivity of organophosphorous pesticide DNAPL alkaline hydrolysis. *Environ. Sci. Pollut. Res. Int.* 23(22), 22658-22666.
- Muller, R.H., Kleinstuber, S. and Babel, W. (2001) Physiological and genetic characteristics of two bacterial strains utilizing phenoxypropionate and phenoxyacetate herbicides. *Microbiol. Res.* 156(2), 121-131.
- Mundle, S.O.C., Johnson, T., Lacrampe-Couloume, G., Perez-de-Mora, A., Duhamel, M., Edwards, E.A., McMaster, M.L., Cox, E., Revesz, K. and Lollar, B.S. (2012) Monitoring Biodegradation of Ethene and Bioremediation of Chlorinated Ethenes at a Contaminated Site Using Compound-Specific Isotope Analysis (CSIA). *Environ. Sci. Technol.* 46(3), 1731-1738.
- Nelson, L.M. (1982) Biologically induced hydrolysis of parathion in soil: isolation of hydrolysing bacteria. *Soil Biol. Biochem.* 14(3), 219-222.
- Nelson, L.M., Yaron, B. and Nye, P.H. (1982) Biologically induced hydrolysis of parathion in soil: kinetics and modelling. *Soil Biol. Biochem.* 14(3), 223-227.
- Nielsen, M.B., Kjeldsen, K.U., Lever, M.A. and Ingvorsen, K. (2014) Survival of prokaryotes in a polluted waste dump during remediation by alkaline hydrolysis. *Ecotoxicology* 23, 404-418.
- Nijenhuis, I., Andert, J., Beck, K., Kastner, M., Diekert, G. and Richnow, H.H. (2005) Stable isotope fractionation of tetrachloroethene during reductive dechlorination

- by *Sulfurospirillum multivorans* and *Desulfitobacterium* sp. strain PCE-S and abiotic reactions with cyanocobalamin. *Appl. Environ. Microb.* 71(7), 3413-3419.
- Nijenhuis, I., Renpenning, J., Kümmel, S., Richnow, H.H. and Gehre, M. (2016) Recent advances in multi-element compound-specific stable isotope analysis of organohalides: Achievements, challenges and prospects for assessing environmental sources and transformation. *Trends Environ. Anal. Chem.* 11, 1-8.
- Nijenhuis, I. and Richnow, H.H. (2016) Stable isotope fractionation concepts for characterizing biotransformation of organohalides. *Curr. Opin. Biotechnol.* 41, 108-113.
- NorthPestClean (2014) Layman reports 2: Demonstration of in situ alkaline hydrolysis as a novel soil remediation technique for a pesticide contamination, Central Denmark Region, Department of Environment, <http://www.eng.northpestclean.dk/publications/layman-reports/>.
- Northrop, D.B. (1981) The expression of isotope effects on enzyme-catalyzed reactions. *Annu. Rev. Biochem.* 50, 103-131.
- OECD (2005) p-chlorotoluene CAS N°: 106-43-4 Screening Information DataSheet - Initial assessment report for SIAM 20, p. 154, UNEP Publication.
- Okai, M., Kubota, K., Fukuda, M., Nagata, Y., Nagata, K. and Tanokura, M. (2010) Crystal structure of gamma-hexachlorocyclohexane Dehydrochlorinase LinA from *Sphingobium japonicum* UT26. *J. Mol. Biol.* 403(2), 260-269.
- Passeport, E., Landis, R., Lacrampe-Couloume, G., Lutz, E.J., Mack, E.E., West, K., Morgan, S. and Lollar, B.S. (2016) Sediment monitored natural recovery evidenced by compound specific isotope analysis and high-resolution pore water sampling. *Environ. Sci. Technol.* 50(22), 12197-12204.
- Passeport, E., Zhang, N., Wu, L., Herrmann, H., Sherwood Lollar, B. and Richnow, H.-H. (2018) Aqueous photodegradation of substituted chlorobenzenes: Kinetics, carbon isotope fractionation, and reaction mechanisms. *Water Res.* 135, 95-103.
- Pehkonen, S.O. and Zhang, Q. (2002) The degradation of organophosphorus pesticides in natural waters: A critical review. *Crit. Rev. Env. Sci. Tec.* 32(1), 17-72.
- Penning, H., Sorensen, S.R., Meyer, A.H., Aamand, J. and Elsner, M. (2010) C, N, and H isotope fractionation of the herbicide isoproturon reflects different microbial transformation pathways. *Environ. Sci. Technol.* 44(7), 2372-2378.
- Pooley, K.E., Blessing, M., Schmidt, T.C., Haderlein, S.B., Macquarrie, K.T.B. and Prommer, H. (2009) Aerobic Biodegradation of Chlorinated Ethenes in a Fractured Bedrock Aquifer: Quantitative Assessment by Compound-Specific Isotope Analysis (CSIA) and Reactive Transport Modeling. *Environ. Sci. Technol.* 43(19), 7458-7464.
- Pope, C.N. (1999) Organophosphorus pesticides: Do they all have the same mechanism of toxicity? *J. Toxicol. Env. Heal. B* 2(2), 161-181.

- Reetz, M.T. (2011) Laboratory evolution of stereoselective enzymes: a prolific source of catalysts for asymmetric reactions. *Angewandte Chemie International Edition* 50(1), 138-174.
- Renpenning, J., Hitzfeld, K.L., Gilevska, T., Nijenhuis, I., Gehre, M. and Richnow, H.H. (2015a) Development and validation of an universal interface for compound-specific stable isotope analysis of chlorine ($^{37}\text{Cl}/^{35}\text{Cl}$) by GC-high-temperature conversion (HTC)-MS/IRMS. *Anal. Chem.* 87(5), 2832-2839.
- Renpenning, J., Horst, A., Schmidt, M. and Gehre, M. (2018) Online isotope analysis of $^{37}\text{Cl}/^{35}\text{Cl}$ universally applied for semi-volatile organic compounds using GC-MC-ICPMS. *J. Anal. Atom. Spectrom.* (33), 314-321.
- Renpenning, J., Keller, S., Cretnik, S., Shouakar-Stash, O., Elsner, M., Schubert, T. and Nijenhuis, I. (2014) Combined C and Cl isotope effects indicate differences between corrinoids and enzyme (*Sulfurospirillum multivorans* PceA) in reductive dehalogenation of tetrachloroethene, but not trichloroethene. *Environ. Sci. Technol.* 48(20), 11837-11845.
- Renpenning, J., Kuemmel, S., Hitzfeld, K.L., Schimmelmann, A. and Gehre, M. (2015b) Compound-Specific Hydrogen Isotope Analysis of Heteroatom-Bearing Compounds via Gas Chromatography-Chromium-Based High-Temperature Conversion (Cr/HTC)-Isotope Ratio Mass Spectrometry. *Anal. Chem.* 87(18), 9443-9450.
- Renpenning, J., Rapp, I. and Nijenhuis, I. (2015c) Substrate hydrophobicity and cell composition influence the extent of rate limitation and masking of isotope fractionation during microbial reductive dehalogenation of chlorinated ethenes. *Environ. Sci. Technol.* 49(7), 4293-4301.
- Romero, A., Santos, A., Vicente, F. and González, C. (2010) Diuron abatement using activated persulphate: Effect of pH, Fe(II) and oxidant dosage. *Chem. Eng. J.* 162(1), 257-265.
- Rosell, M., Gonzalez-Olmos, R., Rohwerder, T., Rusevova, K., Georgi, A., Kopinke, F.D. and Richnow, H.H. (2012) Critical Evaluation of the 2D-CSIA Scheme for Distinguishing Fuel Oxygenate Degradation Reaction Mechanisms. *Environ. Sci. Technol.* 46(9), 4757-4766.
- Said-Ahmad, W., Wong, K., McNall, M., Shawar, L., Jacksier, T., Turich, C., Stankiewicz, A. and Amrani, A. (2017) Compound-Specific Sulfur Isotope Analysis of Petroleum Gases. *Anal. Chem.* 89(5), 3199-3207.
- Sakaguchi-Soder, K., Jager, J., Grund, H., Matthaus, F. and Schuth, C. (2007) Monitoring and evaluation of dechlorination processes using compound-specific chlorine isotope analysis. *Rapid Commun. Mass Sp.* 21(18), 3077-3084.
- Sakellarides, T.M., Siskos, M.G. and Albanis, T.A. (2003) Photodegradation of selected organophosphorus insecticides under sunlight in different natural waters and soils. *Int. J. Environ. An. Ch.* 83(1), 33-50.

- Santos, F.F., Martin-Neto, L., Airoidi, F.P.S. and Rezende, M.O.O. (2005) Photochemical behavior of parathion in the presence of humic acids from different origins. *J. Environ. Sci. Heal. B* 40(5), 721-730.
- Schimmelmann, A., Qi, H.P., Coplen, T.B., Brand, W.A., Fong, J., Meier-Augenstein, W., Kemp, H.F., Toman, B., Ackermann, A., Assonov, S., Aerts-Bijma, A.T., Brejcha, R., Chikaraishi, Y., Darwish, T., Elsner, M., Gehre, M., Geilmann, H., Groing, M., Helie, J.F., Herrero-Martin, S., Meijer, H.A.J., Sauer, P.E., Sessions, A.L. and Werner, R.A. (2016) Organic Reference Materials for Hydrogen, Carbon, and Nitrogen Stable Isotope-Ratio Measurements: Caffeines, n-Alkanes, Fatty Acid Methyl Esters, Glycines, L-Valines, Polyethylenes, and Oils. *Anal. Chem.* 88(8), 4294-4302.
- Schmidt, T.C., Zwank, L., Elsner, M., Berg, M., Meckenstock, R.U. and Haderlein, S.B. (2004) Compound-specific stable isotope analysis of organic contaminants in natural environments: a critical review of the state of the art, prospects, and future challenges. *Anal. Bioanal. Chem.* 378(2), 283-300.
- Schwarzbauer, J. and Ricking, M. (2010) Non-target screening analysis of river water as compound-related base for monitoring measures. *Environ. Sci. Pollut. R.* 17(4), 934-947.
- Sethunathan, N. and Yoshida, T. (1973) A Flavobacterium sp. that degrades diazinon and parathion. *Can. J. Microbiol.* 19(7), 873-875.
- Sharma, P., Pandey, R., Kumari, K., Pandey, G., Jackson, C.J., Russell, R.J., Oakeshott, J.G. and Lal, R. (2011) Kinetic and sequence-structure-function analysis of known LinA variants with different hexachlorocyclohexane isomers. *PLoS One* 6(9), e25128.
- Shelton, D.R., Boyd, S.A. and Tiedje, J.M. (1984) Anaerobic biodegradation of phthalic acid esters in sludge. *Environ. Sci. Technol.* 18(2), 93-97.
- Shimizu, M., Yasui, Y. and Matsumoto, N. (1983) Structural specificity of aromatic compounds with special reference to mutagenic activity in *Salmonella typhimurium*: a series of chloro- or fluoro-nitrobenzene derivatives. *Mutat. Res.* 116(3-4), 217-238.
- Shouakar-Stash, O., Drimmie, R.J., Zhang, M. and Frape, S.K. (2006) Compound-specific chlorine isotope ratios of TCE, PCE and DCE isomers by direct injection using CF-IRMS. *Appl. Geochem.* 21(5), 766-781.
- Shrivastava, N., Macwan, A.S., Kohler, H.E. and Kumar, A. (2017) Important amino acid residues of hexachlorocyclohexane dehydrochlorinases (LinA) for enantioselective transformation of hexachlorocyclohexane isomers. *Biodegradation* 28(2-3), 171-180.
- Siddaramappa, R., Rajaram, K.P. and Sethunathan, N. (1973) Degradation of parathion by bacteria isolated from flooded soil. *Appl. Microbiol.* 26(6), 846-849.

- Simonich, S.L. and Hites, R.A. (1995) Global distribution of persistent organochlorine compounds. *Science* 269(5232), 1851-1854.
- Singh, B.K. and Walker, A. (2006) Microbial degradation of organophosphorus compounds. *Fems Microbiol. Rev.* 30(3), 428-471.
- Sofer, Z. and Schiefelbein, C.F. (1986) Hydrogen isotope ratio determinations in hydrocarbons using the pyrolysis preparation technique. *Anal. Chem.* 58(9), 2033-2036.
- Staples, C.A., Peterson, D.R., Parkerton, T.F. and Adams, W.J. (1997) The environmental fate of phthalate esters: A literature review. *Chemosphere* 35(4), 667-749.
- Suar, M., van der Meer, J.R., Lawlor, K., Holliger, C. and Lal, R. (2004) Dynamics of multiple *lin* gene expression in *Sphingomonas paucimobilis* B90A in response to different hexachlorocyclohexane isomers. *Appl. Environ. Microb.* 70(11), 6650-6656.
- Sun, J.Q., Wu, X.Q. and Gan, J. (2015) Uptake and metabolism of phthalate esters by edible plants. *Environ. Sci. Technol.* 49(14), 8471-8478.
- Swiderek, K. and Paneth, P. (2013) Binding isotope effects. *Chem. Rev.* 113(10), 7851-7879.
- Tang, W.J., Zhang, L.S., Fang, Y., Zhou, Y. and Ye, B.C. (2016) Biodegradation of phthalate esters by newly isolated *Rhizobium* sp. LMB-1 and its biochemical pathway of di-n-butyl phthalate. *J Appl. Microbiol.* 121(1), 177-186.
- Thullner, M., Centler, F., Richnow, H.-H. and Fischer, A. (2012) Quantification of organic pollutant degradation in contaminated aquifers using compound specific stable isotope analysis – Review of recent developments. *Org. Geochem.* 42(12), 1440-1460.
- Tobias, H.J. and Brenna, J.T. (1997) On-line pyrolysis as a limitless reduction source for high-precision isotopic analysis of organic-derived hydrogen. *Anal. Chem.* 69(16), 3148-3152.
- Trapp, S. (2015) Calibration of a plant uptake model with plant- and site-specific data for uptake of chlorinated organic compounds into radish. *Environ. Sci. Technol.* 49(1), 395-402.
- Trova, C., Cossa, G. and Gandolfo, G. (1991) Behavior and fate of chloronitrobenzene in a fluvial environment. *Bull. Environ. Contam. Toxicol.* 47(4), 580-585.
- Tsitonaki, A., Petri, B., Crimi, M., Mosbæk, H., Siegrist, R.L. and Bjerg, P.L. (2010) In situ chemical oxidation of contaminated soil and groundwater using persulfate: A review. *Crit. Rev. Env. Sci. Tec.* 40(1), 55-91.
- Vamsee-Krishna, C. and Phale, P.S. (2008) Bacterial degradation of phthalate isomers and their esters. *Indian J microbiol.* 48(1), 19-34.

- Van Acker, M., Shahar, A., Young, E.D. and Coleman, M.L. (2006) GC/multiple collector-ICPMS method for chlorine stable isotope analysis of chlorinated aliphatic hydrocarbons. *Anal. Chem.* 78(13), 4663-4667.
- Van Breukelen, B.M. (2007) Extending the Rayleigh equation to allow competing isotope fractionating pathways to improve quantification of biodegradation. *Environ. Sci. Technol.* 41(11), 4004-4010.
- Van Keer, I., Bronders, J., Verhack, J., Schwarzbauer, J. and Swennen, R. (2012) Limitations in the use of compound-specific stable isotope analysis to understand the behaviour of a complex BTEX groundwater contamination near Brussels (Belgium). *Environ. Earth Sci.* 66(2), 457-470.
- Vaughan, P.P. and Blough, N.V. (1998) Photochemical formation of hydroxyl radical by constituents of natural waters. *Environ. Sci. Technol.* 32(19), 2947-2953.
- Ventrice, P., Ventrice, D., Russo, E. and De Sarroa, G. (2013) Phthalates: European regulation, chemistry, pharmacokinetic and related toxicity. *Environ. Toxicol. Phar.* 36(1), 88-96.
- Verma, H., Kumar, R., Oldach, P., Sangwan, N., Khurana, J.P., Gilbert, J.A. and Lal, R. (2014) Comparative genomic analysis of nine *Sphingobium* strains: insights into their evolution and hexachlorocyclohexane (HCH) degradation pathways. *BMC Genomics* 15(1), 1014.
- Vetter, W., Armbruster, W., Betson, T.R., Schleucher, J., Kapp, T. and Lehnert, K. (2006) Baseline isotopic data of polyhalogenated compounds. *Anal. Chim. Acta* 577(2), 250-256.
- Vijgen, J. (2006) The Legacy of Lindane HCH Isomer Production. A Global Overview of Residue Management, Formulation and Disposal.
- Vogt, C., Dorer, C., Musat, F. and Richnow, H.H. (2016) Multi-element isotope fractionation concepts to characterize the biodegradation of hydrocarbons - from enzymes to the environment. *Curr. Opin. Biotechnol.* 41, 90-98.
- Wanamaker, E.C., Chingas, G.C. and McDougal, O.M. (2013) Parathion hydrolysis revisited: in situ aqueous kinetics by ¹H NMR. *Environ. Sci. Technol.* 47(16), 9267-9273.
- Weisburger, E.K., Russfield, A.B., Homburger, F., Weisburger, J.H., Boger, E., Vandongen, C.G. and Chu, K.C. (1978) Testing of twenty-one environmental aromatic amines or derivatives for long-term toxicity or carcinogenicity. *J Environ. Pathol. and Toxicol.* 2(2), 325-356.
- Westaway, K.C. (2006) *Advances in Physical Organic Chemistry*, Vol 41. Richard, J.P. (ed), pp. 217-273, Academic Press Ltd-Elsevier Science Ltd, London.
- Wiberg, K., Letcher, R.J., Sandau, C.D., Norstrom, R.J., Tysklind, M. and Bidleman, T.F. (2000) The Enantioselective Bioaccumulation of Chiral Chlordane and r-HCH Contaminants in the Polar Bear Food Chain. *Environ. Sci. Technol.* (34), 2668-2674.

- Wiegert, C., Aeppli, C., Knowles, T., Holmstrand, H., Evershed, R., Pancost, R.D., Machackova, J. and Gustafsson, O. (2012) Dual Carbon-Chlorine Stable Isotope Investigation of Sources and Fate of Chlorinated Ethenes in Contaminated Groundwater. *Environ. Sci. Technol.* 46(20), 10918-10925.
- Wolfsberg, M., Van Hook, W.A., Paneth, P. and Rebelo, L.P.N. (2010) Isotope Effects in the Chemical, Geological, and Bio Sciences. Wolfsberg, M. (ed), pp. 319-324, Springer.
- Wols, B.A. and Hofman-Caris, C.H.M. (2012) Review of photochemical reaction constants of organic micropollutants required for UV advanced oxidation processes in water. *Water Res.* 46(9), 2815-2827.
- Wu, C. and Linden, K.G. (2008) Degradation and byproduct formation of parathion in aqueous solutions by UV and UV/H₂O₂ treatment. *Water Res.* 42(19), 4780-4790.
- Wu, L., Chladkova, B., Lechtenfeld, O.J., Lian, S., Schindelka, J., Herrmann, H. and Richnow, H.H. (2018a) Characterizing chemical transformation of organophosphorus compounds by (13)C and (2)H stable isotope analysis. *Sci. Total. Environ.* 615, 20-28.
- Wu, L., Kummel, S. and Richnow, H.H. (2017) Validation of GC-IRMS techniques for delta13C and delta2H CSIA of organophosphorus compounds and their potential for studying the mode of hydrolysis in the environment. *Anal. Bioanal. Chem.* 409(10), 2581-2590.
- Wu, L., Moses, S., Liu, Y., Renpenning, J. and Richnow, H.H. (2018b) Development of extraction and clean-up methods for multi- element compound specific isotope analysis of hexachlorocyclohexanes for isotope forensic and food web studies. *Anal. Chem.*
- Wu, L., Verma, D., Bondgaard, M., Melvej, A., Vogt, C., Subudhi, S. and Richnow, H.H. (2018c) Carbon and hydrogen isotope analysis of parathion for charactering natural attenuation by hydrolysis at a contaminated site. *Water Res.* 143, 146-154.
- Wu, L., Yao, J., Trebse, P., Zhang, N. and Richnow, H.H. (2014) Compound specific isotope analysis of organophosphorus pesticides. *Chemosphere* 111, 458-463.
- Xie, P.C., Ma, J., Liu, W., Zou, J., Yue, S.Y., Li, X.C., Wiesner, M.R. and Fang, J.y. (2015) Removal of 2-MIB and geosmin using UV/persulfate: contributions of hydroxyl and sulfate radicals. *Water Res.* 69, 223-233.
- Xu, B., Gao, N.Y., Cheng, H., Xia, S.J., Rui, M. and Zhao, D.D. (2009) Oxidative degradation of dimethyl phthalate (DMP) by UV/H₂O₂ process. *J. Hazard. Mater.* 162(2-3), 954-959.
- Xu, B., Gao, N.Y., Sun, X.F., Xia, S.J., Rui, M., Simonnot, M.O., Causserand, C. and Zhao, J.F. (2007) Photochemical degradation of diethyl phthalate with UV/H₂O₂. *J. Hazard. Mater.* 139(1), 132-139.

- Yasunaga, G., Fujise, Y., Zenitani, R., Tanabe, S. and Kato, H. (2015) Spatial and temporal variation of PCBs and organochlorine pesticides in the Antarctic minke whales, *Balaenoptera bonaerensis*, in the period 1987-2005. *Chemosphere* 126, 11-17.
- Zafiriou, O.C. (1974) Sources and reactions of OH and daughter radicals in seawater. *J. Geophys. Res.* 79(30), 4491-4497.
- Zech, M. and Glaser, B. (2009) Compound-specific delta O-18 analyses of neutral sugars in soils using gas chromatography-pyrolysis-isotope ratio mass spectrometry: problems, possible solutions and a first application. *Rapid Commun. Mass. Sp.* 23(22), 3522-3532.
- Zech, M., Saurer, M., Tuthorn, M., Rinne, K., Werner, R.A., Siegwolf, R., Glaser, B. and Juchelka, D. (2013) A novel methodological approach for delta O-18 analysis of sugars using gas chromatography-pyrolysis-isotope ratio mass spectrometry. *Isot. Environ. Healt. S.* 49(4), 492-502.
- Zhang, D., Wu, L., Yao, J., Herrmann, H. and Richnow, H.H. (2018a) Carbon and hydrogen isotope fractionation of phthalate esters during degradation by sulfate and hydroxyl radicals. *Chem. Eng. J.* 347, 111-118.
- Zhang, D., Wu, L., Yao, J., Vogt, C. and Richnow, H. (2018b) Carbon and hydrogen isotope fractionation during abiotic hydrolysis and aerobic biodegradation of phthalate esters. *Environ. Sci. Technol.*
- Zhang, N., Bashir, S., Qin, J.Y., Schindelka, J., Fischer, A., Nijenhuis, I., Herrmann, H., Wick, L.Y. and Richnow, H.H. (2014) Compound specific stable isotope analysis (CSIA) to characterize transformation mechanisms of alpha-hexachlorocyclohexane. *J. Hazard. Mater.* 280, 750-757.
- Zhang, N., Geronimo, I., Paneth, P., Schindelka, J., Schaefer, T., Herrmann, H., Vogt, C. and Richnow, H.H. (2016a) Analyzing sites of OH radical attack (ring vs. side chain) in oxidation of substituted benzenes via dual stable isotope analysis (delta(13)C and delta(2)H). *Sci. Total. Environ.* 542(Pt A), 484-494.
- Zhang, N., Schindelka, J., Herrmann, H., George, C., Rosell, M., Herrero-Martin, S., Klan, P. and Richnow, H.H. (2015) Investigation of Humic Substance Photosensitized Reactions via Carbon and Hydrogen Isotope Fractionation. *Environ. Sci. Technol.* 49(1), 233-242.
- Zhang, X.L., Feng, M.B., Qu, R.J., Liu, H., Wang, L.S. and Wang, Z.Y. (2016b) Catalytic degradation of diethyl phthalate in aqueous solution by persulfate activated with nano-scaled magnetic CuFe₂O₄/MWCNTs. *Chem. Eng. J.* 301, 1-11.
- Zwank, L., Berg, M., Elsner, M., Schmidt, T.C., Schwarzenbach, R.P. and Haderlein, S.B. (2005) New evaluation scheme for two-dimensional isotope analysis to decipher biodegradation processes: Application to groundwater contamination by MTBE. *Environ. Sci. Technol.* 39(4), 1018-1029.

6. Appendix

Appendix 6.1.

Compound specific isotope analysis of organophosphorus pesticides

Published paper: *Wu, L.; Yao, J.; Trebse, P.; Zhang, N.; Richnow, H. H., Chemosphere 2014, 111, 458-63.*



Compound specific isotope analysis of organophosphorus pesticides



Langping Wu^a, Jun Yao^{a,1}, Polonca Trebse^{b,*}, Ning Zhang^c, Hans H. Richnow^c

^a School of Civil and Environmental Engineering, and National International Cooperation Based on Environment and Energy, University of Science and Technology Beijing, Xueyuan Road No. 30, Haidian District, Beijing 100083, PR China

^b Laboratory for Environmental Research, University of Nova Gorica, Vipavska 13, Nova Gorica SI-5000, Slovenia

^c Department of Isotope Biogeochemistry, Helmholtz Centre for Environmental Research-UFZ, Permoserstraße 9 15, Leipzig 04318, Germany

HIGHLIGHTS

- First report on stable carbon isotope fractionation of organophosphorus (OP) pesticides.
- Method development for analyzing carbon isotope composition of OP pesticides.
- Isotope fractionation characterising decomposition pathways of OP pesticides.

ARTICLE INFO

Article history:

Received 14 November 2013

Received in revised form 26 March 2014

Accepted 12 April 2014

Handling Editor: X. Cao

Keywords:

Organophosphorus pesticides

Dichlorvos

Omethoate

Dimethoate

CSIA

ABSTRACT

Compound-specific isotope analysis (CSIA) has been established as a tool to study the environmental fate of a wide range of contaminants. In this study, CSIA was developed to analyse the stable carbon isotope signatures of the widely used organophosphorus pesticides: dichlorvos, omethoate and dimethoate. The linearity of the GC–C–IRMS system was tested for target pesticides and led to an acceptable isotope composition within the uncertainty of the instrument. In order to assess the accuracy of the developed method, the effect of the evaporation procedure on measured carbon isotope composition ($\delta^{13}\text{C}$) values was studied and showed that concentration by evaporation of solvents had no significant isotope effect. The CSIA was then applied to investigate isotope fractionation of the hydrolysis and photolysis of selected pesticides. The carbon isotope fractionation of tested pesticides was quantified by the Rayleigh model, which revealed a bulk enrichment factor (ϵ) of $-0.2 \pm 0.1\text{‰}$ for hydrolysis of dichlorvos, $-1.0 \pm 0.1\text{‰}$ and $-3.7 \pm 1.1\text{‰}$ for hydrolysis and photolysis of dimethoate respectively. This study is a first step towards the application of CSIA to trace the transport and degradation of organophosphorus pesticides in the environment.

© 2014 Elsevier Ltd. All rights reserved.

1. Introduction

A growing food demand in the world forces intensive agriculture accompanied by releasing of a variety of agrochemicals into the environment. There are public concerns regarding the use of pesticides and adequate monitoring of the fate of pesticides is an urgent objective. Today, over 500 compounds are registered worldwide as pesticides, or metabolites of pesticides, of which organophosphorus compounds are a highly diverse family of organic chemicals used in high amounts. For example, the annual production of organophosphorus pesticides (OP pesticides) is more than 100,000 t in China, which accounts for more than 80% of total pesticide production (Liu, 2010). In our study we focused on three

representatives from the group of OP pesticides: dichlorvos, omethoate and dimethoate. These three OP pesticides are widely used in China, are of public concern, and are on the list of Priority Monitoring Pesticides published by the Ministry of Environmental Protection of the People's Republic of China due to their high toxicity, frequent use and appearance (Jiang, 1993).

Dichlorvos (2,2-dichlorovinyl dimethyl phosphate) is a volatile organophosphorus insecticide with fumigant and penetrant action. It is predominantly used as a fumigant or spray for stored grain and for grain handling equipment (Onicescu et al., 2010). Dimethoate (O,O-dimethyl S-[2-(methylamino)-2-oxoethyl] dithiophosphate) is an OP pesticide which has both direct and systemic action against a broad range of insect pests. It is considered as 'moderately hazardous, class II' compound by WHO with a permissible limit of 0.006 mg L^{-1} in drinking water. Omethoate (2-[(dimethoxyphosphoryl)sulfanyl]-N-methyl-acetamide) is an structural analog of dimethoate, and appears to play a dominant role in the

* Corresponding author. Tel.: +386 5 331 5238; fax: +386 5 331 5296.

E-mail addresses: yaojun@ustb.edu.cn (J. Yao), polonca.trebse@ung.si (P. Trebse).

¹ Tel./fax: +86 10 62333305.

toxicity of dimethoate for insects and mammals. These pesticides may be characterised by classical analytical methods, like GC and LC in combination with different detection techniques, like FID, ECD, NPD and MS (Pappas and Kyriakidis, 2003; Evgenidou et al., 2006; Priya et al., 2011). The complexity of aquatic systems always makes it difficult to assess degradation based on concentration data alone, especially, to distinguish degradation from dilution processes in the environment.

Recently, CSIA has opened a promising avenue to study the contaminants behaviours in the environment employing isotope fractionation to trace reactivity. The stability of chemical bonds is dependent on the mass of substituent thus higher activation energy is needed to cleave a bond formed by heavy isotopomers leading to kinetic isotope fractionation in chemical processes (Bigeleisen and Wolfsberg, 1958). This principle controls the reactivity of the individual stable isotopes in the environment and determines isotope fingerprints during synthesis of organic compounds. The isotope composition provides clues that can be used to identify sources, transformation reactions, and sinks of organic compounds in the environment (Meckenstock et al., 2004). The coupling of gas chromatographs with IRMS makes it possible to analyse isotope ratios of individual compounds in complex mixtures and is known as CSIA. CSIA has offered novel avenues to trace transformation processes of contaminants in complex environments because it can be used to identify (Hirschorn et al., 2004; Elsner et al., 2005; Fletcher et al., 2009; Hofstetter and Berg, 2011) and quantify (Abe and Hunkeler, 2006; Aeppli et al., 2010) transformation reactions by determining the isotope composition of organic compound. Over recent years, CSIA has become an increasingly valuable tool and has been applied to study several groups of contaminants, mostly including benzene homologues (Mancini et al., 2003; Fischer et al., 2008), chlorinated ethenes (Vieth et al., 2003; Van Breukelen et al., 2005; Nijenhuis et al., 2007), petroleum hydrocarbons (Richnow et al., 2003a, 2003b), and fuel oxygenates (Mckelvie et al., 2007; Rosell et al., 2007, 2010, 2012). CSIA has been developed for several pesticides, such as Lindane (Badea et al., 2009), isoproturon (Penning et al., 2010) and 2,6-dichlorobenzamide (BAM) (Reinicke et al., 2012). However, to our best knowledge, the evaluation of OP pesticides by CSIA has, to date, not been reported.

The aim of this study was to develop a method for the analysis of carbon isotope signatures of three OP pesticides (dichlorvos, omethoate and dimethoate) extracted from aqueous samples and to explore the applicability of CSIA to characterise the transformation of OP pesticides. For each compound, the precision of the method was tested as well as the detection limits of precise isotope analysis. All measurements were initially analysed by GC–FID in order to find appropriate chromatographic conditions. Organophosphorus esters are susceptible to hydrolysis, therefore this is the most common environmental degradation pathway, so the method was then applied to assess their isotope fractionation changes during hydrolysis. Photolytic degradation of dimethoate was conducted to demonstrate that CSIA could be used to explore different degradation mechanisms by isotope fractionation.

2. Materials and methods

2.1. Chemicals

High purity standards of three pesticides were selected: dichlorvos (PESTANAL[®], analytical standard, 98.8% pure), omethoate (PESTANAL[®], analytical standard, 97.0% pure), dimethoate (PESTANAL[®], analytical standard, 99.6% pure) were purchased from Fluka (Sigma–Aldrich, Germany). Methanol of HPLC gradient grade (purity $\geq 99.8\%$) was supplied by J.T. Baker (Netherlands), while

dichloromethane (Assay (GC), purity > 99.9%) were supplied by Fluka (Sigma–Aldrich, Germany). Stock and standard solutions of pesticides were stored at $-4\text{ }^{\circ}\text{C}$. All other chemicals were analytical grade and used without further purification. $2 \times \text{DI}$ water was obtained by a NANOpure[®] ultrapure water system (Barnstead, USA).

2.2. Pesticides extraction

Solid-phase extraction (SPE) using 3 mL DSC-18 cartridges (Discovery[®], Bellefonte, USA) were used for extraction of pesticides from aqueous solution. Before extraction, the SPE cartridges were activated by passing consecutively 5 mL of dichloromethane, 5 mL of $2 \times \text{DI}$ water, and 5 mL of purified water alkalized to pH 10 with 0.1 M NaOH (or acidified to pH 3 with 0.1 M HCl for control experiments) (Demoliner et al., 2010). Cartridges were then loaded with 6 mL samples and eluted with 1 mL of dichloromethane to 2 mL vials. The extracted phase was stored for subsequent analysis. All extractions were performed in two parallels for each time point of all experiments, one of them was immediately analysed by GC–FID as described below, and the other one was stored at $-4\text{ }^{\circ}\text{C}$ for isotope analysis.

2.3. Evaporation experiment

The evaporation test was conducted to quantify the effect of evaporation procedures on isotope fractionation. Standard dichloromethane solutions of dichlorvos, omethoate and dimethoate mixture (100 mg L^{-1} 1:1:1) were evaporated under a gentle stream of N_2 to volume of 15%, 25%, 40%, 60%, 80% and 100%, respectively, and changes in their carbon isotope compositions were determined.

2.4. Analysis methods

2.4.1. GC–FID analysis

An Agilent 6890 series gas chromatograph (GC, Agilent Technologies, Germany) equipped with a flame ionization detector (FID) was used. OP pesticides were separated in a HP-608 column ($30\text{ m} \times 0.53\text{ mm} \times 0.5\text{ }\mu\text{m}$, USA) with helium as the carrier gas (flow of 6.0 mL min^{-1}). The column was initially held at $60\text{ }^{\circ}\text{C}$ for 1 min, ramped at $30\text{ }^{\circ}\text{C min}^{-1}$ to $300\text{ }^{\circ}\text{C}$, and held for 2 min. Injector and detector temperatures were set to $180\text{ }^{\circ}\text{C}$ and $250\text{ }^{\circ}\text{C}$, respectively. The samples were injected in splitless mode with injection volumes of $1\text{ }\mu\text{L}$. Each sample was measured in triplicate. Calibration of three tested pesticides was measured by diluting it with dichloromethane.

2.4.2. EA–IRMS analysis

To validate the results of the GC–IRMS method, the carbon isotope compositions of the reference compounds were determined with an elemental analyser (EuroVector, Milan, Italy) directly coupled via a ConFlo III (open split, Thermo Fisher Scientific, Bremen, Germany) to a MAT 253 isotope ratio mass spectrometer (Thermo Fisher Scientific), as described elsewhere (Badea et al., 2009).

2.4.3. CSIA analysis

The carbon isotope composition of dichlorvos, omethoate and dimethoate was analysed by a GC–IRMS system consisting of a gas chromatograph (Agilent 6890) coupled via a GC/C III interface to isotope ratio mass spectrometer (Finnigan MAT 252, Thermo Fisher Scientific). The oxidation furnace of the GC/C III interface containing (Pt, Ni, CuO) was set to $980\text{ }^{\circ}\text{C}$. A DB-608 column ($30\text{ m} \times 0.32\text{ mm} \times 0.5\text{ }\mu\text{m}$, USA) was used for pesticides separation, with helium as the carrier gas at a flow rate of 1.3 mL min^{-1} .

The column was initially held at 60 °C for 2 min, ramped at 12 °C min⁻¹ to 225 °C, then up to 280 °C at 7 °C min⁻¹ and finally held for 2 min. The injector was set to 180 °C. Samples were injected in the split injection mode (the split ratio was from 1:1 to 1:5, which was adjusted to concentrations resulting in suitable peak areas). At least three replicates were measured per sample in order to check the reproducibility. If necessary, the samples were reduced under a gentle stream of N₂ to increase the concentration for isotope analysis.

2.5. Hydrolysis experiment

OP pesticides can be hydrolyzed rapidly in alkaline solution, but are more stable in acidic solution. Thus, the hydrolysis experiments of selected pesticides were carried out in buffer solution of pH 10, while hydrolysis in solutions of pH 3 was used as control experiments. Hydrolysis experiments were carried out at 22 °C in 200 mL buffer solution (pH 10) which was prepared with 0.1 M NaOH (purity ≥ 99%) and 0.1 M KCl–boric acid (purity > 99.5%). Control experiments were performed in 50 mL buffer solution (pH 3) which contains 0.1 M HCl (32%, Baker analytical grade) and 0.1 M C₈H₅KO₄ (potassium hydrogen phthalate, 99% purity, Alfa Aesar, Germany). All hydrolysis experiments were conducted in grinding mouth Erlenmeyer flasks with initial concentration of 100 mg L⁻¹ of respective pesticides. Samples were collected at regular time intervals for further analysis. Remaining concentrations of compounds during degradation were determined by GC–FID, and then calculated according to the calibration curve of OP pesticides (see Supporting Information, Fig. S3).

2.6. Photolysis experiment

Photolysis experiment was conducted in a tailor-made chamber photoreactor using six mercury fluorescent lamps as a UVA radiation source (CLEO 20 W, 438 mm × 26 mm, Philips; broad maximum at 355 nm) which was described in details elsewhere (Černigoj et al., 2007). Before starting the degradation experiment, the photoreactor was preheated for 15 min by turning on lamps to keep stable temperature at 35 °C. 200 mL aqueous solution of dimethoate (100 mg L⁻¹) was taken in the reaction tube, and 50 mL of dimethoate solution was performed as dark control experiment. Samples were collected at regular irradiation time intervals for further analysis.

2.7. Quantification of carbon isotope fractionation

The quantification of carbon isotope fractionation has been described in (Meckenstock et al., 2004). Briefly, the isotope ratios measured by CSIA are reported in δ notation in parts per thousand (‰) relative to the international carbon isotope standard (VPDB) (Coplen, 2011). Then bulk isotope enrichment factors (ε) can be obtained from the slope of the Rayleigh equation. Eq. (1):

$$\varepsilon_C = \ln \left[\frac{(\delta_t + 1)}{(\delta_0 + 1)} \right] / \ln \left(\frac{C_t}{C_0} \right) \quad (1)$$

Isotope fractionation occurs during the chemical reaction step. The apparent kinetic isotope effect (AKIE) was calculated to quantify the intrinsic isotope effect of the bond cleavage. AKIE values were calculated by Eq. (2) (Elsner et al., 2005)

$$\text{AKIE}_C = \left(\frac{1}{z \times \frac{n}{x} \times \varepsilon_C + 1} \right) \quad (2)$$

where *n* is the number of carbon atoms in the molecule, *x* is the number of carbon atoms in the reactive position, and *z* is the number of indistinguishable reactive sites.

3. Results and discussion

3.1. CSIA development

The mixtures of OP pesticides were successfully separated by GC–FID and GC–C–IRMS system under selected temperature programs and columns (see Supporting Information, Fig. S1).

The linearity of the method was analysed using a stock solution of OP pesticides, dissolved in DCM to different final concentrations (concentrations of 40, 50, 100, 200, 300, 400, 500, 600, 800, 1000 mg L⁻¹). A new glass liner, 4 mm ID filled with single taper and quartz wool (SGE), was used for split/splitless injection into GC system caused significant shifts in δ¹³C values and gave a poor linearity range, especially for omethoate (see Supporting Information, Fig. S2). Glass liner deactivation using BSTFA gave a better linearity and the isotope composition was almost identical to the elementary analysis coupled to isotope ratio determination. Therefore, we suggest that OP pesticides were decomposed in the liner. In order to circumvent this problem, 1 μL of BSTFA (N,O-bis(trimethylsilyl)trifluoroacetamide, SUPELCO) was injected manually three times into the GC inlet (The Agilent Multimode Inlet (MMI)), adjusted to 100 °C with split ratio of 200:1. Then the injector was heated to 180 °C. After deactivation of the liner, the linearity ranges of OP pesticides was improved (Fig. 1). Linearity ranges were shown for a range of signal areas: 12–35 vs (200–600 mg L⁻¹), 1–68 vs (40–1000 mg L⁻¹) and 5.5–60 vs (100–1000 mg L⁻¹) for dichlorvos, omethoate and dimethoate respectively, showing that the linearity of our method led to an acceptable isotope composition of pesticides within the uncertainty of the instrument. Only signals with this range of areas were used for evaluation of isotope values.

To assess the trueness of the GC–C–IRMS method, the isotope composition of three pure compounds was analysed by EA–IRMS system. The values obtained by two methods were compared in Table 1. The systematic shifts in averaged δ¹³C values determined by the EA–IRMS and GC–C–IRMS systems were 0.8‰, 0.3‰ and 0.7‰ for dichlorvos, omethoate and dimethoate respectively, thus showing relatively good agreement between the two methods.

The isotope effect of the evaporation procedure was evaluated. The evaporation of mixture solution from the original concentration of 100% to 80%, 60%, 40%, 25% and 15% of the original volume shows almost no difference compared with original δ¹³C value of the initial compound (Fig. 2). The standard deviations (2σ) of 6 δ¹³C values of dichlorvos, omethoate and dimethoate were 0.15‰, 0.14‰ and 0.11‰, which fit to the reproducibility by CSIA for carbon isotope (2σ ≤ ± 0.5‰). Therefore, the precision of the measurement was demonstrated as well. The evaporation procedure is unlikely to induce significant isotope effects, thus, concentration of components by evaporation can be used for sample preparation. As the sensitivity of the GC–C–IRMS is relatively low compared to GC–MS techniques, further efforts are needed for isolation of OP pesticides from environmental samples. For example, the limits of the source of drinking water in China are 0.08 and 0.05 mg L⁻¹ for dimethoate and dichlorvos, respectively. For monitoring of environmentally relevant concentration, isolation and enrichment strategies need to be developed. However, as evaporation does not affect the isotope composition, solvent extraction of large sample volume and subsequent enrichment by careful evaporation might be employed.

3.2. Carbon isotope fractionation during degradation

Hydrolysis occurs at several reactive positions in OP pesticide molecules. It can occur by a homogeneous mechanism, where H₂O and OH⁻ act as nucleophiles (Bavcon et al., 2003). OP pesticides can be hydrolyzed rapidly in alkaline solution, but are more

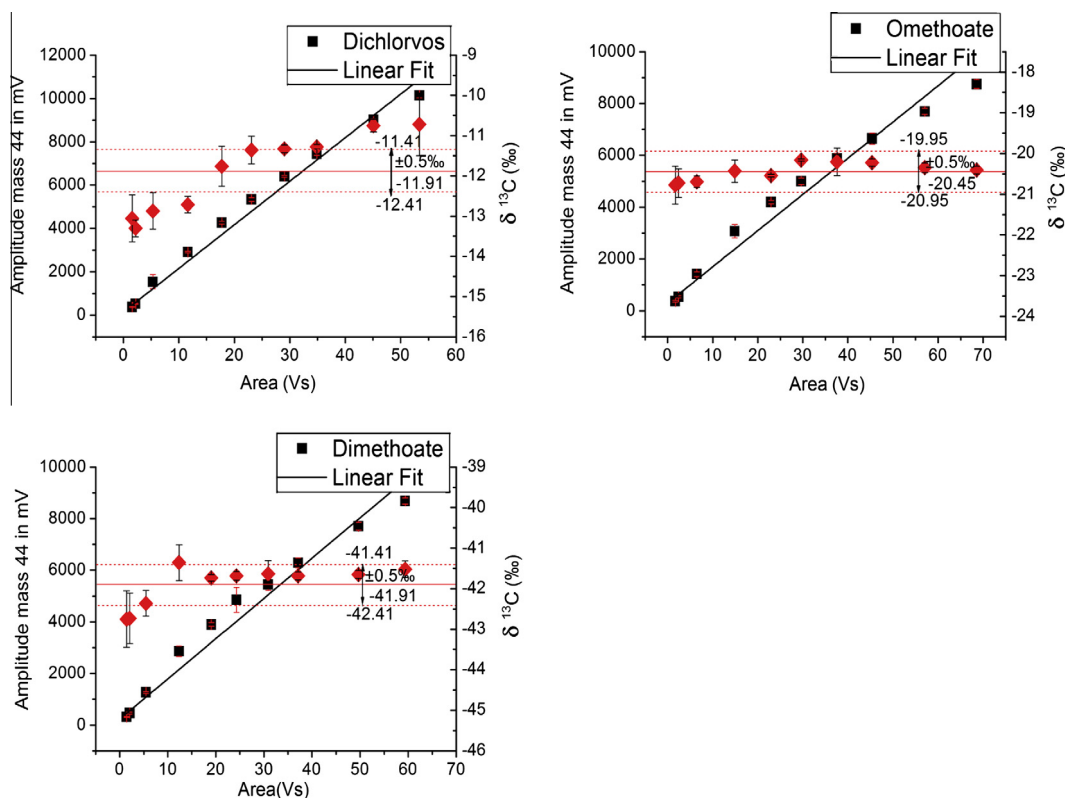


Fig. 1. Linearity test for dichlorvos, omethoate and dimethoate after deactivation of the liner. Signal area represent here correspond to concentrations of 40, 50, 100, 200, 300, 400, 500, 600, 800, 1000 mg L⁻¹. Red diamonds (◆) indicate $\delta^{13}\text{C}$ values and black squares (■) indicate amplitude values. Solid lines represent the means of all measurements; dotted lines represent one standard deviation (2σ) of all measurements. Error bars represent one 2σ of triplicate. (For interpretation of the references to colour in this figure legend, the reader is referred to the web version of this article.)

Table 1
Comparison of mean $\delta^{13}\text{C}$ (‰) values between EA-IRMS and GC-C-IRMS.

Compound	$\delta^{13}\text{C}$ (‰)		$\Delta\delta^{13}\text{C}$ (‰)
	EA-IRMS	GC-C-IRMS	
Dichlorvos	-10.4 ± 0.1	-11.2 ± 0.4	+0.8
Omethoate	-20.8 ± 0.0	-20.5 ± 0.2	-0.3
Dimethoate	-42.6 ± 0.1	-41.7 ± 0.3	-0.7

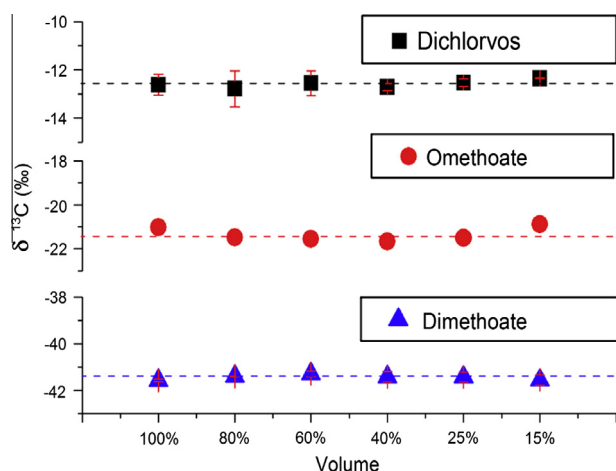


Fig. 2. Evaporation experiment for dichlorvos, omethoate and dimethoate. Isotope composition was determined after reduction of the solvent volume from 100% to 80%, 60%, 40%, 25% and 15%. Dotted lines represent the average value of all measurements. Error bars represent one 2σ of two measurements.

stable in acidic solution. In all of our experiments, the heavier carbon isotope was enriched for tested compounds during the degradation. Data from single experiments are shown in Fig. 3 (data of control experiments are reported in Table S1). After 98.3% was hydrolyzed, dichlorvos was detected with a carbon isotopic composition of $-13.7 \pm 0.2\text{‰}$ (Fig. 3a), which is slightly heavier than the isotopic signature of the parent compound at the beginning of the experiment ($\delta^{13}\text{C} = -14.5 \pm 0.2\text{‰}$). 97.7% of omethoate was degraded within 8 h, and the corresponding carbon isotope signatures were enriched from $-22.2 \pm 0.1\text{‰}$ to $-20.5 \pm 0.2\text{‰}$ (Fig. 3b). Similarly, during the hydrolysis of dimethoate, significant carbon isotope fractionation was observed. The carbon isotope ratio of dimethoate enriched from $-42.8 \pm 0.0\text{‰}$ to $-40.9 \pm 0.2\text{‰}$ (Fig. 3c) within a 96 h experiment. The carbon isotope composition enriched from $-42.5 \pm 0.3\text{‰}$ to $-40.4 \pm 0.2\text{‰}$ upon photolysis of dimethoate over experimental period of 56 h (Fig. 3d).

3.3. AKIE and degradation mechanisms

The isotope fractionation process was quantified by the isotope enrichment factor (ϵ) using the Rayleigh equation (Eq. (1)), obtaining enrichment factors of $-0.2 \pm 0.1\text{‰}$ for hydrolysis of dichlorvos and $-1.0 \pm 0.1\text{‰}$ and $-3.7 \pm 1.1\text{‰}$ for hydrolysis and photolysis dimethoate respectively (Fig. 4). For further elucidation of the reaction mechanism, AKIE values were calculated to characterise the isotope effect of the cleavage of the chemical bond at the reactive positions. According to Oncescu and Oancea (2007), the hydrolysis of dichlorvos may occur by a homogeneous mechanism where $^+\text{H}_3\text{O}/\text{OH}^-$ act as nucleophiles in a $\text{S}_{\text{N}}2$ mechanism. Its a general base-catalyzed reaction and has two parallel routes (Fig. S4). Both routes show no carbon atoms are involved in the reactive

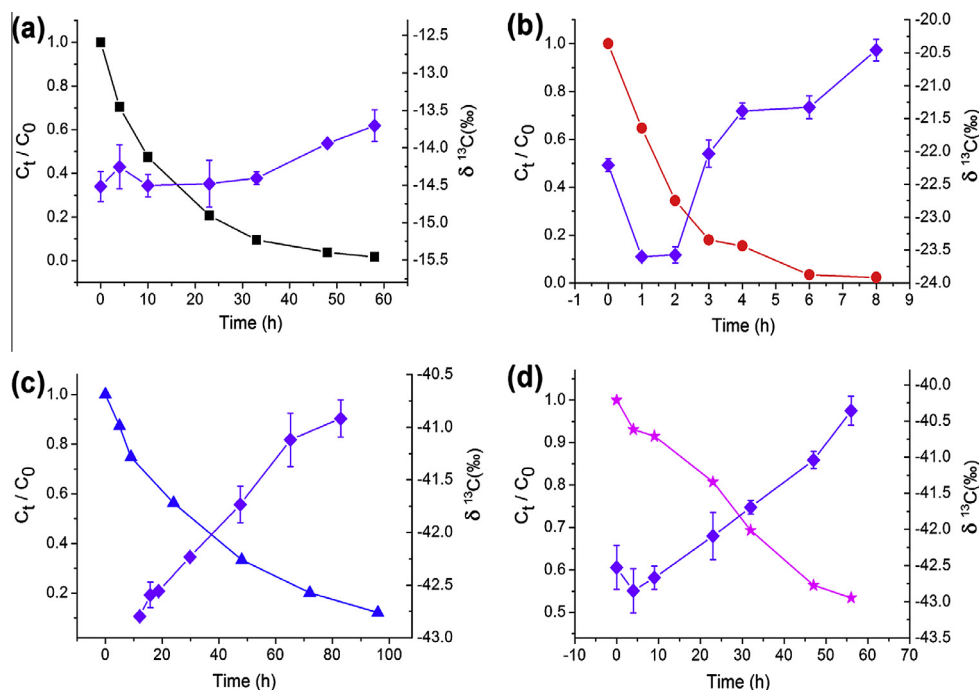


Fig. 3. Changes in concentrations (C_t/C_0) and carbon isotope ratios ($\delta^{13}C$) of OP pesticides during degradation. (a–c) Demonstrate the hydrolysis degradation of dichlorvos (■), omethoate (●) and dimethoate (▲); (d) demonstrates the photolysis of dimethoate (★). (◆) Indicate $\delta^{13}C$ values.

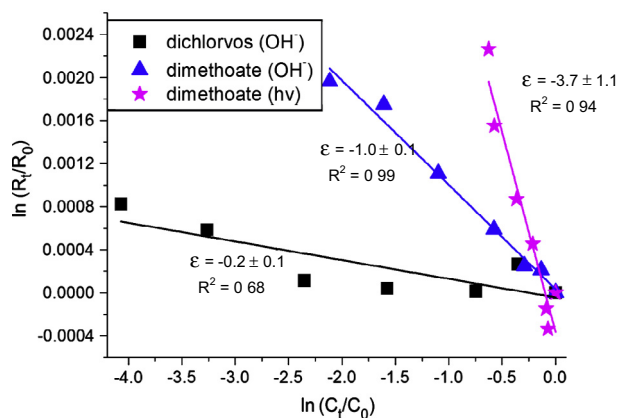


Fig. 4. Double logarithmic plot according to the Rayleigh equation of the isotopic composition vs the residual concentration of dichlorvos (■) from hydrolysis and dimethoate from hydrolysis (▲) and photodegradation (★). ϵ values were calculated according to equation (Eq. (11)) using the slope of the linear regression.

positions. Onescu et al. found that the lowest value (0.61) of bond energy in dichlorvos molecule belongs to phosphate–dichlorvinyl bond, which indicates that this bond has to cleave first by hydrolysis. Thus, we suggest that there is no primary carbon isotope fractionation occurs during the hydrolysis of dichlorvos. The obtained relatively lower enrichment factors of $-0.2 \pm 0.1\%$ may be caused by the secondary isotope effects. Thus, changes in carbon isotope ratios of dichlorvos induced by hydrolysis are expected to be low and the enrichment in isotope signature of dichlorvos may offer opportunities for detection of other processes or source allocation.

The fractionation upon hydrolysis of dimethoate ($-1.0 \pm 0.1\%$) was significantly higher than dichlorvos suggesting a primary isotope effect associated with a carbon bond cleavage in the first unidirectional and irreversible reaction step. In analogy to the proposed mechanism for the hydrolysis of omethoate (Farooq et al., 2004), we propose a similar mechanism proceeding by two

main pathways. A nucleophilic OH^- attacking the phosphorus atom will lead to P–S bond cleavage without any primary carbon isotope effect. A parallel nucleophilic OH^- attack on the C–O bond may lead to a C–O bond fission associated with a primary stable carbon isotope effect and lead to the formation of O-desmethyl-dimethoate. O-desmethyl-dimethoate and O,O-dimethylhydrogen phosphorothioate acid as products of dimethoate hydrolysis at alkaline conditions (WHO, 2012), suggesting that two parallel reactions are at work. The calculation of AKIE value of 1.0050 ± 0.0005 , which is smaller than the theoretical value of KIE (1.061) for C–O bond may reflect that two parallel mechanisms at work and leading to a lower isotope fractionation as expected for an typical $\text{S}_{\text{N}}2$ reaction such as alkaline hydrolysis of a methoxy bond alone (see Supporting Information).

During photolytic degradation, C–O bonds can be broken under direct UV irradiation (Wang et al., 2006). There are two C–O bonds in dimethoate molecule. Assuming that the photolysis of dimethoate was a concerted reaction, where $n = 5$, $x = 2$, $z = 1$, the AKIE calculation gives a value of 1.0094 ± 0.0027 . If the reaction proceeds in stepwise mode, where $n = 5$, $x = 1$, $z = 1$, the AKIE calculation gives a value of 1.0188 ± 0.0054 . Both AKIE values are typically below the theoretical KIE O–C bond cleavages, but still in the similar order. However, as documented so far, this is the first study on CSIA of OP pesticides, therefore, no other values are available to date for comparison. Further mechanistic studies employing CSIA need to be conducted and compared with metabolite studies to identify bond cleavage mechanisms in more details.

4. Conclusion

The GC–IRMS method for CSIA for dichlorvos, omethoate and dimethoate was developed in this study. Linearity test shows that carbon isotope ratios can be obtained for a signal size of area above 12, 1 and 5.5 vs for dichlorvos, omethoate and dimethoate, respectively. The measurements obtained by GC–IRMS system exhibited standard deviations (2σ) that were mostly $< \pm 0.5\%$. To explore the application of the developed CSIA, the degradation

experiments revealed a bulk enrichment factor (ϵ) for hydrolysis of $-0.2 \pm 0.1\text{‰}$ and $-1.0 \pm 0.1\text{‰}$ for dichlorvos and dimethoate, respectively. The photolysis of dimethoate gave a larger enrichment factor of $3.7 \pm 1.1\text{‰}$ and allow to distinct hydrolysis and photolysis. Our study clearly demonstrated that carbon isotope fractionation occurs during degradation of tested pesticides. The isotope enrichment factor may be used to characterise hydrolysis reaction and direct photolysis in field studies.

Monitoring the carbon isotope signatures may be a promising tool for the qualitative and quantitative assessment of the fate of OP pesticides. In order to assess the transport of OP pesticides in the environment and decipher their degradation in more details by CSIA, further laboratory investigations providing reference enrichment factors for degradation mechanisms occurring under different hydrogeochemical conditions are needed. In addition, ^2H , ^{18}O and ^{15}N could also be considered for isotope analysis in order to obtain enhanced insight of OP pesticides from multi-element isotope analysis in future studies.

Acknowledgments

This work is supported in part by grants from International Joint Key Project from National Natural Science Foundation of China (40920134003) and National Natural Science Foundation of China (41273092). We acknowledge financial support from Scholarships of the Republic of Slovenia 2012/13 scheme Mobility Grant. Ning Zhang was supported by CSI: ENVIRONMENT ITN (European Union, 7th Framework Programme, contract number PITN-GA-2010-264329). The isotope analysis was performed in the stable isotope laboratory of the UFZ. We thank M. Gehre, U. Günther for supporting in the laboratory, and thank Dr. Matthew Lee for providing language help.

Appendix A. Supplementary material

Supplementary data associated with this article can be found, in the online version, at <http://dx.doi.org/10.1016/j.chemosphere.2014.04.037>.

References

- Abe, Y., Hunkeler, D., 2006. Does the Rayleigh equation apply to evaluate field isotope data in contaminant hydrogeology. *Environ. Sci. Technol.* 40, 1588–1596.
- Aeppli, C., Hofstetter, T.B., Amaral, H.I.F., Kipfer, R., Schwarzenbach, R.P., Berg, M., 2010. Quantifying in situ transformation rates of chlorinated ethenes by combining compound-specific stable isotope analysis, groundwater dating, and carbon isotope mass balances. *Environ. Sci. Technol.* 44, 3705–3711.
- Badea, S.L., Carsten, V., Stefanie, W., Danet, A.F., Richnow, H.H., 2009. Stable isotope fractionation of α -hexachlorocyclohexane (Lindane) during reductive dechlorination by two strains of sulfate-reducing bacteria. *Environ. Sci. Technol.* 43, 3155–3161.
- Bavcon, M., Trebše, P., Zupančič Kralj, L., 2003. Investigations of the determination and transformations of diazinon and malathion under environmental conditions using gas chromatography coupled with a flame ionisation detector. *Chemosphere* 50, 595–601.
- Bigeleisen, J., Wolfsberg, M., 1958. Theoretical and experimental aspects of isotope effects in chemical kinetics. *Adv. Chem. Phys.*, 15–76.
- Černigoj, U., Štangar, U.L., Trebše, P., 2007. Evaluation of a novel carberry type photoreactor for the degradation of organic pollutants in water. *J. Photochem. Photobiol. A* 188, 169–176.
- Coplen, T.B., 2011. Guidelines and recommended terms for expression of stable-isotope-ratio and gas-ratio measurement results. *Rapid Commun. Mass Spectrom.* 25, 2538–2560.
- Demoliner, A., Caldas, S.S., Costa, F.P., Gonçalves, F.F., Clementin, R.M., 2010. Development and validation of a method using SPE and LC-ESI-MS-MS for the determination of multiple classes of pesticides and metabolites in water samples. *J. Brazil Chem. Soc.* 21, 1424–1433.
- Elsner, M., Zwank, L., Hunkeler, D., 2005. A new concept linking observable stable isotope fractionation to transformation pathways of organic pollutants. *Environ. Sci. Technol.* 39, 6896–6916.
- Evgenidou, E., Konstantinou, I., Fytianos, K., Albanis, T., 2006. Study of the removal of dichlorvos and dimethoate in a titanium dioxide mediated photocatalytic process through the examination of intermediates and the reaction mechanism. *J. Hazard. Mater.* 137, 1056–1064.
- Farooq, R., Lin, F., Wang, Y., Huang, J., Xu, Z., Shaukat, S.F., 2004. Pressure hydrolysis for degradation of omethoate pesticide in water. *J. Shanghai Univ. (Engl. Ed.)* 8, 221–226.
- Fischer, A., Herklotz, I., Herrmann, S., Thollner, M., Weelink, S.A.B., Stams, A.J.M., Schloemann, M., Richnow, H.H., Vogt, C., 2008. Combined carbon and hydrogen isotope fractionation investigations for elucidating benzene biodegradation pathways. *Environ. Sci. Technol.* 42, 4356–4363.
- Fletcher, K.E., Löffler, F.E., Richnow, H.H., Nijenhuis, I., 2009. Stable carbon isotope fractionation of 1,2-dichloropropane during dichloroelimination by dehalococoides populations. *Environ. Sci. Technol.* 43, 6915–6919.
- Hirschorn, S.K., Dinglasan, M.J., Elsner, M., Mancini, S.A., Lacrampe Couloume, G., Edwards, E.A., Sherwood Lollar, B., 2004. Pathway dependent isotopic fractionation during aerobic biodegradation of 1,2-dichloroethane. *Environ. Sci. Technol.* 38, 4775–4781.
- Hofstetter, T.B., Berg, M., 2011. Assessing transformation processes of organic contaminants by compound-specific stable isotope analysis. *TrAC, Trends Anal. Chem.* 30, 618–627.
- Jiang, X.L., 1993. Study on screening of the priority monitoring pesticides. *Adv. Environ. Sci.* 1, 1–15.
- Liu, J.L., 2010. Advance on microbial degradation of organophosphorus pesticides pollution. *J. Biol.* 27, 79–82.
- Mancini, S.A., Ulrich, A.C., Lacrampe-Couloume, G., Sleep, B., Edwards, E.A., Lollar, B.S., 2003. Carbon and hydrogen isotopic fractionation during anaerobic biodegradation of benzene. *Appl. Environ. Microbiol.* 69, 191–198.
- Mckelvie, J.R., Mackay, D.M., de Sieres, N.R., Lacrampe Couloume, G., Sherwood Lollar, B., 2007. Quantifying MTBE biodegradation in the Vandenberg air force base ethanol release study using stable carbon isotopes. *J. Contam. Hydrol.* 94, 157–165.
- Meckenstock, R.U., Morasch, B., Griebler, C., Richnow, H.H., 2004. Stable isotope fractionation analysis as a tool to monitor biodegradation in contaminated aquifers. *J. Contam. Hydrol.* 75, 215–255.
- Nijenhuis, I., Nikolausz, M., Köth, A., Felföldi, T., Weiss, H., Drangmeister, J., Großmann, J., Kästner, M., Richnow, H.H., 2007. Assessment of the natural attenuation of chlorinated ethenes in an anaerobic contaminated aquifer in the Bitterfeld/Wolfen area using stable isotope techniques, microcosm studies and molecular biomarkers. *Chemosphere* 67, 300–311.
- Oncescu, T., Oancea, P., 2007. On the mechanism of dichlorvos hydrolysis. *Rev. Chim.* 58, 232–235.
- Oncescu, T., Stefan, M.I., Oancea, P., 2010. Photocatalytic degradation of dichlorvos in aqueous TiO_2 suspensions. *Environ. Sci. Pollut. Res.* 17, 1158–1166.
- Pappas, C.J., Kyriakidis, N.V., 2003. A comparison of dimethoate degradation in lemons and mandarins on the trees with two GC systems. *Food Chem.* 80, 23–28.
- Penning, H., Sorensen, S.R., Meyer, A.H., Aamand, J., Elsner, M., 2010. C, N, and H isotope fractionation of the herbicide isoproturon reflects different microbial transformation pathways. *Environ. Sci. Technol.* 44, 2372–2378.
- Priya, D.N., Modak, J.M., Trebše, P., Žabar, R., Raichur, A.M., 2011. Photocatalytic degradation of dimethoate using Lbl fabricated TiO_2 /polymer hybrid films. *J. Hazard. Mater.* 195, 214–222.
- Reinicke, S., Simonsen, A., Sørensen, S.R., Aamand, J., Elsner, M., 2012. C and N isotope fractionation during biodegradation of the pesticide metabolite 2,6-dichlorobenzamide (BAM): potential for environmental assessments. *Environ. Sci. Technol.* 46, 1447–1454.
- Richnow, H.H., Annweiler, E., Michaelis, W., Meckenstock, R.U., 2003a. Microbial in situ degradation of aromatic hydrocarbons in a contaminated aquifer monitored by carbon isotope fractionation. *J. Contam. Hydrol.* 65, 101–120.
- Richnow, H.H., Meckenstock, R.U., Ask Reitzel, L., Baun, A., Ledin, A., Christensen, T.H., 2003b. In situ biodegradation determined by carbon isotope fractionation of aromatic hydrocarbons in an anaerobic landfill leachate plume (Vejen, Denmark). *J. Contam. Hydrol.* 64, 59–72.
- Rosell, M., Barcelo, D., Rohwerder, T., Breuer, U., Gehre, M., Richnow, H.H., 2007. Variations in $^{13}\text{C}/^{12}\text{C}$ and D/H enrichment factors of aerobic bacterial fuel oxygenate degradation. *Environ. Sci. Technol.* 41, 2036–2043.
- Rosell, M., Finsterbusch, S., Jechalke, S., Hubschmann, T., Vogt, C., Richnow, H.H., 2010. Evaluation of the effects of low oxygen concentration on stable isotope fractionation during aerobic MTBE biodegradation. *Environ. Sci. Technol.* 44, 309–315.
- Rosell, M., Olmos, R.G., Rohwerder, T., Kopinke, F.D., Richnow, H.H., 2012. Critical evaluation of the 2D-CSIA scheme for distinguishing fuel oxygenate degradation reaction mechanisms. *Environ. Sci. Technol.* 46, 4757–4766.
- Van Breukelen, B.M., Hunkeler, D., Volkering, F., 2005. Quantification of sequential chlorinated ethene degradation by use of a reactive transport model incorporating isotope fractionation. *Environ. Sci. Technol.* 39, 4189–4197.
- Vieth, A., Müller, J., Strauch, G., Kastner, M., Gehre, M., Meckenstock, R.U., Richnow, H.H., 2003. In situ biodegradation of tetrachloroethene and trichloroethene in contaminated aquifers monitored by stable isotope fractionation. *Isot. Environ. Health Stud.* 39, 113–124.
- Wang, D., Chen, J., Su, Y., 2006. Study on photocatalytic degradation of organophosphorus pesticides with nanometer TiO_2 . *Foshan Ceram.* 6, 1–3.
- WHO, 2012. Specifications and evaluations for public health: Dimethoate.

Supporting information**Compound Specific Isotope Analysis of Organophosphorus Pesticides**

Langping Wu^a, Jun Yao^{a**}, Polonca Trebse^{b*}, Ning Zhang^c, Hans H. Richnow^c

^aSchool of Civil and Environmental Engineering, and National International Cooperation Based on Environment and Energy, University of Science and Technology Beijing, Xueyuan Road No.30, Haidian District, Beijing 100083, P.R. China

^bLaboratory for Environmental Research, University of Nova Gorica, Vipavska 13, SI-5000 Nova Gorica, Slovenia

^cDepartment of Isotope Biogeochemistry, Helmholtz Centre for Environmental Research-UFZ, Permoserstraße 9 15, 04318 Leipzig, Germany

* Corresponding author: Laboratory for Environmental Research, University of Nova Gorica, Vipavska 13, SI-5000 Nova Gorica, Slovenia

Tel.: +386-5-331-5238; Fax: +386-5-331-5296.

E-mail address: polonca.trebse@ung.si (P. Trebse).

** Co-corresponding author: University of Science and Technology Beijing, Xueyuan Road No.30, Haidian District, Beijing 100083, P.R. China

Tel: +86-10-62333305; Fax: +86-10- 62333305

E-mail address: yaojun@ustb.edu.cn, yaojun@cug.edu.cn

Chromatographic analysis of OP pesticides

In this study, the concentrations of three OP pesticides were measured by an Agilent 6890 series gas chromatograph (GC, Agilent Technologies, Germany) equipped with a flame ionization detector (FID). OP pesticides were separated in a HP-608 column (30 m × 0.53 mm × 0.5 μm, USA) with helium as the carrier gas (flow of 6.0 mL min⁻¹). The column was initially held at 60 °C for 1 min, ramped at 30 °C min⁻¹ to 300 °C, and held for 2 min. Injector and detector temperatures were 180 °C and 250 °C, respectively. The samples were injected in splitless mode with injection volumes of 1 μL. The chromatograms of selected compounds are showed in Fig. S1(a), with retention time of 3.900 min, 5.828 min and 6.290 min for dichlorvos, omethoate and dimethoate respectively.

The carbon isotope composition of dichlorvos, omethoate and dimethoate was analysed with a GC-C-IRMS system. For gas chromatographic separation of pesticides, a DB-608 column (30 m × 0.32 mm × 0.5 μm, Agilent, USA) was used, with helium as the carrier gas at a flow rate of 1.3 mL min⁻¹. The column was initially held at 60 °C for 2 min, ramped at 12 °C min⁻¹ to 225 °C, then up to 280 °C at 7 °C min⁻¹ and finally held for 2 min. The injector temperature was 180 °C. Samples were injected in the split injection mode (the split ratio was adjusted so as to obtain suitable peak areas). The mixtures of OP pesticides were successfully separated by GC-C-IRMS system (Fig. S1(b)), which indicates that the temperature programs and columns described above were suitable to separate dichlorvos, omethoate and dimethoate.

Linearity test

For the linearity test, stock solutions of OP pesticides mixture, dissolved in dichloromethane to different final concentrations (40 to 1000 mg L⁻¹), were used. First we used a new liner in the split/splitless injector and analyzed the linearity of the method as well as the reproducibility of the measurements. As shown in Fig. S2, dichlorvos has a good linearity range with area signal of 5 to 50 Vs (100 to 1000 mg L⁻¹). A narrow linearity range of 12 to 22 Vs (200 to 400 mg L⁻¹) for dimethoate was obtained. The δ¹³C values of omethoate were not stable and a limited linearity range was observed. We believe that the chromatographic conditions of OP pesticides were not optimal. Possibly the new liner was not completely inert and selected compounds were degraded in the liner of GC system, which caused significant changes in δ¹³C values and affect the linearity range, especially for omethoate. We therefore injected BSTFA several times into the GC inlet to deactivate the liner (see the main manuscript)

Calibration curve

In order to calculate the remaining concentrations of tested pesticides during degradation experiments, calibration curve was carried out by diluting standard solution of mixed pesticides (1:1:1) with dichloromethane to final concentrations of 10, 50, 100, 200, 300, 400, 500, 600, 700, 800 and 1000 mg L⁻¹. Calibration curves of three pesticides shows relatively good linearity, with correlation coefficient of 0.998, 0.994 and 0.997 for dichlorvos, omethoate and dimethoate (Fig. S3).

Experiments for hydrolysis and photolysis of OP pesticides

Hydrolysis could occur at several reactive centers in a given OP pesticide molecule. It can occur by a homogeneous mechanism, where H_2O and OH^- act as nucleophiles (Bavcon et al., 2003). OP pesticides can be hydrolyzed rapidly in alkaline solution, but are more stable in acidic solution. Thus, the hydrolysis experiments of selected pesticides were carried out at $22\text{ }^\circ\text{C}$ in 200 mL buffer solution (pH 10) which was prepared with 0.1 M NaOH (purity $\geq 99\%$) and 0.1 M KCl-boric acid (purity $> 99.5\%$). Control experiments were performed in 50 mL buffer solution (pH 3) which contained 0.1 M HCl (32%, Baker analytical grade) and 0.1 M $\text{C}_8\text{H}_5\text{KO}_4$ (potassium hydrogen phthalate, 99% purity, Alfa Aesar, Germany). All hydrolysis experiments were conducted in grinding mouth Erlenmeyer flasks with initial concentration of 100 mg L^{-1} of respective pesticides.

Photolysis experiment was conducted in a tailor-made chamber photoreactor using six low-pressure mercury fluorescent lamps as a UVA radiation source (CLEO 20W, 438mm \times 26 mm, Philips; broad maximum at 355 nm), described in details elsewhere (Černigoj et al., 2007). Before starting the degradation experiment, the photoreactor was preheated for 15 minutes by turning on lamps to maintain a stable temperature. A 200 mL aqueous solution of dimethoate (100 mg L^{-1}) was taken in the reaction tube, and 50 mL of dimethoate solution was performed as a dark control experiment. The results of control experiment are shown in Table S1.

Omethoate and dimethoate were hydrolyzed by 9% and 4% respectively over the whole period of control experiment (Table S1). In the dichlorvos experiment no degradation was evident, and the slightly higher concentration could be caused by the uncertainty of the analysis method. Correspondingly, the $\delta^{13}\text{C}$ changed $+0.3\text{‰}$, 0‰ and $+0.2\text{‰}$ in the control experiments for hydrolysis of dichlorvos, omethoate and dimethoate are all within the reproducibility by CSIA for carbon isotope ($2\sigma \leq \pm 0.5\text{‰}$). The control experiment for the photolysis of dimethoate showed no concentration or carbon isotope composition changes. The results indicate no detectable carbon isotope fractionation during all control experiments.

Mechanism for the hydrolysis of dichlorvos and dimethoate

The hydrolysis of dichlorvos is a general base-catalyzed reaction and has two parallel routes (Oncescu and Oancea, 2007). The phosphorus atom is electron deficient, and nucleophilic attack is the first step in the hydrolytic reaction. As shown in Fig. S4, both routes show that no carbon atoms are involved in the reactive positions. The calculation of the bond strength in dichlorvos molecule by Oncescu et al (Oncescu and Oancea, 2007) show that the lowest value (0.61) belongs to phosphate-dichlorvinyl bond, which indicates that this bond will cleave first by hydrolysis. Thus, we suggest that there is no significant carbon isotope fractionation during the hydrolysis of dichlorvos as no carbon bond cleavage could lead to a primary isotope effect. The obtained relatively lower enrichment factors of $-0.2 \pm 0.1\text{‰}$ could be a result of a secondary isotope effect.

For dimethoate degradation, hydroxide ions promote the rate of hydrolysis by catalysis. The hydrolytic cleavage of thioester bond leading to the formation of N-(methyl) mercaptoacetamide and O,O-dimethyl phosphorothioate (Yao et al., 2011). It is probable that the reaction proceeds via a metastable pentacoordinate phosphate intermediate formed by nucleophilic attack of OH^- (Farooq et al., 2004). The nucleophilic displacement reaction at the

phosphoryl center occurs with high stereospecificity and takes place with inversion of configuration at phosphorus. The mechanism for the hydrolysis of dimethoate under basic conditions is shown (Fig. S5).

The AKIE of dimethoate was calculated assuming a C-S bond cleavage. Streitwieser semiclassical limits for C-S and C-O bond cleavage are 1.04994 and 1.06142 respectively (Huskey, 1991) and but in reality AKIE values are smaller. C-S bond cleavage may be assumed to be relevant under acidic conditions and may lead to a primary carbon isotope effect. Under alkaline condition the main pathway is the hydrolysis of the P-O bond not associated with a primary carbon isotope effect, whereas the hydrolysis of the methoxy group leading to formation of methanol and O-demethyl-dimethoate by cleavage of a C-O bond may be a relevant side reaction (Farooq et al., 2004). The AKIE for S_{N2} reactions assuming a nucleophilic attack is estimated to have a maximal carbon isotope effect (KIE) in the order of a C-O bond cleavage. The calculated AKIE assuming C-O bond cleavage under alkaline conditions is much lower which may suggest that the AKIE is a result of a side reaction cleaving a C-O bond whereas the P-O bond cleavage is a parallel pathway. Further investigations are needed to substantiate this interpretation.

References:

- Bavcon, M., Trebše, P., Zupančič Kralj, L., 2003. Investigations of the determination and transformations of diazinon and malathion under environmental conditions using gas chromatography coupled with a flame ionisation detector. *Chemosphere* 50, 595-601.
- Černigoj, U., Štangar, U.L., Trebše, P., 2007. Evaluation of a novel carberry type photoreactor for the degradation of organic pollutants in water. *J. Photoch. Photobio. A* 188, 169-176.
- Farooq, R., Lin, F., Wang, Y., Huang, J., Xu, Z., Shaukat, S.F., 2004. Pressure hydrolysis for degradation of omethoate pesticide in water. *Journal of Shanghai University (English Edition)* 8, 221-226.
- Huskey, W.P., 1991. In *Enzyme mechanism from isotope effects*. In: Cook, P.F. (Ed.). CRC Press, Boca Raton, FL, pp. 37-72.
- Oncescu, T., Oancea, P., 2007. On the mechanism of dichlorvos hydrolysis. *Rev. Chim.* 58, 232-235.
- Yao, J.J., Hoffmann, M.R., Gao, N.Y., Zhang, Z., Li, L., 2011. Sonolytic degradation of dimethoate: Kinetics, mechanisms and toxic intermediates controlling. *Water Res* 45, 5886-5894.

Table S1: Changes in concentrations (C_t/C_0) and carbon isotope ratios ($\delta^{13}\text{C}$) of OP pesticides during control experiments. $\Delta\delta^{13}\text{C}$ refers to the change of isotope composition during the experiment.

Compounds	Sampling	C_t / C_0	$\delta^{13}\text{C}$ (‰)	$\Delta\delta^{13}\text{C}$ (‰)
dichlorvos (pH 3)	0	1	-12.9 ± 0.2	+0.3
	58	1.03	-12.6 ± 0.3	
omethoate (pH 3)	0	1	-20.4 ± 0.3	0
	8	0.91	-20.4 ± 0.1	
dimethoate (pH 3)	0	1	-42.7 ± 0.1	+0.2
	96	0.96	-42.5 ± 0.1	
dimethoate (dark controle)	0	1	-41.8 ± 0.1	0
	56	1.00	-41.8 ± 0.7	

Table S2: Carbon isotopic enrichment factors (ϵ) and apparent kinetic isotope effects (AKIEs) of dichlorvos and dimethoate (see Eqn. (2) in manuscript for the definition of n , x , z).

Compound	ϵ (‰)	n	x	z	AKIEs
Dichlorvos (OH ⁻)	-0.2 ± 0.1	-	-	-	-.-
Dimethoate (OH ⁻)	-1.0 ± 0.1	5	1	1	1.0050 ± 0.0005
Dimethoate (photolysis)	-3.7 ± 1.1	5	2	1	1.0094 ± 0.0027

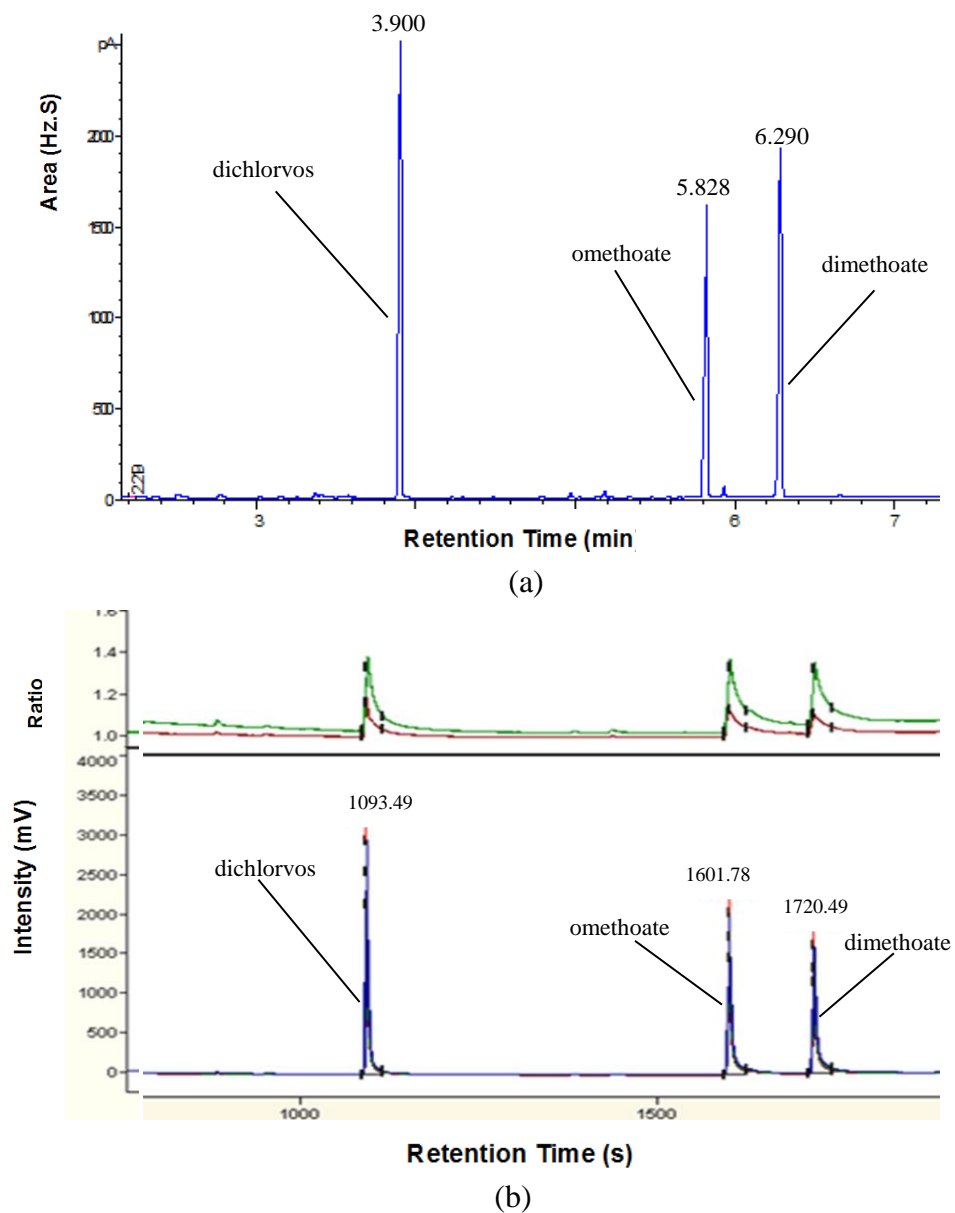


Fig. S1: The separation of standards mixture of dichlorvos, omethoate and dimethoate by GC-FID (a) and GC-C-IRMS (b) methods.

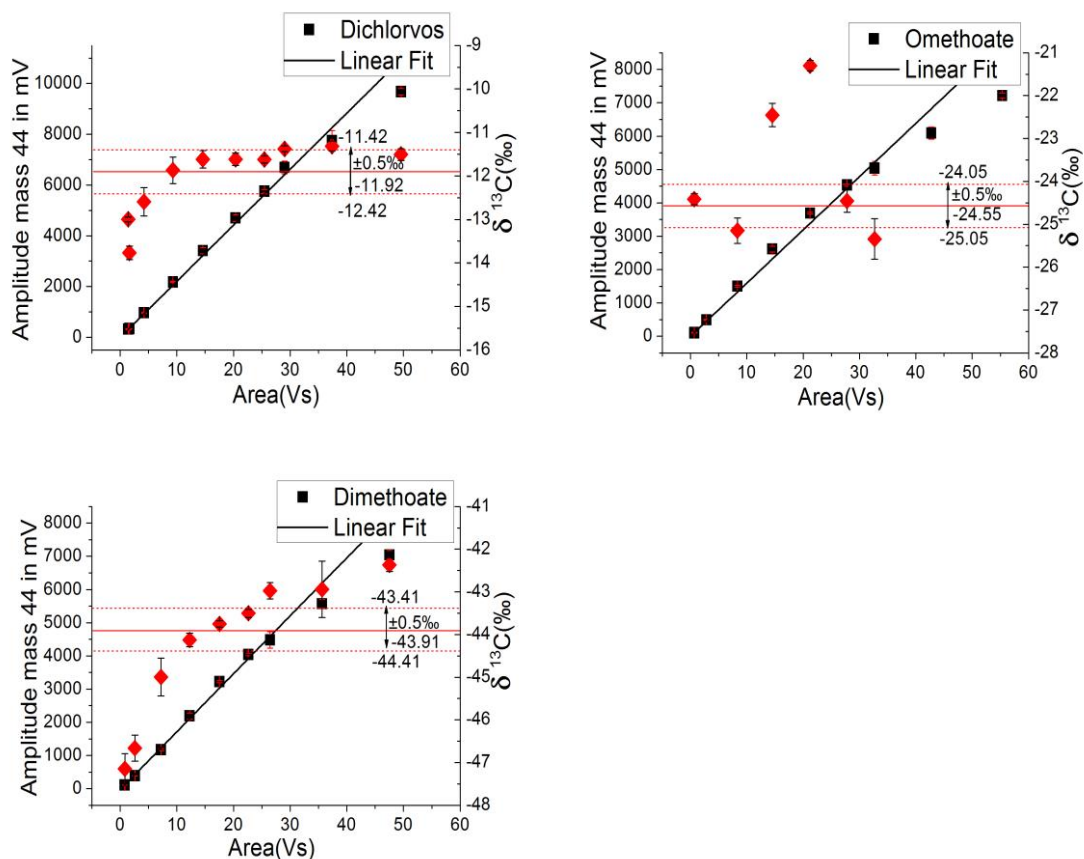


Fig. S2: Linearity test for dichlorvos, omethoate and dimethoate without deactivation of GC injection port. Signal area correspond to concentrations of 40, 50, 100, 200, 300, 400, 500, 600, 800, 1000 mg/L. Red diamonds (\blacklozenge) indicate $\delta^{13}\text{C}$ values and black squares (\blacksquare) indicate amplitude values. Solid lines represent the means of all measurements; dotted lines represent one standard deviation (2σ) of all measurements. Error bars represent one 2σ of triplicate.

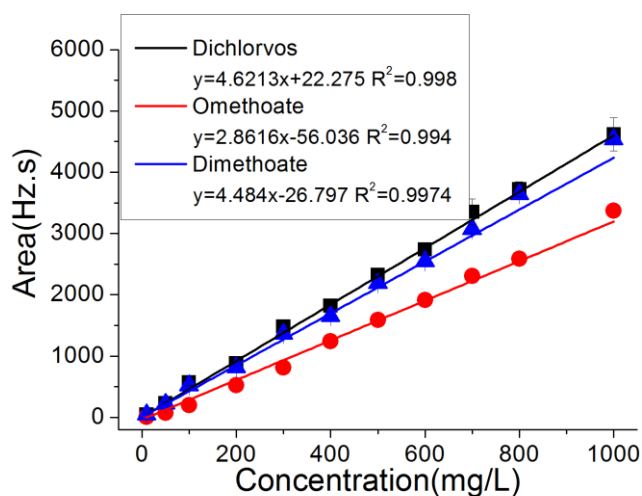


Fig. S3: Calibration curve of dichlorvos, omethoate and dimethoate by GC-FID. Signal areas of three tested pesticides were measured in DCM as solvent.

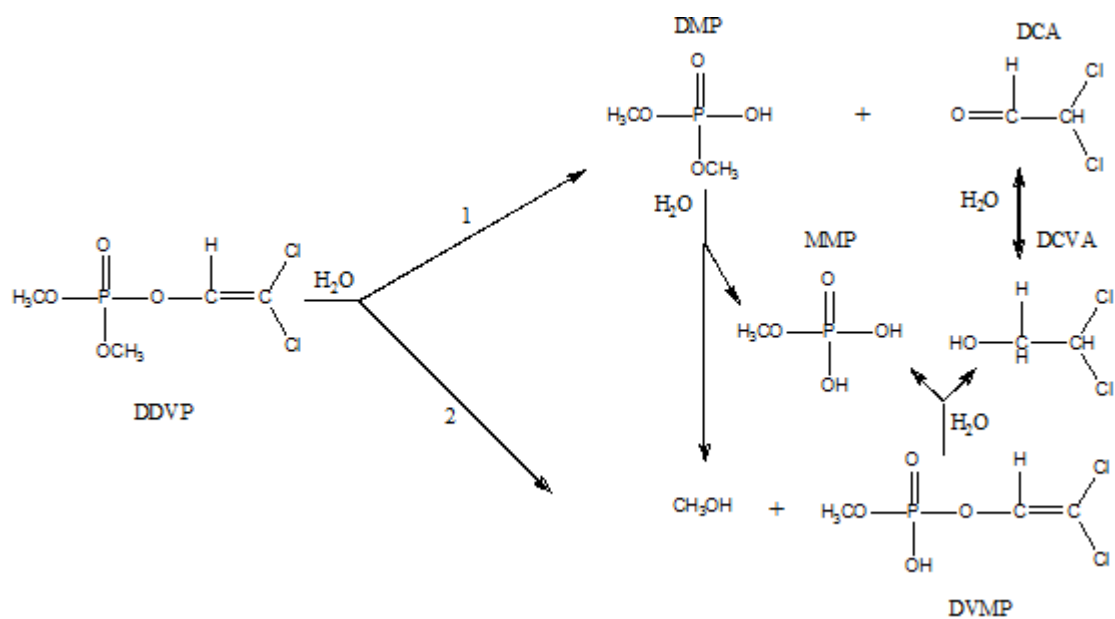


Fig. S4: Hydrolysis pathways of dichlorvos according to reference (Oncescu and Oancea, 2007).

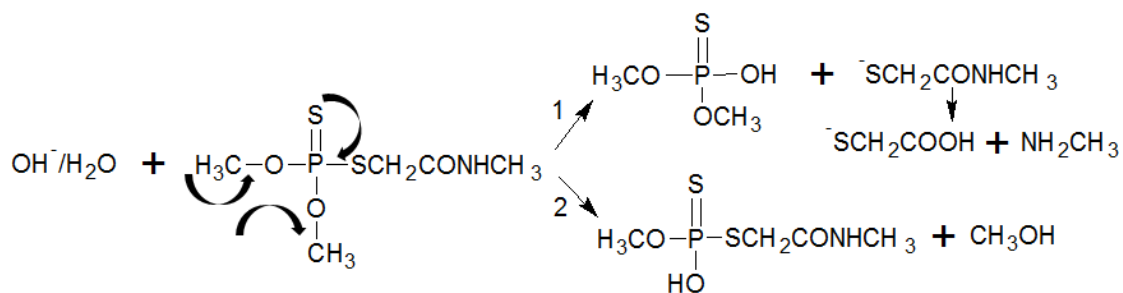


Fig. S5: Mechanism for the hydrolysis of dimethoate at basic conditions according to references (Farooq et al., 2004; Yao et al., 2011).

Appendix 6.2.

Validation of GC-IRMS techniques for $\delta^{13}\text{C}$ and $\delta^2\text{H}$ CSIA of organophosphorus compounds and their potential for studying the mode of hydrolysis in the environment

Published paper: *Wu, L.; Kümmel, S.; Richnow, H. H., Anal. Bioanal. Chem. 2017, 409, (10), 2581-2590.*

Validation of GC–IRMS techniques for $\delta^{13}\text{C}$ and $\delta^2\text{H}$ CSIA of organophosphorus compounds and their potential for studying the mode of hydrolysis in the environment

Langping Wu¹ · Steffen Kümmel¹ · Hans H. Richnow¹

Received: 25 November 2016 / Revised: 3 January 2017 / Accepted: 10 January 2017 / Published online: 6 February 2017
© Springer-Verlag Berlin Heidelberg 2017

Abstract Compound-specific stable isotope analysis (CSIA) is among the most promising tools for studying the fate of organic pollutants in the environment. However, the feasibility of multidimensional CSIA was limited by the availability of a robust method for precise isotope analysis of heteroatom-bearing organic compounds. We developed a method for $\delta^{13}\text{C}$ and $\delta^2\text{H}$ analysis of eight organophosphorus compounds (OPs) with different chemical properties. In particular, we aimed to compare high-temperature conversion (HTC) and chromium-based HTC (Cr/HTC) units to explore the limitations of hydrogen isotope analysis of heteroatom-bearing compounds. Analysis of the amount dependency of the isotope values (linearity analysis) of OPs indicated that the formation of HCl was a significant isotope fractionation process leading to inaccurate $\delta^2\text{H}$ analysis in HTC. In the case of nonchlorinated OPs, by-product formation of HCN, H_2S , or PH_3 in HTC was observed but did not affect the dynamic range of reproducible isotope values above the limit of detection. No hydrogen-containing by-products were found in the Cr/HTC process by use of ion trap mass spectrometry analysis. The accuracy of gas chromatography – isotope ratio mass spectrometry was validated in comparison with elemental analyzer – isotope ratio mass spectrometry. Dual-

isotope fractionation yielded Δ values of 0 ± 0 at pH 7, 7 ± 1 at pH 9, and 30 ± 6 at pH 12, indicating the potential of 2D CSIA to characterize the hydrolysis mechanisms of OPs. This is the first report on the combination of $\delta^2\text{H}$ and $\delta^{13}\text{C}$ isotope analysis of OPs, and this is the first study providing a systematic evaluation of HTC and Cr/HTC for hydrogen isotope analysis using OPs as target compounds.

Keywords Organophosphorus compounds · Compound-specific stable isotope analysis · Hydrogen isotope · Pesticides · Chromium-based high-temperature conversion

Introduction

Synthetic organophosphorus compounds (OPs) have a wide spectrum of applications as plasticizers, flame retardants, and chemical warfare agents, and they are used worldwide as pesticides. The general chemical structure of organophosphorus pesticides described by Sogorb et al. [1] comprises alkyl or aryl groups bound to a phosphorus atom via an oxygen or sulfur atom, forming phosphates, phosphorothioates, or phosphorodithioates. The pesticide properties of OPs were first recognized in 1854 [2], and so far, more than 100,000 OPs have been screened for their insecticidal properties, and more than 100 are available for commercial use [3], which contributed to approximately 30% of the total pesticide use worldwide in 2008 [4]. In general, OPs, especially organophosphorus pesticides, are not considered to be very persistent in the environment as they are relatively quickly degraded in comparison with organochlorine compounds. However, continuous and excessive use of OPs has led to environmental contaminations, with rising public concerns as the residues have repeatedly been detected in soils, sediments,

Electronic supplementary material The online version of this article (doi:10.1007/s00216-017-0203-3) contains supplementary material, which is available to authorized users.

✉ Hans H. Richnow
hans.richnow@ufz.de

¹ Department of Isotope Biogeochemistry, Helmholtz Centre for Environmental Research, UFZ, Permoserstrasse 15, 04318 Leipzig, Germany

waterbodies, and food and drinking water, and have been found in rain, air samples [5], fishes [6], and human urine [7]. To have a more thorough understanding of the fate of OPs, tools are needed to investigate their sources, reactive transport pathways, and sinks in the environment.

At present, compound-specific stable isotope analysis (CSIA) using gas chromatography (GC) – isotope ratio mass spectrometry (IRMS) is one of the most promising tools for studying the fate of organic pollutants in the environment and to assess in situ contaminant degradation [8–11]. CSIA has primarily been applied to study the fate of volatile organic groundwater pollutants such as benzene, toluene, ethylbenzene, and xylene (BTEX) [12–14], chlorinated ethenes and benzenes [15–19], and fuel oxygenates [20–22].

The carbon isotope fractionation associated with the hydrolysis of dichlorvos, omethoate, and dimethoate is to the best of our knowledge the only application of CSIA for studying the fate of OPs [23]. The changes of the isotopic signatures of two elements are compared, leading to a mechanistic interpretation of CSIA results [24–27], and consequently may allow a more accurate interpretation of the underlying degradation pathways in the environment. Until recently, the feasibility of multidimensional CSIA was limited by the low availability of a robust method for precise hydrogen isotope analysis of heteroatom-bearing organic compounds, which is a major drawback.

The high-temperature conversion (HTC) technique is a widely used method for hydrogen isotope analysis of water and many organic materials. However, it becomes more challenging for nitrogen-, chlorine-, and sulfur-containing organics because of the formation of hydrogen-containing by-products such as HCN, HCl, and H₂S. This incomplete conversion of organically bound hydrogen to molecular H₂ can lead to inaccurate $\delta^2\text{H}$ values. Many efforts have been made to overcome these limitations [28, 29]. Gehre et al. [30] developed a concept that uses a pyrolysis unit filled with chromium in an elemental analyzer (EA) coupled to an IRMS system. Caused by quantitative scavenging of the heteroatoms by the chromium, complete conversion of the organically bound hydrogen to molecular hydrogen was observed. Moreover, Renpenning et al. [31] demonstrated successfully the feasibility of the chromium-based HTC (Cr/HTC) concept for CSIA by transferring the Cr/HTC principle to a GC–IRMS system. These findings imply that conventional HTC units for CSIA need critical evaluation as hydrogen-containing by-products may be formed, preventing the robust determination of hydrogen isotopes.

In this study, we aimed to compare HTC and Cr/HTC units to explore the limitations of hydrogen isotope analysis of heteroatom-bearing compounds, particularly nitrogen-, sulfur, oxygen, and chlorine-containing compounds. OPs are complex heteroatom-bearing compounds that may contain nitrogen, sulfur, oxygen, and chlorine in a single molecule. Some

OPs are thermally labile and can disintegrate in the injector system, complicating analysis. Our first aim was to develop analytical methods for $\delta^{13}\text{C}$ and $\delta^2\text{H}$ analysis of eight OPs as model compounds for phosphates, phosphorothioates, or phosphorodithioates for multi-isotope CSIA and to explore the detection limits. The second aim was comparison of HTC and Cr/HTC for complex heteroatom compounds to validate the reliability of these methods with use of OPs as model substrates. Finally, the methods developed were used for the determination of carbon and hydrogen enrichment factors of dimethoate hydrolysis at different pH values to explore the potential of 2D CSIA for characterizing hydrolysis pathways. To the best of our knowledge, this is the first report on the combination of $\delta^2\text{H}$ and $\delta^{13}\text{C}$ isotope analysis of OPs, and this is the first study providing a systematic evaluation of the analytical characteristics of HTC and Cr/HTC for hydrogen isotope analysis using OPs as target compounds.

Materials and methods

Target OPs

The target OPs used for this study were dichlorvos (2,2-dichlorovinyl dimethyl phosphate; purity greater than 98.8%), omethoate (2-[(dimethoxyphosphoryl)sulfanyl]-*N*-methylacetamide; purity greater than 97.0%), dimethoate (*O,O*-dimethyl *S*-[2-(methylamino)-2-oxoethyl] dithiophosphate; purity greater than 99.6%), parathion methyl (*O,O*-dimethyl-*O*-(4-nitrophenyl) phosphorothioate; purity greater than 99.8%), parathion (*O,O*-diethyl-*O*-(4-nitrophenyl) phosphorothioate; purity greater than 99.7%), chlorpyrifos (*O,O*-diethyl *O*-3,5,6-trichloropyridin-2-yl phosphorothioate; purity greater than 99.8%), tris(1,3-dichloropropan-2-yl) phosphate (TDCPP; purity greater than 95.7%), and tris(2-chloroethyl) phosphate (TCEP; purity greater than 97.0%), which were purchased from Sigma-Aldrich. The molecular structures of the target OPs are shown in Table S1. OP stock solutions were prepared in dichloromethane (high-performance liquid chromatography grade, purity greater than 99.9%).

Concentration determination by GC–FID

An 6890 series gas chromatograph (Agilent Technologies, USA) equipped with a flame ionization detector (GC–FID) was used to determine the concentration of OPs throughout the study. OPs were separated on an HP-5 column (30 m × 0.32 mm × 0.25 μm, Agilent, USA) with a helium flow rate of 1.5 mL min⁻¹. The temperature program used was as follows: hold for 2 min at 60 °C, then increase the temperature at 10 °C min⁻¹ to 160 °C, at 5 °C min⁻¹ to 220 °C, and at 15 °C min⁻¹ to 280 °C, with a 2-min hold. Injector and detector

temperatures were set to 180 °C and 250 °C respectively. The samples were injected in split mode (1:10) with injection volumes of 1 μL .

Isotope measurement by EA–IRMS

To validate the results of the GC–IRMS method, $\delta^{13}\text{C}$ values of target OPs were determined by a EuroEA3000 EA (EuroVector, Italy) coupled to an IRMS system as described elsewhere [32]. The reference $\delta^2\text{H}$ values were measured by the newly developed chromium-filled EA (EA–Cr/HTC) method [30]. To reduce the evaporation of the samples on the metal surface, approximately 5 mg of Com-Aid for liquids (aluminum oxide powder, Leco, St Joseph, MI, USA) was added together with the liquid sample in a tin cup before analysis. All results were calibrated against international standards by a two-point calibration method [33, 34]. The following international isotope standards from the International Atomic Energy Agency (IAEA) were used: IAEA-CH-6 (sucrose, $\delta^{13}\text{C} = -10.4\text{‰}$) and IAEA-CH-7 (polyethylene, $\delta^{13}\text{C} = -32.2\text{‰}$) for $\delta^{13}\text{C}$ calibration, and VSMOW2 (water, $\delta^2\text{H} = 0\text{‰}$) and SLAP2 (water, $\delta^2\text{H} = -428\text{‰}$) for $\delta^2\text{H}$ calibration.

Carbon isotope analysis by GC– combustion–IRMS

The $\delta^{13}\text{C}$ values of target OPs were measured with a GC–combustion–IRMS (GC-C-IRMS) system [35]. A 7890A gas chromatograph (Agilent Technologies, Palo Alto, CA, USA) was coupled via a ConFlo IV interface (Thermo Fisher Scientific, Germany) to a MAT 253 IRMS system (Thermo Fisher Scientific, Germany) via an open split. A DB-608 column (30 m \times 0.32 mm \times 0.5 μm , Agilent J&W, USA) was used for separation of OPs with an oven temperature program of a 2-min hold at 60 °C, then an increase of the temperature at 20 °C min^{-1} to 210 °C, at 1 °C min^{-1} to 220 °C, and at 20 °C min^{-1} to a final temperature 280 °C, followed by a 5-min hold. For each analysis, an aliquot of 2 μL per sample was injected into the system in split injection mode (1:5). To avoid thermal decomposition of OPs in the injector, the temperature of the split/splitless injector was adjusted according to the temperature range of the boiling points of the target OPs, which was 180 °C for dimethoate, omethoate, parathion, and parathion methyl, 195 °C for dichlorvos and TCEP, 220 °C for chlorpyrifos, and 260 °C for TDCPP. Samples were run in triplicate.

Hydrogen isotope analysis by GC–HTC–IRMS and GC–Cr/HTC–IRMS

High-temperature pyrolysis was used to convert organically bound hydrogen into molecular hydrogen at 1400 °C for $\delta^2\text{H}$ measurement. Samples were analyzed via the same setup and

separated on a DB-608 column with use of the same temperature program as described for $\delta^{13}\text{C}$ analysis. Aliquots (1–3 μL) of samples were injected into a split/splitless injector, which was set at 180–260 °C. Samples were run in triplicate. For GC–HTC–IRMS, samples were converted in nonporous tubular ceramic reactors (0.8-mm inner diameter, 320 mm long, Degussit AL23 aluminum oxide ceramic, Friatec, Germany) with a carrier gas flow rate of 1.2 mL min^{-1} to achieve reaction time required for complete conversion. For GC–Cr/HTC–IRMS, the same ceramic reactor was filled with chromium powder (particle size of 250–300 μm , purity greater than 99%, Cr Patinal®, Merck, Germany) along the length of the high-temperature oven. The design of the Cr/HTC reactor was as described elsewhere [31] with some minor modifications: the tubular ceramic reactor was filled for a length of approximately 215 mm with chromium powder, resulting in an empty space of roughly 65 mm at the beginning of the reactor (gas flow direction). This modification was used to reduce tar formation on surfaces at lower temperature at the inflow leading to incomplete conversion of organic compounds. Additionally, only the end of the chromium powder bed was abutted by a 5-mm plug of quartz wool (HEKAtech, Germany) to fix the chromium in the ceramic tube. The carrier gas flow rate was adjusted to 1.1 mL min^{-1} at the outlet of the Cr/HTC reactor. All results were calibrated by a two-point calibration method against two reference compounds—hexadecane A ($\delta^2\text{H} = -167\text{‰}$) and hexadecane B ($\delta^2\text{H} = -11\text{‰}$)—as described elsewhere [31].

Characterization of by-product formation during HTC and Cr/HTC via ITMS

The formation of pyrolytic by-products was analyzed by a PolarisQ ion trap mass spectrometer (Thermo Finnigan, Germany). The instrumental setup was described elsewhere [36]. Omethoate, dimethoate, parathion methyl, and parathion were used as model compounds for characterization of by-product formation by an either empty (HTC) or a chromium-filled (Cr/HTC) reactor at 1400 °C. The gas chromatograph was equipped with a BPX-5 column (30 m \times 0.25 mm \times 0.25 μm , SGE, Australia). Samples were injected in splitless mode by an autosampler (A200S, CTC Analytics, Switzerland) and with a gas flow rate of 1.1 mL min^{-1} . All conversion products were transferred online to the ITMS system, where the molecular and fragment ions of gases in a range of 10–200 m/z were quantitatively analyzed.

Effect of sample pretreatment on the isotope composition

To quantify the effect of evaporation on the isotope composition, 100 mL of solutions of standard target OPs dissolved in dichloromethane were evaporated to 0.5 mL or dryness by an evaporator (TurboVap® II, Biotage, Sweden). The

evaporation was performed at a pressure of 8–12 psi (55–83 kPa) and 25 °C. $\delta^{13}\text{C}$ and $\delta^2\text{H}$ values of OPs were determined before and after evaporation (see the [electronic supplementary material](#)).

Hydrolysis of dimethoate

Dimethoate hydrolysis experiments were performed in phosphate buffer solution of pH 7, pH 9 and pH 12 respectively, and hydrolysis in acidic buffer solution of pH 3 was conducted as a control experiment [23]. To adjust the reaction time, the incubation temperature was set at 60 °C for pH 7, at 30 °C for pH 9, and at 4 °C for pH 12. All experiments were conducted as batch experiments in 50 mL buffer solution with an initial dimethoate concentration of 100 mg L⁻¹. At different times, the hydrolysis was stopped by adjustment of the pH of the aqueous sample to 3 with 6 N HCl. The remaining dimethoate was extracted with 2 mL dichloromethane under continuous shaking at 120 rpm for 2 h. Dichlorvos (1000 mg L⁻¹) serving as an internal standard was added to the dichloromethane used for extraction. Afterward, the organic phase was transferred into 2-mL vials and stored at -20 °C until analysis. Calculation and quantification of isotope fractionation have been described elsewhere [37] and are briefly reported in the [electronic supplementary material](#).

Results and discussion

Decomposition of OPs in the GC injector

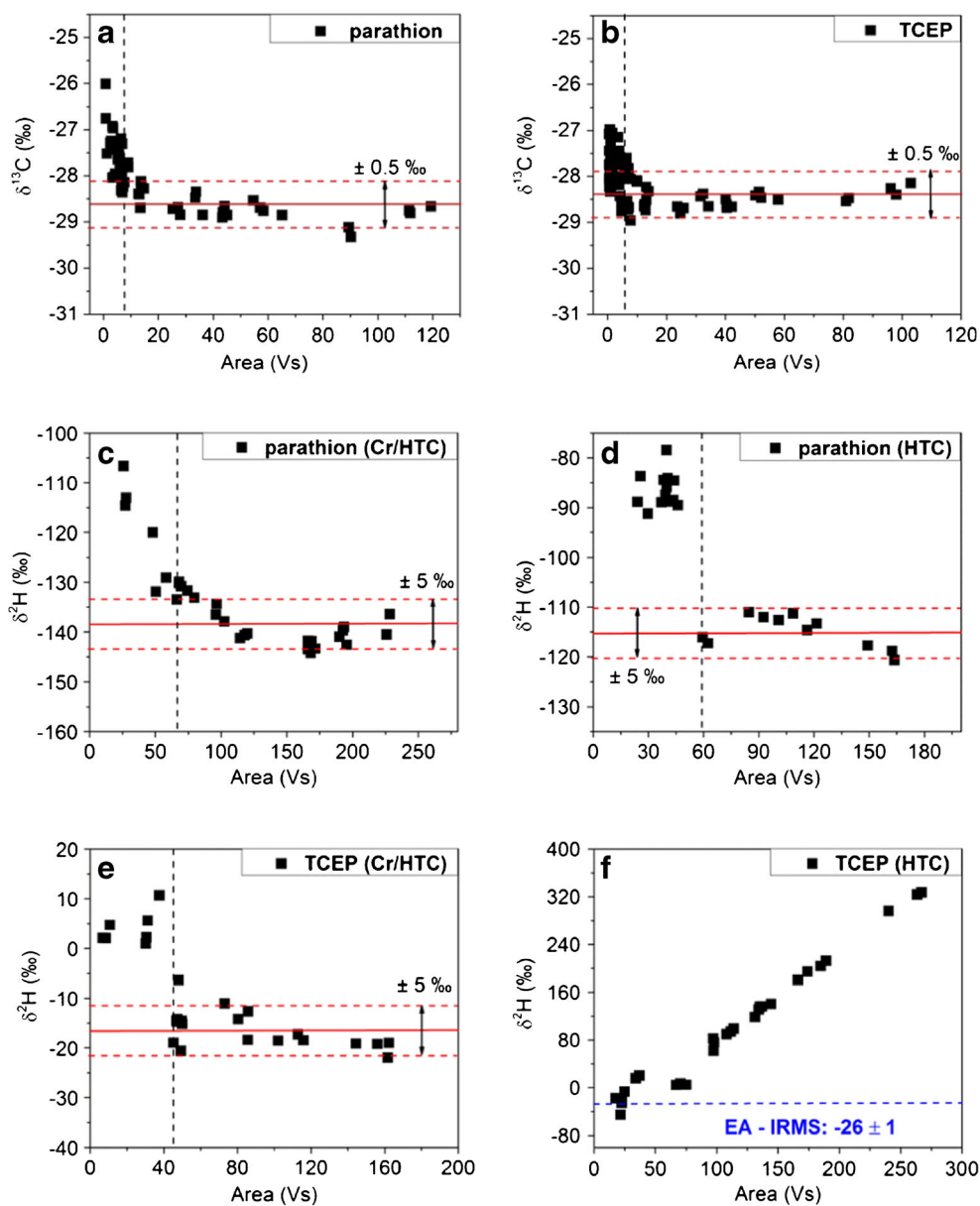
Isotope fractionation on thermal decomposition in the injector is one of the challenges for stable isotope analysis of OPs since many OPs, including parathion, dimethoate, and omethoate, are thermally unstable and decompose at relatively low temperatures. For example, parathion decomposes above 200 °C [38] and omethoate can start to decompose at about 135 °C [39]. To avoid thermal decomposition of OPs in the injector, the GC injector temperature was optimized for each compound tested, and was 180 °C for omethoate, dimethoate, parathion methyl, and parathion, 195 °C for dichlorvos and TCEP, 220 °C for chlorpyrifos, and 260 °C for TDCPP. However, omethoate isotope measurement at 180 °C is still critical since omethoate can react with the glass liner in the GC injector when the liner is not completely deactivated. This decomposition reaction is expected to increase with higher injector temperatures and higher sample concentrations, which can become critical for $\delta^2\text{H}$ measurements. From the GC-IRMS chromatograms (Fig. S1), omethoate decomposition by-product peaks were observed when the omethoate injection amount was higher than approximately 2000 ng. Additionally, higher omethoate concentrations lead to increasing by-product peaks, which then affected the isotope ratio

more significantly. When the omethoate injection amount was 1000, 2000, and 3000 ng respectively, the corresponding $\delta^2\text{H}$ values were -116‰, -134‰, and -152‰. To get more reliable isotope measurements especially regarding $\delta^2\text{H}$ measurements for OPs, the following suggestions can be applied: (1) lower the injector temperature; (2) as long as $\delta^2\text{H}$ values can be measured precisely, avoid a high absolute amount of target analytes transferred to the column; (3) use a glass liner without glass wool; (4) deactivate the liner with *N,O*-bis(trimethylsilyl)trifluoroacetamide [23]. The deactivation procedure is briefly reported in the [supplementary material](#). As shown in Fig. S1d, the deactivation of the liner by *N,O*-bis(trimethylsilyl)trifluoroacetamide leads to the disappearance of the decomposition products, and the $\delta^2\text{H}$ values were -117‰ after deactivation.

Dependency of isotope values on amount of OPs (linearity ranges)

The lower limits of precise CSIA and the dynamic range of concentrations needed for reproducible $\delta^{13}\text{C}$ and $\delta^2\text{H}$ values were investigated for the eight target OPs with use of a stock solution dissolved in dichloromethane. The dynamic range of concentrations in which the isotope value is stable is often defined as the linearity range, and was obtained for parathion as a model compound for nonchlorinated OPs and TCEP as a model compound for chlorinated OPs; the remaining OPs are reported in the [electronic supplementary material](#). For nonchlorinated OPs, measurements of parathion documented a dependency of $\delta^{13}\text{C}$ values on the injected amount and defined a required parathion sample amount for an area signal of 7 V s or more of approximately 1.1 nmol parathion, or 11.0 nmol C (Fig. 1a). For chlorinated OPs, measurements of TCEP also documented a dependency of $\delta^{13}\text{C}$ on the injected amount, and defined a required TCEP sample size for an area signal of 4.5 V s or greater of approximately 0.7 nmol TCEP, or 4.2 nmol C (Fig. 1b). The $\delta^2\text{H}$ values obtained via GC-Cr/HTC-IRMS become linear for an area signal of 42–120 V s for the eight OPs tested. The significant variation in the lower limits of precise CSIA for different OPs could be caused by the compound-specific transformation efficiency of the Cr/HTC reactor. For example, the linearity range of parathion isotope analysis allows determination of $\delta^2\text{H}$ values down to 66 V s, leading to a required sample amount of approximately 3.4 nmol parathion, or 48 nmol H (Fig. 1c). The linearity range of TCEP isotope analysis extended down to 45 V s, which corresponds to a required sample amount of approximately 12.6 nmol TCEP, or 151 nmol H (Fig. 1e). In contrast, linearity ranges for $\delta^2\text{H}$ obtained via GC-HTC-IRMS were obtained only for nonchlorinated OPs. For example, the linearity range of parathion isotope analysis allows determination of $\delta^2\text{H}$ values down to 60 Vs, corresponding to a required sample amount of approximately

Fig. 1 Linearity analysis of $\delta^{13}\text{C}$ (a, b) and $\delta^2\text{H}$ (c–f) values of parathion and tris(2-chloroethyl) phosphate (TCEP) to correlate isotope composition with the signal intensity. The linearity of $\delta^2\text{H}$ measurements was assessed with gas chromatography (GC)–chromium-based high-temperature conversion (Cr/HTC)–isotope ratio mass spectrometry (IRMS) (c, e) and GC–high-temperature conversion (HTC)–IRMS (d, f). Dotted black lines indicate the lower limits of precise compound-specific stable isotope analysis; dotted red lines indicate the analytical uncertainty for carbon and hydrogen isotope analysis; solid lines represent the mean values of all measurements within the linearity ranges. EA elemental analyzer



6.6 nmol parathion, or 92 nmol H (Fig. 1d). However, in the case of TCEP, a clear dependency of $\delta^2\text{H}$ values on the injected amount was observed; with increasing area signals from 34 to 260 V s, $\delta^2\text{H}$ increased from -5‰ to 273‰ ; consequently, no concentration range for amount-independent isotope analysis (acceptable linearity) was obtained (Fig. 1f). A similar dependency of the isotope value on concentration was observed for all the chlorinated OPs analyzed (Fig. S4).

The linearity of $\delta^{13}\text{C}$ and $\delta^2\text{H}$ measurements is defined here as an acceptable isotope composition for the OPs tested within the uncertainty of the instrument independent of the concentration of the substrate. Only area signals within the linearity ranges obtained can be used for evaluation of isotope values. Nonlinearity of $\delta^2\text{H}$ for the chlorinated compounds analyzed may be due to the conversion process and by-product

formation via GC–HTC–IRMS, but within the linearity ranges obtained, $\delta^2\text{H}$ values for nonchlorinated organic compounds can be measured by GC–HTC–IRMS.

Characterization of the conversion process by analysis by-product formation

The molecular background scan of the HTC and Cr/HTC (1400 °C) effluent gas stream was monitored with an ion trap mass spectrometer. Except for H_2O (m/z 18), N_2 (m/z 28, 29), and O_2 (m/z 32), which are mainly caused by the background of the system, the major by-products after conventional HTC of parathion resulted in strong formation of HCN (m/z 27), H_2S or PH_3 (m/z 34), COS (m/z 60), and CS_2 (m/z 76) (Fig. 2a), suggesting that hydrogen species other than H_2 were

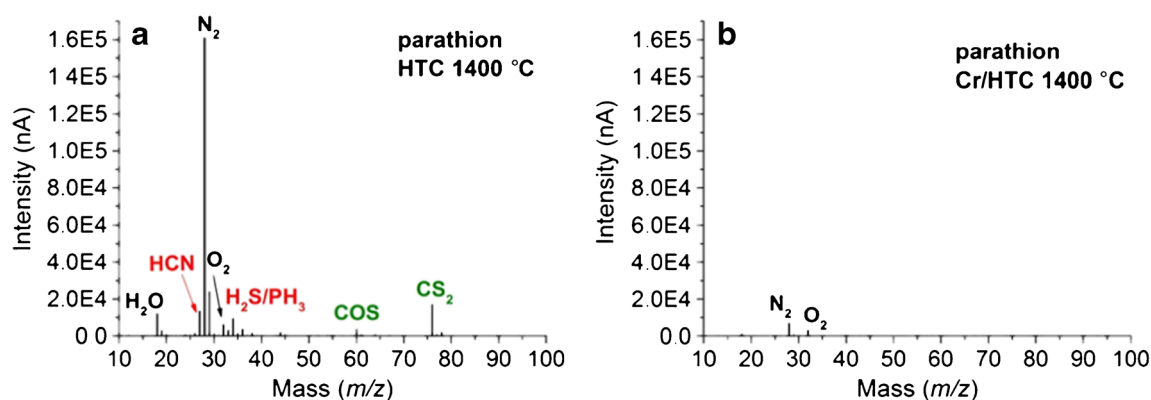


Fig. 2 By-product formation during conventional HTC (a) versus Cr/HTC (b) monitored with an ion trap mass spectrometer. HTC of parathion at 1400 °C resulted in the formation of HCN (m/z 27), H₂S or PH₃ (m/z 34), COS (m/z 60), and CS₂ (m/z 76) (a). No relevant formation of by-

products from parathion was observed via Cr/HTC at 1400 °C (b). H₂O (m/z 18), N₂ (m/z 28), and O₂ (m/z 32) are typical atmospheric background signals of the system

formed, potentially leading to isotope fractionation. In comparison, no by-product formation from parathion was observed via Cr/HTC (Fig. 2b). Formation of by-products occurred during conventional HTC of all the OPs tested. Additionally, the formation of HCl (m/z 35–38) as a by-product was observed for all the chlorinated organic compounds tested in previous studies but not when Cr/HTC was used [31]. In comparison with HTC as the current routine technique, conversion of heteroatom-bearing compounds to H₂ at hot chromium could benefit from a significant reduction of by-product formation. Chromium reacts with heteroatoms (especially Cl, N, S, and O) quantitatively to form chromium salts and remains irreversibly scavenged in the Cr/HTC reactor as described previously [30, 31].

Because of the formation of hydrogen-bearing by-products, the yield of H₂ for isotope analysis is reduced. However, H₂ yields obtained via Cr/HTC compared with conventional HTC can differ for different compounds and are dependent on the age of the conversion reactor, suggesting that carbon residues might be formed by the precipitation of elementary carbon within the hot zone of the reactor, leading to a changed reactivity. The linearity measurement of the investigated OPs indicated that the formation of HCl was a significant isotope fractionating process leading to inaccurate measurement of $\delta^2\text{H}$. In the case of TCEP, $\delta^2\text{H}$ shifted from -5‰ to 273‰ depending on the amounts injected, and no linearity range was observed (Fig. 1f). The mean $\delta^2\text{H}$ value of parathion obtained via HTC, (-115 ± 3)‰, differs from that obtained via Cr/HTC, (-138 ± 4)‰, which is mostly probably due to the typical peak shape of parathion via HTC, which usually shows peak fronting and peak tailing in the chromatogram. The comparison of peak shapes for hydrogen isotope analysis of parathion using the HTC and Cr/HTC interface is shown in Fig. S5. Good linearity for nonchlorinated OPs was obtained via conventional HTC, which indicates that hydrogen-bearing by-products might not be associated with

isotope fractionation even though two by-products are formed or the fractionation during thermal decomposition is minor and stable. The isotope fractionation associated with the by-product formation was not affected by concentration, leading to a dynamic range with a relatively acceptable linearity. Thus, a critical analysis of the linearity is needed; if good linearity can be achieved, hydrogen isotope fractionation processes may be reproducibly analyzed by both conventional HTC and Cr/HTC.

Validation and comparison of methods

To evaluate the accuracy of isotope measurement, the $\delta^{13}\text{C}$ and $\delta^2\text{H}$ values for the eight OPs obtained via GC-IRMS were compared with the respective reference data obtained by EA-IRMS. $\delta^{13}\text{C}$ and $\delta^2\text{H}$ values obtained via GC-IRMS were calculated from the mean values of all measurements ($n \geq 15$) within the corresponding linearity ranges. Carbon isotope analysis of the OPs revealed good agreement between GC-C-IRMS and EA-IRMS analysis (slope 0.98, $R^2 = 0.996$, shift of scale 31.3‰; Fig. 3a). Hydrogen isotope analysis also resulted in good agreement between GC-Cr/HTC-IRMS and EA-Cr/HTC-IRMS as well as in comparison with 18 reference materials analyzed by Renpenning et al. [31] (slope 1.06, $R^2 = 0.997$, interval of $\delta^2\text{H}$ 896‰; Fig. 3b). The hydrogen isotope composition of nonchlorinated OPs obtained by GC-HTC-IRMS fit to the correlation obtained by the analysis using EA-Cr/HTC-IRMS (Fig. 3b). However, because of formation of HCl, the calculation of mean $\delta^2\text{H}$ values for chlorinated OPs measured via GC-HTC-IRMS was not performed.

Effect of evaporation process on the isotope composition

Because of the low sensitivity of GC-IRMS systems, samples usually need to be concentrated before their analysis.

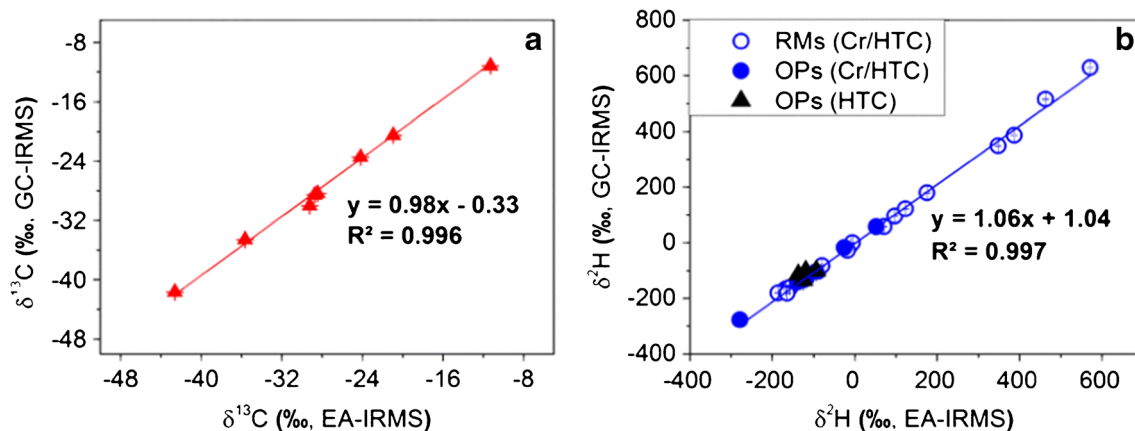


Fig. 3 $\delta^{13}\text{C}$ (a) and $\delta^2\text{H}$ (b) values for the eight organophosphorus compounds (OPs) measured by GC-IRMS are compared with respective data obtained by EA-IRMS to evaluate the accuracy. Error bars are smaller

Concerning the measurement of reliable isotope compositions, the preconcentration of the sample should in the end deliver an amount above the lower limits of precise isotope measurement. One of the commonest methods used to concentrate experimental samples is solvent evaporation. Especially for the monitoring of environmentally relevant samples, solvent extraction of large sample volumes and subsequent enrichment of the analyte via careful evaporation is inevitable in most cases. Thus, evaporation effects on the isotope composition have to be considered for the development of a CSIA method. Therefore, an evaporation experiment was conducted, and the isotopic composition of the target OPs was determined before and after the evaporation procedure. After the solvent volume had been reduced by 200 times, the observed shifts of $\delta^{13}\text{C}$ and $\delta^2\text{H}$ for the OPs tested were negligible. In addition, a solution of target OPs was evaporated to dryness twice and the residue was dissolved in same amount of solvent again, but no significant shifts were observed for $\delta^{13}\text{C}$ and $\delta^2\text{H}$ (the original data are shown in Tables S4 and Table S5). Consequently, our results suggest that evaporation is unlikely to induce any significant shift of the isotope composition and can thus be regarded as an isotope-effect-free approach that might be used for the preparation of OP samples.

Carbon and hydrogen isotope fractionation during dimethoate hydrolysis

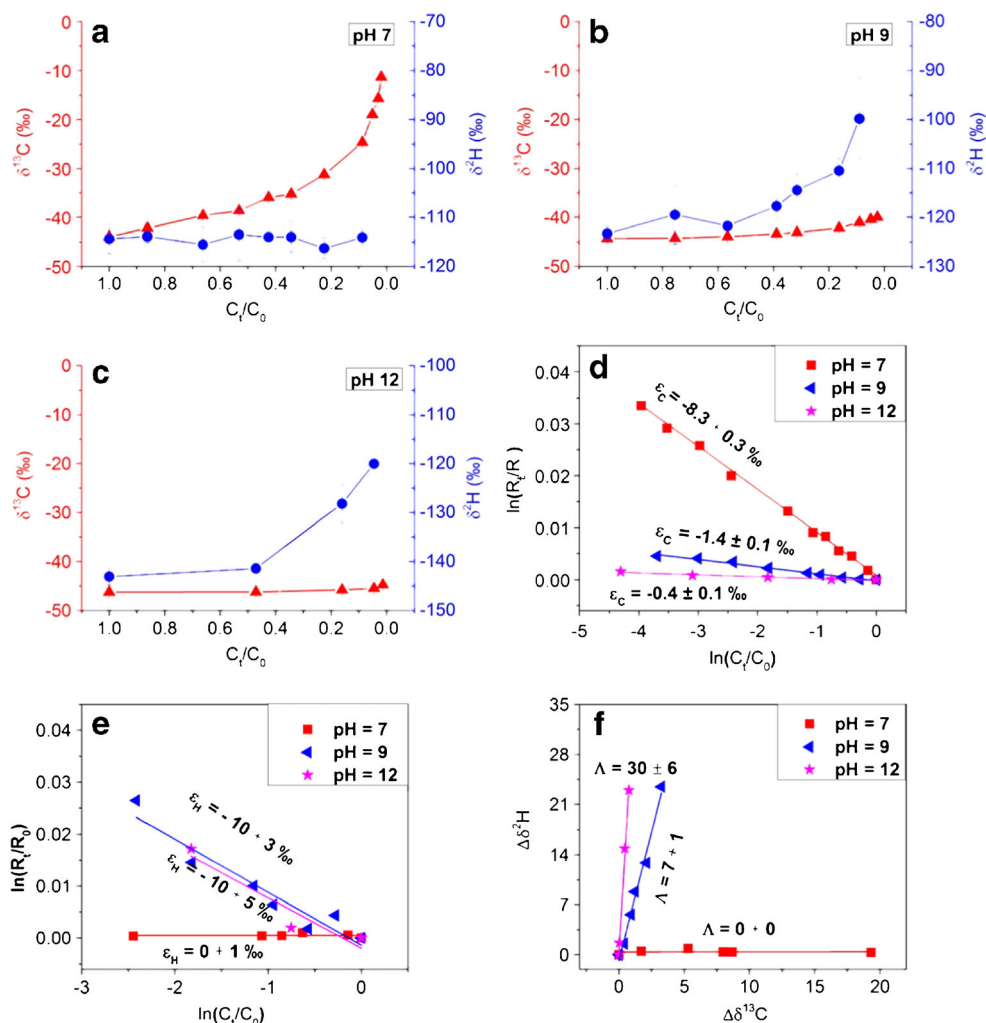
During chemical hydrolysis at pH 7, $\delta^{13}\text{C}$ of dimethoate shifted from -43.9‰ to -11.4‰ with 98% degradation (Fig. 4a). This isotope shift of 32.5‰ is 65 times larger than the instrument uncertainty ($\pm 0.5\text{‰}$), which demonstrates that carbon isotope analysis might be applied for the tracking in situ hydrolysis of dimethoate, in particular in neutral or slightly acidic/alkaline conditions. In contrast, hydrolysis at pH 9

than the symbols. The isotope compositions of the eight OPs are reported in Table S2. $\delta^2\text{H}$ values for reference materials (RMs) are reported in Table S3 and were taken from Renpenning et al. [31]

resulted in only a small shift of 4.3‰ with 98% degradation (Fig. 4b), whereas hydrolysis at pH 12 revealed an overall difference of 1.5‰ with 99% degradation (Fig. 4c), which is hardly significant considering the analytical uncertainty of the method ($\pm 0.5\text{‰}$). However, no change in $\delta^2\text{H}$ was observed at pH 7 (Fig. 4a), a small shift from -123‰ to -100‰ with 91% degradation was observed at pH 9 (Fig. 4b), and a shift from -143‰ to -120‰ with 95% degradation was observed at pH 12 (Fig. 4c). Regarding the control experiment at pH 3, no significant change in $\delta^{13}\text{C}$ and $\delta^2\text{H}$ was observed (Table S6). The enrichment factors for carbon (ϵ_{C}) were $(-8.3 \pm 0.3)\text{‰}$ at pH 7, $(-1.4 \pm 0.1)\text{‰}$ at pH 9, and $(-0.4 \pm 0.1)\text{‰}$ at pH 12 (Fig. 4d). The enrichment factors for hydrogen (ϵ_{H}) were $(0 \pm 1)\text{‰}$ at pH 7, $(-10 \pm 3)\text{‰}$ at pH 9, and $(-10 \pm 5)\text{‰}$ at pH 12 (Fig. 4e). The dual-isotope fractionation of carbon versus hydrogen yielded Δ values ($=\Delta\delta^2\text{H}/\Delta\delta^{13}\text{C}$) of 0 ± 0 at pH 7, 7 ± 1 at pH 9, and 30 ± 6 at pH 12 (Fig. 4f).

Using dimethoate as a model compound for OPs, we evaluated for the first time the potential of carbon and hydrogen isotope fractionation to investigate the hydrolysis mechanisms of OPs at different pH values. The differences in ϵ_{C} obtained indicate that there are clearly two different pathways during neutral and alkaline hydrolysis. We propose that in alkaline conditions, a nucleophilic OH^- attacking the phosphorus atom will lead to P-S bond cleavage without any primary carbon isotope effect; however, a parallel nucleophilic OH^- attack on the C-O bond may lead to a C-O bond fission associated with a primary stable carbon isotope effect in neutral and acidic conditions. The reaction scheme is shown in Scheme S1. Our conclusion is supported by previous analysis of hydrolysis products of dimethoate. Hydrolysis at pH 5 and pH 7 yielded *O*-demethyl dimethoate; and *O*-demethyl dimethoate and *O,O*-dimethyl hydrogen phosphorothioate acid were found at pH 9 [40]. At pH 9, ϵ_{C} of $(-1.4 \pm 0.1)\text{‰}$ showed good agreement with ϵ_{C} of $(-1.0 \pm 0.1)\text{‰}$ at pH 10 that we obtained

Fig. 4 Changes in carbon (triangles) and hydrogen (circles) isotope ratios during hydrolysis of dimethoate at pH 7 (a), pH 9 (b), and pH 12 (c). Rayleigh plots of carbon (d) and hydrogen (e) isotope fractionation for dimethoate hydrolysis at pH 7 (squares), pH 9 (triangles), and pH 12 (stars). The logarithmic plots were calculated according to the modified Rayleigh equation given in the [electronic supplementary material](#). Two-dimensional plots (f) of hydrogen versus carbon discrimination for dimethoate hydrolysis at pH 7 (squares), pH 9 (triangles), and pH 12 (stars). Error bars display the accuracy of $\delta^{13}\text{C}$ and $\delta^2\text{H}$ measurements, which were always better than $\pm 0.5\%$ and $\pm 5\%$ respectively



in a previous study. The relative small carbon enrichment factors suggest that two parallel pathways are active during hydrolysis in weak alkaline conditions. In contrast, ϵ_H obtained at pH 9 and pH 12 indicates that a hydrogen atom next to the position of bond cleavage might give a secondary isotope effect in alkaline conditions. Thus, neutral and alkaline hydrolysis can be distinguished by use of combined carbon and hydrogen isotope fractionation. As indicated by our data, dual-isotope fractionation can elucidate differences in alkaline hydrolysis more precisely; hydrolysis at pH 9 showed a significantly smaller Λ value compared with hydrolysis at pH 12 (Fig. 4e).

Conclusions

A method to measure $\delta^{13}\text{C}$ and $\delta^2\text{H}$ values of OPs was developed and evaluated. The method developed allows accurate and precise isotope analysis of OPs and is applicable for analysis of degradation reactions associated with isotope fractionation such as hydrolysis. Hydrogen isotope analysis of

chlorinated OPs is impossible with conventional GC-HTC-IRMS; in contrast this can be achieved for nonchlorinated OPs. Cr/HTC is a promising approach for routine hydrogen isotope analysis and has the potential to replace the routine HTC as the standard method.

The method promises great potential for future investigations regarding the fate of OPs using CSIA. Because of the high detection limit of IRMS, it remains a challenge to enrich and clean up OPs from environmental samples with residual levels of micrograms; for example, the OP residues in surface water of agriculture intensive areas in India were $0.46 \mu\text{g L}^{-1}$ for chlorpyrifos [41]. However, at a typical waste dump site with parathion concentration up to $31,000 \text{ mg kg}^{-1}$ (wet weight) in soil samples [42] or in a contaminated groundwater area with parathion concentration up to 4 mg L^{-1} [43], CSIA can be easily applied and has great potential to analyze hydrolysis reactions in the environment using a combination of carbon and hydrogen isotope analysis.

Acknowledgements L.W. was financially supported by the China Scholarship Council (file no. 201306460007). We are thankful to M.

Gehre and U. Günther for support in the Isotope Laboratory of the Department of Isotope Biogeochemistry and for the support by the graduate school of the Helmholtz Centre for Environmental Research (HiGrade).

Compliance with ethical standards

Conflict of interest The authors declare that they have no conflict of interest.

References

- Sogorb MA, Vilanova E. Enzymes involved in the detoxification of organophosphorus, carbamate and pyrethroid insecticides through hydrolysis. *Toxicol Lett.* 2002;128(1-3):215–28.
- Minton NA, Murray VS. A review of organophosphate poisoning. *Med Toxicol Adverse Drug Exp.* 1988;3(5):350–75.
- Organophosphate insecticides fact sheet (1996) <http://www.pan-uk.org/pestnews/Actives/organoph.htm>.
- He HB. The status and trend of development of organophosphorus pesticide industry. *World Pestic.* 2008;30(6):29–34.
- Aston LS, Seiber JN. Exchange of airborne organophosphorus pesticides with pine needles. *J Environ Sci Health Part B.* 1996;31(4):671–98.
- Kim JW, Isobe T, Chang KH, Amano A, Maneja RH, Zamora PB, et al. Levels and distribution of organophosphorus flame retardants and plasticizers in fishes from Manila Bay, the Philippines. *Environ Pollut.* 2011;159(12):3653–9.
- Bravo R, Caltabiano LM, Weerasekera G, Whitehead RD, Fernandez C, Needham LL, et al. Measurement of dialkyl phosphate metabolites of organophosphorus pesticides in human urine using lyophilization with gas chromatography-tandem mass spectrometry and isotope dilution quantification. *J Exposure Anal Environ Epidemiol.* 2004;14(3):249–59.
- Elsner M, Jochmann MA, Hofstetter TB, Hunkeler D, Bernstein A, Schmidt TC, et al. Current challenges in compound-specific stable isotope analysis of environmental organic contaminants. *Anal Bioanal Chem.* 2012;403(9):2471–91.
- Hofstetter TB, Berg M. Assessing transformation processes of organic contaminants by compound-specific stable isotope analysis. *Trends Anal Chem.* 2011;30(4):618–27.
- Hofstetter TB, Schwarzenbach RP, Bernasconi SM. Assessing transformation processes of organic compounds using stable isotope fractionation. *Environ Sci Technol.* 2008;42(21):7737–43.
- Elsner M. Stable isotope fractionation to investigate natural transformation mechanisms of organic contaminants: principles, prospects and limitations. *J Environ Monit.* 2010;12(11):2005–31.
- Mak KS, Griebler C, Meckenstock RU, Liedl R, Peter A. Combined application of conservative transport modelling and compound-specific carbon isotope analyses to assess in situ attenuation of benzene, toluene, and o-xylene. *J Contam Hydrol.* 2006;88(3-4):306–20.
- Van Keer I, Bronders J, Verhack J, Schwarzbauer J, Swennen R. Limitations in the use of compound-specific stable isotope analysis to understand the behaviour of a complex BTEX groundwater contamination near Brussels (Belgium). *Environ Earth Sci.* 2012;66(2):457–70.
- Fischer A, Bauer J, Meckenstock RU, Stichler W, Griebler C, Maloszewski P, et al. A multitracer test proving the reliability of Rayleigh equation-based approach for assessing biodegradation in a BTEX contaminated aquifer. *Environ Sci Technol.* 2006;40(13):4245–52.
- Mundle SOC, Johnson T, Lacrampe-Couloume G, Perez-de-Mora A, Duhamel M, Edwards EA, et al. Monitoring biodegradation of ethene and bioremediation of chlorinated ethenes at a contaminated site using compound-specific isotope analysis (CSIA). *Environ Sci Technol.* 2012;46(3):1731–8.
- Pooley KE, Blessing M, Schmidt TC, Haderlein SB, Macquarrie KTB, Prommer H. Aerobic biodegradation of chlorinated ethenes in a fractured bedrock aquifer: quantitative assessment by compound-specific isotope analysis (CSIA) and reactive transport modeling. *Environ Sci Technol.* 2009;43(19):7458–64.
- Wiegert C, Aeppli C, Knowles T, Holmstrand H, Evershed R, Pancost RD, et al. Dual carbon-chlorine stable isotope investigation of sources and fate of chlorinated ethenes in contaminated groundwater. *Environ Sci Technol.* 2012;46(20):10918–25.
- Bashir S, Hitzfeld KL, Gehre M, Richnow HH, Fischer A. Evaluating degradation of hexachlorocyclohexane (HCH) isomers within a contaminated aquifer using compound-specific stable carbon isotope analysis (CSIA). *Water Res.* 2015;71:187–96.
- Zhang N, Bashir S, Qin JY, Schindelka J, Fischer A, Nijenhuis I, et al. Compound specific stable isotope analysis (CSIA) to characterize transformation mechanisms of alpha-hexachlorocyclohexane. *J Hazard Mater.* 2014;280:750–7.
- Rosell M, Gonzalez-Olmos R, Rohwerder T, Rusevova K, Georgi A, Kopinke FD, et al. Critical evaluation of the 2D-CSIA scheme for distinguishing fuel oxygenate degradation reaction mechanisms. *Environ Sci Technol.* 2012;46(9):4757–66.
- Youngster LKG, Rosell M, Richnow HH, Haggblom MM. Assessment of MTBE biodegradation pathways by two-dimensional isotope analysis in mixed bacterial consortia under different redox conditions. *Appl Microbiol Biotechnol.* 2010;88(1):309–17.
- Zhang N, Schindelka J, Herrmann H, George C, Rosell M, Herrero-Martin S, et al. Investigation of humic substance photosensitized reactions via carbon and hydrogen isotope fractionation. *Environ Sci Technol.* 2015;49(1):233–42.
- Wu L, Yao J, Trebse P, Zhang N, Richnow HH. Compound specific isotope analysis of organophosphorus pesticides. *Chemosphere.* 2014;111:458–63.
- Fischer A, Herklotz I, Herrmann S, Thullner M, Weelink SAB, Stams AJM, et al. Combined carbon and hydrogen isotope fractionation investigations for elucidating benzene biodegradation pathways. *Environ Sci Technol.* 2008;42(12):4356–63.
- Kuder T, Wilson JT, Kaiser P, Kolhatkar R, Philp P, Allen J. Enrichment of stable carbon and hydrogen isotopes during anaerobic biodegradation of MTBE: Microcosm and field evidence. *Environ Sci Technol.* 2005;39(1):213–20.
- Zwank L, Berg M, Elsner M, Schmidt TC, Schwarzenbach RP, Haderlein SB. New evaluation scheme for two-dimensional isotope analysis to decipher biodegradation processes: Application to groundwater contamination by MTBE. *Environ Sci Technol.* 2005;39(4):1018–1029.
- Kuder T, van Breukelen BM, Vanderford M, Philp P. 3D-CSIA: carbon, chlorine, and hydrogen isotope fractionation in transformation of TCE to ethene by a Dehalococcoides culture. *Environ Sci Technol.* 2013;47(17):9668–77.
- Vetter W, Armbruster W, Betson TR, Schleucher J, Kapp T, Lehnert K. Baseline isotopic data of polyhalogenated compounds. *Anal Chim Acta.* 2006;577(2):250–6.
- Chartrand MMG, Hirschorn SK, Lacrampe-Couloume G, Sherwood Lollar B. Compound-specific hydrogen isotope analysis of 1,2-dichloroethane: potential for delineating source and fate of chlorinated hydrocarbon contaminants in groundwater. *Rapid Commun Mass Spectrom.* 2007;21(12):1841–7.
- Gehre M, Renpenning J, Gilevska T, Qi H, Copley TB, Meijer HA, et al. On-line hydrogen-isotope measurements of organic samples using elemental chromium: an extension for high temperature

- elemental-analyzer techniques. *Anal Chem.* 2015;87(10):5198–205.
31. Renpenning J, Kuemmel S, Hitzfeld KL, Schimmelmann A, Gehre M. Compound-specific hydrogen isotope analysis of heteroatom-bearing compounds via gas chromatography-chromium-based high-temperature conversion (Cr/HTC)-isotope ratio mass spectrometry. *Anal Chem.* 2015;87(18):9443–50.
 32. Gehre M, Strauch G. High-temperature elemental analysis and pyrolysis techniques for stable isotope analysis. *Rapid Commun Mass Spectrom.* 2003;17(13):1497–503.
 33. Coplen TB, Brand WA, Gehre M, Groning M, Meijer HAJ, Toman B, et al. After two decades a second anchor for the VPDB delta C-13 scale. *Rapid Commun Mass Spectrom.* 2006;20(21):3165–6.
 34. Coplen TB. Guidelines and recommended terms for expression of stable-isotope-ratio and gas-ratio measurement results. *Rapid Commun Mass Spectrom.* 2011;25(17):2538–60.
 35. Herrero-Martin S, Nijenhuis I, Richnow HH, Gehre M. Coupling of a headspace autosampler with a programmed temperature vaporizer for stable carbon and hydrogen isotope analysis of volatile organic compounds at microgram per liter concentrations. *Anal Chem.* 2015;87(2):951–9.
 36. Renpenning J, Hitzfeld KL, Gilevska T, Nijenhuis I, Gehre M, Richnow HH. Development and validation of an universal interface for compound-specific stable isotope analysis of chlorine ($^{37}\text{Cl}/^{35}\text{Cl}$) by GC-high-temperature conversion (HTC)-MS/IRMS. *Anal Chem.* 2015;87(5):2832–9.
 37. Meckenstock RU, Morasch B, Griebler C, Richnow HH. Stable isotope fractionation analysis as a tool to monitor biodegradation in contaminated aquifers. *J Contam Hydrol.* 2004;75(3-4):215–55.
 38. International Programme on Chemical Safety. ICSC 0006 - parathion <http://www.inchem.org/documents/icsc/icsc/eics0006.htm> (2004).
 39. US National Library of Medicine. HSDB: omethoate. <https://toxnet.nlm.nih.gov/cgi-bin/sis/search2/f?/.temp/~0ULjae:1> (2004).
 40. Food and Agriculture Organization. Dimethoate (27). http://www.fao.org/fileadmin/templates/agphome/documents/Pests_Pesticides/JMPR/Evaluation03/Dimethoate_2003.pdf (2003).
 41. Lari SZ, Khan NA, Gandhi KN, Meshram TS, Thacker NP. Comparison of pesticide residues in surface water and ground water of agriculture intensive areas. *J Environ Health Sci Eng.* 2014;12(1):173–83.
 42. Nielsen MB, Kjeldsen KU, Lever MA, Ingvorsen K. Survival of prokaryotes in a polluted waste dump during remediation by alkaline hydrolysis. *Ecotoxicology.* 2014;23(3):404–18.
 43. Andersen L, Jørgensen C, Holm J (2007) In situ biologisk nedbrydning som oprensningmetode ved Høfde 42. <http://www2.mst.dk/Udgiv/publikationer/2007/978-87-7052-608-1/pdf/978-87-7052-609-8.pdf>.

Supplementary material

Validation of GC-IRMS techniques for $\delta^{13}\text{C}$ and $\delta^2\text{H}$ CSIA of organophosphorus compounds and their potential for studying the mode of hydrolysis in the environment

Langping Wu, Steffen Kümmel, Hans H. Richnow*

Department of Isotope Biogeochemistry, Helmholtz Centre for Environmental Research – UFZ, Permoserstrasse 15, D-04318, Leipzig, Germany.

*Email: hans.richnow@ufz.de, Tel: 0049 341 235 1212 Fax: 0341-450822**Table S1:** Molecular structures of the target OPs.

	compound	molecular Formula	molecular structures	density (g/cm ³)	CAS number
1	dichlorvos	C ₄ H ₇ Cl ₂ O ₄ P		1.42, liquid	62-73-7
2	dimethoate	C ₅ H ₁₂ NO ₃ PS ₂		1.28, solid	60-51-5
3	omethoate	C ₅ H ₁₂ NO ₄ PS		1.32, liquid	1113-02-6
4	chlorpyrifos	C ₉ H ₁₁ Cl ₃ NO ₃ PS		1.40, solid	2921-88-2
5	parathion	C ₁₀ H ₁₄ NO ₅ PS		1.27, liquid	56-38-2
6	parathion-methyl	C ₈ H ₁₀ NO ₅ PS		1.36, solid	298-00-0
7	TDCPP	C ₉ H ₁₅ Cl ₆ O ₄ P		1.52, liquid	13674-87-8
8	TCEP	C ₆ H ₁₂ Cl ₃ O ₄ P		1.42, liquid	115-96-8

1. Decomposition of omethoate in the GC Injector

Omethoate starts to decompose at 135 °C and can react with the glass liner in the GC injector when the liner is not completely deactivated. The reaction is expected to increase strongly with higher injector temperatures and higher sample concentrations. Fig. S1 shows screen shots of GC-IRMS chromatograms of omethoate isotope measurements for $\delta^2\text{H}$ (via Cr/HTC) at injector temperature of 180 °C. 1 μL , 2 μL and 3 μL of 1000 mg L^{-1} omethoate in DCM were injected in splitless mode yielding an injection of 1000 ng, 2000 ng and 3000 ng omethoate, respectively. Omethoate elute at retention time (RT) of 804 to 807s, whereas no byproduct peaks appeared when 1000 ng omethoate were injected (Fig. S1a), a very small peak prior to omethoate appeared when the injected concentration was increased to 2000 ng (Fig. S1b). Moreover, this byproduct peak significantly increased when 3000 ng omethoate were injected (FigS1c) indicating that higher omethoate concentrations lead to increased byproduct formation caused by decomposition of omethoate in the injector. As shown in Figure S1d, the deactivation of the liner by BSTFA leads to disappearance of the decomposition products. 2000 ng omethoate injection is still sufficient for routine $\delta^{13}\text{C}$ analysis, however for reliable $\delta^2\text{H}$ analysis, much higher amounts of substrates are needed. Therefore, in order to avoid a decomposition of omethoate in the injector a completely deactivated liner is important and any potential formation of decomposition products should be carefully monitored. For precise analysis the activity of the liner need to be tested prior isotope analysis with individual pure OPs.

2. Deactivation of the glass liner with N,O-Bis(trimethylsilyl)trifluoroacetamide (BSTFA).

In order to avoid the decomposition of OPs in the injector of GC, the glass liner needs to be deactivated prior to isotope measurements [1]. To deactivate the liner, 1 μL of BSTFA (N,O-bis(trimethylsilyl) trifluoroacetamide, SUPELCO) was injected manually 3 times into the GC inlet. The detailed steps are as follows: 1) adjust the injector temperature to 100 °C, and the split ratio to 1:200; 2) inject 1 μL of BSTFA manually for 3 times, wait for 5 min between each injection; 3) wait for 10 min; 4) reduce the split ratio to normal conditions and increase the injector temperature to 200 °C, heat up the GC column to its upper temperature limit for 30 min.

3. Dependency of isotope values in the amount of target OP (linearity of the analytical system)

The dependency of $\delta^{13}\text{C}$ and $\delta^2\text{H}$ values on the amount of analyt (linearity) was analyzed along ranges of concentrations for 8 target OPs using a stock solution of OPs dissolved in DCM. For reliable isotope analysis without correction the isotope value should be independent of the concentration which is the concentration interval where the system is linear with respect to constant isotope composition. The analytical methods are reported in the main text. Significant variety of linearity ranges for different OPs were obtained; the possible reasons were discussed in the main text. Here we document the linearity ranges of the OPs which were not reported in the manuscript. Linearity of $\delta^{13}\text{C}$ values for parathion-methyl, chlorpyrifos and TDCPP are shown in Figure S2. Measurements of different amounts of parathion-methyl, chlorpyrifos and TDCPP documented a linearity range starting from an area signal of 9 Vs, 7 Vs and 5 Vs, respectively, which correspond to an injection of ~ 2.5 nmol parathion-methyl, ~ 1.1 nmol chlorpyrifos and ~ 0.7 nmol TDCPP. The linearity ranges of $\delta^{13}\text{C}$ for dichlorvos, omethoate and dimethoate were reported previously.[1]

Linearity of $\delta^2\text{H}$ values for non-chlorinated OPs is shown in Figure S3. Measurements of parathion-methyl and omethoate via GC-Cr/HTC-IRMS documented a linearity range starting from an area signal of 53 Vs and 42 Vs, respectively, which correspond to an injection of ~ 11.4 nmol parathion-methyl and ~ 2.8 nmol omethoate. However, measurements of parathion-methyl and omethoate via GC-HTC-IRMS documented a linearity range starting from an area signal of 45 Vs and 12 Vs, respectively, which correspond to an injection of ~ 14.2 nmol parathion-methyl and ~ 1.7 nmol omethoate. In contrast, linearity ranges of $\delta^2\text{H}$ for chlorinated OPs were only obtained via GC-Cr/HTC-IRMS (Fig. S4). Measurements of dichlorvos, chlorpyrifos and TDCPP via GC-Cr/HTC-IRMS documented a linearity range starting from an area signal of 66 Vs, 70 Vs and 120 Vs, respectively, which correspond to an injection of ~ 13.6 nmol dichlorvos, ~ 11.4 nmol chlorpyrifos and ~ 16.2 nmol TDCPP. However, in case of measurements via GC- HTC-IRMS, a clear dependency of $\delta^2\text{H}$ values on the sample intensities was observed due to the formation of HCl. Consequently, no linearity ranges were obtained.

The linearity of $\delta^{13}\text{C}$ and $\delta^2\text{H}$ lead to an acceptable isotope composition for tested OPs within the uncertainty of the instrument. Only area signals within the obtained linearity ranges can be used for evaluation of isotope values.

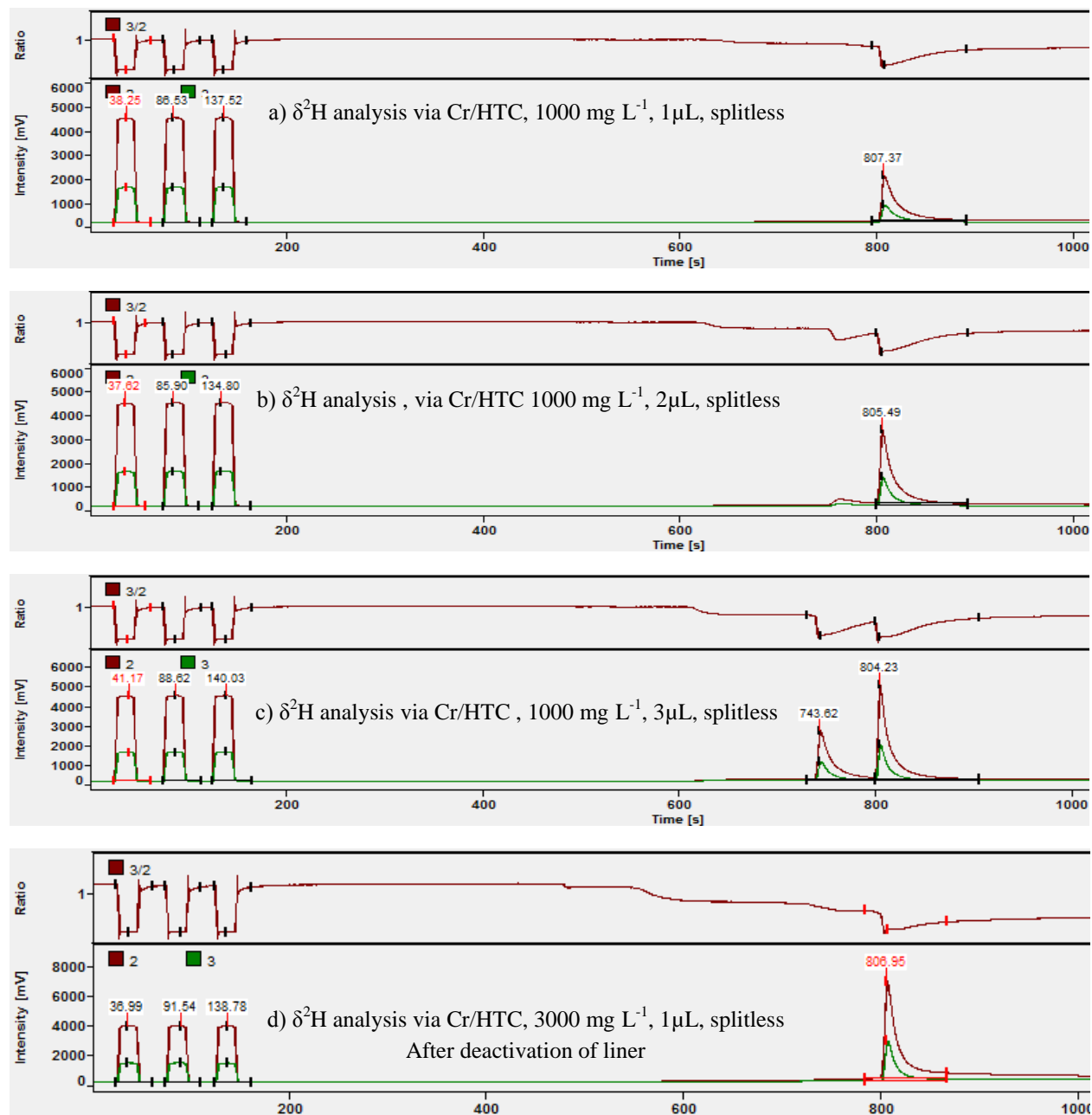


Fig. S1 GC-IRMS chromatograms of $\delta^2\text{H}$ analysis of omethoate standard solutions. By-product peaks (RT 743.62s) appearing before omethoate (RT 804.23s) indicate a thermal decomposition of omethoate in the injector.

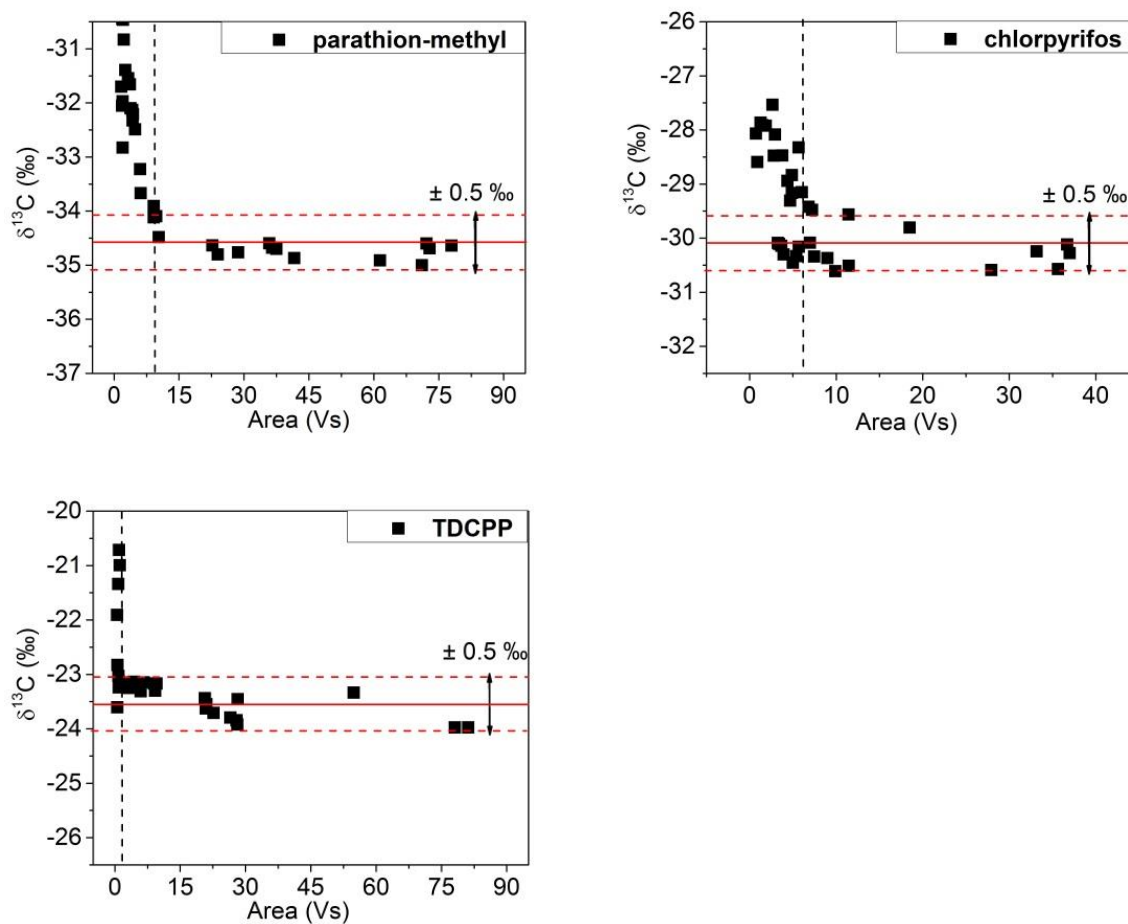


Fig. S2 Linearity analysis of $\delta^{13}\text{C}$ values for parathion-methyl, chlorpyrifos and TDCPP correlating isotope compositions to signal intensities. Black dotted lines indicate the lower limits of precise CSIA; red dotted lines indicate the analytical uncertainty for carbon isotope analysis; solid lines represent the mean values of all measurements within the linearity ranges.

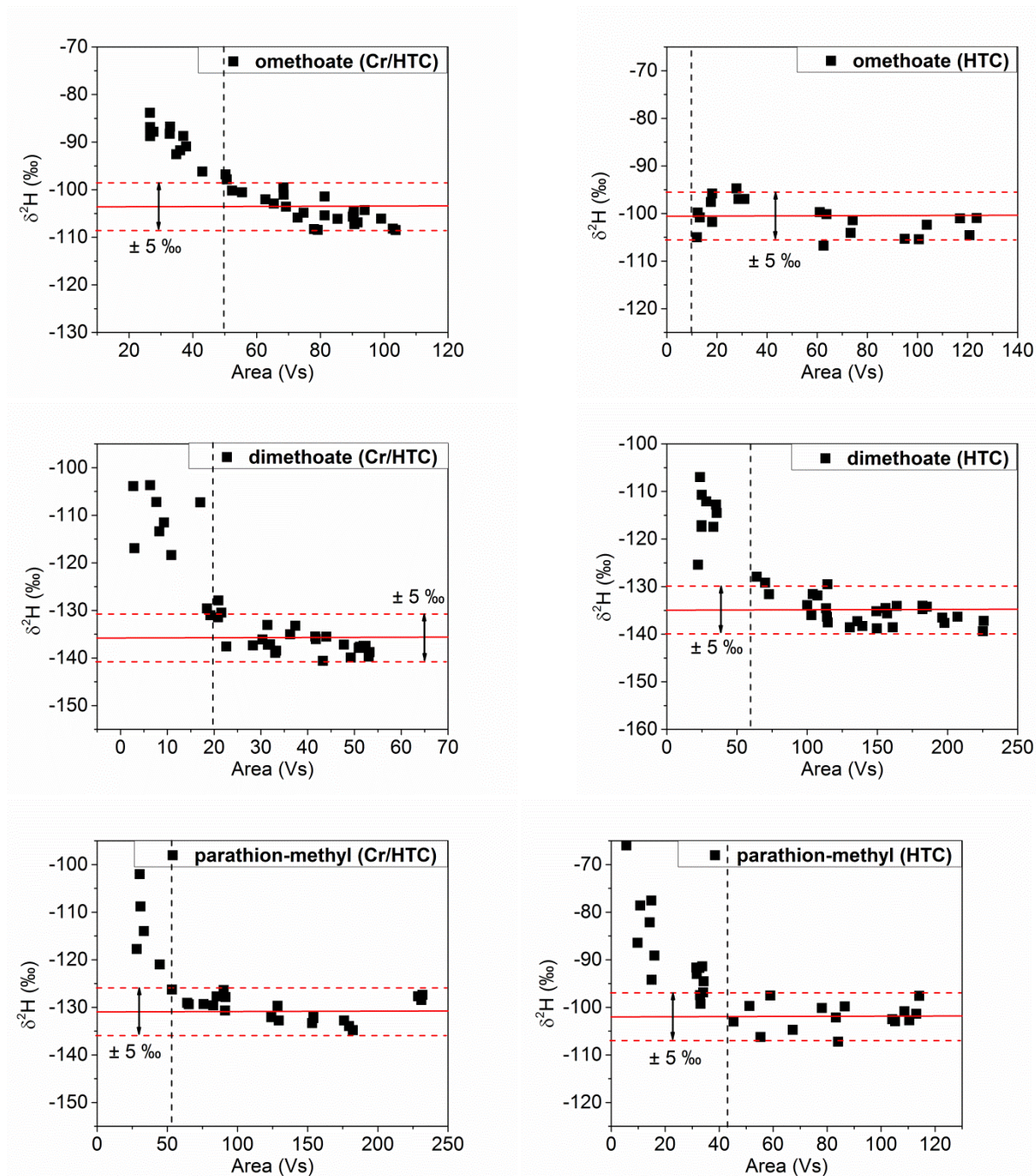


Fig. S3 Linearity analysis of $\delta^2\text{H}$ values for non-chlorinated OPs (omethoate, dimethoate and parathion-methyl) correlating isotope compositions to signal intensities. The linearity of $\delta^2\text{H}$ measurements were assessed with GC-Cr/HTC-IRMS and GC-HTC-IRMS. Black dotted lines indicate the lower limits of precise CSIA; red dotted lines indicate the analytical uncertainty for carbon and hydrogen isotope analysis; solid lines represent the mean values of all measurements within the linearity ranges.

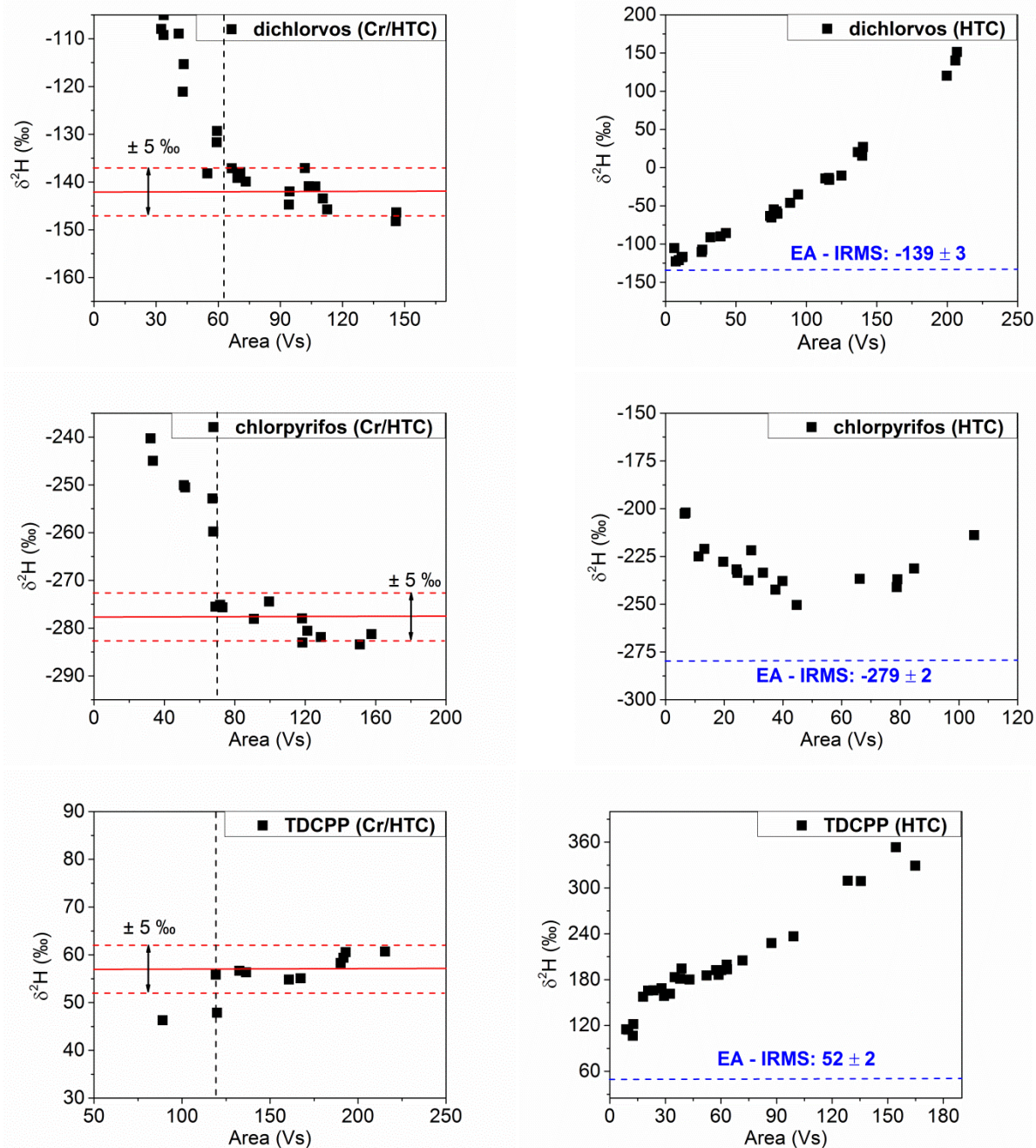


Fig. S4 Linearity analysis of $\delta^2\text{H}$ values for chlorinated OPs (dichlorvos, chlorpyrifos and TDCPP) correlating isotope compositions to signal intensities. The linearity of $\delta^2\text{H}$ measurements were assessed with GC-Cr/HTC-IRMS and GC-HTC-IRMS. Black dotted lines indicate the lower limits of precise CSIA; red dotted lines indicate the analytical uncertainty for hydrogen isotope analysis; solid lines represent the mean values of all measurements within the linearity ranges; blue dotted lines indicate the mean values obtained via EA-Cr/HTC-IRMS.

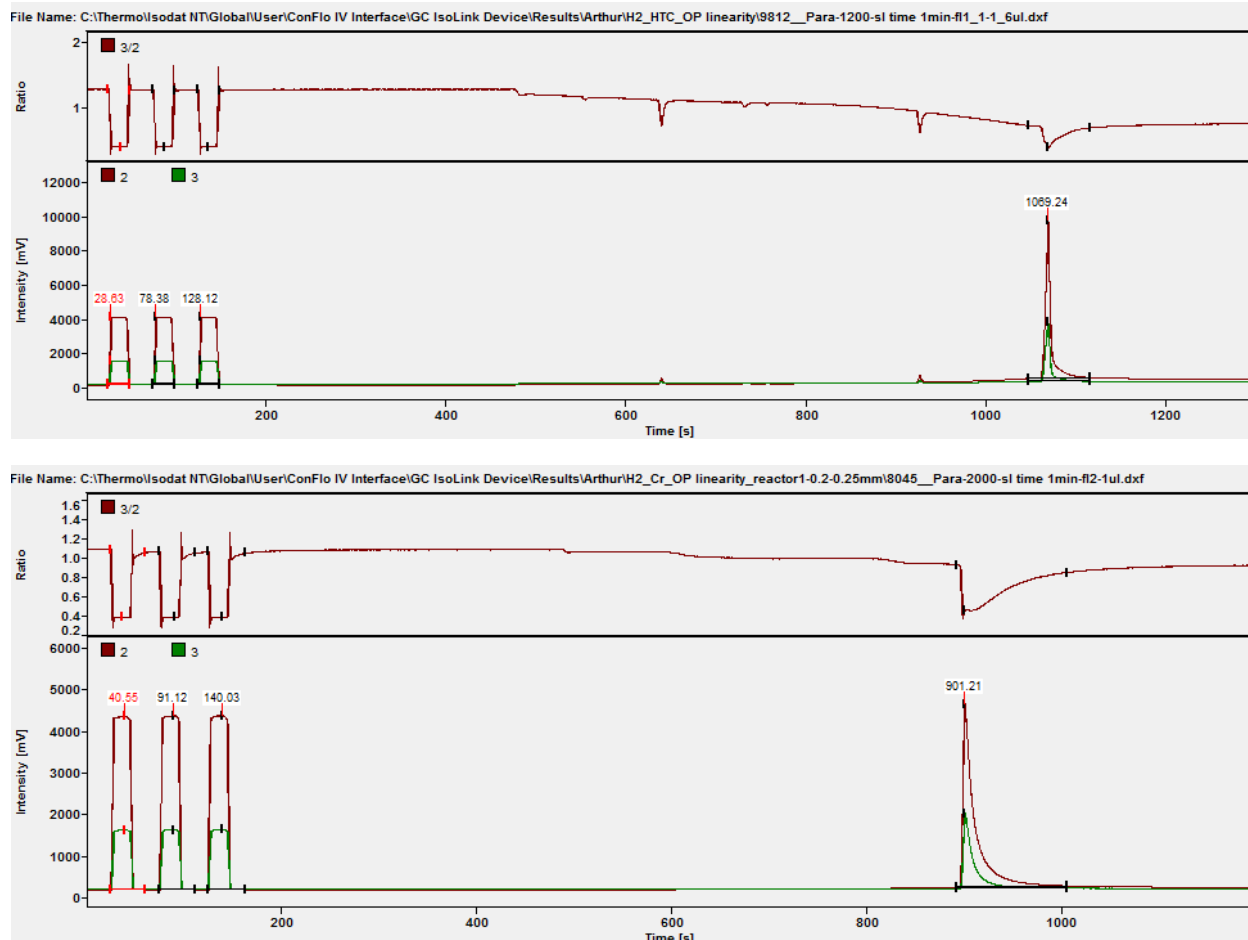


Fig. S5 Comparison of peak shapes in chromatograms for hydrogen isotope analysis of parathion using the HTC (above) and Cr/HTC interface (below).

4. Validation and Comparison of Methods

In order to evaluate the accuracy of isotope measurement, the $\delta^{13}\text{C}$ and $\delta^2\text{H}$ values for 8 OPs analyzed *via* GC-IRMS were compared to the respective data obtained by an elementary analyzer with a chromium reactor coupled to an isotope mass spectrometer (EA-Cr/HTC-IRMS) as a reference values. The reference values *via* EA-Cr/HTC-IRMS were obtained from the mean value of triplicates for $\delta^{13}\text{C}$ and four replicates for $\delta^2\text{H}$. The $\delta^{13}\text{C}$ and $\delta^2\text{H}$ values analyzed *via* GC-IRMS were calculated from the mean values of all measurements ($n \geq 15$) within the corresponding linearity ranges. Raw data of target OPs are shown in Table S2, raw data of other oxygen-, nitrogen-, chlorine-, and sulfur-containing materials used for reference are shown in Table S3 which is obtained from elsewhere[2].

Table S2: Comparison of $\delta^2\text{H}$ Values of target OPs determined via online EA-Cr/HTC-IRMS, GC-HTC-IRMS and GC-Cr/HTC-IRMS. This data are used in Fig. 3 (main text).

OPs	$\delta^{13}\text{C}$ (‰)		$\delta^2\text{H}$ (‰)		
	EA-IRMS	GC-C-IRMS	EA-Cr/HTC-IRMS	GC-Cr/HTC-IRMS	GC-HTC-IRMS
chlorpyrifos	-29.2 ± 0.0	-30.0 ± 0.5	-279 ± 2	-278 ± 4	n.d.
dichlorvos	-11.3 ± 0.1	-11.2 ± 0.4	-139 ± 3	-142 ± 3	n.d.
parathion	-28.7 ± 0.1	-28.6 ± 0.4	-137 ± 1	-138 ± 4	-115 ± 3
dimethoate	-42.6 ± 0.1	-41.7 ± 0.3	-125 ± 1	-135 ± 3	-135 ± 3
parathion-methyl	-35.7 ± 0.0	-34.6 ± 0.3	-119 ± 1	-130 ± 3	-102 ± 3

omethoate	-20.9 ± 0.0	-20.5 ± 0.2	-94 ± 2	-104 ± 4	-101 ± 4
TCEP	-28.4 ± 0.1	-28.4 ± 0.3	-26 ± 1	-17 ± 3	n.d.
TDCPP	-24.2 ± 0.0	-23.4 ± 0.3	52 ± 2	58 ± 2	n.d.

Table S3: $\delta^2\text{H}$ values for oxygen-, nitrogen-, chlorine-, and sulfur-containing materials used for reference via GC-Cr/HTC-IRMS are compared to respective data from online EA-Cr/HTC-IRMS to evaluate accuracy[2]. This data are used in Fig. 3 (main text).

	$\delta^2\text{H}$ (‰)	
	EA-Cr/HTC-IRMS	GC-Cr/HTC-IRMS
C ₁₆ #A	-167 ± 1	-167
C ₁₆ #B	-11 ± 1	-9 ± 1
C ₁₆ #C	387 ± 2	387
FAME #A	-186 ± 1	-181 ± 2
FAME #B	-6 ± 2	0 ± 1
FAME #C	348 ± 2	349 ± 2
IAEA 600	-158 ± 1	-161 ± 1
caffeine #1	97 ± 1	96 ± 1
caffeine #2	-157 ± 1	-162 ± 1
caffeine #3	175 ± 1	180 ± 2
DDD	71 ± 3	58 ± 1
DDE	-89 ± 2	-103 ± 1
DDT	-18 ± 2	-27 ± 1
HCH	-80 ± 1	-82 ± 4
TCE-PPG	463 ± 9	516 ± 2
TCE-Merck	571 ± 6	629 ± 2
DMSO ₂	123 ± 1	122 ± 1
Ph ₂ S ₂	-164 ± 1	-182 ± 1

5. Effect of evaporation process on the isotope composition

The carbon and hydrogen isotope fractionation associated with evaporation was evaluated as evaporation of solvents is commonly used in preparation procedures. After reducing the solvent volume for 200 times, the observed shifts of $\delta^{13}\text{C}$ for 8 tested OPs ranged between 0.1 ‰ and 0.5 ‰, the respective shifts of $\delta^2\text{H}$ for 4 tested OPs ranged between 1 ‰ and 5 ‰ (Table S4). Regarding the analytical uncertainty of carbon (± 0.5 ‰) and hydrogen (± 5 ‰) isotope analysis, all observed shifts can be considered to be negligible. After evaporating tested OPs to dryness twice and dissolved in same amount of solvent again, no significant shifts were observed (Table S5). In case evaporation to dryness is used in an extraction and isolation procedure the used technique need to be tested as distillation processes lead to isotope fractionation.

Table S4: Effect of evaporation (reduce solvent volume for 200 times) on the isotope composition.

Compound	$\delta^{13}\text{C}$ (‰)		$\Delta\delta^{13}\text{C}$ (‰)	$\delta^2\text{H}$ (‰)		$\Delta\delta^2\text{H}$ (‰)
	before	after		before	after	
dichlorvos	-10.2 ± 0.1	-10.3 ± 0.2	-0.1	n.d.	n.d.	n.d.
omethoate	-20.2 ± 0.1	-20.7 ± 0.5	-0.5	-104 ± 8	-109 ± 4	-5
dimethoate	-40.2 ± 0.3	-40.3 ± 0.3	-0.1	-131 ± 2	-128 ± 5	3
parathion-methyl	-34.2 ± 0.4	-34.7 ± 0.2	-0.5	-54 ± 7	-53 ± 1	1
parathion	-28.3 ± 0.1	-28.6 ± 0.2	-0.3	-106 ± 5	-101 ± 1	5
chlorpyrifos	-30.3 ± 0.0	-30.1 ± 0.1	0.2	n.d.	n.d.	n.d.
TCEP	-28.7 ± 0.1	-28.6 ± 0.2	0.1	n.d.	n.d.	n.d.
TDCPP	-22.5 ± 0.1	-22.3 ± 0.1	0.2	n.d.	n.d.	n.d.

Table S5: Effect of evaporation (evaporate to dry) on the isotope composition.

Compound	$\delta^{13}\text{C}$ (‰)		$\Delta\delta^{13}\text{C}$ (‰)	$\delta^2\text{H}$ (‰)		$\Delta\delta^2\text{H}$ (‰)
	before	after		before	after	
dimethoate	-40.2 ± 0.3	-40.5 ± 0.3	-0.3	-131 ± 2	-135 ± 1	-4
parathion	-28.3 ± 0.1	-28.5 ± 0.2	-0.2	-106 ± 5	-104 ± 1	2
chlorpyrifos	-30.3 ± 0.0	-30.3 ± 0.1	0.0	-237 ± 5	-240 ± 0	-3
TCEP	-28.7 ± 0.1	-29.1 ± 0.4	-0.4	-6 ± 5	-7 ± 2	-1

6. Effect of temperature on the isotope composition

In general OPs are thermal labile components which can easily decompose at certain temperatures. In order to conduct hydrolysis experiments at higher temperatures, the thermal stability of OPs in solvents was investigated. Therefore, 1000 mg L⁻¹ of target OPs solutions dissolved in DCM were exposed at 60°C for 8 days, and stable carbon and hydrogen isotopic compositions were determined before and after thermal incubation. After incubation, shifts in the carbon isotope composition for 8 tested OPs ranged between 0.0 ‰ and 0.5 ‰ and observed shifts for hydrogen isotope composition for 4 OPs ranged between 1 ‰ and 3 ‰ (Table S4). Losses of components due to thermal composition were not observed (data not shown). As in the case of the evaporation experiment the observed shifts of isotopic composition caused by thermal incubation were also within the analytical uncertainty of carbon and hydrogen isotope analysis. Thus, an exposure to temperature of 60°C does not cause any carbon and hydrogen isotopic effect for tested OPs.

Table S6: Effect of temperature on the isotope composition. Compounds were dissolved in DCM and were exposed at 60°C for 8 days.

Compound	$\delta^{13}\text{C}$ (‰)		$\Delta\delta^{13}\text{C}$ (‰)	$\delta^2\text{H}$ (‰)		$\Delta^2\text{H}$ (‰)
	before	after		before	After	
dichlorvos	-10.9 ± 0.1	-11.1 ± 0.4	-0.2	n.d.	n.d.	n.d.
omethoate	-18.9 ± 0.0	-18.4 ± 0.0	0.5	-109 ± 6	-109 ± 4	0
dimethoate	-39.4 ± 0.2	-39.3 ± 0.1	0.1	-103 ± 2	-106 ± 2	-3
parathion-M	-36.6 ± 0.5	-36.6 ± 0.3	0.0	$-58. \pm 2$	-58 ± 4	0
parathion	-27.7 ± 0.1	-27.9 ± 0.2	-0.3	-107 ± 2	-106 ± 1	1
chlorpyrifos	-28.3 ± 0.6	-28.5 ± 0.2	-0.2	n.d.	n.d.	n.d.
TCEP	-28.7 ± 0.3	-28.6 ± 0.0	0.1	n.d.	n.d.	n.d.
TDCPP	-23.6 ± 0.1	-23.5 ± 0.1	0.1	n.d.	n.d.	n.d.

n.d. = not determined

7. Hydrolysis of dimethoate

The hydrolysis experiments of dimethoate were carried out in phosphate buffer solution at pH 7, pH 9 and pH 12, respectively. The preparation of buffer solution is shown below:

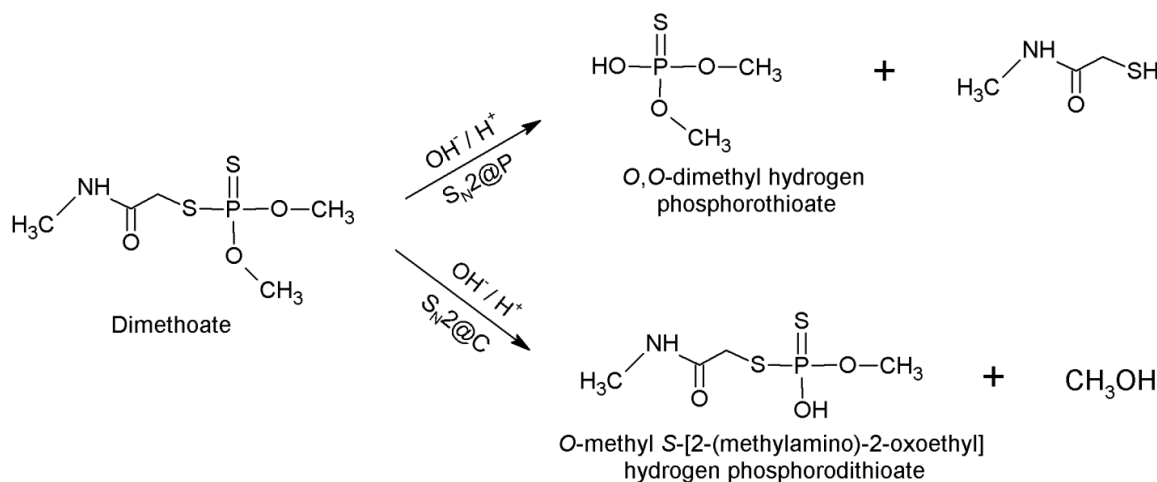
pH = 3 (control): 102.75 mL of 0.2 mol L⁻¹ Na₂HPO₄ + 397.25 mL of 0.1 mol L⁻¹ C₆H₈O₇·H₂O (citric acid), fill the volume to 500mL with double-distilled water;

pH = 7: 35 mL of 0.1 mol L⁻¹ NaOH + 500 mL of 0.1 mol L⁻¹ NaH₂PO₄, fill the volume to 1000mL with double-distilled water;

pH = 9: 213 mL of 0.1 mol L⁻¹ NaOH + 500mL of 0.1 mol L⁻¹ KCl-H₃BO₃ (boric acid), fill the volume to 1000mL with double-distilled water;

pH = 12: 269 ml of 0.1 mol L⁻¹ NaOH + 500 ml of 0.05 mol L⁻¹ Na₂HPO₄, fill the volume to 1000mL with double-distilled water.

Since hydrolysis of dimethoate at acidic condition is expected to be very slow, control experiments were conducted at pH 3 in buffer solution. As shown in table S5, no significant changes in concentration in carbon isotope ratios during all three control experiments were 0.2 ‰, 0.8 ‰, and 0.2 ‰, respectively, and changes in hydrogen isotope ratios were -3 ‰, -4 ‰, and -3 ‰, respectively. Considering the analytical uncertainty of ± 0.5 ‰ for $\delta^{13}\text{C}$ and ± 5 ‰ for $\delta^2\text{H}$, no carbon and hydrogen isotope fractionation occurred during the control experiments for dimethoate hydrolysis. No significant losses of substrates were observed in the control experiments.



Scheme 1. Hydrolysis pathways of dimethoate. $\text{S}_{\text{N}}2@P$ hydrolysis reaction of dimethoate at high pH to produce O,O-dimethyl hydrogen phosphorothioate, and the $\text{S}_{\text{N}}2@C$ reaction at low pH to produce O-demethyl-dimethoate (O-methyl S-[2-(methylamino)-2-oxoethyl] hydrogen phosphorodithioate).

Table S7: Changes in concentrations (C_t/C_0) and carbon ($\delta^{13}\text{C}$) and hydrogen ($\delta^2\text{H}$) isotope ratios of dimethoate during control experiments at pH3. $\Delta\delta^{13}\text{C}$ and $\Delta\delta^2\text{H}$ refers to the changes of isotope composition during the experiment.

	time(h)	C_t / C_0	$\delta^{13}\text{C}$ (‰)	$\Delta\delta^{13}\text{C}$ (‰)	$\Delta^2\text{H}$ (‰)	$\Delta\delta^2\text{H}$ (‰)
Control for pH 7	0	1.00	-44.3 ± 0.6	0.2	-103 ± 2	-3
	195	0.98	-44.1 ± 0.1		-106 ± 2	
Control for pH 9	0	1.00	-44.3 ± 0.6	0.8	-96 ± 1	-4
	288	0.93	-43.5 ± 0.2		-100 ± 3	
Control for pH 12	0	1.00	-46.3 ± 0.0	0.2	-119 ± 2	-3
	1	1.00	-46.1 ± 0.1		-122 ± 5	

8. Definition and calculation of isotope enrichment factors

The carbon and hydrogen isotopic compositions are reported as δ values in parts per thousand (‰) relative to international standards (Pee Dee Belemnite (PDB) and Standard Mean Ocean Water (SMOW) for carbon and hydrogen, respectively) according to Eq. (1), where E indicates ^{13}C or ^2H and R indicates the isotope ratio of $^{13}\text{C}/^{12}\text{C}$ or $^2\text{H}/^1\text{H}$.

$$\delta E_{\text{sample}} = \frac{R_{\text{sample}}}{R_{\text{standard}}} - 1 \quad (1)$$

The isotope enrichment factors (ϵ) are determined from the logarithmic form of the Rayleigh equation according to Eq. (2), where δ is the measured stable isotope compositions at time t and time 0 and C is the concentration of target compound at time t and time 0.

$$\epsilon = \ln \left[\frac{(\delta_t + 1)}{(\delta_0 + 1)} \right] / \ln \left[\frac{C_t}{C_0} \right] \quad (2)$$

References

1. Wu L, Yao J, Trebse P, Zhang N, Richnow HH (2014) Compound specific isotope analysis of organophosphorus pesticides. *Chemosphere* 111:458-463. doi:10.1016/j.chemosphere.2014.04.037
2. Renpenning J, Kuemmel S, Hitzfeld KL, Schimmelmann A, Gehre M (2015) Compound-Specific Hydrogen Isotope Analysis of Heteroatom-Bearing Compounds via Gas Chromatography-Chromium-Based High-Temperature Conversion (Cr/HTC)-Isotope Ratio Mass Spectrometry. *Anal Chem* 87 (18):9443-9450. doi:10.1021/acs.analchem.5b02475

Appendix 6.3.

Characterizing chemical transformation of organophosphorus compounds by ^{13}C and ^2H stable isotope analysis

Published paper: *Wu, L.; Chladkova, B.; Lechtenfeld, O. J.; Lian, S.; Schindelka, J.; Herrmann, H.; Richnow, H. H., Sci. Total. Environ. 2018, 615, 20-28.*



Characterizing chemical transformation of organophosphorus compounds by ^{13}C and ^2H stable isotope analysis \star



Langping Wu^a, Barbora Chládková^{a,1}, Oliver J. Lechtenfeld^b, Shujuan Lian^a, Janine Schindelka^c, Hartmut Herrmann^c, Hans H. Richnow^{a,*}

^a Department of Isotope Biogeochemistry, Helmholtz Centre for Environmental Research-UFZ, Permoserstraße 15, 04318 Leipzig, Germany

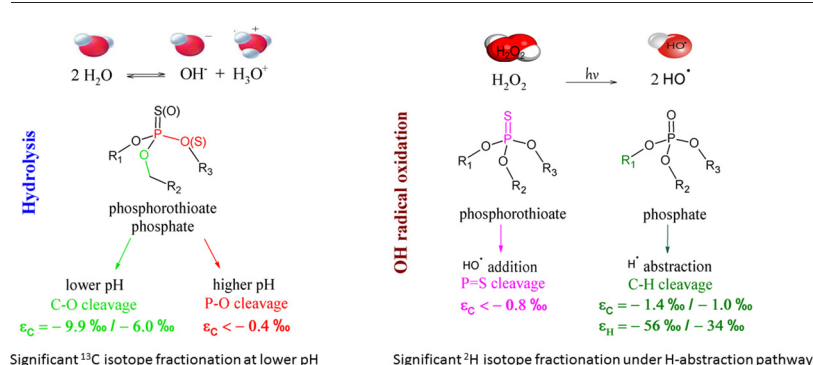
^b Department of Analytical Chemistry, Helmholtz Centre for Environmental Research-UFZ, Permoserstraße 15, 04318 Leipzig, Germany

^c Atmospheric Chemistry Department (ACD), Leibniz Institute for Tropospheric Research (TROPOS), Permoserstraße 15, 04318 Leipzig, Germany

HIGHLIGHTS

- Concept using C and H isotope fractionation to analyze degradation of OPs is developed.
- Isotope fractionation patterns upon hydrolysis and radical oxidation are compared.
- Dependence of isotope fractionation patterns on the chemical structure of OPs.
- Isotope fractionation pattern has potential to study the OPs in the environment.

GRAPHICAL ABSTRACT



ARTICLE INFO

Article history:

Received 9 August 2017

Received in revised form 21 September 2017

Accepted 21 September 2017

Available online xxx

Editor: D. Barcelo

Keywords:

Compound specific isotope analysis

Parathion

TCEP

Hydrolysis

Photolysis

Transformation products

ABSTRACT

Continuous and excessive use of organophosphorus compounds (OPs) has led to environmental contaminations which raise public concerns. This study investigates the isotope fractionation patterns of OPs in the aquatic environment dependence upon hydrolysis, photolysis and radical oxidation processes. The hydrolysis of parathion (EP) and methyl parathion (MP) resulted in significant carbon fractionation at lower pH (pH 2–7, $\epsilon_C = -6.9 \sim -6.0\text{‰}$ for EP, $-10.5 \sim -9.9\text{‰}$ for MP) but no detectable carbon fractionation at higher pH (pH 12). Hydrogen fractionation was not observed during any of the hydrolysis experiments. These results indicate that compound specific isotope analysis (CSIA) allows distinction of two different pH-dependent pathways of hydrolysis. Carbon and hydrogen isotope fractionation were determined during UV/ H_2O_2 photolysis of EP and tris(2-chloroethyl) phosphate (TCEP). The constant $\delta^2\text{H}$ values determined during the OH radical reaction of EP suggested that the rate-limiting step proceeded through oxidative attack by OH radical on the P=S bond. The significant H isotope enrichment suggested that OH radical oxidation of TCEP was caused by an H-abstraction during the UV/ H_2O_2 processes ($\epsilon_H = -56 \pm 3\text{‰}$). Fenton reaction was conducted to validate the H isotope enrichment of TCEP associated with radical oxidation, which yielded ϵ_H of $-34 \pm 5\text{‰}$. Transformation products of OPs during photodegradation were identified using Fourier Transform Ion Cyclotron Resonance Mass Spectrometry (FT-ICR MS). This study

\star All authors declare that there is no conflict of interest.

* Corresponding author.

E-mail address: hans.richnow@ufz.de (H.H. Richnow).

¹ Present address: Department of Polymer Engineering, Faculty of Technology, Tomas Bata University in Zlín, Vavrečkova 275, 760 01 Zlín, Czech Republic.

highlights that the carbon and hydrogen fractionation patterns have the potential to elucidate the transformation of OPs in the environment.

© 2017 Elsevier B.V. All rights reserved.

1. Introduction

Organophosphorus compounds (OPs) are often used as pesticides, warfare agents, flame retardants, plasticizers, or flotation agents. The OPs discussed in the present study are esters of phosphoric acids, thiophosphoric acids and dithiophosphoric acids forming a wide variety of phosphates, phosphorothioates, or phosphorodithioates (Fig. S1 in Supplementary material (SM)), each of them has different reactivity towards hydrolysis, oxidation and biodegradation (Pehkonen and Zhang, 2002; Singh and Walker, 2006). Many OP derivatives are associated with acute toxicity by inhibiting acetylcholinesterase (AChE) in the nervous system, hence they are used as pesticides for control of insects and other higher organisms (Colovic et al., 2013). OP pesticides are less persistent in the environment when compared with organochlorine pesticides and thus have been widely used throughout the world. However, continuous and excessive use of OPs has led to environmental contaminations which raise public concerns (EPA US, 2006).

Parathion (*O,O*-diethyl *O*-(4-nitrophenyl) phosphorothioate), also known as ethyl parathion (EP), was one of the most widely applied organophosphorus insecticides in agriculture in the past decades, and was primarily used as an insecticide on fruit, cotton, wheat, vegetables, and nut crops (FAO, 1990b). The average half-life time of EP during hydrolysis, degradation in aerobic soil and anaerobic soil are 302 days, 58 days and 21 days respectively (Kegley et al., 2016b), which leads to a huge potential for EP and its metabolic products to contaminate surface water and groundwater. Its use is banned or restricted in many countries but continues in many other developing countries including China and India, where the application is still legal for crops.

Methyl parathion (*O,O*-dimethyl-*O*-(4-nitrophenyl) phosphorothioate, MP) is structurally very similar to EP and less persistent in the environment, with an average half-life time during hydrolysis, degradation in aerobic soil and anaerobic soil of 45 days, 12 days and 1 day, respectively (Kegley et al., 2016a). Due to its severe hazardous potential classified by the Rotterdam Convention, MP is not allowed for sale and import in nearly all countries around the world (RotterdamConvention, 2004).

Tris(2-chloroethyl) phosphate (TCEP) is an anthropogenic organic compound used as flame retardant, plasticizer, and viscosity regulator in various types of polymers, and is commonly listed among a class of emerging contaminants associated with wastewater pollution of freshwater resources (Andresen et al., 2004; Stackelberg et al., 2007). TCEP is considered as almost non-biodegradable and not expected to hydrolyze significantly under environmental conditions, thus advanced oxidation processes (AOP), such as Fenton reaction and UV/H₂O₂, have been studied as a possible remediation strategy (Ou et al., 2017; Watts and Linden, 2008; Watts and Linden, 2009; Yuan et al., 2015).

Compound specific stable isotope analysis (CSIA) can provide additional information on the organic pollutants' transformation pathways in complex environments (Elsner et al., 2005; Hofstetter and Berg, 2011; Thullner et al., 2012). Previous studies have shown the potential use of stable isotope fractionation to characterize transformation mechanisms of organic compounds (Elsner, 2010; Elsner and Imfeld, 2016; Elsner et al., 2012; Nijenhuis and Richnow, 2016; Vogt et al., 2016; Wu et al., 2014), as this approach is a valuable tool to analyze the rate-limiting step in reaction mechanisms such as the mode of chemical bond cleavage (Northrop, 1981).

Hydrolysis is one pathway controlling the fate of OPs in the environment and react by a common mechanism, where H₂O and OH⁻ act as nucleophiles in a bimolecular nucleophilic substitution mechanism (S_N2 mechanism) (Pehkonen and Zhang, 2002). The esters of phosphates, phosphorothioates, and phosphorodithioates can be hydrolyzed

under acidic and alkaline conditions by two different pathways but the relative contribution of each hydrolysis pathway is pH-dependent. Photodegradation and chemical oxidation are other important degradation processes. Several studies investigated the reaction mechanisms of OPs during photodegradation, in which simultaneous pathways including oxidation of P=S to P=O, elimination of nitro group, remethylation and oxidation of the alkyl substituent were proposed (Araújo et al., 2007; Durand et al., 1994; Kanmoni et al., 2012; Sakellarides et al., 2003; Santos et al., 2005; Wu and Linden, 2008). Although several types of transformation products were typically determined, it is difficult to confirm photodegradation pathways via identified transformation products, as short-lived intermediates could be missed.

Previous studies reported OPs contamination in natural waters (Pehkonen and Zhang, 2002) and atmosphere (Kawahara et al., 2005). OP residues have been found in rain, snow, fog and air samples (Aston and Seiber, 1996). Oxidation of OPs by OH radical is likely in surface water and atmosphere (aerosols). OH radical can be generated by natural presented photosensitizers such as humic substances (Zhang et al., 2015). The photosensitizers promoted indirect photolysis is a naturally occurring degradation process. It may be an important factor governing the fate of organic contaminants in the environment. The multi-isotope fractionation pattern allows characterize the bond cleavage mechanisms of photosensitization, and is thus a valuable tool for studying the fate of OPs in surface waters and atmospheric media containing photosensitizers.

The main objective of this study is to evaluate the carbon and hydrogen isotope fractionation patterns associated with hydrolysis and photolysis which are considered to be important chemical transformation reactions of OPs in the environment. We selected EP, MP and dimethoate (Wu et al., 2017) as model compounds of phosphorothioates and phosphorodithioates representing typical esters of phosphoric acids and analyzed the carbon and hydrogen isotope fractionation patterns upon hydrolysis at various pH values to study the different mode of hydrolysis by CSIA. Radical oxidation and photolysis of EP (model of phosphorothioates) were investigated to compare isotope fractionation patterns with those obtained from hydrolysis. In addition, OH radical oxidation of TCEP (model of phosphate) by Fenton reaction (the iron catalyzed hydrogen peroxide) and via indirect photolysis (UV/H₂O₂) was performed to understand the isotope fractionation associated by an H-abstraction step. The transformation products were further identified using Fourier Transform Ion Cyclotron Resonance Mass Spectrometry (FT-ICR MS) to analyze the transformation mechanisms.

2. Materials and methods

2.1. Chemicals

Parathion (*O, O*-diethyl *O*-(4-nitrophenyl) phosphorothioate, purity >99.7%), methyl parathion (*O, O*-dimethyl-*O*-(4-nitrophenyl) phosphorothioate; purity > 99.8%), TCEP (tris(2-chloroethyl) phosphate, purity > 97.0%) and dichlorvos (2,2-dichlorovinyl dimethyl phosphate, purity >98.8%) were purchased from Sigma-Aldrich (Munich, Germany) and used without further purification. Tributyl phosphate (TBP, purity 99%) was purchased in Xiya Company in China. Hydrogen peroxide (30% w/w) was supplied by Merck (Darmstadt, Germany).

2.2. Hydrolysis experiment

Hydrolysis of EP and MP were carried out at up to 60 °C (to reduce the reaction time) in 100 mM phosphate buffer solution at pH 2, pH 5, pH 7,

pH 9 and pH 12, respectively. All experiments were conducted as batch experiments in 100 mL buffer solution, with an initial concentration of 24 mg L^{-1} for EP and 50 mg L^{-1} for MP. At different time intervals, the hydrolysis was stopped by adjusting the whole 100 mL aqueous sample to pH 7 using 6 N HCl or 5 M NaOH. The residues of EP and MP were extracted by 2 mL dichloromethane containing 400 mg L^{-1} of dichlorvos as internal standard, shaking at 180 rpm for 2 h. Afterwards, the organic phase was transferred into 2 mL vials for concentration and isotope analysis.

2.3. Direct photolysis and OH radical reaction

The photolysis of EP was conducted in a photochemical reactor system consisting of a 2 L Pyrex cylindrical flask and a circulating water system. Irradiation was achieved using a 150-W xenon lamp as the light source (Type L2175, wavelength: 185–2000 nm, Hamamatsu, Japan). The light spectrum is shown in Fig. S2. A filter with a 280 nm cut-off wavelength (Schott WG 280 long pass filter, 3.15 mm thick, Galvoptics Ltd., United Kingdom) was applied to provide emission spectrum with wavelengths $\geq 280 \text{ nm}$ typical of the sun at the Earth's surface. All EP experiments were conducted in phosphate buffer (10 mM, pH 7) at 25°C , with initial concentration of 10 mg L^{-1} . For the OH radical oxidation experiments, 30% H_2O_2 was used to obtain initial molar ratio of H_2O_2 : EP to 500:1. The direct photolysis of EP was performed at the same conditions without H_2O_2 and without 280 nm filter as EP has maximum absorption at 277 nm in MilliQ water and maximum absorption at 289 nm in phosphate buffer (Fig. S3). Dark control experiments were conducted in the same system without UV irradiation.

The OH radical reaction of TCEP was conducted in the same photochemical reactor system as for EP, but using a 200 mL Pyrex cylindrical flask. All TCEP experiments were conducted in phosphate buffer (100 mM, pH 7) at 20°C , with initial concentration of 500 mg L^{-1} , 30% H_2O_2 was used to obtain initial molar ratio of H_2O_2 : TCEP to 50:1. Dark control experiments were conducted in the same system without UV irradiation in order to investigate the oxidation of TCEP by H_2O_2 . Another control experiment was performed at the same condition but without H_2O_2 in order to investigate the direct photolysis of TCEP. More detailed information is described in SM.

2.4. Fenton reaction

The OH radical oxidation by Fenton reaction of TCEP was investigated at room temperature in 200 mL well-stirred phosphate buffer (100 mM, pH 3) with an initial molar ratio of TCEP: H_2O_2 : FeSO_4 to 1:50:10. The initial concentration of TCEP was 500 mg L^{-1} . To attain homogeneous reaction, required amount of TCEP and Fe^{2+} stock solution was first dissolved into buffer and stirred for 30 min. The Fenton reaction was then initiated by sequential addition of 1.8 mL of 30% H_2O_2 (30 min sequencing intervals). The solution was continuously mixed at 400 rpm during 2-h reaction. At 30 min intervals, 10 mL of aqueous sample was taken for the extraction of TCEP residues by adding 0.5 mL of dichloromethane containing 2000 mg L^{-1} TBP as internal standard and shaken at 180 rpm at 4°C for 2 h. The excessed OH radicals were quenched by an addition of 1 mL of isopropanol to stop the reaction during extraction procedure.

2.5. Analytical methods

2.5.1. Concentration determination

An Agilent 6890 series GC (Agilent Technologies, USA) equipped with a flame ionization detector (FID) was used to determine the concentration throughout the study. Analytes were separated in an HP-5 column ($30 \text{ m} \times 320 \mu\text{m} \times 0.25 \mu\text{m}$, Agilent 19091J-413, USA) with helium flow of 1.5 mL min^{-1} as the carrier gas. The oven was first held at 60°C for 2 min, then increased at $10^\circ\text{C min}^{-1}$ to 160°C , at 5°C min^{-1} to 220°C , and finally at $15^\circ\text{C min}^{-1}$ to 280°C and held for 2 min. Each TCEP sample containing internal standard was measured once with a

split ratio of 50:1, EP and MP samples were measured with a split ratio of 10:1.

2.5.2. Isotope analysis

The carbon and hydrogen isotope compositions were analyzed by gas chromatograph-combustion-isotope ratio mass spectrometer (GC-C-IRMS) and gas chromatograph chromium based high temperature conversion-isotope ratio mass spectrometer (GC-Cr/HTC-IRMS) system using the same methods as described by Wu et al. (2017) but with modifications on oven temperature programs: the column was initially held at 60°C for 2 min, ramped at 8°C min^{-1} to 280°C , and then held for 2 min. All samples were run in triplicates and errors are reported in SM. All hydrogen isotope results were calibrated by two-point calibration against two reference compounds using hexadecane A ($\delta^2\text{H} = -167\text{‰}$) and hexadecane B ($\delta^2\text{H} = -11\text{‰}$) which were described elsewhere (Renpenning et al., 2015). The quantification of isotope fractionation was evaluated by isotope enrichment factors (ϵ) using Rayleigh equation which is reported previously (Elsner et al., 2005; Hofstetter et al., 2008) and described briefly in SM.

2.5.3. Transformation product analysis

Transformation products of EP and TCEP during photodegradation were tentatively identified analyzing the precise mass via ultra-high resolution FT-ICR MS (Solarix XR 12 T, Bruker Daltonics) based on accurate masses allowing calculating elemental compositions of ions. 10 mL of aqueous solution was extracted by solid phase extraction (SPE) using Bond Elut PPL cartridges (50 mg, Agilent). The SPE extraction procedures followed the manufacturer guidelines and the transformation products were eluted with 0.5 mL methanol. The methanolic extract was diluted 1:100 or 1:1000 (v/v) with MilliQ water/MeOH (1:1, v/v) before analysis. A FT-ICR MS equipped with a dynamically harmonized analyzer cell was used for the analysis of the methanolic extracts. Samples were measured with positive and negative mode electrospray ionization in direct infusion mode with a 4 MWord time domain using typical electrospray ionization (ESI) conditions. For each sample, 16 (TCEP) or 128 to 256 scans (EP, 10–100 ms ion accumulation time) were co-added in a range of 73–3000 m/z and the spectra externally calibrated with fatty acids present in the samples between m/z 83 and m/z 353. The high mass accuracy and resolution (450,000 at m/z 200) allowed for a tentative assignment of possible transformation products via their exact mass and calculated molecular formulas where the molecular formulas of the parent compounds were used as an upper element limit for the calculation. For further method details, refer to the SM.

3. Results and discussion

3.1. Isotope fractionation patterns of EP and MP during hydrolysis

More than 90% of MP and EP were hydrolyzed in phosphate buffer at pH 2–12 and C and H isotope ratios were analyzed (Fig. 1). The hydrolysis of MP and EP is a homogeneous reaction following pseudo-first-order kinetics (Fig. S6), the rate constants under all examined conditions are shown in Table 1. As shown in Fig. 1, significant C isotope fractionation was observed during MP hydrolysis at lower pH and could be quantified by the Rayleigh model, corresponding to isotope enrichment factors of $\epsilon_C = -10.0 \pm 0.7\text{‰}$ at pH 2, $\epsilon_C = -10.5 \pm 1.1\text{‰}$ at pH 5 and $\epsilon_C = -9.9 \pm 0.7\text{‰}$ at pH 7. The C isotope fractionation upon EP hydrolysis corresponding to isotope enrichment factors of $\epsilon_C = -6.9 \pm 0.8\text{‰}$ at pH 2, $-6.7 \pm 0.4\text{‰}$ at pH 5 and $-6.0 \pm 0.2\text{‰}$ at pH 7 were described by the Rayleigh model as well. Smaller but significant C isotope fractionation corresponding to isotope enrichment factor of $\epsilon_C = -6.5 \pm 0.4\text{‰}$ for MP and $\epsilon_C = -3.5 \pm 0.4\text{‰}$ for EP were observed during hydrolysis at pH 9, however, no C isotope fractionation was observed for both MP and EP hydrolysis at pH 12, indicating a different pathway.

The reduction of C isotope fractionation by almost 50% at pH 9 suggests compared to neutral conditions that two pathways of hydrolysis

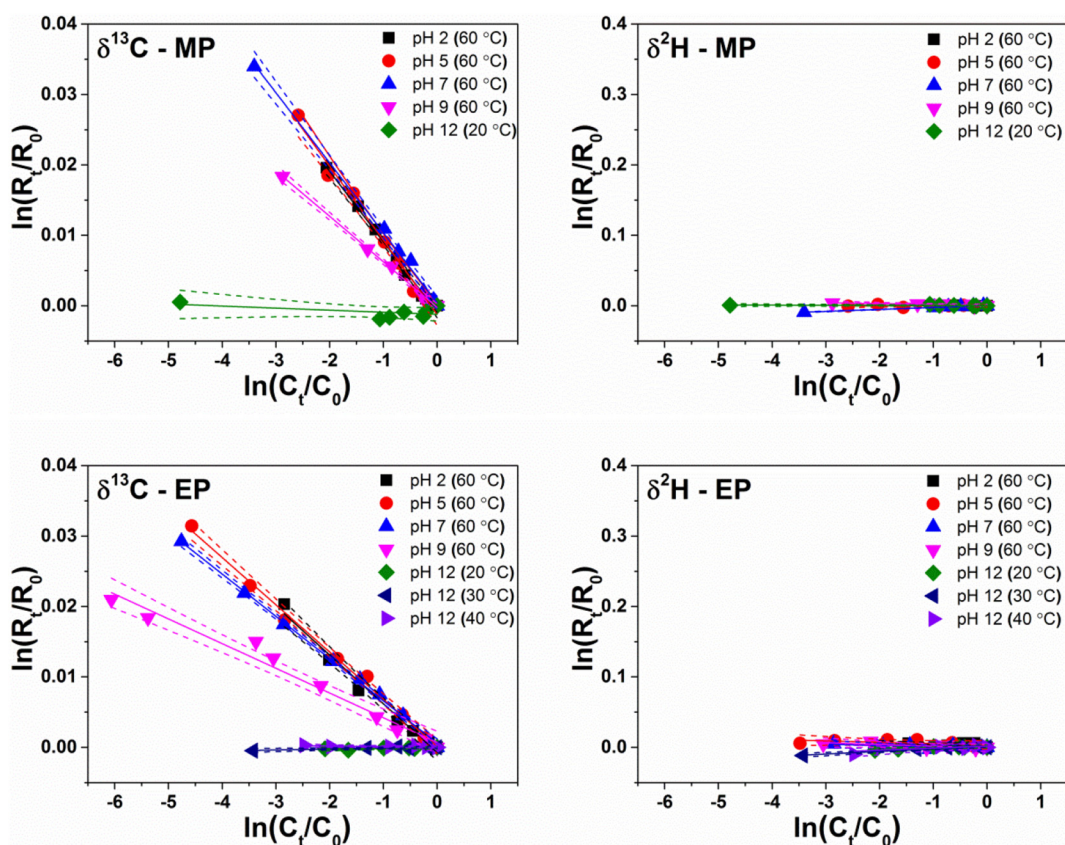


Fig. 1. Rayleigh plots for Carbon and hydrogen stable isotope fractionation of EP and MP during hydrolysis at different pH. Dashed lines indicate the 95% confidence intervals. The ϵ values were reported in Table 1.

take place. If a substrate is being degraded via two competing pathways and following first-order kinetics, the rate ratio (F) of two competing pathways can be calculated from the observed isotope enrichment factor and the isotope enrichment factors associated with the two pathways. The extended Rayleigh-type equation derived by Van Breukelen (2007) was employed to calculate the contribution of each pathway. According to the calculation (described in SM), MP hydrolysis at pH 9 has a contribution of 62–66% compared to the reaction pathway under acidic

condition, while EP hydrolysis at pH 9 has a contribution of 51–58% compared to the pathway under acidic condition.

Furthermore, we did not observe significant changes in H isotope ratios of MP and EP during hydrolysis at any pH, indicating no H bond cleavage is involved during the rate limiting step of the hydrolysis. The combination of negligible H and significant C isotope fractionation indicates that hydrolysis under acidic and neutral conditions undergoes the same transformation mechanism which involves C bond cleavage.

Table 1

Summary of the reaction rate constants (k), isotope enrichment factors (ϵ), and the 95% confidence intervals (CI 95%) for chemical transformation of OPs.

Reaction	T (°C)	$K (\times 10^{-5} \text{ s}^{-1})$	R^2	$t_{1/2}$ (h)	$\epsilon_C \pm 95\% \text{CI} (\%)$	R^2	$\epsilon_H \pm 95\% \text{CI} (\%)$	R^2
hydro_dime_pH7 ^a	60	0.57	0.999	37.7	-8.3 ± 0.3	0.998	n.d.	
hydro_dime_pH9 ^a	30	0.35	0.999	56.3	-1.4 ± 0.1	0.987	-10 ± 3	0.924
hydro_dime_pH12 ^a	4	121.31	0.997	0.2	-0.4 ± 0.1	0.950	-10 ± 5	0.901
hydro_MP_pH 2	60	0.78	0.993	23.2	-10.0 ± 0.7	0.995	n.d.	
hydro_MP_pH 5	60	1.00	0.997	17.3	-10.5 ± 1.1	0.989	n.d.	
hydro_MP_pH 7	60	1.36	0.995	16.2	-9.9 ± 0.7	0.997	n.d.	
hydro_MP_pH 9	60	1.53	0.995	13.0	-6.5 ± 0.4	0.998	n.d.	
hydro_MP_pH 12	20	5.58	0.999	3.7	n.d.	n.d.	n.d.	
hydro_EP_pH 2	60	0.25	0.997	70.1	-6.9 ± 0.8	0.985	n.d.	
hydro_EP_pH 5	60	0.28	0.996	71.8	-6.7 ± 0.4	0.996	n.d.	
hydro_EP_pH 7	60	0.31	0.997	74.9	-6.0 ± 0.2	0.999	n.d.	
hydro_EP_pH 9	60	0.42	0.995	49.5	-3.5 ± 0.4	0.976	n.d.	
hydro_EP_pH 12	20	0.64	0.993	27.3	n.d.	n.d.	n.d.	
hydro_EP_pH 12	30	2.19	0.993	8.3	n.d.	n.d.	n.d.	
hydro_EP_pH 12	40	7.92	0.991	2.8	n.d.	n.d.	n.d.	
UV/no filter_EP	25	0.36	0.976	72.8	-0.6 ± 0.1	0.979	n.d.	
UV/H ₂ O ₂ _EP	25	4.61	0.992	4.4	-0.8 ± 0.1	0.993	n.d.	
UV/H ₂ O ₂ _TCEP	20	7.86	0.999	2.6	-1.4 ± 0.1	0.996	-56 ± 3	0.997
Fenton_TCEP	25	35.75	0.908	0.6	-1.0 ± 0.2	0.982	-34 ± 5	0.986

hydro is short for "hydrolysis"; dime is short for "dimethoate"; n.d. is short for "not determined".

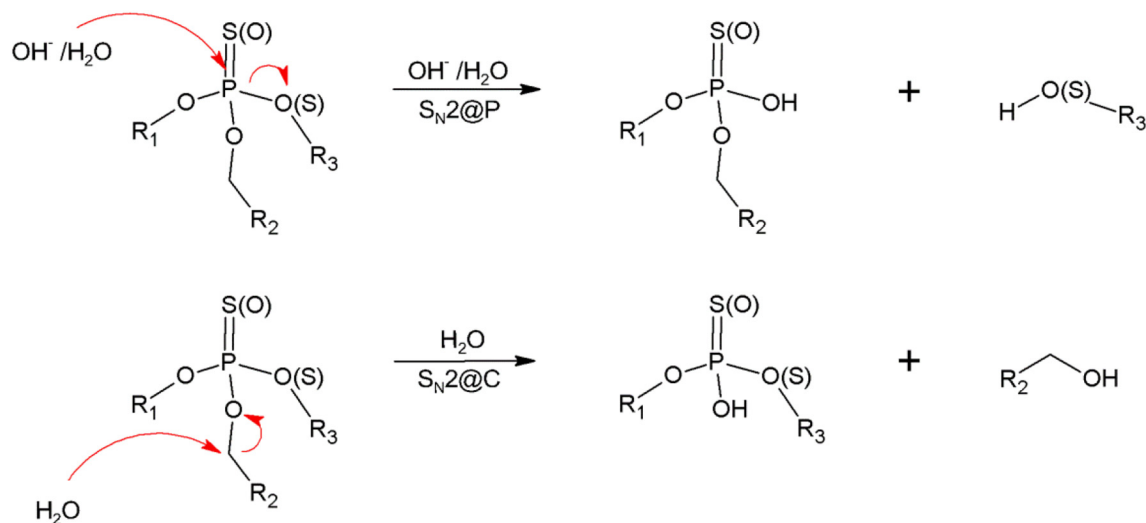
^a Experimental details and results of hydrolysis of dimethoate are reported by Wu et al. (2017).

Transformation mechanism changes under strong alkaline condition, suggesting no C bond cleavage in the rate limiting step at pH 12. Thus, C isotope fractionation can be used to distinguish different types of hydrolysis of MP and EP. The observed similar isotope fractionation patterns during the hydrolysis suggest the same transformation mechanisms for MP and EP. The smaller ϵ_C obtained in EP hydrolysis at the same pH can be explained by isotope dilution effects, as EP molecules contain two more carbon atoms in comparison to MP molecules.

3.2. Exploring the hydrolysis mechanisms of OPs

General hydrolysis pathways of OPs were proposed in Scheme 1. Two pathways have been reported previously for EP hydrolysis (Wanamaker et al., 2013). The previous reported pathways can be characterized by isotope fractionation analysis. Under acidic/neutral conditions, the product O-ethyl O-(4-nitrophenol) hydrogen phosphorothioate is formed through C—O bond cleavage, which results in a significant C isotope enrichment. The major transformation products of 4-nitrophenol and O, O-diethyl hydrogen phosphorothioate at higher pH suggest a P—O bond cleavage which supports our interpretation that no C isotope fractionation is observed at pH 12 due to no C bond cleavage in the rate limiting step of the reaction. An enrichment factor of $\epsilon_C = -3.5 \pm 0.4\%$ obtained during hydrolysis at pH 9 indicates that two hydrolysis pathways of EP are active simultaneously. The P—O bond cleavage has no effect on isotope composition of EP and lower the isotope fractionation contributed from the O—C bond cleavage mechanism. No H isotope fractionation is observed during EP hydrolysis at any pH since no H bond cleavage is involved in the rate determining step of the first irreversible reaction.

The similar hydrolysis pathways are reported for MP, where the dominant product of acid hydrolysis is O-methyl O-(4-nitrophenol) hydrogen phosphorothioate while under alkaline hydrolysis the main product is 4-nitrophenol (FAO, 1990a). The interpretation of the reaction mechanisms suggested in former studies appears to be consistent with the isotope fractionation results of the present study: O-methyl O-(4-nitrophenol) hydrogen phosphorothioate is formed through C—O bond cleavage during acid hydrolysis, leading to significant C isotope enrichment in the remaining phase; 4-nitrophenol is produced through P—O bond cleavage during alkaline hydrolysis and gives no C isotope fractionation. The same hydrolysis pathways were investigated using isotope fractionation for dimethoate in a previous study from our laboratory (Wu et al., 2017), where the enrichment factor of $\epsilon_C = -8.3 \pm 0.3\%$ at pH 7 indicated a C—O bond cleavage; and a P—S bond cleavage at pH 12 resulted in a negligible enrichment factor of $\epsilon_C = -0.4 \pm 0.1\%$.



Scheme 1. Proposed transformation mechanisms of OPs during hydrolysis at different pH. Hydrolysis of OPs can occur via two pathways: attack by OH^- and H_2O at the phosphorus atom at high pH and attack by H_2O at the α carbon of the alkoxy group at low pH. R_1 and R_2 are predominantly aryl or alkyl group. R_3 can be diverse and may belong to a wide range of aliphatic, aromatic or heterocyclic group.

In summary, we propose two general hydrolysis pathways of OPs including phosphates, phosphorothioates and phosphorodithioates (Scheme 1): one is P—O (S) bond cleavage by nucleophilic attack at the phosphorus atom, resulting in no C (and H) isotope fractionation; another one is C—O bond cleavage by nucleophilic attack at the carbon atom, resulting in a significant C (and no H) isotope fractionation. Therefore, C isotope fractionation can be used to distinguish different hydrolysis pathways of OPs.

3.3. Isotope fractionation patterns of EP during direct photolysis and OH radical reaction

EP shows a maximum absorption at 289 nm when dissolved in phosphate buffer (Fig. S3). Up to 99% of EP was converted slowly after 359 h during direct photolysis without applying a 280 nm cut-off filter. The same amount of EP was transformed much faster, within 23 h, during the indirect photolysis ($\text{UV}/\text{H}_2\text{O}_2$) at wavelengths above 280 nm. The obtained rate constants of $0.36 \times 10^{-5} \text{ s}^{-1}$ with R^2 of 0.976 for direct photolysis and $4.61 \times 10^{-5} \text{ s}^{-1}$ with R^2 of 0.992 for indirect photolysis indicate that photolysis and the OH radical oxidation of EP follows pseudo-first-order kinetics (Fig. S8). C isotope fractionation associated with direct photolysis and OH radical reaction of EP was low but still could be quantified by the Rayleigh model. The $\delta^{13}\text{C}$ was enriched by 2.8‰ after >99% of EP degradation during direct photolysis, corresponding to a ϵ_C of $-0.6 \pm 0.1\%$ (Fig. 2). The $\delta^{13}\text{C}$ only enriched by 1.5‰ after >98% of EP conversion during OH radical oxidation induced by $\text{UV}/\text{H}_2\text{O}_2$ photolysis, corresponding to a ϵ_C of $-0.8 \pm 0.1\%$ (Fig. 2). No detectable H isotope fractionation was observed during both experiments of EP, suggesting no H bond breaking occurs.

3.4. Isotope fractionation patterns of TCEP during OH radical reaction

TCEP is transparent in the wide range of 200–800 nm wavelengths (Fig. S3) and thus has no potential to harvest light for direct photolysis. The OH radical oxidation and corresponding C and H isotope fractionation of TCEP was investigated using $\text{UV}/\text{H}_2\text{O}_2$ and Fenton reagents $\text{FeSO}_4/\text{H}_2\text{O}_2$, respectively. In the $\text{UV}/\text{H}_2\text{O}_2$ system, the $\delta^{13}\text{C}$ value of TCEP was enriched from $-31.5 \pm 0.2\%$ to $-26.3 \pm 0.3\%$ after 13 h (97% of degradation) and $\delta^2\text{H}$ value was enriched from $-25 \pm 5\%$ to $185 \pm 5\%$ (Fig. S9). Rate constant of $7.86 \times 10^{-5} \text{ s}^{-1}$ with R^2 of 0.999 indicates a pseudo-first-order kinetic reaction (Fig. S8). The C and H isotope fractionation can be quantified by the Rayleigh equation yielding a small ϵ_C of $-1.4 \pm 0.1\%$, and a large ϵ_H of $-56 \pm 3\%$. The hydrogen

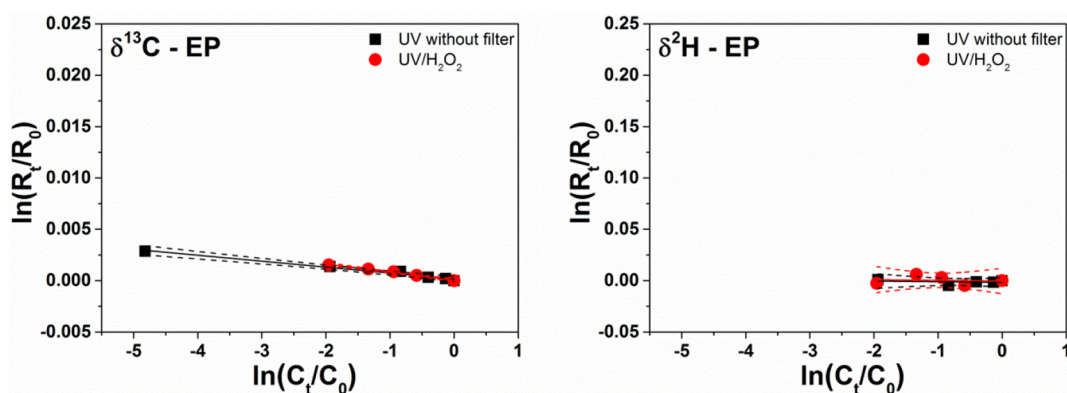


Fig. 2. Rayleigh plots for carbon and hydrogen stable isotope fractionation of EP during direct photolysis (without filter) and OH radical reaction (UV/H₂O₂). Dashed lines indicate the 95% confidence intervals. No hydrogen isotope fractionation was obtained. The ϵ_c values were reported in Table 1.

and carbon fractionation are linearly correlated yielding a dual isotope enrichment factor (Λ) of 43 ± 5 (Fig. 3). Λ is the slope of the linear relationship of isotope composition shifts of both elements ($\Delta\delta^2\text{H}$ vs $\Delta\delta^{13}\text{C}$), expressed as $\Lambda = \Delta\delta^2\text{H}/\Delta\delta^{13}\text{C}$, where $\Delta\delta^2\text{H} = \delta^2\text{H}_t - \delta^2\text{H}_0$, $\Delta\delta^{13}\text{C} = \delta^{13}\text{C}_t - \delta^{13}\text{C}_0$. The control experiment without adding H₂O₂ clearly showed no loss of TCEP after 136 h, indicating that no direct photolysis of TCEP occurred.

Fenton reaction of TCEP is a pseudo-first-order kinetic reaction too. The $\delta^{13}\text{C}$ value was enriched from $-29.4 \pm 0.3\%$ to $-26.2 \pm 0.2\%$ and $\delta^2\text{H}$ was enriched from $-28 \pm 3\%$ to $87 \pm 4\%$ after 96% degradation (Fig. S9), yielding a fractionation factor of ϵ_c of $-1.0 \pm 0.2\%$ and ϵ_H of $-34 \pm 5\%$. The hydrogen and carbon fractionation are linearly correlated by a Λ factor of 35 ± 5 (Fig. 3).

3.5. Exploring the OH radical reaction mechanisms of OPs

The FT-ICR MS analysis was used to identify photodegradation products of EP and TCEP to confirm proposed OP transformation pathways using transformation products patterns. Photodegradation of EP yielded five major transformation products (Table S1). The rate-limiting step of photodegradation of EP involves OH radical addition to the central phosphorus atom to yield an phosphorenyl radical, this OH adduct radical may be prone to stabilization by two different pathways as illustrated in Scheme 2a: (A) stabilization by the elimination of sulfhydryl radical to produce P=O bond to form Paraoxon (P1) (C₁₀H₁₄NO₆P, *m/z* pos: 276.0632) which was one of the major products determined in the reaction solution. Previous studies shows that the oxidative attack of the OH

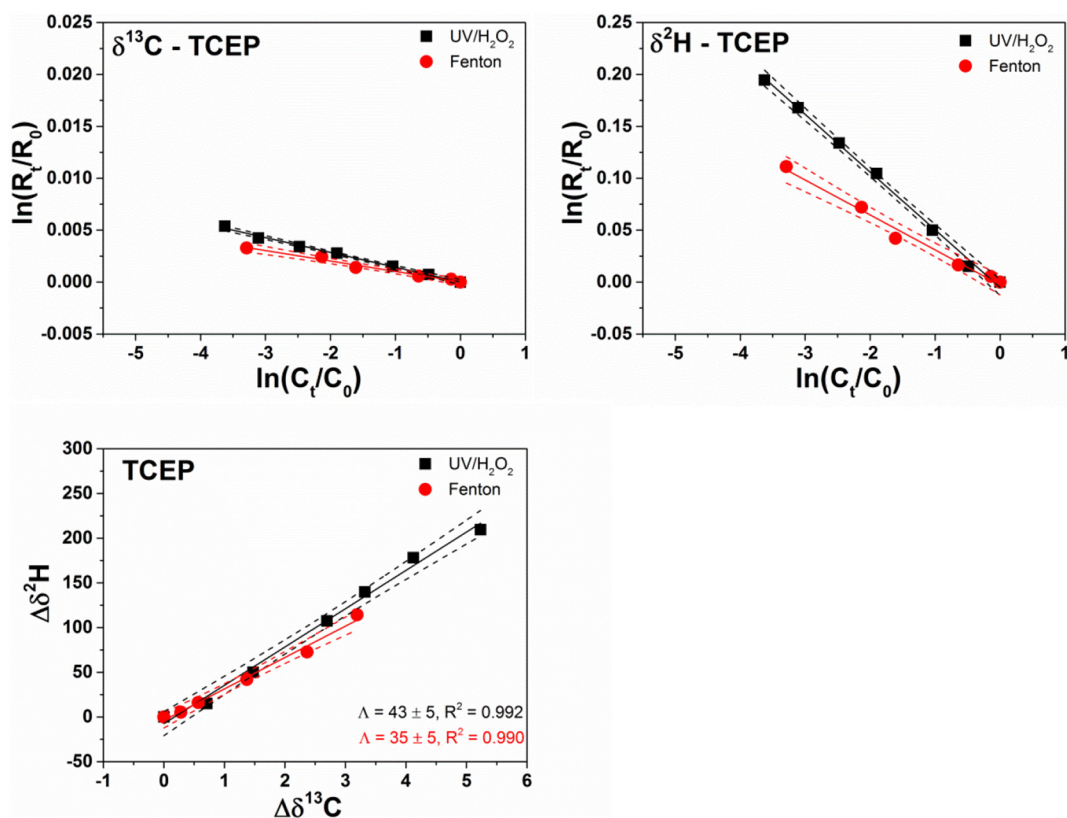
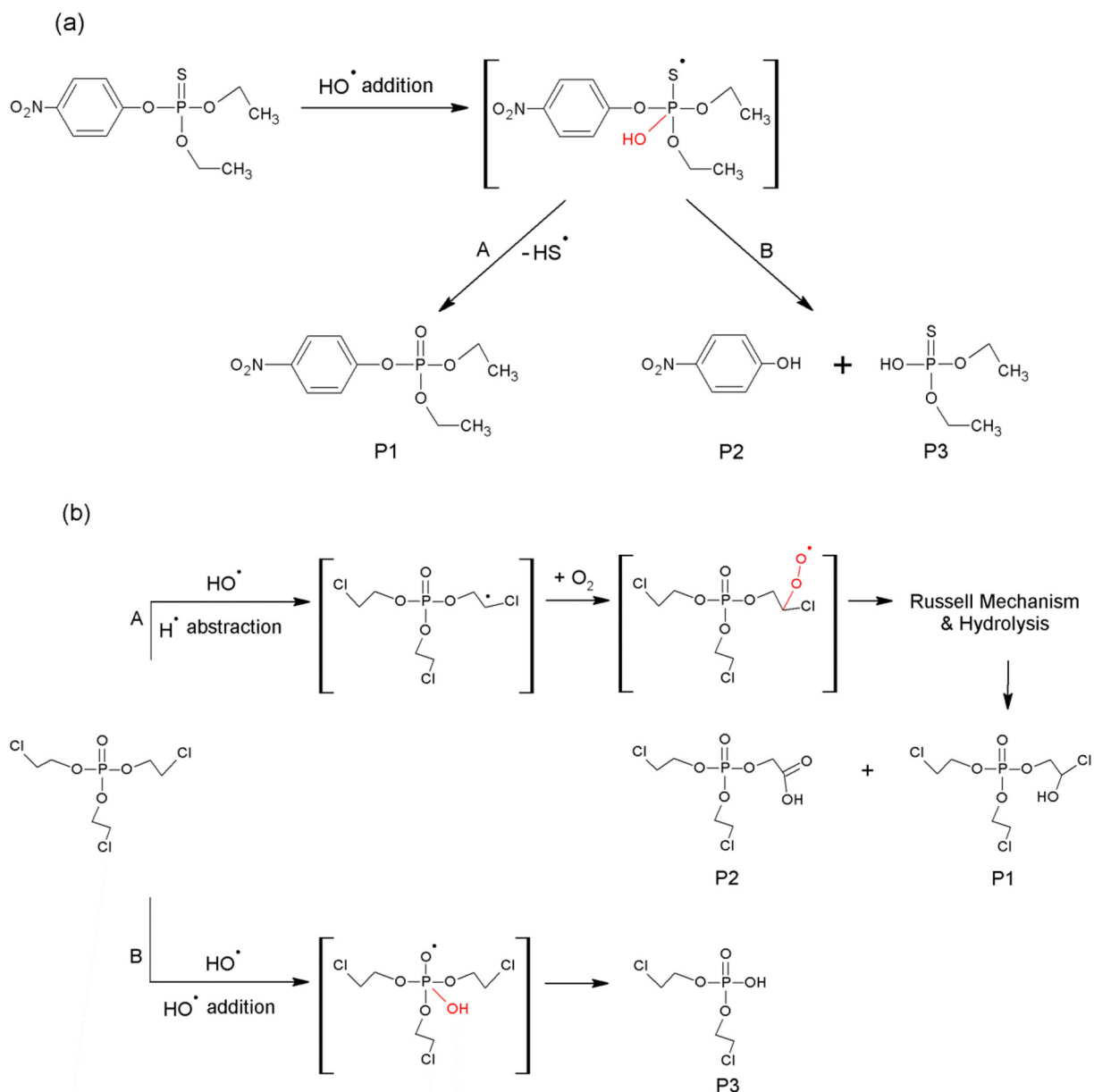


Fig. 3. Rayleigh plots quantifying ²H and ¹³C fractionation of TCEP and the correlation of ²H and ¹³C fractionation during OH radical oxidation by UV/H₂O₂ and Fenton reaction. Dashed lines indicate the 95% confidence intervals. The ϵ_c and ϵ_H values were reported in Table 1.



Scheme 2. Proposed transformation mechanisms of OH radical reaction with EP (a) and TCEP (b). Scheme 2a illustrates the rate-limiting step of the photodegradation of EP, which involves OH radical addition to the central phosphorus atom and stabilized by two different pathways: (A) the elimination of sulfhydryl radical to produce P=O bond to form paraoxon (P1); (B) the elimination of nitrophenol from the phosphoric center to form P2 and P3. Scheme 2b illustrates the first step reactions of TCEP may simultaneously occur over two different pathways: (A) involves hydrogen abstraction by OH radical, followed by oxygen addition and then undergo Russell Mechanism and hydrolysis to form P1 and P2; (B) involves OH radical addition to the central phosphorus atom, followed by the elimination of an ethyl chlorine arm from the phosphoric center to form P3.

radicals on the P=S bond occurs firstly in the case of phosphorothioates, such as dichlofenthion (Konstantinou et al., 2001), pirimiphos-methyl (Herrmann et al., 1999), fenitrothion (Kerzhentsev et al., 1996) and dimethoate (Evgenidou et al., 2006). Wu and colleagues studied desulfurization of phosphorothioate and proposed that the sulfur atom can be replaced by an oxygen atom via a radical mechanism (Wu et al., 2012). (B) Stabilization by the elimination of nitrophenol from the phosphoric center to form P2 ($C_6H_5NO_3$, m/z neg: 138.0197) and P3 ($C_4H_{11}O_3PS$, m/z neg: 169.0094). The subsequent reaction of Paraoxon (P1) may lead to the formation of P2 and P4 ($C_4H_{11}O_4P$, m/z neg: 153.0322) through a P—O bond cleavage.

Transformation product analysis showed no difference between direct photolysis and OH radical oxidation of EP, indicating the same transformation mechanisms starting with the oxidation of the sulfur. The proposed mechanisms are consistent with isotope fractionation results, as no significant C or H isotope fractionation was observed (Fig. 2). Wu

and Linden proposed a third pathway where a hydroxyl radical attacks the nitrophenyl bond which results in a formation of *O,O*-diethyl-phenyl thiophosphate (Wu and Linden, 2008). The observed ϵ_c of $-0.6 \pm 0.1\%$ from direct photolysis and ϵ_c of $-0.8 \pm 0.1\%$ from OH radical oxidation (Fig. 2, Table 1) are too small to be indicative of C—N bond cleavage. In addition, P5 (*O,O*-diethyl phenyl thiophosphate, $C_{10}H_{15}O_3PS$) with expected m/z pos: 247.0552 or m/z neg: 245.0407 was not detected as a transformation product by FT-ICR MS analysis in the present study.

Eight transformation products (P1 to P8) were detected in the photodegradation of TCEP using UV/ H_2O_2 , the tentative structure of the products are shown in Table S2. Scheme 2b illustrates the proposed first step transformation of TCEP during OH radical reaction. Pathway A involves hydrogen abstraction from the alkyl-C position by OH radical to produce carbon-centered radical, which is followed by oxygen addition to generate the peroxy radical. Peroxy radicals typically undergo a bimolecular Russell Mechanism (Miyamoto et al., 2003) leading to

the corresponding alcohol, P1 ($C_6H_{12}Cl_3O_5P$, m/z pos (Na): 322.9380), and aldehyde which are expected to be readily hydrolyzed to P2 ($C_6H_{11}Cl_2O_6P$, m/z neg: 278.9598). Pathway B involves OH radical addition to the central phosphorus atom to yield an oxygen-centered phosphorenyl radical, which is followed by the elimination of an ethyl chlorine arm from the phosphoric center to form P3 ($C_4H_9Cl_2O_4P$, m/z neg: 220.9543). In addition, P4 ($C_6H_{13}Cl_2O_5P$, m/z neg: 264.9805) was detected with a lower intensity compared to other transformation products, which is likely formed by the hydrolysis of TCEP resulting a substitution of one chlorine terminal by a carboxyl. Further breakdown products formed in subsequent reactions are found (P5 to P8 see SM) which are not discussed in this study.

Hydrogen abstraction and addition-elimination are the primary mechanisms for the photocatalytic oxidation of dimethyl methylphosphonate (DMMP) via hydroxyl radical attack (Aguila et al., 2001; O Shea et al., 1997). Similar mechanisms are proposed for the degradation of TCEP via persulfate radical attack (Ou et al., 2017). The significant isotope fractionation of TCEP of $\epsilon_H = -56 \pm 3\%$ combined with $\epsilon_C = -1.4 \pm 0.1\%$ suggests a C—H bond cleavage, which supports the H abstraction mechanism as well.

Our results suggest that the major reaction mechanisms of OPs during OH radical reaction are related to their chemical structures as illustrated in Scheme 2: (1) The P=S bond is oxidized to P=O in case of phosphorothioate structure (e.g. EP) in the rate determining step yielding very low or no carbon and hydrogen fractionation in contrast to (2) C—H bond breaking through H abstraction step in case of phosphate structure substitution by alkyl groups (e.g. TCEP). These two major chemical structures-dependent reaction mechanisms of OPs can be distinct when applying C and H isotope fractionation approach diagnostically.

4. Conclusions

Carbon and hydrogen stable isotope fractionation can be used diagnostically to characterize degradation pathways of phosphates, phosphorothioates and phosphorodithioates which are core structural elements of large variety of OPs. The variation of carbon isotope fractionation pattern has a potential for characterizing different modes of hydrolysis. The hydrogen isotope fractionation is low when a P—O(S) bond in phosphates, phosphorothioates and phosphorodithioates is hydrolyzed. The characteristic isotope fractionation upon hydrolysis may be used for evaluation of remediation approaches using alkaline hydrolysis in contaminated groundwater (LRSB L, 2014; Nielsen et al., 2014), whereas the isotope fractionation pattern of the residual fraction may give information about which mode of hydrolysis was at work. The isotope fractionation may be used to characterize hydrolytic reaction in plumes of contaminated aquifers or in the vicinity of industrial dump sites.

In case of OH radical oxidation or direct photolysis, cleavage of a C—H bond can lead to a characteristic correlation of hydrogen and carbon fractionation for exploring predominant degradation pathways in surface water bodies or in aerosols. However, phosphorothioates and phosphorodithioates will become desulfurized in the rate limiting step not yielding a larger isotope fractionation which limits the CSIA concept for tracing the process under environmental conditions. Possible radical oxidation reaction cannot be analyzed by 2H and ^{13}C fractionation when the degradation process is initiated with a desulfurization step in the first irreversible reaction which is a clear limitation for the multi isotope fractionation analysis. Thus, the isotope fractionation might be used for evaluating In Situ Chemical Oxidation (ISCO) of phosphate derivatives but has limitation for phosphorothioates and phosphorodithioates.

Hydrolysis and oxidation are concerned to be major degradation pathways for OPs. Our systematic study on 2H and ^{13}C fractionation of OPs shows the potential for analyzing chemical degradation reactions in aquatic environments using the isotope fractionation concept. For further exploring the diagnostic potential of tracing reaction mechanisms in the environment using isotope fractionation, systematic studies on

microbial degradation are needed and 2H and ^{13}C fractionation patterns need to be compared with those of chemical transformation reactions.

Acknowledgments

Langping Wu and Shujuan Lian are financially supported by the China Scholarship Council (File No. 201306460007 and 201404910520). Barbora Chládková was financially supported by Tomas Bata University in Zlín Internal Grant IGA/FT/2017/008. The authors are grateful for using the analytical facilities of the Centre for Chemical Microscopy (ProVIS) at the Helmholtz Centre for Environmental Research, Leipzig which is supported by the European Regional Development Funds (EFRE - Europe funds Saxony) and the Helmholtz Association. We are thankful to M. Gehre and S. Kümmel for support in the Isotope Laboratory of the Department of Isotope Biogeochemistry and for the support by the graduate school of the UFZ (HIGRADE).

Appendix A. Supplementary data

Supplementary data to this article can be found online at <https://doi.org/10.1016/j.scitotenv.2017.09.233>.

References

- Aguila, A., O'Shea, K.E., Tobien, T., Asmus, K.D., 2001. Reactions of hydroxyl radical with dimethyl methylphosphonate and diethyl methylphosphonate. A fundamental mechanistic study. *J. Phys. Chem. A* 105, 7834–7839.
- Andresen, J.A., Grundmann, A., Bester, K., 2004. Organophosphorus flame retardants and plasticisers in surface waters. *Sci. Total Environ.* 332, 155–166.
- Araújo, T.M., Campos, M.N.N., Canela, M.C., 2007. Studying the photochemical fate of methyl parathion in natural waters under tropical conditions. *Int. J. Environ. Anal. Chem.* 87, 937–947.
- Aston, L.S., Seiber, J.N., 1996. Exchange of airborne organophosphorus pesticides with pine needles. *J. Environ. Sci. Health B* 31, 671–698.
- Colovic, M.B., Krstic, D.Z., Lazarevic-Pasti, T.D., Bondzic, A.M., Vasic, V.M., 2013. Acetylcholinesterase inhibitors: pharmacology and toxicology. *Curr. Neuropharmacol.* 11, 315–335.
- Durand, G., Abad, J.L., Sanchezbaeza, F., Messeguer, A., Barcelo, D., 1994. Unequivocal identification of compounds formed in the photodegradation of fenitrothion in water-methanol and proposal of selected transformation pathways. *J. Agric. Food Chem.* 42, 814–821.
- Elsner, M., 2010. Stable isotope fractionation to investigate natural transformation mechanisms of organic contaminants: principles, prospects and limitations. *J. Environ. Monit.* 12, 2005–2031.
- Elsner, M., Imfeld, G., 2016. Compound-specific isotope analysis (CSIA) of micropollutants in the environment - current developments and future challenges. *Curr. Opin. Biotechnol.* 41, 60–72.
- Elsner, M., Zwank, L., Hunkeler, D., Schwarzenbach, R.P., 2005. A new concept linking observable stable isotope fractionation to transformation pathways of organic pollutants. *Environ. Sci. Technol.* 18, 6896–6916.
- Elsner, M., Jochmann, M.A., Hofstetter, T.B., Hunkeler, D., Bernstein, A., Schmidt, T.C., et al., 2012. Current challenges in compound-specific stable isotope analysis of environmental organic contaminants. *Anal. Bioanal. Chem.* 403, 2471–2491.
- EPA US, 2006. Organophosphorus Cumulative Risk Assessment (2006 Update). U.S. Environmental Protection Agency, pp. 1–189.
- Evgenidou, E., Konstantinou, I., Fytianos, K., Albanis, T., 2006. Study of the removal of dichlorvos and dimethoate in a titanium dioxide mediated photocatalytic process through the examination of intermediates and the reaction mechanism. *J. Hazard. Mater.* 137, 1056–1064.
- FAO, 1990a. Parathion-methyl (059). Food and Agriculture Organization of the United Nations.
- FAO, 1990b. Parathion (58). Food and Agriculture Organization of the United Nations.
- Herrmann, J.M., Guillard, C., Arguello, M., Aguera, A., Tejedor, A., Piedra, L., et al., 1999. Photocatalytic degradation of pesticide pirimiphos-methyl - Determination of the reaction pathway and identification of intermediate products by various analytical methods. *Catal. Today* 54, 353–367.
- Hofstetter, T.B., Berg, M., 2011. Assessing transformation processes of organic contaminants by compound-specific stable isotope analysis. *Trac-Trend. Anal. Chem.* 30, 618–627.
- Hofstetter, T.B., Spain, J.C., Nishino, S.F., Bolotin, J., Schwarzenbach, R.P., 2008. Identifying competing aerobic nitrobenzene biodegradation pathways by compound-specific isotope analysis. *Environ. Sci. Technol.* 42, 4764–4770.
- Kanmonji, V.G.G., Daniel, S., Raj, G.A.G., 2012. Photocatalytic degradation of chlorpyrifos in aqueous suspensions using nanocrystals of ZnO and TiO₂. *React. Kinet. Mech. Catal.* 106, 325–339.
- Kawahara, J., Horikoshi, R., Yamaguchi, T., Kumagai, K., Yanagisawa, Y., 2005. Air pollution and young children's inhalation exposure to organophosphorus pesticide in an agricultural community in Japan. *Environ. Int.* 31, 1123–1132.

- Kegley, S.E., Hill, B.R., S., C., A.H., 2016a. Parathion - identification, toxicity, use, water pollution potential, ecological toxicity and regulatory information. PAN Pesticide Database. Pesticide Action Network, North America, Oakland, CA.
- Kegley, S.E., Hill, B.R., O., S., C., A.H., 2016b. Methyl parathion - identification, toxicity, use, water pollution potential, ecological toxicity and regulatory information. PAN Pesticide Database. Pesticide Action Network, North America, Oakland, CA.
- Kerzhentsev, M., Guillard, C., Herrmann, J.M., Pichat, P., 1996. Photocatalytic pollutant removal in water at room temperature: case study of the total degradation of the insecticide fenitrothion (phosphorothioic acid O,O-dimethyl-O(3-methyl-4-nitro-phenyl ester). *Catal. Today* 27, 215–220.
- Konstantinou, I.K., Sakellarides, T.M., Sakkas, V.A., Albanis, T.A., 2001. Photocatalytic degradation of selected s-triazine herbicides and organophosphorus insecticides over aqueous TiO₂ suspensions. *Environ. Sci. Technol.* 35, 398–405.
- LRSB L, 2014. Pilot Experiments on the Remediation Technology In Situ Alkaline Hydrolysis at Groyne 42, Final report. NorthPestClean, Kongens Lyngby, Denmark.
- Miyamoto, S., Martinez, G.R., Medeiros, M.H.G., Di Mascio, P., 2003. Singlet molecular oxygen generated from lipid hydroperoxides by the Russell mechanism: studies using O-18-labeled linoleic acid hydroperoxide and monomol light emission measurements. *J. Am. Chem. Soc.* 125, 6172–6179.
- Nielsen, M.B., Kjeldsen, K.U., Lever, M.A., Ingvorsen, K., 2014. Survival of prokaryotes in a polluted waste dump during remediation by alkaline hydrolysis. *Ecotoxicology* 23, 404–418.
- Nijenhuis, I., Richnow, H.H., 2016. Stable isotope fractionation concepts for characterizing biotransformation of organohalides. *Curr. Opin. Biotechnol.* 41, 108–113.
- Northrop, D.B., 1981. The expression of isotope effects on enzyme-catalyzed reactions. *Annu. Rev. Biochem.* 50, 103–131.
- Oshea, K.E., Beightol, S., Garcia, I., Aguilar, M., Kalen, D.V., Cooper, W.J., 1997. Photocatalytic decomposition of organophosphonates in irradiated TiO₂ suspensions. *J. Photochem. Photobiol., A* 107, 221–226.
- Ou, H., Liu, J., Ye, J., Wang, L., Gao, N., Ke, J., 2017. Degradation of tris(2-chloroethyl) phosphate by ultraviolet-persulfate: kinetics, pathway and intermediate impact on proteome of *Escherichia coli*. *Chem. Eng. J.* 308, 386–395.
- Pehkonen, S.O., Zhang, Q., 2002. The degradation of organophosphorus pesticides in natural waters: a critical review. *Crit. Rev. Environ. Sci. Technol.* 32, 17–72.
- Renpenning, J., Kuemmel, S., Hitzfeld, K.L., Schimmelmann, A., Gehre, M., 2015. Compound-specific hydrogen isotope analysis of heteroatom-bearing compounds via gas chromatography-chromium-based high-temperature conversion (Cr/HTC)-isotope ratio mass spectrometry. *Anal. Chem.* 87, 9443–9450.
- RotterdamConvention, 2004. PIC Chemicals - Rotterdam Convention.
- Sakellarides, T.M., Siskos, M.G., Albanis, T.A., 2003. Photodegradation of selected organophosphorus insecticides under sunlight in different natural waters and soils. *Int. J. Environ. Anal. Chem.* 83, 33–50.
- Santos, F.F., Martin-Neto, L., Airoidi, F.P.S., Rezende, M.O.O., 2005. Photochemical behavior of parathion in the presence of humic acids from different origins. *J. Environ. Sci. Health B* 40, 721–730.
- Singh, B.K., Walker, A., 2006. Microbial degradation of organophosphorus compounds. *FEMS Microbiol. Rev.* 30, 428–471.
- Stackelberg, P.E., Gibs, J., Furlong, E.T., Meyer, M.T., Zaugg, S.D., Lippincott, R.L., 2007. Efficiency of conventional drinking-water-treatment processes in removal of pharmaceuticals and other organic compounds. *Sci. Total Environ.* 377, 255–272.
- Thullner, M., Centler, F., Richnow, H.-H., Fischer, A., 2012. Quantification of organic pollutant degradation in contaminated aquifers using compound specific stable isotope analysis – review of recent developments. *Org. Geochem.* 42, 1440–1460.
- Van Breukelen, B.M., 2007. Extending the Rayleigh equation to allow competing isotope fractionating pathways to improve quantification of biodegradation. *Environ. Sci. Technol.* 41, 4004–4010.
- Vogt, C., Dorer, C., Musat, F., Richnow, H.H., 2016. Multi-element isotope fractionation concepts to characterize the biodegradation of hydrocarbons - from enzymes to the environment. *Curr. Opin. Biotechnol.* 41, 90–98.
- Wanamaker, E.C., Chingas, G.C., McDougal, O.M., 2013. Parathion hydrolysis revisited: in situ aqueous kinetics by (1)h NMR. *Environ. Sci. Technol.* 47, 9267–9273.
- Watts, M.J., Linden, K.G., 2008. Photooxidation and subsequent biodegradability of recalcitrant tri-alkyl phosphates TCEP and TBP in water. *Water Res.* 42, 4949–4954.
- Watts, M.J., Linden, K.G., 2009. Advanced oxidation kinetics of aqueous tri alkyl phosphate flame retardants and plasticizers. *Environ. Sci. Technol.* 8, 2937–2942.
- Wu, C., Linden, K.G., 2008. Degradation and byproduct formation of parathion in aqueous solutions by UV and UV/H₂O₂ treatment. *Water Res.* 42, 4780–4790.
- Wu, L.M., White, D.E., Ye, C., Vogt, F.G., Terfloth, G.J., Matsuhashi, H., 2012. Desulfurization of phosphorothioate oligonucleotides via the sulfur-by-oxygen replacement induced by the hydroxyl radical during negative electrospray ionization mass spectrometry. *J. Mass Spectrom.* 47, 836–844.
- Wu, L., Yao, J., Trebbe, P., Zhang, N., Richnow, H.H., 2014. Compound specific isotope analysis of organophosphorus pesticides. *Chemosphere* 111, 458–463.
- Wu, L., Kummel, S., Richnow, H.H., 2017. Validation of GC-IRMS techniques for delta¹³C and delta²H CSIA of organophosphorus compounds and their potential for studying the mode of hydrolysis in the environment. *Anal. Bioanal. Chem.* 409, 2581–2590.
- Yuan, X., Lacorte, S., Cristale, J., Dantas, R.F., Sans, C., Esplugas, S., et al., 2015. Removal of organophosphate esters from municipal secondary effluent by ozone and UV/H₂O₂ treatments. *Sep. Purif. Technol.* 156, 1028–1034.
- Zhang, N., Schindelka, J., Herrmann, H., George, C., Rosell, M., Herrero-Martin, S., et al., 2015. Investigation of Humic Substance Photosensitized Reactions via Carbon and Hydrogen Isotope Fractionation. *Environ. Sci. Technol.* 49, 233–242.

Supplementary material

Characterizing chemical transformation of organophosphorus compounds by ^{13}C and ^2H stable isotope analysis

Langping Wu^a, Barbora Chládková^{a,b}, Oliver J. Lechtenfeld^c, Shujuan Lian^a, Janine Schindelka^d, Hartmut Herrmann^d, Hans H. Richnow^{a,*}

^a Department of Isotope Biogeochemistry, Helmholtz Centre for Environmental Research-UFZ, Permoserstraße 15, 04318 Leipzig, Germany.

^b Department of Polymer Engineering, Faculty of Technology, Tomas Bata University in Zlín, Vavrečkova 275, 760 01 Zlín, Czech Republic, (Present address).

^c Department of Analytical Chemistry, Helmholtz Centre for Environmental Research-UFZ, Permoserstraße 15, 04318 Leipzig, Germany.

^d Atmospheric Chemistry Department (ACD), Leibniz Institute for Tropospheric Research (TROPOS), Permoserstraße 15, 04318 Leipzig, Germany.

*Email: hans.richnow@ufz.de, Tel: 0049 341 235 1212 Fax: 0341-450822

21 pages

10 figures

2 tables

Contents

1. Structural Elements of Organophosphorus Compounds (OPs).....	2
2. Light Spectrum of the Xenon Lamp and UV Absorption Spectra of EP and TCEP	2
3. Hydrolysis of Methyl Parathion (MP).....	3
4. Hydrolysis of Parathion (EP)	3
5. Direct Photolysis and OH Radical Oxidation of EP	6
6. UV/H ₂ O ₂ Photolysis and Fenton Reaction of TCEP.....	7
7. Quantification of Isotope Fractionation	9
8. Identification of Transformation Products of EP and TCEP during OH Radical Reaction	9
9. References	12

1. Structural Elements of Organophosphorus Compounds (OPs)

OPs as discussed in this study are esters of phosphoric acids, thiophosphoric acids and dithiophosphoric acids forming a wide variety of phosphates, phosphorothioates, or phosphorodithioates (Fig. S1). Their general structural element is a phosphorus atom in an oxidation state +5 (P (V)) substituted by oxygen or sulfur. R_1 and R_2 are mainly the aryl or alkyl group, which can be attached to a phosphorus atom via oxygen. R_3 can be diverse and may consist to a wide range of aliphatic, aromatic or heterocyclic structural units. (Singh and Walker, 2006)

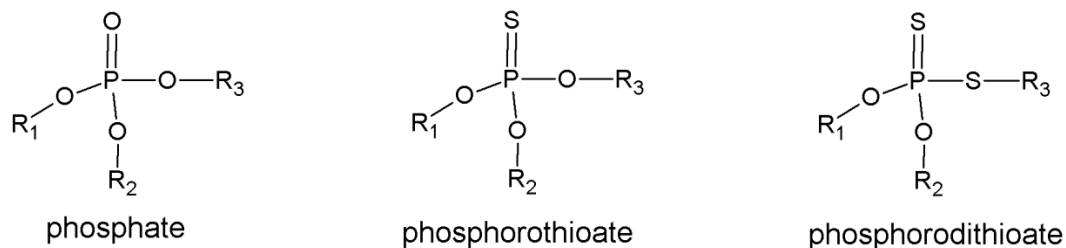


Fig. S1: Core structures of OPs discussed in this study.

2. Light Spectrum of the Xenon Lamp and UV Absorption Spectra of EP and TCEP

For the photolysis experiments in this study, irradiation was achieved using a 150-W xenon lamp as the light source (Type L2175, wavelength: 185-2000 nm, Hamamatsu, Japan). The xenon lamp is filled with xenon gas that emits “white light” at a high color temperature of 6000K, which is close to that of sunlight and covers a broad continuous spectrum from the ultraviolet to infrared region (185-2000 nm). The light spectrum is shown in Fig. S2. The UV absorption of the EP and TCEP was measured in triplicate on a UV/VIS/NIR spectrophotometer (Lambda 900, Perkin-Elmer, Waltham, U.S.). TCEP was dissolved in MilliQ water at a concentration of 100 mg L⁻¹. EP was prepared at a concentration of 24 mg L⁻¹ in MilliQ water and phosphate buffer (100 mM, pH 7), respectively. TCEP has no light absorption in the wide range of 200 – 800 nm (Fig. S3). On the contrary, EP has maximum absorption at 277 nm in MilliQ water, and at 289 nm when dissolved in phosphate buffer (100 mM, pH 7).

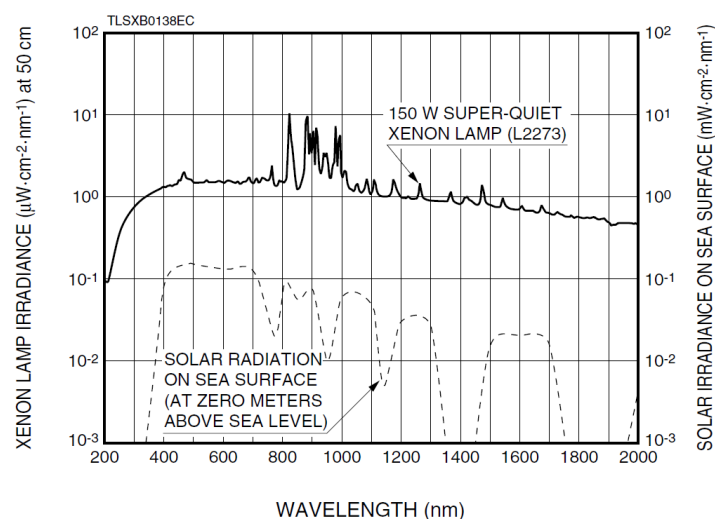


Fig. S2. Light spectrum of the xenon lamp. The original source of the spectrum is obtained from the website of Hamamatsu (Xenon lamp L2175): http://www.hamamatsu.com/resources/pdf/etd/Xe-HgXe_TLSX1044E.pdf

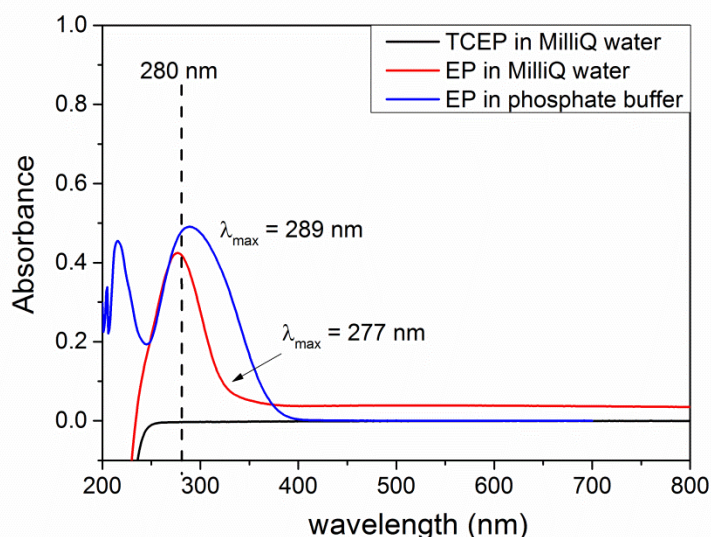


Fig. S3. UV absorption spectra of EP and TCEP.

3. Hydrolysis of Methyl Parathion (MP)

Hydrolysis experiments of MP were carried out at 60°C to reduce the reaction time in 100mM phosphate buffer solution at pH 2, pH 5, pH 7, pH9 and at 20°C for alkaline hydrolysis at pH 12. All experiments were conducted as batch experiments using 120 mL serum bottles which were filled with 100 mL buffer solution and closed with Teflon coated butyl rubber septa and crimped. 0.5 mL of stock solution of MP in acetone was added into each preheated serum bottle through rubber septa (shaken immediately) to achieve an initial concentration of 50 mg L⁻¹ to initiate hydrolysis reaction. Gastight vials containing 2 ml of 1000 mg L⁻¹ MP solution in hexane/acetone (1:1) was also put into an oven at 60°C as controls for thermal degradation. At different time intervals, the hydrolysis was stopped by adjusting the aqueous sample to pH 7 using 6N HCl or 5M NaOH. For extraction of the remaining MP, 2 mL of DCM containing 400 mg L⁻¹ of dichlorvos as internal standard was added through a rubber septa and shaken at 180 rpm for 2h at 4 °C. Afterwards, the organic phase was transferred into 2mL vials for concentration measurement as soon as possible, and the samples were stored at -20 °C for further isotope analysis.

The results of the hydrolysis experiments are summarized in Fig. S4. After 70 h of reaction, the δ¹³C of MP become enriched from -37.9 ± 0.1‰ to -18.9 ± 0.1‰ for 87% of degradation at pH 2, from -38.0 ± 0.1‰ to -11.7 ± 0.3‰ for 93% of degradation at pH 5, and from -38.5 ± 0.0‰ to -5.3 ± 0.3‰ for 97% of degradation at pH 7. 94% of MP degradation was observed at pH 9 after 52 h, with δ¹³C enrichment from -38.1 ± 0.1‰ to -20.3 ± 0.2‰. However, 99% of MP degradation was obtained at pH 12 after 24 h but without any δ¹³C changes. During all MP hydrolysis experiments, no δ²H shift was observed. The hydrolysis of MP could be described by degradation rate constants (× 10⁻⁵ s⁻¹) of 0.78 (R² = 0.993) at pH 2 (60°C), 1.00 (R² = 0.997) at pH 5 (60°C), 1.36 (R² = 0.995) at pH 7 (60°C), 1.53 (R² = 0.995) at pH 9 (60°C), and 5.58 (R² = 0.999) at pH 12 (20°C) indicating homogeneous reactions and pseudo-first-order kinetics (Fi. S4).

4. Hydrolysis of Parathion (EP)

Hydrolysis experiments of EP were carried out at the same conditions as described for MP except with an initial concentration of 24 mg L⁻¹. To investigate the effect of temperature on hydrolysis mechanisms, the hydrolysis of EP at pH 12 was conducted at 20 °C, 30 °C and 40 °C, respectively. The δ¹³C of EP

enriched from $-29.4 \pm 0.6\text{‰}$ to $-9.4 \pm 0.3\text{‰}$ for 94% of degradation at pH 2 after 306 h, from $-29.8 \pm 0.0\text{‰}$ to $1.2 \pm 0.2\text{‰}$ for 99% of degradation at pH 5 after 426 h from $-30.0 \pm 0.0\text{‰}$ to $-1.2 \pm 0.1\text{‰}$ for 99% of degradation at pH 7 after 426 h, and from $-29.7 \pm 0.1\text{‰}$ to $-9.2 \pm 0.1\text{‰}$ for 99% of degradation at pH 9 after 401 h (Fig. S5). During hydrolysis at pH 12, 88% of EP degradation was obtained after 92 h at 20 °C, 97% degradation was obtained after 42 h at 30 °C, and 92% degradation was obtained after 9 h at 40 °C, all without any $\delta^{13}\text{C}$ changes. No $\delta^2\text{H}$ shifts were observed during all EP hydrolysis experiments ($\delta^2\text{H}$ values for samples of more than 95% degradation were not measured due to the low concentration of EP). The hydrolysis of EP can be described by pseudo-first-order kinetics resulting in degradation rate constants ($\times 10^{-5} \text{ s}^{-1}$) of 0.25 ($R^2 = 0.997$) at pH 2 (60°C), 0.28 ($R^2 = 0.996$) at pH 5 (60°C), 0.31 ($R^2 = 0.997$) at pH 7 (60°C), 0.42 ($R^2 = 0.995$) at pH 9 (60°C), 0.64 ($R^2 = 0.993$) at pH 12 (20°C), 2.19 ($R^2 = 0.993$) at pH 12 (30°C), and 7.92 ($R^2 = 0.991$) at pH 12 (40°C), indicating homogeneous reactions (Fig. S6).

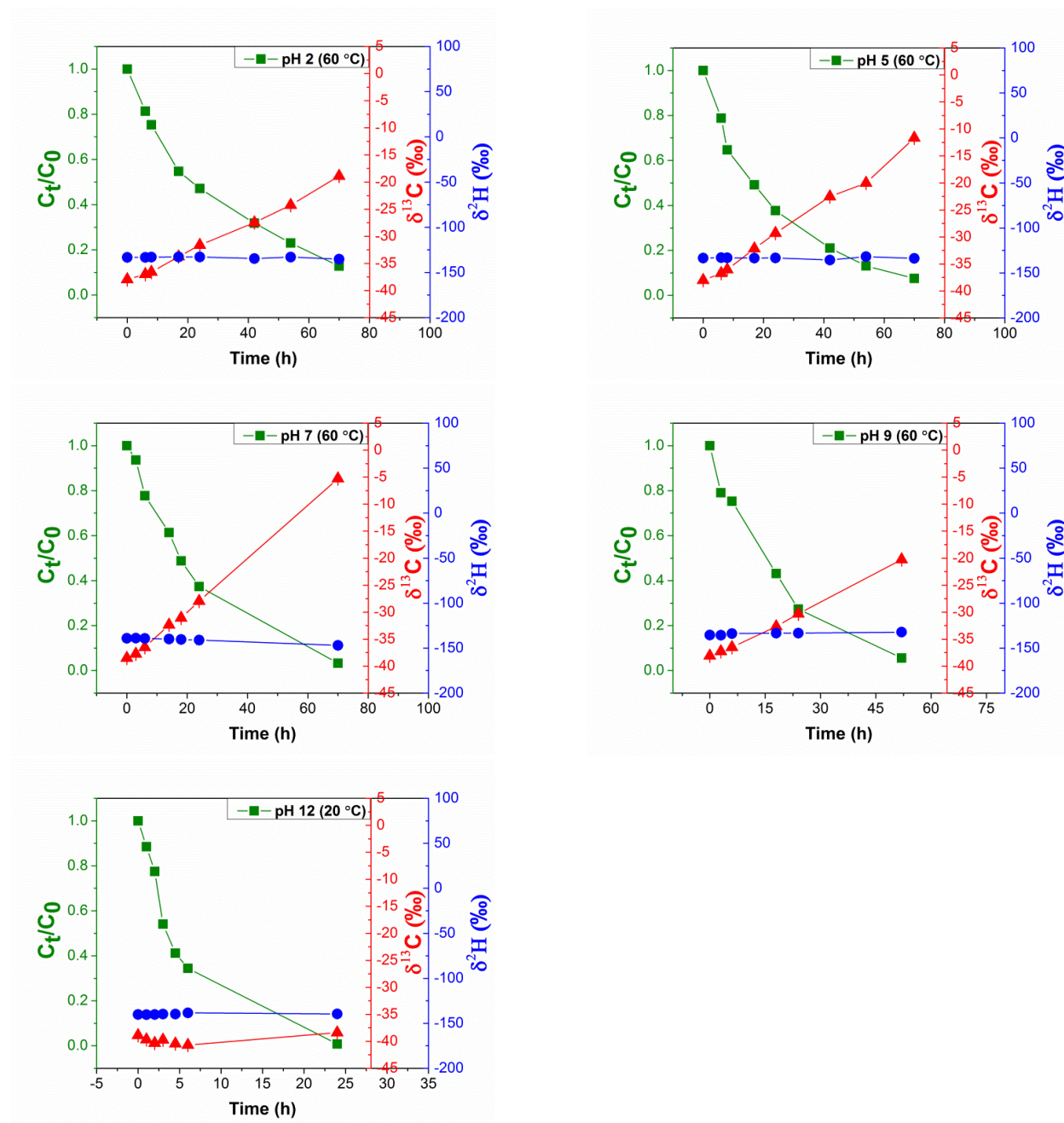
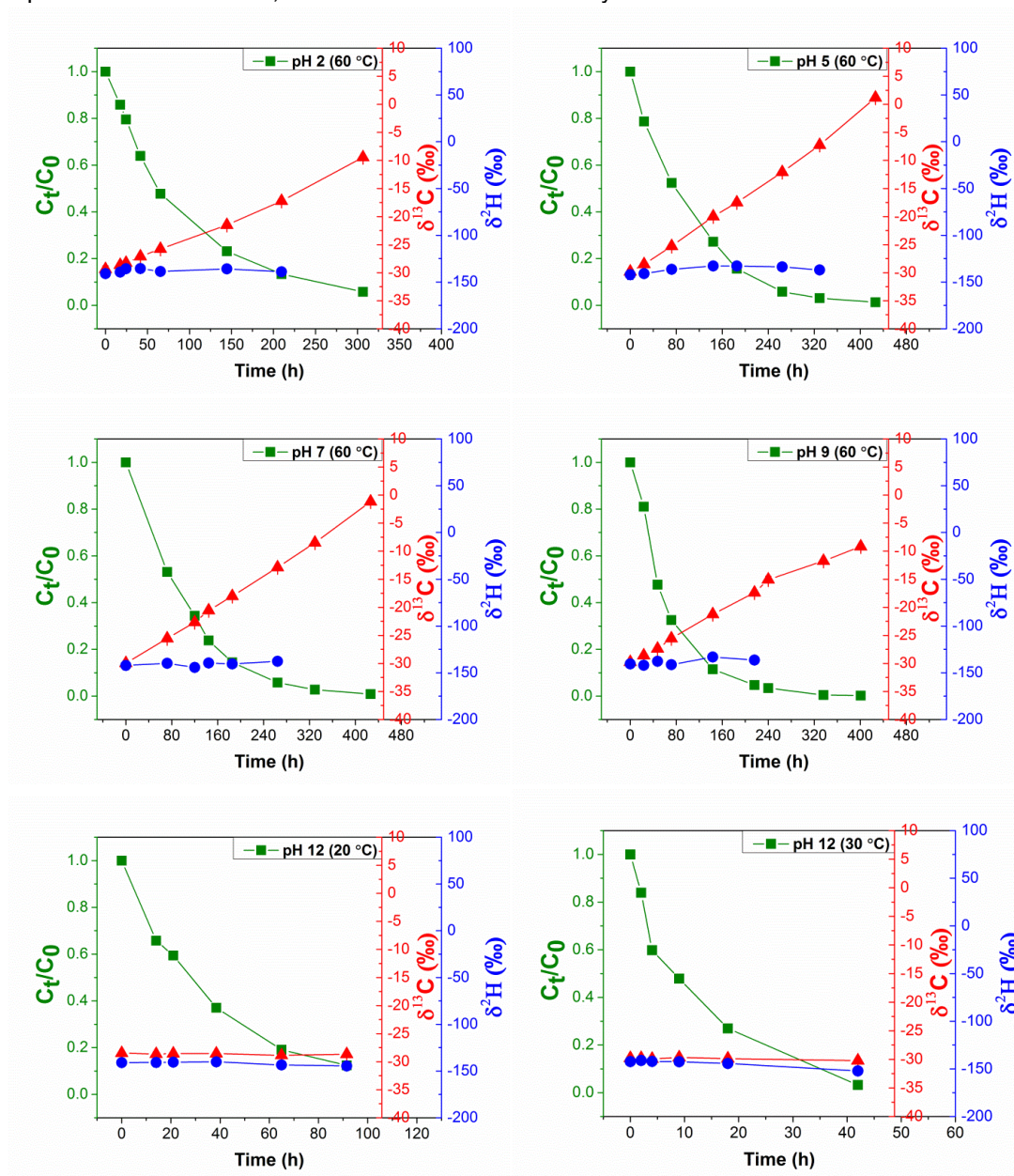


Fig. S4. Transformation of MP by hydrolysis at different pH. Carbon and hydrogen isotope signatures ($\delta^{13}\text{C}$ signified by red triangles, $\delta^2\text{H}$ signified by blue circles) vs the fraction of remaining substrate (C_t/C_0 signified by green squares) are shown. Uncertainties of isotope analysis represent standard deviations of triplicate measurements; error bars are smaller than symbols.



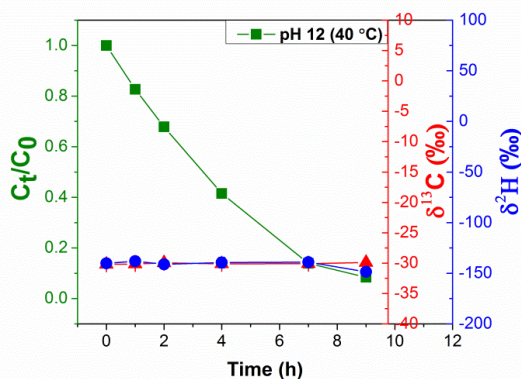


Fig. S5. Transformation of EP by hydrolysis at different pH. Carbon and hydrogen isotope signatures ($\delta^{13}C$ signified by red triangles, δ^2H signified by blue circles) vs. the fraction of remaining substrate (C_t/C_0 signified by green squares) are shown. Uncertainties of isotope analysis represent standard deviations of triplicate measurements; error bars are smaller than symbols.

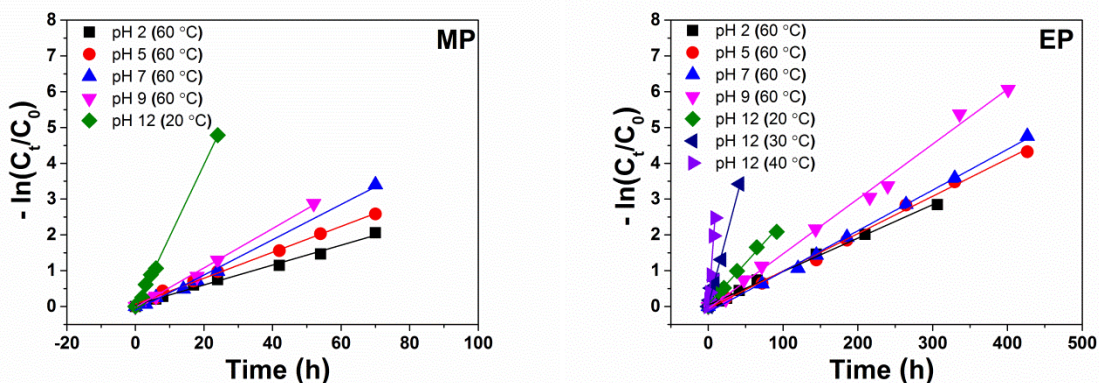


Fig. S6. Kinetics of EP and MP during hydrolysis at different pH. Solid lines show pseudo-first-order kinetics.

5. Direct Photolysis and OH Radical Oxidation of EP

The photolysis of EP was conducted in a photochemical reactor system consisting of a 2000 mL Pyrex cylindrical flask with a quartz window whose surface area was approximately 160 cm². Irradiation was achieved using a 150-W xenon lamp as the light source (Type L2175, wavelength: 185-2000 nm, Hamamatsu, Japan). The temperature was controlled by a circulating water system positioned around the Pyrex reactor to guarantee constant reaction conditions at 25 °C. The distance between the quartz window of the reactor and the light source was approximately 13 cm. A filter with a 280-nm cut-off wavelength (Schott WG 280 long pass filter, 3.15mm thick, Galvoptics Ltd, United Kingdom) was applied to provide emission spectrum with a wavelengths ≥ 280 nm typical of the sun at the Earth's surface. EP stock solution was prepared at 20 mg mL⁻¹ in acetone. For the OH radical reaction, 1 mL of EP stock solution was mixed into 2000 mL of phosphate buffer (10 mM, pH 7) for overnight in the photo reactor to achieve an initial concentration of 10 mg L⁻¹. The reaction was started by addition of 2.68 mL of 30% H₂O₂ into the EP buffer solution, resulting in a 500:1 initial molar ratio of H₂O₂ to EP. The solution was continuously stirred and maintained at a constant temperature of 25 °C. At different time intervals, 200 mL of aqueous sample was taken into a serum bottle. 4 mL of DCM containing 200 mg L⁻¹ of dichlorvos as an internal standard was added to extract the remaining reactants. The direct photolysis of EP was

performed at the same condition without H_2O_2 and without 280 nm filter. Dark control experiments were conducted in the same system without UV irradiation.

The $\delta^{13}\text{C}$ values only enriched 2.8‰ (from $-34.5 \pm 0.2\text{‰}$ to $-31.7 \pm 0.1\text{‰}$) for more than 99% of substrate conversion after 359 h of direct photolysis. An enrichment of 1.5‰ (from $-34.9 \pm 0.5\text{‰}$ to $-33.3 \pm 0.3\text{‰}$) for more than 98% of substrate conversion after 23 h was found during OH radical oxidation with H_2O_2 (Fig. S7). No $\delta^2\text{H}$ shifts were observed during both photolysis experiments. The photolysis of EP could be described with pseudo-first-order kinetics (Fig. S8), resulting in degradation rate constants ($\times 10^{-5} \text{ s}^{-1}$) of 0.36 ($R^2 = 0.976$) during direct photolysis and 4.61 ($R^2 = 0.992$) during OH radical reaction.

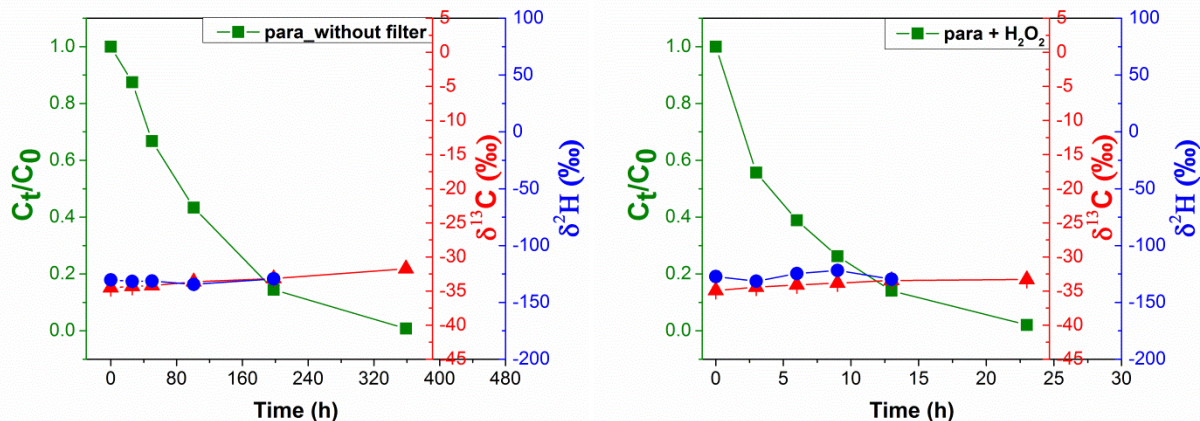


Fig. S7. Carbon and hydrogen enrichment during the direct photolysis and OH radical reaction of parathion. Carbon and hydrogen isotope signatures ($\delta^{13}\text{C}$ signified by red triangles, $\delta^2\text{H}$ signified by blue circles) vs. the fraction of remaining substrate (C_t/C_0 signified by green squares) are shown. Uncertainties of isotope analysis represent standard deviations of triplicate measurements; error bars are smaller than symbols.

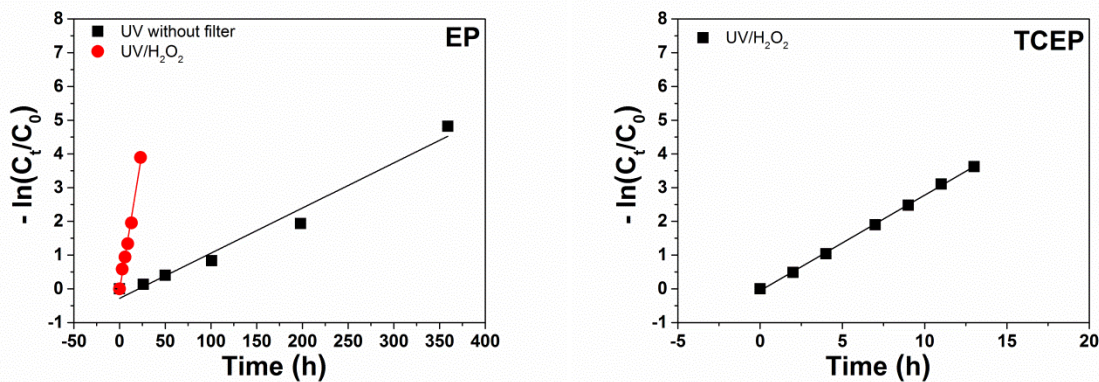


Fig. S8. Kinetics of EP and TCEP during direct photolysis and OH radical reaction. Solid lines show pseudo-first-order kinetics.

6. UV/ H_2O_2 Photolysis and Fenton Reaction of TCEP

The photolysis of TCEP was conducted in the same photochemical reactor system described above except for in a 200 mL Pyrex cylindrical flask with a quartz window whose surface area was approximately 64 cm^2 . The TCEP stock solution was prepared with a concentration of 500 mg mL^{-1} in

acetonitrile. For the OH radical oxidation by photolysis of H_2O_2 , 0.2 mL of TCEP stock solution was dissolved in a 200 mL phosphate buffer (100 mM, pH 7) preheated at 20 °C and stirred overnight in the photo reactor to achieve an initial concentration of 500 mg L^{-1} . And then 1.8 mL of 30% H_2O_2 was added into the TCEP buffer solution, resulting in a 50:1 initial molar ratio of H_2O_2 to TCEP. The solution was continuously mixed on a magnetic stirrer at 500 rpm during the experiment and the temperature was maintained at 20 °C with cooling system. After 15 min of mixing, the UV lamp source was turned on to start the photoreaction. At different time intervals, 10 mL of aqueous sample was taken through a rubber septum of the reactor using a syringe and transferred into a gas-tight vial. 0.5 mL of DCM containing 2000 mg L^{-1} of TBP as an internal standard was added to extract the remaining reactants by shaking at 180 rpm at 4 °C for 2h. The organic phase was transferred into 2 mL vials afterwards for further analysis. The direct photolysis of TCEP was performed at the same condition without H_2O_2 . Dark control experiments were conducted in the same system without UV irradiation.

Fenton reaction of TCEP was carried out at room temperature in 200 mL well-stirred solution under no light exposure and an initial selected mole ratio of $\text{TCEP}:\text{H}_2\text{O}_2:\text{FeSO}_4 = 1:50:10$ (1.75 mM:87.5 mM:17.5 mM). The initial concentration of TCEP was 500 mg L^{-1} . To attain sufficient dissolution of the degraded compound, 100 mg of TCEP was dissolved into 200 mL phosphate buffer (100mM, pH 3) and stirred for 30 min. Then required amount of Fe^{2+} stock solution was added to the reaction mixture. The Fenton reaction was initiated by sequential addition of 1.8 mL of 30% H_2O_2 (30min sequencing intervals). The solution was continuously mixed at 400 rpm during 2-hour reaction. The initial sample was taken before the initiation of the Fenton reaction by H_2O_2 (with Fe^{2+} already added in the solution, before H_2O_2 addition). At 30 min intervals, 10 mL of aqueous sample was taken for the extraction of TCEP residues by adding 0.5 mL of DCM containing 2000 mg L^{-1} of TBP as internal standard and shaken at 180 rpm at 4 °C for 2h. The excessed OH radicals were quenched by an addition of 1 mL of isopropanol to stop the reaction during extraction procedure.

The OH radical oxidation and corresponding C and H isotope fractionation of TCEP were investigated using UV/ H_2O_2 and $\text{FeSO}_4/\text{H}_2\text{O}_2$ system to generate OH radicals. In the UV/ H_2O_2 system, the $\delta^{13}\text{C}$ composition of TCEP enriched from $-31.5 \pm 0.2\text{‰}$ to $-26.3 \pm 0.3\text{‰}$ for 97% of degradation after 13 h and $\delta^2\text{H}$ composition enriched from $-25 \pm 5\text{‰}$ to $185 \pm 5\text{‰}$ (Fig. S9). A rate constant of $7.86 \times 10^{-5} \text{ s}^{-1}$ with $R^2 = 0.999$ indicates a pseudo-first-order kinetic reaction (Fig. S8). During Fenton reaction, the rate constant of $35.75 \times 10^{-5} \text{ s}^{-1}$ with $R^2 = 0.908$ indicates a pseudo-first-order kinetic reaction. The $\delta^{13}\text{C}$ of TCEP enriched from $-29.4 \pm 0.3\text{‰}$ to $-26.2 \pm 0.2\text{‰}$ and $\delta^2\text{H}$ enriched from $-28 \pm 3\text{‰}$ to $87 \pm 4\text{‰}$ within 96% of degradation (Fig. S9).

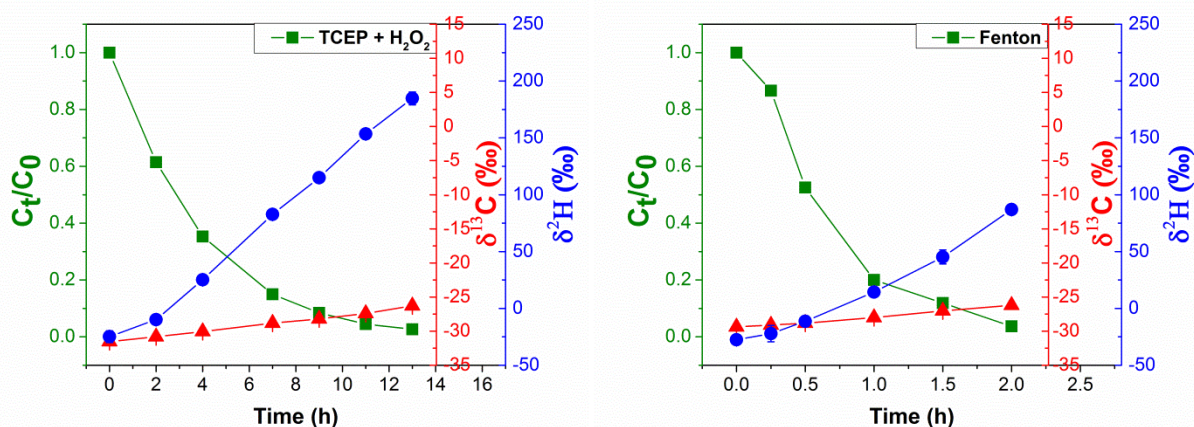


Fig. S9. Carbon and hydrogen enrichment during OH radical oxidation induced by photosensitization of H_2O_2 and Fenton reaction of TCEP. Carbon and hydrogen isotope signatures ($\delta^{13}\text{C}$ signified by red triangles, $\delta^2\text{H}$ signified by blue circles) vs. the fraction of remaining substrate (C_t/C_0 signified by green

squares) are shown. Uncertainties of isotope analysis represent standard deviations of triplicate measurements; error bars are smaller than symbols.

7. Quantification of Isotope Fractionation

7.1 Isotope Enrichment Factor (ϵ)

The carbon and hydrogen isotopic signatures are reported as δ values in parts per thousand (‰) relative to international reference materials, Vienna PeeDee Belemnite (VPDB) for carbon and Standard Mean Ocean Water (SMOW) for hydrogen. The isotope enrichment factor (ϵ) can be determined from the logarithmic form of the Rayleigh equation (eq. S1). δE_t and δE_0 are the isotopic signatures of the compound for the element E at a given time t and at the beginning of the reaction; while C_t/C_0 is the fraction of the remaining compound.

$$\ln\left(\frac{\delta E_t + 1}{\delta E_0 + 1}\right) = \epsilon \times \ln\left(\frac{C_t}{C_0}\right) \quad \text{S1}$$

7.2 Rate Ratio of Two Competing Degradation Pathways (F)

Van Breukelen (Van Breukelen, 2007) derived extended Rayleigh-type equations to improve quantification of isotopic fractionation expressed during substrate consumption via competing pathways. If a substrate is being degraded via two pathways and following first-order kinetics, the rate ratio of two competing degradation pathways (F) can be calculated from the observed isotope enrichment factor (ϵ_A) and the isotope enrichment factor values associated with the two pathways ϵ_1 and ϵ_2 , which is shown in eq. S2:

$$F = \frac{\epsilon_A - \epsilon_2}{\epsilon_1 - \epsilon_2} \quad (\text{S2})$$

F indicates the isotope fractionation contribution of pathway 1 to the observed isotope fractionation ϵ_A . Note that eq. S2 is applicable for only two competing pathways, for three or more pathways unique solutions are not possible (Van Breukelen, 2007). Similar C isotope enrichment factors observed during hydrolysis of MP and EP at lower pH indicate one pathway ($\epsilon_1 = -10.5 \sim -9.9\text{‰}$ for MP and $\epsilon_1 = -6.9 \sim -6.0\text{‰}$ for EP), no C isotope fractionation observed for both MP and EP hydrolysis at pH 12 indicates another pathway ($\epsilon_2 = 0$). The reduction of C isotope fractionation by almost the half at pH 9 suggests that two pathways of hydrolysis are at work whereas $\epsilon_A = -6.5 \pm 0.4\text{‰}$ for MP and $\epsilon_A = -3.5 \pm 0.4\text{‰}$ for EP. Therefore, calculated from eq. S3, MP hydrolysis at pH9 have a contribution of 62 ~ 66% of pathway 1, while EP hydrolysis at pH9 have a contribution of 51 ~ 58% of pathway 1.

8. Identification of Transformation Products of EP and TCEP during OH Radical Reaction

In order to analyze the transformation products of EP and TCEP during OH radical reaction using UV/H₂O₂, experiments were conducted under the same conditions as described above. After achieving 51% degradation of EP during UV/H₂O₂ reaction, 99% degradation of EP during direct photolysis, 11% degradation of TECP during UV/H₂O₂ reaction, respectively, 10 mL of aqueous solution was extracted by solid phase extraction (SPE) using Bond Elut PPL cartridges (50 mg, Agilent). The SPE extraction procedures followed the manufacturer guidelines and were: cleaning with 1 mL methanol; conditioning with the cartridges with 2 mL acidic water (pH 2 adjusted with HCl); loading of 10 mL aqueous sample solution adjusted to pH 2 using HCl; washing with 1 mL acidic water to remove the residual buffer salts; drying the cartridges with a nitrogen steam and elution of the transformation products with 0.5 mL methanol. The methanolic extract was collected and diluted 1:100 or 1:1000 (v/v) with MilliQ water /MeOH (1:1, v/v) before analysis. Parallel experiments were conducted under the same conditions but in MilliQ water for direct analysis of aqueous solution, in order to investigate the SPE extraction efficiency by PPL cartridges.

A Fourier-transform ion cyclotron resonance mass spectrometer (FT-ICR MS, Solarix XR 12T, Bruker Daltonics) equipped with a dynamically harmonized analyzer cell was used for the analysis of the methanolic extracts. Samples were measured with positive and negative mode electrospray ionization in direct infusion mode with a 4 MWord time domain using typical ESI conditions. For each sample, 16 (TCEP) or 128 to 256 scans (EP, 10 – 100 ms ion accumulation time) were co-added in a range of 73-3000 m/z and the spectra externally calibrated with fatty acids. The high mass accuracy and resolution (450000 at m/z 200) allowed for a tentative assignment of possible transformation products via their exact mass and calculated molecular formulas where the molecular formulas of the parent compounds were used as an upper element limit for the calculation. For instance, as shown in Fig. S10, a transformation product of TCEP was found in negative mode with m/z 278.9598 and ion formula of $C_6H_{10}Cl_2O_6P^-$, which was clearly not present in the 0h samples extracted by PPL and in the aqueous solution. Paraoxon (m/z pos: 276.0632) was not detected in sample from direct photolysis of EP, however, the formation of O,O-diethyl phosphate (m/z neg: 153.0322) during direct photolysis of EP suggests that paraoxon was further degraded, considering the sample was extracted after 99% degradation of EP (Table S1). Therefore, same transformation products of EP were detected from the direct photolysis and OH radical reaction. Comparing the performance of SPE extraction using PPL cartridges to direct aqueous solution analysis, our results indicate that the SPE using PPL cartridges is efficient enough to extract all known transformation products. All detected transformation products of EP and TCEP are listed in Tables S1 and S2, respectively.

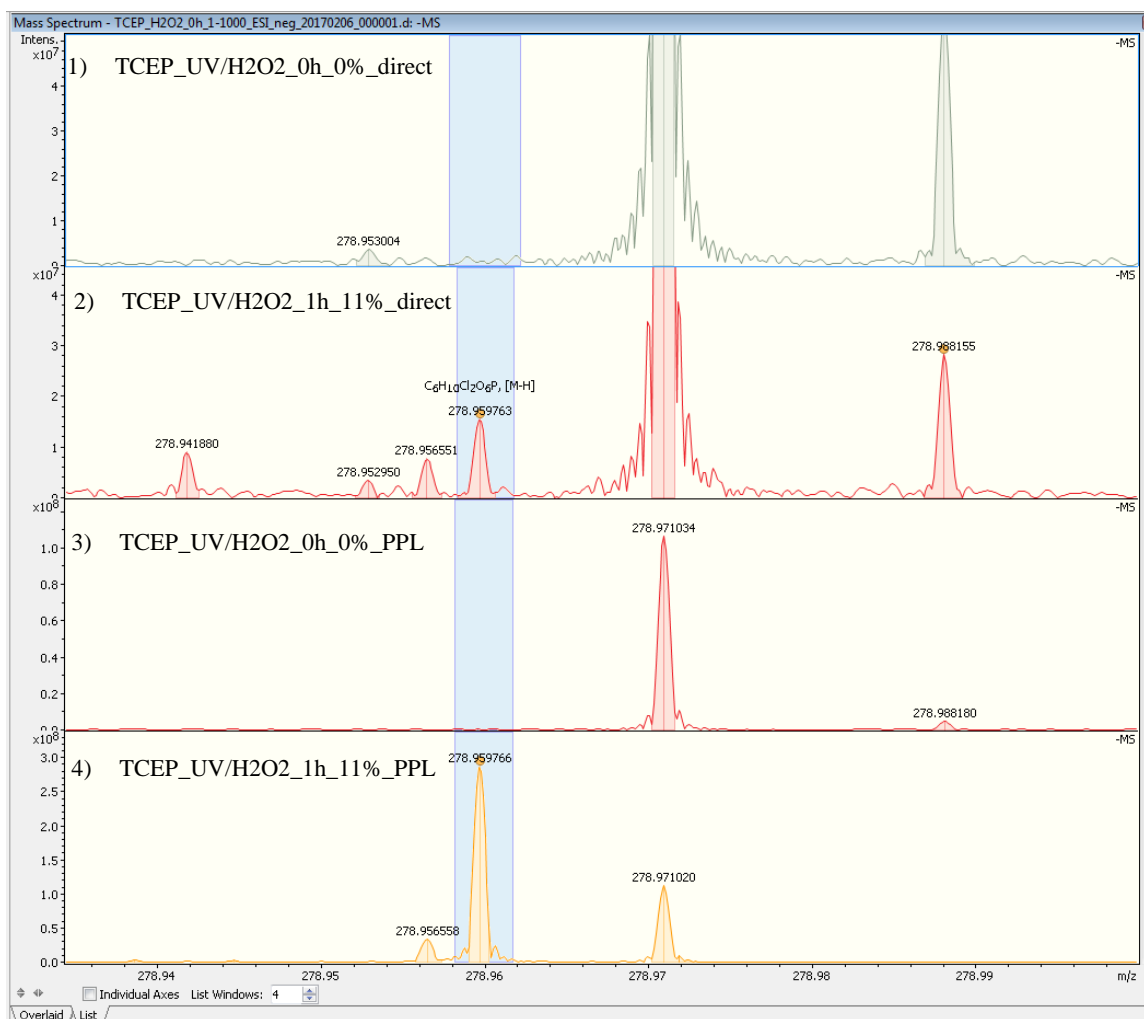


Fig. S10: Mass spectra of transformation products analysis of TCEP via FT-ICR MS. Spectra with same acquisition conditions were compared.

Table S1: List of tentatively characterized transformation products detected during direct photolysis and OH radical reaction of EP using FT-ICR MS.

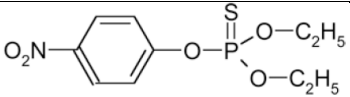
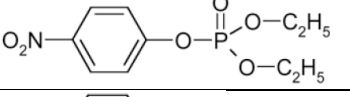
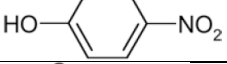
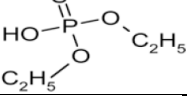
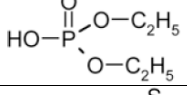
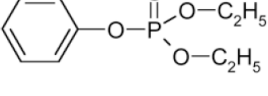
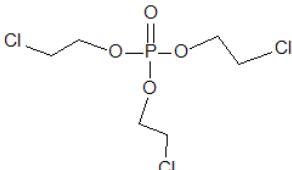
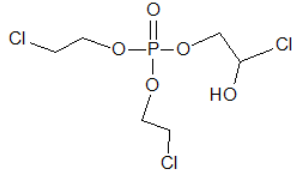
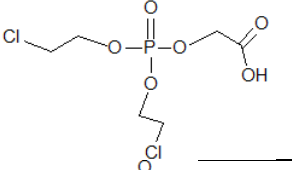
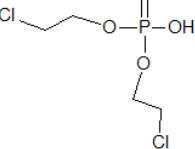
name	neutral formula	tentative structure	m/z pos	m/z neg	Detected? (pos/neg)	photolysis experiment
Parathion	C ₁₀ H ₁₄ NO ₅ PS		292.0403 (H)		pos (H)/- (lock mass)	
P1 (Paraoxon)	C ₁₀ H ₁₄ NO ₆ P		276.0632 (H)		pos (H)/- < 0.25 ppm	UV/H ₂ O ₂
P2 (4-nitro-phenol)	C ₆ H ₅ NO ₃			138.0197 (H)	-/neg (H) < 0.1 ppm	direct and UV/H ₂ O ₂
P3 (O,O-diethyl thiophosphate)	C ₄ H ₁₁ O ₃ PS			169.0094 (H)	-/neg (H) < 0.3 ppm	direct and UV/H ₂ O ₂
P4 (O,O-diethyl phosphate)	C ₄ H ₁₁ O ₄ P			153.0322 (H)	-/neg (H) < 0.1 ppm	direct and UV/H ₂ O ₂
P5 (O,O-diethyl phenyl thiophosphate)	C ₁₀ H ₁₅ O ₃ PS		247.0552 (H)	245.0407 (H)	-/-	

Table S2: List of tentatively characterized transformation products detected during OH radical reaction of TCEP using FT-ICR MS.

name	neutral formula	tentative structure	m/z pos	m/z neg	Detected? (pos/neg)
TCEP	C ₆ H ₁₂ Cl ₃ O ₄ P		284.9612 (H) 306.9431 (Na)		pos (H,Na)/- <0.009 ppm
P1	C ₆ H ₁₂ Cl ₃ O ₅ P		322.9380 (Na)		pos (Na)/- <0.403 ppm
P2	C ₆ H ₁₁ Cl ₂ O ₆ P			278.9598 (H)	-/neg (H) <-0.053ppm
P3	C ₄ H ₉ Cl ₂ O ₄ P			220.9543 (H)	-/neg (H) <0.037 ppm

P4	$C_6H_{13}Cl_2O_5P$			264.9805 (H)	-/neg (H) <0.528 ppm
P5	$C_4H_9Cl_2O_6P$			252.9441 (H)	-/neg (H) <0.045 ppm
P6	$C_4H_8ClO_6P$			216.9674 (H) 238.9494 (Na)	-/neg (H,Na) <-0.006 ppm
P7	$C_4H_{11}O_6P$			185.0220 (H)	-/neg (H) < -0.396 ppm
P8	$C_2H_6ClO_4P$			180.9439 (Na)	-/neg(Na) <-0.032ppm

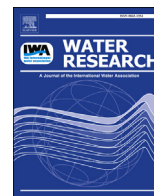
9. References

- Singh BK, Walker A. Microbial degradation of organophosphorus compounds. *Fems Microbiol. Rev.* 2006; 30: 428-471.
- Van Breukelen BM. Extending the Rayleigh equation to allow competing isotope fractionating pathways to improve quantification of biodegradation. *Environ. Sci. Technol.* 2007; 41: 4004-4010.

Appendix 6.4.

Aqueous photodegradation of substituted chlorobenzenes: Kinetics, carbon isotope fractionation, and reaction mechanisms

Published paper: *Passeport, E.; Zhang, N.; Wu, L.; Herrmann, H.; Sherwood Lollar, B.; Richnow, H. H., Water Res. 2018, 135, 95-103.*



Aqueous photodegradation of substituted chlorobenzenes: Kinetics, carbon isotope fractionation, and reaction mechanisms

Elodie Passeport^{a,*,1,2}, Ning Zhang^{b,3}, Langping Wu^b, Hartmut Herrmann^c, Barbara Sherwood Lollar^a, Hans-Hermann Richnow^b

^a Department of Earth Sciences, University of Toronto, 22 Russell Street, Toronto, ON M5S 3B1, Canada

^b Department of Isotope Biogeochemistry, Helmholtz Center for Environmental Research UFZ, Permoserstrasse 15, 04318 Leipzig, Germany

^c TROPOS Leibniz Institute for Tropospheric Research, Atmospheric Chemistry Department (ACD), Permoserstrasse 15, 04318 Leipzig, Germany

ARTICLE INFO

Article history:

Received 18 December 2017

Received in revised form

3 February 2018

Accepted 5 February 2018

Available online 9 February 2018

Keywords:

Photodegradation

Water quality

Chlorobenzenes

Stable isotope

OH radicals

ABSTRACT

Substituted chlorobenzenes are the basic substructure of many surface water contaminants. In this study, the isotope fractionation and reaction mechanisms involved during the aqueous direct and indirect photodegradation of CH₃-, Cl-, and NO₂- substituted chlorobenzenes were investigated in laboratory experiments. Only 4-nitrochlorobenzene showed slow but isotopically fractionating direct photolysis. During indirect photodegradation using UV/H₂O₂-generated OH radicals, the pseudo first-order reaction rate constants increased in the order of the NO₂- < Cl- < CH₃- substituted chlorobenzenes. The most pronounced carbon enrichment factors were observed for nitrochlorobenzenes (up to $-4.8 \pm 0.5\%$), whereas the lowest were for chlorotoluenes ($\leq -1.0 \pm 0.1\%$). As the substituents became more electron-withdrawing, the activation energy barrier increased, leading to slower reaction rates, and the transition state changed to a more symmetrical or less reactant-like structure, resulting in larger apparent kinetic isotope effects. The results suggest that the rate-determining step in the reaction with OH radicals was the addition of the electrophile to the benzene ring. Even though further research is needed to quantify isotope fractionation during other transformation processes, these results showed evidence that compound specific isotope analysis can be used as a diagnostic tool for the fate of substituted chlorobenzenes in water.

© 2018 Elsevier Ltd. All rights reserved.

1. Introduction

Substituted chlorobenzenes are the basic chemical structure of many environmental contaminants such as herbicides 2,4-D, dichlorprop, chlortoluron, and drugs and personal care products like triclosan and diclofenac. In their simplest form, substituted chlorobenzenes, such as isomers of dichlorobenzene (DCB), chloromethylbenzene (or chlorotoluene, CMB), and nitrochlorobenzene (NCB), are widely distributed in surface waters (Schwarzbauer and

Ricking, 2010) in the low ng L⁻¹ or μg L⁻¹ range (Bester et al., 1998; Lekkas et al., 2004; Trova et al., 1991), due to their use as chemical intermediates in the production of dyes, solvents, pesticides, and pharmaceuticals. They have all been listed as substances which could belong to List I of European Council Directive 76/464/EEC (European Commission, 1982) due to their known or suspected toxicity to aquatic organisms and mutagenic and carcinogenic potentials (Calamari et al., 1983; OECD, 2005; Shimizu et al., 1983; Weisburger et al., 1978). The dichlorobenzene isomers also belong to the U.S. EPA List of Priority Pollutants (USEPA, 1979). Characterizing the transfer and transformation processes of substituted chlorobenzenes in surface waters is therefore essential to protect human and aquatic life and develop effective remediation strategies. One method that can be used to evaluate *in situ* transformation, Compound Specific Isotope Analysis (CSIA), is based on the faster reaction rates of molecules containing light (e.g., ¹²C) versus heavy (e.g., ¹³C) isotopes. While CSIA is widely used to study the fate and removal of traditional groundwater contaminants, to

* Corresponding author. 35 St George Street, Room GB319F, M5S 1A4 Toronto ON Canada.

E-mail address: elodie.passeport@utoronto.ca (E. Passeport).

¹ Present address: Department of Civil Engineering, University of Toronto, 35 St George Street, Toronto, ON M5S 1A4, Canada.

² Present address: Department of Chemical Engineering and Applied Chemistry, University of Toronto, 200 College Street, Toronto, ON M5S 3E5, Canada.

³ Present address: Department of Chemistry and Pharmaceutical Engineering, Qilu University of Technology, Jinan 250353, China.

date, its application to other environments such as sediments (Passeport et al., 2016) and surface waters is limited, e.g., Elsayed et al. (2014), Hartenbach et al. (2008), Maier et al. (2016), and Ratti et al. (2015a). In some cases, CSIA can help identify transformation processes that involve the breaking of chemical bonds. It can also be used to quantify degradation and gain insight into contaminant reaction mechanisms without the need to identify transformation products (Hunkeler et al., 2008).

In natural environments such as lakes and rivers, and in water treatment plants where UV/H₂O₂ advanced oxidation processes are used, organic compounds can be eliminated via direct photolysis and indirect photolysis induced by reactive species such as hydroxyl (OH) radicals (Boreen et al., 2003; Wols and Hofman-Caris, 2012). Hydroxyl radicals are naturally generated in all surface water environments from the photolysis of dissolved organic (Vaughan and Blough, 1998) and inorganic compounds (Zafriou, 1974). Therefore, there is great potential to evaluate the attenuation of contaminants with OH radicals in various aquatic systems using CSIA, which could be a promising tool for water quality monitoring and assessment. One of the limitations of stable carbon isotope analysis is the need for about 0.2–20 ng of carbon to be injected on-column (Giebel et al., 2010), resulting in typically moderately high detection limits of 5–10 µg/L (Dempster et al., 1997; Hunkeler and Aravena, 2000; Zwank et al., 2005), even though accurate carbon isotope analysis has been successfully conducted down to 0.1–1 µg/L (Schreglmann et al., 2013). The reaction mechanisms governing the direct and indirect photodegradation of substituted chlorobenzenes are not well understood. In addition, the potential of isotope fractionation during photodegradation reactions, and the extent to which it can contribute to deciphering reaction pathways have not been the subject of many studies. Previous research showed that stable carbon enrichment factors ranged from negligible values to ~ -5‰, e.g. during direct aqueous photolysis of polybrominated diphenyl ethers (Rosenfelder et al., 2011), organophosphorus pesticide dimethoate (Wu et al., 2014), herbicide atrazine (Hartenbach et al., 2008), and α -hexachlorocyclohexane (Zhang et al., 2014). Previous studies showed that direct photolytic dechlorination of the three chloroaniline isomers was associated with highly variable carbon and nitrogen isotope effects, which depended on pH and excited spin state populations (Ratti et al., 2015b, 2015c). Aqueous reactions of organic compounds with OH radicals also led to a similar range of stable carbon enrichment factors (Hartenbach et al., 2008; Ratti et al., 2015a; Wu et al., 2018; Zhang et al., 2014, 2016, 2015). For example, a negligible carbon enrichment factor (< -0.5‰) was found during the reaction of OH radicals with atrazine (Hartenbach et al., 2008), as well as for toluene, ethylbenzene, xylenes, and anisole (Zhang et al., 2016); moderate values were obtained for α -hexachlorocyclohexane (-1.9‰) (Zhang et al., 2014) and fuel oxygenates (-1.0 to -1.6‰); while larger values, up to -3.9‰, were observed for anilines and nitrobenzene (Zhang et al., 2016). In some cases, the determination of isotope fractionation for two or more elements proved efficient to distinguish among degradation processes. The apparent kinetic isotope effect values for carbon and nitrogen for the direct (Ratti et al., 2015b, 2015c) and indirect (Ratti et al., 2015a) photodegradation of chloroanilines correlated differently showing potential for the use of CSIA to differentiate between these chemical degradation pathways. However, the variability of isotope fractionation during aqueous photodegradation as a function of environmental conditions such as the type of reactive species, pH, and oxygen concentration (Hartenbach et al., 2008; Ratti et al., 2015a; Zhang et al., 2015), makes it difficult to predict reaction mechanisms and isotope effect for new molecules.

The objectives of this study were: 1) to estimate the extent of direct photolysis and indirect photolysis using OH radicals for

substituted chlorobenzenes in aqueous solutions; 2) to quantify stable carbon isotope fractionation during photodegradation, 3) to evaluate the potential to use CSIA to differentiate aqueous photodegradation from other environmentally-relevant processes such as biodegradation; and 4) to propose reaction mechanisms based on isotopic and kinetics data.

2. Materials and methods

2.1. Chemicals

Hydrogen peroxide (H₂O₂, 30% w/w), *n*-pentane, and sodium chloride (NaCl) were obtained from Merck (Darmstadt, Germany). The 1,2-, 1,3-, and 1,4-dichlorobenzene (1,2-, 1,3-, and 1,4-DCB), 3- and 4-nitrochlorobenzene (3- and 4-NCB), and 3- and 4- chloromethylbenzene (3- and 4-CMB) isomers were purchased from Sigma Aldrich. All chemicals were of analytical grade. A solution of phosphate buffer (10 mM, pH = 7.3) was made with Na₂HPO₄ and NaH₂PO₄. Ultrapure water (Milli-Q System, Millipore GmbH, Schwalbach/Ts. Germany) was used to prepare the standards and pH buffer.

2.2. Photodegradation experiments

All experiments were conducted using a 215-mL Pyrex cylindrical reactor vessel with a 28-cm² quartz window. The double-layer reactor wall allowed for controlling the reactor temperature at 20 °C. A 150-W xenon lamp (185–2000 nm, L2175, Hamamatsu, Japan) was used with a filter to cut-off radiations below 280 nm to better represent typical wavelengths at the Earth's surface. The lamp was placed 10-cm away from the reactor. A schematic of the experimental system is provided in Zhang et al. (2016). Each experiment was conducted with one of the studied compounds with initial concentrations ranging from 2×10^{-4} to 7×10^{-4} M, similar to other studies (Maier et al., 2016; Ratti et al., 2015a) and sufficiently low for the solutions to be considered as optically dilute as per OECD Guideline 316 (OECD, 2008) while guaranteeing proper quantification of parent compounds and potential degradation products, and accurate determination of stable carbon isotope signatures. Each solution was prepared in a pH = 7.3 aqueous phosphate buffer solution. For the indirect photodegradation experiments, 0.25 mL of 30% H₂O₂ was added to the solution at the start of the experiment, resulting in initial H₂O₂ concentrations of 12.5 mM, and contaminant to H₂O₂ molar ratios ranging between 1:50 and 1:25, similar to former studies (Daifullah and Mohamed, 2004; Zhang et al., 2016) and approximately one order of magnitude higher than for typical UV/H₂O₂ advanced oxidation treatment processes (Collins and Bolton, 2016). This ensured the formation of excess OH radicals therefore guaranteeing that direct photolysis and reactions with OH radicals would dominate in the reactors. A 200-mL volume of buffered solution was introduced in the reactor, leaving an initial reactor headspace of 15 mL. The solution was continuously stirred at 500 rpm during the experiment. Control dark experiments with 0.25 mL of 30% H₂O₂ were conducted for each compound without light and covering the reactor with aluminum foil to prevent light penetration. At each time step, 2 and 3 mL samples were collected for concentration and stable carbon isotope analysis, respectively. At the end of each experiment, a 10-mL sample was collected for product identification by gas chromatography mass spectrometry (GC/MS). The UV absorbance peaks of all studied compounds were determined using a UV/VIS/NIR Lambda 900 spectrophotometer (Perkin Elmer Instruments) (Supplemental Information (SI) Fig. S1 and Table S1). Only a portion of 3-NCB and 4-NCB showed significant absorbance above 280 nm.

2.3. Analytical methods

Concentrations. Concentrations of DCB, CMB, and NCB isomers were measured by gas chromatography coupled to a flame ionization detector (GC/FID). Details on temperature programs, sample preparation, and error estimation are provided in SI Section S2.

Stable carbon isotope analysis. For all compounds, the 3-mL samples collected for CSIA were extracted with 0.5 mL of *n*-pentane by shaking on an orbital shaker for 1 h at 200 rpm. The extracts were immediately transferred to 2-mL vials with inserts and kept at -20°C until analysis. Stable carbon isotope values were determined by gas chromatography – combustion – isotope ratio mass spectrometry (GC/C/IRMS, GC Isolink, ConFlo IV, and MAT 253), using a ZB-1 column ($60\text{ m} \times 0.32\text{ mm} \times 1\text{ }\mu\text{m}$). The temperature program started at 40°C , held for 5 min, then increased up to 280°C at $20^{\circ}\text{C min}^{-1}$ and held for 2 min. A total error of $\pm 0.5\%$ encompassing accuracy and reproducibility was accounted for on each $\delta^{13}\text{C}$ value (Sherwood Lollar et al., 2007).

Product identification. Photodegradation products were identified by gas chromatography (GC, 7890A, Agilent, Palo Alto, USA) mass spectrometry (MS, 5975C, Agilent, Palo Alto, USA). The GC column was a HP-5 ($30\text{ m} \times 0.32\text{ mm} \times 0.25\text{ }\mu\text{m}$, Agilent), and the GC temperature program started at 40°C and held for 5 min, the temperature was then increased up to 90°C at $3^{\circ}\text{C min}^{-1}$ and held at 90°C for 2 min, and increased up to 300°C at $20^{\circ}\text{C min}^{-1}$ and held for 5 min. Samples from the last sampling time of the direct and indirect photodegradation experiments were analyzed after derivatization. Derivatization was conducted to identify potential phenolic products as follows: 10 mg of NaHCO_3 was mixed into 1 mL of aqueous sample, and 5 μL of acetic anhydride (0.05 M) was then added to acetylate phenolic groups. The mixture was shaken for 20 min at 150 rpm and 0.5 mL of dichloromethane (DCM) was added before shaking again at 500 rpm for 1 h. The DCM extracts were analyzed by GC/MS. Selected samples, collected before the last sampling time for concentration measurement of the parent products, were also analyzed by GC/MS without prior derivatization.

2.4. Hammett relationship

A Hammett plot was constructed using the pseudo first-order rate constants with respect to the aromatic compound (k_X) obtained from the indirect photodegradation experiments for each chlorobenzene with substituent X placed in *meta* or *para* positions, i.e., X = Cl for 1,3-DCB and 1,4-DCB, CH_3 for the CMB isomers, and NO_2 for NCBs. The rate constants were normalized by the chlorobenzene indirect photodegradation pseudo first-order rate constant, $k_H = 0.173\text{ h}^{-1}$, determined under the same experimental conditions by Zhang et al. (2016). The Hammett equation, $\log(k_X/k_H) = \rho \times \sigma$, was fitted to the data and parameter ρ , expressing the effect of a substituent on the rate constant, was determined graphically. The Hammett substituent constants, σ^+ , for *meta* (σ_m^+) and *para* (σ_p^+) substituents, representing the total polar effect exerted by a substituent on the reaction center when a positive charge is delocalized, were obtained from Hansch et al. (1991). Due to steric hindrance, the Hammett relationship is not applicable to *ortho*-substituted compounds such as 1,2-DCB.

2.5. Isotope data analysis

Carbon enrichment factors (ϵ_C) were determined from the Rayleigh equation, Eq. (1), using the linear regression of $\ln(R/R_0)$ as a function of $\ln(f)$, without forcing through zero, where R and R_0 are the isotopic compositions at any time $t > 0$ and the initial time t_0 , and f is the fraction of remaining compound at time t , calculated based on the stepwise correction method reported by Buchner et al.

(2017), even though virtually no difference were observed in the enrichment factors when determined using the ratio of the concentrations at times t and t_0 for f :

$$\frac{R}{R_0} = (f)^{\epsilon_C} \quad (1)$$

The enrichment factors represent carbon isotope effects for the whole molecule. To characterize the isotope effect at the reactive position for each substituted chlorobenzene, apparent kinetic isotope effect values for carbon ($AKIE_C$) were calculated as in Eq. (2) (Elsner et al., 2005):

$$\frac{1}{AKIE_C} = \frac{z \cdot n \cdot \epsilon_C}{x \cdot 1000} + 1 \quad (2)$$

where, for a given postulated reaction mechanism, n is the number of carbon atoms in the molecule, x is the number of carbon atoms at reactive positions, and z is the number of carbon atoms at reactive positions with equal reactivity. Assuming negligible contribution from secondary kinetic isotope effects (KIE_C), i.e., the reactive positions are associated with primary isotope effect only, $x = z$.

3. Results

3.1. Control dark experiments

The control dark experiments were conducted for each of the studied chemicals in presence of H_2O_2 . No significant concentration decrease was observed other than the expected headspace losses of $<7\%$ due to liquid – gas phase re-equilibration after each sampling (SI Fig. S2). This suggests that the sole presence of H_2O_2 does not induce degradation of the studied chemicals under the experimental conditions used.

3.2. Direct photolysis

In general, direct photolysis through UV light absorption (for $\lambda \geq 280\text{ nm}$) did not significantly affect concentrations and isotope values ($\pm 0.5\%$) of most studied compounds with two exceptions (SI Fig. S3). Direct photolysis of 1,4-DCB did not seem to produce significant concentration decrease except during the 4 h and 19 h sampling times (Fig. S3) during which the light was off. Given that the subsequent samples showed constant concentrations, and that the $\delta^{13}\text{C}$ values were within $\pm 0.5\%$ for times 0 h, 19 h, and 24 h, this concentration decrease is not due to direct photolysis. For the direct photolysis of 4-NCB, the $\delta^{13}\text{C}$ values remained within $\pm 0.5\%$ of the initial value of -32.9% for 2 days. However, subsequently, 4-NCB $\delta^{13}\text{C}$ values became significantly enriched in ^{13}C by up to 2.2‰ after 4 days, when 34% of the initial concentration had disappeared (SI Fig. S3 (d) and S4). This is due to the potential of 4-NCB to partially absorb light at wavelengths higher than the cut-off filter at 280 nm (see SI Fig. S1), with a maximum absorbance at 281 nm, and a corresponding molar absorption coefficient $\epsilon_{281\text{nm}}$ of $3242\text{ M}^{-1}\text{ cm}^{-1}$ applying the Beer-Lambert law. The 4-NCB direct photolysis was associated with a first-order degradation rate constant of $0.0043 \pm 0.0003\text{ h}^{-1}$ ($R^2 = 0.97$) and an enrichment factor of $-5.1 \pm 0.4\%$ ($R^2 = 0.96$) over the reduction of 34% of the initial compound (SI Fig. S4 and Table S2).

3.3. Indirect photolysis

Figure 1 presents the kinetics of indirect photodegradation of the studied compounds reacting with OH radicals. The reactions followed pseudo first-order kinetics with respect to each

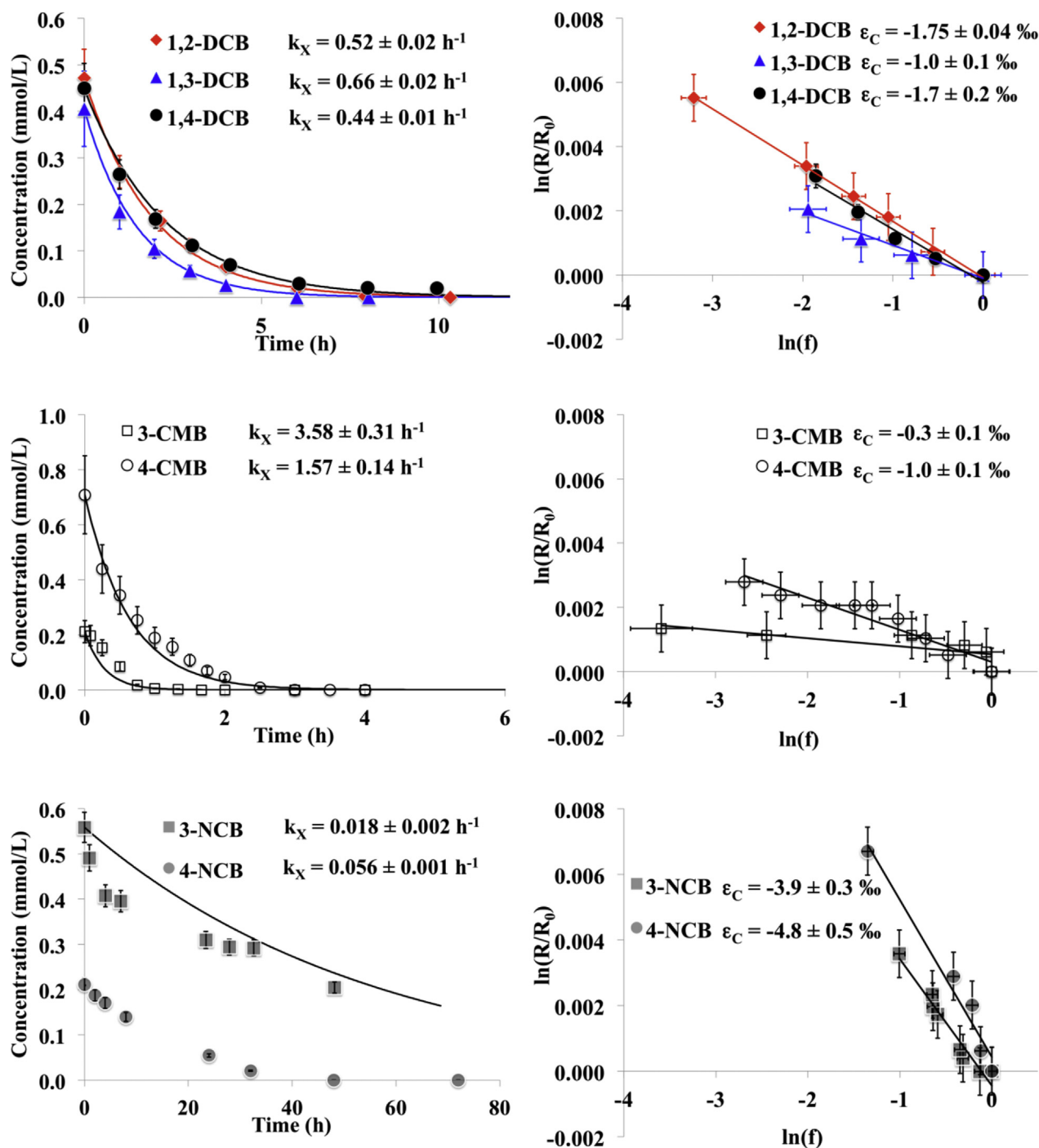


Fig. 1. Kinetics and Rayleigh plots of the studied substituted chlorobenzenes during indirect photodegradation.

Concentrations (left panels) and stable carbon isotope results (linear form of the Rayleigh plot, right panels) during the reaction of the studied substituted chlorobenzenes with OH radicals. The pseudo first-order rate constants (k_X) and enrichment factors (ϵ_C) are presented with 95% confidence interval errors. The error bars on concentrations ($2 \times \text{COV}$, i.e. $2 \times$ coefficient of variation) were 13% (1,2-DCB), 20% (1,3-DCB), 12% (1,4-DCB), 19% (3-CMB), 20% (4-CMB), 6% (3-NCB), and 7% (4-NCB). The error bars on stable isotope $\delta^{13}\text{C}$ values were $\pm 0.5\%$, accounting for both accuracy and reproducibility (Sherwood Lollar et al., 2007). The error bars on the Rayleigh plots were determined from error propagation. Note the differences in time intervals for the X-axis and concentration range for the Y-axis in the kinetics plots (left panels).

contaminant, with R^2 values greater than 0.94 and pseudo first-order rate constants (k_X) that increased in the order of NCBs (0.018 and 0.056 h^{-1}), DCBs (0.44 – 0.66 h^{-1}), and CMBs (1.57 and 3.58 h^{-1}) (see SI Table S2). This is in agreement with previously reported pseudo first-order rate constants of related compounds at similar initial concentrations reacting in UV/ H_2O_2 systems, with similar molar ratio and H_2O_2 initial concentrations, such as substituted benzenes (Ghaly et al., 2001; Sundstrom et al., 1989;

Weir et al., 1987), e.g. with values ranging from 0.01 h^{-1} for nitrobenzene to 0.50 h^{-1} for N,N -dimethylaniline (Zhang et al., 2016). The CMBs degraded at the fastest rates with concentrations reaching below detection limit levels after 2 h for 3-CMB and 3.5 h for 4-CMB. The calculated indirect photodegradation half-life ($\ln(2)/k_X$) were 1.0–1.6 h for DCBs, 0.2 h for 3-CMB and 0.4 h for 4-CMB, and 39 and 12 h for 3-NCB and 4-NCB, respectively.

The Hammett plot is shown in Fig. 2. The linear relationship

between $\log(k_X/k_H)$ vs. σ^+ showed a good fit ($R^2 = 0.85$), and displayed a negative Hammett ρ value of -2.1 , suggesting that the reaction rate increases with electron-donating groups. This is in line with the observed lower half-life of CMBs compared to DCBs and NCBs, and with previous similar studies of the reaction of substituted benzenes with OH radicals (Mohan et al., 1991).

The Rayleigh equation was applied as described in Eq. (1) to determine stable carbon isotope enrichment factors. The CMB isotope enrichment factors were insignificant ($< -1.0 \pm 0.1\%$), those for the DCB isomers were -1.75 ± 0.04 (1,2-DCB), $-1.0 \pm 0.1\%$ (1,3-DCB), and $-1.7 \pm 0.2\%$ (1,4-DCB), whereas those for the NCBs were the highest, $-3.9 \pm 0.3\%$ (3-NCB) and $-4.8 \pm 0.5\%$ (4-NCB) (SI Table S2 and Fig. 1). The ϵ_C values of NCBs were consistent with the $-3.9 \pm 0.2\%$ value obtained by Zhang et al. (2016) for nitrobenzene aqueous reaction with OH radicals.

3.4. Transformation products

For each experiment, selected samples were analyzed by GC/MS to identify remaining degradation products (SI Table S3). The analysis did not reveal any phenolic products except for the reaction of the two CMB isomers with OH radicals for which 2-chloro-6 (or 5)-methylphenol were detected. These results are not consistent with the reported phenolic products obtained from OH radical reactions with substituted benzenes. This is likely due to a combination of two factors: first, the samples that underwent derivatization prior to analysis were those from the last sampling points, when the proportions of remaining parent contaminant and intermediate metabolites such as phenolic products were low; second, the samples collected at intermediate sampling points were analyzed without prior derivatization, which would have limited the potential to detect phenolic compounds.

4. Discussion

4.1. Substituted chlorobenzenes are subject to aqueous photodegradation

The first finding of this research is that the complete

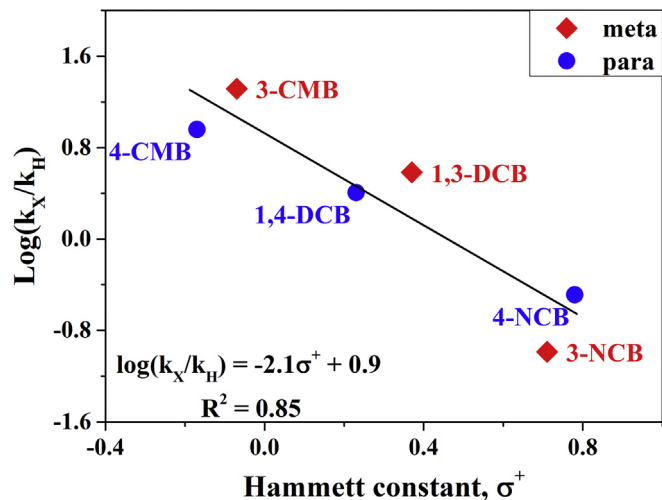


Fig. 2. Hammett plot.

Hammett plot presenting the logarithm of the ratio of the pseudo first-order rate constants for the reaction between OH radicals and the non-substituted chlorobenzene (k_H , chlorobenzene), and the X-substituted chlorobenzenes (k_X , X = Cl, CH₃, and NO₂). The Hammett constant, σ^+ , is the substituent constant obtained from Hansch et al. (1991).

disappearance of the compounds within 2–48 h – up to ~315 h for 3-NCB, the generation of some phenolic degradation products in the case of the CMB isomers, and the observed stable carbon isotope fractionation all demonstrate that substituted chlorobenzenes are able to react with photo-induced OH radicals in aqueous solution. The absence of significant amounts of degradation intermediates was partly explained by the absence of derivatization for intermediate samples, but could also show that the degradation products further degrade as well. The pseudo first-order degradation rate constants of 2,4-dichlorophenol, a potential product of the reaction of 1,3-DCB with OH radicals, were found to be 3.1 h^{-1} in H₂O₂/UV processes and 3.0 and 10.4 h^{-1} during direct photolysis under similar initial concentration and pH conditions as those used in this study (Pera-Titus et al., 2004). This is 5–16 times larger than that of 1,3-DCB at $0.66 \pm 0.02 \text{ h}^{-1}$ measured here, and therefore suggests that detection of phenolic products would have been difficult due to their fast degradation in the reactor.

The second finding of this study is that 4-NCB can also degrade directly via photolysis even in the absence of reactive species such as OH radicals. However, this process was much slower ($k = 0.0043 \pm 0.0003 \text{ h}^{-1}$) than the reaction of 4-NCB with OH radicals ($k = 0.056 \pm 0.001 \text{ h}^{-1}$) and therefore might not be relevant when both processes occur concurrently.

4.2. Insight into reaction mechanisms

4.2.1. Hammett plot

The kinetics results showed a linear relationship between $\log(k_X/k_H)$ and σ^+ with a good correlation coefficient ($R^2 = 0.85$) (Fig. 2). This suggests that the reaction of substituted chlorinated benzenes with OH radicals involves one main rate-determining step. The relatively high magnitude of the proportionality constant, ρ , with an absolute value greater than 1, shows that the effect of the substituents on the reaction rate is significant. The fact that the ρ value is negative, -2.1 , indicates that the reaction rates increase with electron-donating groups (CH₃) and decrease with electron-withdrawing groups (Cl, NO₂). This is simply another way to note that the reaction rates increase in the order of NO₂-, Cl-, and CH₃-substituted chlorobenzenes. Mohan et al. (1991) studied OH radical addition to substituted chlorobenzenes, with -CH₃ and -OCH₃ as electron-donating groups, and -CF₃, -CHCl₂, and -CH₂Cl as electron-withdrawing groups. Using a similar Hammett plot approach, they also obtained a negative but smaller slope of -0.52 . Other studies reported ρ values of -0.41 and -0.5 for the reaction of monosubstituted benzenes with OH radicals (Anbar et al., 1966; Neta and Dorfman, 1968). A negative value for ρ suggests that a positive charge develops at the reaction center in the transition state of the rate-determining step of the reaction of substituted chlorinated benzenes with OH radicals. This is a characteristic of Electrophilic Aromatic Substitution (EAS) reactions. It is well established that OH radical attack on aromatic compounds proceeds via a mechanism analogous to EAS (Anbar et al., 1966). For such reactions, electron-withdrawing groups (e.g., Cl, NO₂) increase the energy barrier for the addition of an electrophile, in this case the OH radical, to the aromatic ring. This is due to a combination of transition state destabilization and ground state stabilization, and results in a decrease in the reaction rate. Electrophilic aromatic substitution reactions are a two-step process. For the reaction of substituted chlorobenzenes with OH radicals, the first step is rate determining and involves the formation of a π complex transition state followed by the addition of the OH radical and results in the formation of a sigma complex hydroxycyclohexadienyl radical intermediate. The second step consists of the fast elimination of a H atom from the ring to regain its aromaticity leaving a chlorophenolic product (Smith and Norman, 1963).

The addition of OH radical to the ring and further elimination of a hydrogen atom to recover the ring's aromaticity have been observed during the aqueous reaction of chlorotoluene (Mohan et al., 1991) and nitrochlorobenzene with OH radicals that produced phenolic intermediate compounds (Guittonneau et al., 1990). Zhang et al. (2016) also identified phenolic intermediates in the reaction of substituted benzenes with OH radicals. In the present study, phenolic products were observed in the early stage (<2 h) of the reaction of 3- and 4-CMB with OH radicals, with the production of 2-chloro-6-methylphenol and 2-chloro-5-methylphenol, respectively. This confirms that OH addition to the ring is the most likely rate-determining step in the reaction of the studied substituted chlorobenzenes with OH radicals.

4.2.2. Isotope effects

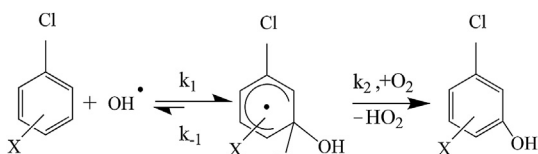
To further elucidate reaction mechanisms, AKIE_C values were calculated to characterize the isotope effect of the cleavage of the chemical bond at the reactive positions. Based on the kinetics results discussed above, and former results on CMB and NCB (Guittonneau et al., 1990; Mohan et al., 1991), OH radical aromatic substitution is expected to be the dominant mechanism for the indirect photodegradation of the substituted chlorobenzenes. However, Zhang et al. (2016) showed that the methyl group in toluene could also undergo H abstraction during reaction with OH radicals, which could be expected for the CMB isomers. However, reaction products following attack on the methyl group, such as 3- and 4-chlorobenzaldehyde and benzyl alcohols, were not observed in the present study, while chlorophenols were observed for 3- and 4-CMBs. To further evaluate if H abstraction was significant, in the AKIE_C value calculations, two main reaction pathways were hypothesized: OH radical substitution to a H atom attached to one of the unsubstituted carbon atom of the benzene ring, and H abstraction from the methyl group in the CMB isomers. In addition, instead of only considering all unsubstituted carbon atoms from the benzene ring as potential reactive positions, the values for x and z in Eq. (2) for the calculation of the AKIE_C values were determined by considering the substituents' *ortho*-, *meta*-, or *para*-directing effect, and whether they were activating or deactivating substituents on the benzene ring (see details in SI Section S5). The calculated AKIE_C values are summarized in SI Table S2.

By analogy with the conceptual framework developed for enzyme-catalyzed reactions, we can represent the reaction of the X-substituted chlorobenzenes with OH radicals as shown in Scheme 1, where a hydroxycyclohexadienyl radical intermediate is formed:

This let us introduce a commitment factor, C, such that $C = k_2/k_{-1}$ in the expression of AKIE_C:

$$AKIE_C = \frac{KIE_C + C}{1 + C} \quad (3)$$

where KIE_C is the intrinsic kinetic isotope effect that depends only on the irreversible reaction step:



Scheme 1. OH radical ring substitution on X-substituted chlorobenzenes (X = CH₃, Cl, or NO₂).

$$KIE_C = \frac{k_2^L}{k_2^H} \quad (4)$$

Equation (3) assumes that the first reversible step is associated with negligible isotope effects.

As it is not expected for k_{-1} to be significant, i.e., the addition of the OH radical to the aromatic ring is not easily reversible, $k_2 \gg k_{-1}$, resulting in large values for C regardless of the substituent and its position. With large C values – equivalent to a very efficient enzymatic reaction – the AKIE_C values are reduced (masked) and tend to be closer to unity rather than representing the intrinsic KIE_C.

All AKIE_C values showed normal kinetic isotope effects (AKIE_C > 1) (SI Table S2). Under the assumption of OH radical electrophilic aromatic substitution, the AKIE_C values were very close to unity for the DCB and CMB isomers, and somewhat higher for 3-NCB (1.024 ± 0.004) and 4-NCB (1.030 ± 0.004).

The absolute magnitude of the enrichment factors and the AKIE_C values for the *meta*-substituted chlorobenzenes were always lower than those of their *para*-substituted counterparts. Given that the *meta*-substituted chlorobenzenes reacted faster than their *para*-substituted counterparts, $C_{meta} > C_{para}$, this resulted in the observed lower AKIE_{Cmeta} than AKIE_{Cpara} and therefore more masking of the intrinsic KIE_C in the *meta*-substituted chlorobenzenes compared to their *para*-substituted counterparts.

Theoretical and experimental KIE_C values obtained for C–O bond formation on alkenes typically range from 0.998 to 1.024 for chemical oxidations with permanganate and epoxidation reactions (Elsner et al., 2005; Singleton et al., 1997; Singleton and Wang, 2005). The oxidation on a ring can be expected to be associated with even larger KIE_C values due to the larger energy barrier of the reaction to break a ring's aromaticity. Indeed, reported experimental AKIE_C values for C–O bond formation during ring hydroxylation ranged from 1.005 to 1.026 in biodegradation experiments, and from 1.029 to 1.051 for abiotic experiments of gas-phase OH radical addition to various aromatic compounds (SI Table S4). To the best of our knowledge, the only theoretical KIE_C values calculated for the ring addition of OH radicals are those reported in Zhang et al. (2016) for OH addition to the *para* position of various substituted benzenes, and ranged from 1.0239 to 1.0316. While the AKIE_C values of the two NCB isomers were within these ranges, those for the CMB and the DCB isomers were lower (1.002–1.011), possibly due to a masking effect. Given that the reactor was continuously stirred, the reaction rates were expected to be diffusion-controlled. Possible explanations proposed for the masking of the KIE_C in substituted benzenes (Zhang et al., 2016) could apply here as well, such as the formation of the π complex transition state prior to OH radical addition in Step 1 of Scheme 1, and pre-equilibrium between the substituted chlorobenzene and the OH radical prior to the rate-determining step. A recent study proposed that the creation of a water cage could account for masking of intrinsic KIE (Kopinke and Georgi, 2017). This cage effect was explained by the trapping of the OH radical and substrate in the water shell formed by complex interaction of the hydrophobic solute with the surrounding water molecules. The correlation between AKIE_C values and molecules' hydrophobicity ($\log(K_{ow})$ values) was used to evaluate this assumption. A good correlation ($r^2 = 0.83$) was found for the molecules studied in the present study (SI Fig. S5). However a poor correlation ($r^2 = 0.46$) was obtained when analyzing the dependency of AKIE_C of substituted benzenes using data from Zhang et al. (2016) (SI Fig. S5) suggesting that the molecular structure of the organic substrate was the main factor driving fractionation. The relationship between AKIE_C values and substituents' Hammett constants suggests that the electronic

structure of the organic molecules was the major factor governing isotope fractionation for radical reactions in water. More research may be needed to validate the cage effect as a potential contributor to KIE_C masking in OH radical aqueous reactions.

Under the scenario of OH radical addition to a substituted carbon atom, involving the breaking of a C–Cl, C–N, or C–C bond, the same values for $AKIE_C$ as those for OH radical addition to an unsubstituted carbon atom were obtained (SI Section S5). However, these $AKIE_C$ values were significantly lower than the theoretical KIE_C Streitwieser limits for these cleavages, i.e. 1.057 for C–Cl, 1.060 for C–N, and 1.049 for C–C (Elsner et al., 2005), which were obtained under the assumption that the bond is broken during the transition state. When considering a more realistic assumption, e.g. that the bond is 50% broken, half these limits can be considered. Even in this case, the theoretical KIE_C values are still higher than the calculated $AKIE_C$ values, except for C–N cleavage in the NCB isomers, confirming that the breaking of a C–X bond in the rate-determining step is unlikely.

Finally, $AKIE_C$ values of 1.002 and 1.007 for 3- and 4-CMB, respectively, were obtained when assuming H abstraction on the CH_3 group of the CMB isomers. These were lower than theoretical KIE_C values of 1.020 expected for C–H bond cleavage (Elsner et al., 2005), suggesting that OH radical addition to an unsubstituted carbon atom likely played a more dominant role than H abstraction in the reaction of the CMB isomers with OH radicals. This is in line with the higher contribution of OH addition relative to H abstraction observed for toluene (Zhang et al., 2016). It is also confirmed by the detection of phenol intermediates in the indirect photodegradation experiments with CMB isomers, which supports a preferential attack of the OH radicals to the ring rather than the methyl group. Finally, this is also the main reaction mechanism proposed for the reaction of chlorotoluene isomers with OH radicals in distilled water (Mohan et al., 1991).

The ϵ_C and $AKIE_C$ values increased with increasing Hammett substituent constants σ^+ (Fig. 3). The most electron-withdrawing substituents led to the highest carbon isotope fractionation. This suggests that the transition state might be more symmetrical for the reaction of OH radicals with the NCB and DCB isomers than for the CMBs. More data are needed to propose a quantitative

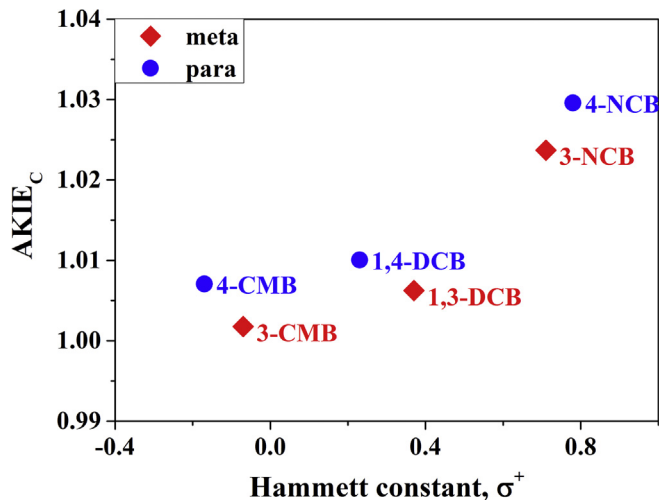


Fig. 3. Relationship between $AKIE_C$ values and substituents' Hammett constants. Correlation between $AKIE_C$ values and Hammett substituent constants for the reaction between OH radicals and the X-substituted chlorobenzenes (k_X , X = Cl, CH_3 , and NO_2). The Hammett constant, σ^+ , is the substituent constant obtained from Hansch et al. (1991); CMB is chloromethylbenzene, DCB is dichlorobenzene, and NCB is nitrochlorobenzene.

relationship between isotope fractionation and substituent constants, and to provide a mechanistic interpretation for such a relationship. The influence of the electronic properties of aromatic substituents on isotope effects was observed for nitrogen isotope fractionation during the oxidation of substituted anilines (Ratti et al., 2015a; Skarpeli-Liati et al., 2011; Skarpeli-Liati et al., 2012) while no substituent effect was observed for the abiotic reduction of nitroaromatic compounds (Hofstetter et al., 2008a).

Based on these kinetics and isotope results, the proposed dominant reaction pathway for the studied compounds involves the initial formation of a C–O bond at one of the unsubstituted carbon atoms on the benzene ring during the rate-determining step, followed by the release of a H atom (Scheme 1).

4.3. Potential to use CSIA to distinguish between aqueous photodegradation and other processes

The negligible isotope fractionation observed for the CMB isomers prevents stable carbon isotope analysis to be used as an identification tool for CMB aqueous photodegradation. Conversely, the NCBs, and to a lower extent the DCBs, showed quantifiable carbon isotope fractionation during their reaction with OH radicals. While transformation reactions may produce significant isotope fractionation, typically, negligible carbon isotope fractionation is associated with transfer mechanisms such as equilibrium adsorption (Harrington et al., 1999; Passeport et al., 2014), diffusion (Passeport et al., 2014; Xu et al., 2016), and volatilization (Harrington et al., 1999), at least at scales relevant to most field sampling strategies (Xu et al., 2016, 2017). Table S5 in SI summarizes published carbon isotope enrichment factors for various transformation processes of substituted chlorobenzenes that could occur concurrently with indirect photodegradation, e.g., microbial degradation under aerobic and anaerobic conditions, abiotic processes, and direct photodegradation. Because significant gaps still exist in the assessment of carbon isotope enrichment factors for these compounds, those of related compounds were reported as well.

During anaerobic microbial degradation, 1,3-DCB and 1,4-DCB produce significant isotope fractionation with ϵ_C values of -5.4 ± 0.4 and $-6.3 \pm 0.2\%$, respectively, while 1,2-DCB is associated with a low enrichment factor of $-0.8 \pm 0.1\%$ (Liang et al., 2014). While the large ϵ_C values of 1,3- and 1,4-DCB would prevent the use of stable carbon isotope analysis to distinguish between anaerobic biodegradation and reaction with OH radicals, situations where both processes occur simultaneously are rare. Indeed, indirect aqueous photodegradation is only relevant in surface waters, where oxygenated conditions dominate. In aquatic surface environments such as rivers, wetlands, and oceans, the concentrations in oxygen (Tao et al., 2006) and OH radicals (Zhou and Mopper, 1990) decrease with depth, and anaerobic zones are usually limited to the sediment phase or water depths at which reactions with OH radicals are not expected. No carbon isotope enrichment factors have been reported for the aerobic biodegradation of DCB isomers; however, negligible carbon isotope fractionation ($< -0.4 \pm 0.1\%$) was observed for chlorobenzene (Kaschl et al., 2005) and 1,2,4-trichlorobenzene (Griebler et al., 2004; Liang et al., 2011), suggesting that DCBs might also be associated with small ϵ_C values during aerobic biodegradation. There is therefore potential to use CSIA to identify indirect aqueous photodegradation of the DCB isomers.

For NCBs, the only other published ϵ_C value, -0.65% , is that associated with the abiotic reduction of 4-NCB in suspensions of Fe(II)/goethite (Hartenbach et al., 2006). No information on stable carbon isotope fractionation exists for the aerobic or anaerobic biodegradation of NCB isomers. However, nitrobenzene was

studied under aerobic conditions, and exhibited ϵ_C values of $-0.57 \pm 0.06\text{‰}$ during aerobic partial reduction by *Pseudomonas pseudoalcaligenes* strain JS45 (Hofstetter et al., 2008b), and between -3.5 ± 0.2 and $-3.9 \pm 0.2\text{‰}$ for nitrobenzene aerobic oxidation with various bacteria strains, cell extracts, and enzymes (Hofstetter et al., 2008b; Pati et al., 2014). Smaller ϵ_C values were obtained for the aerobic oxidation of 2-, 3-, 4-, and 2,6-di-nitro-toluene, ranging from -0.4 ± 0.2 and $-1.4 \pm 0.4\text{‰}$ (Pati et al., 2016). Altogether, these results suggest that the aerobic biodegradation of NCB isomers could produce stable carbon isotope fractionation within a similar range as that reported here for their reaction with OH radicals. These effects should be evaluated in future studies before CSIA can be used as a diagnostic tool for NCB fate in surface water environments.

5. Conclusions

- Results from (i) the Hammett relationship, (ii) the stable carbon isotope analysis, (iii) degradation product analysis, and (iv) former literature studies provided multiple lines of evidence that the reaction of OH radicals with substituted chlorobenzenes proceeds primarily via OH aromatic substitution, involving first the rate-determining C–O bond formation, followed by H release.
- The substituents on the chlorobenzene structure affected both reactivity and stable carbon isotope fractionation.
- While the carbon isotope enrichment factors obtained in this study were small, they will likely be sufficient to identify indirect photodegradation of the NCB and potentially the DCB isomers provided that at least 40% of the NCBs and 70–87% of the DCBs degrade via reaction with OH radicals.
- In order to conclusively assess the diagnostic capabilities of CSIA for substituted chlorobenzenes, further research should be conducted with more complex water matrices.

Acknowledgements

This research has been financially supported by the European Union under the 7th Framework Program (project acronym CSI:ENVIRONMENT, contract number PITN-GA-2010-264329), and a Collaborative Research and Development grant from the Natural Sciences and Engineering Research Council of Canada (#497236).

Appendix A. Supplementary data

Supplementary data related to this article can be found at <https://doi.org/10.1016/j.watres.2018.02.008>.

References

Anbar, M., Meyerstein, D., Neta, P., 1966. The reactivity of aromatic compounds toward hydroxyl radicals. *J. Phys. Chem.* 70 (8), 2660–2662.

Bester, K., Gatermann, R., Huhnerfuss, H., Lange, W., Theobald, N., 1998. Results of non target screening of lipophilic organic pollutants in the German Bight. IV: identification and quantification of chloronitrobenzenes and dichloronitrobenzenes. *Environ. Pollut.* 102 (2–3), 163–169.

Boreen, A.L., Arnold, W.A., McNeill, K., 2003. Photodegradation of pharmaceuticals in the aquatic environment: a review. *Aquat. Sci.* 65 (4), 320–341.

Buchner, D., Jin, B., Ebert, K., Rolle, M., Elsner, M., Haderlein, S.B., 2017. Experimental determination of isotope enrichment factors – bias from mass removal by repetitive sampling. *Environ. Sci. Technol.* 51 (3), 1527–1536.

Calamari, D., Galassi, S., Setti, F., Vighi, M., 1983. Toxicity of selected chlorobenzenes to aquatic organisms. *Chemosphere* 12 (2), 253–262.

Collins, J., Bolton, J.R., 2016. *Advanced Oxidation Handbook*. American Water Works Association, Denver, CO, USA.

Daifullah, A.H.A., Mohamed, M.M., 2004. Degradation of benzene, toluene ethylbenzene and p-xylene (BTEX) in aqueous solutions using UV/H₂O₂ system. *J. Chem. Technol. Biotechnol.* 79 (5), 468–474.

Dempster, H.S., Sherwood Lollar, B., Feenstra, S., 1997. Tracing organic contaminants

in groundwater: a new methodology using compound-specific isotopic analysis. *Environ. Sci. Technol.* 31 (11), 3193–3197.

Elsayed, O.F., Maillard, E., Vuilleumier, S., Nijenhuis, I., Richnow, H.H., Imfeld, G., 2014. Using compound-specific isotope analysis to assess the degradation of chloroacetanilide herbicides in lab-scale wetlands. *Chemosphere* 99, 89–95.

Elsner, M., Zwank, L., Hunkeler, D., Schwarzenbach, R.P., 2005. A new concept linking observable stable isotope fractionation to transformation pathways of organic pollutants. *Environ. Sci. Technol.* 39 (18), 6896–6916.

European Commission, 1982, 14 July 1982. Official Journal of the European Communities C176, Communication from the Commission to the Council on Dangerous Substances Which Might be Included in List I of Council Directive 76/464/EEC, vol. 25, p. 14.

Ghaly, M.Y., Hartel, G., Mayer, R., Haseneder, R., 2001. Photochemical oxidation of p-chlorophenol by UV/H₂O₂ and photo-Fenton process. A comparative study. *Waste Manag.* 21 (1), 41–47.

Giebel, B.M., Swart, P.K., Riemer, D.D., 2010. Delta 13-C table isotope analysis of atmospheric oxygenated volatile organic compounds by gas chromatography-isotope ratio mass spectrometry. *Anal. Chem.* 82 (16), 6797–6806.

Griebler, C., Safinowski, M., Vieth, A., Richnow, H.H., Meckenstock, R.U., 2004. Combined application of stable carbon isotope analysis and specific metabolites determination for assessing in situ degradation of aromatic hydrocarbons in a tar oil-contaminated aquifer. *Environ. Sci. Technol.* 38 (2), 617–631.

Guittonneau, S., De Laat, J., Guguet, J.-P., Bonnel, C., Dore, M., 1990. Oxidation of parachloronitrobenzene in dilute aqueous solution by O₃ UV and H₂O₂ UV: a Comparative Study. *Ozone: Sci. Eng.* 12 (1), 73–94.

Hansch, C., Leo, A., Taft, R.W., 1991. A survey of Hammett substituent constants and resonance and field parameters. *Chem. Rev.* 91 (2), 165–195.

Harrington, R.R., Poulson, S.R., Drever, J.I., Colberg, P.J.S., Kelly, E.F., 1999. Carbon isotope systematics of monoaromatic hydrocarbons: vaporization and adsorption experiments. *Org. Geochem.* 30 (8A), 765–775.

Hartenbach, A., Hofstetter, T.B., Berg, M., Bolotin, J., Schwarzenbach, R.P., 2006. Using nitrogen isotope fractionation to assess abiotic reduction of nitroaromatic compounds. *Environ. Sci. Technol.* 40 (24), 7710–7716.

Hartenbach, A.E., Hofstetter, T.B., Tentscher, P.R., Canonica, S., Berg, M., Schwarzenbach, R.P., 2008. Carbon, hydrogen, and nitrogen isotope fractionation during light-induced transformations of atrazine. *Environ. Sci. Technol.* 42 (21), 7751–7756.

Hofstetter, T.B., Neumann, A., Arnold, W.A., Hartenbach, A.E., Bolotin, J., Cramer, C.J., Schwarzenbach, R.P., 2008a. Substituent effects on nitrogen isotope fractionation during abiotic reduction of nitroaromatic compounds. *Environ. Sci. Technol.* 42 (6), 1997–2003.

Hofstetter, T.B., Spain, J.C., Nishino, S.F., Bolotin, J., Schwarzenbach, R.P., 2008b. Identifying competing aerobic nitrobenzene biodegradation pathways by compound-specific isotope analysis. *Environ. Sci. Technol.* 42 (13), 4764–4770.

Hunkeler, D., Aravena, R., 2000. Determination of compound-specific carbon isotope ratios of chlorinated methanes, ethanes, and ethenes in aqueous samples. *Environ. Sci. Technol.* 34 (13).

Hunkeler, D., Meckenstock, R.U., Sherwood Lollar, B., Schmidt, T.C., Wilson, J.T., 2008. A Guide for Assessing Biodegradation and Source Identification of Organic Ground Water Contaminants Using Compound Specific Isotope Analysis (CSIA). United States Environmental Protection Agency, Ada, OK, p. 67.

Kaschl, A., Vogt, C., Uhlig, S., Nijenhuis, I., Weiss, H., Kastner, M., Richnow, H.H., 2005. Isotopic fractionation indicates anaerobic monochlorobenzene biodegradation. *Environ. Toxicol. Chem.* 24 (6), 1315–1324.

Kopinke, F.D., Georgi, A., 2017. What controls selectivity of hydroxyl radicals in aqueous solution? Indications for a cage effect. *J. Phys. Chem.* 121 (41), 7947–7955.

Lekkas, T., Kolokythas, G., Nikolaou, A., Kostopoulou, M., Kotrikla, A., Gatidou, G., Thomaidis, N.S., Goulinopoulos, S., Makri, C., Babos, D., Vagi, M., Stasinakis, A., Petsas, A., Lekkas, D.F., 2004. Evaluation of the pollution of the surface waters of Greece from the priority compounds of List II, 76/464/EEC Directive, and other toxic compounds. *Environ. Int.* 30 (8), 995–1007.

Liang, X., Howlett, M.R., Nelson, J.L., Grant, G., Dworatzek, S., Lacrampe-Couloume, G., Zinder, S.H., Edwards, E.A., Sherwood Lollar, B., 2011. Pathway-dependent isotope fractionation during aerobic and anaerobic degradation of monochlorobenzene and 1,2,4-trichlorobenzene. *Environ. Sci. Technol.* 45 (19), 8321–8327.

Liang, X., Mundle, S.O.C., Nelson, J.L., Passeport, E., Chan, C.C.H., Lacrampe-Couloume, G., Zinder, S.H., Sherwood Lollar, B., 2014. Distinct carbon isotope fractionation during anaerobic degradation of dichlorobenzene isomers. *Environ. Sci. Technol.* 48 (9), 4844–4851.

Maier, M.P., Prasse, C., Pati, S.G., Nitsche, S., Li, Z., Radke, M., Meyer, A., Hofstetter, T.B., Ternes, T.A., Elsner, M., 2016. Exploring trends of C and N isotope fractionation to trace transformation reactions of diclofenac in natural and engineered systems. *Environ. Sci. Technol.* 50 (20), 10933–10942.

Mohan, H., Mudaliar, M., Aravindakumar, C.T., Rao, B.S.M., Mittal, J.P., 1991. Studies on structure reactivity in the reaction of OH radicals with substituted halobenzenes in aqueous solutions. *J. Chem. Soc. Perkin Trans. 2* (9), 1387–1392.

Neta, P., Dorfman, L.M., 1968. Pulse Radiolysis Studies. XIII. Rate constants for the reaction of hydroxyl radicals with aromatic compounds in aqueous solutions. *Adv. Chem.* 81, 222–230.

OECD, 2005. p-chlorotoluene CAS N°: 106-43-4 Screening Information DataSheet - Initial Assessment Report for SIAM 20. UNEP Publication, p. 154.

OECD, 2008. Organisation for Economic Co-operation and Development (OECD). Test Guideline 316, Phototransformation of Chemicals in Water - Direct

- Photolysis, p. 53.
- Passeport, E., Landis, R., Lacrampe-Couloume, G., Lutz, E.J., Mack, E.E., West, K., Morgan, S., Lollar, B.S., 2016. Sediment monitored natural recovery evidenced by compound specific isotope analysis and high-resolution pore water sampling. *Environ. Sci. Technol.* 50 (22), 12197–12204.
- Passeport, E., Landis, R., Mundle, S.O., Chu, K., Mack, E.E., Lutz, E., Sherwood Lollar, B., 2014. Diffusion sampler for compound specific carbon isotope analysis of dissolved hydrocarbon contaminants. *Environ. Sci. Technol.* 48 (16), 9582–9590.
- Pati, S.G., Kohler, H.P.E., Bolotin, J., Parales, R.E., Hofstetter, T.B., 2014. Isotope effects of enzymatic dioxygenation of nitrobenzene and 2-nitrotoluene by nitrobenzene dioxygenase. *Environ. Sci. Technol.* 48 (18), 10750–10759.
- Pati, S.G., Kohler, H.P.E., Pabis, A., Paneth, P., Parales, R.E., Hofstetter, T.B., 2016. Substrate and enzyme specificity of the kinetic isotope effects associated with the dioxygenation of nitroaromatic contaminants. *Environ. Sci. Technol.* 50 (13), 6708–6716.
- Pera-Titus, M., Garcia-Molina, V., Banos, M.A., Gimenez, J., Esplugas, S., 2004. Degradation of chlorophenols by means of advanced oxidation processes: a general review. *Appl. Catal. B Environ.* 47 (4), 219–256.
- Ratti, M., Canonica, S., McNeill, K., Bolotin, J., Hofstetter, T.B., 2015a. Isotope fractionation associated with the indirect photolysis of substituted anilines in aqueous solution. *Environ. Sci. Technol.* 49 (21), 12766–12773.
- Ratti, M., Canonica, S., McNeill, K., Bolotin, J., Hofstetter, T.B., 2015b. Isotope fractionation associated with the photochemical dechlorination of chloroanilines. *Environ. Sci. Technol.* 49 (16), 9797–9806.
- Ratti, M., Canonica, S., McNeill, K., Erickson, P.R., Bolotin, J., Hofstetter, T.B., 2015c. Isotope fractionation associated with the direct photolysis of 4-chloroaniline. *Environ. Sci. Technol.* 49 (7), 4263–4273.
- Rosenfelder, N., Bendig, P., Vetter, W., 2011. Stable carbon isotope analysis (δ -C-13 values) of polybrominated diphenyl ethers and their UV-transformation products. *Environ. Pollut.* 159 (10), 2706–2712.
- Schreglmann, K., Hoeche, M., Steinbeiss, S., Reinnicke, S., Elsner, M., 2013. Carbon and nitrogen isotope analysis of atrazine and desethylatrazine at sub-microgram per liter concentrations in groundwater. *Anal. Bioanal. Chem.* 405 (9), 2857–2867.
- Schwarzbauer, J., Ricking, M., 2010. Non-target screening analysis of river water as compound-related base for monitoring measures. *Environ. Sci. Pollut. Control Ser.* 17 (4), 934–947.
- Sherwood Lollar, B., Hirschorn, S.K., Chartrand, M.M.G., Lacrampe-Couloume, G., 2007. An approach for assessing total instrumental uncertainty in compound-specific carbon isotope analysis: implications for environmental remediation studies. *Anal. Chem.* 79 (9), 3469–3475.
- Shimizu, M., Yasui, Y., Matsumoto, N., 1983. Structural specificity of aromatic compounds with special reference to mutagenic activity in *Salmonella typhimurium*: a series of chloro- or fluoro-nitrobenzene derivatives. *Mutat. Res.* 116 (3–4), 217–238.
- Singleton, D.A., Merrigan, S.R., Liu, J., Houk, K.N., 1997. Experimental geometry of the epoxidation transition state. *J. Am. Chem. Soc.* 119 (14), 3385–3386.
- Singleton, D.A., Wang, Z.H., 2005. Isotope effects and the nature of enantioselectivity in the shi epoxidation. The importance of asynchronicity. *J. Am. Chem. Soc.* 127 (18), 6679–6685.
- Skarpeli-Liati, M., Jiskra, M., Turgeon, A., Garr, A.N., Arnold, W.A., Cramer, C.J., Schwarzenbach, R.P., Hofstetter, T.B., 2011. Using nitrogen isotope fractionation to assess the oxidation of substituted anilines by manganese oxide. *Environ. Sci. Technol.* 45 (13), 5596–5604.
- Skarpeli-Liati, M., Pati, S., Bolotin, J., Hofstetter, T.B., 2012. Carbon, hydrogen, and nitrogen isotope fractionation associated with oxidative transformation of substituted aromatic N-alkyl amines. *Environ. Sci. Technol.* 46 (13), 7189–7198.
- Smith, J.R.L., Norman, R.O.C., 1963. Hydroxylation. Part I. The oxidation of benzene and toluene by Fenton's reagent. *J. Chem. Soc.* 2897–2905.
- Sundstrom, D.W., Weir, B.A., Klei, H.E., 1989. Destruction of aromatic pollutants by UV light catalyzed oxidation with hydrogen peroxide. *Environ. Prog.* 8 (1), 6–11.
- Tao, W.D., Hall, K.J., Duff, S.J.B., 2006. Performance evaluation and effects of hydraulic retention time and mass loading rate on treatment of wastewater leachate in surface-flow constructed wetlands. *Ecol. Eng.* 26 (3), 252–265.
- Trova, C., Cossa, G., Gandolfo, G., 1991. Behavior and fate of chloronitrobenzene in a fluvial environment. *Bull. Environ. Contam. Toxicol.* 47 (4), 580–585.
- USEPA, 1979. United States Environmental Protection Agency, List of Priority Pollutants, 40 Code of Federal Regulations Part 423, Appendix a, p. 1.
- Vaughan, P.P., Blough, N.V., 1998. Photochemical formation of hydroxyl radical by constituents of natural waters. *Environ. Sci. Technol.* 32 (19), 2947–2953.
- Weir, B.A., Sundstrom, D.W., Klei, H.E., 1987. Destruction of benzene by ultraviolet light-catalyzed oxidation with hydrogen peroxide. *Hazard Waste Hazard. Mater.* 4 (2), 165–176.
- Weisburger, E.K., Russfield, A.B., Homburger, F., Weisburger, J.H., Boger, E., Vandongen, C.G., Chu, K.C., 1978. Testing of twenty-one environmental aromatic amines or derivatives for long-term toxicity or carcinogenicity. *J. Environ. Pathol. Toxicol.* 2 (2), 325–356.
- Wols, B.A., Hofman-Caris, C.H.M., 2012. Review of photochemical reaction constants of organic micropollutants required for UV advanced oxidation processes in water. *Water Res.* 46 (9), 2815–2827.
- Wu, L.P., Chladkova, B., Lechtenfeld, O.J., Lian, S.J., Schindelka, J., Herrmann, H., Richnow, H.H., 2018. Characterizing chemical transformation of organophosphorus compounds by C-13 and H-2 stable isotope analysis. *Sci. Total Environ.* 615, 20–28.
- Wu, L.P., Yao, J., Trebse, P., Zhang, N., Richnow, H.H., 2014. Compound specific isotope analysis of organophosphorus pesticides. *Chemosphere* 111, 458–463.
- Xu, B.S., Sherwood Lollar, B., Passeport, E., Sleep, B.E., 2016. Diffusion related isotopic fractionation effects with one-dimensional advective-dispersive transport. *Sci. Total Environ.* 550, 200–208.
- Xu, S., Sherwood Lollar, B., Sleep, B.E., 2017. Rethinking aqueous phase diffusion related isotope fractionation: contrasting theoretical effects with observations at the field scale. *Sci. Total Environ.* 607–608, 1085–1095.
- Zafriou, O.C., 1974. Sources and reactions of OH and daughter radicals in seawater. *J. Geophys. Res.* 79 (30), 4491–4497.
- Zhang, N., Bashir, S., Qin, J., Schindelka, J., Fischer, A., Nijenhuis, I., Herrmann, H., Wick, L.Y., Richnow, H.H., 2014. Compound specific stable isotope analysis (CSIA) to characterize transformation mechanisms of alpha-hexachlorocyclohexane. *J. Hazard Mater.* 280, 750–757.
- Zhang, N., Geronimo, I., Paneth, P., Schindelka, J., Schaefer, T., Herrmann, H., Vogt, C., Richnow, H.H., 2016. Analyzing sites of OH radical attack (ring vs. side chain) in oxidation of substituted benzenes via dual stable isotope analysis (δ -C-13 and δ -H-2). *Sci. Total Environ.* 542, 484–494.
- Zhang, N., Schindelka, J., Herrmann, H., George, C., Rosell, M., Herrero-Martin, S., Klan, P., Richnow, H.H., 2015. Investigation of humic substance photosensitized reactions via carbon and hydrogen isotope fractionation. *Environ. Sci. Technol.* 49 (1), 233–242.
- Zhou, X.L., Mopper, K., 1990. Determination of photochemically produced hydroxyl radicals in seawater and fresh water. *Mar. Chem.* 30 (1–3), 71–88.
- Zwank, L., Berg, M., Elsner, M., Schmidt, T.C., Schwarzenbach, R.P., Haderlein, S.B., 2005. New evaluation scheme for two-dimensional isotope analysis to decipher biodegradation processes: application to groundwater contamination by MTBE. *Environ. Sci. Technol.* 39 (4).

Supplemental Information

Aqueous photodegradation of substituted chlorobenzenes: Kinetics, carbon isotope fractionation, and reaction mechanisms

Elodie Passeport^{*1,†‡}, Ning Zhang^{2, §}, Langping Wu², Hartmut Herrmann³, Barbara Sherwood Lollar¹, Hans-Hermann Richnow²

¹ Department of Earth Sciences, University of Toronto, 22 Russell Street, Toronto, ON M5S 3B1, Canada
Present addresses:

†Department of Civil Engineering, University of Toronto, 35 St George Street, Toronto, ON M5S 1A4, Canada

‡Department of Chemical Engineering and Applied Chemistry, University of Toronto, 200 College Street, Toronto, ON M5S 3E5, Canada

² Department of Isotope Biogeochemistry, Helmholtz Center for Environmental Research UFZ, Permoserstrasse 15, 04318 Leipzig, Germany

Present address:

§ Department of Chemistry and Pharmaceutical Engineering, Qilu University of Technology, Jinan 250353, China

³ TROPOS Leibniz Institute for Tropospheric Research, Atmospheric Chemistry Department (ACD), Permoserstrasse 15, 04318 Leipzig, Germany

* Corresponding author

Address: 35 St George Street, Room GB319F, M5S 1A4 Toronto ON Canada

Phone number: 001 416 978 5747

Fax number: 001 416 978 6813

Email address: elodie.passeport@utoronto.ca

Content

Section S1. UV molar attenuation coefficients for all studied compounds as a function of the wavelength

Section S2. Analytical methods

Section S3. Control dark experiments

Section S4. Direct photolysis experiments

Section S5. Summary of kinetics and isotope experimental results

Section S6. Degradation products detected

Section S7. Experimental carbon isotope results for reactions involving a C–O bond formation

Section S8. Literature review on ϵ_C for various processes affecting the studied compounds and related ones in surface water environments

Section S1. UV molar attenuation coefficients for all studied compounds as a function of the wavelength

Figure S1: UV molar attenuation coefficients versus wavelength

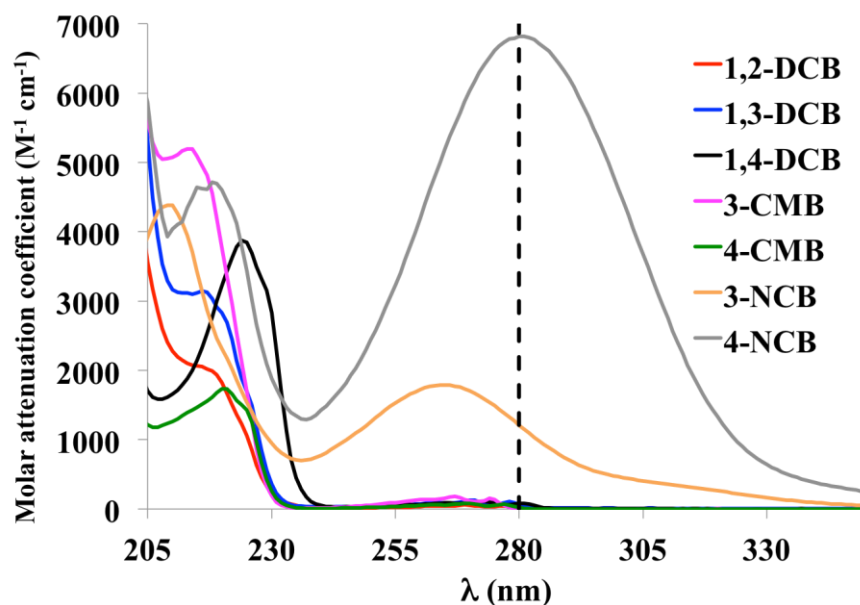


Figure S1. Molar attenuation coefficient ($\text{mol}^{-1} \text{ L cm}^{-1}$) for 1,2-dichlorobenzene (1,2-DCB), 1,3-dichlorobenzene (1,3-DCB), 1,4-dichlorobenzene (1,4-DCB), 3-chloromethylbenzene (3-CMB), 4-chloromethylbenzene (4-CMB), 3-nitrochlorobenzene (3-NCB), and 4-nitrochlorobenzene (4-NCB) in phosphate buffer (10 mM, pH = 7.3). The vertical dashed line at 280 nm indicates that wavelengths below 280 nm were filtered out of the lamp and did not reach the reactor.

Table S1: Wavelengths at maximum absorbance.

Compound	Maximum wavelength (nm)	absorbance
1,2-DCB	215	
1,3-DCB	216	
1,4-DCB	224	
3-CMB	213	
4-CMB	220	
3-NCB	265	
4-NCB	281	

Section S2. Analytical methods

Concentration determination. Concentrations of DCB and CMB isomers were measured from headspace injections (250 μL) by gas chromatography coupled to a flame ionization detector (GC/FID) (Agilent, G1530A), using a HP-5 column (30 m \times 0.32 mm \times 0.25 μm) and helium as the carrier gas. For each of the DCB and CMB samples, 0.6 g of NaCl was added into a 10-mL vial before the addition of the 2 mL sample, to enhance partitioning to the gas phase. The temperature program started at 55 $^{\circ}\text{C}$ and held for 1 min, increased up to 90 $^{\circ}\text{C}$ at 10 $^{\circ}\text{C min}^{-1}$, then up to 130 $^{\circ}\text{C}$ at 6 $^{\circ}\text{C min}^{-1}$, and finally up to 220 $^{\circ}\text{C}$ at 30 $^{\circ}\text{C min}^{-1}$.

Concentrations of NCBs were determined from liquid injections (1 μL) of extracts on an Agilent 7820A GC/FID using a HP-5 column (30 m \times 0.32 mm \times 0.25 μm) and helium as a carrier flow. Liquid-liquid extractions of 2-mL samples were conducted with 0.5 mL of *n*-pentane containing chlorobenzene (CB) as an internal standard (1-h shaking at 215 rpm). The extract was then immediately collected and placed in small vials at -20 $^{\circ}\text{C}$ until analysis. The temperature program started at 40 $^{\circ}\text{C}$ held for 8 min, then increased to 140 $^{\circ}\text{C}$ at 5 $^{\circ}\text{C min}^{-1}$ and held for 2 min, increased up to 250 $^{\circ}\text{C}$ at 45 $^{\circ}\text{C min}^{-1}$ and held 2 min.

Estimation of error on concentrations. The DCB and CMB concentrations were determined using a calibration curve made with external standards at 4 to 6 concentration levels. For each concentration level, the coefficient of variation (COV) of the peak area was calculated from at least three replicate injections. The error on sample concentration was determined as twice the highest value of the COV for a 95% confidence interval: 13% (1,2-DCB), 20% (1,3-DCB), 12% (1,4-DCB), 19% (3-CMB), and 20% (4-CMB). For NCBs, test aqueous solutions of 3-NCB and 4-NCB at known concentrations were prepared and extracted with the CB-spiked *n*-pentane similarly as done with the samples. The 3-NCB/CB and 4-NCB/CB ratios were calculated for each test solution, and were 1.76 ± 0.05 (3-NCB/CB) and 1.23 ± 0.04 (4-NCB/CB), corresponding to $2 \times \text{COV}$ of 6% (3-NCB) and 7% (4-NCB). These values for $2 \times \text{COV}$ were used as the errors on concentrations for 3-NCB and 4-NCB in the samples.

Section S3. Control dark experiments

Figure S2: Concentrations of substituted chlorobenzenes during the control dark experiments

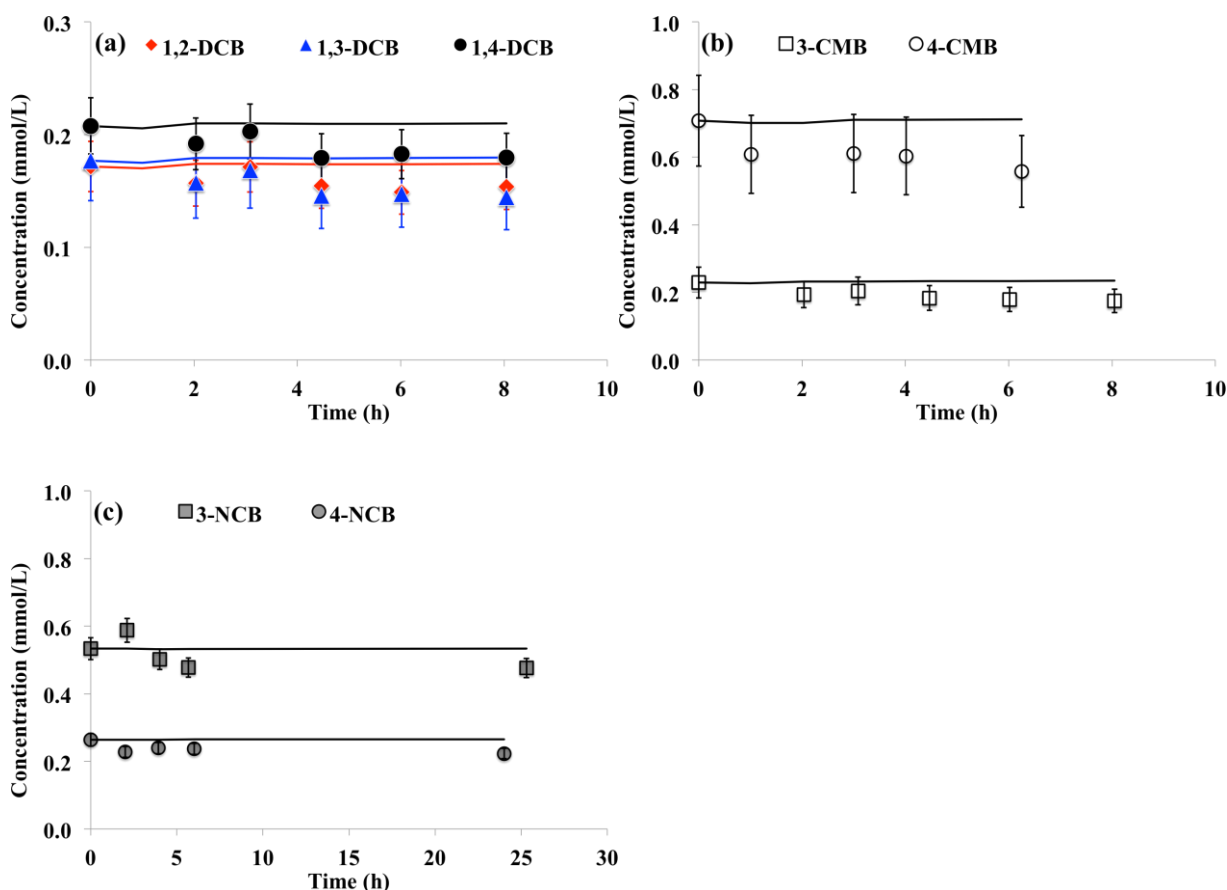


Figure S2. Concentrations of (a) 1,2-dichlorobenzene (1,2-DCB), 1,3-dichlorobenzene (1,3-DCB), and 1,4-dichlorobenzene (1,4-DCB); (b) 3-chloromethylbenzene (3-CMB) and 4-chloromethylbenzene (4-CMB); and (c) 3-nitrochlorobenzene (3-NCB) and 4-nitrochlorobenzene (4-NCB) during the dark experiments in presence of H_2O_2 . In each graph, the lines correspond to the theoretical concentration changes due to liquid – gas re-equilibration calculated after each sample taken. The error bars on

concentrations ($2\times\text{COV}$, i.e. $2\times$ coefficient of variation) were 13% (1,2-DCB), 20% (1,3-DCB), 12% (1,4-DCB), 19% (3-CMB), 20% (4-CMB), 6% (3-NCB), and 7% (4-NCB).

Section S4. Direct photolysis experiments

Figure S3: Kinetics results for the direct photolysis of the studied compounds

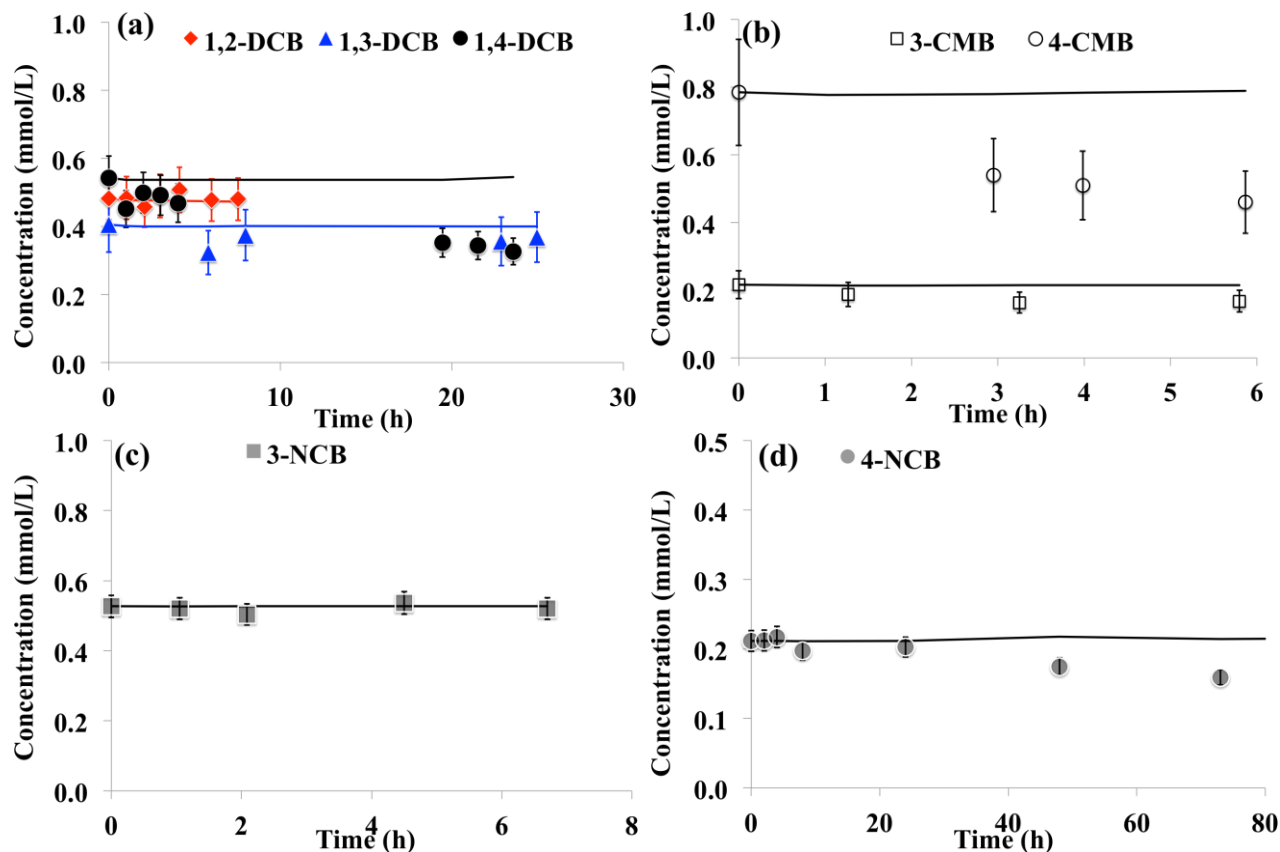


Figure S3. Concentrations of (a) 1,2-dichlorobenzene (1,2-DCB), 1,3-dichlorobenzene (1,3-DCB), and 1,4-dichlorobenzene (1,4-DCB); (b) 3-chloromethylbenzene (3-CMB) and 4-chloromethylbenzene (4-CMB); (c) 3-nitrochlorobenzene (3-NCB); and (d) 4-nitrochlorobenzene (4-NCB) during the direct photolysis experiments in the absence of H_2O_2 . In each graph, the lines correspond to the theoretical concentration changes due to liquid – gas re-equilibration after each sample taken. Note that for safety reasons, the light was turned off between times 8 h and 23 h for 1,3-DCB, and between 4 h and 19 h for 1,4-DCB. The error bars on concentrations ($2\times\text{COV}$, i.e. $2\times$ coefficient of variation) were 13% (1,2-DCB), 20% (1,3-DCB), 12% (1,4-DCB), 19% (3-CMB), 20% (4-CMB), 6% (3-NCB), and 7% (4-NCB). Note the differences in axis scales for the four graphs.

Note for Figure S3 (b): For 4-CMB, a sharp concentration decrease, corresponding to 31% of the initial concentration, was noted after 3 hours. However, the $\delta^{13}\text{C}$ values of 4-CMB at times 0 and 6 h were the same: -27.4‰ . Therefore, the sudden decrease in concentration at 3 hours was likely due to the fact that the t_0 sample was collected before liquid – headspace equilibrium occurred.

Figure S4: Rayleigh plot for the direct photolysis of 4-NCB

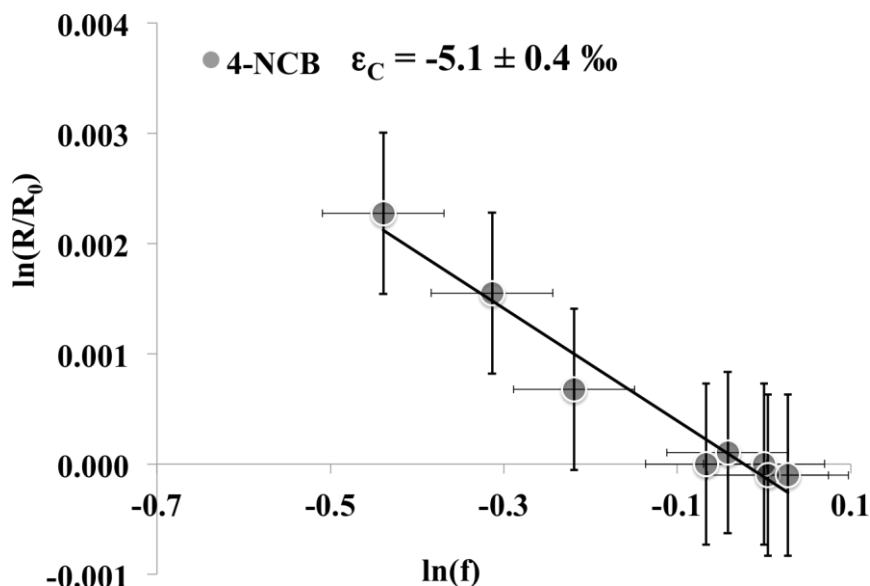


Figure S4: Rayleigh plot for the direct photolysis of 4-nitrochlorobenzene (4-NCB). The enrichment factors (ϵ_C) is presented with 95% confidence interval error. The error bars on the Rayleigh plot were determined from error propagation, using a total error of 0.5‰, accounting for both accuracy and reproducibility (Sherwood Lollar et al. 2007), on stable isotope $\delta^{13}\text{C}$ values, and 7% ($2 \times \text{COV}$, i.e. $2 \times$ coefficient of variation) for the 4-NCB concentration data.

Section S5. Summary of kinetics and isotope experimental results

Table S2: Pseudo first-order degradation rate constants (k_X), measured carbon isotope bulk enrichment factors (ϵ_C), and apparent kinetic isotope effects for carbon (AKIE_C) for the direct and indirect photodegradation of substituted chlorobenzenes.

Compound	k_X (h^{-1}) ^a	R^{2a}	ϵ_C (‰) ^b	R^{2b}	n^c	x^c	z^c	AKIE_C ^d
<i>Direct photolysis</i>								
4-NCB	0.0043 ± 0.0003	0.97	-5.1 ± 0.4	0.96	-	-	-	-
<i>Indirect photolysis: reaction with OH radicals</i>								
1,2-DCB	0.52 ± 0.02	0.99	-1.75 ± 0.04	1.00	6	4	4	1.011 ± 0.003
1,3-DCB	0.66 ± 0.02	1.00	-1.0 ± 0.1	0.97	6	3	3	1.006 ± 0.029
1,4-DCB	0.44 ± 0.01	1.00	-1.7 ± 0.2	0.97	6	4	4	1.010 ± 0.014
3-CMB	3.58 ± 0.31	0.96	-0.3 ± 0.1	0.58	7	3	3	1.002 ± 1.311
4-CMB	1.57 ± 0.14	0.94	-1.0 ± 0.1	0.90	7	2	2	1.007 ± 0.024
3-NCB	0.018 ± 0.002	0.94	-3.9 ± 0.3	0.96	6	3	3	1.024 ± 0.004
4-NCB	0.056 ± 0.001	1.00	-4.8 ± 0.5	0.97	6	2	2	1.030 ± 0.004

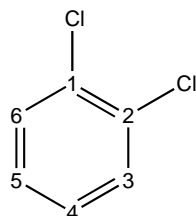
^a k_X : Pseudo first-order degradation rate constants for X-substituted chlorobenzenes with 95% confidence interval uncertainties, and R^2 : correlation coefficients for the regression of $\ln(f)$ vs. time; ^b ϵ_C : stable carbon enrichment factors, and R^2 : correlation coefficients for the regression of $\ln(R/R_0)$ vs. $\ln(f)$. Uncertainties on k_X and ϵ_C represent 95% confidence intervals calculated from the standard deviation of the regression slopes. ^c Parameters from Equation (2) assuming OH radical aromatic substitution for the indirect photodegradation experiments. ^d AKIE_C : Apparent Kinetic Isotope Effect for carbon with uncertainties representing 95% confidence intervals calculated from error propagation.

Calculations of AKIE values

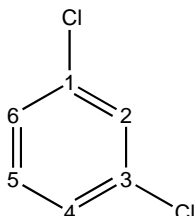
1. Identification of reactive sites

1.1 Dichlorobenzenes

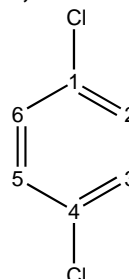
1,2-DCB



1,3-DCB



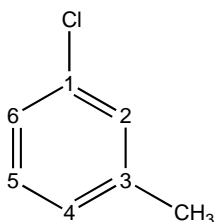
1,4-DCB



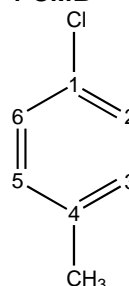
Chlorine is an ortho- and para- directing deactivator due to both an inductive electron withdrawing effect that lowers DCB reactivity, and a resonance donating effect from Cl lone pairs of electrons that determines the regiochemistry. In 1,2- and 1,4-DCB, all four unsubstituted carbons are equivalent for the addition of an OH radical and further release of a H atom; conversely, the directing effects of both chlorine groups reinforce one another in 1,3-DCB preferentially leading to OH substitution on carbon # 2, 4, and 6. The values for x and z ($x = z$) are therefore 4 for 1,2- and 1,4-DCB, and 3 for 1,3-DCB. These results are in line with the observed highest rate constant for 1,3-DCB compared to the other two DCB isomers. The corresponding $AKIE_C$ values are therefore 1.011 ± 0.003 (1,2-DCB), 1.006 ± 0.029 (1,3-DCB), and 1.010 ± 0.014 (1,4-DCB) (SI Table S2). The same $AKIE_C$ values are obtained under the scenario of OH addition to a carbon attached to one of the Cl substituents, using $n = 6$, $x = z = 2$.

1.2 Chlorotoluenes

3-CMB

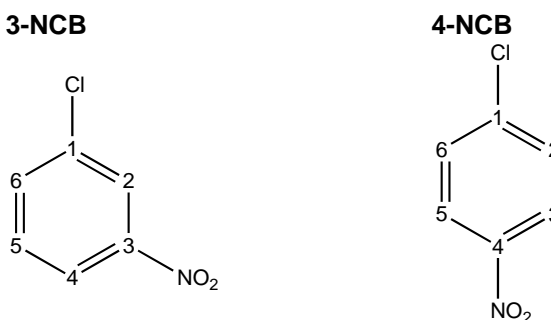


4-CMB



The methyl group is an ortho- and para- directing activator due to an inductive donating effect. In 3-CMB, the directing effects of both the Cl and CH_3 groups reinforce one another leading to $x = z = 3$ main reaction sites on carbons # 2, 4, and 6. Conversely, the directing influences of the Cl and CH_3 groups oppose one another in 4-CMB. Because CH_3 is an activating group, contrary to Cl, which is deactivating, the OH radical is expected to preferentially substitute on carbons # 3 and 5 preferentially in 4-CMB, leading to $x = z = 2$. If no assumptions are made on the preferred sites of attack in 4-CMB, then $x = z = 4$. In both cases, whether $x = z = 2$ or $x = z = 4$ is selected, the same $AKIE_C$ value of 1.007 is obtained. These predictions are consistent with 3-CMB exhibiting a higher degradation rate constant than 4-CMB. The corresponding $AKIE_C$ values are therefore 1.002 ± 1.311 (3-CMB) and 1.007 ± 0.024 (4-CMB) (SI Table S2). The same $AKIE_C$ values are obtained for the two isomers under the scenarios of either OH addition to a carbon attached to one of the benzene substituents (CH_3 or Cl), or when considering H abstraction from the CH_3 group, in both cases using $n = 7$, $x = z = 1$.

1.3 Nitrochlorobenzenes



The nitro group is a meta-directing deactivator through a resonance withdrawing effect. In 3-NCB, the Cl and NO₂ directing influences oppose one another. Given that Cl is the least deactivating of the two substituents, it will preferentially direct the reaction to carbons # 2, 4, and 6, resulting in $x = z = 3$. Whether this assumption of preferential OH attack on these three carbon atoms is made ($x = z = 3$), or all four unsubstituted carbon atoms are considered as associated with equal probabilities of attack ($x = z = 4$), the same $AKIE_C$ values of 1.024 is obtained for 3-NCB. In 4-NCB, the directing effects of the Cl and NO₂ substituents reinforce one another leading to carbons #2 and #6 as the preferential sites for the attack of the OH radical ($x = z = 2$). Again, these results are consistent with 4-NCB showing a higher degradation rate constant than 3-NCB. The corresponding $AKIE_C$ values are 1.024 ± 0.004 (3-NCB) and 1.030 ± 0.004 (4-NCB) (SI Table S2). The same $AKIE_C$ values for each DCB isomer are obtained under the scenario of OH addition to a carbon attached to either the Cl or NO₂ substituent, using $n = 6$, $x = z = 1$.

2. Potential for reaction at substituted carbon atoms

If the rate-determining step for the reaction of OH radicals with substituted chlorobenzenes involves the breaking of a chemical bond at one of the substituted carbon atoms, i.e., C–Cl, C–N, or C–C, the corresponding $AKIE_C$ values would be 1.011 (1,2-DCB), 1.006 (1,3-DCB), 1.010 (1,4-DCB), 1.002 and 1.007 for 3- and 4-CMB, respectively, and 1.024 and 1.030 for 3- and 4-NCB, respectively.

Figure S5: Correlation between $AKIE_C$ values and molecules hydrophobicity to evaluate Kopinke and Georgi (2017)'s water cage effect hypothesis

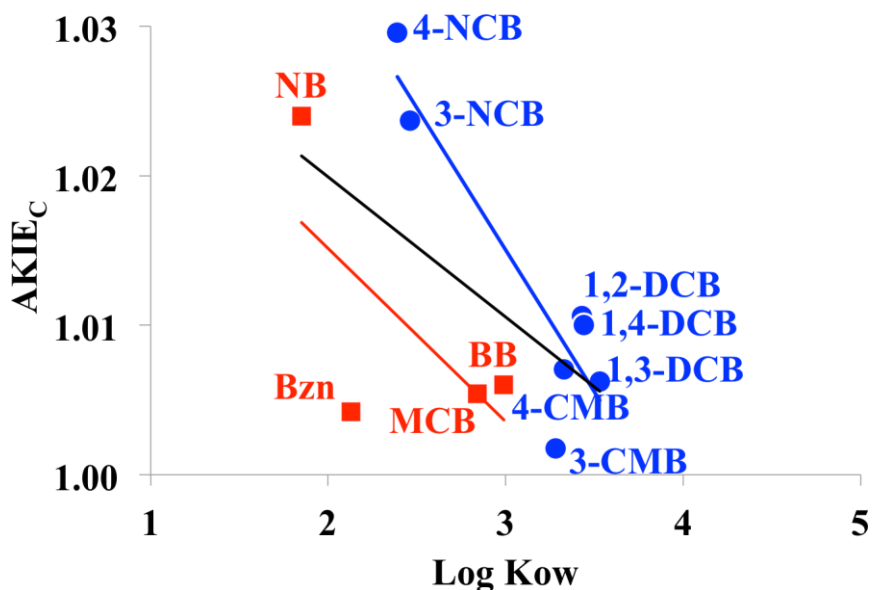


Figure S5: $AKIE_C$ values for OH radical ring addition using data from the present study (blue circles) and those from Zhang et al. (2016) (red squares) as a function of the log Kow (octanol – water partition coefficient) of the molecules. The equations represent the linear relationships for data from the present study in blue ($y = -0.02x + 1.07$, $R^2 = 0.83$), from Zhang et al. (2016) in red ($y = -0.01x + 1.04$, $R^2 = 0.46$), and for all the data together in black ($y = -0.01x + 1.04$, $R^2 = 0.34$), with 1,2-DCB: 1,2-dichlorobenzene, 1,3-DCB: 1,3-dichlorobenzene, 1,4-DCB: 1,4-dichlorobenzene, 3-CMB: 3-chloromethylbenzene, 4-CMB: 4-chloromethylbenzene, 3-NCB: 3-nitrochlorobenzene, 4-NCB: 4-nitrochlorobenzene, Bzn: benzene, MCB: chlorobenzene, BB: bromobenzene, NC: nitrobenzene.

Section S6. Degradation products detected

Table S3: Summary of qualitative GC/MS analysis of selected samples

Compound	Derivatization	Direct photolysis	Indirect photolysis
1,2-DCB	Yes	8 h / 0 % ^(a) : - No products ^(b)	10 h / 100 %: - No products
	No	N/A	2 h / 43 %: - No products
1,3-DCB	Yes	10 h / 8 %: - No products	Sample broken
	No	N/A	2 h / 55 %: - No products
1,4-DCB	Yes	8 h / 40 %: - No products	10 h / 96 %: - No products
	No	N/A	2 h / 41 %: - No products
3-CMB	Yes	6 h / 22 %: - No products	4 h / 100 %: - No products
	No	N/A	0.75 h / 92 %: - Small amounts of 2-chloro-6-methylphenol
4-CMB	Yes	6 h / 41 %: - No products	3.5 h / 100 %: - No products
	No	N/A	1.5 h / 85 %: - Small amounts of 2-chloro-5-methylphenol
3-NCB	Yes	N/A	48 h / 63 %: - No products
	No	6 h / 1 %: - No products	24 h / 45 %, 28 h / 47%, 32 h / 48 %: - No products
4-NCB	Yes	96 h / 34 %: - No products	98 h / 100 %: - No products
	No	96 h / 34 %: - No products	8 h / 34 %, 24 h / 74 %, 32 h / 90 %: - No products

^(a) Duration of irradiation / percent concentration decrease since start of the experiment at that sampling time; ^(b) No degradation products observed.

Section S7. Experimental carbon isotope results for reactions involving a C–O bond formation

Table S4: Summary of carbon isotope enrichment factors and $AKIE_C$ values for biotic and abiotic experiments involving the formation of a C–O bond on an aromatic ring.

Compound	Transformation type	Pathway	ϵ_C (‰)	$AKIE_C$ (reported or calculated)	Comments	Reference
Biodegradation experiments						
Benzene	Methanogenic	Ring hydroxylation?	-0.8 ± 0.2	1.005 ± 0.083	Mixed culture OR CH4-1b	(Mancini et al. 2008)
Benzene	Methanogenic	Ring hydroxylation?	-1.1 ± 0.1	1.007 ± 0.019	Enrichment culture Cart CH4-1	(Mancini et al. 2008)
Benzene	Sulphate-reducing	Ring hydroxylation?	-3.6 ± 0.3	1.022 ± 0.004	Enrichment culture Cart SO4-1a	(Mancini et al. 2008)
Benzene	Aerobic	Monohydroxylation	-1.7 ± 0.2	1.010 ± 0.0012	<i>R. pickettii</i> PKO1	(Fischer et al. 2008)
Benzene	Aerobic	Monohydroxylation	-4.3 ± 0.4	1.026 ± 0.0025	<i>C. necator</i> ATCC	(Fischer et al. 2008)
Benzene	Sulphate-reducing	Unknown	-1.9 ± 0.3	1.011 ± 0.0018	Enrichment culture	(Fischer et al. 2008)
Benzene	Sulphate-reducing	Unknown	-3.0 ± 0.4	1.018 ± 0.008	Mixed culture	(Fischer et al. 2009)
Benzene	Aerobic	Ring monohydroxylation?	-2.6 ± 0.8	1.016 ± 0.0050	<i>A. denitrificans</i> BC	(Fischer et al. 2008)
Benzene	Aerobic	Unknown	-1.46 ± 0.06	1.009 ± 0.006	<i>Acinetobacter</i> sp.	(Hunkeler et al. 2001)
Benzene	Aerobic	Unknown	-3.53 ± 0.26	1.022 ± 0.004	<i>Burkholderia</i> sp.	(Hunkeler et al. 2001)
Toluene	Aerobic	Ring monooxygenation	-1.1 ± 0.2	1.008 ± 0.031	<i>R. pickettii</i> PKO1	(Morasch et al. 2002)
Abiotic experiments						
Benzene	Abiotic, gas phase	Ring OH radical addition	-7.47 ± 0.44	1.047 ± 0.001	Atmospheric chemistry	(Anderson et al. 2004)
Benzene	Abiotic, gas phase	Ring OH radical addition	-8.07 ± 1.36	1.051 ± 0.004	Atmospheric chemistry	(Rudolph et al. 2000)
Toluene	Abiotic, gas phase	Ring OH radical addition	-5.91 ± 0.23	1.043 ± 0.001	Atmospheric chemistry	(Anderson et al. 2004)
Ethylbenzene	Abiotic, gas phase	Ring OH radical addition	-4.32 ± 0.38	1.036 ± 0.003	Atmospheric chemistry	(Anderson et al. 2004)
o-xylene	Abiotic, gas phase	Ring OH radical addition	-4.25 ± 0.04	1.035 ± 0.0003	Atmospheric	(Anderson et al.

Compound	Transformation type	Pathway	ϵ_C (‰)	AKIE _C (reported or calculated)	Comments	Reference
					chemistry	(2004)
p-xylene	Abiotic, gas phase	Ring OH radical addition	-4.81 ± 1.13	1.040 ± 0.006	Atmospheric chemistry	(Anderson et al. 2004)
1,2,4-trimethylbenzene	Abiotic, gas phase	Ring OH radical addition	-3.17 (n = 1)	1.029	Atmospheric chemistry	(Anderson et al. 2004)
o-ethyltoluene	Abiotic, gas phase	Ring OH radical addition	-4.69 (n = 1)	1.044	Atmospheric chemistry	(Anderson et al. 2004)
Benzene	Abiotic, liquid phase	Ring OH radical addition	-7.98	1.0316	Indirect aqueous photodegradation	(Zhang et al. 2016)
Toluene	Abiotic, liquid phase	Ring OH radical addition	-6.05	1.0285	Indirect aqueous photodegradation	(Zhang et al. 2016)
Ethylbenzene	Abiotic, liquid phase	Ring OH radical addition	-5.49	1.0286	Indirect aqueous photodegradation	(Zhang et al. 2016)
o-xylene	Abiotic, liquid phase	Ring OH radical addition	-5.41	1.0286	Indirect aqueous photodegradation	(Zhang et al. 2016)
Chlorobenzene	Abiotic, liquid phase	Ring OH radical addition	-7.24	1.0295	Indirect aqueous photodegradation	(Zhang et al. 2016)
Nitrobenzene	Abiotic, liquid phase	Ring OH radical addition	-7.52	1.0308	Indirect aqueous photodegradation	(Zhang et al. 2016)

Section S8. Literature review on ϵ_C for various processes affecting the studied compounds and related ones in surface water environments

Table S5: Summary of carbon isotope enrichment factors (ϵ_C , in ‰) for the studied compounds

Compound	Reaction with OH radicals	Ref ^a	Anaerobic biodegradation	Ref ^a	Aerobic biodegradation	Ref ^a	Other processes	Ref ^a
Compounds studied in this work								
1,2-dichlorobenzene	-1.75 ± 0.04	This study	-0.8 ± 0.1	1				
1,3- dichlorobenzene	-1.0 ± 0.1	This study	-5.4 ± 0.4	1				
1,4- dichlorobenzene	-1.7 ± 0.2	This study	-6.3 ± 0.2	1				
3-chlorotoluene	-0.3 ± 0.1	This study						
4- chlorotoluene	-1.0 ± 0.1	This study						
3-nitrochlorobenzene	-3.9 ± 0.3	This study						
4- nitrochlorobenzene	-4.8 ± 0.5	This study					Reduction by Fe(II) /goethite: -0.65	2
Related compounds								
Chlorobenzene	-0.9 ± 0.1	3	-5.0 ± 0.2	4	-0.4 ± 0.1 for <i>Ralstonia</i> sp	5		
Chlorobenzene			Field suggests ¹³ C enrichment	5				
Chlorobenzene					-0.3 ± 0.04 for <i>R. erythropolis</i>	5		
Chlorobenzene					-0.2 ± 0.2 for <i>P. veronii</i>	5		
Chlorobenzene					-0.1 ± 0.1 for <i>A. facilis</i>	5		
1,2,4-trichlorobenzene			-3.2 ± 0.5	6	Negligible	6, 7		
1,2,4-trichlorobenzene			-3.0 ± 0.4	7	Negligible	6, 7		
1,2,3-trichlorobenzene			-3.4 ± 0.3 and -3.4 ± 0.5	6				
Nitrobenzene	-3.9 ± 0.2	3			-3.9 ± 0.1 for aerobic oxidation by <i>Comamonas</i> sp. strain JS765	8		
Nitrobenzene					-0.57 ± 0.06 for aerobic	8		

Compound	Reaction with OH radicals	Ref ^a	Anaerobic biodegradation	Ref ^a	Aerobic biodegradation	Ref ^a	Other processes	Ref ^a
					reduction by <i>Pseudomonas pseudoalcaligenes</i> strain JS45			
Nitrobenzene					-3.7 ± 0.2 for aerobic oxidation by <i>E. Coli</i> clones	9		
Nitrobenzene					-3.6 ± 0.3 for aerobic oxidation by cell extracts of <i>E. Coli</i> clones	9		
Nitrobenzene					-3.5 ± 0.2 for aerobic oxidation by purified nitrobenzene dioxygenase (NBDO)	9		
Nitrobenzene					-3.9 ± 0.2 for aerobic oxidation by <i>Comamonas</i> sp. strain JS765	9		
2-nitrotoluene					-1.3 ± 0.1 for aerobic oxidation by <i>E. Coli</i> clones	9		
2-nitrotoluene					-1.2 ± 0.3 for aerobic oxidation by cell extracts of <i>E. Coli</i> clones	9		
3-nitrotoluene					-0.4 ± 0.2 by nitrobenzene dioxygenase (NBDO) and -0.6 ± 0.2 by 2-nitrotoluene dioxygenase (2NTDO)	10		
4-nitrotoluene					-1.4 ± 0.4 by nitrobenzene dioxygenase (NBDO) and -0.1 ± 0.1 by 2-nitrotoluene dioxygenase (2NTDO)	10		
2,6-dinitrotoluene					-1.1 ± 0.4 by	10		

Compound	Reaction with OH radicals	Ref ^a	Anaerobic biodegradation	Ref ^a	Aerobic biodegradation	Ref ^a	Other processes	Ref ^a
					nitrobenzene dioxygenase (NBDO)			
Naphthalene					-0.4 ± 0.3 by nitrobenzene dioxygenase (NBDO)	10		
Aniline	-3.6 ± 0.06	3					Indirect photodegradation reaction with ³ AQDS*: -1.4 ± 0.5	11
Aniline							Indirect photodegradation reaction with ³ MB**: 0.7 ± 1.1	11
4-chloroaniline							Direct photolysis: between -0.8 ± 0.2‰ to -2.7 ± 0.2‰	12
4-chloroaniline							Indirect photodegradation reaction with ³ AQDS*: -1.0 ± 0.1	11
4-chloroaniline							Indirect photodegradation reaction with ³ MB**: -0.2 ± 0.4	11
4-methylaniline							Indirect photodegradation reaction with ³ AQDS*: from -0.2 ± 0.2 to 1.4 ± 0.8	11
4-methylaniline							Indirect photodegradation reaction with ³ MB**: 0.5 ± 1.0	11
4-methoxyaniline							Indirect photodegradation reaction with ³ AQDS*: -0.2 ± 0.4	11
4-methoxyaniline							Indirect photodegradation reaction with ³ MB**: -1.4 ± 2.3	11

^a Ref: reference: 1: (Liang et al. 2014); 2: (Hartenbach et al. 2006); 3: (Zhang et al. 2016); 4: (Liang et al. 2011); 5: (Kaschl et al. 2005); 6: (Griebler et al. 2004); 7: (Liang et al. 2011); 8: (Hofstetter et al. 2008); 9: (Pati et al. 2014); 10: (Pati et al. 2016); 11: (Ratti et al. 2015a); 12: (Ratti et al. 2015b).

References

- Anderson, R.S., Iannone, R., Thompson, A.E., Rudolph, J. and Huang, L. (2004) Carbon kinetic isotope effects in the gas-phase reactions of aromatic hydrocarbons with the OH radical at 296 +/- 4 K. *Geophysical Research Letters* 31(15).
- Fischer, A., Gehre, M., Breitfeld, J., Richnow, H.H. and Vogt, C. (2009) Carbon and hydrogen isotope fractionation of benzene during biodegradation under sulfate-reducing conditions: a laboratory to field site approach. *Rapid Communications in Mass Spectrometry* 23(16), 2439-2447.
- Fischer, A., Herklotz, I., Herrmann, S., Thullner, M., Weelink, S.A.B., Stams, A.J.M., Schlömann, M., Richnow, H.-H. and Vogt, C. (2008) Combined carbon and hydrogen isotope fractionation investigations for elucidating benzene biodegradation pathways. *Environmental Science & Technology* 42(12), 4356-4363.
- Griebler, C., Safinowski, M., Vieth, A., Richnow, H.H. and Meckenstock, R.U. (2004) Combined application of stable carbon isotope analysis and specific metabolites determination for assessing in situ degradation of aromatic hydrocarbons in a tar oil-contaminated aquifer. *Environmental Science & Technology* 38(2), 617-631.
- Hartenbach, A., Hofstetter, T.B., Berg, M., Bolotin, J. and Schwarzenbach, R.P. (2006) Using nitrogen isotope fractionation to assess abiotic reduction of nitroaromatic compounds. *Environmental Science & Technology* 40(24), 7710-7716.
- Hofstetter, T.B., Spain, J.C., Nishino, S.F., Bolotin, J. and Schwarzenbach, R.P. (2008) Identifying competing aerobic nitrobenzene biodegradation pathways by compound-specific isotope analysis. *Environmental Science & Technology* 42(13), 4764-4770.
- Hunkeler, D., Anderson, N., Aravena, R., Bernasconi, S.M. and Butler, B.J. (2001) Hydrogen and carbon isotope fractionation during aerobic biodegradation of benzene. *Environmental Science & Technology* 35(17), 3462-3467.
- Kaschl, A., Vogt, C., Uhlig, S., Nijenhuis, I., Weiss, H., Kastner, M. and Richnow, H.H. (2005) Isotopic fractionation indicates anaerobic monochlorobenzene biodegradation. *Environmental Toxicology and Chemistry* 24(6), 1315-1324.
- Kopinke, F.D. and Georgi, A. (2017) What controls selectivity of hydroxyl radicals in aqueous solution? Indications for a cage effect. *Journal of Physical Chemistry A* 121(41), 7947-7955.
- Liang, X., Howlett, M.R., Nelson, J.L., Grant, G., Dworatzek, S., Lacrampe-Couloume, G., Zinder, S.H., Edwards, E.A. and Sherwood Lollar, B. (2011) Pathway-dependent isotope fractionation during aerobic and anaerobic degradation of monochlorobenzene and 1,2,4-trichlorobenzene. *Environmental Science & Technology* 45(19), 8321-8327.
- Liang, X., Mundle, S.O.C., Nelson, J.L., Passeport, E., Chan, C.C.H., Lacrampe-Couloume, G., Zinder, S.H. and Sherwood Lollar, B. (2014) Distinct carbon isotope fractionation during anaerobic degradation of dichlorobenzene isomers. *Environmental Science & Technology* 48(9), 4844-4851.
- Mancini, S.A., Devine, C.E., Elsner, M., Nandi, M.E., Ulrich, A.C., Edwards, E.A. and Sherwood Lollar, B. (2008) Isotopic evidence suggests different initial reaction mechanisms for anaerobic benzene biodegradation. *Environmental Science & Technology* 42(22).
- Morasch, B., Richnow, H.H., Schink, B., Vieth, A. and Meckenstock, R.U. (2002) Carbon and hydrogen stable isotope fractionation during aerobic bacterial degradation of aromatic hydrocarbons. *Applied and Environmental Microbiology* 68(10).
- Pati, S.G., Kohler, H.P.E., Bolotin, J., Parales, R.E. and Hofstetter, T.B. (2014) Isotope effects of enzymatic dioxygenation of nitrobenzene and 2-nitrotoluene by nitrobenzene dioxygenase. *Environmental Science & Technology* 48(18), 10750-10759.
- Pati, S.G., Kohler, H.P.E., Pabis, A., Paneth, P., Parales, R.E. and Hofstetter, T.B. (2016) Substrate and enzyme specificity of the kinetic isotope effects associated with the dioxygenation of nitroaromatic contaminants. *Environmental Science & Technology* 50(13), 6708-6716.
- Ratti, M., Canonica, S., McNeill, K., Bolotin, J. and Hofstetter, T.B. (2015a) Isotope fractionation associated with the indirect photolysis of substituted anilines in aqueous solution. *Environmental Science & Technology* 49(21), 12766-12773.
- Ratti, M., Canonica, S., McNeill, K., Erickson, P.R., Bolotin, J. and Hofstetter, T.B. (2015b) Isotope fractionation associated with the direct photolysis of 4-chloroaniline. *Environmental Science & Technology* 49(7), 4263-4273.

- Rudolph, J., Czuba, E. and Huang, L. (2000) The stable carbon isotope fractionation for reactions of selected hydrocarbons with OH-radicals and its relevance for atmospheric chemistry. *Journal of Geophysical Research-Atmospheres* 105(D24), 29329-29346.
- Sherwood Lollar, B., Hirschorn, S.K., Chartrand, M.M.G. and Lacrampe-Couloume, G. (2007) An approach for assessing total instrumental uncertainty in compound-specific carbon isotope analysis: Implications for environmental remediation studies. *Analytical Chemistry* 79(9), 3469-3475.
- Zhang, N., Geronimo, I., Paneth, P., Schindelka, J., Schaefer, T., Herrmann, H., Vogt, C. and Richnow, H.H. (2016) Analyzing sites of OH radical attack (ring vs. side chain) in oxidation of substituted benzenes via dual stable isotope analysis ($\delta^{13}\text{C}$ and $\delta^2\text{H}$). *Science of the Total Environment* 542, 484-494.

Appendix 6.5.

Carbon and hydrogen isotope fractionation of phthalate esters during degradation by sulfate and hydroxyl radicals

Published paper: *Zhang, D.; Wu, L.; Yao, J.; Herrmann, H.; Richnow, H. H., Chem. Eng. J. 2018, 347, 111-118.*



Carbon and hydrogen isotope fractionation of phthalate esters during degradation by sulfate and hydroxyl radicals



Dan Zhang^{a,b}, Langping Wu^b, Jun Yao^{c,*}, Hartmut Herrmann^d, Hans-Hermann Richnow^{b,c,*}

^a School of Energy and Environmental Engineering, University of Science and Technology Beijing, Xueyuan Road No. 30, Haidian District, Beijing 100083, PR China

^b Department of Isotope Biogeochemistry, Helmholtz Centre for Environmental Research-UFZ, Permoserstraße 15, Leipzig 04318, Germany

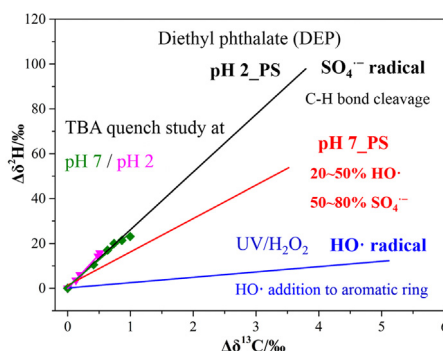
^c School of Water Resources and Environment, China University of Geosciences (Beijing), Xueyuan Road No. 29, Haidian District, Beijing 100083, PR China

^d Atmospheric Chemistry Department (ACD), Leibniz Institute for Tropospheric Research (TROPOS), Permoserstraße 15, Leipzig 04318, Germany

HIGHLIGHTS

- Dual isotope fractionation characterized persulfate oxidation and UV/H₂O₂ reaction.
- Radical quench study and CSIA were combined to explore the contribution of radicals.
- SO₄^{•-} was the predominant radical species for persulfate oxidation of DEP at pH 2.
- SO₄^{•-} and HO[•] contributed to DEP degradation during persulfate oxidation at pH 7.
- The mechanism of HO[•] reaction with DEP tended to be radical addition to aromatic ring.

GRAPHICAL ABSTRACT



ARTICLE INFO

Keywords:

Compound-specific stable isotope analysis
Phthalate esters
Isotope fractionation
Sulfate radical
Hydroxyl radical

ABSTRACT

This study investigated ¹³C and ²H isotope fractionation associated with oxidation of three phthalate esters (PAEs) by radical species, including sulfate radical (SO₄^{•-}) induced by heat-activated persulfate (PS) and hydroxyl radical (HO[•]) induced by UV/H₂O₂. For persulfate oxidation at pH = 2 and pH = 7, similar carbon isotope fractionation (ε_C) but distinct hydrogen isotope enrichment factors (ε_H) were observed. The UV/H₂O₂ reaction of three PAEs showed smaller ε_H values in comparison with persulfate oxidation. The correlation of ²H and ¹³C fractionation (λ) allows to distinguish the persulfate oxidation (25.7 ± 2.6) and UV/H₂O₂ oxidation (2.4 ± 0.2) of diethyl phthalate (DEP) highlighting the potential of compound-specific stable isotope analysis (CSIA) to characterize chemical oxidation mechanism of PAEs. Moreover, study of radical quenching and CSIA were combined to explore the dominant radical species during persulfate oxidation of DEP. SO₄^{•-} was found to be the predominant radical at pH = 2. Both SO₄^{•-} and HO[•] contributed to DEP degradation at pH = 7 and HO[•] was estimated to have a contribution of 21–63% according to dual C–H isotope fractionation values. Carbon and hydrogen apparent kinetic isotope effects (AKIEs) (¹³C-AKIE = 1.017, ²H-AKIE = 2.41) obtained from dominating sulfate radical reaction of DEP both supported the hypothesis of C–H bond cleavage. Thus, carbon and hydrogen isotope enrichment factors clearly distinguish the different reaction mechanisms and hence, are a promising approach to improve understanding of radical species reaction pathways for chemical oxidation of PAEs.

* Corresponding authors at: School of Water Resources and Environment, China University of Geosciences (Beijing), Xueyuan Road No. 29, Haidian District, Beijing 100083, PR China.
E-mail addresses: yaojun@cugb.edu.cn (J. Yao), hans.richnow@ufz.de (H.-H. Richnow).

<https://doi.org/10.1016/j.cej.2018.04.047>

Received 7 November 2017; Received in revised form 4 April 2018; Accepted 7 April 2018

Available online 07 April 2018

1385-8947/ © 2018 Elsevier B.V. All rights reserved.

1. Introduction

Phthalate esters (PAEs) are widely used as plasticizers and additives in numerous products, such as polyvinylchloride (PVC), cosmetics, medical devices, plastic toys and detergents [1]. Worldwide production of PAEs is more than 8 million tons per year [2]. PAEs are not linked by covalent bonds within the product matrix. Therefore, they can be leached out from the matrix e.g. by organic solvents or by diffusion [3,4]. Previous studies [5,6] reported contamination of PAEs in environmental compartments such as atmosphere (in and out door air, aerosols), water, sediment, soil, tissues and fluids of wildlife and humans. Consequently, PAEs have caused increasing concerns due to the potential hepatotoxic, teratogenic and carcinogenic effects [7]. Dimethyl phthalate (DMP), diethyl phthalate (DEP) and dibutyl phthalate (DBP) have been listed as priority pollutants by US Environmental Protection Agency (EPA) [8]. Several other environmental agencies from the European Union, China and Canada either classify some commonly occurring PAEs as priority pollutants or limit their use in children's toys [9]. Therefore, knowledge about the different degradation processes is needed for efficient and economic removal of PAEs in the environment.

In situ chemical oxidation (ISCO) has become a promising technique for the removal of organic contaminants in soil, groundwater and aquifers making use of radical oxidation reactions [10]. Hydrogen peroxide (H_2O_2) and persulfate (PS) are widely used oxidants in ISCO [11,12]. UV/ H_2O_2 is an efficient approach to produce hydroxyl radicals ($\text{HO}\cdot$) and has been used to degrade organic compounds such as PAEs, BPA, dyes, benzene and PAHs [13–17]. Over the last few years, sulfate radicals ($\text{SO}_4^{\cdot-}$) generated by PS or peroxymonosulfate (PMS) are considered as an alternative to $\text{HO}\cdot$ due to its long lifetime and high redox potential [10,18]. Heat-activation is a commonly used activation method and it becomes attractive when combined with in situ thermal remediation [19]. It has been reported that $\text{SO}_4^{\cdot-}$ is able to oxidize a variety of compounds, including PAEs, BTEX, PCBs, PAHs etc. [11,20–22]. Meanwhile it is well demonstrated that the formation of $\text{SO}_4^{\cdot-}$ and $\text{HO}\cdot$ is pH dependent in activated PS system [10,23,24]. Radical quenching studies are mainly used to distinguish dominant radical species according to different reactivities to probe potential radicals and their reaction with compounds. However, it is still not clear how to quantify the relative contribution of $\text{SO}_4^{\cdot-}$ and $\text{HO}\cdot$. Only few studies calculated the relative contribution of $\text{SO}_4^{\cdot-}$ and $\text{HO}\cdot$ to the oxidation reaction based on different transformation yields or rate constants [25–27]. Hence, it would be important to explore other possible ways on radical contribution estimation in order to investigate the complex interaction of radicals with PAEs and utilize the full potential of ISCO processes.

Compound-specific stable isotope analysis (CSIA) has received increasing attention in monitoring the fate of organic contaminants based on isotope fractionation concepts [28]. CSIA has been successfully applied to identify sources, assess natural attenuation of contaminants and investigate reaction mechanisms on both chemical reaction and biodegradation in contaminant hydrology and organic (bio)-geochemistry [29,30]. In the last decades, several studies showed the potential of multi-element CSIA ($\delta^{13}\text{C}$, $\delta^2\text{H}$, $\delta^{37}\text{Cl}$, $\delta^{15}\text{N}$ etc.) to explore different transformation processes [31]. For example, dual element stable isotope analysis of $\delta^{13}\text{C}$ and $\delta^2\text{H}$ was found sensitive to analyze sites of C–H bond cleavage (ring vs side chain) during oxidation of substituted benzenes [32]. In previous studies, the application of CSIA on PAEs mainly focused on the carbon isotope fractionation during photolysis and biodegradation [33–36]. To our best knowledge, studies on multi-element CSIA during PS oxidation and UV/ H_2O_2 have not yet been reported for PAEs. This knowledge is essential for the application of stable isotope techniques to identify and quantify the removal of PAEs by advanced oxidation processes in remediation applications.

The main objectives of this study were (i) to investigate the potential of ^{13}C and ^2H isotope analysis for characterizing different oxidation processes (heat-activated PS oxidation and UV/ H_2O_2) of three

PAEs, (ii) to estimate the role of $\text{SO}_4^{\cdot-}$ and $\text{HO}\cdot$ during DEP oxidation and (iii) to explore apparent kinetic isotope effects (AKIEs) of two radicals' reaction with DEP. Isotope enrichment factors of ϵ_{C} and ϵ_{H} for all reactions were determined. A combined method based on radical quenching and CSIA was established to identify potential radical species which are responsible for the degradation of DEP. Moreover, extended Rayleigh-type equations and 2D-CSIA were used for the first time to estimate the relative contribution of $\text{SO}_4^{\cdot-}$ and $\text{HO}\cdot$ induced degradation of DEP. The reported ^2H and ^{13}C fractionation factors have the potential to be a reference for characterizing different degradation processes in environmental studies.

2. Materials and methods

2.1. Chemicals

DMP, DEP and DBP with 99.5% purity (analytical grade) were purchased from Sinopharm Chemical Reagent Co., Ltd. (Shanghai, China) and used without further purification. Potassium persulfate ($\text{K}_2\text{S}_2\text{O}_8$), hydrogen peroxide (30% H_2O_2), naphthalene (99%), di-potassium hydrogen phosphate (K_2HPO_4) and potassium dihydrogen phosphate (KH_2PO_4) were obtained from Merck (Guaranteed reagent quality, Darmstadt, Germany). Hydrochloric acid solution (HCl, 6 M), hexane and ethanol were supplied by Carl Roth GmbH + Co. KG (Karlsruhe, Germany). Ortho-xylene and *tert*-butyl alcohol (TBA, 99.5%) were purchased from Sigma-Aldrich (Munich, Germany). Sulfuric acid (25%, w/w), acetone, acetonitrile and dichloromethane (DCM) were supplied by Chem solute, Th. Geyer (Germany). Deionized water was produced by a Milli-Q system ($> 18.2 \text{ M}\Omega \text{ cm}^{-1}$, Millipore GmbH, Schwalbach/Ts. Germany) and used to prepare all experimental solutions.

2.2. Experimental procedures

2.2.1. Heat-activated persulfate oxidation

Persulfate oxidation reactions were conducted as batch experiments in a series of glass vials. A phosphate buffer solution was used to keep pH values stable and to maintain degradation condition constant during the whole reaction [37]. Potassium persulfate ($\text{K}_2\text{S}_2\text{O}_8$) was used to generate $\text{SO}_4^{\cdot-}$ at pH = 2 and pH = 7. The pH value was adjusted by sulfuric acid (25% H_2SO_4). Preliminary experiment with persulfate at pH = 10 showed the degradation kinetic of DEP was similar to the one obtained for alkaline hydrolysis at the same pH (data not shown), thus we do not further analyze persulfate oxidation at alkaline pH. An activation temperature of 35 °C was chosen for persulfate oxidation. Initial concentrations of PAEs were 1.09 mM DMP, 0.97 mM DEP and 0.037 mM DBP, respectively, considering different solubilities in water and to achieve adequate signal intensity for isotope measurements. The molar ratio of persulfate and PAEs was 50:1. Control experiments were conducted without addition of persulfate under identical conditions simultaneously. At different time intervals, reaction vials were removed and three PAEs were extracted by liquid–liquid extraction. 2 mL of DCM containing 500 mg L^{-1} ortho-xylene (as internal standard) was added to extract DMP and DEP from the aqueous solution. For DBP, 1 mL of hexane containing 100 mg L^{-1} naphthalene (as internal standard) was used as solvent in order to obtain good extraction efficiency.

To investigate the roles of $\text{SO}_4^{\cdot-}$ and $\text{HO}\cdot$ species formed in PS oxidation at pH = 2 and pH = 7, radical quenching experiments were carried out separately in the presence of ethanol (EtOH) and *tert*-butyl alcohol (TBA). The radical scavengers (EtOH and TBA) were added to obtain a concentration of 195 mM, which corresponded to a 200:1 molar ratio of the radical scavengers compared to target compound (DEP). The second order rate constant of $\text{HO}\cdot$ with TBA ($k_{\text{TBA}/\text{HO}\cdot} = 6 \times 10^8 \text{ M}^{-1}\text{s}^{-1}$) is almost 3 orders of magnitude faster than that of $\text{SO}_4^{\cdot-}$ with TBA ($k_{\text{TBA}/\text{SO}_4^{\cdot-}} = 4 \times 10^5 \text{ M}^{-1}\text{s}^{-1}$) [38]. TBA was always used as a chemical probe to quench $\text{HO}\cdot$ completely but $\text{SO}_4^{\cdot-}$

partially and thus differentiate these two radicals. EtOH was considered to quench $\text{SO}_4^{\cdot-}$ and $\text{HO}\cdot$ simultaneously [39,40].

2.2.2. UV/H₂O₂ photolysis

The reactions of three PAEs in UV/H₂O₂ system were carried out as the representative experiment of $\text{HO}\cdot$ dominant reactions. The photodegradation system consisted of a 200-mL Pyrex cylindrical flask with quartz window and was equipped with a 150 W xenon lamp (Hamamatsu, Japan). The xenon lamp covered a broad continuous spectrum from 185 nm to 2000 nm. A filter was used to cut off wavelengths shorter than 280 nm and to avoid reactions in this range. DEP in water showed no significant UV absorption at wavelengths longer than 280 nm, suggesting the absence of direct photolysis when a filter was used (Fig. S2). The reaction solution consisted of 200 mL phosphate buffer solution at pH = 7. Initial concentrations of PAEs were the same as those in PS oxidation experiments. $\text{HO}\cdot$ were generated by adding 30% H₂O₂, producing a molar ratio of 30:1 between H₂O₂ and PAEs. The experiment was carried out at 20 ± 1 °C using a temperature-controlled cooling system. The reaction solution was mixed with a magnetic stirrer at 250 rpm throughout the whole experiment. At different time intervals, aliquots of the reaction solution were withdrawn using a syringe and extracted by liquid-liquid extraction as described in Section 2.2.1.

2.3. Concentration and isotope analysis

2.3.1. GC-FID and GC-MS analysis

Gas chromatography (7820A, Agilent, USA) coupled with flame ionization detection (GC-FID) was applied to determine the concentration of PAEs (DMP, DEP and DBP). A HP-5 column (30 m × 0.32 mm i.d., 0.25 μm, Agilent, USA) was used to separate compounds. The oven temperature program was 60 °C (held 2 min) followed by a ramp of 10 °C min⁻¹ to 290 °C (held 2 min). The carrier gas was helium (1.5 mL min⁻¹). Samples were injected in split mode with a split ratio of 30:1 (1 μL) and the injector temperature was set at 250 °C. An Agilent GC-MS (7890A-5975C) system with the same column and GC parameters was used to identify potential degradation products.

2.3.2. Carbon and hydrogen isotope analysis

Carbon and hydrogen isotope compositions of PAEs were measured by gas chromatography-isotope ratio mass spectrometry (GC-IRMS, MAT 253, Thermo-Finnigan, Germany). Samples were injected in split mode (5:1, 1 μL) for carbon isotope measurement, and splitless mode was used for hydrogen isotope analysis to obtain optimum signal intensity. Good separation and peak shape of analytes were achieved using a ZB-1 column (60 m × 0.32 mm i.d., 1 μm, Phenomenex Inc., USA). The GC oven temperature program and other GC parameters were the same as those used for the GC-FID (see above). Reproducibility of δ¹³C and δ²H values was monitored by triplicate injections for each sample. The uncertainties of all samples were within typical analytical uncertainties (δ¹³C: ± 0.5‰, δ²H: ± 5‰).

2.4. Data evaluation

2.4.1. Evaluation of isotope fractionation

Carbon and hydrogen isotope fractionation of PAEs during chemical reactions were evaluated using the Rayleigh equation which is expressed as follows [33]:

$$\ln \frac{\delta_t + 1}{\delta_0 + 1} = \varepsilon \times \ln f \quad (1)$$

where δ_t and δ₀ are the isotope compositions of substrate at time t and zero, f is the remaining fraction of substrate at time t (f = C_t/C₀), and ε is obtained as the bulk isotope enrichment factor. For the correlation of ²H and ¹³C isotope values the isotopic shifts of hydrogen (δ²H) and

carbon (δ¹³C) were presented as Δδ²H vs Δδ¹³C during degradation process. A linear regression of Δδ²H and Δδ¹³C was used to calculate the slope (Λ) for the relationship between hydrogen and carbon isotope fractionation.

2.4.2. Extended Rayleigh-type equations

An extended Rayleigh-type equation (Eq. (2)) was derived to calculate the contribution of two processes degrading the same substrate simultaneously by two different mechanisms [41]. F is the rate ratio of the first process to the overall reaction where two competing degradation pathways occurred, ε_A, ε₁ and ε₂ are the kinetic isotope enrichment factors of the overall reaction, the individual process 1 and 2, respectively.

$$F = \frac{\varepsilon_A - \varepsilon_2}{\varepsilon_1 - \varepsilon_2} \quad (2)$$

For improved two-dimensional isotope analysis, dual element stable isotope data was used in a modified version of the Rayleigh equation to estimate the individual contributions of two competing pathways to the overall degradation [41,42]. The rate ratio F is obtained as

$$F = \frac{\Lambda \varepsilon_{C_2} - \varepsilon_{H_2}}{(\varepsilon_{H_1} - \varepsilon_{H_2}) - \Lambda (\varepsilon_{C_1} - \varepsilon_{C_2})} \quad (3)$$

where Λ is the relationship of isotope shifts of two isotope pairs (H-C), and the ε values are the corresponding isotope enrichment factors associated with two individual processes.

2.4.3. Apparent kinetic isotope effect (AKIE) calculation

For the Rayleigh equation, ε values are calculated from compound-average isotope data whereas the intrinsic isotope effect is position specific associated with the reaction step [43]. Therefore, in order to investigate underlying reaction mechanisms and degradation pathways, it is crucial to convert observable ε values into AKIEs. Eq. (4) is used to correct bulk isotope enrichment factors for isotopic dilution, the number of reactive sites within the molecule, as well as intra-molecular isotopic competition [44].

$$\text{AKIE} = \frac{1}{1 + \frac{n}{x} z \cdot \varepsilon_{\text{bulk}} (\text{‰}) / 1000} \quad (4)$$

where ε_{bulk} is the bulk isotope enrichment factor, n is the number of atoms of the element considered in the molecule, x is the number of atoms at reactive positions and z is the number of indistinguishable reactive positions.

3. Results and discussion

3.1. Degradation kinetics of PAEs

Three PAEs (DMP, DEP and DBP) with different lengths of alkyl side chain were selected in this study. The chemical oxidation processes of three PAEs followed pseudo-first order kinetics in all experiments (R² ≥ 0.965, Table 1). Control experiments of DEP by direct UV radiation, UV radiation with filter and hydrolysis at 35 °C showed negligible degradation compared to chemical oxidation (Figs. S1, S2). Rate constants (k) for the UV/H₂O₂ reaction of DMP (0.0528 h⁻¹), DEP (0.0541 h⁻¹) and DBP (0.1115 h⁻¹) were determined to describe the reaction (Table 1). A previous study [45] showed that the calculated k values increased with the number of carbon atom in the alkyl side chain of PAEs during ·OH-initiated photodegradation using transition-state theory. The activation energies for the reaction of the three PAEs differ with the chemical structure and the rate constants of the PAEs degradation due to UV/H₂O₂ reaction are probably related to the ·OH reaction with the aromatic ring and the side chain. During persulfate oxidation of PAEs, the temperature was chosen at 35 °C for milder reaction condition. The pH value is considered to be an important factor for reaction kinetics and radical species, therefore the removal of three

Table 1
Degradation kinetic and isotope fractionation parameters of PAEs during chemical oxidation.

Conditions	k (h ⁻¹)	R ²	ε _C (‰)	R ²	ε _H (‰)	R ²	Λ	f
DMP_pH 2_PS	0.0024	0.986	-2.09 ± 0.21 ^a	0.994	-23.9 ± 2.4	0.995	13.1 ± 1.4	0.252
DMP_pH 7_PS	0.0037	0.983	-2.08 ± 0.10	0.998	-8.7 ± 1.2	0.985	4.8 ± 0.5	0.055
DMP_pH 7_UV/H ₂ O ₂	0.0528	0.980	-2.76 ± 0.25	0.996	-4.8 ± 0.5	0.994	2.0 ± 0.1	0.075
DEP_pH 2_PS	0.0057	0.999	-1.39 ± 0.13	0.995	-41.8 ± 2.4	0.998	25.7 ± 2.6	0.066
DEP_pH 7_PS	0.0025	0.973	-1.57 ± 0.18	0.993	-28.3 ± 3.3	0.993	14.9 ± 3.0	0.112
DEP_pH 7_UV/H ₂ O ₂	0.0541	0.993	-2.30 ± 0.42	0.990	-6.8 ± 1.3	0.989	2.4 ± 0.2	0.101
DBP_pH 2_PS	0.015	0.995	-0.73 ± 0.10	0.983	-31.0 ± 2.0	0.997	39.0 ± 3.4	0.080
DBP_pH 7_PS	0.0039	0.987	-0.63 ± 0.07	0.989	-24.6 ± 1.8	0.996	35.3 ± 4.5	0.136
DBP_pH 7_UV/H ₂ O ₂	0.1115	0.985	-0.92 ± 0.16	0.974	-9.3 ± 2.0	0.960	9.0 ± 2.3	0.093
DEP_pH 7_TBA PS	0.0007	0.970	-1.35 ± 0.12	0.996	-39.8 ± 5.7	0.989	24.1 ± 4.3	0.478
DEP_pH 2_TBA PS	0.0007	0.965	-1.07 ± 0.29	0.989	-38.8 ± 7.7	0.988	30.5 ± 2.2	0.606

^a Uncertainty given as 95% confidence interval.

PAEs by persulfate oxidation was studied at pH = 2 and pH = 7. Three PAEs presented different degradation kinetic behaviors. For DEP and DBP, rate constants at pH = 2 are larger than those at pH = 7, which is consistent with previous results of Li et al. [46] indicating that acidic condition had positive effect on DBP degradation due to the predominant radical species of SO₄^{•-}. However, DMP seems to show a different kinetic trend, resulting in a slightly smaller removal rate at pH = 2. Wang et al. [47] reported similar rate constants of DMP at pH = 3.1 and pH = 7.0 by thermally activated persulfate oxidation, which indicated that initial pH values had a minor effect on the rate constants of DMP. The different reaction kinetic of DMP compared to DEP and DBP could be probably related to different dominant radical species and their affinity to react with the longer alkyl side chain of the PAE molecules.

3.2. Carbon and hydrogen isotope fractionation patterns of PAEs during chemical oxidation

Both carbon and hydrogen isotopic values of three PAEs from all investigated reactions showed the trend to more positive values during the degradation, which indicates a normal isotope effect (Fig. S3). The carbon and hydrogen isotope enrichment factors of DMP, DEP and DBP can be quantified using Rayleigh equation (Fig. 1). The Rayleigh regression of all three PAEs exhibited high correlation coefficients (R² ≥ 0.960) for δ²H and δ¹³C and the uncertainty was within the 95% confidence interval (C.I.) (Table 1). For the UV/H₂O₂ reaction, carbon isotope enrichment factors (ε_C) of DMP, DEP and DBP ranged from -2.76 ± 0.25‰, to -2.30 ± 0.42‰, to -0.92 ± 0.16‰, respectively. ε_C values decreases with increasing length of the alkyl side chain in the PAE molecules. This result is likely related to the isotope dilution effect caused by carbon atoms in non-reactive positions [33]. During heat-activated persulfate oxidation, as shown in Table 1, degradation rate constants of three PAEs vary at pH = 2 and pH = 7. However, ε_C values remain similar for each PAE compared to those obtained from the UV/H₂O₂ reaction. The isotope dilution effect is also observed for DMP, DEP and DBP. Therefore, carbon isotope fractionation patterns alone are not sufficient to distinguish between UV/H₂O₂ and PS oxidation processes. In contrast, ε_H values obtained from the degradation of three PAEs in the UV/H₂O₂ reaction are much smaller than those from PS oxidation. Furthermore, for reaction with heat-activated PS oxidation, ε_H values range from -8.7 ± 1.2‰ (pH = 7) to -23.9 ± 2.4‰ (pH = 2) for DMP, from -28.3 ± 3.3‰ (pH = 7) to -41.8 ± 2.4‰ (pH = 2) for DEP and from -24.6 ± 1.8‰ (pH = 7) to -31.0 ± 2.0‰ (pH = 2) for DBP. In this case, δ²H values of three PAEs show a similar trend to a larger hydrogen isotope fractionation at pH = 2 compared to pH = 7. Thus, distinctly different hydrogen enrichment factors could be used to distinguish different reaction processes. The increase of ²H fractionation might be an indication that SO₄^{•-} become a major species at low pH in persulfate oxidation reactions leading to larger hydrogen isotope fractionation compared to

high pH where SO₄^{•-} and HO[•] coexist (see discussion below). Contrary to the carbon isotope fractionation pattern, ε_H values of DMP, DEP and DBP do not show a consistent trend for an isotope dilution effect with increasing length of the alkyl side chain during PS oxidation experiments. This is due to the possibility that different dominant pathways are responsible for the decomposition of three PAEs with different alkyl side chain lengths, as suggested in a previous computational study on HO[•]-initiated photochemical transformation of four PAEs [45].

3.3. Correlation of ²H and ¹³C isotope fractionation to differentiate reaction processes

The correlation of hydrogen and carbon isotopic values of three PAEs undergoing different reactions was compared individually in dual isotope plots. All investigated experiments showed a well-fitted linear correlation (Fig. 2). For reaction with UV/H₂O₂ and PS oxidation of DMP, different slopes (Λ = Δδ²H/Δδ¹³C) are observed ranging from 2.0 ± 0.1 to 13.1 ± 1.4 (Table 1), which is attributable to different ε_H values (ranging from -4.8 ± 0.5‰ to -23.9 ± 2.4‰) and similar ε_C values (ranging from -2.08 ± 0.10‰ to -2.76 ± 0.25‰). Similarly, significant variations of Λ values (2.4 ± 0.2, 14.9 ± 3.0 and 25.7 ± 2.6) are obtained for DEP during three reactions. In this case, distinct dual H-C isotope slopes of DMP and DEP for radical oxidation processes open the possibility of 2D-CSIA to differentiate chemical oxidation reactions of PAEs in the field. However, DBP showed a different trend with almost identical Λ values at pH = 2 (39.0 ± 3.4) and pH = 7 (35.3 ± 4.5) during persulfate oxidation. Despite this, the correlation of ²H and ¹³C isotope fractionation obtained for DBP also could be used to distinguish between UV/H₂O₂ (9.0 ± 2.3) and persulfate oxidation reaction. Even if distinct ε_H values have the potential to distinguish reactions, the dual element isotope approach may be recommended for field studies. A significant advantage is that possible transport and retardation processes on the extent of isotope fractionation can be canceled out because they may have a similar influence on both elements [48]. The difference between dual element isotope fractionation patterns of UV/H₂O₂ and PS oxidation could be due to distinct dominant radical species leading to the degradation of PAEs. In addition, significant isotope discrimination of DMP and DEP for PS oxidation at pH = 2 and pH = 7 is likely associated with different radical species. Interestingly, the similar Λ values at pH = 2 and pH = 7 for DBP were not observed for DMP and DEP, which might be partly explained with the influence of the chemical structure, particularly the alkyl side chain which is a potential target for radicals. It is conceivable that the competing reactions at the side chain and aromatic rings are changing with chain length but we cannot quantify the reaction to prove this hypothesis. Therefore, more research is needed to understand the precise mechanisms of free radical reactions with the alkyl side chain of PAEs and which affect the Λ values.

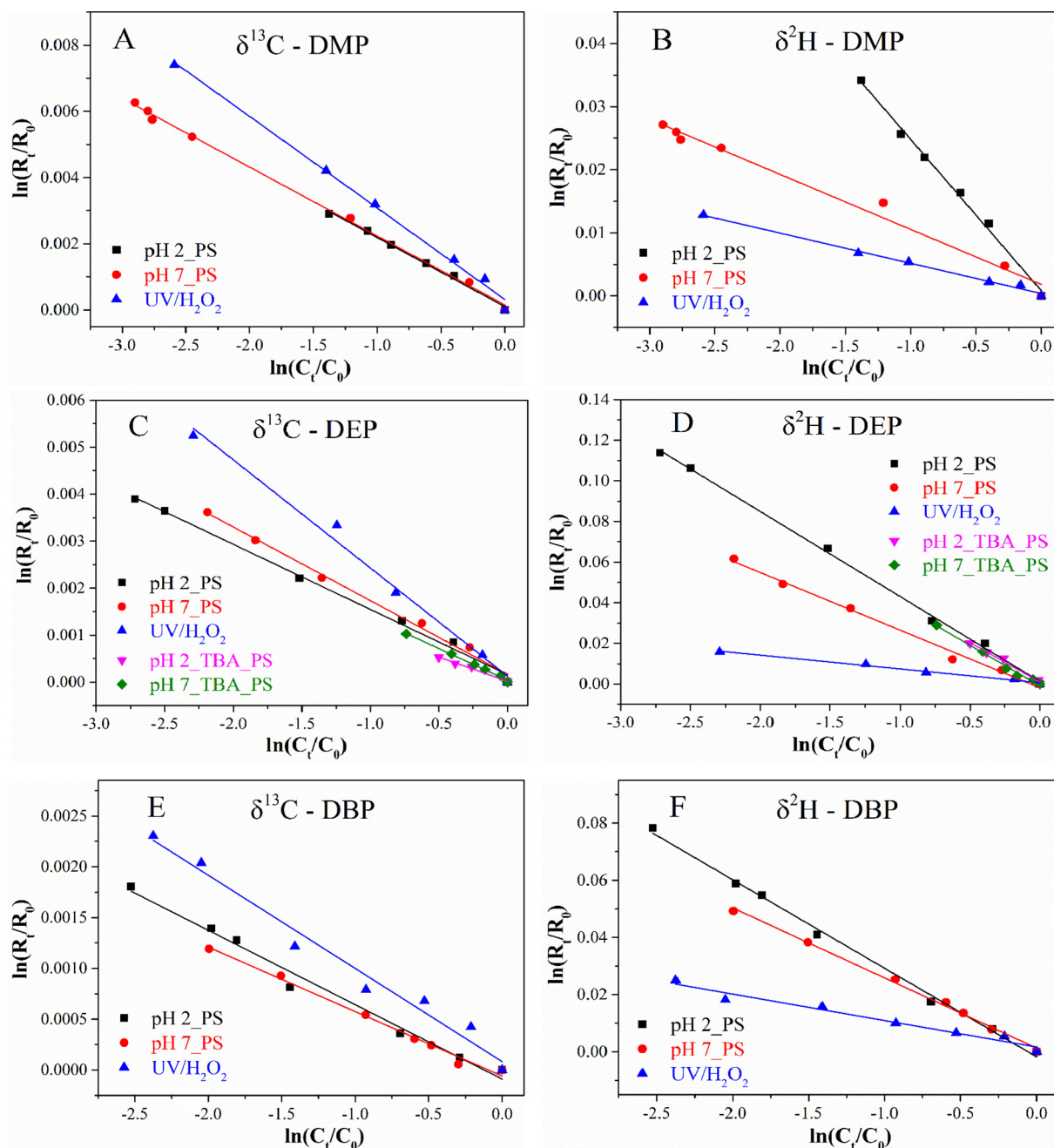


Fig. 1. Rayleigh regression of carbon (left panels, A, C, E) and hydrogen (right panels, B, D, F) isotope data during chemical oxidation reactions of PAEs (DMP, DEP and DBP).

3.4. Identification of predominant radical species by studying radical quenching combined with CSIA

Previous studies have demonstrated that $\text{SO}_4^{\cdot-}$ and $\text{HO}\cdot$ were probably generated and responsible for the decomposition of organic contaminants in persulfate oxidation system [24,25,40,46,49]. Predominant radical species during heat-activated PS oxidation were investigated using two alcoholic radical scavengers. EtOH and TBA were added to the solution, respectively and corresponded to a 200:1 molar ratio of the radical scavengers and DEP. Both $\text{SO}_4^{\cdot-}$ and $\text{HO}\cdot$ could be quenched by EtOH due to the second-order rate constants of $1.2\text{--}2.8 \times 10^9 \text{ M}^{-1}\text{s}^{-1}$ for EtOH/ $\text{HO}\cdot$ system and $1.6\text{--}7.7 \times 10^7 \text{ M}^{-1}\text{s}^{-1}$ for EtOH/ $\text{SO}_4^{\cdot-}$ system [50]. TBA is considered as an efficient scavenger of $\text{HO}\cdot$, because TBA reacts relatively slowly with $\text{SO}_4^{\cdot-}$ ($k = 4\text{--}9.1 \times 10^5 \text{ M}^{-1}\text{s}^{-1}$) compared to high

reactivity of TBA/ $\text{HO}\cdot$ system ($k = 3.8\text{--}7.6 \times 10^8 \text{ M}^{-1}\text{s}^{-1}$) [46]. After the addition of EtOH, the removal of DEP by persulfate could be neglected compared to experiments without scavenger at pH = 2 and pH = 7 (Fig. 3), which indicates that PS oxidation processes are mostly attributed to free radical reactions of $\text{SO}_4^{\cdot-}$ and $\text{HO}\cdot$. In the presence of TBA, strong inhibiting effects on the degradation of DEP were observed. A slightly smaller degree of inhibition than that of EtOH possibly indicates the presence of $\text{SO}_4^{\cdot-}$ during PS oxidation of DEP. However, results for degradation kinetics of radical quenching experiments in this study are not sufficient to identify dominant radical species at pH = 2 and pH = 7 due to strong inhibition of EtOH and TBA. In order to explore predominant reactive species responsible for the degradation of DEP, carbon and hydrogen isotope fractionations of TBA quenching experiments were investigated. Contrary to the distinct ϵ_{H} and Λ values of PS oxidation with DEP at pH = 2 and pH = 7, the

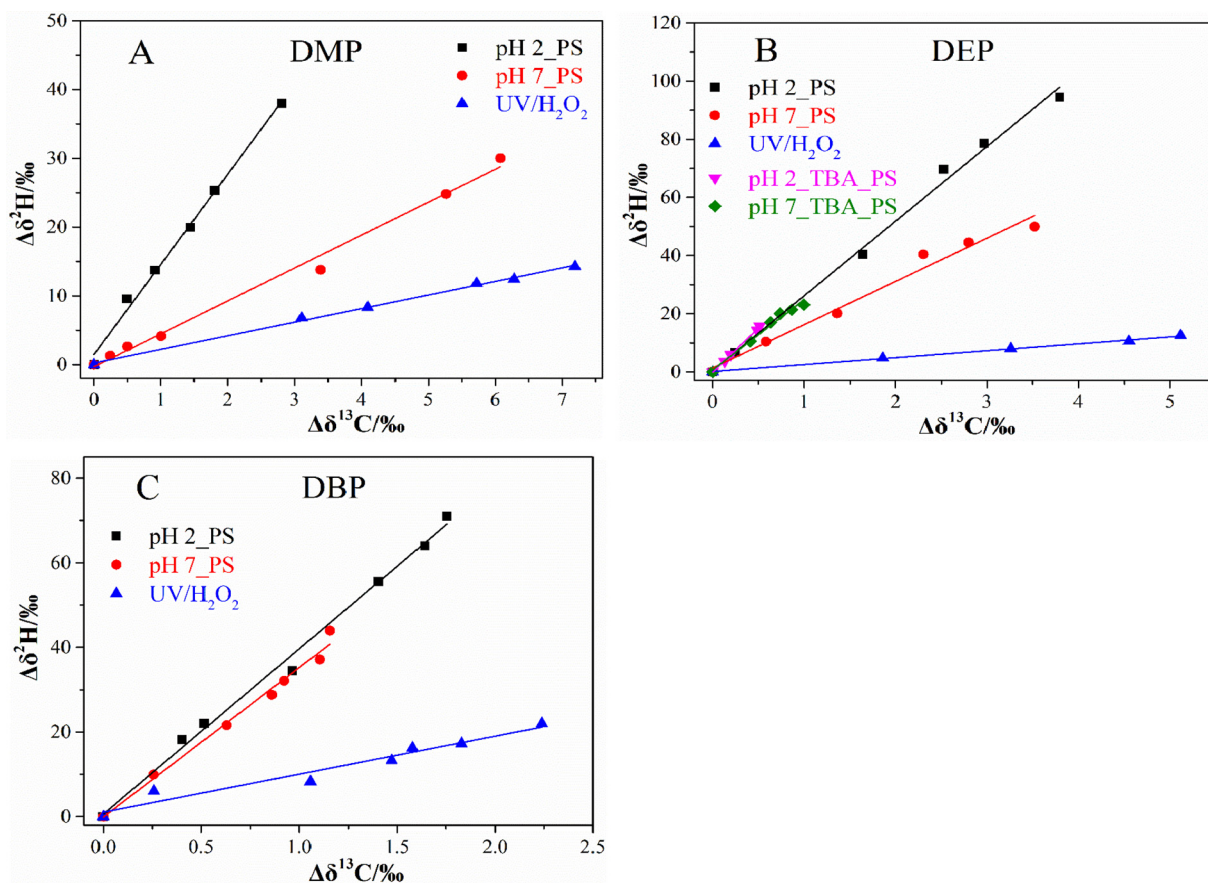


Fig. 2. Correlation of ^2H and ^{13}C isotope fractionation for DMP (A), DEP (B) and DBP (C) during chemical oxidation reactions.

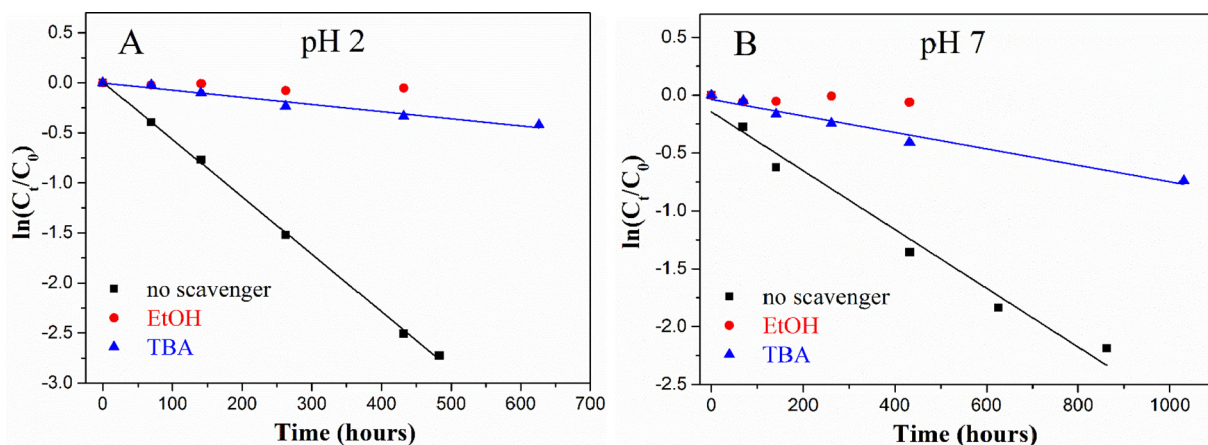


Fig. 3. Degradation kinetic curves of DEP during the study of radical quenching at pH = 2 (A) and pH = 7 (B).

obtained ε_{H} and Λ values after the addition of TBA were very similar (Table 1, Fig. 2). The difference between PS oxidation and TBA quenching experiments could be due to different radical species contributing to the overall reaction. In the presence of TBA, $\text{SO}_4^{\cdot-}$ becomes the predominant radical species which is responsible for the degradation of DEP at pH = 2 and pH = 7 and which is consistent with isotope fractionation results. In addition, Λ values of DEP quenching experiments ($\Lambda = 24.1 \pm 4.3$ at pH = 7, $\Lambda = 30.5 \pm 2.2$ at pH = 2) are almost identical to that of PS oxidation at pH = 2 ($\Lambda = 25.7 \pm 2.6$). This result suggests that $\text{SO}_4^{\cdot-}$ is the dominant radical at pH = 2 during PS oxidation of DEP, while $\text{SO}_4^{\cdot-}$ as well as $\text{HO}\cdot$ probably contribute to the degradation at pH = 7 with a smaller Λ value of 14.9 ± 3.0 .

3.5. Estimating the relative contribution of $\text{SO}_4^{\cdot-}$ and $\text{HO}\cdot$ in the overall reaction using isotope fractionation analysis

In previous studies [41,42], Rayleigh-type equations were modified to derive an equation for estimating the contribution of two simultaneous pathways to the overall degradation. To estimate the relative contribution of $\text{SO}_4^{\cdot-}$ and $\text{HO}\cdot$, it is assumed that the impact of phosphate buffer on major radical species during PS oxidation is small. Phosphate buffer has been widely used to maintain a constant pH value in many studies due to low reactivity with sulfate and hydroxyl radicals [37,51–53]. A phosphate buffer of up to 100 mM was used to keep the pH value constant. Still, the radical chain reaction with phosphate anions (HPO_4^{2-} and H_2PO_4^-) might affect the reaction. The potential

formation of HPO_4^{2-} and H_2PO_4^- with respect to pH value and concentration of the phosphate buffer used in the experiments was estimated according to literature data (Excel SI). The potential contribution of phosphate radicals in the experiments of DEP was minor (< 8%) and did not affect the discussion below (Text SI). Therefore, the contribution of secondary inorganic radical species was not considered further for the estimation of the relative contribution of $\text{SO}_4^{\cdot-}$ and $\text{HO}\cdot$.

$\text{HO}\cdot$ is the predominant radical species in the UV/ H_2O_2 reaction, whereas the TBA quenching experiment of DEP at pH = 7 suggests that $\text{SO}_4^{\cdot-}$ are the dominant radicals. In addition, distinct ^2H and ^{13}C isotope enrichment factors allow to estimate the relative contribution of $\text{SO}_4^{\cdot-}$ and $\text{HO}\cdot$ on the removal of DEP during PS oxidation at pH = 7 according to the extended Rayleigh-type equation. Error propagation was used to calculate the 95% confidence intervals of the estimated contribution (F) of $\text{HO}\cdot$ vs $\text{SO}_4^{\cdot-}$. $\text{HO}\cdot$ has a contribution of 0–47% and 20–50% based on the uncertainty of carbon and hydrogen isotope analyses, respectively. Moreover, Eq. (3) was also applied to calculate the value of F using carbon and hydrogen isotope signatures simultaneously. A contribution of 21–63% for $\text{HO}\cdot$ was obtained, which is in agreement with hydrogen isotope result. The reason is that the reaction of DEP with $\text{SO}_4^{\cdot-}/\text{HO}\cdot$ shows similar carbon enrichment factors, but different hydrogen enrichment factors. In this case, it is recommended to estimate the relative contribution using hydrogen isotope data differently than data from carbon isotope analysis. Even though a wide range of variability is observed due to the uncertainty of Λ and ϵ values, preliminary results indicate that a combination of radical quenching experiments and CSIA has the potential to estimate the relative contribution of $\text{SO}_4^{\cdot-}$ and $\text{HO}\cdot$ in persulfate oxidation systems.

3.6. Apparent kinetic isotope effects of DEP with $\text{HO}\cdot$ and $\text{SO}_4^{\cdot-}$

The intermediate products from DEP reaction with UV/ H_2O_2 were investigated using GC–MS analysis. The main transformation product is tentatively identified as diethyl 3-hydroxyphthalate (Fig. S4) by the molecular ion, mass fragment peak and also by comparison with a previous study [54]. $\text{HO}\cdot$ can oxidize organic compounds in aqueous media via three possible reaction mechanisms: (i) $\text{HO}\cdot$ addition leading to the radical adducts formation (RAF pathway), (ii) hydrogen atom transfer by $\text{HO}\cdot$ (HAT pathway) and (iii) single electron transfer by $\text{HO}\cdot$ (SET pathway) [55]. Based on the identified transformation product, $\text{HO}\cdot$ addition to the aromatic ring of DEP is assumed to be the main reaction mechanism, which is consistent with Gauss computational results on $\text{HO}\cdot$ -initiated degradation of PAEs in a previous study [45]. The values of $\delta^{13}\text{C}$ and $\delta^2\text{H}$ are measured as average isotope compositions in the compound, thus obtained ϵ_{C} and ϵ_{H} values are considered as bulk isotope fractionation factors. According to Eq. (4), ϵ_{C} and ϵ_{H} can be converted into position specific apparent kinetic isotope effects (^{13}C -AKIE and ^2H -AKIE) considering the reactive sites and nonreactive positions in the molecule. Experimentally determined kinetic isotope effect (KIE) values which are typical for oxidation reactions involving C–H bond cleavage are in the range of 1.01–1.03 for carbon isotopes and 2–8 for hydrogen isotopes [44,56]. For calculation of ^{13}C -AKIE during UV/ H_2O_2 reaction of DEP, the values of n , x and z are 12, 2 and 2, respectively. The calculated ^{13}C -AKIE of 1.028 falls in the range of 1.01–1.03 (Table 2), which supports the speculation of the RAF

pathway. However, for ^2H , an AKIE of 1.11 was obtained, which is lower than the previously reported KIE_{H} of 2–8. Much smaller experimental kinetic isotope effect (AKIE_{H}) might be likely associated with a sp^2 to sp^3 hybridization change at the reacting carbon in the aromatic ring as reported elsewhere [32].

For the reaction of $\text{SO}_4^{\cdot-}$ with DEP, degradation products could not be identified by GC–MS analysis. The concentration of the metabolites was possibly very low and rapid degradation of metabolites in subsequent radical reaction may prevent detection of the products which would indicate hydroxylation of the side chain or the aromatic ring. Previous mechanistic studies on the reaction of sulfate radicals with PAEs suggested that the first step of $\text{SO}_4^{\cdot-}$ oxidation was likely the radical attack on the aromatic ring or oxidation of the aliphatic chain [46,47,57]. Therefore, AKIEs were calculated for the reaction of DEP with $\text{SO}_4^{\cdot-}$ considering radical attack at the side chain and at the aromatic ring. In the presence of TBA, $\text{SO}_4^{\cdot-}$ becomes the predominant radical species responsible for DEP decomposition. ^{13}C -AKIE and ^2H -AKIE at pH = 2 were 1.013 and 2.19, respectively, and considered to be identical for both pathways, because the number of reactive positions (x) and indistinguishable reactive positions (z) lead to calculation of identical AKIEs in this simplified approach (Eq. (4)). Additionally, corresponding AKIEs for PS oxidation at pH = 2 and TBA quenching experiment at pH = 7 were shown in Table 2. As $\text{HO}\cdot$ and $\text{SO}_4^{\cdot-}$ are both involved at pH = 7 during PS oxidation, it is difficult to confirm exact values of n , x and z for the radical reaction due to competing mechanisms. Therefore, ^{13}C -AKIE and ^2H -AKIE values are not calculated for PS oxidation at pH = 7 in this study. Although the obtained ^{13}C -AKIE and ^2H -AKIE values of $\text{SO}_4^{\cdot-}$ dominant reactions are both in accordance with expected KIE ranges for C–H bond oxidation (C:1.01–1.03, H: 2–8), it supports the hypothesis of C–H bond cleavage but cannot be used to predict degradation mechanisms at the side chain or aromatic ring of DEP with $\text{SO}_4^{\cdot-}$. More information on intermediate products may be needed for further elucidation of reaction mechanisms.

4. Conclusions

In present study, dual isotope fractionation of radical reactions was systematically investigated in heat-activated PS oxidation and UV/ H_2O_2 for three PAEs (DMP, DEP and DBP). Distinct Λ values ($\Delta\delta^2\text{H}/\Delta\delta^{13}\text{C}$) indicate the potential of CSIA to characterize PS oxidation and UV/ H_2O_2 reaction in field studies as an example for environmental remediation measures or technical systems. The combination of radical quenching analysis and CSIA suggests that $\text{SO}_4^{\cdot-}$ is the dominant radical species to oxidize DEP at pH = 2 during PS oxidation, while both $\text{SO}_4^{\cdot-}$ and $\text{HO}\cdot$ are the major species at pH = 7. Additionally, it provides a novel approach to estimate the relative contribution of $\text{SO}_4^{\cdot-}$ and $\text{HO}\cdot$ to the overall reaction using isotope fractionation for characterizing radical reactions. Carbon and hydrogen isotope fractionation patterns are of fundamental importance to evaluate ISCO processes for the removal of PAEs. The results of this study are an important step forward in understanding degradation mechanisms of organic compounds with $\text{SO}_4^{\cdot-}$ and $\text{HO}\cdot$ in the aqueous phase.

Table 2
Carbon and hydrogen AKIEs of DEP for investigated experimental systems.

Conditions	Dominant radical	ϵ_{C} (‰)	^{13}C - AKIE	ϵ_{H} (‰)	^2H - AKIE
UV/ H_2O_2 at pH 7	$\text{HO}\cdot$	-2.30 ± 0.42	1.028	-6.8 ± 1.3	1.11
TBA quench at pH 2	$\text{SO}_4^{\cdot-}$	-1.07 ± 0.29	1.013	-38.8 ± 7.7	2.19
TBA quench at pH 7	$\text{SO}_4^{\cdot-}$	-1.35 ± 0.12	1.016	-39.8 ± 5.7	2.26
PS oxidation at pH 2	$\text{SO}_4^{\cdot-}$	-1.39 ± 0.13	1.017	-41.8 ± 2.4	2.41
PS oxidation at pH 7	$\text{SO}_4^{\cdot-} + \text{HO}\cdot$	-1.57 ± 0.18	n.d. ^a	-28.3 ± 3.3	n.d. ^a

^a n.d.: not determined.

Acknowledgments

This work was supported by the China Scholarship Council (File No. 201506460058 for Dan Zhang, and File No. 201306460007 for Langping Wu) and in part by grants from the Key project from National Science Foundation of China (41430106, 41720104007). We are grateful to Steffen Kümmel for his help in the Isotope Laboratory of the UFZ.

Appendix A. Supplementary data

Supplementary data associated with this article can be found, in the online version, at <http://dx.doi.org/10.1016/j.cej.2018.04.047>.

References

- C.A. Staples, D.R. Peterson, T.F. Parkerton, W.J. Adams, The environmental fate of phthalate esters: a literature review, *Chemosphere* 35 (1997) 667–749.
- Y. Zhang, Q. Liang, R.T. Gao, H.B. Hou, W.B. Tan, X.S. He, H. Zhang, M.D. Yu, L. Ma, B.D. Xi, X.W. Wang, Contamination of phthalate esters (PAEs) in typical wastewater-irrigated agricultural soils in Hebei, North China, *PLoS One* 10 (2015) e0137998.
- C. Vamsee-Krishna, P.S. Phale, Bacterial degradation of phthalate isomers and their esters, *Indian J. Microbiol.* 48 (2008) 19–34.
- J.Q. Sun, X.Q. Wu, J. Gan, Uptake and metabolism of phthalate esters by edible plants, *Environ. Sci. Technol.* 49 (2015) 8471–8478.
- H. Chen, R. Zhuang, J. Yao, F. Wang, Y. Qian, A comparative study on the impact of phthalate esters on soil microbial activity, *Bull. Environ. Contam. Toxicol.* 91 (2013) 217–223.
- S. Net, R. Sempere, A. Delmont, A. Paluselli, B. Ouddane, Occurrence, fate, behavior and ecotoxicological state of phthalates in different environmental matrices, *Environ. Sci. Technol.* 49 (2015) 4019–4035.
- W.J. Tang, L.S. Zhang, Y. Fang, Y. Zhou, B.C. Ye, Biodegradation of phthalate esters by newly isolated *Rhizobium* sp. LMB-1 and its biochemical pathway of di-n-butyl phthalate, *J. Appl. Microbiol.* 121 (2016) 177–186.
- United States Environmental Protection Agency (USEPA), Electronic code of federal regulations, Title 40-Protection of environment, Appendix A to Part 423-126, Priority pollutants 2013.
- D.W. Gao, Z.D. Wen, Phthalate esters in the environment: a critical review of their occurrence, biodegradation, and removal during wastewater treatment processes, *Sci. Total Environ.* 541 (2016) 986–1001.
- P. Devi, U. Das, A.K. Dalai, In-situ chemical oxidation: principle and applications of peroxide and persulfate treatments in wastewater systems, *Sci. Total Environ.* 571 (2016) 643–657.
- A. Tsitonaki, B. Petri, M. Crimi, H. Mosbæk, R.L. Siegrist, P.L. Bjerg, In situ chemical oxidation of contaminated soil and groundwater using persulfate: a review, *Crit. Rev. Environ. Sci. Technol.* 40 (2010) 55–91.
- M. Cheng, G.M. Zeng, D.L. Huang, C. Lai, P. Xu, C. Zhang, Y. Liu, Hydroxyl radicals based advanced oxidation processes (AOPs) for remediation of soils contaminated with organic compounds: a review, *Chem. Eng. J.* 284 (2016) 582–598.
- M. Gmurek, M. Olak-Kucharczyk, S. Ledakowicz, Photochemical decomposition of endocrine disrupting compounds - A review, *Chem. Eng. J.* 310 (2017) 437–456.
- B. Xu, N.Y. Gao, X.F. Sun, S.J. Xia, M. Rui, M.O. Simonnot, C. Causserand, J.F. Zhao, Photochemical degradation of diethyl phthalate with UV/H₂O₂, *J. Hazard. Mater.* 139 (2007) 132–139.
- B. Xu, N.Y. Gao, H. Cheng, S.J. Xia, M. Rui, D.D. Zhao, Oxidative degradation of dimethyl phthalate (DMP) by UV/H₂O₂ process, *J. Hazard. Mater.* 162 (2009) 954–959.
- D.L. Huang, Y. Wang, C. Zhang, G.M. Zeng, C. Lai, J. Wan, L. Qin, Y. Zeng, Influence of morphological and chemical features of biochar on hydrogen peroxide activation: implications on sulfamethazine degradation, *RSC Adv.* 6 (2016) 73186–73196.
- D.L. Huang, C.J. Hu, G.M. Zeng, M. Cheng, P. Xu, X.M. Gong, R.Z. Wang, W.J. Xue, Combination of Fenton processes and biotreatment for wastewater treatment and soil remediation, *Sci. Total Environ.* 574 (2017) 1599–1610.
- F. Ghanbari, M. Moradi, Application of peroxymonosulfate and its activation methods for degradation of environmental organic pollutants: review, *Chem. Eng. J.* 310 (2017) 41–62.
- Y.F. Ji, C.X. Dong, D.Y. Kong, J.H. Lu, Q.S. Zhou, Heat-activated persulfate oxidation of atrazine: implications for remediation of groundwater contaminated by herbicides, *Chem. Eng. J.* 263 (2015) 45–54.
- X.L. Zhang, M.B. Feng, R.J. Qu, H. Liu, L.S. Wang, Z.Y. Wang, Catalytic degradation of diethyl phthalate in aqueous solution by persulfate activated with nano-scaled magnetic CuFe₂O₄/MWCNTs, *Chem. Eng. J.* 301 (2016) 1–11.
- S. Waclawek, H.V. Lutze, K. Grübel, V.V.T. Padil, M. Černík, D.D. Dionysiou, Chemistry of persulfates in water and wastewater treatment: a review, *Chem. Eng. J.* 330 (2017) 44–62.
- J.L. Wang, S.Z. Wang, Activation of persulfate (PS) and peroxymonosulfate (PMS) and application for the degradation of emerging contaminants, *Chem. Eng. J.* 334 (2018) 1502–1517.
- A. Romero, A. Santos, F. Vicente, C. González, Diuron abatement using activated persulfate: effect of pH, Fe(II) and oxidant dosage, *Chem. Eng. J.* 162 (2010) 257–265.
- C.J. Liang, H.-W. Su, Identification of sulfate and hydroxyl radicals in thermally activated persulfate, *Ind. Eng. Chem. Res.* 48 (2009) 5558–5562.
- G.P. Anipsitakis, D.D. Dionysiou, Radical generation by the interaction of transition metals with common oxidants, *Environ. Sci. Technol.* 38 (2004) 3705–3712.
- S. Yuan, P. Liao, A.N. Alshawabkeh, Electrolytic manipulation of persulfate reactivity by iron electrodes for trichloroethylene degradation in groundwater, *Environ. Sci. Technol.* 48 (2014) 656–663.
- M. Ahmad, A.L. Teel, O.S. Furman, J.I. Reed, R.J. Watts, Oxidative and reductive pathways in iron-ethylenediaminetetraacetic acid-activated persulfate systems, *J. Environ. Eng.* 138 (2012) 411–418.
- M. Elsner, G. Imfeld, Compound-specific isotope analysis (CSIA) of micropollutants in the environment-current developments and future challenges, *Curr. Opin. Biotechnol.* 41 (2016) 60–72.
- M. Elsner, Stable isotope fractionation to investigate natural transformation mechanisms of organic contaminants: principles, prospects and limitations, *J. Environ. Monit.* 12 (2010) 2005–2031.
- I. Nijenhuis, H.H. Richnow, Stable isotope fractionation concepts for characterizing biotransformation of organohalides, *Curr. Opin. Biotechnol.* 41 (2016) 108–113.
- C. Vogt, C. Dorer, F. Musat, H.H. Richnow, Multi-element isotope fractionation concepts to characterize the biodegradation of hydrocarbons-from enzymes to the environment, *Curr. Opin. Biotechnol.* 41 (2016) 90–98.
- N. Zhang, I. Geronimo, P. Paneth, J. Schindelka, T. Schaefer, H. Herrmann, C. Vogt, H.H. Richnow, Analyzing sites of OH radical attack (ring vs. side chain) in oxidation of substituted benzenes via dual stable isotope analysis (^δ13C and ^δ2H), *Sci. Total Environ.* 542 (2016) 484–494.
- H. Liu, Z. Wu, X.Y. Huang, C. Yarnes, M.J. Li, L. Tong, Carbon isotopic fractionation during biodegradation of phthalate esters in anoxic condition, *Chemosphere* 138 (2015) 1021–1027.
- X.W. Peng, X.G. Li, L.J. Feng, Behavior of stable carbon isotope of phthalate acid esters during photolysis under ultraviolet irradiation, *Chemosphere* 92 (2013) 1557–1562.
- X.W. Peng, L.J. Feng, X.G. Li, Pathway of diethyl phthalate photolysis in sea-water determined by gas chromatography-mass spectrometry and compound-specific isotope analysis, *Chemosphere* 90 (2013) 220–226.
- X.W. Peng, X.G. Li, Compound-specific isotope analysis for aerobic biodegradation of phthalate acid esters, *Talanta* 97 (2012) 445–449.
- C.Q. Tan, N.Y. Gao, Y. Deng, Y.J. Zhang, M.H. Sui, J. Deng, S.Q. Zhou, Degradation of antipyrine by UV, UV/H₂O₂ and UV/PS, *J. Hazard. Mater.* 260 (2013) 1008–1016.
- L.S. Lian, B. Yao, S.D. Hou, J.Y. Fang, S.W. Yan, W.H. Song, Kinetic study of hydroxyl and sulfate radical-mediated oxidation of pharmaceuticals in wastewater effluents, *Environ. Sci. Technol.* 51 (2017) 2954–2962.
- Y. Yang, J. Jiang, X.L. Lu, J. Ma, Y.Z. Liu, Production of sulfate radical and hydroxyl radical by reaction of ozone with peroxymonosulfate: a novel advanced oxidation process, *Environ. Sci. Technol.* 49 (2015) 7330–7339.
- P.C. Xie, J. Ma, W. Liu, J. Zou, S.Y. Yue, X.C. Li, M.R. Wiesner, J.y. Fang, Removal of 2-MIB and geosmin using UV/persulfate: contributions of hydroxyl and sulfate radicals, *Water Res.* 69 (2015) 223–233.
- B.M. van Breukelen, Extending the Rayleigh equation to allow competing isotope fractionating pathways to improve quantification of biodegradation, *Environ. Sci. Technol.* 41 (2007) 4004–4010.
- F. Centler, F. Hesse, M. Thullner, Estimating pathway-specific contributions to biodegradation in aquifers based on dual isotope analysis: theoretical analysis and reactive transport simulations, *J. Contam. Hydrol.* 152 (2013) 97–116.
- C.M. Aelion, P. Höhener, D. Hunkeler, R. Aravena, Environmental Isotopes in Biodegradation and Bioremediation, CRC Press, 2009.
- M. Elsner, L. Zwank, D. Hunkeler, R.P. Schwarzenbach, A new concept linking observable stable isotope fractionation to transformation pathways of organic pollutants, *Environ. Sci. Technol.* 39 (2005) 6896–6916.
- Y. Gao, T. An, Y. Ji, G. Li, C. Zhao, Eco-toxicity and human estrogenic exposure risks from OH-initiated photochemical transformation of four phthalates in water: a computational study, *Environ. Pollut.* 206 (2015) 510–517.
- H. Li, J. Wan, Y. Ma, Y. Wang, Reaction pathway and oxidation mechanisms of dibutyl phthalate by persulfate activated with zero-valent iron, *Sci. Total Environ.* 562 (2016) 889–897.
- Z. Wang, D.Y. Deng, L.L. Yang, Degradation of dimethyl phthalate in solutions and soil slurries by persulfate at ambient temperature, *J. Hazard. Mater.* 271 (2014) 202–209.
- J. Palau, P. Jamin, A. Badin, N. Vanhecke, B. Haerens, S. Brouyere, D. Hunkeler, Use of dual carbon-chlorine isotope analysis to assess the degradation pathways of 1,1,1-trichloroethane in groundwater, *Water Res.* 92 (2016) 235–243.
- D.H. Han, J.Q. Wan, Y.W. Ma, Y. Wang, Y. Li, D.Y. Li, Z.Y. Guan, New insights into the role of organic chelating agents in Fe(II) activated persulfate processes, *Chem. Eng. J.* 269 (2015) 425–433.
- P. Neta, R.E. Huie, A.B. Ross, Rate constants for reactions of inorganic radicals in aqueous solution, *J. Phys. Chem. Ref. Data* 17 (1988) 1027–1284.
- C.J. Liang, Z.S. Wang, N. Mohanty, Influences of carbonate and chloride ions on persulfate oxidation of trichloroethylene at 20 °C, *Sci. Total Environ.* 370 (2006) 271–277.
- X.G. Gu, S.G. Lu, L. Li, Z.F. Qiu, Q. Sui, K.F. Lin, Q.S. Luo, Oxidation of 1,1,1-trichloroethane stimulated by thermally activated persulfate, *Ind. Eng. Chem. Res.* 50 (2011) 11029–11036.
- A. Ghauch, A.M. Tuqan, N. Kibbi, Ibuprofen removal by heated persulfate in aqueous solution: a kinetics study, *Chem. Eng. J.* 197 (2012) 483–492.
- K.S. Tay, N.A. Rahman, M.R. Bin Abas, Fenton degradation of dialkylphthalates: products and mechanism, *Environ. Chem. Lett.* 9 (2011) 539–546.
- T. An, Y. Gao, G. Li, P.V. Kamat, J. Peller, M.V. Joyce, Kinetics and mechanism of OH mediated degradation of dimethyl phthalate in aqueous solution: experimental and theoretical studies, *Environ. Sci. Technol.* 48 (2014) 641–648.
- P.F. Cook, Enzyme Mechanism from Isotope Effects, CRC Press, 1991.
- L.J. Xu, W. Chu, L. Gan, Environmental application of graphene-based CoFe₂O₄ as an activator of peroxymonosulfate for the degradation of a plasticizer, *Chem. Eng. J.* 263 (2015) 435–443.

Supporting Information

Carbon and hydrogen isotope fractionation of phthalate esters during degradation by sulfate and hydroxyl radicals

Dan Zhang^{1,2}, Langping Wu², Jun Yao^{3**}, Hartmut Herrmann⁴, Hans-Hermann Richnow^{2,3*}

¹School of Energy and Environmental Engineering, University of Science and Technology Beijing, Xueyuan Road No.30, Haidian District, Beijing 100083, PR China

²Department of Isotope Biogeochemistry, Helmholtz Centre for Environmental Research-UFZ, Permoserstraße 15, Leipzig 04318, Germany

³School of Water Resources and Environment, China University of Geosciences (Beijing), Xueyuan Road No.29, Haidian District, Beijing 100083, PR China

⁴Leibniz Institute for Tropospheric Research (TROPOS), Permoserstraße 15, Leipzig 04318, Germany

* To whom correspondence should be addressed

* hans.richnow@ufz.de Tel.: +49 (0) 341 235 1212, Fax: +49 (0) 341 235 1443

** yaojun@cugb.edu.cn Tel.: +86 (0)10 82321958, Fax: +86 (0)10 82321958

11 pages

4 figures

Content

Control experiments of DEP	S2
Carbon and hydrogen isotope fractionation of PAEs	S3-S5
Estimation of potential influence of secondary radicals generated by the reaction of phosphate ions with $\text{SO}_4^{\cdot-}$ / $\text{HO}\cdot$	S5-S6
Identification of degradation product of DEP in the UV/ H_2O_2 reaction by GC-MS	S6
References	S7

Control experiments of DEP

For PS oxidation of DEP, control experiments without PS addition (hydrolysis) at pH = 2 and pH = 7 were conducted at 35 °C. The remaining fraction of DEP showed no obvious decrease in concentration over the time course of the experiments (Fig. S1), which proved that the reduction in DEP concentration during PS oxidation was exclusively a result of degradation.

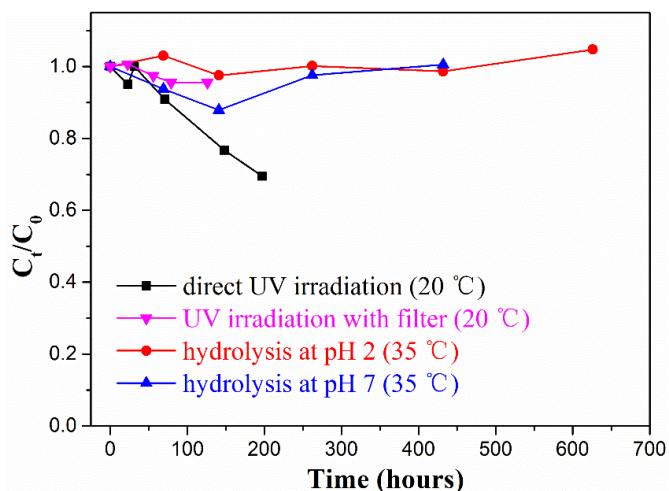


Fig. S1. Remaining fraction of DEP in control experiments.

Control experiment of DEP reaction only with UV irradiation ($\lambda \geq 185$ nm, direct photolysis) showed less than 10% decrease within 50 hours whereas more than 90% of DEP degraded in 40 hours for UV/H₂O₂ reaction. Rate constants of direct photolysis and UV/H₂O₂ were 0.0018 h⁻¹ and 0.0541 h⁻¹, respectively, which indicated that degradation rate of direct photolysis was much slower than that of UV/H₂O₂. The degradation of DEP under direct photolysis can be explained by UV absorption spectrum of DEP, which was shown in Fig. S2. The measurement was performed with DEP dissolved in water using a UV spectrometer. The maximum absorption peak was observed at $\lambda = 229$ nm, which was in agreement with previous studies on PAEs [1, 2]. This indicates that direct photolysis is unlikely when a UV filter with cut off at $\lambda \geq 280$ nm is used. Control experiment of UV radiation with filter ($\lambda \geq 280$ nm) for cut of the shortwave UV irradiation showed almost stable concentration and suggested that photolysis at $\lambda \geq 280$ nm does not affect the concentration of DEP under the experimental conditions.

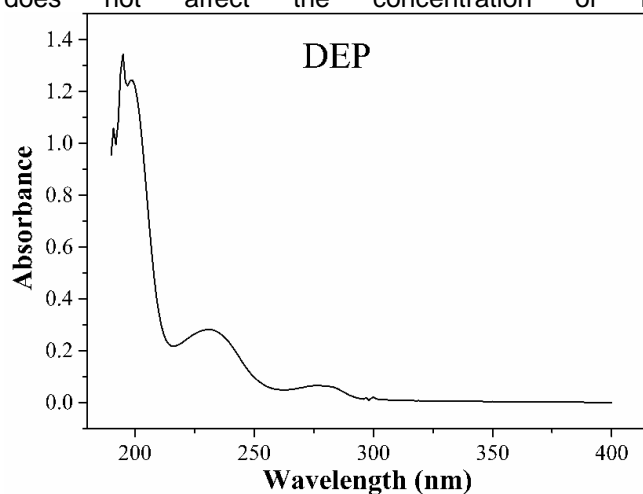
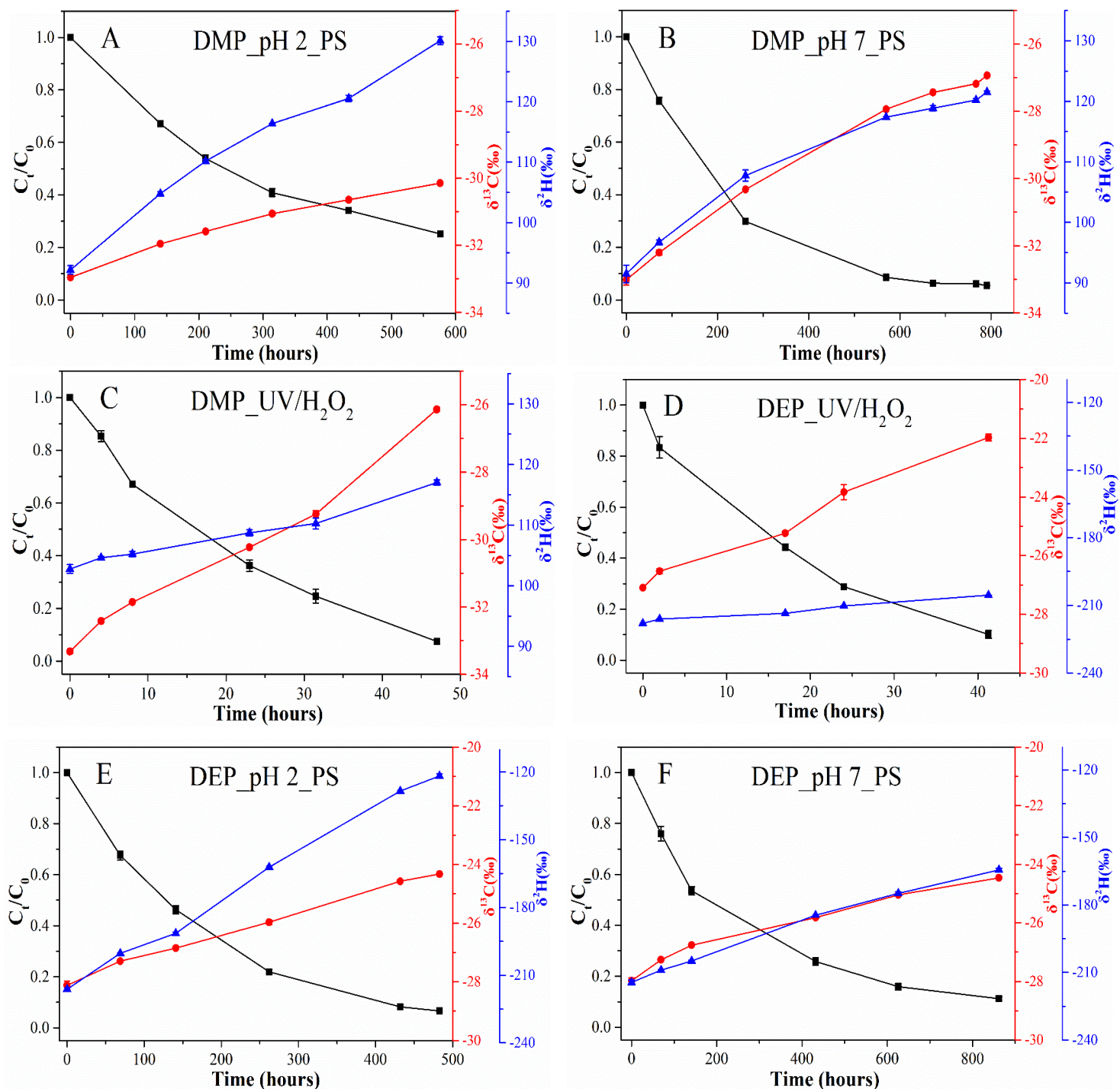


Fig. S2. UV absorption spectrum of DEP in water.

Carbon and hydrogen isotope fractionation of PAEs

The remaining fraction, carbon and hydrogen isotope composition of DMP, DEP and DBP in the degradation experiments were shown in Fig. S3. For all investigated reactions, $\delta^{13}\text{C}$ and $\delta^2\text{H}$ values of three PAEs showed a trend to more positive isotope values in the time course of degradation, which indicated a normal isotope effect.



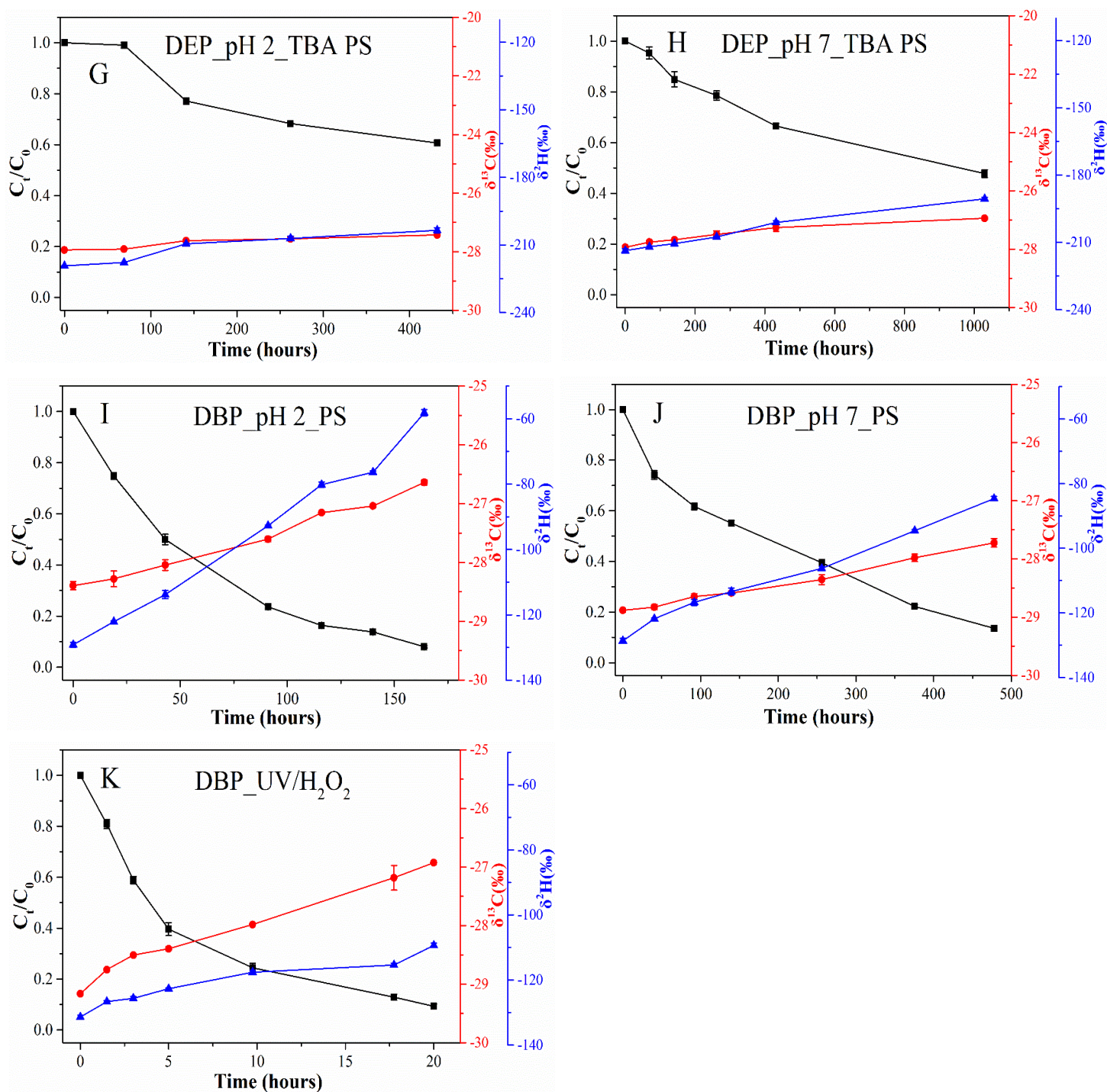


Fig. S3. Remaining fraction (black squares), carbon isotope ratios (red circles) and hydrogen isotope ratios (blue triangles) of three PAEs (DMP, DEP and DBP) during transformation reactions catalyzed by persulfate oxidation at pH 2 (A, E and I), persulfate oxidation at pH 7 (B, F and J), UV/H₂O₂ process (C, D and K), quenching experiment with TBA at pH 2 (G) and quenching experiment with TBA at pH 7 (H).

Carbon isotope composition of DMP exhibited ^{13}C enrichment from $-32.96 \pm 0.04\text{‰}$ to $-30.15 \pm 0.02\text{‰}$ after 75% degradation by persulfate oxidation at pH 2, from $-33.01 \pm 0.16\text{‰}$ to $-26.94 \pm 0.02\text{‰}$

after 95% degradation by persulfate oxidation at pH 7 and from $-33.32 \pm 0.05\text{‰}$ to $-26.14 \pm 0.06\text{‰}$ after 93% degradation by UV/H₂O₂ reaction, respectively. The hydrogen isotope composition of DMP showed a distinct ²H enrichment from $92.2 \pm 0.7\text{‰}$ to $130.1 \pm 0.6\text{‰}$ after 75% degradation by PS oxidation at pH 2, from $91.5 \pm 1.5\text{‰}$ to $121.5 \pm 0.2\text{‰}$ after 95% degradation by PS oxidation at pH 7, and from $102.8 \pm 0.7\text{‰}$ to $117.0 \pm 0.5\text{‰}$ after 93% degradation by UV/H₂O₂.

The changes in ¹³C and ²H values of DEP during different batch experiments were shown in Fig. S3 (D ~ H). Radical quenching experiments with TBA at pH = 2 and pH = 7 were conducted to obtain further information on predominant radical species. For persulfate oxidation of DEP at pH 7 without and with TBA, hydrogen isotope ratios were enriched from $-214.4 \pm 1.1\text{‰}$ to $-164.5 \pm 0.8\text{‰}$ after 89% degradation and from $-213.7 \pm 0.9\text{‰}$ to $-190.6 \pm 0.7\text{‰}$ after 52% degradation. In these experiments, carbon isotope ratios were enriched from $-27.98 \pm 0.10\text{‰}$ to $-24.46 \pm 0.02\text{‰}$ after 89% degradation and from $-27.94 \pm 0.02\text{‰}$ to $-26.94 \pm 0.05\text{‰}$ after 52% degradation. During the degradation experiments of DEP at pH 2 with persulfate oxidation but without TBA, ²H values were enriched from $-216.2 \pm 0.6\text{‰}$ to $-121.8 \pm 1.0\text{‰}$ after 93% degradation. In the parallel batch experiment using persulfate oxidation with TBA, ²H isotope value became isotopically heavier from $-219.3 \pm 0.1\text{‰}$ to $-203.5 \pm 1.1\text{‰}$ after 40% degradation. Carbon isotope ratios were enriched in ¹³C from $-28.12 \pm 0.14\text{‰}$ to $-24.32 \pm 0.01\text{‰}$ after 93% degradation and from $-27.94 \pm 0.04\text{‰}$ to $-27.43 \pm 0.03\text{‰}$ after 40% degradation, respectively (Fig. S3, E and G).

Estimation of potential influence of secondary radicals generated by the reaction of phosphate ions with SO₄^{•-}/HO[•].

Potential effect of phosphate buffer on chemical reactions of DEP was investigated and radical reactions of SO₄^{•-}/HO[•] with phosphate (HPO₄²⁻ and H₂PO₄⁻) were considered to form secondary phosphate radicals (HPO₄^{•-} and H₂PO₄^{•-}). For the experiments a 61.6 and 100 mM phosphate buffer was used (see excel script for individual experiments). Potential contributions to the degradation of DEP with secondary radicals were estimated in order to evaluate if isotope fractionation of DEP could be affected. An excel script with the calculation was attached for the formation of phosphate radicals with experimental parameters, such as concentrations and pH (SI). For simplification of the model calculation, we considered a preferential reaction of radicals with the aromatic system of DEP. Absolute rate constants for the reaction of SO₄^{•-} with aromatic compounds were found in the range of $10^9 \text{ M}^{-1}\text{s}^{-1}$ [3], therefore, the rate constant of SO₄^{•-} with DEP was estimated to be $1.0 \times 10^9 \text{ M}^{-1}\text{s}^{-1}$. Initial concentration of DEP was 0.97 mM and the first-order rate constant of SO₄^{•-} with DEP representing the sink strength (S [SO₄^{•-} + DEP]) was calculated to be $9.7 \times 10^5 \text{ s}^{-1}$. According to different phosphate buffer compositions at pH = 2 and pH = 7, potential reactions of SO₄^{•-} with phosphate anions (HPO₄²⁻ and H₂PO₄⁻) were estimated and absolute second-order rate constants were obtained from previous study of Maruthamuthu and Neta [4]. Rate constants for the formation of phosphate radicals were estimated to be in the range of $2.0 \times 10^4 \text{ M}^{-1}\text{s}^{-1}$ to $1.2 \times 10^6 \text{ M}^{-1}\text{s}^{-1}$ and were considerably smaller than the rate constants for DEP reaction with HO[•] ($4.4 \times 10^9 \text{ M}^{-1}\text{s}^{-1}$) and SO₄^{•-} ($1.0 \times 10^9 \text{ M}^{-1}\text{s}^{-1}$).

Thus, maximal contribution of secondary radicals can be considered to be small compared to primary radical species during PS oxidation at pH = 2 and pH = 7. It was calculated to contribute between 0.7% and 7.9%, respectively assuming that they react with DEP. In addition, second-order rate constant of HO[•]-initiated DEP transformation was calculated to be $4.4 \times 10^9 \text{ M}^{-1}\text{s}^{-1}$ using transition-state theory [5]. The corresponding first-order rate constant of HO[•] with DEP representing the sink strength (S [HO[•] + DEP]) was estimated to be $4.3 \times 10^6 \text{ s}^{-1}$ considering initial concentration of DEP. Similarly, secondary reactions of HO[•] with HPO₄²⁻/H₂PO₄⁻ were considered according to literature data [4] and the effect of generated phosphate radicals on HO[•] was estimated to be 0.2%. The estimation showed that potential effects of phosphate radicals on SO₄^{•-} and HO[•] were lower than 8%. It is known that oxidation capability of radical species decreases in the order: SO₄^{•-} > H₂PO₄^{•-} > HPO₄^{•-} [4]. Therefore, we considered that the contribution of phosphate radicals was not significant in the investigated experiments of DEP.

In addition, estimated calculation method was applied to the experiments of DMP with the assumption that second-order rate constant of SO₄^{•-} with DMP was $1.0 \times 10^9 \text{ M}^{-1}\text{s}^{-1}$. To our best knowledge, accurate value of k [SO₄^{•-} + DMP] was not available from literature. Hence, we assumed the

value according to previous study [3] and used it to roughly estimate the potential influence of secondary phosphate radicals on the reaction of HO· with DMP. The contribution of secondary radicals during PS oxidation experiments with DMP were estimated to be 0.6% (pH 2) and 7.0% (pH 7), respectively (see excel script). Moreover, potential contribution of secondary phosphate radicals on HO· catalyzed radical reaction was calculated as 0.3% when the value of k [HO· +DMP] was $2.7 \times 10^9 \text{ M}^{-1} \text{ s}^{-1}$ based on literature data [5]. Thus, the estimated results indicated that potential influence of secondary phosphate radicals was not significant for DMP in this study.

We did not estimate the contribution of secondary radical for DBP experiments because absolute second-order rate constant for the reaction of $\text{SO}_4^{\cdot -}$ with DBP was lacking and it was difficult to estimate. Possible contribution of $\text{SO}_4^{\cdot -}$ reaction with long alkyl side chain of DBP needed to take into consideration. For PAEs molecules, the reaction of radical species with the side chain became more significant with the increasing length of the alkyl side chain in HO·-initiated reactions [5]. More research on the reaction of phosphate radicals with PAEs is needed and will be conducted in the future study.

Identification of degradation product of DEP in the UV/H₂O₂ reaction by GC-MS.

Transformation products of DEP reaction with UV/H₂O₂ were tentatively identified by GC-MS. Based on the molecular ion, mass fragment peak and also through comparison with literature, the peak at retention time of 14.31 min was identified as diethyl 3-hydroxyphthalate according to the previous study of Tay et al. [6] (Fig. S4). The mass spectrum could be clearly distinct from the mass spectrum of diethyl 4-hydroxyphthalate.

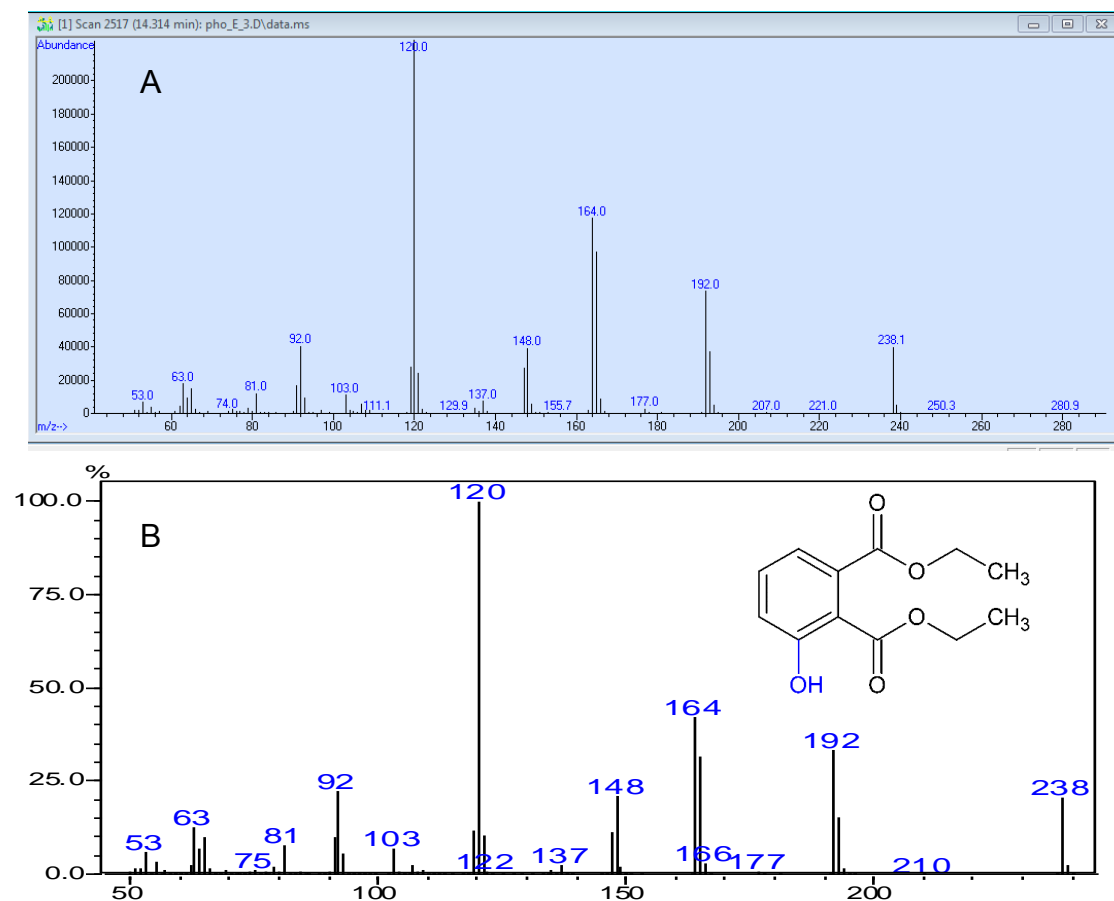


Fig. S4. Mass spectra of identified degradation product (A) and diethyl 3-hydroxyphthalate (B) from Tay et al. [6].

References

- [1] B. Xu, N.Y. Gao, X.F. Sun, S.J. Xia, M. Rui, M.O. Simonnot, C. Causserand, J.F. Zhao, Photochemical degradation of diethyl phthalate with UV/H₂O₂, *J. Hazard. Mater.* 139 (2007) 132-139.
- [2] O. Bajt, G. Mailhot, M. Bolte, Degradation of dibutyl phthalate by homogeneous photocatalysis with Fe(III) in aqueous solution, *Applied Catalysis B: Environmental* 33 (2001) 239-248.
- [3] P. Neta, V. Madhavan, H. Zemel, R.W. Fessenden, Rate constants and mechanism of reaction of sulfate radical anion with aromatic compounds, *J. Am. Chem. Soc.* 99 (1977) 163-164.
- [4] P. Maruthamuthu, P. Neta, Phosphate radicals. Spectra, acid-base equilibriums, and reactions with inorganic compounds, *The Journal of Physical Chemistry* 82 (1978) 710-713.
- [5] Y. Gao, T. An, Y. Ji, G. Li, C. Zhao, Eco-toxicity and human estrogenic exposure risks from OH-initiated photochemical transformation of four phthalates in water: A computational study, *Environ. Pollut.* 206 (2015) 510-517.
- [6] K.S. Tay, N.A. Rahman, M.R. Bin Abas, Fenton degradation of dialkylphthalates: products and mechanism, *Environ Chem Lett* 9 (2011) 539-546.

Appendix 6.6.

Development of extraction and clean-up methods for multi- element compound specific isotope analysis of hexachlorocyclohexanes for isotope forensic and food web studies

Submitted manuscript: *Wu, L.; Moses, S.; Liu, Y.; Renpenning, J.; Richnow, H. H., Anal. Chem. 2018.*

Development of Extraction and Clean-up Methods for Multi- element Compound Specific Isotope Analysis of Hexachlorocyclohexanes for Isotope Forensic and Food Web Studies

Langping Wu, Sonya Moses, Yaqing Liu, Julian Renpenning, Hans H. Richnow*

Department of Isotope Biogeochemistry, Helmholtz Centre for Environmental Research-UFZ, Permoserstraße 15, 04318 Leipzig, Germany

*Email: hans.richnow@ufz.de, Tel: 0049 341 235 1212 Fax: 0341-450822

ABSTRACT

We have developed methods for the extraction and clean-up of hexachlorocyclohexane isomers (HCHs) from water, soil, plant, milk, fish oil and liver for studying sources and reactive transport processes of HCHs using multi-element compound specific isotope analysis (CSIA) approach. The extraction and clean-up methods were evaluated for recovery efficiency and isotope effects. The recovery resulted in sufficient precision and accuracy for carbon, hydrogen and chlorine isotope analysis within the analytical uncertainty of $\pm 0.5\%$, $\pm 5\%$ and $\pm 0.2\%$, respectively. The developed method was applied for stable isotope analysis of HCHs in soil, plant and liver samples from a contaminated landscape in Bitterfeld, Germany. The enrichment of isotope compositions of up to 14.1‰ for carbon and 2.6‰ for chlorine demonstrates the potential for analyzing reactive transport processes of HCHs in the food web. The methods can be applied for multi-element stable isotope analysis of HCHs for sources identification, characterization of degradation mechanisms, and particularly contaminant accumulation in the food web.

Keywords: hexachlorocyclohexane isomers, extraction, isotope fractionation, food web, reactive transport.

INTRODUCTION

γ -hexachlorocyclohexane (γ -HCH) is one of the most produced and extensively used organochlorine pesticides of the past. Its application and production were banned by the Stockholm Convention in 2009 due to its persistent, toxic, cancerogenic and mutagenic properties.^{1,2} Today official use continues only in pharmaceutical treatment for lice and scabies.¹ Hexachlorocyclohexane isomers (HCHs) are commercially manufactured by the reaction between benzene and chlorine in the presence of UV light. Except for γ -HCH, the other isomers lack of specific insecticidal properties. The production of one ton of γ -HCH generates 8 to 12 tons of HCH containing waste, the so called "HCH muck". α -HCH forms the major portion of technical HCH, while β -, and δ -HCH are chemically significantly more stable.³ Huge amounts of HCH muck was produced and largely deposited in an uncontrolled manner, which leads to serious environmental pollution world wide,^{4,5} and especially in Germany,^{6,7} Italy,⁸ Spain,⁹ China¹⁰ and India.¹¹ HCHs are considered as persistent organic pollutants due to their relative long-life in the environment. Due to the low water solubility HCHs tend to accumulate in the soil and enter the food web through plant uptake from the roots and air.^{12,13} HCHs can be transported over long distances by natural processes like global distillation. Today HCHs residues can be found in elevated concentration in Arctic and Antarctic animals at the end of the food chain.¹⁴⁻¹⁷

Compound specific isotope analysis (CSIA) appears to be a promising method to assess sources and fate of organic pollutants in the environment.¹⁸⁻²⁰ Hydrogen, carbon and chlorine isotope compositions allow to identify sources of HCHs.²¹ The carbon isotope fractionation can be used to characterise *in situ* (bio)degradation.²²⁻²⁴ One main bottleneck for CSIA is, however, the moderate analytical sensitivity and purity requirements for isotope analysis. In particular, the low

detection limit of CSIA makes the investigation of bioaccumulated contaminants in the food web challenging, since large amounts of samples are required to enable isolation of sufficient compound quantities. To date, the first and only study using CSIA to investigate reactive bioaccumulation of contaminants was conducted by Holmstrand et al.,²⁵ where aromatic compounds were extracted from 16 kg of seal blubber by continuous partitioning with acetonitrile in 2.2 L lipid batches using a Wallenberg perforator. This approach is not feasible for routine investigations of contaminants in the food web as it is limited by the availability of large amount of samples as well as laboratory equipments or spaces. Furthermore, the high lipophilicity of HCHs makes the separation from remaining lipids highly challenging. Thus, methods for extraction, separation and clean-up of HCHs from biota matrixes, as well as routine laboratory preparation methods are needed for implementation of CSIA.

The main objective of this study is to develop methods for HCHs extraction and purification from environmental and particularly for biological samples for ¹³C, ²H and ³⁷Cl stable isotope analysis in order to explore the potential for food web studies. The method development includes isolation of lipophilic HCHs from proteinaceous and fat-rich biological materials. The extraction and clean-up protocols were provided in details. The HCHs extraction efficiency from different matrixes (water, soil, plants, milk, oil, tissue) was evaluated through spiking experiments. The recovery and isotope artefact of the methods were critically examined. In order to conclude the potential of CSIA for the investigation of bioaccumulation and degradation at individual trophic levels in the food web, extracted HCHs samples from a contaminated site (Bitterfeld/Wolfen, Germany) were used for isotope analysis.

EXPERIMENTAL SECTION

Chemicals and Reference Matrixes

α -, β -, δ -HCH (99.5% purity, Fluka) were purchased from Sigma-Aldrich. HCHs stock solution containing 10 g L⁻¹ of α -, β -, δ -HCH (1:1:1) was prepared in acetone (ROTISOLV® \geq 99.9 %, UV/IR-Grade) for spiking water and soil samples. A stock solution prepared in hexane was used for spiking lipid rich material including plant, fish oil, milk and liver samples. Stock solution was stored in the refrigerator at 4°C before use. High purity of acetonitrile (\geq 99.9%, Carl Roth GmbH & Co. KG, Germany), n-hexane (for pesticide residue analysis, Sigma-Aldrich) and dichloromethane (DCM, \geq 99.9%, Carl Roth GmbH & Co. KG, Germany) were used for HCHs extraction. Florisil (for chromatography, ROTH, 100-200 mesh) was used as stationary phase for liquid column chromatography, glass wool (untreated, SUPELCO Analytical) and sea sand were used for packing the column. 7,12-dimethyl-benz[α]anthracene (p. A, Reagent Grade) was used as an internal standard to track elution of HCH fractions from the Florisil column. An UVA lamp (320-420 nm) was used to visualize the 7, 12-dimethyl-benz[α]anthracene elution. HCH-free soil and grass (*Calamagrostis epigejos*) obtained from residential garden, fish oil (Den originale Moeller's Tran), fresh milk (3.5% fat) and pork liver purchased from supermarket were used as matrixes to evaluate the extraction.

Extraction of HCHs from Different Matrixes

Water. HCHs stock solution was spiked into 1 L of distilled water in a separation funnel at concentration levels between 2900 and 10150 μ g L⁻¹. The spiked HCHs were extracted 3 times with 90 mL DCM in total (30 mL each time) by shaking thoroughly. The organic phases were combined and evaporated to \sim 0.5 mL under a gentle stream of nitrogen in a TurboVap concentrator (TurboVap II, Biotage, Sweden). At the end, the concentrated sample was transferred into a glass vial by a glass pipette and reconstituted into 1 mL hexane for further analysis.

Soil. HCHs stock solution was spiked into 10 g (wet weight) of HCH-free garden soil at concentration levels between 290 and 1015 μ g g⁻¹. 10g of spiked soil were extracted by accelerated solvent extraction (Dionex ASE 200, Thermo Scientific) equipped with 11 mL

stainless steel extraction cells. The extraction conditions are as following: solvent: hexane/acetone (1:1, v:v); oven heat up time: 6 min; final temperature: 100 °C; static time: 3 min; pressure: 1500 psi; purge time: 60 s; flush volume: 60%; static extraction cycles: 3. The extracted solution containing HCHs were combined and dried with ~ 5 g anhydrous Na₂SO₄. The HCH extracts were evaporated to dryness using a TurboVap concentrator and then re-dissolved to 1 mL of n-hexane for further clean-up.

Plants. Plant sample from residential garden was first cut into small pieces and fully dried in a freeze-dryer (Christ Beta-2-16 Freeze Dryer, Martin Christ Gefriertrocknungsanlagen GmbH, Germany) at -35°C and 0.310 mbar. The dry sample was mechanically ground into a fine powder in a grinder. About 6 g of powdered plant was filled into a 22 mL stainless steel extraction cell (Dionex, Thermo Scientific) in which cellulose filters were placed on the both side of the cell. During filling of plant powder into cells, 1 mL of HCHs stock solution was spiked drop by drop (to ensure homogeneously distribution) until the target concentrations between 10 and 166 µg g⁻¹ were adjusted. The cell was then placed overnight in the fume hood for solvent evaporation before extraction. ASE extraction conditions are the same as for soil sample extraction, but temperature was adjusted to 125 °C. The extract from plant was transferred into a 50 mL round bottom flask, and then solvent was evaporated in a rotary evaporator at 40°C. A small amount of activated Florisil and DCM were added to re-dissolve the extracted materials. The extracted materials were adsorbed on Florisil by evaporation of DCM to dryness for further clean-up.

Fish Oil. HCHs stock solution was spiked into 100 mL fish oil at concentration levels between 1 and 100 µg g⁻¹. 100 mL of spiked fish oil was extracted with 100 mL of acetonitrile in a 500 mL centrifuge bottle (PP Copolymer, Thermo Fisher Nalgene®) which was placed in ultrasonic bath for 1h. Acetonitrile and oil phases were separated by centrifugation at 10.000 rpm at 4°C for 20min, and then acetonitrile phase was carefully transferred into a TurboVap vial using glass pipette. The same extraction procedures were repeated three times again with 50 mL, 25 mL, 25 mL of acetonitrile, respectively. After which the acetonitrile phase were combined and evaporated in a TurboVap concentrator (25 °C, 9-14 psi) until the sample was concentrated to about 2 mL. If the co-extracted lipids were more than 10 mL, the sample was re-extracted three times with an equal volume of acetonitrile in an ultrasonic bath for 30 min. The same procedures were applied as described above.

Liver. Fresh pork liver was first homogenized using a hand blender (VH007, Voche, UK), and then HCHs stock solution was spiked into 100 g liver to obtain a concentration of 10 µg g⁻¹. The HCHs extraction procedures were same as described for fish oil.

Milk. HCHs stock solution was spiked into 500 mL milk to obtain a concentration of 100 µg L⁻¹. 500 mL of milk are extracted with 50 mL of hexane in a 1L separation funnel. 5~10 mL ethanol was added to the hexane phase in order to obtain a better phase separation. The hexane phase was collected in a TurboVap vial. After repeating the extraction procedures 3 times, the emulsion layer on top of aqueous phase was collected into a 500 mL centrifuge bottle and centrifuged at 10.000 rpm for 20 min at 4°C, in order to obtain a phase separation. All hexane phases were combined and evaporated in a TurboVap concentrator (25 °C, 9-14 psi) until only co-extracted lipids remained. If the co-extracted lipids were more than 10 mL, the lipid phase was re-extracted 3 times with an equal volume of acetonitrile in an ultrasonic bath for 30 min, as described for fish oil.

Clean-up of HCHs Extracts

Water and Soil. The clean-up method was modified from US EPA method 3620C.²⁶ A glass Pasteur pipette (0.7 cm diameter × 15 cm length) was used as chromatographic column. The pipette was packed from bottom to top with a little glass wool, 1 cm clean sea sand, 1 g activated Florisil, and 0.5 cm layer of activated anhydrous Na₂SO₄. The column was first pre-eluted with 1 mL of n-hexane. Then 50 µg of 7,12-Dimethyl-benz[a]anthracene (2 mg mL⁻¹ in hexane, 25 µL) was added on top of the column as UV-tracer. The 7,12-dimethyl-benz[a]anthracene can co-

elute with HCHs and thus can be used as an indicator for the elution of HCHs. The extracted sample dissolving in hexane was loaded onto column and eluted continuously by 5 mL hexane (1st fraction) and 5 mL hexane/DCM mixture (v/v 1:1) (2nd fraction) at the natural gravity flow velocity. A 360 nm UVA lamp was used to monitor the fluorescence. The eluate from 1st fraction containing mainly hydrocarbons was disposed. The eluate from 2nd fraction was evaporated to ~0.5 mL under a gentle nitrogen stream in a TurboVap concentrator, and then transferred and reconstituted into 1 mL DCM into glass vials for further concentration and isotope analysis.

Plants. The final extract adsorbed to Florisil (as described above) was purified by column chromatography. The glass column (2.2 cm diameter x 32.5 cm length) was packed, from bottom to top, with a little glass wool, 1 cm of cleaned sea sand, 15 cm of activated Florisil and 4 cm of activated anhydrous Na₂SO₄. Anhydrous Na₂SO₄ was activated by heating at 200 °C overnight and saved in a closed container; Florisil was activated at 120°C for 12 h just before usage. Florisil was packed into column as slurry in hexane to ensure that the column is tightly and homogeneously packed. 15 mL hexane was passed through to wash the packed column (keep 1 mL hexane above the upper surface of column). Then 100 µg of 7, 12-Dimethylbenz[a]anthracene (2 mg mL⁻¹ in hexane, 50 µL) was added on top of the column as UV-tracer. The extracted sample adsorbed to Florisil was loaded onto column and eluted continuously by 30 mL hexane (1st fraction) and 45 mL hexane/DCM (v/v 1:1) (2nd fraction). The fractions were collected as above, the 1st fraction was disposed and the 2nd fraction containing HCHs were subjected for further analysis.

Fish Oil, Milk and Liver. The co-extracted lipids (about 2 mL) were transferred and mixed with 3 times volume of 95% concentrated H₂SO₄ in a 20 mL glass bottle closed with Teflon coated screw cap. The mixed solution was reacted at 70°C in an ultrasonic bath for 2h to remove co-extracted lipids by acidic hydrolysis. The hydrolyzed solution was transferred into a separation funnel with 100 mL of distilled water and 30 mL of hexane, and then shaken carefully for approximately 2 mins. The acidic aqueous phase was discharged after getting clear phase separation. The hexane phase was then washed with 50 mL distilled water. After that, 20 mL of 0.5 M NaOH were added to the hexane phase to remove the remaining lipids by saponification. The mixture was shaken for 30 s, after 0.5 M NaOH were added to promote saponification of the lipids, until the hexane phase was transparent yellow and no further color change occurred on addition of NaOH solution. The solution mixture was then transferred and centrifuged at 4°C for 20 min at 10k rpm to ensure a good phase separation. The hexane phase was collected and the remaining alkaline solution was extracted once more with 30 mL hexane under same conditions. Finally, the combined hexane phase was evaporated to ~1 mL with a TurboVap concentrator. The extract was then purified by column chromatography as described for plant sample.

HCHs Contaminated Site and Sampling

Soil, ground water, plant and wild animal tissue samples were obtained at a large-scale HCHs contaminated mega site which is located at Bitterfeld/Wolfen in the eastern part of Germany. The field site history and contamination have been described elsewhere.^{23,27} Four soil samples were taken from different locations at the contaminated site. Plants samples of two different species, *Plantago lanceolate* and *Phragmites australis*, were taken in October 2015 from two different locations at heavily contaminated "Area C".²³ Wild boar and deer (about one year old) feeding in this area were hunted in November 2015 with the support of the Environmental Agency in Bitterfeld. Liver and brain samples were collected for further studies. All samples were stored at -20 °C until HCHs extraction. The HCHs extraction and purification methods described above were applied for preparation of each sample (10 g of soil, 6 g of dried plant, 150 g of liver and 86 g of brain).

Analytical Methods

Concentration Analysis. An Agilent 6890 series GC (Agilent Technologies, USA) equipped with a flame ionization detector (FID) was used to determine the concentration throughout the study.

HCHs were separated with a HP-5 column (30 m × 320 μm × 0.25 μm, Agilent 19091J-413, USA) using helium flow of 1 mL min⁻¹ as the carrier gas. The oven temperature can be found in the supporting information. Samples were measured with a split ratio of 1:1 with injector temperature of 250 °C and injection volume of 1 μL. Each sample was measured in triplicates.

Isotope Analysis. Isotope composition of element (E) is reported as δ notation in parts per thousand (‰) and expressed as the deviation from international standards according to the following equation:

$$\delta E_{\text{sample}} = \frac{R_{\text{sample}}}{R_{\text{standard}}} - 1$$

R indicates the isotope ratio of ¹³C/¹²C, ²H/¹H or ³⁷Cl/³⁵Cl. International standards for carbon, hydrogen and chlorine are Vienna Pee Dee Belemnite (VPDB), Vienna Standard Mean Ocean Water (VSMOW) and Standard Mean Ocean Chloride (SMOC), respectively.

Carbon isotope composition (δ¹³C) was analyzed using a gas chromatograph-combustion-isotope ratio mass spectrometer (GC-C-IRMS) system, where a GC (7890A, Agilent Technologies, USA) was coupled via a ConFlo IV interface (Thermo Fisher Scientific, Germany) to a MAT 253 IRMS system (Thermo Fisher Scientific, Germany). A Zebtron ZB1 column (60 m × 0.32 mm × 1 μm; Phenomenex, Germany) with a constant carrier gas flow of 1.5 mL min⁻¹ was applied for chromatographic separation. All samples were injected in splitless mode and injection temperature at 250 °C. The oven temperature was described in supporting information. Subsequently, compounds were converted to CO₂ in the combustion reactor (Thermo Fisher Scientific, Germany) operating at 1000 °C. Samples were analyzed as triplicates. Corresponding analytical precision for δ¹³C was below ±0.5‰. All δ¹³C values were normalized to VPDB scale by a two-point calibration using characterized in-house standards β-HCH (δ¹³C = -34.1‰) and γ-HCH (δ¹³C = -25.3‰). A third standard α-HCH (δ¹³C = -29.1‰) was used for validation of the calibration.

Hydrogen isotope composition (δ²H) was analyzed via a gas chromatograph-chromium based high temperature conversion-isotope ratio mass spectrometer (GC-Cr/HTC-IRMS) system, as previously described elsewhere.²⁸⁻³⁰ Briefly, Cr/HTC makes use of the combination of high temperature conversion and reduction at hot elemental chromium at 1200 °C. While hetero-elements (i.e. N, S, halogens) are scavenged at elevated temperatures as chromium salts, H₂ is released into the carrier stream and subsequently isotopically analyzed with the IRMS. Chromatographic separation was carried out using identical GC column and temperature program as described in the supporting information. Samples were analyzed as triplicates. Corresponding analytical precision for δ²H was below ±5‰. All δ²H values were normalized to VSMOW scale by a two-point calibration using characterized in-house standards: tetradecane (δ²H = -230‰) and hexadecane (δ²H = +381‰, reference ID: USGS69³¹). A third standard heptadecane (δ²H = -73‰) was used for validation of the calibration.

Chlorine isotope composition (δ³⁷Cl) was determined online using gas chromatography coupled with multiple-collector inductively coupled plasma mass spectrometry (GC-MC-ICPMS), as recently described elsewhere.³² A gas chromatograph (Trace 1310, Thermo Fisher Scientific, Germany), equipped with an auto-sampler (TriPlus RSH, Thermo Fisher Scientific, Germany) was used for analyte separation. Samples were injected with a split ratio of 1:10 and a constant carrier gas flow of 2 mL min⁻¹. All samples were analyzed as triplicates and separated on a Zebtron ZB-1 capillary column using temperature programming as described in the supporting information. Solvent peak cut was done with a SilFlow GC Dean Switch (SGE Analytical Science, Austria) at the end of the GC column. Once separated, the analyte was directed to the ICP torch via a Thermo Elemental Transferline AE2080 (Aquitaine Electronique, France). Several modifications were introduced to the transfer line. The interface was specifically modified for the transport of semi-volatile organics from the GC to the cold ICP torch. The MC-ICPMS was operating in low

resolution mode ($m/\Delta m = 300$) using a super dry plasma reducing interferences from protonation. Parameters for the MC-ICPMS are described in detail before.^{32,33} After atomization and ionization in the dry argon plasma, chlorine isotopes were analysed directly at mass 35 and 37 ($^{35}\text{Cl}^+$, $^{37}\text{Cl}^+$) at low resolution mode ($m/\Delta m = 300$). Generated transient signals ("peaks") were transformed into isotopic ratios after acquisition. All isotopic ratios were calculated using regression analysis. Linear regression of these plots yields a straight line whose slope represents the isotope ratio.

All samples were spiked with an in-house reference (TCE No.2) as an internal isotopic reference for compensation of potential instrumental drifts. The $\delta^{37}\text{Cl}$ was determined in two steps: (1) the deviation of a sample from an internal isotopic reference with a known $\delta^{37}\text{Cl}$ value was calculated, and (2) obtained raw $\delta^{37}\text{Cl}$ values were normalized to SMOC scale by applying a two-point calibration approach. Calibration to SMOC scale was done using in-house standards with characterized chlorine isotope composition, including methyl chloride (MC, $\delta^{37}\text{Cl} = +6.02\text{‰}$) and trichloroethene no.2 (TCE2, $\delta^{37}\text{Cl} = -1.19\text{‰}$). In addition trichloroethene no.6 (TCE6, $\delta^{37}\text{Cl} = +2.17\text{‰}$) was used for the validation of calibration, as described by Horst et al.³²

RESULTS AND DISCUSSIONS

Development of Protocols for HCH Extraction from Different Matrixes

Compound-specific stable isotope analyses of carbon, hydrogen and chlorine are several orders or magnitude less sensitive than modern GC or HPLC analysis and thus require larger amount of samples to enrich and clean up sufficient material for analysis. A central step of clean up and enrichment strategies are evaporation of solvent for concentrating target components. Insignificant isotope effects associated with solvent evaporation were observed by Ivdra et al.³⁴ We rigorously tested the recovery and potential isotope effects after evaporation of solvent with HCH isomers to dryness and found not statistically relevant changes in the $\delta^{13}\text{C}$ and $\delta^2\text{H}$ isotope compositions. Evaporation processor does not change isotope composition of HCHs and thus large amount solvents can be used for extraction. Column chromatography packed with Florisil slurry and pre-eluted by hexane gives almost complete recovery. The use of co-eluting fluorescent aromatic tracer (7, 12-Dimethyl-benz[a]anthracene) allows visual inspection of the chromatography and precise cut of the fraction containing HCH isomers. The tracer can be used as internal standard for recovery if intended.

Water and Soil. HCHs contaminated water samples were extracted simply by liquid-liquid extraction method using DCM. The extraction procedure was repeated three times to increase HCHs recoveries. Accelerated solvent extraction was applied for extraction of HCHs from soil. The extraction conditions are reported elsewhere³⁵ with modification of three static cycles in order to improve the recovery rate. Interference from humic substances and co-extracted organic substances are expected. For example, fatty acids are very often co-extracted by organic solvent; therefore the HCHs extracts from water and soil were further separated by Florisil column chromatography. Florisil was selected in the present study due to its potential to retain lipids and high polar materials, as well as its capability of effecting clean-up of apolar pesticide residues from food samples.³⁶ Overall recoveries of 88 - 95% and 86 - 94% were obtained from water and soil for α -, β -, δ -HCH, respectively (Table 1).

Plants. In most crop species the typical leaf relative water content at initial wilting is about 60 - 70%.³⁷ Accordingly, 15 - 20 g of fresh plant is need for extracting sufficient HCH residues for $\delta^{13}\text{C}$ measurement of HCH residues at a contaminated site,¹³ where residues of 2.5 - 18.7 mg kg^{-1} α -HCH and 0.9 - 40.3 mg kg^{-1} β -HCH from 18 studied leaf samples (dry weight) were reported. Plants were first freeze-dried rather than air-dried in order to minimize the losses as HCHs are relatively volatile hydrophobic compounds. The clean-up method using Florisil column was modified from elsewhere.²⁵

ASE with hexane/acetone (1:1, v:v) at 125 °C was used for extraction. Hydrophobic compounds such as plant waxes, chlorophyll and lipids can be co-extracted from plants, which could form a

lipid-layer and block the Florisil column during HCHs separation by column chromatography. The HCHs extracts after ASE step were, therefore, first adsorbed to a small amount of Florisil before loading on the column. Overall recoveries of 36 - 66% were achieved for α -, β -, δ -HCH from plants (Table 1). The losses during extraction of HCHs from plants samples were evaluated step by step (data is shown in supporting information, Table S1). The recoveries of 98 - 107% after solvent evaporation and 92 - 98% after column chromatography indicated that almost no significant losses of HCHs were observed during these two steps. Only 12 - 17% of HCHs recoveries were obtained after ASE using hexane as extraction solvent, which is likely due to the polarity of hexane is too low to extract HCHs from the organic plant matrix. HCHs recoveries were significantly increased to 43 - 50% when ASE extraction solvent was changed to acetone/hexane 1:1 (v/v), and furthermore slightly improved to 52 - 61% when same ASE extraction procedure was repeated twice. HCH extracts from ASE using acetone alone were difficult to be purified by column chromatography due to the co-extraction of large amounts of interfering compounds such as pigments.

Fish Oil, Milk and Liver. The methods of HCHs extraction and clean-up from fish oil, milk and liver were adapted from elsewhere.^{25,38} Fish oil was selected to represent extreme lipids-enriched samples. Acetonitrile was applied to remove large amounts of lipids in the first extraction step as lipids have relative lower solubility in acetonitrile comparing to hexane. Instead of using phase partitioning in a separation funnel, we homogenize the sample solvent mixture in an ultrasonic bath and centrifugation was applied for better HCHs extraction and good phase separation between acetonitrile and oil phase. The extraction procedure using acetonitrile was repeated three times in order to improve the HCHs recoveries. A recovery of 75 - 89% was achieved after repeating the acetonitrile extraction three times (Table S2). Milk was selected to represent fatty samples containing a large amount of water. Milk contains typically 88 % water and is rich in fat (3.4 %) and protein (3.3%). Hexane extraction was applied to remove water and hydrophilic substances in the first extraction step from the milk. Fresh pork liver was chosen as a representative sample of animal tissues containing high amounts of fat and protein. The homogenization of this tissue is achieved with a food blender before acetonitrile can be used in order to increase the extraction recovery. Fish oil, milk and liver contain fatty matrixes which are co-extracted. The separation of lipophilic HCHs is challenging.

We choose a strategy to remove co-extracted lipids by acidic hydrolysis using 95% concentrated H_2SO_4 , followed by saponification process using 0.5 M NaOH solution. The majority of hydrolyzed carboxylic acids are deprotonated and polar hydrolysis products (glycerol) are dissolved in the water phase, thus HCH can be extracted with n-hexane. Obtaining a clear phase separation in each step is essential to improve the HCHs recoveries. The overall HCHs recoveries of 16 - 30%, 33 - 44% and 16 - 25% were obtained from Fish oil, milk and liver, respectively (Table 1).

Table 1: HCHs Recoveries from Different Matrixes.

sample code	spiking concentration	α -HCH	β -HCH	δ -HCH
water 10	water 2900 $\mu\text{g L}^{-1}$	93%	90%	88%
water 20	water 5800 $\mu\text{g L}^{-1}$	94%	91%	93%
water 35	water 10150 $\mu\text{g L}^{-1}$	95%	94%	94%
soil 10	soil 290 $\mu\text{g g}^{-1}$	91%	88%	86%
soil 20	soil 580 $\mu\text{g g}^{-1}$	92%	92%	92%
soil 35	soil 1015 $\mu\text{g g}^{-1}$	94%	92%	93%
Grass Sp-3 10 F2	grass 10 $\mu\text{g g}^{-1}$	38%	36%	66%
Grass Sp 1000 ug F2	grass 166 $\mu\text{g g}^{-1}$	39%	48%	40%
FO Sp 10 F2	fish oil 10 $\mu\text{g g}^{-1}$	30%	21%	16%
FO Sp10000 ug F2	fish oil 100 $\mu\text{g g}^{-1}$	26%		18%
GM Sp 1ug/g F2	milk 100 $\mu\text{g L}^{-1}$	40%	44%	33%
Liver Sp 10 F2	liver 10 $\mu\text{g g}^{-1}$	16%	25%	20%

Effects of Sample Treatment on Stable Isotope Composition

The HCH molecule contains carbon, hydrogen and chlorine, which can be applied for the compound-specific stable isotope analysis. The corresponding isotope compositions of $\delta^{13}\text{C}$, $\delta^2\text{H}$ and $\delta^{37}\text{Cl}$ were determined using the highest HCHs concentrations of each sample matrix and compared before and after extraction. As shown in Table 2, isotopic shifts were from -0.6 to +0.6‰ for carbon, from -8 to +10‰ for hydrogen and from -0.12 to +0.27‰ for chlorine. Considering the typical analytical uncertainty of $\pm 0.5\text{‰}$ for $\delta^{13}\text{C}$, $\pm 5\text{‰}$ for $\delta^2\text{H}$ and $\pm 0.2\text{‰}$ for $\delta^{37}\text{Cl}$, the shifts of isotope compositions before and after HCHs extraction from different matrixes are within the analytical uncertainty and within acceptable range. Conclusively, negligible stable isotope fractionation could be observed after extraction and separation of HCH from biological samples.

The molecules remain intact under physical extraction processes; leading to negligible alteration of the isotope compositions of HCHs. Transformation processes involving breaking of chemical bonds could lead to kinetic isotope fractionation. Among the procedures applied in the present study, HCHs transformation process could occur during saponification step using NaOH solution, since HCHs can be hydrolyzed under alkaline condition.³⁹ However, the observed slight shifts of isotope compositions were within analytical uncertainty, indicating that the isotope fractionation occurring during the short time period of the saponification process was negligible. Despite of the lower extraction recoveries achieved above, the main contribution of present study is to prove that the modified methods are able to extract and purify HCHs from complicated matrixes, and most importantly they are isotope effect free, and therefore can be applied to investigate the reactive transformation of HCHs in food web.

Evaluation of the Isotope Effects of Matrix on ^{37}Cl Analysis

The bottle neck for $\delta^{13}\text{C}$ and $\delta^2\text{H}$ analysis is the clean-up step to obtain analytes containing fractions that allow base line separation from other organic compounds. In contrast, the analysis of $\delta^{37}\text{Cl}$ requires base line separation of only chlorine-containing analytes. Therefore, carbon/hydrogen containing matrix should not affect the $\delta^{37}\text{Cl}$ analysis. In order to evaluate potential interference of chlorine-free matrix on $\delta^{37}\text{Cl}$ analysis, analytical standards of HCHs and different amount of diesel were dissolved in hexane, representing HCHs in middle and high concentration level of a complex diesel matrix. The samples were first measured by GC-MS and then subjected to GC-MC-ICPMS for $\delta^{37}\text{Cl}$ analysis. The GC-MS chromatography indicated that HCHs peaks were overlapped with matrixes (Figure S1). Detailed information can be found in supporting information. However, when the same samples were injected to GC-MC-ICPMS for $\delta^{37}\text{Cl}$ analysis, a clear base line separation could be achieved (Figure S2). No significant changes in $\delta^{37}\text{Cl}$ composition were observed for HCHs isotope analysis within a complex diesel matrix (Table S3). The large carbon and hydrogen background from the diesel component in the dry plasma do not interfere with determination of chlorine isotopes. Conclusively, chlorine-free matrixes will not affect the performance of the $\delta^{37}\text{Cl}$ analysis. The $\delta^{37}\text{Cl}$ analysis requires thus not rigorous clean-up steps by column chromatography. The analytical precision (1σ) was usually below $\pm 0.2\text{‰}$ for single compound as found before and with high sensitivity typically in the range of 2-3 nmol Cl on column.³³

Table 2: Changes in isotope compositions of HCHs after sample treatment procedures.

sample		α -HCH	offset	β -HCH	offset	δ -HCH	offset
HCH std		-29.3 ± 0.4		-28.8 ± 0.2		-28.8 ± 0.2	
water	$\delta^{13}\text{C}$ [‰ vs VPDB]	-29.1 ± 0.3	+0.2	-29.4 ± 0.3	-0.6	-28.9 ± 0.1	-0.1
soil		-28.7 ± 0.2	+0.6	-29.0 ± 0.1	-0.2	-28.9 ± 0.2	-0.2
grass		-29.7 ± 0.0	-0.4	-28.7 ± 0.4	+0.1	-28.4 ± 0.2	+0.4
fish oil		-29.5 ± 0.1	-0.1	-28.4 ± 0.1	+0.4	-28.3 ± 0.1	+0.5
milk		-29.3 ± 0.3	+0.1	-28.4 ± 0.2	+0.5	-28.2 ± 0.3	+0.6
liver		-29.8 ± 0.2	-0.4	-28.9 ± 0.0	-0.1	-28.7 ± 0.1	+0.1

HCH std		-102 ± 3		-112 ± 5		-105 ± 6	
water	$\delta^2\text{H}$ [‰ vs VSMOW]	-101 ± 3	+1	-110 ± 5	+2	-108 ± 4	-3
soil		-102 ± 1	0	-113 ± 3	-1	-106 ± 0	-1
grass							
fish oil		-106 ± 5	-4	-112 ± 3	0	-105 ± 8	0
milk							
liver		-110 ± 4	-8	-102 ± 2	+10	-111 ± 4	-6
HCH std		-0.67 ± 0.14		-2.64 ± 0.13		-0.34 ± 0.28	
soil	$\delta^{37}\text{Cl}$ [‰ vs SMOC]	-0.56 ± 0.06	+0.11	-2.57 ± 0.13	+0.07	-0.30 ± 0.18	+0.04
grass		-0.40 ± 0.03	+0.27	-2.50 ± 0.10	+0.14	-0.31 ± 0.05	+0.03
fish oil		-0.55 ± 0.27	+0.12	-2.60 ± 0.15	+0.04	-0.34 ± 0.30	+0.00
milk		-0.47 ± 0.17	+0.20	-2.63 ± 0.08	+0.01	-0.26 ± 0.07	+0.08
liver		-0.42 ± 0.10	+0.25	-2.59 ± 0.40	+0.05	-0.46 ± 0.43	-0.12

Environmental Applications

The methods were tested to analyse the isotope composition of α and β -HCH in a contaminated landscape in order to evaluate the potential for analysing reactive transport in food webs. Multi isotope analysis allows the identification of chemical and biological transformation processes,¹⁹ as well as allows obtaining information on dehalogenation reactions.⁴⁰ Thus it can provide evidence for developing a concept for studying multi element isotope fractionation to characterise degradation processes in the food web at a field site.

Surface and ground water in the area of Bitterfeld/Wolfen are heavily polluted by HCHs, which have been already described in several studies.^{7,27} However, only few studies focused on the contamination and transformation of HCHs in soil, uptake to plants, as well as transfer to higher organisms. We analyzed the isotope composition of HCHs from various samples in order to validate the potential for isotope forensics and food web studies. The concentration of HCH residues (without consideration of extraction recovery) were ranging from 0.7 to 833.5 $\mu\text{g g}^{-1}$ for α -HCH and 1.4 to 406.8 $\mu\text{g g}^{-1}$ for β -HCH in soil, ranging from 0.5 to 22.4 $\mu\text{g g}^{-1}$ for α -HCH and 1.0 to 14.8 $\mu\text{g g}^{-1}$ for β -HCH in plants (dry weight), ranging from 0.03 to 0.15 $\mu\text{g g}^{-1}$ for α -HCH and 0.01 to 0.06 $\mu\text{g g}^{-1}$ for β -HCH in pork/deer liver and brain. HCH muck, gray to white crystals contains of more than 90% (weight percent) of HCH isomers in industrial waste deposits and in former loading, is considered to represent the original source of waste material from HCH production and therefore represent the initial isotope composition of the source in Bitterfeld.²³ Stable carbon and chlorine isotope compositions ($\delta^{13}\text{C}$, $\delta^{37}\text{Cl}$) of α - and β -HCH from contaminated soil, plants, liver and brain were determined (Figure 1). The carbon isotope compositions of α -HCH and β -HCH in muck varied from -29.2‰ to -27.5‰, and from -28.4‰ to -27.2‰ in, respectively. The $\delta^{13}\text{C}$ of α -HCH shifted from -29.9‰ to -25.2‰ in soil, -26.8‰ to -25.5‰ in plants, -20.9‰ to -15.1‰ in liver and -25.5‰ in brain; $\delta^{13}\text{C}$ of β -HCH changed from -28.0‰ to -23.4‰ in plants and -25.8‰ to -18.7‰ in liver.

The chlorine isotope compositions ($\delta^{37}\text{Cl}$) of α -HCH and β -HCH in muck varied from -0.83‰ to -0.51‰, and from -1.46‰ to -0.80‰, respectively. The $\delta^{37}\text{Cl}$ of α -HCH shifted from -0.92‰ to -0.84‰ in soil, -0.23‰ to 1.16‰ in plants; the $\delta^{37}\text{Cl}$ of β -HCH shifted from -0.95‰ to -0.01‰ in plants. $\delta^{37}\text{Cl}$ was not determined from liver and brain samples due to low HCHs concentrations. Compare to HCH muck, the shifts of $\delta^{13}\text{C}$ and $\delta^{37}\text{Cl}$ in contaminated plants indicated that uptake of HCHs in plants were associated with isotope fractionation, suggesting biodegradation in the rhizosphere or in the plants. In addition, strong carbon isotope enrichment of HCHs (up to 14.1‰ for α -HCH and 9.7‰ for β -HCH) in the liver suggests that only a residual fraction was accumulated in the fat of the liver after intensive metabolism. The isotope enrichment in the residual HCHs fraction reflects the metabolic degradation in the higher organisms. This implies that the concentration of residual fraction does not reflect the exposure process in the organisms adequately as the enrichment is based on the hypothesis that phase partitioning into the lipid

governs accumulation. In contrast, the isotope fractionation of the residual HCHs fraction indicates that the exposure of the organisms might be higher as a major fraction of the HCHs have been degraded. The isotope enrichment of the HCHs suggests active degradation probably by liver enzymes.

Based on the Rayleigh approach, significant isotope enrichment combined with specific stable isotope enrichment factors can be applied to quantify the *in situ* degradation of contaminants. For example, based on the carbon isotope fractionation of HCHs and an enrichment factor for microbial degradation the range of HCHs biodegradation could be estimated within contaminated aquifer at Bitterfeld/Wolfen. Bashir et al. calculated that microbial degradation has removed 30 to 86% on reactive transport pathways at a HCH contaminated site.²² The same approach using CSIA holds great potential to quantify the reactive transport of HCHs from soil to plant, and to higher organisms. Correlation of hydrogen, carbon and chlorine isotope fractionation may be used to identify bond cleavage reaction of degradation processes of halogenated contaminants.⁴¹⁻⁴³

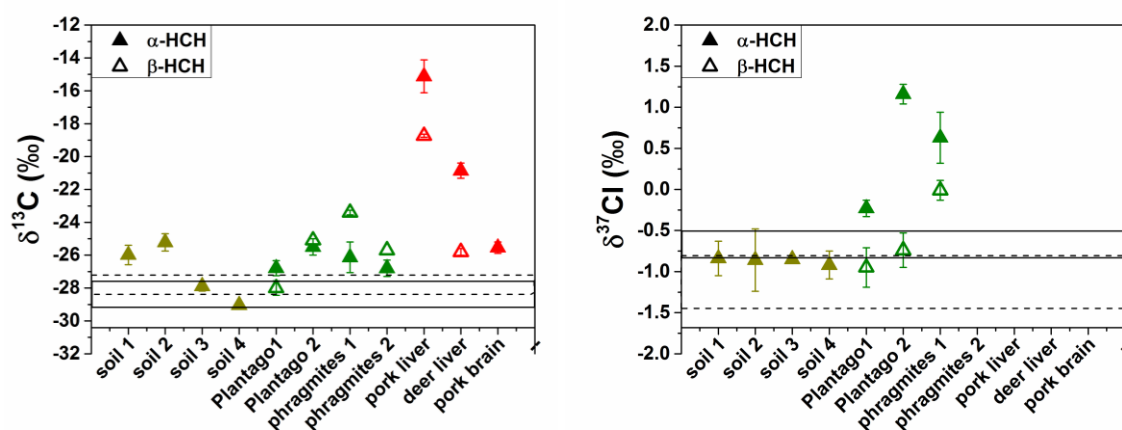


Figure 1: Isotope composition ($\delta^{13}\text{C}$, $\delta^{37}\text{Cl}$) of α - and β -HCH from contaminated soil, plants, liver and brain. Solid lines indicate the isotope composition variation of α -HCH muck; dotted lines indicate the isotope composition variation of β -HCH muck. The isotope compositions of α - and β -HCH are indicated by solid and open symbol, respectively.

CONCLUSIONS

A method for extraction and purification of HCHs for the analysis of carbon, hydrogen and chlorine isotope composition of HCHs in various environmental compartments was developed and evaluated. All steps of sample preparation have been shown to be free of isotope fractionation concerning the typical uncertainty of the $\delta^{13}\text{C}$, $\delta^2\text{H}$ and $\delta^{37}\text{Cl}$ analysis. The method allows an accurate and precise isotope analysis of HCHs and is applicable for analyzing degradation reaction associated with isotope fractionation in water, soil, plants, milk and animal tissues. Furthermore, this is a great advantage for investigating the transformation of chlorinated compounds using stable chlorine isotope especially in food web, as residual lipids and hydrocarbons will not affect the performance of the $\delta^{37}\text{Cl}$ analysis.

Experientially, the minimum concentration of HCHs for reliable carbon isotope analysis is 15 mg L^{-1} for injection (assume at least $1.5 \text{ }\mu\text{g}$ of HCH was extracted into $100 \text{ }\mu\text{L}$ of solvent for measurement). Similar quantity of HCH is required for reliable chlorine isotope analysis, and 5 ~ 10 times higher quantity is needed for reliable hydrogen isotope analysis. Based on the developed extraction and clean-up methods in the present study, 75 g of liver contaminated with $0.1 \text{ }\mu\text{g g}^{-1}$ of HCH is sufficient for carbon isotope analysis, even with a low extraction efficiency of 20%. With a low extraction efficiency of 40%, 4 g of dried plant contaminated with $1 \text{ }\mu\text{g g}^{-1}$ of HCH

is recommended for carbon isotope analysis. The methods have potential for monitoring HCH in food web to develop sustainable management options of contaminated sites as well as in risk assessment and public health studies.

ORCID

Langping Wu: 0000-0003-0599-7172

Sonya Moses: 0000-0002-2984-4851

Julian Renpenning: 0000-0002-5487-1640

Hans H. Richnow: 0000-0002-6144-4129

Notes

The authors declare no competing financial interest.

ACKNOWLEDGMENT

Langping Wu (File No. 201306460007) and Yaqing Liu (File No. 201301542002) are financially supported by the China Scholarship Council. We acknowledge the financial support from the German-Israeli Foundation for Research and Development (GIF) Grant no. I-1368-307.8/2016 (“Prediction of chiral and isotope enrichment during the transformations of halo-organic pollutants: Mechanistic and QSAR approaches”)

REFERENCES

- (1) UNEP. Stockholm Convention on Persistent Organic Pollutants. **2009**, 12.
- (2) Vijgen, J.; Abhilash, P. C.; Li, Y. F.; Lal, R.; Forter, M.; Torres, J.; Singh, N.; Yunus, M.; Tian, C. G.; Schaffer, A.; Weber, R. *Environ. Sci. Pollut. Res.* **2011**, *18*, 152-162.
- (3) Lal, R.; Pandey, G.; Sharma, P.; Kumari, K.; Malhotra, S.; Pandey, R.; Raina, V.; Kohler, H. P. E.; Holliger, C.; Jackson, C.; Oakeshott, J. G. *Microbiol. Mol. Biol. Rev.* **2010**, *74*, 58-80.
- (4) Li, Y. F. *Sci. Total. Environ.* **1999**, *232*, 121-158.
- (5) Vijgen, J. *A Global Overview of Residue Management, Formulation and Disposal* **2006**.
- (6) Schwartz, R.; Gerth, J.; Neumann-Hensel, H.; Förstner, U. *J. Soils Sediments* **2006**, *6*, 145-155.
- (7) Wycisk, P.; Stollberg, R.; Neumann, C.; Gossel, W.; Weiss, H.; Weber, R. *Environ. Sci. Pollut. Res. Int.* **2013**, *20*, 1907-1917.
- (8) Fuscoletti, V.; Achene, L.; Gismondi, F.; Lamarra, D.; Lucentini, L.; Spina, S.; Veschetti, E.; Turrio-Baldassarri, L. *Bull. Environ. Contam. Toxicol.* **2015**, *95*, 108-115.
- (9) Fernandez, J.; Arjol, M. A.; Cacho, C. *Environ. Sci. Pollut. Res. Int.* **2013**, *20*, 1937-1950.
- (10) Lammel, G.; Ghim, Y.-S.; Grados, A.; Gao, H.; Hühnerfuss, H.; Lohmann, R. *Atmos. Environ.* **2007**, *41*, 452-464.
- (11) Nayyar, N.; Lal, R. *J. Bioremediat. Biodegrad.* **2016**, *07*.
- (12) Trapp, S. *Environ. Sci. Technol.* **2015**, *49*, 395-402.
- (13) Calvelo Pereira, R.; Camps-Arbestain, M.; Rodriguez Garrido, B.; Macias, F.; Monterroso, C. *Environ. Pollut.* **2006**, *144*, 210-217.
- (14) Yasunaga, G.; Fujise, Y.; Zenitani, R.; Tanabe, S.; Kato, H. *Chemosphere* **2015**, *126*, 11-17.
- (15) Lana, N. B.; Berton, P.; Covaci, A.; Ciocco, N. F.; Barrera-Oro, E.; Atencio, A.; Altamirano, J. *C. Sci. Total. Environ.* **2014**, *499*, 89-98.
- (16) Wiberg, K.; Letcher, R. J.; Sandau, C. D.; Norstrom, R. J.; Tysklind, M.; Bidleman, T. F. *Environ. Sci. Technol.* **2000**, *2668-2674*.
- (17) Carlsson, P.; Warner, N. A.; Hallanger, I. G.; Herzke, D.; Kallenborn, R. *Environ. Pollut.* **2014**, *192*, 154-161.
- (18) Thullner, M.; Centler, F.; Richnow, H.-H.; Fischer, A. *Org. Geochem.* **2012**, *42*, 1440-1460.
- (19) Vogt, C.; Dorer, C.; Musat, F.; Richnow, H. H. *Curr. Opin. Biotechnol.* **2016**, *41*, 90-98.
- (20) Elsner, M.; Imfeld, G. *Curr. Opin. Biotechnol.* **2016**, *41*, 60-72.
- (21) Ivdra, N.; Fischer, A.; Herrero-Martin, S.; Giunta, T.; Bonifacie, M.; Richnow, H. H. *Environ. Sci. Technol.* **2017**, *51*, 446-454.

- (22) Bashir, S.; Hitzfeld, K. L.; Gehre, M.; Richnow, H. H.; Fischer, A. *Water Res.* **2015**, *71*, 187-196.
- (23) Liu, Y.; Bashir, S.; Stollberg, R.; Trabitsh, R.; Weiss, H.; Paschke, H.; Nijenhuis, I.; Richnow, H. H. *Environ. Sci. Technol.* **2017**, *51*, 8909-8916.
- (24) Chartrand, M.; Passeport, E.; Rose, C.; Lacrampe-Couloume, G.; Bidleman, T. F.; Jantunen, L. M.; Sherwood Lollar, B. *Rapid Commun. Mass. Sp.* **2015**, *29*, 505-514.
- (25) Holmstrand, H.; Mandalakis, M.; Zencak, Z.; Andersson, P.; Gustafsson, O. *Chemosphere* **2007**, *69*, 1533-1539.
- (26) Agency, U. S. E. P.; United States Environmental Protection Agency, 2014.
- (27) Wycisk, P. *Toxicol. Lett.* **2003**, *140-141*, 343-351.
- (28) Renpenning, J.; Kuemmel, S.; Hitzfeld, K. L.; Schimmelmann, A.; Gehre, M. *Anal. Chem.* **2015**, *87*, 9443-9450.
- (29) Gehre, M.; Renpenning, J.; Geilmann, H.; Qi, H. P.; Coplen, T. B.; Kummel, S.; Ivdrá, N.; Brand, W. A.; Schimmelmann, A. *Rapid Commun. Mass. Sp.* **2017**, *31*, 475-484.
- (30) Wu, L. P.; Kummel, S.; Richnow, H. H. *Anal. Bioanal. Chem.* **2017**, *409*, 2581-2590.
- (31) Schimmelmann, A.; Qi, H. P.; Coplen, T. B.; Brand, W. A.; Fong, J.; Meier-Augenstein, W.; Kemp, H. F.; Toman, B.; Ackermann, A.; Assonov, S.; Aerts-Bijma, A. T.; Brejcha, R.; Chikaraishi, Y.; Darwish, T.; Elsner, M.; Gehre, M.; Geilmann, H.; Groing, M.; Helie, J. F.; Herrero-Martin, S.; Meijer, H. A. J.; Sauer, P. E.; Sessions, A. L.; Werner, R. A. *Anal. Chem.* **2016**, *88*, 4294-4302.
- (32) Horst, A.; Renpenning, J.; Richnow, H. H.; Gehre, M. *Anal. Chem.* **2017**, *89*, 9131-9138.
- (33) Renpenning, J.; Horst, A.; Schmidt, M.; Gehre, M. *J. Anal. Atom. Spectrom.* (submitted) **2018**.
- (34) Ivdrá, N.; Herrero-Martin, S.; Fischer, A. *J. Chromatogr. A* **2014**, *1355*, 36-45.
- (35) Scientific, T.; Thermo Fisher Scientific Inc., 2012.
- (36) Koc, F.; Karakus, E. *Kafkas Univ. Vet. Fak. Derg.* **2011**, *17*, 65-70.
- (37) Plantstress. Plantstress.com.
- (38) Jensen, S.; Athanasiadou, M.; Bergman, A. *Organohalogen Compd.* **1992**, *8*, 79-80.
- (39) Zhang, N.; Bashir, S.; Qin, J. Y.; Schindelka, J.; Fischer, A.; Nijenhuis, I.; Herrmann, H.; Wick, L. Y.; Richnow, H. H. *J. Hazard. Mater.* **2014**, *280*, 750-757.
- (40) Nijenhuis, I.; Richnow, H. H. *Curr. Opin. Biotechnol.* **2016**, *41*, 108-113.
- (41) Kuder, T.; van Breukelen, B. M.; Vanderford, M.; Philp, P. *Environ. Sci. Technol.* **2013**, *47*, 9668-9677.
- (42) Renpenning, J.; Keller, S.; Cretnik, S.; Shouakar-Stash, O.; Elsner, M.; Schubert, T.; Nijenhuis, I. *Environ. Sci. Technol.* **2014**, *48*, 11837-11845.
- (43) Franke, S.; Lihl, C.; Renpenning, J.; Elsner, M.; Nijenhuis, I. *FEMS Microbiol Ecol* **2017**.



For TOC only

Supporting Information

Development of Extraction and Clean-up Methods for Multi- element Compound Specific Isotope Analysis of Hexachlorocyclohexanes for Isotope Forensic and Food Web Studies

Langping Wu, Sonya Moses, Yaqing Liu, Julian Renpenning, Hans H. Richnow*

Department of Isotope Biogeochemistry, Helmholtz Centre for Environmental Research-UFZ, Permoserstraße 15, 04318 Leipzig, Germany

*Email: hans.richnow@ufz.de, Tel: 0049 341 235 1212 Fax: 0341-450822

6 pages

3 Tables

3 Figures

GC Oven Temperature Program for HCH analysis

Concentration Analysis. The oven temperature was held at 70 °C for 1 min, increased at 8 °C min⁻¹ to 180 °C and then at 2 °C min⁻¹ to 195 °C, finally increased at 8 °C min⁻¹ to 280 °C and held for 5 min. Samples were measured with a split ratio of 1:1 with injector temperature of 250 °C and injection volume of 1 µL. Each sample was measured in triplicates.

Isotope Analysis. For $\delta^{13}\text{C}$, $\delta^2\text{H}$ and $\delta^{37}\text{Cl}$ analysis the the same oven temperature program was used. The oven temperature was initially held at 70 °C for 2 min, ramped at 10 °C min⁻¹ to 175 °C and then at 1 °C min⁻¹ to 200 °C for 8 min, and finally ramped at 15 °C min⁻¹ to 300 °C and held for 1 min.

Evaluation of HCHs Losses during Extraction from Plants.

The losses during extraction of HCHs from plants samples were evaluated step by step. As shown in Table S1, the recoveries of $104 \pm 5\%$ after solvent evaporation and $95 \pm 3\%$ after column chromatography indicated that almost no significant losses of HCHs were observed during these two steps. Only $15 \pm 3\%$ of HCHs recoveries were obtained after ASE using hexane as extraction solvent. Probably the polarity of hexane is too low to extract HCHs efficiently from the organic plant matrix. HCHs recoveries were significantly increased to $47 \pm 4\%$ when ASE extraction solvent was changed to acetone/hexane 1:1 (v/v), and furthermore slightly improved to $58 \pm 5\%$ when same ASE extraction procedure was repeated twice. HCH extracts from ASE using acetone alone were difficult to be purified by column chromatography due to the co-extraction of large amounts of interfering compounds such as pigments.

Table S1: Recoveries of HCHs during Extraction from Plants.

	α -HCH	β -HCH	δ -HCH	methods	Note
extraction of HCHs from 6 g of plants ($17 \mu\text{g g}^{-1}$ spiking concentration)					
1	98%	106%	107%	solvent evaporation	45 mL solvent were evaporated to 0.5 mL
2	98%	92%	96%	column chromatography	HCHs were spiked into co-extracted plants residues before loading on column
3	12%	17%	16%	ASE using hexane	sample was extracted once
4	43%	49%	50%	ASE using acetone/hexane 1:1	sample was extracted once
5	52%	60%	61%	ASE using acetone/hexane 1:1	sample was extracted twice

Evaluation of HCHs Losses during Extraction from Fish Oil using Acetonitrile.

100 mL of spiked fish oil was extracted with 100 mL of acetonitrile in a 500 mL centrifuge bottle which was placed in ultrasonic bath for 1h. Acetonitrile and oil phases were separated by centrifugation at 10,000 rpm at 4°C for 20min, and then acetonitrile phase was subjected to HCHs concentration analysis. The same extraction procedures were repeated with 50 mL and 25 mL of acetonitrile, respectively, and the acetonitrile phases were analyzed to evaluate the HCHs concentrations after each extraction. The extraction procedure using acetonitrile was repeated three times in order to improve the HCHs recoveries. A recovery of 75% ~ 89% was achieved after repeating the acetonitrile extraction three times (Table S2).

Table S2: Recoveries of HCHs during Extraction from Fish Oil.

	α -HCH	β -HCH	δ -HCH	methods	Note
extraction of HCHs from 100 g of fish oil ($1 \mu\text{g g}^{-1}$ spiking concentration) using acetonitrile					
1	47%	56%	58%	1 st extraction using acetonitrile	
2	32%	36%	37%	2 nd extraction using acetonitrile	
3	23%	23%	25%	3 rd extraction using acetonitrile	
	75%	86%	89%		total recovery of three extraction

Evaluation of the Isotope Effects of Matrix on ^{37}Cl analysis.

In order to evaluate the isotope effects of matrix on $\delta^{37}\text{Cl}$ analysis, HCHs were dissolved in hexane with addition of different amount of diesel fuel, representing HCHs in middle (300 mg L^{-1} HCHs + 25 mL L^{-1} diesel fuel) and high (200 mg L^{-1} HCHs + 40 mL L^{-1} diesel fuel) concentration level of diesel matrix representatively. The two samples were first analyse by GC-MS (TIC, SIM) and then subjected to GC-MC-ICPMS for $\delta^{37}\text{Cl}$ analysis.

An Agilent 7890A series gas chromatograph (GC, Agilent Technologies, Palo Alto, USA) equipped with a quadrupole mass spectrometer (MS) was used for identification of HCHs isomers. HCHs isomers were separated by BPX-5 capillary column ($30 \text{ m} \times 0.25 \text{ mm ID} \times 0.25 \mu\text{m}$, SGE, Darmstadt, Germany) with helium as the carrier gas (flow of 2.0 mL min^{-1}). The oven temperature program started at 60°C , was held for 3 min isothermally, increased by 3°C min^{-1} to 180°C , then increase at $20^\circ\text{C min}^{-1}$ to 300°C , and finally increased at $10^\circ\text{C min}^{-1}$ to 350°C , where it was held for 10 min. The samples were injected in splitless mode. $\delta^{37}\text{Cl}$ was measured via GC-MC-ICPMS as described in the main text.

The GC-MS analysis of α -, β -, δ -HCH isomers in diesel matrixes are shown in Figure S1. For concentration level of HCH similar to the diesel matrix (Figure S1 a), HCHs were separated from diesel however not by base line separation. Quantification of HCHs under this condition can cause bias. At high concentration of diesel matrix (Figure S1 b), HCHs peaks were overlapped with matrixes and

quantification was not possible using the TIC with poor base line separation. The broadening of peaks is a result of intentionally overloading the column with diesel fuel for demonstrating the selectivity for chlorine analysis with the GC-MC-ICPMS.

However, when the same samples were injected to GC-MC-ICPMS for $\delta^{37}\text{Cl}$ analysis, a clear base line separation was observed (Figure S2), demonstrating the selectivity of chlorine analysis. The hydrocarbon matrix was not visible although the chromatographic column was overloaded. The first peak was TCE of known $\delta^{37}\text{Cl}$ composition which was used as reference compound for $\delta^{37}\text{Cl}$ analysis (Figure S2 a, b). The other three peaks were α -, β -, δ -HCH, respectively. All hydrocarbons from diesel matrix do not appear in the GC-MC-ICPMS chromatography, and therefore will not interfere with determination of the chlorine isotope composition. $\delta^{37}\text{Cl}$ values of HCHs before and after the addition of diesel matrix were compared, no significant $\delta^{37}\text{Cl}$ changes were observed (Table S3). Therefore, non-chlorine containing matrixes will not affect the performance of the $\delta^{37}\text{Cl}$ analysis.

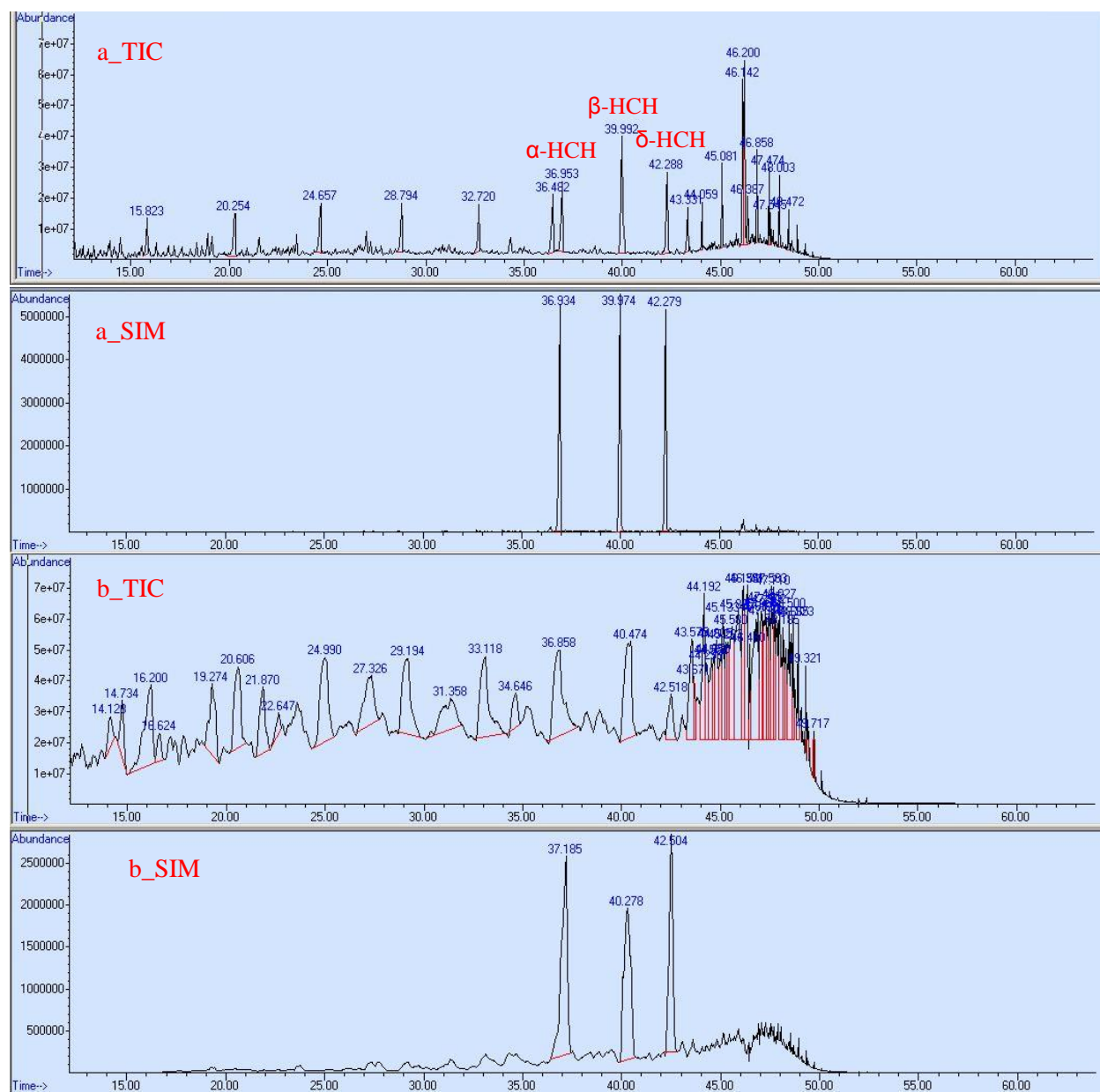


Figure S1: Total ion counts (TIC) and selected ions mass (SIM, m/z xxx) chromatographs of α -, β -, δ -HCH isomers in diesel matrixes. (a) indicates HCHs in the similar concentration level of the diesel fuel (300 mg L^{-1} HCHs + 25 mL L^{-1} diesel fuel); (b) indicates HCHs in high concentration level of diesel fuel (200 mg L^{-1} HCHs + 40 mL L^{-1} diesel fuel). The broadening of peaks is a result of intentionally overloading the column with diesel fuel for demonstrating the selectivity for chlorine analysis with the GC-MC-ICPMS.

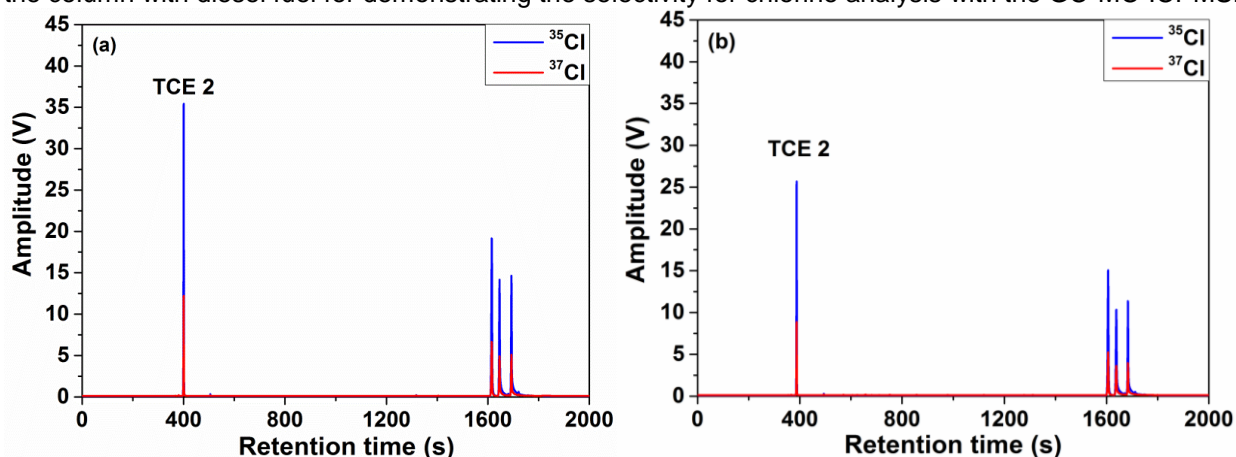


Figure S2: GC-MC-ICPMS chromatogram of α -, β -, δ -HCH isomers in diesel matrixes for $\delta^{37}\text{Cl}$ analysis. (a) indicates HCHs in the similar concentration level with diesel fuel (300 mg L^{-1} HCHs + 25 mL L^{-1} diesel fuel); (b) indicates HCHs in high concentration of diesel fuel (200 mg L^{-1} HCHs + 40 mL L^{-1} diesel fuel). The first peak (TCE 2) is trichoroethene which was used as reference compound for $\delta^{37}\text{Cl}$ analysis.

Table S3: Changes in $\delta^{37}\text{Cl}$ isotope compositions of HCHs in diesel matrix.

sample	α -HCH (‰)	offset (‰)	β -HCH (‰)	offset (‰)	δ -HCH (‰)	offset (‰)
HCHs std in clean hexane	-1.29 ± 0.22		-2.80 ± 0.12		-1.09 ± 0.18	
HCHs in low level diesel matrix	-1.45 ± 0.01	-0.16	-2.92 ± 0.12	-0.12	-1.01 ± 0.07	0.08
HCHs in high level diesel matrix	-1.35 ± 0.16	-0.06	-2.93 ± 0.15	-0.13	-1.28 ± 0.2	-0.19

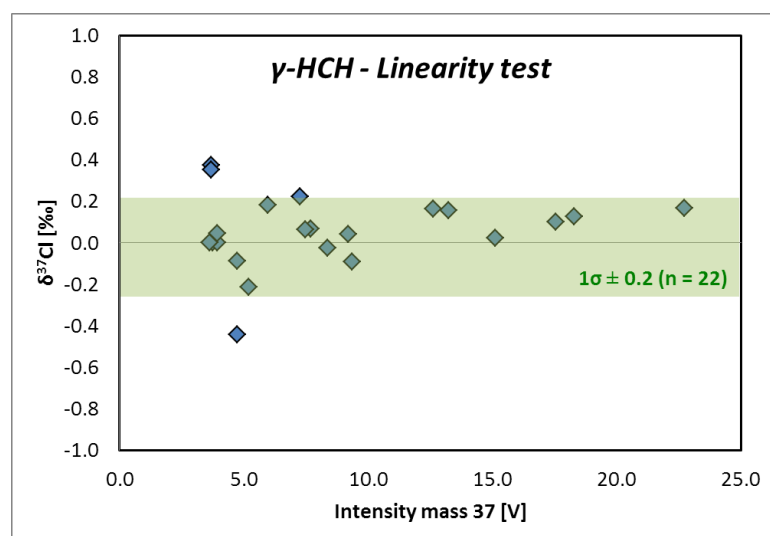
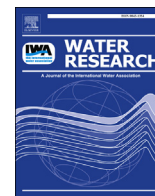


Figure S3: Linearity test for γ -HCH for transient peak signals. The mean value was normalized to zero for better comparability. Standard deviation (1σ) of ± 0.2 ‰ was determined for all 21 data points above the isotopic limit of detection (3V).

Appendix 6.7.

Carbon and hydrogen isotope analysis of parathion for characterizing natural attenuation by hydrolysis at a contaminated site

Published paper: *Wu, L.; Verma, D.; Bondgaard, M.; Melvej, A.; Vogt, C.; Subudhi, S.; Richnow, H. H., Water Res. 2018, 143, 146-154.*



Carbon and hydrogen isotope analysis of parathion for characterizing its natural attenuation by hydrolysis at a contaminated site

Langping Wu^a, Dipti Verma^b, Morten Bondgaard^c, Anja Melvej^c, Carsten Vogt^a, Sanjukta Subudhi^b, Hans H. Richnow^{a,*}

^a Department of Isotope Biogeochemistry, Helmholtz Centre for Environmental Research-UFZ, Permoserstraße 15, 04318 Leipzig, Germany

^b Environmental and Industrial Biotechnology Division, The Energy and Resources Institute, New Delhi 110003, India

^c Department of Environment, Central Denmark Region, Lægårdvej 10, 7500 Holstebro, Denmark

ARTICLE INFO

Article history:

Received 15 March 2018

Received in revised form

7 June 2018

Accepted 16 June 2018

Available online 18 June 2018

Keywords:

Isotope fractionation

Parathion

In situ hydrolysis

Field application

CSIA

ABSTRACT

The applicability of compound-specific isotope analysis (CSIA) for assessing *in situ* hydrolysis of parathion was investigated in a contaminated aquifer at a former pesticide wastes landfill site. Stable isotope analysis of parathion extracted from groundwater taken from different monitoring wells revealed a maximum enrichment in carbon isotope ratio of +4.9‰ compared to the source of parathion, providing evidence that *in situ* hydrolysis took place. Calculations based on the Rayleigh-equation approach indicated that the natural attenuation of parathion was up to 8.6% by hydrolysis under neutral and acidic conditions. In degradation experiments with aerobic and anaerobic parathion-degrading microbes, no carbon and hydrogen isotope fractionation of parathion were observed. For the first time, CSIA has been applied for the exclusive assessment of the hydrolysis of phosphorothioate-containing organophosphorus pesticides at a contaminated field site.

© 2018 Elsevier Ltd. All rights reserved.

1. Introduction

Organophosphorus pesticides (OPs) have been used mainly as insecticides throughout the world since the decline in the use of organochlorine pesticides in the 1960s and 1970s. OPs exhibit acute toxicity by inhibiting acetylcholinesterase (AChE) in the nervous system. Today the consumption of OPs ranks second relative to the total global pesticide usage (Fenner et al., 2013). OPs are considered to be degradable in the environment in contrast to organochlorines, however, continuous and excessive use of OPs has led to environmental contaminations which raise public concerns (USEPA, 2006) as the residues have repeatedly been detected in soils, sediments, waterbodies, air samples, fishes and humans (Aston and Seiber, 1996; Kawahara et al., 2005; Pehkonen and Zhang, 2002). Parathion (O,O-diethyl O-(4-nitrophenyl) phosphorothioate) was one of the most widely used organophosphorus insecticides in agriculture in the past decades, and was primarily used on fruit, cotton, wheat, vegetables, and nut crops (FAO, 1990). Due to its toxicity, parathion has been banned or restricted in many countries; however,

stockpiles and waste from previous manufacturing and former landfill sites often contain parathion (LRSB, 2014; Nielsen et al., 2014) forming serious point source contaminations which require management strategies. Thus, it is important to understand the chemical fate of parathion for properly environmental risks assessment at landfill sites and for groundwater quality protection and management.

Hydrolysis is believed to be one of the major pathways controlling the fate of OPs in the environment. Hydrolysis of OPs proceeds by a common mechanism, where H₂O and OH⁻ act as nucleophiles in a bimolecular nucleophilic substitution mechanism (S_N2 mechanism) (Pehkonen and Zhang, 2002; Thatcher and Kluger, 1989). The ester bonds of OPs can be hydrolyzed under acidic and alkaline conditions by two different pathways whereas the relative contribution of each hydrolysis pathway is pH-dependent (Wu et al., 2018). Alkaline hydrolysis is much faster compared to acidic and neutral hydrolysis. For example, the half-life of parathion is reported to be 133 days at pH 5 (25 °C), 247 days at pH 7 (25 °C), 102 days at pH 9 (25 °C) (FAO, 1990), and only 1.14 days at pH 12 (20 °C) (Wu et al., 2018). Generally, alkaline hydrolysis is unlikely to contribute significantly to the natural attenuation of parathion, since mostly neutral and slightly acidic conditions are prevailing in the environment. Therefore, hydrolysis

* Corresponding author.

E-mail address: hans.richnow@ufz.de (H.H. Richnow).

under neutral or slightly acidic environmental conditions will lead to long half-life of parathion. The pH of seawater is typically limited to a range between 7.5 and 8.4 and seawater ingressions in dumpsites affected by tidal fluctuation may potentially contribute to increase *in situ* hydrolysis.

Compound specific isotope analysis (CSIA) opens the door to the development of field-based assessment of degradation reactions. CSIA is one of the most promising fate investigative tools which enable the detection of *in situ* biodegradation of organic contaminants (Nijenhuis and Richnow, 2016; Vogt et al., 2016). It has been used to estimate the extent of biodegradation of a specific compound from changes in isotope ratios of field samples if the isotope enrichment factor (ϵ) of that compound is determined in laboratory experiments based on the Rayleigh equation (Bashir et al., 2015; Hofstetter et al., 2008; Liu et al., 2017; Thullner et al., 2012). The molecular size of many micropollutants, such as pesticides, consumer care products or pharmaceuticals, is greater than of typical legacy contaminants (chlorinated-compounds, benzene, and toluene) thus limiting the sensitivity of CSIA. As only bond change reactions induce kinetic isotope effects which are used for characterizing degradation reactions, large molecules exhibit more atoms which are not reacting. Thus, changes in single element isotope ratios (e.g. $\delta^{13}\text{C}$) tend to become smaller with larger molecular size due to isotope dilution effects of non-reacting atoms. Moreover, single element isotope ratios in the field can be always influenced by masking of isotope fractionation which makes the identification of degradation pathways by single element isotope analysis more difficult (Elsner, 2010). Multi-element isotope analysis offers an opportunity to circumvent the problem associated with single-element CSIA as it allows characterizing bond change reactions of several elements.

In previous studies, we analyzed the carbon and hydrogen isotope fractionation of several OPs upon chemical oxidation and hydrolysis in laboratory experiments (Wu et al. 2014, 2018). We could show that the rate-limiting step of the UV/H₂O₂ reaction of parathion is the oxidative attack of the OH radical on the P=S bond, as indicated by negligible carbon and hydrogen isotope fractionation. The hydrolysis of parathion under acidic and alkaline conditions resulted in distinct but different carbon isotope fractionation patterns, principally allowing the distinction of the two different pH-dependent pathways and giving the possibility for characterizing natural attenuation of parathion by hydrolysis in the environment using isotope fractionation concepts.

CSIA has been widely used for biodegradation assessment of different contaminant groups (Elsner, 2010; Thullner et al., 2012). Recently Vogt and colleagues summarized the concepts for applying CSIA for characterization of natural attenuation of hydrocarbons in field studies (Vogt et al., 2016). In addition, CSIA has been proposed as a useful approach for characterizing degradation processes of micropollutants such as pesticides at field scale (Elsner and Imfeld, 2016); however, only in a few field studies CSIA has been applied to assess microbial degradation of different pesticides or herbicides (Bashir et al., 2015; Liu et al., 2017; Milosevic et al., 2013). To our best knowledge, CSIA has not yet been applied in field studies to assess the *in situ* degradation of OPs. In order to fill this research gap, we selected parathion as a model compound of OPs and investigated its natural attenuation by hydrolysis at a contaminated site using carbon and hydrogen isotope analysis.

2. Materials and methods

2.1. Chemicals

Parathion (*O,O*-diethyl *O*-(4-nitrophenyl) phosphorothioate, >99.7%) was purchased from Sigma-Aldrich and dichloromethane

(DCM, $\geq 99.9\%$) and 25% HCl solution were purchased from Carl Roth GmbH & Co. KG, Germany. Anhydrous Na₂SO₄ ($\geq 99\%$) was obtained from Bernd Kraft GmbH, Germany.

2.2. Field site and sampling

Groyne 42 is situated at Harboøre Tongue in Denmark facing the North Sea. Between 1950 and 1960, waste chemicals were disposed at the site. The area is still heavily contaminated by approximately 100 tons of primarily OPs, mainly the highly toxic parathion (NorthPestClean, 2014a). A complex dense non-aqueous phase liquid (DNAPL) presenting in Groyne 42 is a mixture of OPs and intermediate products, reactants, and solvents used or produced in the manufacturing of OPs. The background information of this site has been described elsewhere (Bondgaard et al., 2012; Hvidberg et al., 2008). In 2006 the contaminated area (20,000 m²) was encapsulated by installing a 600 m long and 14 m deep steel sheet piling and a plastic membrane cap in order to prevent further leaching of toxins to the seawater (Fig. S1, (NorthPestClean, 2014a)). From 2007 to 2014 the Central Denmark Region and the Danish Environmental Protection Agency conducted research to develop a new *in situ* treatment of the site. The treatment consisted of *in situ* alkaline hydrolysis (ISAH) combined with pump-and-treat. The demonstration experiments were carried out on site in controlled test cells (TCs) and test pipes (TPs). More information can be found in the online reports from North Pest Clean (NorthPestClean). Because of the demonstration experiments in the NorthPestClean project, the site contained discrete areas which are the treated areas with sodium hydroxide (pH 13) and the untreated areas with neutral to acidic conditions (pH 2–7). By 2014, the total removal of contaminants from TCs and TPs in treated areas is up to 85% from water and 76% from sediment by ISAH combined with pump-and-treat (NorthPestClean, 2014b). However, the natural attenuation of parathion in the untreated area remains unknown due to the lack of efficient assessment methods.

The locations of monitoring wells are indicated in Fig. 1. Two free phase samples from the Groyne 42 DNAPL were taken in 2011 and 2014 and used to characterize the isotopic composition of the source of parathion. The Groyne 42 DNAPL has a density of 1.16 g mL⁻¹ and viscosity of 13.9 cP at 10 °C (Muff et al., 2016). The composition by weight of the DNAPL was characterized to be 62% parathion, 9% methyl-parathion (*O,O*-dimethyl-*O-p*-nitrophenylphosphorothioate), 7% mercury, 5% sulfotep (diethoxyphosphinothioxyloxy-diethoxy-sulfanylidene- λ 5-phosphane), 3% malathion (diethyl 2-[(dimethoxyphosphorothioyl)sulfanyl]butanedioate) and 14% other unknown contaminants (NorthPestClean, 2014a). The free phase samples were dissolved in DCM and directly subjected for carbon and hydrogen isotope analysis to be used as the source signature of parathion.

19 samples were collected from monitoring wells installed in the treated area and 17 samples were collected from the untreated area using a submersible electrical pump. 1 L of brown glass bottles (Schott, Germany) were used for sampling from the treated area where high concentrations of parathion were expected. In order to avoid evaporation of parathion, bottles were filled with groundwater almost completely and sealed with Teflon-coated caps (Schott, Germany) without headspace. The pH of groundwater samples was adjusted to neutral or slightly acidic conditions using 25% HCl solution to inhibit alkaline hydrolysis. Neutralization was monitored by universal pH indicator strips (0–14 pH Indicator Strips, Macherey-Nagel). 2.5 L of brown glass bottles (Schott, Germany) were used for sampling from the untreated area using the same procedures as described above but without adjusting the pH, because parathion has a relative slow hydrolysis rate at neutral to acidic conditions. The ground water level was measured on-site by

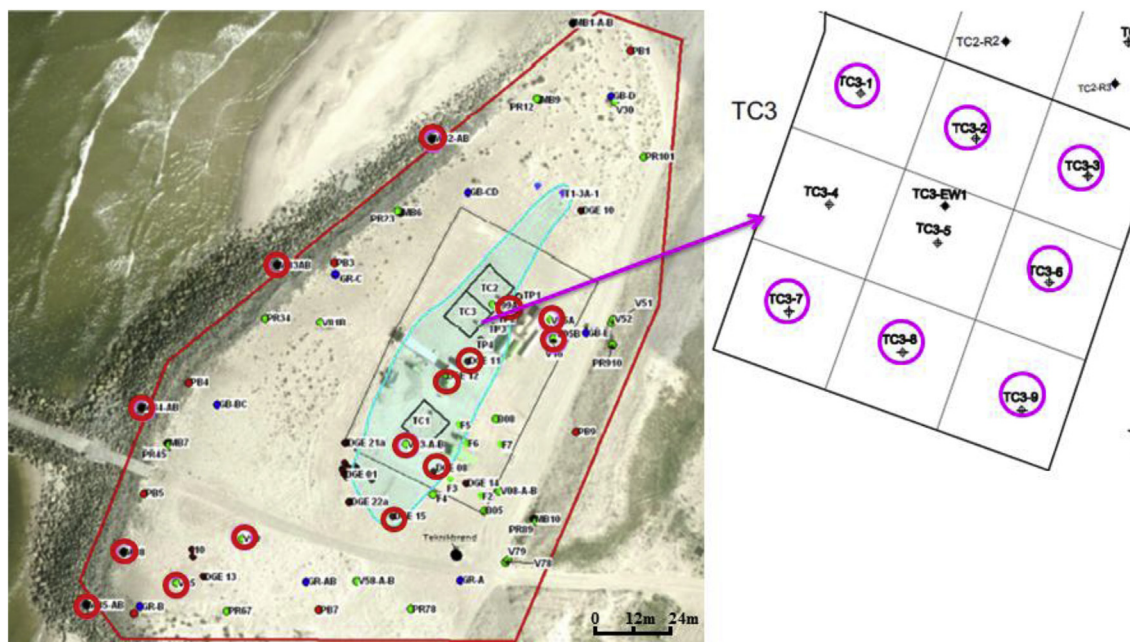


Fig. 1. Map of the “Groyne 42” field site showing the areas of *in situ* treatment by alkaline hydrolysis (TC1–TC3) and the locations of the sampling wells within the treated (pink circles) and untreated area (red circles). The area colored in blue indicates the location of the contamination hotspot. (For interpretation of the references to color in this figure legend, the reader is referred to the Web version of this article.)

an EL-WA water level meters. The concentrations of dissolved oxygen, temperature, pH, and electrical conductivity (EC) were measured on-site during sampling using a Multimeter (WTW, Weilheim, Germany). Samples were sent to the laboratory and stored at 4 °C until extraction. The extraction of samples was processed within 2 weeks after sampling.

2.3. Sample preparation

Groundwater samples were transferred into a 2 L glass-separation funnel. Each sample was extracted three times with 100 mL, 50 mL, and 50 mL of DCM, respectively, by shaking thoroughly. The organic phases were combined and evaporated to ~2 mL under a gentle stream of N₂ in a TurboVap concentrator (TurboVap II, Biotage, Sweden). The extraction and evaporation procedure did not result in significant changes in carbon and hydrogen isotope ratios of parathion as shown elsewhere (Wu et al., 2017). The concentrated sample from the untreated area was then transferred into a 4 mL glass vial by a glass pipette and reconstituted into 3 mL of DCM. The concentrated sample from the treated area was transferred into a 20 mL glass vial by a glass pipette and reconstituted into 10 mL of DCM due to the high concentration of parathion. Before analysis approximately 1.5 g (untreated area) or 5 g (treated area) of anhydrous Na₂SO₄ were added in each vial to remove water.

2.4. Aerobic and anaerobic degradation of parathion

In order to investigate the isotopic profiles of parathion during biodegradation, experiments were conducted using two isolated aerobic strains (TERI OP1, TERI OP2) and one anaerobic strain (TERI ANA-1), respectively. The strains were isolated from soil samples collected from nearby garden located in Gwal Pahari (Gurgaon, Haryana), India. The aerobic strains were isolated in mineral salt (MS) medium with compositions as described elsewhere (Rokade and Mali, 2013). Enrichment and isolation of anaerobic parathion

degraders was carried out under strictly anoxic conditions. MS medium was prepared under anaerobic condition as described elsewhere (Jungheer et al., 2012), by simultaneous boiling for 10 min and purging with nitrogen flush to remove the dissolved oxygen. 0.1% of resazurin was added as redox indicator and L-cysteine HCL (2.5%) was added as a reducing agent to maintain the anoxic conditions. More details of the enrichment and isolation of strains were described in the Supporting Information (section 3.1, 3.2 and 4.1). Batch experiments were conducted under oxic and anoxic conditions in 500 mL flasks containing 250 mL MS medium for studying parathion degradation kinetics. For each batch experiment, seven flasks containing 34 μM parathion-spiked MS medium were inoculated with 1 mL of inoculum. More information about inoculum preparation is provided in the Supporting Information (section 3.3). Sterile control flasks were prepared by the same procedures except adding inoculum. All control and culture flasks were incubated at 150 rpm and 30 °C in the dark. At different time intervals, 1 mL culture broth was taken for optical density and pH variation measurement. Residual parathion and potential metabolites in the medium were extracted by 10 mL of DCM containing naphthalene (6.5 mg L⁻¹) as internal standard for further analysis.

2.5. Analytical methods and quantification

2.5.1. Concentration measurement

Parathion was quantified using an Agilent 6890 series GC (Agilent Technologies, USA) equipped with a flame ionization detector (FID) as described elsewhere (Wu et al. 2017, 2018). A modified temperature program was used: the column was initially held at 60 °C for 2 min, and increased at 8 °C min⁻¹ to 280 °C, and then held for 2 min.

2.5.2. Isotope analysis

The carbon isotope compositions of parathion were analyzed by a gas chromatography-combustion-isotope ratio mass

spectrometer (GC-C-IRMS) system, which consists of a GC 7890A (Agilent Technologies, Palo Alto, CA, USA) coupled via a ConFlo IV interface (Thermo Fisher Scientific, Germany) to a MAT 253 IRMS (Thermo Fisher Scientific, Germany) via an open split. High-temperature pyrolysis was used to convert organically bound hydrogen into molecular hydrogen at 1200 °C for hydrogen isotope composition measurement via the gas chromatograph-high temperature conversion-isotope ratio mass spectrometer system (GC-HTC-IRMS). A DB-608 column (30 m × 0.32 mm × 0.5 μm, Agilent J&W, USA) was used for sample separation, the column was initially held at 60 °C for 2 min, and increased at 8 °C min⁻¹ to 280 °C, and then held for 2 min. All samples were measured in triplicate. The other analytical details are the same as described elsewhere (Wu et al., 2017).

2.5.3. Quantification of parathion degradation in the field

The carbon and hydrogen isotopic signatures are reported as δ values in parts per thousand (‰) relative to international reference materials which are Vienna PeeDee Belemnite (VPDB) for carbon and Standard Mean Ocean Water (SMOW) for hydrogen (Coplen, 2011; Coplen et al., 2006; Schimmelmann et al., 2016). A main objective of CSIA is to quantify the amount of (chemical or biological) degradation in the field supporting monitored natural attenuation (MNA) as a site remedy. The extent of degradation can be estimated for individual compounds using the isotope shifts between the source and the residual not yet degraded fraction of the reacting compound using Eq. (1) which is derived from the rearrangement of the logarithmic form of the Rayleigh equation Eq. (2) (Meckenstock et al., 2004):

$$D (\%) = \left(1 - \frac{C_t}{C_0}\right) \times 100 = \left[1 - \left(\frac{\delta_t + 1}{\delta_0 + 1}\right)^{\left(\frac{1}{\epsilon}\right)}\right] \times 100 \quad (1)$$

$$\ln\left(\frac{\delta_t + 1}{\delta_0 + 1}\right) = \epsilon \times \ln\left(\frac{C_t}{C_0}\right) \quad (2)$$

where C_t is the concentration at a given reaction time t or on a flow path downgradient a source; C_0 is the concentration at the beginning of a reaction or in source area; δ_t and δ_0 are the corresponding carbon and hydrogen isotope ratios of the reacting compound; ϵ is the isotope enrichment factor for a degradation process, which can be obtained from reference experiment under laboratory condition using Rayleigh equation Eq. (2). Thus, the extent of degradation (D %) in the field can be retrieved from isotope values alone, without additional information on concentrations or transformation products.

3. Results and discussion

3.1. Parathion distribution and hydrogeochemical conditions

The physicochemical parameters of the groundwater samples are listed in Table 1. The groundwater level in the monitoring wells ranged from 1.40 to 5.15 m below surface. The temperature was between 11.4 and 13.0 °C. Concentrations of dissolved oxygen were always below 0.1 mg L⁻¹, indicating almost anoxic conditions. In the untreated area, the pH ranged from 3.2 to 6.5, the acidic conditions were likely due to acid chemical waste deposition. Only one well in this area showed an alkaline pH of 9.4 (well V03-2). Parathion concentrations of samples from the untreated area were always lower than 5 mg L⁻¹. In the treated area, the pH ranged from 6.9 to 12.4, demonstrating the effectiveness of the remediation measure. Samples from well TC3-9-3 in the treated area were strongly acidic (pH 2.2) indicating that this well is very close to the core of acid

waste deposition and mixing of alkaline solutions with DNAPL did not result in alkaline conditions. The concentrations of parathion varied from 0.76 to 155.33 mg L⁻¹ in the wells within the treated area (Table 1). The solubility of parathion is 10.4 mg L⁻¹ in water at 8 °C (the average temperature of ground water in Denmark), which is calculated using the enthalpy of fusion for parathion as described elsewhere (Polatoğlu et al., 2015). Most of the parathion concentrations levels in the treated area are above its solubility. This is due to that the treated area is located at the contamination hotspot (Fig. 1) where free organic phases of a mixture of OPs, intermediate products, reactants, as well as solvents used in the manufacturing of OPs are present. Free contaminant phases probably fill pore space of the sediment implying a limited contact to water phases, thus reducing the mixing with alkaline water in the treated area. The large variations of pH values and parathion concentrations in both areas illustrate rather heterogenic biogeochemical conditions at the investigated site.

Potential transformation products of parathion were investigated in different treated and untreated areas of the site (Fig. S2 and Table S1). The relative abundance and frequency of detected aminoparathion (4-diethoxyphosphinothioxyaniline) suggested reduction of the nitro group of parathion by chemical or microbial processes (see also below). Compared to the treated area, the higher abundance of aminoparathion in the untreated area (Table S1) showing neutral and acidic conditions indicates that the reduction of the nitro group is preferentially a biological process. The presence of aminoparathion may point to reducing conditions prevailing at the dumpsite. Aminoparathion was detected in our biological degradation experiments under aerobic conditions using strain TERI OP1 and under anoxic conditions using strain TERI ANA-1 as described below in section 3.4, which is also in line with previous studies (Singh and Walker, 2006). *p*-nitrophenol (4-nitrophenol) is a typical alkaline hydrolysis product of parathion and was detected in both untreated and treated areas. The relative abundance and detection frequency were higher in the treated area (Table S1), showing the hydrolytic cleavage of the O-P bond. The abundance of *p*-nitrophenol in biodegradation studies suggests that biological hydrolysis may contribute to transformation of parathion.

3.2. Carbon and hydrogen isotope analysis of parathion from field samples

The average value of all isotope analyses of source samples was taken as source signature of parathion, resulting in $-22.9 \pm 0.8\%$ for $\delta^{13}\text{C}$ ($n = 10$) and $-212 \pm 15\%$ for $\delta^2\text{H}$ ($n = 12$). In the untreated area, the obtained $\delta^{13}\text{C}$ values differed from -22.1% to -18.0% and $\delta^2\text{H}$ values differed from -226% to -208% (Table 1). In the treated area, the $\delta^{13}\text{C}$ values varied from -23.6% to 20.1% and $\delta^2\text{H}$ values varied from -227% to -201% (Table 1).

Compared to the source signature of parathion, the $\delta^{13}\text{C}$ enrichment of 0.8% – 4.9% was obtained from the wells in the untreated area (Fig. 2a), indicating *in situ* acidic and neutral hydrolysis was taking place. In the treated area, the $\delta^{13}\text{C}$ values were almost identical with the source signature (Fig. 2a) showing that no carbon isotope fractionation of parathion occurs under strong alkaline conditions, which is in agreement with the results of laboratory hydrolysis experiments (Wu et al., 2018). $\delta^{13}\text{C}$ enrichments of 2.8% and 2.1% were observed in samples from wells TC3-6-3 and TC3-7-2, respectively, which are characterized by strongly alkaline pH values (11.7–12.4). This result might be explained by mixing of alkaline water and plumes during sampling. Mixing of water in porous media under laminar flow conditions in sandy aquifers is restricted, which imply that alkaline solution will not mix easily with contaminant phases or highly contaminated water.

Table 1
Physicochemical parameters of groundwater samples, parathion concentrations, parathion isotope values and qualitative assessment of *in situ* hydrolysis of parathion. Samples containing parathion concentrations below detection limit are not listed.

Well ID	water level (m)	Temp. (°C)	O ₂ (mg L ⁻¹)	conductivity (mS cm ⁻¹)	pH	sample volumn (L)	Parathion (mg L ⁻¹)	δ ¹³ C (‰)	δ ² H (‰)	<i>In situ</i> hydrolysis at pH 2, 5 and 7 ^a (%)	<i>In situ</i> hydrolysis at pH 9 ^b (%)	C ₀ (mg L ⁻¹)
samples from treated area												
TC3-1-1	5.15	12.5	0.01	19.31	9.2	1.00	107.90	-23.6 ± 0.5	b.d.			
TC3-1-2	2.94	12.4	0.04	23.50	11.2	0.98	0.78	b.d. ^c	b.d.			
TC3-1-3	3.96	12.6	0.05	10.03	6.9	1.01	133.65	-22.8 ± 0.1	b.d.			
TC3-2-2	3.06	12.2	0.09	33.00	11.9	0.98	0.76	b.d.	b.d.			
TC3-2-3	3.04	12.4	0.04	12.70	10.3	0.98	1.37	b.d.	b.d.			
TC3-3-3	3.12	13.0	0.03	12.23	9.5	1.00	56.99	-22.1 ± 0.1	-210 ± 2			
TC3-6-3	3.19	12.6	0.04	12.51	11.7	0.98	5.75	-20.1 ± 0.4	b.d.	3.7–5.0	7.4–9.3	5.97 -6.34
TC3-7-2	2.95	11.6	0.05	27.50	12.4	0.87	155.33	-20.8 ± 0.0	-227 ± 3	2.8–3.7	5.5–7.0	
TC3-7-3	2.97	12.2	0.05	12.26	8.1	0.94	124.46	-22.4 ± 0.2	-211 ± 6			
TC3-8-3	4.00	12.3	0.06	9.28	9.4	0.96	132.51	-23.0 ± 0.1	-201 ± 2			
TC3-9-3	3.07	12.2	0.11	13.91	2.2	1.00	33.97	-22.7 ± 0.1	-211 ± 2			
samples from untreated area												
T1-3-1	3.59	11.4	0.09	20.20	4.4	2.19	2.64	-22.1 ± 0.1	b.d.	1.1–1.4	2.2–2.7	2.67 -2.72
TP2-1-1	1.40	11.4	0.07	5.47	3.8	2.18	3.22	-21.1 ± 0.3	b.d.	2.4–3.2	4.7–5.9	3.30 -3.42
F5	3.81	12.7	0.08	5.46	4.1	2.00	3.16	-21.7 ± 0.2	-211 ± 1	1.6–2.1	3.1–3.9	3.21 -3.29
V03-2	3.85	11.8	0.05	6.73	9.4	2.13	1.86	-21.7 ± 0.0	-215 ± 4	1.6–2.1	3.1–3.9	1.88 -1.93
DGE15	3.88	12.0	0.08	6.81	4.0	2.33	4.94	-21.5 ± 0.6	-226 ± 0	1.8–2.4	3.6–4.5	5.03 -5.17
V05 A	4.03	11.4	0.09	17.23	3.2	2.50	0.58	-18.3 ± 0.4	-208 ± 1	6.1–8.1	12.0–15.1	0.62 -0.68
DGE13	3.51	12.5	0.10	9.34	6.5	2.50	0.01	-21.8 ± 0.0	b.d.	1.5–2.0	2.9–3.7	0.01 -0.01
V81 B	3.49	12.4	0.10	14.64	3.5	2.27	0.12	-18.0 ± 0.6	-214 ± 5	6.5–8.6	12.7–16.0	0.13 -0.14

^a Quantitative assessment of *in situ* hydrolysis of parathion under neutral and acidic conditions using ϵ_C of -6.0 ± 0.2 at pH 7, ϵ_C of -6.7 ± 0.4 at pH 5 and ϵ_C of -6.9 ± 0.8 at pH 2. The ϵ_C values were obtained from lab experiments (Wu et al., 2018).

^b Quantitative assessment of *in situ* hydrolysis of parathion under slightly alkaline condition using ϵ_C of -3.5 ± 0.4 at pH 9 obtained from (Wu et al., 2018).

^c b.d.: below detection limit.

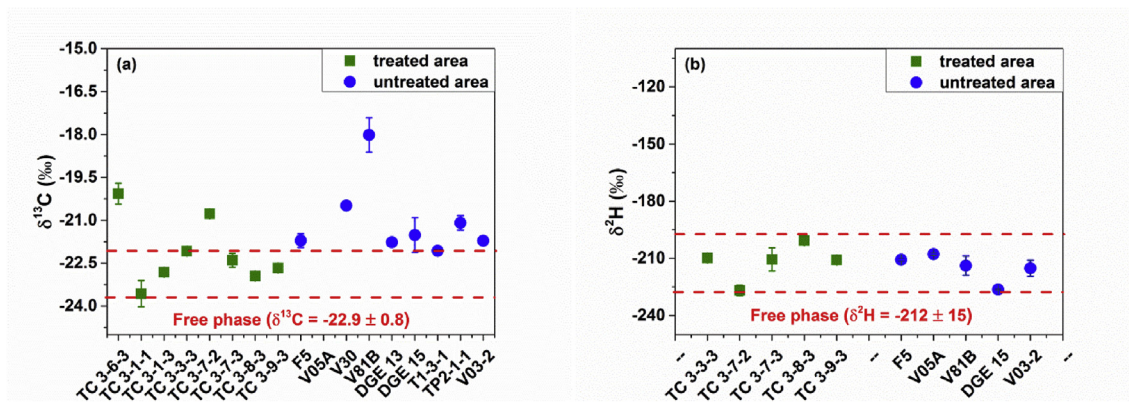


Fig. 2. Carbon (a) and hydrogen (b) isotope ratios of parathion obtained from the groundwater from the “Groyne 42” field site. Green squares indicate the samples from the treated area; blue circles indicate the samples from untreated area; Red dotted lines indicate the carbon and hydrogen source signatures of parathion. (For interpretation of the references to color in this figure legend, the reader is referred to the Web version of this article.)

Mass transfer processes are widely controlled by diffusive transport resulting in transversal dispersion along a flow path. Convective mixing in porous sediments practically can be neglected. For example mixing of contaminants with electron donor or acceptor under laminar flow conditions can be limiting for biodegradation. Mixing during sampling need to be taken into account for interpreting isotope composition and lead to an underestimation of degradation reactions (Kopinke et al., 2005). Mixing of water bodies from different sections of an aquifer with specific reaction conditions should be considered for quantitative interpretation of isotope fractionation pattern (Thullner et al., 2012). The isotope fractionation is an indication that the hydrolysis may have taken place under acidic, neutral or slight alkaline conditions explaining the carbon isotope enrichment. However, in both treated and untreated areas, the $\delta^2\text{H}$ values were all overlapping with the source signature (Fig. 2b) because the hydrolysis of parathion is not associated to a detectable hydrogen isotope fractionation effect, independent of the pH value.

3.3. Isotopic profiles of parathion during hydrolysis and chemical oxidation

Carbon and hydrogen isotope fractionation patterns of hydrolysis and chemical oxidation of parathion have been investigated systematically in our previous study (Wu et al., 2018). Chemical oxidation of parathion occurs via oxidation of the P=S bond to a P=O bond by an OH radical in the first rate-determining irreversible step (Fig. 3B); the reaction is not linked to detectable hydrogen or carbon isotope fractionation. In contrast, the hydrolysis of parathion results in no detectable H isotope fractionation but significant C isotope fractionation, corresponding to isotope enrichment factors of $\epsilon_{\text{C}} = -6.9 \pm 0.8\%$ at pH 2, $-6.7 \pm 0.4\%$ at pH 5, $-6.0 \pm 0.2\%$ at pH 7, $-3.5 \pm 0.4\%$ at pH 9, and no detectable carbon isotope fractionation at pH 12. The different isotope fractionation patterns are due to two hydrolysis pathways of parathion (Fig. 3A): one is P-O bond cleavage by nucleophilic attack at the phosphorus atom under strong alkaline condition, resulting in no C and H isotope fractionation; another one is C-O bond cleavage by nucleophilic attack at the carbon atom under acidic, neutral and slightly alkaline conditions, resulting in a significant C but no H isotope fractionation.

The obtained ϵ_{C} at pH 2, pH 5 and pH 7 are identical when considering the confidence intervals. This is due to the similar pathway taking place under neutral and acidic hydrolysis (Fig. 3A1) which cannot be distinct by isotope fractionation analysis. In the case of lower pH < 7, the changes of pH have effects on the reaction rates, for instance, the hydrolysis half-life of parathion at 25 °C is reported to be 133 days at pH 5 and 247 days at pH 7 (FAO, 1990). However, no effects of pH changes on the reaction pathway and therefore the identical ϵ_{C} were obtained. Two hydrolysis pathways take place simultaneously in the range of $7 < \text{pH} < 10$. With the increase of pH, the contribution from C-O bond cleavage pathway decreases, resulting in smaller ϵ_{C} . The reduction of the ϵ_{C} at pH 9 revealed that the contribution to parathion degradation via C-O bond cleavage pathway is 51–58% (Wu et al., 2018) using the extended Rayleigh-type equation derived by Van Breukelen (Van Breukelen, 2007). Parathion is hydrolyzed completely by the P-O bond cleavage pathway at pH > 10, as shown experimentally (Wanamaker et al., 2013), which is in agreement with the result that no detectable ϵ_{C} was obtained during hydrolysis at pH 12. Therefore, C isotope fractionation can be expected and applied to characterize parathion hydrolysis at pH < 10.

3.4. Isotopic profiles of parathion during biodegradation

Isotopic profiles of parathion during biodegradation were

investigated under laboratory cultivation using two isolated aerobic strains (TERI OP1, TERI OP2) and one anaerobic strain (TERI ANA-1). Experimental details with regard to the microbiological investigations are described in the Supporting Information. During aerobic degradation of more than 80% parathion, no carbon and hydrogen isotope enrichment could be observed (Table S2). Similarly under anoxic conditions, no carbon and hydrogen isotope enrichment of parathion could be observed after 90% degradation (Table S3). Thus, the reactions were not associated with detectable carbon and hydrogen isotope fractionation of parathion using the three tested strains. The potential biodegradation metabolites of parathion were tentative analyzed via GC-MS (for analytical details see supporting information). The tentative metabolites analyses suggested that *p*-nitrophenol, formed through the hydrolysis of the ester bond, was one initial reaction product under aerobic conditions using strain TERI OP2. Aminoparathion was detected in degradation experiments under aerobic conditions and anoxic conditions using strain TERI OP1 and strain TERI ANA-1, respectively. This indicates that the biodegradation leads to the reduction of the nitro group to form the amino group.

In previous studies, several microbial strains have been isolated capable of degrading parathion, affiliated e.g. to the genera *Flavobacterium*, *Bacillus*, *Pseudomonas* or *Arthrobacter* (Singh and Walker, 2006). The previously proposed biodegradation mechanisms of parathion were summarized in Fig. 3C, which are (C1) hydrolysis of the phosphotriester bond to form *p*-nitrophenol (P-O bond cleavage), which is the major pathway; (C2) reduction of the nitro group acting as electron acceptor to form aminoparathion (N-O bond cleavage); (C3) oxidation of the sulfur group of parathion to form paraoxon (diethyl (4-nitrophenyl) phosphate) (P=S bond cleavage). No carbon or hydrogen bonds breaking is involved in the first rate-determining irreversible step of all three proposed pathways, thus, no significant carbon and/or hydrogen isotope fractionation is expected to be associated with the biodegradation of parathion. Therefore, the microbial degradation is not likely to be characterized by carbon and hydrogen isotope fractionation. However, only a limited number of studies exist on aerobic and anaerobic degradation of parathion, it cannot be fully excluded that microorganisms could attack parathion by oxidizing a carbon entity leading to carbon and hydrogen isotope fractionation.

3.5. Quantitative assessment of in situ hydrolysis at the investigated field site

Even though the formation of OH radicals is unlikely in an anoxic or oxygen-limited aquifer, the chemical oxidation of parathion leads to desulfurization in the rate-limiting step and would not yield significant carbon or hydrogen isotope fractionation (Wu et al., 2018). As discussed above, it is unlikely that significant carbon or hydrogen isotope fractionation is associated with the biodegradation of parathion, and moreover, no carbon isotope fractionation can be expected during the hydrolysis of parathion at pH > 10. Hence, the carbon isotope enrichment obtained in parathion at the Groyne 42 site can be contributed exclusively to hydrolysis at pH < 10.

The extent of hydrolysis can be estimated by Eq. (1) using the ϵ_{C} determined in laboratory experiments based on the Rayleigh equation. However, the accuracy of the degradation estimation in the field is highly dependent on the choice of an appropriate ϵ_{C} for the given field situation (USEPA, 2008). The extent of *in situ* hydrolysis of parathion in the untreated area at the Groyne 42 site was estimated using ϵ_{C} of -6.0 ± 0.2 (pH 7), -6.7 ± 0.4 (pH 5) and -6.9 ± 0.8 (pH 2), respectively. The estimation using carbon isotope enrichment revealed the evidence that up to 8.6% natural attenuation of parathion was contributed by hydrolysis under

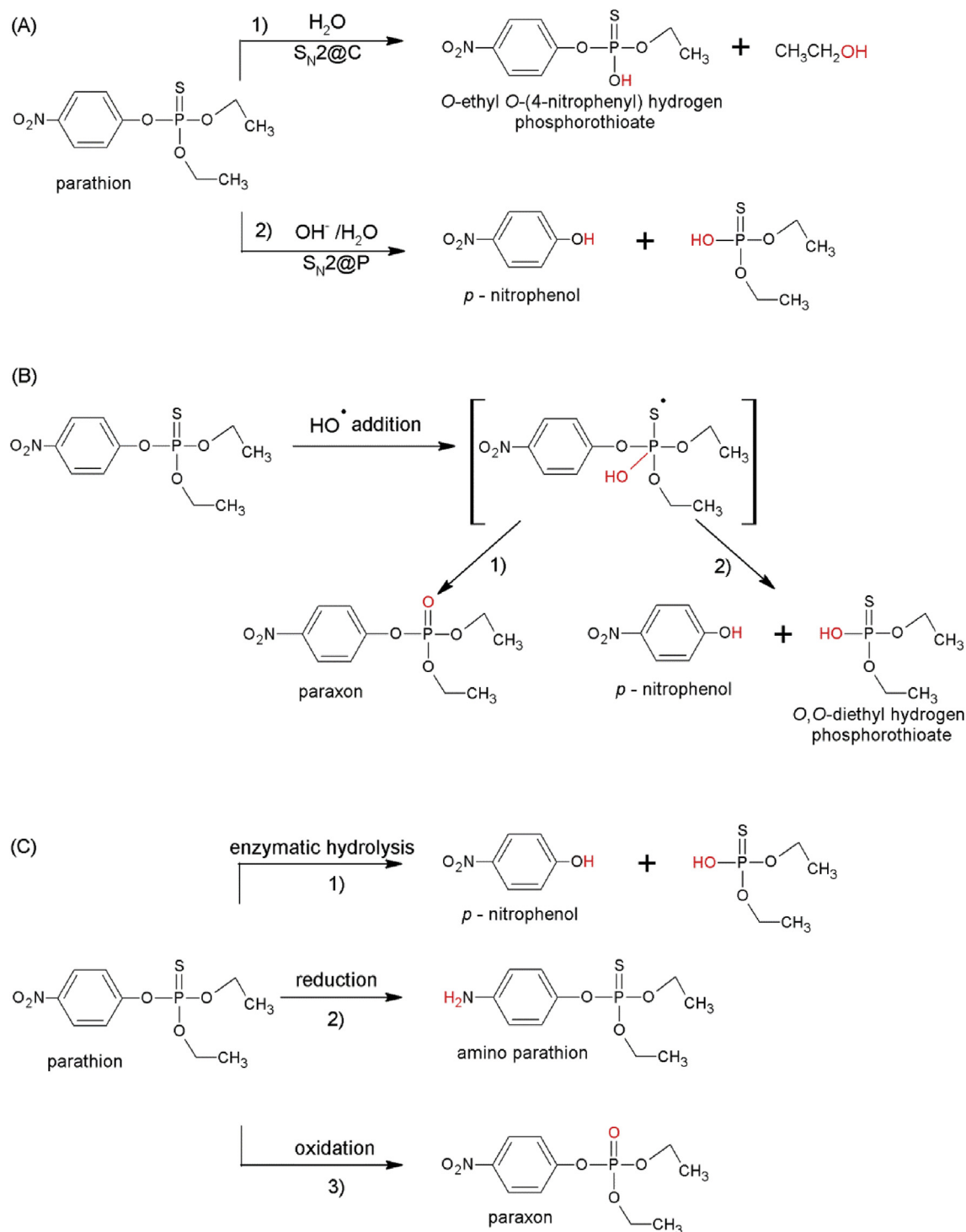


Fig. 3. Proposed reaction schemes with transformation mechanisms of parathion during (A) hydrolysis at different pH, (B) chemical oxidation by OH radical and (C) biodegradation. Scheme (A) illustrates that hydrolysis of parathion occurs via two pathways: (A1) nucleophilic attack by H_2O at the α -carbon of the alkoxy group at acidic/neutral condition; (A2) nucleophilic attack by OH^- and H_2O at the phosphorus atom at alkaline condition. Scheme (B) illustrates that the first rate-limiting step of the chemical oxidation of parathion by OH radical occurs via OH radical addition to the central phosphorus atom and stabilized by two different pathways: (B1) the elimination of sulfhydryl radical to produce $\text{P}=\text{O}$ bond to form paraxon; (B2) the elimination of nitrophenol from the phosphoric center to form *p*-nitrophenol. Scheme (C) summarizes biodegradation pathways of parathion: (C1) enzymatic hydrolysis of the phosphotriester bond to form *p*-nitrophenol; (C2) reduction of the nitro group to form amino parathion; (C3) oxidation of parathion to paraxon.

neutral and acidic conditions (Table 1). The ϵ_C of -3.5 ± 0.4 (pH 9) was used to estimate the extent of degradation in the untreated area considering the mixed hydrolysis pathways, which resulted in up to 16% of natural attenuation of parathion was contributed by hydrolysis under slightly alkaline conditions (Table 1). The low

extent of *in situ* hydrolysis is due to long half-life of parathion under acidic and neutral conditions and low ground water temperature at the field site (11–13 °C). The initial concentration of parathion (C_0) in the untreated area was calculated by applying Eq. (1) using the measured concentrations (C_t) and estimated extent of hydrolysis

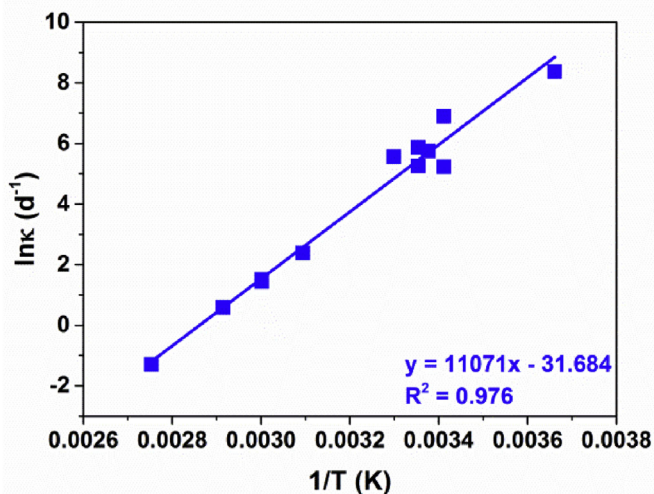


Fig. 4. The Arrhenius plot of parathion hydrolysis using collected data in Table S4.

(Table 1). The initial concentrations of parathion in monitored wells in the untreated area were calculated to be below 5.17 mg L^{-1} , which is below the solubility of 10.4 mg L^{-1} in water at 8°C (the average temperature of ground water in Denmark).

Muff and colleagues investigated the influence of co-solvents on the aqueous solubility and reactivity of the OPs in the complex Groyne 42 DNAPL. Their results suggest that the hydrolysis reactions are limited by the rate of hydrolysis rather than NAPL dissolution (Muff et al., 2016). Chemical hydrolysis of parathion follows pseudo-first-order kinetics within the accuracy of measurement. Half-life of the reactions conducted at pH 1 to 7.8 and temperatures from 0 to 90°C under different conditions from different studies are summarized in Table S4. Arrhenius plots are often used to analyze the effect of temperature on the rates of chemical reactions which displays the logarithm of kinetic constants ($\ln(\kappa)$) plotted against inverse temperature ($1/T$). The Arrhenius plot of parathion hydrolysis using collected data in Table S4 gave a straight line with R^2 of 0.976 (Fig. 4), from which the activation energy (E_a) $92.04 \text{ kJ mol}^{-1}$ was determined. The obtained E_a is in the same order of the previous reported value of $22.35 \text{ kcal mol}^{-1} = 93.52 \text{ kJ mol}^{-1}$ which was calculated from the hydrolysis of parathion at pH 7.8 at different temperatures (Weber, 1976). The equation obtained in Fig. 3 shows the correlation of temperature and the rate constants of parathion hydrolysis at $\text{pH} < 7.8$. From this, a half-life of 1521 days at the average ground water temperature in Denmark (8°C) can be roughly predicted. The relative low temperature at the Groyne 42 field site would lead to long retention time of parathion in the untreated area. A previous study suggested that the enhancement of the average rate of hydrolysis could be achieved by a factor of 1.4–4.8 by increasing the reaction temperature from 10 to 30°C (Muff et al., 2016). Our results contradicts to some extent with the assumption that the rate of hydrolysis is the rate limiting step in the *in situ* degradation, and believe that mixing is a major factor. Firstly, we found indication for neutral and acidic hydrolysis even in the treated areas where someone would expect prevailing alkaline conditions. Secondly, the high parathion concentrations clearly over the water solubility suggest that phases are present which are obviously not assessable to hydrolysis. Thirdly, in spite of long half-life, the high concentrations suggest that phases not assessable to hydrolysis still provide a source of contamination leaching into the ground water.

Thus, the kinetic of hydrolytic transformation is expected to be controlled by mixing of alkaline water in the subsurface, and

mixing in porous media is slow. Similar assumption could be made for neutral and acidic hydrolysis. Mixing of alkaline solutions with DNAPL seems to be a challenge for all *in situ* measures. Heterogenic reaction conditions could be expected as suggested by the carbon isotope enrichment of parathion even at places with high pH pointing to a predominance of neutral or acidic hydrolysis.

4. Conclusions

Carbon isotope fractionation can be used to characterize acidic and neutral hydrolysis of parathion at contaminated field sites. Anaerobic and aerobic biodegradation of parathion proceed via reduction of the nitro group to aminoparathion and/or via enzymatic hydrolysis to *p*-nitrophenol, and chemical oxidation by radicals occurs via desulfurization of parathion to paraoxon; both reaction mechanisms were shown to be not associated with carbon and hydrogen isotope fractionation. Therefore, the extent of hydrolysis under typical environmental pH values (3–10) can be quantified robustly using the Rayleigh concept and the isotope enrichment factors obtained in laboratory hydrolysis experiments.

At pH smaller than 7 where the C-O bond cleavage is the dominant hydrolysis pathway, the pH changes will affect the reaction rate but has no effects on the carbon isotope enrichment factors of parathion. In addition, hydrolysis rates increase with increasing temperature, for instance, the half-life of parathion at pH 7 is 247 days at 25°C (FAO, 1990) and 75 h at 60°C (Wu et al., 2018). However, the mechanisms will not change and the isotope fractionation of $\text{S}_\text{N}2$ reaction is considered to be not much effected by temperature. A previous study reported that the hydrolysis rates of methyl halides increased with increasing temperature, while carbon kinetic isotope effects for halide substitution were almost independent of temperature (Baesman and Miller, 2005). This suggest that when both temperature and pH adjustments are required for technical measures to improve parathion hydrolysis at contaminated sites, the isotope enrichment factors obtained in laboratory hydrolysis experiments are still applicable to analyze the mode of hydrolysis.

Conflicts of interest

None.

Acknowledgment

Langping Wu is financially supported by the China Scholarship Council (File No. 201306460007). The work was partially financially supported by BMBF-DBT Cooperation Science Program (project No: 01DQ15006 and BT/IN/Germany-BMBF/02/BL/2015-16). We are thankful to Steffen Kümmel and Matthias Gehre for support in the Isotope Laboratory of the Department of Isotope Biogeochemistry. Banwari Lal and Subhasis Das are acknowledged for supporting this work.

Appendix A. Supplementary data

Supplementary data related to this article can be found at <https://doi.org/10.1016/j.watres.2018.06.039>.

References

- Aston, L.S., Seiber, J.N., 1996. Exchange of airborne organophosphorus pesticides with pine needles. *J. Environ. Sci. Heal. B* 31 (4), 671–698.
- Baesman, S.M., Miller, L.G., 2005. Laboratory determination of the carbon kinetic isotope effects (KIEs) for reactions of methyl halides with various nucleophiles in solution. *J. Atmos. Chem.* 52 (2), 203–219.
- Bashir, S., Hitzfeld, K.L., Gehre, M., Richnow, H.H., Fischer, A., 2015. Evaluating

- degradation of hexachlorocyclohexane (HCH) isomers within a contaminated aquifer using compound-specific stable carbon isotope analysis (CSIA). *Water Res.* 71, 187–196.
- Bondgaard, M., Hvidberg, B., Ramsay, L., 2012. Remediation of Pesticide Contamination by in Situ Alkaline Hydrolysis - a New Soil Remediation Technology. In: *Eight International Conference on Remediation of Chlorinated and Recalcitrant Compounds*, Monterey, California.
- Coplen, T.B., 2011. Guidelines and recommended terms for expression of stable-isotope-ratio and gas-ratio measurement results. *Rapid Commun. Mass. Sp.* 25 (17), 2538–2560.
- Coplen, T.B., Brand, W.A., Gehre, M., Groning, M., Meijer, H.A.J., Toman, B., Verkouteren, R.M., 2006. After two decades a second anchor for the VPDB delta C-13 scale. *Rapid Commun. Mass. Sp.* 20 (21), 3165–3166.
- Elsner, M., 2010. Stable isotope fractionation to investigate natural transformation mechanisms of organic contaminants: principles, prospects and limitations. *J. Environ. Monit.* 12 (11), 2005–2031.
- Elsner, M., Imfeld, G., 2016. Compound-specific isotope analysis (CSIA) of micro-pollutants in the environment - current developments and future challenges. *Curr. Opin. Biotechnol.* 41, 60–72.
- FAO, 1990. Parathion (58). Food and Agriculture Organization of the United Nations.
- Fenner, K., Canonica, S., Wackett, L.P., Elsner, M., 2013. Evaluating pesticide degradation in the environment: blind spots and emerging opportunities. *Science* 341 (6147), 752–758.
- Hofstetter, T.B., Schwarzenbach, R.P., Bernasconi, S.M., 2008. Assessing transformation processes of organic compounds using stable isotope fractionation. *Environ. Sci. Technol.* 42 (21), 7737–7743.
- Hvidberg, B., Ramsay, L., Kirkegaard, C., Elkjær, L., Jørgensen, C., Oberender, A., Kiilerich, O., 2008. Remediation Technologies for a Large Pesticide-contaminated Site: Enclosure, Alkaline Hydrolysis and Bioventing.
- Junghare, M., Subudhi, S., BL, 2012. Improvement of hydrogen production under decreased partial pressure by newly isolated alkaline tolerated anaerobe, *Clostridium butyricum* TM9A: optimization of process parameters. *Int. J. Hydrogen. Energ.* 4 (37), 3160–3168.
- Kawahara, J., Horikoshi, R., Yamaguchi, T., Kumagai, K., Yanagisawa, Y., 2005. Air pollution and young children's inhalation exposure to organophosphorus pesticide in an agricultural community in Japan. *Environ. Int.* 31 (8), 1123–1132.
- Kopinke, F.D., Georgi, A., Voskamp, M., Richnow, H.H., 2005. Carbon isotope fractionation of organic contaminants due to retardation on humic substances: implications for natural attenuation studies in aquifers. *Environ. Sci. Technol.* 39 (16), 6052–6062.
- Liu, Y., Bashir, S., Stollberg, R., Trabitzsch, R., Weiss, H., Paschke, H., Nijenhuis, I., Richnow, H.H., 2017. Compound specific and enantioselective stable isotope analysis as tools to monitor transformation of hexachlorocyclohexane (HCH) in a complex aquifer system. *Environ. Sci. Technol.* 51 (16), 8909–8916.
- LRSB, L., 2014. Pilot Experiments on the Remediation Technology in Situ Alkaline Hydrolysis at Groyne 42. Final Report. NorthPestClean, Kongens Lyngby, Denmark.
- Meckenstock, R.U., Morasch, B., Griebler, C., Richnow, H.H., 2004. Stable isotope fractionation analysis as a tool to monitor biodegradation in contaminated aquifers. *J. Contam. Hydrol.* 75 (3–4), 215–255.
- Milosevic, N., Qiu, S., Elsner, M., Einsiedl, F., Maier, M.P., Bensch, H.K., Albrechtsen, H.J., Bjerg, P.L., 2013. Combined isotope and enantiomer analysis to assess the fate of phenoxy acids in a heterogeneous geologic setting at an old landfill. *Water Res.* 47 (2), 637–649.
- Muff, J., MacKinnon, L., Durant, N.D., Bennedsen, L.F., Rugge, K., Bondgaard, M., Pennell, K., 2016. The influence of cosolvent and heat on the solubility and reactivity of organophosphorus pesticide DNAPL alkaline hydrolysis. *Environ. Sci. Pollut. Res. Int.* 23 (22), 22658–22666.
- Nielsen, M.B., Kjeldsen, K.U., Lever, M.A., Ingvorsen, K., 2014. Survival of prokaryotes in a polluted waste dump during remediation by alkaline hydrolysis. *Ecotoxicology* 23, 404–418.
- Nijenhuis, I., Richnow, H.H., 2016. Stable isotope fractionation concepts for characterizing biotransformation of organohalides. *Curr. Opin. Biotechnol.* 41, 108–113.
- NorthPestClean Projects related to the toxic waste site at Groyne 42 <http://www.eng.northpestclean.dk/publications/>.
- NorthPestClean, 2014a. Layman Reports 2: Demonstration of in Situ Alkaline Hydrolysis as a Novel Soil Remediation Technique for a Pesticide Contamination, Central Denmark Region. Department of Environment. <http://www.eng.northpestclean.dk/publications/layman-reports/>.
- NorthPestClean, 2014b. Pilot Experiments on the Remediation Technology in Situ Alkaline Hydrolysis at Groyne 42-Final Report. <http://www.northpestclean.dk/publikationer/rapporter-fra-northpestclean-perioden-2011-2014/>.
- Pehkonen, S.O., Zhang, Q., 2002. The degradation of organophosphorus pesticides in natural waters: a critical review. *Crit. Rev. Env. Sci. Tec.* 32 (1), 17–72.
- Polatoğlu, İ., Yürekli, Y., Baştürk, S.B., 2015. Estimating solubility of parathion in organic solvents. *AKU J. Sci. Eng.* 15 (3), 1–5.
- Rokade, K.B., Mali, G.V., 2013. Biodegradation of chlorpyrifos by *Pseudomonas desmolyticum* NCIM 2112. *Int. J. Pharm. Bio. Sci.* (B) 2 (4), 609–616.
- Schimmelmann, A., Qi, H.P., Coplen, T.B., Brand, W.A., Fong, J., Meier-Augenstein, W., Kemp, H.F., Toman, B., Ackermann, A., Assonov, S., Aerts-Bijma, A.T., Brejcha, R., Chikaraishi, Y., Darwish, T., Elsner, M., Gehre, M., Geilmann, H., Groing, M., Helie, J.F., Herrero-Martin, S., Meijer, H.A.J., Sauer, P.E., Sessions, A.L., Werner, R.A., 2016. Organic reference materials for hydrogen, carbon, and nitrogen stable isotope-ratio measurements: caffeine, n-alkanes, fatty acid methyl esters, glycines, L-valines, polyethylenes, and oils. *Anal. Chem.* 88 (8), 4294–4302.
- Singh, B.K., Walker, A., 2006. Microbial degradation of organophosphorus compounds. *FEMS Microbiol. Rev.* 30 (3), 428–471.
- Thatcher, G.R.J., Kluger, R., 1989. Mechanism and catalysis of nucleophilic substitution in phosphate esters. *Adv. Phys. Org. Chem.* 25, 99–265.
- Thullner, M., Centler, F., Richnow, H.-H., Fischer, A., 2012. Quantification of organic pollutant degradation in contaminated aquifers using compound specific stable isotope analysis - review of recent developments. *Org. Geochem.* 42 (12), 1440–1460.
- USEPA, 2006. Organophosphorus Cumulative Risk Assessment (2006 Update). U.S. Environmental Protection Agency, pp. 1–189.
- USEPA, 2008. In: N.R.M.R.L. (Ed.), *A Guide for Assessing Biodegradation and Source Identification of Organic Ground Water Contaminants Using Compound Specific Isotope Analysis (CSIA)*. U.S. EPA Office of Research and Development, p. 67 (ADA OK).
- Van Breukelen, B.M., 2007. Extending the Rayleigh equation to allow competing isotope fractionating pathways to improve quantification of biodegradation. *Environ. Sci. Technol.* 41 (11), 4004–4010.
- Vogt, C., Dorer, C., Musat, F., Richnow, H.H., 2016. Multi-element isotope fractionation concepts to characterize the biodegradation of hydrocarbons - from enzymes to the environment. *Curr. Opin. Biotechnol.* 41, 90–98.
- Wanamaker, E.C., Chingas, G.C., McDougal, O.M., 2013. Parathion hydrolysis revisited: in situ aqueous kinetics by ¹H NMR. *Environ. Sci. Technol.* 47 (16), 9267–9273.
- Weber, K., 1976. Degradation of parathion in seawater. *Water Res.* 10 (3), 237–241.
- Wu, L., Chladkova, B., Lechtenfeld, O.J., Lian, S., Schindelka, J., Herrmann, H., Richnow, H.H., 2018. Characterizing chemical transformation of organophosphorus compounds by ¹³C and ²H stable isotope analysis. *Sci. Total Environ.* 615, 20–28.
- Wu, L., Kummel, S., Richnow, H.H., 2017. Validation of GC-IRMS techniques for delta C-13 and delta H-2 CSIA of organophosphorus compounds and their potential for studying the mode of hydrolysis in the environment. *Anal. Bioanal. Chem.* 409 (10), 2581–2590.
- Wu, L., Yao, J., Trebse, P., Zhang, N., Richnow, H.H., 2014. Compound specific isotope analysis of organophosphorus pesticides. *Chemosphere* 111, 458–463.

Supplementary information

Carbon and hydrogen isotope analysis of parathion for characterizing natural attenuation by hydrolysis at a contaminated site

Langping Wu^a, Dipti Verma^b, Morten Bondgaard^c, Anja Melvej^c, Carsten Vogt^a, Sanjukta Subudhi^b, Subhasis Das^b, Banwari Lal^b Hans H. Richnow^{a,*}

^a Department of Isotope Biogeochemistry, Helmholtz Centre for Environmental Research-UFZ, Permoserstraße 15, 04318 Leipzig, Germany

^b Environmental and Industrial Biotechnology Division, The Energy and Resources Institute, New Delhi 110003, India

^c Department of Environment, Central Denmark Region, Lægårdvej 10, 7500 Holstebro, Denmark

*Email: hans.richnow@ufz.de Tel: 0049 341 235 1212 Fax: 0341-450822

13 pages

4 figures

4 tables

Contents

1. Groyne 42 site	2
2. Tentative transformation products of parathion at field site	2
3. Aerobic degradation of parathion	4
3.1. Enrichment for isolation of parathion-degrading bacteria	4
3.2. Screening and selection of parathion-degrading aerobic bacteria	5
3.3. Aerobic degradation of parathion using selected isolates TERI OP1 and TERI OP2	5
3.4. Carbon and hydrogen isotope analysis of parathion during aerobic degradation	6
4. Anaerobic degradation of parathion	6
4.1. Enrichment and selection of parathion-degrading microbes under anoxic conditions	6
4.2 Anaerobic degradation of parathion using isolate TERI ANA-1	7
4.3. Carbon and hydrogen isotope analysis of parathion during anaerobic degradation	7
5. Biodegradation mechanisms of parathion	8
6. Half-life of parathion hydrolysis	8
7. References	8

1. Groyne 42 site

Groyne 42 is situated at Harbøre Tongue in Denmark facing the North Sea and was used to dispose of waste from production of chemicals between 1950 and 1960. The area is heavily contaminated by approx. 100 tons of primarily organophosphates (OPs), mainly the highly toxic parathion. The background information of this site has been described elsewhere (Bondgaard et al. 2012, Hvidberg et al. 2008). In 2006, the contaminated area (20,000 m²) was encapsulated by installing a 600 m long and 14 m deep steel sheet piling and a plastic membrane cap in order to prevent further leaching of toxins to the seawater (Fig. S1, (NorthPestClean 2014)). The Sheet piling is embedded in an impermeable clay layer at a depth of 14 meters. At a depth of 7.5 m below surface level is a silty clay layer with form a barrier to the vertical migration of the OP plume. The geology in the contaminated area consists of fine- to medium grained sand. Infiltration of precipitation for recharge of ground water in the containment is prevented by a plastic membrane and the water table in the enclosed area is controlled. The contaminant plume is located 4-8 meters below ground. The integrity of iron sheet piling guaranteed isolation of the plume at least to the year 2021 but is expected to last even much longer.

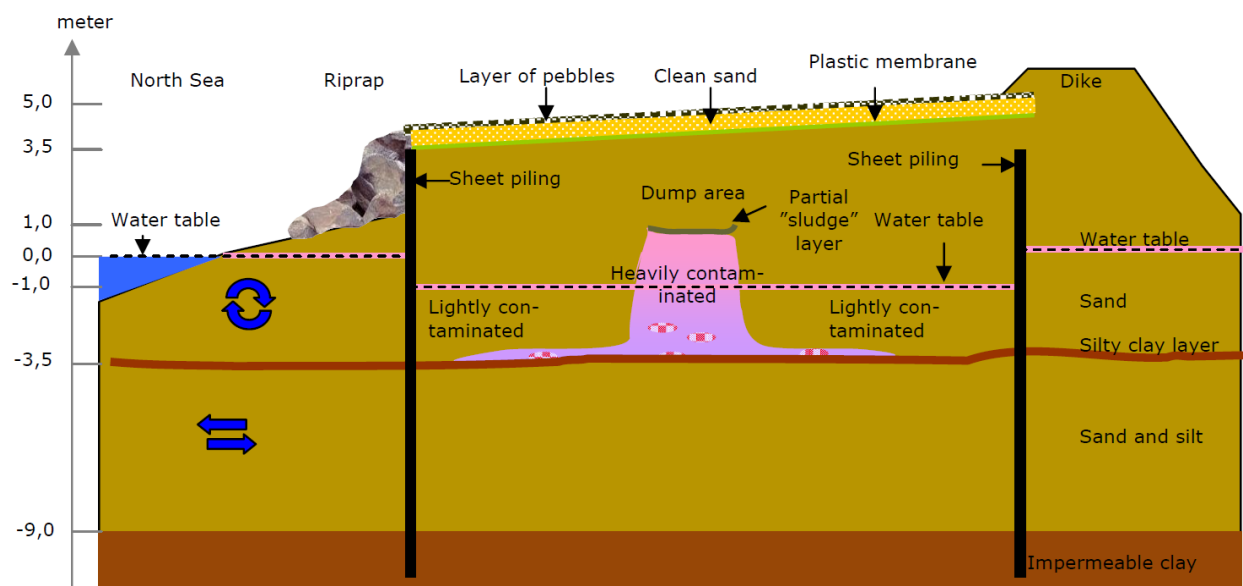


Fig. S1: Schematic profile of the geological situation and the containment (NorthPestClean 2014).

2. Tentative transformation products of parathion at field site

Tentative transformation products of parathion at field site were measured by GC-MS using the same methods as described below in section 5. The relative abundance and frequency of detection are listed in Table S1.

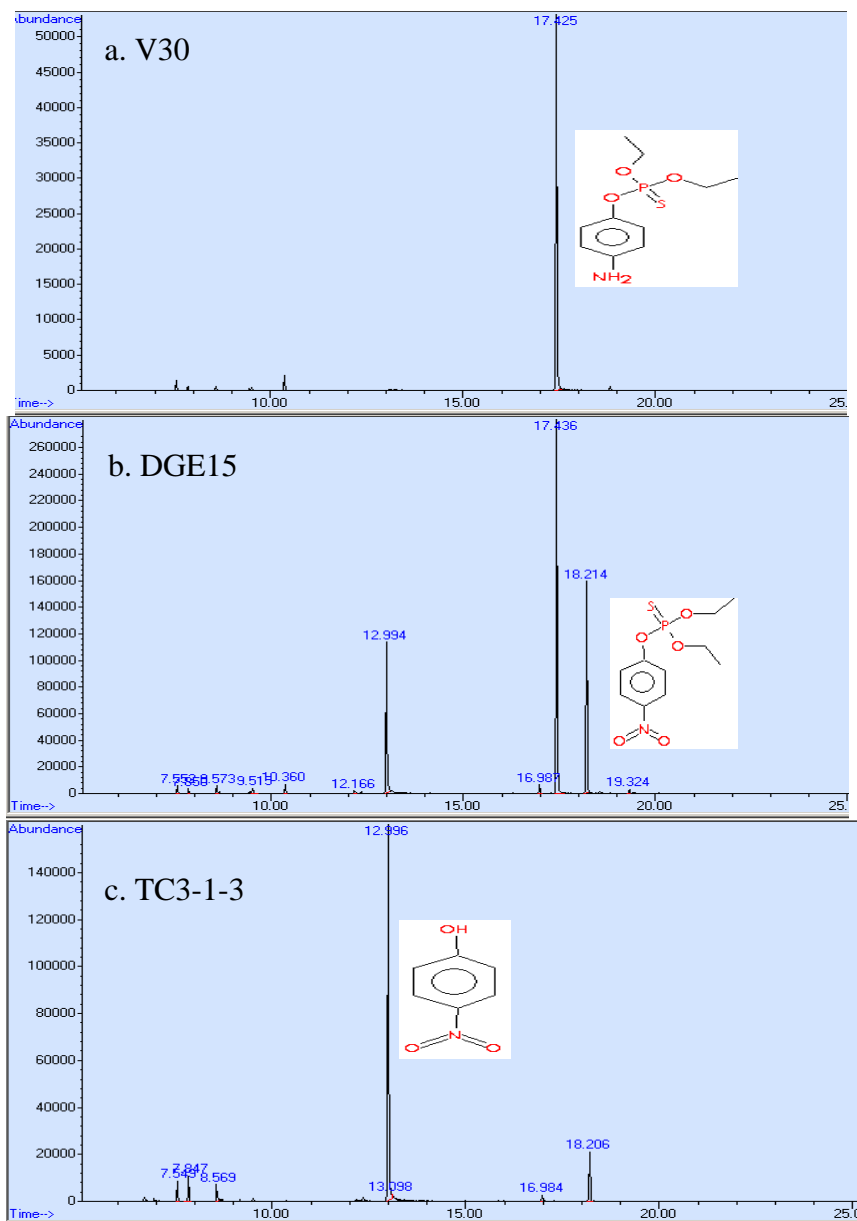


Fig. S2: GC-MS chromatography of major transformation products of parathion at the Groyne 42 site. The dominant peaks indicate *p*-nitrophenol (retention time at 12.994-12.996 min), aminoparathion (retention time at 17.425-17.436 min) and parathion (retention time at 18.206-18.214 min).

Table S1: The relative abundance and detection frequency of *p*-nitrophenol, aminoparathion and parathion in the field site samples. “+” indicates that the compound was detected; “++” indicates the relative more abundant compound as shown in Fig. S2.

Well ID	<i>p</i> -nitrophenol	aminoparathion	parathion
untreated area			
MB1-2		++	
MB4-1		++	
MB4-2		++	
MB5-1		++	

MB5-2		++	
T1-3-1		++	+
TP2-1-1		++	+
F5	++	+	+
V03-1		++	+
V03-2	++	+	+
DGE15	+	++	+
V05A	+	++	+
V30		++	
V81B	+	+	+
treated area			
TC3-1-1	++	++	+
TC3-1-2	++	+	
TC3-1-3	++		+
TC3-2-1	++		
TC3-2-2	++		
TC3-2-3	++		
TC3-3-1	++		
TC3-3-2	++		
TC3-3-3	++	+	+
TC3-6-1	++		
TC3-6-2	++		
TC3-6-3	++	+	+
TC3-7-1	++	+	
TC3-7-2		++	+
TC3-7-3	++	+	+
TC3-8-3	++	+	+
TC3-9-2	+	+	
TC3-9-3	++		+

3. Aerobic degradation of parathion

3.1. Enrichment for isolation of parathion-degrading bacteria

Soil samples were collected from nearby garden located in Gwal pahari (Gurgaon, Haryana), India. These soil samples were enriched into the microcosms prepared by amendment of soil along with mineral salt (MS) medium supplemented with technical grade parathion as sole carbon source. The MS medium was composed of (in g per liter): NaNO_3 , 3 g; KCl, 0.5 g; MgSO_4 , 0.5 g; FeSO_4 , 0.001g; K_2HPO_4 , 1g; KH_2PO_4 , 0.05g, as described elsewhere (Rokade and Mali 2013). For isolation of potential parathion degrading microbe(s), 10 g of microcosm soil sample, was enriched further into 100 mL of Erlenmeyer screw capped conical flask containing 50 mL MS medium which was pre-spiked with 34 μM parathion and homogenized overnight at 150 rpm, 25 °C. The flask was then incubated at 30 °C and 150 rpm in the dark. After 120 h incubation, 2.5 mL of culture broth from first enrichment cycle was further transferred to 50 mL of fresh prepared parathion-amended medium as described above for the next enrichment step, and 10 mL of culture liquid was extracted using 2 mL of DCM by shaking at 25 °C for 2 h followed by agitation of 150rpm to avoid soil partials. The DCM extract was then analyzed for the residual parathion concentration. After the 3rd enrichment cycle, aliquots of 100 μL culture broth were spread on MS medium agar plates

pre-spiked with 34 μM of parathion and the plates were incubated at 30 °C. Morphologically different colonies were picked and streaked till the purified colonies were obtained.

3.2. Screening and selection of parathion-degrading aerobic bacteria

The purified isolates were picked and cultured in MS medium supplemented with 34 μM parathion as sole carbon source. Incubation was done at 150 rpm and 30 °C in the dark. An aliquot of cell culture was withdrawn at late log phase and centrifuged at 8000 rpm at 4 °C for 10 min. The cell pellet was washed with freshly prepared MS medium to remove traces of parathion and re-suspended in 5 mL freshly prepared MS medium to use as starter culture for further experimental investigations. 1 mL of the pre-grown starter culture was transferred into 50 mL MS medium which was pre-spiked with 34 μM of parathion; the culture was subsequently incubated at 150 rpm and 30 °C in the dark. 10 mL of culture liquid was extracted and analyzed for the residual parathion concentration at different time intervals. Two isolates showing parathion-degrading capability named as TERI OP1 and TERI OP2 were selected for further investigation.

3.3. Aerobic degradation of parathion using selected isolates TERI OP1 and TERI OP2

Batch experiments were conducted in 500 mL flasks containing 250 mL MS medium for studying parathion degradation kinetics. In order to increase the production of biomass, cells were grown in 1000 mL of flasks containing 500 mL MS medium supplemented with 34 μM parathion, and then cells were harvested at 8000 rpm, 4 °C for 10 min. The cell pellet was washed with freshly prepared MS medium and re-suspended in around 7 ml of fresh MS medium. The cell suspension was used as starter culture for bath experiment for studying the isotope fractionation of parathion. Seven flasks containing 34 μM parathion-spiked MS medium were inoculated with 1 mL of bacterial cell suspension. Sterile control flasks were prepared by the same procedures except adding inoculum. All control and culture flasks were incubated at 150 rpm and 30 °C in the dark. At different time intervals, 1 mL culture broth was taken for optical density and pH variation measurement. Residual parathion and potential metabolites in the rest of the whole spent medium were extracted by 10 mL of DCM containing naphthalene (6.5 mg L⁻¹) as internal standard for further analysis.

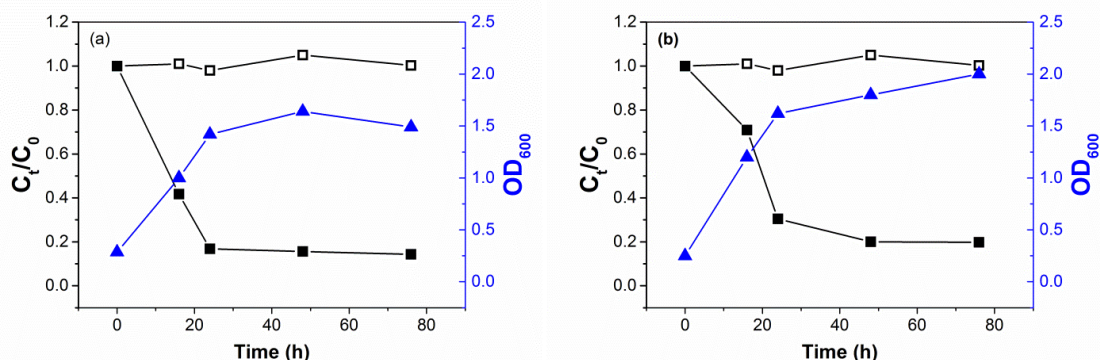


Fig. S3: Aerobic biodegradation experiments of parathion, showing the parathion degradation (solid squares), growth of strains (OD_{600} , solid triangles) and degradation in abiotic controls (open squares) during aerobic biodegradation by TERI OP1 (a) and TERI OP2 (b).

Analysis of results demonstrated that maximum parathion degradation by TERI OP1 and TERI OP2 was observed at 76 h. Further increase of parathion degradation was not observed with increase in incubation time beyond 76 h. Increasing of OD_{600} during incubation suggests that both aerobic strains can grow on parathion as the sole source of carbon (Fig. S3 a-b). After 76 h incubation, 86% and 80% of parathion were degraded in experiments using TERI OP1 (Fig. S3a) and TERI OP2 (Fig. S3b), respectively. No removal of parathion was observed in the abiotic control experiments, indicating parathion was not chemically hydrolyzed in the control during the experimental period.

3.4. Carbon and hydrogen isotope analysis of parathion during aerobic degradation

Extracted samples were further concentrated to about 300 μl under a gentle stream of N_2 to increase the concentration of parathion for carbon and hydrogen isotope analysis. The results of carbon and hydrogen isotope analysis of parathion are summarized in Table S2. Within more than 80% degradation of parathion, $\delta^{13}\text{C}$ changed from -28.1‰ to -27.9‰ and from -28.1‰ to -28.0‰ during incubation using TERI OP1 and TERI OP2, respectively. Considering the $\delta^{13}\text{C}$ analytical uncertainty of $\pm 0.5\text{‰}$, no carbon isotope enrichment was observed during aerobic degradation of parathion. Similar to carbon isotope fractionation, no significant hydrogen isotope enrichment was observed during aerobic degradation of parathion (Table S2) when considering the $\delta^2\text{H}$ analytical uncertainty of $\pm 5\text{‰}$. These results indicate that carbon and hydrogen isotope fractionation is not associated with the aerobic degradation of parathion by TERI OP1 and TERI OP2.

Table S2: Changes in carbon and hydrogen isotope compositions of parathion during aerobic degradation by TERI OP1 and TERI OP2.

Time (h)	OP1			OP2		
	C_t/C_0	$\delta^{13}\text{C}$ (‰)	$\delta^2\text{H}$ (‰)	C_t/C_0	$\delta^{13}\text{C}$ (‰)	$\delta^2\text{H}$ (‰)
0	1.00	-28.1 ± 0.2	-135 ± 4	1.00	-28.1 ± 0.1	-135 ± 1
16	0.42	-27.9 ± 0.2	-132 ± 3	0.71	-28.1 ± 0.1	-138 ± 0
24	0.17	-27.9 ± 0.2	-130 ± 1	0.30	-28.3 ± 0.2	-137 ± 1
48	0.16	-28.1 ± 0.2	-134 ± 1	0.20	-28.1 ± 0.2	-136 ± 1
76	0.14	-27.9 ± 0.1	-128 ± 1	0.20	-28.0 ± 0.3	-135 ± 1

4. Anaerobic degradation of parathion

4.1. Enrichment and selection of parathion-degrading microbes under anoxic conditions

Enrichment of anaerobic parathion degraders in the soil sample was carried out in MS medium as elaborated in section 3.1. However, in this case all the studies were performed under strictly anoxic conditions. MS medium as mentioned above was prepared under anaerobic condition as described elsewhere (Junghare et al. 2012), by simultaneous boiling for 10 min and purging with nitrogen flush to remove the dissolved oxygen. To this 0.1% of resazurin was added as redox indicator and L-cysteine HCL (2.5 %) was added as a reducing agent to maintain the anoxic conditions. The serum bottles were sealed with rubber septum and crimped with aluminium seal. Nitrate (3 g/L) was electron acceptor for the anaerobic degradation of parathion. Followed this nitrogen sparged medium bottles were autoclaved for 15 min for 121 °C. Following sterilization, 100 mL of anaerobic MS medium was spiked with 34 μM of parathion with the help of 1 mL syringe and subsequently homogenized overnight at 25 °C in a horizontal shaker at 150 rpm. Inoculated bottle were further incubated at 30 °C by shaking at 150 rpm. All the experiments were performed in anaerobic chamber (Bactron IV) under anoxic condition. The anaerobic gas chamber atmosphere consists of mixture of Nitrogen (90 %), hydrogen (5 %) and carbon dioxide (5 %) to maintain the oxygen free atmosphere.

Enriched broth was further plated out on MSM agar plates supplemented with 34 μM of parathion. Medium was prepared as mentioned in section 3.1 and plated out in anaerobic chamber. Volume of 100 μL enriched broth was transferred by 1 mL syringe to MS agar plates and spread out with the help of glass spreader. Anaerobic chamber was used to incubate the inoculated plates. After incubation at 30 °C, morphologically different colonies were picked and streaked further to isolate pure colonies. The purified anaerobic bacterial isolates were picked and cultured in anaerobically prepared MS medium spiked with 34 μM parathion as sole carbon source for monitoring their parathion degradation potential under anoxic condition. The protocols were followed as mentioned in section 3.2, except for the fact that these experiments were performed under anoxic conditions. One isolate showing best parathion-degrading capability named as TERI ANA-1 was selected for further investigation.

4.2 Anaerobic degradation of parathion using isolate TERI ANA-1

The inoculum was pre-grown in parathion (34 μM) pre-spiked agar plates at 30° C in the anaerobic chamber and then re-suspended in 10 mL of liquid MS medium prepared anaerobically as mentioned above. Degradation experiments were carried out in 500 mL bottles containing 250 ml anoxic MS medium by following the protocols as mentioned in section 3.3 except for the anoxic condition. Control experiment was set without adding any inoculum culture. No response for oxygen was observed by color change of resazurin during degradation experiment with the living culture.

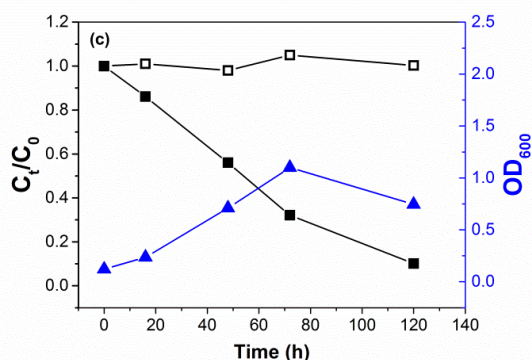


Fig. S4: Anaerobic biodegradation experiment of parathion, showing the parathion degradation (solid squares), growth of strains (OD_{600} , solid triangles) and degradation in abiotic controls (open squares) during anaerobic biodegradation by TERI ANA-1.

Increasing of OD_{600} during incubation suggests the anaerobic strain can grow on parathion as the sole source of carbon (Fig. S4). 90% degradation of parathion was achieved after 120 h incubation using TERI ANA-1 (Fig. S4). No removal of parathion was observed in anaerobic abiotic control experiment, indicating that parathion is biodegradable rapidly by the purified anaerobic strain.

4.3. Carbon and hydrogen isotope analysis of parathion during anaerobic degradation

The results of carbon and hydrogen isotope analysis of parathion of anaerobic degradation experiment are summarized in Table S3. The initial concentration of parathion was 34 μM . The concentration of the sterile control maintained stable at 34 μM . During the whole incubation period, $\delta^{13}\text{C}$ changed from -31.8‰ to -32.2‰ and $\delta^2\text{H}$ changed from -138‰ to -130‰ . Therefore, no detectable carbon and hydrogen isotope enrichment were observed when considering the analytical uncertainty of $\pm 0.5\text{‰}$ for $\delta^{13}\text{C}$ and $\pm 5\text{‰}$ for $\delta^2\text{H}$. Thus, there is no carbon and hydrogen isotope fractionation associated with the anaerobic degradation of parathion using TERI ANA-1.

Table S3: Changes in carbon and hydrogen isotope compositions of parathion during anaerobic degradation by TERI ANA-1.

Time (h)	C_t/C_0	$\delta^{13}\text{C}$ (‰)	$\delta^2\text{H}$ (‰)
0	1.00	-31.8 ± 0.1	-138 ± 1
16	0.86	-32.2 ± 0.5	-137 ± 2
48	0.56	-32.2 ± 0.5	-133 ± 2
72	0.32	-32.4 ± 0.2	n.m. ^a
120	0.10	-32.2 ± 0.2	-130 ± 1

^a n.m.: not measured.

5. Biodegradation mechanisms of parathion

Parathion and potential biodegradation metabolites were extracted as described above after 24 h incubation under aerobic conditions using strain TERI OP1 and TERI OP2, and after 72 h incubation under anoxic conditions using strain TERI ANA-1. An Agilent GC-MS (7890A-5975C) system was used to identify potential biodegradation metabolites of parathion. A DB-608 column (30 m × 0.32 mm × 0.5 µm, Agilent J&W, USA) was used for sample separation with helium flow of 1.5 mL min⁻¹ as the carrier gas. The GC oven was initially held at 60 °C for 2 min, and increased at 8 °C min⁻¹ to 280 °C, and then held for 2 min. 1 µL of sample was injected with a split ratio of 10:1 for each analysis. The tentative metabolites analyses suggested that p-nitrophenol was the initial reaction product under aerobic conditions using strain TERI OP2. Aminoparathion was detected under aerobic conditions using strain TERI OP1 and under anoxic conditions using strain TERI ANA-1 (data not shown). This may suggest that reduction of the nitro group may be a degradation mechanism and probably not leading to carbon or hydrogen isotope fractionation.

6. Half-life of parathion hydrolysis

Chemical hydrolysis of parathion follows pseudo-first-order kinetics within the accuracy of measurement. Half-life of the reactions conducted at pH < 7.8 under different conditions from different studies is listed in Table S4.

Table S4. Half-life of parathion hydrolysis at pH < 7.8 under different conditions.

T (°C)	pH	half-life (days)	reference
0	1-5	3000	(CES and IISc)
20	1-5	690	(CES and IISc)
20	7	130	(ATSDR 2017)
23	7.8	218	(Weber 1976)
25	5	133	(FAO 1990)
25	7	247	(FAO 1990)
30	1-5	180	(CES and IISc)
50	7.8	7.5	(Weber 1976)
60	2	2.9	(Wu et al. 2018)
60	5	3.0	(Wu et al. 2018)
60	7	3.1	(Wu et al. 2018)
70	7.8	1.3	(Weber 1976)
90	7.8	0.2	(Weber 1976)

7. References

- ATSDR (2017) Toxicological profile for parathion. Breysse, P.N. (ed), Agency for Toxic Substances and Disease Registry, Atlanta, Georgia.
- Bondgaard, M., Hvidberg, B. and Ramsay, L. (2012) Remediation of pesticide contamination by in situ alkaline hydrolysis - a new soil remediation technology, Monterey, California.
- CES and IISc Parathion <http://wgbis.ces.iisc.ernet.in/energy/HC270799/HDL/ENV/enven/vol356.htm>, Centre for Ecological Sciences, Bangalore, India.
- FAO (1990) Parathion (58), Food and Agriculture Organization of the United Nations.
- Hvidberg, B., Ramsay, L., Kirkegaard, C., Elkjær, L., Jorgensen, C., Oberender, A. and Kiilerich, O. (2008) Remediation technologies for a large pesticide-contaminated site: enclosure, alkaline hydrolysis and bioventing.

- Junghare, M., Subudhi, S. and B., L. (2012) Improvement of hydrogen production under decreased partial pressure by newly isolated alkaline tolerated anaerobe, *Clostridium butyricum* TM9A: optimization of process parameters. *Int. J. Hydrogen. Energ.* 4(37), 3160-3168.
- NorthPestClean (2014) Layman reports 2: Demonstration of in situ alkaline hydrolysis as a novel soil remediation technique for a pesticide contamination, Central Denmark Region, Department of Environment, <http://www.eng.northpestclean.dk/publications/layman-reports/>.
- Rokade, K.B. and Mali, G.V. (2013) Biodegradation of chlorpyrifos by *Pseudomonas desmolyticum* NCIM 2112. *Int. J Pharm. Bio. Sci.* 2(4), (B) 609 - 616.
- Weber, K. (1976) Degradation of parathion in seawater. *Water Res.* 10(3), 237-241.
- Wu, L., Chladkova, B., Lechtenfeld, O.J., Lian, S., Schindelka, J., Herrmann, H. and Richnow, H.H. (2018) Characterizing chemical transformation of organophosphorus compounds by (¹³C and (²H) stable isotope analysis. *Sci. Total. Environ.* 615, 20-28.

Appendix 6.8.

Carbon and hydrogen stable isotope analysis for characterizing the chemical degradation of tributyl phosphate

Published paper: *Liu, J.; Wu, L.; Kümmel, S.; Yao, J.; Schaefer, T.; Herrmann, H.; Richnow, H. H., Chemosphere 2018, 212, 133-142.*



Carbon and hydrogen stable isotope analysis for characterizing the chemical degradation of tributyl phosphate

Jia Liu ^{a, b, 1}, Langping Wu ^{b, 1}, Steffen Kümmel ^b, Jun Yao ^c, Thomas Schaefer ^d, Hartmut Herrmann ^d, Hans-Hermann Richnow ^{b, c, *}

^a School of Energy and Environmental Engineering, University of Science and Technology Beijing, Xueyuan Road No.30, Haidian District, Beijing 100083, PR China

^b Department of Isotope Biogeochemistry, Helmholtz Centre for Environmental Research-UFZ, Permoserstraße15, Leipzig 04318, Germany

^c School of Water Resources and Environment, China University of Geosciences (Beijing), Xueyuan Road No.29, Haidian District, Beijing 100083, PR China

^d Atmospheric Chemistry Department (ACD), Leibniz Institute for Tropospheric Research (TROPOS), Permoserstraße15, Leipzig 04318, Germany

HIGHLIGHTS

- Quantification of ²H and ¹³C isotope enrichment factors of TBP.
- Comparison of isotope fractionation patterns upon hydrolysis and radical oxidation.
- Characterizing the C–O, C–H bond cleavage of TBP using apparent kinetic isotope effect.

ARTICLE INFO

Article history:

Received 6 April 2018

Received in revised form

6 August 2018

Accepted 8 August 2018

Available online 10 August 2018

Handling Editor: J. de Boer

Keywords:

Tributyl phosphate

Isotope fractionation

Hydrolysis

Radical oxidation

Apparent kinetic isotope effect

ABSTRACT

Tributyl phosphate (TBP) belongs to the group of trialkyl substituted organophosphate esters. Its chemical reactivity depends on the stability of various chemical bonds. TBP was used as a model compound for the development of a concept using stable isotope fractionation associated with bond cleavage reactions for better understanding the fate of TBP in the environment. Carbon isotope enrichment factors (ϵ_C) of TBP hydrolysis were found to be pH dependent ($-3.8 \pm 0.3\%$ at pH 2, $-4.6 \pm 0.5\%$ at pH 7, $-2.8 \pm 0.1\%$ at pH 9, no isotope fractionation at pH 12), which is in accordance with the mode of a S_N2 hydrolytic bond cleavage. Hydrogen isotope fractionation was negligible as no H bond cleavage is involved during hydrolysis. The apparent carbon kinetic isotope effect ($AKIE_C$) ranged from 1.045 to 1.058. In contrast to hydrolysis, both carbon and hydrogen isotope fractionation were observed during radical oxidation of TBP by $\cdot OH$ and $SO_4^{\cdot -}$, yielding ϵ_C from $-0.9 \pm 0.1\%$ to $-0.5 \pm 0.1\%$ and ϵ_H from $-20 \pm 2\%$ to $-11 \pm 1\%$. $AKIE_C$ and $AKIE_H$ varied from 1.007 to 1.011 and from 1.594 to 2.174, respectively. The correlation of ²H and ¹³C isotope fractionation revealed Δ values ranging from 17 ± 1 to 25 ± 6 . Results demonstrated that the correlation of ²H and ¹³C isotope fractionation of TBP allowed to identify radical reactions and to distinguish them from hydrolysis. The presented dual isotope analysis approach has diagnostic value for characterizing the chemical transformation of TBP in the environment.

© 2018 Elsevier Ltd. All rights reserved.

1. Introduction

Tributyl phosphate (TBP) is an organophosphorus compound widely used as flame retardant, plasticiser, anti-foamer, component

of herbicides and hydraulic fluids (Regnery et al., 2011). In addition, it was extensively used as a solvent for plutonium/uranium redox extraction (PUREX) for nuclear fuel reprocessing (Mincher et al., 2008). The production of commercially used TBP is about 3000–5000 tons/year in Europe (Nancharaiyah et al., 2015). Due to its extensive use, TBP is frequently detected in the aquatic environment of many countries, including Germany (Fries and Püttmann, 2003; Regnery and Püttmann, 2010), Austria (Martinez-Carballo et al., 2007), Italy (Bacaloni et al., 2008), Spain (Rodil et al., 2012), Korea (Lee et al., 2016), and China (He et al., 2014; Shi et al., 2016).

* Corresponding author. Department of Isotope Biogeochemistry, Helmholtz Centre for Environmental Research-UFZ, Permoserstraße15, Leipzig 04318, Germany.

E-mail address: hans.richnow@ufz.de (H.-H. Richnow).

¹ Dual-first authorship: the two authors have contributed equally to this work.

TBP can inhibit the enzyme acetylcholine esterase (AChE), resulting in cholinergic toxicity of the autonomic system and can thus lead to respiratory paralysis and even death (Bergman et al., 2012; Greget et al., 2016). Given these adverse effects, TBP has been an environmental concern for decades, especially in aquatic systems. The main degradation pathways are hydrolysis, indirect photo-oxidation or microbial degradation (Berne et al., 2005; Watts and Linden, 2009; Nanchaiah et al., 2015; Su et al., 2016). These are probably the key processes how TBP is degraded or attenuated in the environment. Direct chemical oxidation is effective for the removal of organic contaminants in waste water. In particular, chemicals, such as hydrogen peroxide, persulfate, permanganate and ozone, have been applied for *in situ* chemical oxidation (ISCO) for the treatment of subsurface TBP or similar contamination (Watts and Teel, 2006). Hydroxyl radicals ($\cdot\text{OH}$) are an effective oxidant with redox potential of 1.7–2.8 V and are frequently used for wastewater remediation (Waclawek et al., 2017). Similar to $\cdot\text{OH}$, the sulfate radical ($\text{SO}_4^{\cdot-}$) with a redox potential of 2.5–3.1 V is efficient for the oxidation of many organic compounds (Neta et al., 1988). $\text{SO}_4^{\cdot-}$ can be generated for example from peroxydisulfate ($\text{S}_2\text{O}_8^{2-}$, PS) or peroxymonosulfate (HS_2O_5) salts by the activation of the persulfate anion ($\text{S}_2\text{O}_8^{2-}$, $E_0 = 2.01$ V) using light (Herrmann, 2007; Yang et al., 2017) or heat (House, 1962; Liang and Su, 2009). Over the past ten years, considerable attention has been paid to potassium peroxydisulfate (KPS) because of its lower cost compared to H_2O_2 or O_3 and the high efficiency for organic mineralization (Lau et al., 2007; Waclawek et al., 2017).

Conventionally, degradation pathways are chemically analyzed by measuring the concentrations decrease of reactants and the appearance of degradation products. However, this approach often has large uncertainties in field studies because of the influence of physical processes (such as dilution, volatility and sorption), the challenges of detecting unknown products and the difficulties to establish mass balances. As an alternative technology, compound specific isotope analysis (CSIA) making use of isotope fractionation processes of degradation reactions can be used for the qualitative characterisation and quantitative estimation of processes involved in organic compound degradation in the environment. This technique is becoming a routine and practical approach in biogeochemistry and environmental science (Elsner, 2010; Thullner et al., 2012; Nijenhuis and Richnow, 2016; Vogt et al., 2016).

For better understanding of the transformation mechanisms, the kinetic isotope effect (KIE) based on chemical bond change reactions can be analyzed. The KIE characterizes the rate limitation of a bond change reaction posed by isotopologues. The rate limitation is equivalent to the stability of heavy and light isotope substituted bonds and characterizes the transition state of a chemical reaction (Northrop, 1981; Wolfsberg et al., 2009). The apparent kinetic isotope effect (AKIE) can be calculated to normalize the isotope enrichment factor (ϵ) for non-reacting positions and intermolecular competition to compensate for “dilution” of the isotope composition in reacting isotopologues. The AKIE can be used to compare the kinetic isotope effect of bond cleavage reactions of different molecules. Multi-element isotope fractionation analysis correlating the isotope fractionation of two (or more) elements can be used to evaluate the degradation pathways (Gray et al., 2002; Elsner et al., 2005). Previous studies demonstrated the potential use of stable isotope fractionation for characterizing the transformation mechanisms of organophosphorus compounds, such as dichlorvos, dimethoate, methyl parathion, parathion and tris(2-chloroethyl) phosphate (Wu et al., 2014, 2017, 2018a).

In the present study, we systematically examined the carbon and hydrogen isotope fractionation upon hydrolysis of TBP under acidic, neutral and alkaline conditions to characterise the reaction

pathways. The isotope fractionation patterns of TBP by radical oxidation ($\text{SO}_4^{\cdot-}$ and $\cdot\text{OH}$) were also examined. The objectives of this study were to (1) investigate the kinetic reaction rate constant k_{obs} of hydrolysis and radical oxidation; (2) characterise the stable carbon and hydrogen isotope fractionation of TBP during hydrolysis and radical oxidation; (3) distinguish different mechanisms by using the AKIE values and correlating ^2H and ^{13}C isotope fractionation to obtain Δ values, which may be used diagnostically for tracing TBP degradation in the field.

2. Materials and methods

A detailed description of the analytical methods is provided in the [Supplementary Information \(SI\)](#).

2.1. Chemicals

All chemicals were of analytical grade quality and used without further purification. Tributyl phosphate (TBP, 99% purity) and dibutyl phthalate (DBP, >99% purity) were purchased from Xiya Company (China). Dichloromethane (DCM) was supplied by Carl Roth GmbH + Co. KG (Karlsruhe, Germany). Potassium peroxydisulfate ($\text{K}_2\text{S}_2\text{O}_8$), hydrogen peroxide (30% H_2O_2), di-potassium hydrogen phosphate (K_2HPO_4), potassium dihydrogen phosphate (KH_2PO_4), sodium hydrogen carbonate (NaHCO_3), sodium hydrate (NaOH), and disodium hydrogen phosphate (Na_2HPO_4) were supplied by Merck (Guaranteed reagent quality, Darmstadt, Germany). Solutions and pH buffers were prepared in ultrapure water obtained by a Milli-Q System (Millipore GmbH, Germany).

2.2. Hydrolysis and radical oxidation experiments

The following buffer solutions were used to obtain hydrolysis at different pH conditions: KCl–HCl (50 mM for pH 2), K_2HPO_4 – KH_2PO_4 (100 mM for pH 7), NaHCO_3 – NaOH (45.5 mM for pH 9), and Na_2HPO_4 – NaOH (32.5 mM for pH 12).

Hydrolysis experiments: TBP is hydrolyzed with very slow reaction rates at room temperature under neutral to acidic conditions but rapidly hydrolyzed under strong alkaline condition (Su et al., 2016). In order to adjust the hydrolysis rates in the same order of magnitude for a better comparison of the isotope fractionation patterns associated with different reaction pathways, hydrolysis experiments were carried out at 80 °C to accelerate the hydrolysis rate at pH 2, pH 7 and pH 9, respectively. Hydrolysis experiments at pH 12 were performed at 35 °C to slow down the reaction. All experiments were conducted in 40 mL buffer solutions in 150-mL serum bottles with 100 mg L⁻¹ TBP as initial concentration. At different time intervals, the reaction solutions were extracted by adding 1 mL DCM containing 1000 mg L⁻¹ DBP as internal standard and shaking for at least 4 h at 10 °C. Extracts were stored at 4 °C prior to analysis. The extraction recovery and effect of the extraction procedure on carbon and hydrogen isotope signature were evaluated as described in [Section 3 of the Supplementary Information](#).

Potassium peroxydisulfate (KPS) oxidation: For KPS oxidation experiments a molar ratio of TBP to KPS of 1:20 was used. The KPS oxidation reaction was not conducted at pH 2 due to the exclusive formation of secondary radicals and complicating subsequent reactions. At pH 2, the $\text{SO}_4^{\cdot-}$ reacts exclusively with the Cl^- from the HCl/KCl buffer to produce a Cl atom, which will subsequently react to form $\text{Cl}_2^{\cdot-}$, a dichloride radical anion (Herrmann, 2003). Therefore, the KPS oxidation reactions were only conducted at pH 7, pH 9 and pH 12, respectively. The initial concentration of TBP was 100 ppm. Buffer solutions with different pH values were prepared as described above. All KPS oxidation reactions were carried out at

35 °C. Control experiments were carried out without the addition of KPS. Remaining TBP was extracted and analyzed as described in the hydrolysis experiment.

UV/H₂O₂ oxidation experiment: Photolysis experiments were carried out at pH 7 in phosphate buffer with 200 mg L⁻¹ initial TBP concentration. Irradiation was achieved by a 150 W xenon lamp (Type no. L2175, Hamamatsu, Japan), which covered a broad continuous spectrum from 185 nm to 2000 nm. A long-pass filter with a cut-off of short UV wavelengths below 280 nm (20CGA-280, Newport Corporation, Irvine, U.S.) was applied. Direct photolysis is not expected at the applied UV wavelengths due to the almost negligible photon absorption by TBP (Watts and Linden, 2009). The molar ratio of TBP to H₂O₂ was 1:5. In order to investigate the effects of buffer solution concentrations and reaction rates on the isotope fractionation of TBP, three experiments were carried out in 100 mM buffer solution at 20 °C (UV/H₂O₂_1), 100 mM buffer solution at 15 °C (UV/H₂O₂_2) and 10 mM buffer solution at 15 °C (UV/H₂O₂_3), respectively. 100 mM buffer solution was applied to make sure that the pH will remain stable at 7 during the reaction. Lower buffer concentration of 10 mM was applied to minimize the formation of the secondary radicals (SI, section 5). The experiments were conducted at different temperature of 20 °C and 15 °C to slow down the reaction rate. For direct photolysis, experiments were conducted under the same conditions but without the addition of H₂O₂ in a 100 mM buffer solution at 20 °C. Dark control experiments were conducted under identical experimental conditions without UV exposure (100 mM buffer solution). More information on the experimental setup of the UV degradation experiments are described elsewhere (Zhang et al., 2016). The transformation products of TBP in UV/H₂O₂ experiments were tentatively characterized by a Fourier-transform ion cyclotron resonance mass spectrometer (FT-ICR MS, Solarix XR 12T, Bruker Daltonics), the analytical procedures were described in SI.

2.3. Data analysis

Isotope ratios were expressed as delta notation (δ^hE) in parts per thousand (‰) based on Eq. [1]. Here, R_{sample} is the ratio of the heavy (hE) to the light isotopes (lE) of a sample and R_{ref} corresponds to the ratio of the respective isotopes of reference. For stable carbon isotope analyses the Vienna Pee Dee Belemnite (V-PDB) is used as reference, whereas for stable hydrogen isotope analyses the Vienna Standard Mean Ocean Water (V-SMOW) is applied (Coplen, 1996).

$$\delta^hE = \left(\frac{R_{sample}}{R_{ref}} - 1 \right) = \left(\frac{h_E/l_E}{h_{Eref}/l_{Eref}} - 1 \right) \quad [1]$$

The isotope enrichment factor (ϵ_E) can be determined from the logarithmic form of the Rayleigh equation, as shown in Eq. [2] (Rayleigh, 1896; Elsner, 2010). The variables δ^hE_t and δ^hE_0 are the isotope compositions of a compound for the element E at time t and time zero, respectively, and f is the residual substrate fraction. The changes in concentration during the reaction (C_t/C_0) can be related to the changes in isotope composition by ϵ_E .

$$\ln \left(\frac{\delta^hE_t + 1}{\delta^hE_0 + 1} \right) = \epsilon_E \cdot \ln f = \epsilon_E \cdot \ln \left(\frac{C_t}{C_0} \right) \quad [2]$$

The AKIE_E value of the bond cleavage at the reactive position can be calculated with Eq. [3], where n is the total number of atoms for element E in the molecule, x is the number of reactive sites, and z is the number of indistinguishable reactive sites (Elsner et al., 2005). The normalisation of AKIE_E corrects the bulk isotope enrichment for non-reactive positions and the intramolecular isotopic

competition.

$$AKIE = \frac{1}{1 + \frac{n}{x} \times z \times \epsilon} \quad [3]$$

Assuming that two processes (process 1 and 2) are reacting with the same substrate simultaneously and both processes follow first-order kinetics, the contribution of the individual processes in the mixed reaction can be estimated by an extended Rayleigh-type equation using the individual isotope enrichment factors of the particular reaction (ϵ_1 and ϵ_2). The observable ϵ_i of the mixed reaction and the ϵ_1 and ϵ_2 of the individual pathway 1 and 2 are needed for this calculation. The rate ratio of two competing degradation pathways (F) can be calculated by Eq. (4) (Van Breukelen, 2007), indicating the isotope fractionation contributed by pathway 1 to the observed ϵ_i .

$$F = \frac{\epsilon_i - \epsilon_2}{\epsilon_1 - \epsilon_2} \quad [4]$$

3. Results

3.1. Effects of extraction on isotope signature

The recovery of the liquid/liquid DCM extraction method was $91.2 \pm 10.2\%$ (Fig. S2 (a)). The isotope shifts of TBP before and after DCM extraction were 0.05–0.65‰ for $\delta^{13}C$, and 1–4‰ for δ^2H (Fig. S2 (b)), respectively. Considering the analytical uncertainty of carbon and hydrogen isotope compositions, which is $< \pm 0.5\%$ and $< \pm 5\%$, respectively, carbon and hydrogen isotope shifts due to the extraction process are insignificant. A detailed description was provided in SI, section 3.

3.2. Isotope fractionation of TBP during hydrolysis

The degradation curves and changes in carbon and hydrogen isotope compositions of TBP are illustrated in Fig. 1, and the obtained k_{obs} and ϵ values for TBP hydrolysis are summarized in Table 1. All hydrolysis experiments followed pseudo-first order kinetics with R^2 better than 0.97, alkaline conditions resulted in higher reaction rates compared to neutral and acidic conditions (pH 12 > pH 9 > pH 7 \approx pH 2) (Table 1). The stable carbon isotope enrichment could be quantified by the Rayleigh equation. At pH 2, 90% degradation was achieved within 1236 h, resulting in a carbon enrichment factor (ϵ_C) of $-3.8 \pm 0.3\%$. 88% degradation was achieved within 1140 h at pH 7, yielding an ϵ_C of $-4.6 \pm 0.5\%$. 94% degradation was achieved within 864 h and yielding an ϵ_C of $-2.8 \pm 0.1\%$ at pH 9. At pH 12, 80% degradation was achieved after 1464 h and no carbon enrichment was observed. Hydrogen isotope fractionation was not observed in all hydrolysis experiments (Fig. 1).

3.3. Isotope fractionation of TBP during KPS oxidation

The degradation curves and changes in carbon and hydrogen isotope compositions of TBP are illustrated in Fig. 2, and the corresponding k_{obs} and ϵ values are summarized in Table 1. All oxidation experiments followed pseudo-first order kinetics and the k_{obs} values decreased with increasing pH (Table 1). The stable carbon and hydrogen isotope fractionation could be quantified by the Rayleigh equation. About 95% TBP was degraded within 292 h at pH7/KPS, resulting in a $\epsilon_C = -0.9 \pm 0.1\%$ and $\epsilon_H = -16 \pm 2\%$, respectively. At pH9/KPS, 95% degradation was achieved within 332 h, yielding an ϵ_C of $-0.8 \pm 0.1\%$ and an ϵ_H of $-20 \pm 2\%$. At

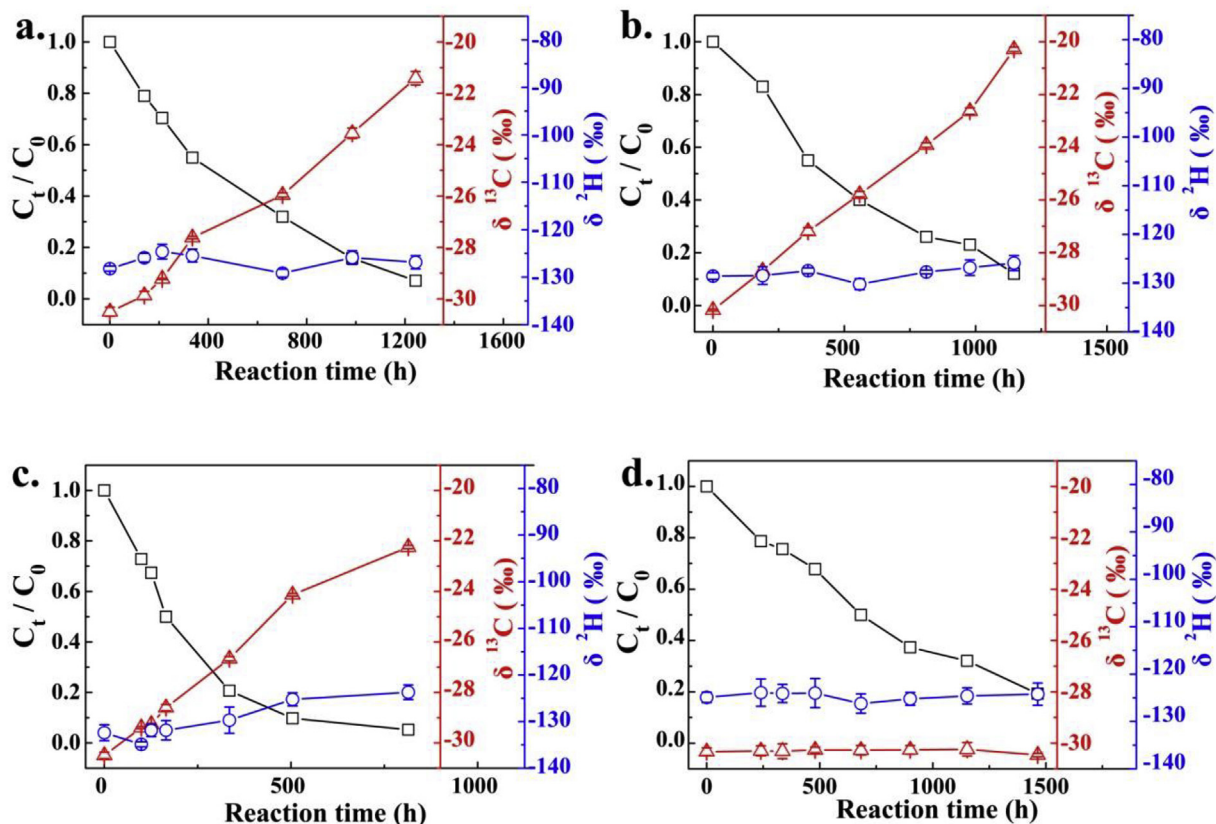


Fig. 1. TBP degradation via hydrolysis at (a) pH 2, (b) pH 7, (c) pH 9, and (d) pH 12. Changes in concentrations (C_t/C_0 , black squares) are correlated with the changes of the carbon ($\delta^{13}\text{C}$, red triangles) and hydrogen isotope ratios ($\delta^2\text{H}$, blue circles). (For interpretation of the references to colour in this figure legend, the reader is referred to the Web version of this article.)

Table 1
Pseudo-first order kinetic rate constants (k_{obs}), isotope enrichment factors (ϵ), AKIE and Λ values obtained from the hydrolysis and the radical oxidation of TBP at different pH.

Conditions	k_{obs} ($\times 10^{-3}\text{h}^{-1}$)	Temp. °C	TBP:oxidant molar ratio	Major radicals	$\Delta\delta^{13}\text{C}^h$ (‰)	$\Delta\delta^2\text{H}^h$ (‰)	ϵ_C (‰)	R^2_C	ϵ_H (‰)	R^2_H	AKIE _C	AKIE _H	Λ	R^2_Λ
Hydrolysis														
pH 2	2.0 ± 0.3^a	80			9.1		-3.8 ± 0.3	0.990	n.d. ^b		1.048 ± 0.004	n.c. ^c	n.d.	
pH 7	1.8 ± 0.2	80			9.9		-4.6 ± 0.5	0.990	n.d.		1.058 ± 0.007	n.c.	n.d.	
pH 9	4.0 ± 0.5	80			8.3		-2.8 ± 0.1	0.997	n.d.		n.c.	n.c.	n.d.	
pH 12	1.1 ± 0.2	35					n.d.		n.d.		n.c.	n.c.	n.d.	
Radical oxidation														
pH7/KPS	10.4 ± 0.4	35	1:20	SO_4^-	2.7	52	-0.9 ± 0.1	0.986	-16 ± 2	0.987	1.011 ± 0.001	1.761 ± 0.167	17 ± 1	0.996
pH9/KPS	8.8 ± 1.1	35	1:20	SO_4^- , $\cdot\text{OH}$	2.1	51	-0.8 ± 0.1	0.989	-20 ± 2	0.991	1.010 ± 0.001	2.174 ± 0.255	23 ± 1	0.990
pH12/KPS	5.5 ± 0.3	35	1:20	$\cdot\text{OH}$	1.1	21	-0.5 ± 0.1	0.980	-11 ± 1	0.993	n.c.	n.c.	19 ± 1	0.991
^d pH7/UV/ H_2O_2 _1	474.2 ± 11.4	20	1:5	$\cdot\text{OH}$	2.4	38	-0.8 ± 0.1	0.995	-14 ± 1	0.993	1.010 ± 0.001	1.608 ± 0.070	17 ± 1	0.996
^e pH7/UV/ H_2O_2 _2	27.9 ± 2.4	15	1:5	$\cdot\text{OH}$	1.3	23	-0.6 ± 0.3	0.928	-13 ± 3	0.985	1.007 ± 0.004	1.610 ± 0.209	19 ± 7	0.956
^e pH7/UV/ H_2O_2 _3	6.8 ± 0.5	15	1:5	$\cdot\text{OH}$	1.6	40	-0.6 ± 0.2	0.972	-17 ± 7	0.983	1.007 ± 0.004	1.761 ± 0.418	25 ± 6	0.994
^f pH7/UV/ H_2O_2 -ave.							-0.7 ± 0.1^f		-15 ± 2^f				20 ± 4^f	
^g average							-0.7 ± 0.1^g		-16 ± 3^g				20 ± 4^g	

^a “±” indicates the 95% confidence interval.

^b “n.d.” is short for not detected.

^c “n.c.” is short for not calculated.

^d The distance between the photo-reactor and light source was 13 cm.

^e The distance between the photo-reactor and light source was 22 cm.

^f Average values of ϵ and Λ for UV/ H_2O_2 experiment, calculating from the three individual UV/ H_2O_2 experiments.

^g Average values of ϵ and Λ for radical oxidation of TBP, calculating from all individual radical oxidation experiments except pH 12/KPS.

^h Isotope shifts of the $\delta^{13}\text{C}$ and $\delta^2\text{H}$ values from the first and last sampling points during the degradation period.

pH12/KPS, TBP was depleted to 90% within 400 h, corresponding to an $\epsilon_C = -0.5 \pm 0.1\%$ and $\epsilon_H = -11 \pm 1\%$. No degradation took place

in control experiments except for pH12/KPS (Fig. S2). Due to the hydrolysis at pH 12, 35% of TBP was degraded within 400 h.

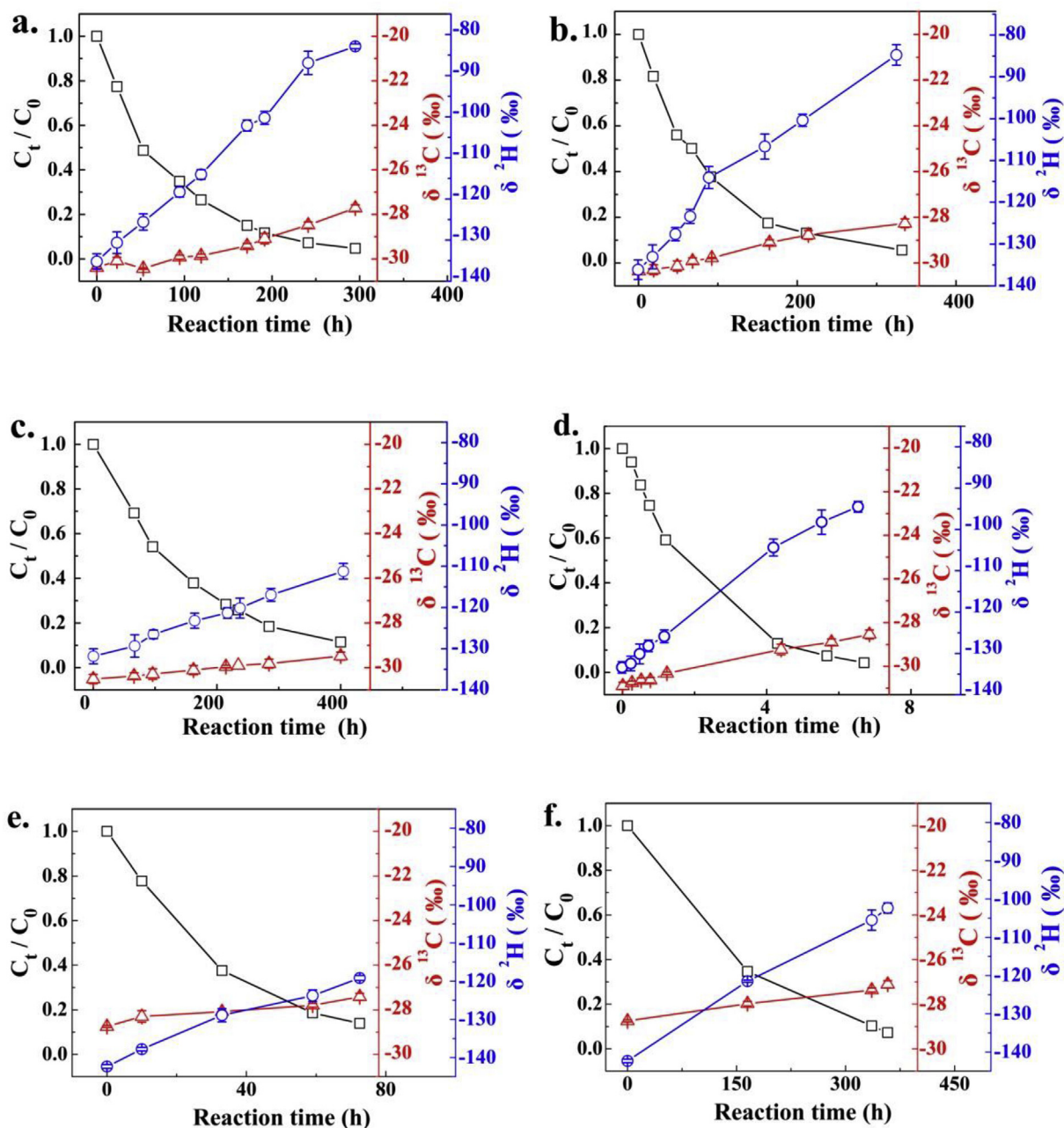


Fig. 2. TBP degradation via radical oxidation. Reaction conditions were as follows: (a) pH7/KPS; (b) pH9/KPS; (c) pH12/KPS; (d) UV/H₂O₂_1; (e) UV/H₂O₂_2; (f) UV/H₂O₂_3. Changes in concentrations (C_t/C_0 , black squares) are correlated with changes of the carbon ($\delta^{13}\text{C}$, red triangles) and hydrogen isotope ratios ($\delta^2\text{H}$, blue circles). (For interpretation of the references to colour in this figure legend, the reader is referred to the Web version of this article.)

3.4. Isotope fractionation of TBP during UV/H₂O₂ oxidation

Degradation curves and changes in carbon and hydrogen isotope compositions of TBP are illustrated in Fig. 2. All experiments followed pseudo-first order kinetics, and the k_{obs} values ($\times 10^{-3} \text{ h}^{-1}$) were 474.2 ± 11.4 in UV/H₂O₂_1, 27.9 ± 2.4 in UV/H₂O₂_2 and 6.8 ± 0.5 in UV/H₂O₂_3, respectively (Table 1). All coefficients of determination (R^2) were larger than 0.99. In the experiment UV/H₂O₂_1, 96% TBP was degraded within 6.7 h, yielding a ϵ_C of $-0.8 \pm 0.1\text{‰}$ and ϵ_H of $-14 \pm 1\text{‰}$. In the degradation experiment UV/H₂O₂_2, 85% TBP was depleted in 72.5 h, resulting in a ϵ_C of $-0.6 \pm 0.3\text{‰}$ and ϵ_H of $-13 \pm 3\text{‰}$. In the degradation experiment

UV/H₂O₂_3, 93% TBP was transformed within 385 h, and an ϵ_C of $-0.6 \pm 0.2\text{‰}$ and ϵ_H of $-17 \pm 7\text{‰}$ were obtained. In the control experiment without H₂O₂ employing the conditions used in UV/H₂O₂_1, no significant change of the TBP concentration was observed (Fig.S2 d), suggesting that direct photolysis did not take place during these experiments.

3.5. Analysis of transformation products of TBP in the UV/H₂O₂ experiment

Three potential transformation products were tentatively characterized as di-*n*-butylphosphate (P1), keto-tri-butylphosphate

(P2), and hydroxy-tri-butylphosphate (P3) (Table S1 and Fig. S3). The detailed information of characterized transformation products is given in the SI, section 7. The precise position of the hydroxyl or keto group at the side chain of the TBP molecule could not be confirmed, however, it is likely that the functional group is formed by radical attack at the sub-terminal carbon of the butyl chain.

3.6. Two dimensional isotope fractionation (C–H)

In order to explore the diagnostic potential of two dimensional isotope fractionation analysis, the hydrogen and carbon isotope fractionation were plotted to obtain Δ values ($\Delta = \frac{\Delta^2H}{\Delta^{13}C} \approx \frac{\epsilon_H}{\epsilon_C}$, $\Delta^{13}C = \delta_f^{13}C - \delta_0^{13}C$, $\Delta^2H = \delta_f^2H - \delta_0^2H$). However, due to the absence of hydrogen isotope fractionation Δ could not be defined for hydrolysis. The radical oxidation of TBP under pH7/KPS, pH9/KPS and pH12/KPS conditions resulted in Δ values of 17 ± 1 , 23 ± 1 , 19 ± 1 , respectively (Table 1). The reactions of TBP by UV/H₂O₂ (dominant \bullet OH reaction, described in SI, section 5) yielded an average Δ value of 20 ± 4 (Table 1), which is statistically identical with the ones obtained from KPS oxidation experiments. The two dimensional isotope fractionation analysis of all radical oxidation experiments including SO₄^{•−} and \bullet OH gave an average Δ value of 20 ± 4 (Table 1).

4. Discussion

4.1. Insight of the isotope fractionation during hydrolysis

A previous study proposed two hydrolysis pathways of organophosphorus compounds (OPs) (Fig. 3a and b): the first one is OH[−] or H₂O attacks the phosphorus atom; the second one is H₂O attacks the carbon atom (Wu et al., 2006). The acid-catalysed hydrolysis of esters mainly proceeds via an A_{AC}2 mechanism suggesting an acyl-oxygen fission (AC) in a bimolecular reaction (Day and Ingold, 1941). For instance, under acidic and neutral conditions, trimethyl phosphate may lead to a C–O bond split as demonstrated in experiments with ¹⁸O-labelled water as indicator (Blumenthal and Herbert, 1945). Consequently, the C–O bond cleavage leads to carbon isotope fractionation of TBP. At high pH (e.g., pH > 10), OH[−] attacks the phosphorus atom through simple nucleophile displacement (S_N2-type) leading to a P–O bond cleavage (Wanamaker et al., 2013). The reaction may proceed via a two-step addition-elimination pathway involving a pentacoordinate intermediate, such as TS1 and TS2 (Fig. 3b) (Kirby et al., 2013). The observed negligible carbon and hydrogen isotope fractionation of TBP at pH 12 highly supports a P–O bond split.

At pH 9, the observed carbon isotope fractionation of TBP provided evidence for a C–O bond split. However, the ϵ_C value at pH 9 was lower than that of pH 2 and pH 7. The same phenomenon was observed during methyl parathion and ethyl parathion hydrolysis (Wu et al., 2018a). Given that hydrolysis of OPs is pH dependent, no precise pH boundary can be used for the identification of C–O or P–O bond split. The two major degradation pathways occurred simultaneously at pH 9. The P–O bond cleavage is not associated with carbon isotope fractionation, and thus carbon isotope fractionation can be solely attributed to the splitting of the C–O bond. Considering that the carbon fractionation observed in experiments for acid hydrolysis (pH 2) and alkaline hydrolysis (pH 12) are representative for the mechanism for C–O and P–O bond split respectively, and both processes follow the first-order kinetics, Eq. [4] can be applied for the calculation of the contribution of the two pathways acting during the hydrolysis at pH 9. The carbon isotope enrichment factors of hydrolysis at pH 2 ($\epsilon_1 = -3.8 \pm 0.3\%$) and the ϵ_2 value of 0‰ representing hydrolysis at pH 12 were used for calculation. Within the uncertainty of isotope enrichment factors

observed in the experiments, the enrichment factor of TBP at pH 9 ($\epsilon_i = -2.8 \pm 0.1\%$) suggests that 67–80% of TBP was hydrolyzed via the C–O bond cleavage pathway, and the remaining 20–33% was attributed to the P–O bond split. The mechanism of acidic and neutral hydrolysis is almost identical, and the calculation is also valid for comparing contributions at neutral conditions.

The hydrolysis pathways for OPs have been well studied previously as discussed above, and the determination of hydrolysis products give no further information. Therefore, the hydrolysis products of TBP were not determined in present study. For testing the hypothesis of the degradation mechanisms the AKIE values were compared to intrinsic KIE reactions. For TBP hydrolysis, AKIE_C (calculation is described in SI, section 6) ranged from 1.048 to 1.058, which is in line with the intrinsic KIE values of nucleophilic substitution (1.03–1.09; S_N2 type on C–O bond) (Paneth et al., 1992), supporting the conclusion of C–O bond cleavage during TBP hydrolysis.

4.2. pH-dependency of radical oxidation

In this study, either SO₄^{•−} or \bullet OH was involved in persulfate oxidation, which is a pH-dependent reaction. Once SO₄^{•−} was generated by S₂O₈^{2−} scission, it could propagate a chain of reactions involving the formation of other reactive species. SO₄^{•−} can react with water at all pH levels, forming \bullet OH (Eq. [S1]) (Neta et al., 1988; Herrmann et al., 1995). With the increase of pH, SO₄^{•−} preferentially reacts with OH[−] forming \bullet OH with an increasing rate constant (Eq. [S2]) (Neta et al., 1988; Herrmann et al., 1995). Hence, at low pH (i.e. pH 7), SO₄^{•−} is the predominant reactive species, whereas at pH 9, both SO₄^{•−} and \bullet OH could coexist and at pH 12, \bullet OH is predominant (Liang and Su, 2009). Considering both radical species can be quenched to some extent by the PO₄^{3−} and CO₃^{2−} components in the buffer, the contributions of secondary radicals formed during the reaction and subsequent reaction with TBP were taken into account and the contributions were estimated to be minor (description in SI, section 5).

During radical oxidation of TBP, the rate constants have the following order: pH 7 > pH 9 > pH 12 (Table 1), demonstrating that the reaction can be retarded by increasing pH. The rate constants are associated with the reactivity of the radicals as SO₄^{•−} has a stronger redox potential than \bullet OH (Buxton et al., 1988; Neta et al., 1988), and thus may result in larger kinetic rate constants. The TBP oxidation by KPS at pH 12 had a 5 times larger rate constant compared to the hydrolysis at pH 12 (Table 1) suggesting that radical oxidation was dominating the degradation reaction. Nevertheless, two degradation processes co-existed in the degradation of TBP in the pH12/KPS system, namely, radical oxidation and alkaline hydrolysis. The contribution of alkaline hydrolysis on the TBP degradation was 35% based on the control experiment without the addition of KPS (Fig. S2).

4.3. Insight of isotope fractionation during \bullet OH and SO₄^{•−} reaction with TBP

\bullet OH which can be generated by H₂O₂ under UV irradiation has a high tendency to react non-selectively on functional groups via electron transfer, hydrogen abstraction or electrophilic/radical addition (Buxton et al., 1988). The transformation products formed in the UV/H₂O₂ reaction with TBP were tentatively identified as keto and hydroxylated derivatives (Table S1), suggesting a hydrogen abstraction from the alkyl chain at sub-terminal positions. This suggests a formation of a radical at the side chain which is quenched by oxygen forming a meta stable intermediate radical followed by a Russell mechanism (Russell, 1957) to form keto and hydroxyl TBP (Fig. 3c). In subsequent steps further reactions may

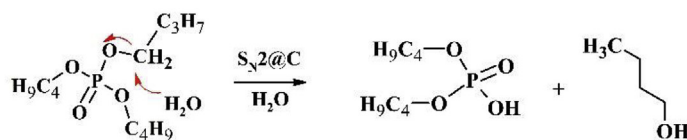
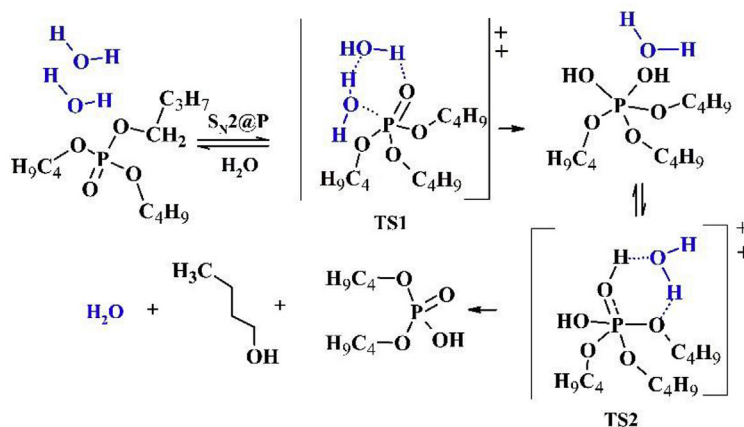
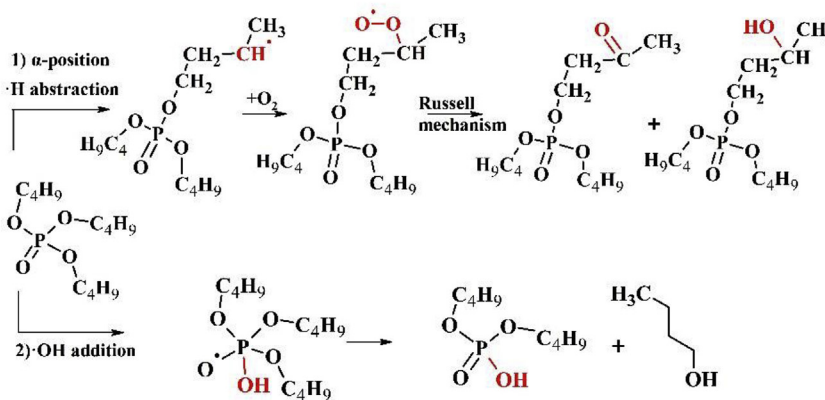
a. Low pH hydrolysis:**b. High pH hydrolysis:****c. Radical oxidation**

Fig. 3. Proposed transformation mechanisms of TBP via hydrolysis and radical oxidation. Hydrolysis of TBP occurs via two pathways: (a) attacked by H_2O at the α -carbon with $\text{S}_{\text{N}}2$ -type substitution at low pH or (b) attacked by H_2O at the P atom with $\text{S}_{\text{N}}2$ -type substitution at high pH. The latter reaction is accompanied with two transition states. Three water molecules assisting the hydrolysis reaction by allowing two proton transfers, via a concerted six-membered cyclic activated complex (TS1) that includes general base catalysis in the first step and the cleavage of the pentacoordinated intermediate in the second step (TS2). The radical oxidation by $\cdot\text{OH}$ can process via two mechanisms. Both processes can occur simultaneously: (1). H-abstraction by $\cdot\text{OH}$, followed by an oxygen addition and finally undergoing the Russell mechanism; (2). The $\cdot\text{OH}$ addition formed the $(\text{BuO})_2\text{PO}\cdot\text{HC}_3\text{H}_7$ radical followed by the elimination of butanol.

lead to the formation of dibutyl phosphate. The hydrogen abstraction mechanism will lead to ^2H and ^{13}C isotope fractionation of TBP. Alternatively, radical addition, for example $\cdot\text{OH}$ addition to the central phosphorus atom, may form a $(\text{C}_4\text{H}_9\text{O})_3\text{PO}\cdot\text{OH}$ radical leading to elimination of butanol and resulting in dibutyl phosphate (Fig. 3c). However, $\cdot\text{OH}$ addition to phosphate will lead to P–O cleavage and is unlikely to induce ^2H and ^{13}C isotope fractionation. Similar mechanisms have been observed in previous studies during the $\cdot\text{OH}$ reaction with tri-(2chloroethyl) phosphate (Wu et al., 2018a) and dimethyl phenylphosphonate (Oh et al., 2003). According to the reaction mechanisms of $\text{SO}_4^{\cdot-}$ and tri-(2chloroethyl) phosphate, $\text{SO}_4^{\cdot-}$ was reported to react with phosphorus and carbon atoms, thereby causing a P–O and C–H bond split (Ou et al., 2017). Similarly, two pathways were proposed to be

involved in TBP oxidation induced by $\text{SO}_4^{\cdot-}$. One pathway involves the addition to the phosphorus centre and rupturing of $-\text{OCH}_2\text{CH}_2\text{CH}_2\text{CH}_3$ chains and the other one involves the addition to the $-\text{CH}_2-$ moieties causing the C–H bond split. Similar isotope fractionation pattern of TBP in reactions with both $\cdot\text{OH}$ and $\text{SO}_4^{\cdot-}$ radicals was observed, indicating that both reaction processes had similar mechanisms. Therefore, the transformation products of TBP in reaction with $\text{SO}_4^{\cdot-}$ were not determined in detail in this study.

The radical reaction with the alkane side chain at the sub-terminal position cleaving a C–H bond in the transition state leads to ^2H and ^{13}C isotope fractionation. The observed ^2H and ^{13}C isotope fractionation in our experiments showed that this pathway took place during radical oxidation of TBP by $\cdot\text{OH}$ and $\text{SO}_4^{\cdot-}$. The obtained ϵ_{C} and ϵ_{H} at pH7/KPS ($\text{SO}_4^{\cdot-}$ dominating) and pH9/KPS

(SO_4^- and $\cdot\text{OH}$ co-existing) were very similar with the ones from UV/ H_2O_2 (pure $\cdot\text{OH}$) (Table 1). The slightly smaller ϵ_C of $-0.5 \pm 0.1\text{‰}$ and ϵ_H of $-11 \pm 1\text{‰}$ at pH12/KPS ($\cdot\text{OH}$ dominating) is due to the effect of alkaline hydrolysis of TBP at pH 12. Considering 35% of TBP degradation was contributed by alkaline hydrolysis (process 1) at pH12/KPS (Fig. S2), the ϵ associated with the $\cdot\text{OH}$ oxidation process (process 2) can be estimated using Eq. (4) where $F=0.35$, $\epsilon_1 = -0.5 \pm 0.1\text{‰}$ for carbon and $-11 \pm 1\text{‰}$ for hydrogen, $\epsilon_2 = 0\text{‰}$. Thus, ϵ_2 was calculated to be $-0.8 \pm 0.2\text{‰}$ for carbon and $-17 \pm 2\text{‰}$ for hydrogen, which were identical with the ones obtained from radical oxidation of TBP at pH7/KPS, pH9/KPS and UV/ H_2O_2 conditions (Table 1). The average values of $\epsilon_C = -0.7 \pm 0.1\text{‰}$, $\epsilon_H = -16 \pm 3\text{‰}$, and $\Lambda = 20 \pm 4$ calculated from all individual radical oxidation experiments suggest that SO_4^- and $\cdot\text{OH}$ radical oxidation processes of TBP could not be distinguished based on isotope enrichment factors within the uncertainty of our results, and it may suggest that both reaction processes had similar mechanisms of attacking carbon atoms and cleaving C–H bonds. However, the precise position of the hydrogen abstraction from the carbon atoms at the side chain of the TBP molecule could not be confirmed without further structural investigation of the transformation products. In addition, the P–O bond splitting pathway cannot be characterized by the ^2H and ^{13}C isotope fractionation of TBP in this study, therefore, ^2H and ^{13}C isotope fractionation studies cannot provide direct evidence to evaluate the process of P–O bond cleavage.

The AKIE_C which ranged from 1.007 to 1.011 for all radical oxidation experiments (Table 1) is consistent with those reported for *n*-alkanes' chemical transformation (1.01–1.02) (Bouchard et al., 2008) and lower than the Streitwieser Limits for a C–H bond (1.021) cleavage (Elsner et al., 2005). A series of studies yield AKIE_H values between 2 and 23 that are typical for H-bond cleavage (Elsner et al., 2005). The AKIE_H values reported in this study were lower and ranged from 1.608 to 2.174, indicating that steps other than the C–H bond cleavage were also rate-determining for radical oxidation of TBP. Potentially a radical reaction at the phosphate moiety may contribute to TBP degradation (Fig. 3c 2) but do not contribute to ^2H and ^{13}C isotope fractionation. This may explain why the calculated AKIE values are lower than those typically expected for C–H bond cleavage. In our case the calculated AKIE values do not describe the KIE of the C–H bond cleavage at the side chain of TBP because the overall transformation reaction has a contribution of OH addition to the phosphate. However our current data do not allow validating this hypothesis in more detail.

4.4. Identification of degradation pathways by 2D-plot to analyse Λ values

The SO_4^- and $\cdot\text{OH}$ resulted in a characteristic isotope fractionation pattern (Λ values) for radical oxidation reactions of TBP. As hydrolysis did not lead to primary hydrogen isotope effects, hydrolysis and radical oxidation of TBP can be clearly distinguished by the correlation of ^2H and ^{13}C fractionation (Fig. 4). Similar results have been reported for radical oxidation of tris(2-chloroethyl) phosphate by $\cdot\text{OH}$ formed in Fenton reactions and UV/ H_2O_2 (Wu et al., 2018a). However, considering the obtained identical Λ values (section 3.5), the Λ values do not allow for separating the mechanisms of SO_4^- and $\cdot\text{OH}$ reactions with TBP. The Λ values are not affected when non-isotope-fractionating processes such as alkaline hydrolysis are influencing overall degradation, showing that mechanisms can also be identified when non-isotope-fractionating processes are at work. This may imply that the extent of isotope fractionation can be used for the assessment of radical reactions and may allow for the selection of an isotope enrichment factor representative for radical reactions. This isotope

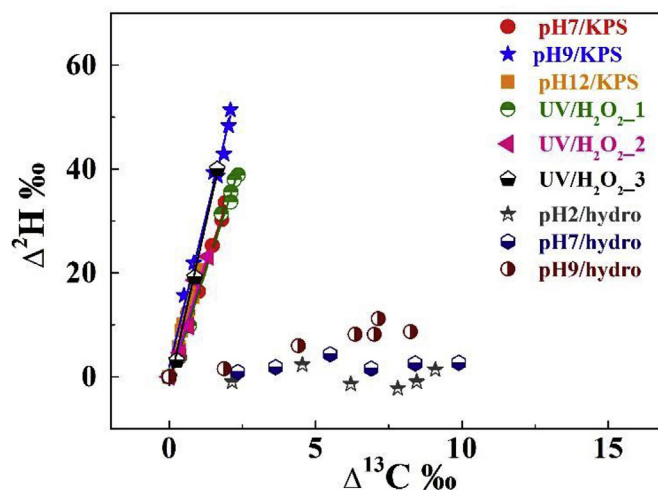


Fig. 4. Two dimensional isotope plots for TBP degradation via hydrolysis and radical oxidation.

enrichment factor could then be used to calculate the contribution of degradation of TBP by radical reactions to the overall degradation in the environment. For example the hydrogen enrichment factor could be used to quantify the contribution of radical reactions because hydrolysis does not exhibit ^2H fractionation. The ^2H and ^{13}C isotope fractionation pattern of parathion has been used at an industrial dumpsite to characterise the contribution of neutral and acidic hydrolysis of parathion in a remediation measure (Wu et al., 2018b). Similarly, the Λ values determined throughout the current study could be used in the future to characterise degradation reaction in field studies for quantifying hydrolysis or chemical oxidation reactions. Further information for quantification of degradation reactions in the environment using enrichment factors have been summarized previously (Thullner et al., 2012).

5. Conclusions

In this study, the carbon and hydrogen isotope fractionation caused by hydrolysis and radical oxidation of TBP were systematically examined at different pH conditions. The AKIE_C of the hydrolysis under neutral and acidic conditions was 1.048–1.058, which was consistent with an $\text{S}_\text{N}2$ -type displacement reaction cleaving the C–O bond. At pH 12, a $\text{S}_\text{N}2$ -type nucleophilic displacement reaction cleaving the P–O bond was characterized by the absence of carbon and hydrogen isotope fractionation. During hydrolysis at pH 9, the $\text{S}_\text{N}2$ -type displacement reaction cleaving the C–O bond affects the carbon isotope fractionation and contributes to 67–80% of the overall reaction. The radical oxidation of TBP results in AKIE_C and AKIE_H of 1.007–1.011 and 1.608–2.174, respectively, which is consistent with a major contribution of a C–H bond cleavage. The correlation of ^2H and ^{13}C isotope fractionation of TBP allows identifying radical reactions and distinguishing radical reactions from hydrolysis.

Conflicts of interest

None.

Acknowledgements

Jia Liu and Langping Wu were financially supported by the China Scholarship Council (File No. 201506460057 and 201306460007,

respectively). The work was partially supported by the National Science Foundation of China [grant number 41430106, 2014 and 41573080, 2015]. The authors are grateful for using the analytical facilities of the Centre for Chemical Microscopy (ProVIS) at the Helmholtz Centre for Environmental Research – UFZ, which is supported by the European Regional Development Funds (EFRE – Europe funds Saxony) and the Helmholtz Association. The authors thank Dr. Oliver J. Lechtenfeld for his support on transformation products analysis in ProVIS, and thank Dr. Matthias Gehrre for his help in the Isotope Laboratory of the UFZ. We are grateful to Axel Horst for critical reading of our manuscript.

Appendix A. Supplementary data

Supplementary data related to this article can be found at <https://doi.org/10.1016/j.chemosphere.2018.08.034>.

References

- Bacaloni, A., Cucci, F., Guarino, C., Nazzari, M., Samperi, R., Laganà, A., 2008. Occurrence of organophosphorus flame retardant and plasticizers in three volcanic lakes of central Italy. *Environ. Sci. Technol.* 42, 1898–1903.
- Bergman, A., Ryden, A., Law, R.J., de Boer, J., Covaci, A., Alae, M., Birnbaum, L., Petreas, M., Rose, M., Sakai, S., Van den Eede, N., van der Veen, I., 2012. A novel abbreviation standard for organobromine, organochlorine and organophosphorus flame retardants and some characteristics of the chemicals. *Environ. Int.* 49, 57–82.
- Berne, C., Allainmat, B., Garcia, D., 2005. Tributyl phosphate degradation by *Rhodospirillum rubrum* and other photosynthetic bacteria. *Biotechnol. Lett.* 27, 561–566.
- Blumenthal, E., Herbert, J., 1945. The mechanism of the hydrolysis of trimethyl orthophosphate. *Trans. Faraday Soc.* 41, 611–617.
- Bouchard, D., Hunkeler, D., Höhener, P., 2008. Carbon isotope fractionation during aerobic biodegradation of n-alkanes and aromatic compounds in unsaturated sand. *Org. Geochem.* 39, 23–33.
- Buxton, G.V., Greenstock, C.L., Helman, W.P., Ross, A.B., 1988. Critical review of rate constants for reactions of hydrated electrons, hydrogen atoms and hydroxyl radicals ($\cdot\text{OH}/\cdot\text{O}$) in aqueous solution. *J. Phys. Chem. Ref. Data* 17, 513–886.
- Coplen, T.B., 1996. New guidelines for reporting stable hydrogen, carbon, and oxygen isotope-ratio data. *Geochim. Cosmochim. Acta* 60, 3359–3360.
- Day, J.N.E., Ingold, C.K., 1941. Mechanism and kinetics of carboxylic ester hydrolysis and carboxyl esterification. *Trans. Faraday Soc.* 686–705, 1941.
- Elsner, M., 2010. Stable isotope fractionation to investigate natural transformation mechanisms of organic contaminants: principles, prospects and limitations. *J. Environ. Monit.* 12, 2005–2031.
- Elsner, M., Zwank, L., Hunkeler, D., Schwarzenbach, R.P., 2005. A new concept linking observable stable isotope fractionation to transformation pathways of organic pollutants. *Environ. Sci. Technol.* 39, 6896–6916.
- Fries, E., Püttmann, W., 2003. Monitoring of the three organophosphate esters TBP, TCEP and TBEP in river water and ground water (Oder, Germany). *J. Environ. Monit.* 5, 346–352.
- Gray, J.R., Lacrampe-Couloume, G., Gandhi, D., Scow, K.M., Wilson, R.D., Mackay, D.M., Sherwood Lollar, B., 2002. Carbon and hydrogen isotopic fractionation during biodegradation of methyl tert-butyl ether. *Environ. Sci. Technol.* 36, 1931–1938.
- Greget, R., Dadak, S., Barbier, L., Lauga, F., Linossier-Pierre, S., Pernot, F., Legendre, A., Ambert, N., Bouteiller, J.M., Dorandeu, F., Bischoff, S., Baudry, M., Fagni, L., Moussaoui, S., 2016. Modeling and simulation of organophosphate-induced neurotoxicity: prediction and validation by experimental studies. *Neurotoxicology* 54, 140–152.
- He, X., Mezyk, S.P., Michael, I., Fatta-Kassinos, D., Dionysiou, D.D., 2014. Degradation kinetics and mechanism of beta-lactam antibiotics by the activation of H₂O₂ and Na₂S₂O₈ under UV-254nm irradiation. *J. Hazard Mater.* 279, 375–383.
- Herrmann, H., 2003. Kinetics of aqueous phase reactions relevant for atmospheric chemistry. *Chem. Rev.* 103, 4691–4716.
- Herrmann, H., 2007. On the photolysis of simple anions and neutral molecules as sources of O \cdot /OH, SO \cdot - and Cl in aqueous solution. *Phys. Chem. Chem. Phys.* 9, 3935–3964.
- Herrmann, H., Reese, A., Zellner, R., 1995. Time-resolved UV/VIS diode array absorption spectroscopy of SO \cdot - (x=3, 4, 5) radical anions in aqueous solution. *J. Mol. Struct.* 348, 183–186.
- House, D.A., 1962. Kinetics and mechanism of oxidations by peroxydisulfate. *Chem. Rev.* 62, 185–&.
- Kirby, A.J., Mora, J.R., Nome, F., 2013. New light on phosphate transfer from triesters. *Biochim. Biophys. Acta* 1834, 454–463.
- Lau, T.K., Chu, W., Graham, N.J., 2007. The aqueous degradation of butylated hydroxyanisole by UV/S₂O₈²⁻: study of reaction mechanisms via dimerization and mineralization. *Environ. Sci. Technol.* 41, 613–619.
- Lee, S., Jeong, W., Kannan, K., Moon, H.B., 2016. Occurrence and exposure assessment of organophosphate flame retardants (OPFRs) through the consumption of drinking water in Korea. *Water Res.* 103, 182–188.
- Liang, C., Su, H.-W., 2009. Identification of sulfate and hydroxyl radicals in thermally activated persulfate. *Ind. Eng. Chem. Res.* 48, 5558–5562.
- Martinez-Carballo, E., Gonzalez-Barreiro, C., Sitka, A., Scharf, S., Gans, O., 2007. Determination of selected organophosphate esters in the aquatic environment of Austria. *Sci. Total Environ.* 388, 290–299.
- Mincher, B.J., Mezyk, S.P., Martin, L.R., 2008. A pulse radiolysis investigation of the reactions of tributyl phosphate with the radical products of aqueous nitric acid irradiation. *J. Phys. Chem.* 112, 6275–6280.
- Nancharaiyah, Y.V., Reddy, G.K.K., Mohan, T.V.K., Venugopalan, V.P., 2015. Biodegradation of tributyl phosphate, an organophosphate triester, by aerobic granular biofilms. *J. Hazard Mater.* 283, 705–711.
- Neta, P., Huie, R.E., Ross, A.B., 1988. Rate constants for reactions of inorganic radicals in aqueous solution. *J. Phys. Chem. Ref. Data* 17, 1027–1284.
- Nijenhuis, I., Richnow, H.H., 2016. Stable isotope fractionation concepts for characterizing biotransformation of organohalides. *Curr. Opin. Biotechnol.* 41, 108–113.
- Northrop, D.B., 1981. The expression of isotope effects on enzyme-catalyzed reactions. *Annu. Rev. Biochem.* 50, 103–131.
- Oh, Y.-C., Bao, Y., Jenks, W.S., 2003. Isotope studies of photocatalysis: TiO₂-mediated degradation of dimethyl phenylphosphonate. *J. Photochem. Photobiol. Chem.* 161, 69–77.
- Ou, H.s., Liu, J., Ye, J.s., Wang, L.L., Gao, N.y., Ke, J., 2017. Degradation of tris(2-chloroethyl) phosphate by ultraviolet-persulfate: kinetics, pathway and intermediate impact on proteome of *Escherichia coli*. *Chem. Eng. J.* 308, 386–395.
- Paneth, P., Buncel, E., Saunders Jr., W., 1992. *Isotopes in Organic Chemistry*, vol. 8. Elsevier, New York.
- Rayleigh, L., 1896. Theoretical considerations respecting the separation of gases by diffusion and similar processes. *Philos. Mag.* 42, 493–498.
- Regnery, J., Puttmann, W., 2010. Occurrence and fate of organophosphorus flame retardants and plasticizers in urban and remote surface waters in Germany. *Water Res.* 44, 4097–4104.
- Regnery, J., Puttmann, W., Merz, C., Berthold, G., 2011. Occurrence and distribution of organophosphorus flame retardants and plasticizers in anthropogenically affected groundwater. *J. Environ. Monit.* 13, 347–354.
- Rodil, R., Quintana, J.B., Concha-Grana, E., Lopez-Mahia, P., Muniategui-Lorenzo, S., Prada-Rodriguez, D., 2012. Emerging pollutants in sewage, surface and drinking water in Galicia (NW Spain). *Chemosphere* 86, 1040–1049.
- Russell, G.A., 1957. Deuterium-isotope effects in the autoxidation of aralkyl hydrocarbons. Mechanism of the interaction of peroxy radicals. *J. Am. Chem. Soc.* 79, 3871–3877.
- Shi, Y., Gao, L., Li, W., Wang, Y., Liu, J., Cai, Y., 2016. Occurrence, distribution and seasonal variation of organophosphate flame retardants and plasticizers in urban surface water in Beijing, China. *Environ. Pollut.* 209, 1–10.
- Su, G., Letcher, R.J., Yu, H., 2016. Organophosphate flame retardants and plasticizers in aqueous solution: pH-dependent hydrolysis, kinetics, and pathways. *Environ. Sci. Technol.* 50, 8103–8111.
- Thullner, M., Centler, F., Richnow, H.-H., Fischer, A., 2012. Quantification of organic pollutant degradation in contaminated aquifers using compound specific stable isotope analysis – review of recent developments. *Org. Geochem.* 42, 1440–1460.
- Van Breukelen, B.M., 2007. Extending the Rayleigh equation to allow competing isotope fractionating pathways to improve quantification of biodegradation. *Environ. Sci. Technol.* 41, 4004–4010.
- Vogt, C., Dorer, C., Musat, F., Richnow, H.H., 2016. Multi-element isotope fractionation concepts to characterize the biodegradation of hydrocarbons - from enzymes to the environment. *Curr. Opin. Biotechnol.* 41, 90–98.
- Waclawek, S., Lutze, H.V., Grubel, K., Padil, V.V.T., Cernik, M., Dionysiou, D.D., 2017. Chemistry of persulfates in water and wastewater treatment: a review. *Chem. Eng. J.* 330, 44–62.
- Wanamaker, E.C., Chingas, G.C., McDougal, O.M., 2013. Parathion hydrolysis revisited: in situ aqueous kinetics by ¹H NMR. *Environ. Sci. Technol.* 47, 9267–9273.
- Watts, M.J., Linden, K.G., 2009. Advanced oxidation kinetics of aqueous tri alkyl phosphate flame retardants and plasticizers. *Environ. Sci. Technol.* 43, 2937–2942.
- Watts, R.J., Teel, A.L., 2006. Treatment of contaminated soils and groundwater using ISCO. *Pract. Period. Hazard. Toxic. Radioact. Waste Manag.* 10, 2–9.
- Wolfsberg, M., Van Hook, W.A., Paneth, P., Rebelo, L.P.N., 2009. *Isotope Effects: in the Chemical, Geological, and Bio Sciences*. Springer Science & Business Media.
- Wu, L., Chládková, B., Lechtenfeld, O.J., Lian, S., Schindelka, J., Herrmann, H., Richnow, H.H., 2018a. Characterizing chemical transformation of organophosphorus compounds by ¹³C and ²H stable isotope analysis. *Sci. Total Environ.* 615, 20–28.
- Wu, L., Kummel, S., Richnow, H.H., 2017. Validation of GC-IRMS techniques for $\delta^{13}\text{C}$ and $\delta^2\text{H}$ CSIA of organophosphorus compounds and their potential for studying the mode of hydrolysis in the environment. *Anal. Bioanal. Chem.* 409, 2581–2590.
- Wu, L., Verma, D., Bondgaard, M., Melvej, A., Vogt, C., Subudhi, S., Richnow, H.H., 2018b. Carbon and hydrogen isotope analysis of parathion for characterizing its natural attenuation by hydrolysis at a contaminated site. *Water Res.* 143, 146–154.
- Wu, L., Yao, J., Trebse, P., Zhang, N., Richnow, H.H., 2014. Compound specific isotope analysis of organophosphorus pesticides. *Chemosphere* 111, 458–463.
- Wu, T., Gan, Q., Jans, U., 2006. Nucleophilic substitution of phosphorothionate ester

- pesticides with bisulfide (HS⁻) and polysulfides (Sn²⁻). *Environ. Sci. Technol.* 40, 5428–5434.
- Yang, Y., Lu, X., Jiang, J., Ma, J., Liu, G., Cao, Y., Liu, W., Li, J., Pang, S., Kong, X., Luo, C., 2017. Degradation of sulfamethoxazole by UV, UV/H₂O₂ and UV/persulfate (PDS): formation of oxidation products and effect of bicarbonate. *Water Res.* 118, 196–207.
- Zhang, N., Geronimo, I., Paneth, P., Schindelka, J., Schaefer, T., Herrmann, H., Vogt, C., Richnow, H.H., 2016. Analyzing sites of OH radical attack (ring vs. side chain) in oxidation of substituted benzenes via dual stable isotope analysis ($\delta^{13}\text{C}$ and $\delta^2\text{H}$). *Sci. Total Environ.* 542, 484–494.

Supplementary Information

Carbon and hydrogen stable isotope analysis for characterizing the chemical degradation of tributyl phosphate

Jia Liu^{1,2§}, Langping Wu^{2§}, Steffen Kümmel², Jun Yao³, Thomas Schaefer⁴, Hartmut Herrmann⁴, Hans-Hermann Richnow^{2,3*}

¹School of Energy and Environmental Engineering, University of Science and Technology Beijing, Xueyuan Road No.30, Haidian District, Beijing 100083, PR China

²Department of Isotope Biogeochemistry, Helmholtz Centre for Environmental Research-UFZ, Permoserstraße15, Leipzig 04318, Germany

³School of Water Resources and Environment, China University of Geosciences (Beijing), Xueyuan Road No.29, Haidian District, Beijing 100083, PR China

⁴Atmospheric Chemistry Department (ACD), Leibniz Institute for Tropospheric Research (TROPOS), Permoserstraße15, Leipzig 04318, Germany

§ Dual-first authorship: the two authors have contributed equally to this work.

* To whom correspondence should be addressed

E-mail: hans.richnow@ufz.de

Tel.: +49 (0) 341 235 1212, Fax: +49 (0) 341 2351443

11 pages

4 figures

1 table

Contents

1. Concentration analysis of Tributylphosphate (TBP).....	1
2. Carbon and hydrogen isotope analysis.....	1
3. Extraction recovery and isotope effects.....	1
4. Control experiments.....	2
5. Calculation of secondary radical reactions in buffer solution.....	3
6. AKIE calculation.....	4
7. Analysis of transformation products of TBP via $\bullet\text{OH}$ oxidation.....	5
8. References.....	7

1. Concentration analysis of Tributylphosphate (TBP)

TBP concentrations were determined by gas chromatography (GC, Agilent 6890, Agilent Technologies, Germany) coupled with a flame ionization detector (FID). Samples were separated on a HP-5 column (30 m length, 0.32 mm inner diameter, 0.25 μm film thickness, Agilent Technologies, Germany) at a constant helium carrier gas flow of 1.5 mL/min with the following temperature program: 60 $^{\circ}\text{C}$ for 2 min, 20 $^{\circ}\text{C}/\text{min}$ to 160 $^{\circ}\text{C}$, 5 $^{\circ}\text{C}/\text{min}$ to 220 $^{\circ}\text{C}$, and 15 $^{\circ}\text{C}/\text{min}$ to 280 $^{\circ}\text{C}$ for 2 min. An aliquot of the sample (1 μL) was injected in split mode with a split ratio of 1:25. The injector temperature was set to 250 $^{\circ}\text{C}$.

2. Carbon and hydrogen isotope analysis

2.1 Analytical methods

Stable carbon and stable hydrogen isotope compositions of TBP were measured by gas chromatography – combustion – isotope ratio mass spectrometry (GC-C-IRMS) (Wu et al., 2017b) and gas chromatography – chromium-based high temperature conversion – isotope ratio mass spectrometry (GC-Cr/HTC-IRMS) (Renpenning et al., 2015; Renpenning et al., 2017), respectively. A GC 7890A (Agilent Technologies, Germany) coupled via a GC IsoLink and a ConFlo IV open split system to a MAT 253 IRMS (Thermo Scientific, Germany) was used. Aliquots of the samples (1-4 μL) were injected with a split ratio of 1:5. Samples were separated on a ZB-1 column (60 m length, 0.32 mm inner diameter, 1 μm film thickness, Phenomenex Inc., USA) at a constant helium carrier gas flow of 2.0 mL/min with the following temperature program: 60 $^{\circ}\text{C}$ for 2 min, 10 $^{\circ}\text{C}/\text{min}$ to 160 $^{\circ}\text{C}$, 5 $^{\circ}\text{C}/\text{min}$ to 220 $^{\circ}\text{C}$, and 15 $^{\circ}\text{C}/\text{min}$ to 280 $^{\circ}\text{C}$ for 2 min. The injector temperature was set to 280 $^{\circ}\text{C}$.

2.2 Linearity

The linearity; that is, the dependence of the isotopic ratios from the amount of sample material, was analyzed using stock solutions of TBP dissolved in DCM to different concentrations. Sample aliquots (1-4 μL) were injected in split (for carbon) or splitless (for hydrogen) mode. Measurements of different amounts of TBP documented a dependence of $\delta^{13}\text{C}$ on the injected amount and defined the required TBP sample amplitude for a ≥ 1500 mV signal as 0.2 nmol TBP on column, or 2.4 nmol C on column; $\delta^2\text{H}$ on the injected amount and defined the required TBP sample size for a ≥ 7500 mV signal as 7.5 nmol TBP on column, or 202 nmol H on column (Fig. S1).

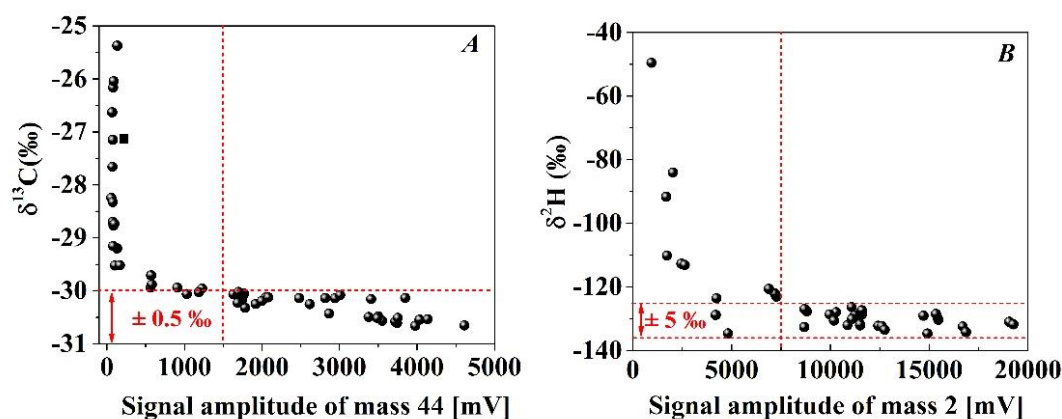


Fig. S1 Linearity of $\delta^{13}\text{C}$ values (A) and $\delta^2\text{H}$ values (B) measured along ranges of injection sizes for TBP.

3. Extraction recovery and isotope effects

3.1 Extraction recovery

TBP standard solutions with six concentrations levels of 400, 1000, 2000, 4000, 5000 and 6000 mg L⁻¹ were prepared by dissolving in 1 mL of DCM containing 1000 mg L⁻¹ DBP (as internal standard). The standard solutions were stored at 4 °C before analysis.

TBP aqueous solutions were prepared by dissolving TBP in 40 mL of water in 50-mL bottles, obtaining final concentrations of 10, 25, 50, 100, 125 and 150 ppm, respectively. Each bottle was closed with a Teflon-coated butyl rubber septum and a crimp cap. The solutions were shaken overnight at room temperature to ensure complete dissolution of TBP. Afterwards, dissolved TBP were extracted with 1 mL of DCM containing 1000 mg L⁻¹ DBP as internal standard by shaking for at least 4 h at 10 °C. The concentrations of the extracts and TBP standard solutions were analyzed by GC-FID as described above, and extraction recovery was calculated. The recovery of the liquid/liquid DCM extraction method was 91.2 ± 10.2% (Fig. S2 (a)).

3.2 Effects of extraction on isotope signature

To ensure that the liquid-liquid extraction method does not cause any isotope fractionation effect, the isotope signature of TBP was determined before and after DCM extraction. As shown in Fig S2 (b), the isotope shifts before and after DCM extraction were 0.05 – 0.65‰ for δ¹³C, and 1 – 4‰ for δ²H, respectively. Considering the analytical uncertainty of carbon and hydrogen isotope compositions, which is < ±0.5‰ for carbon and < ±5‰ for hydrogen (Sessions, 2006; Sherwood Lollar et al., 2007), carbon and hydrogen isotope shifts due to the extraction process are insignificant.

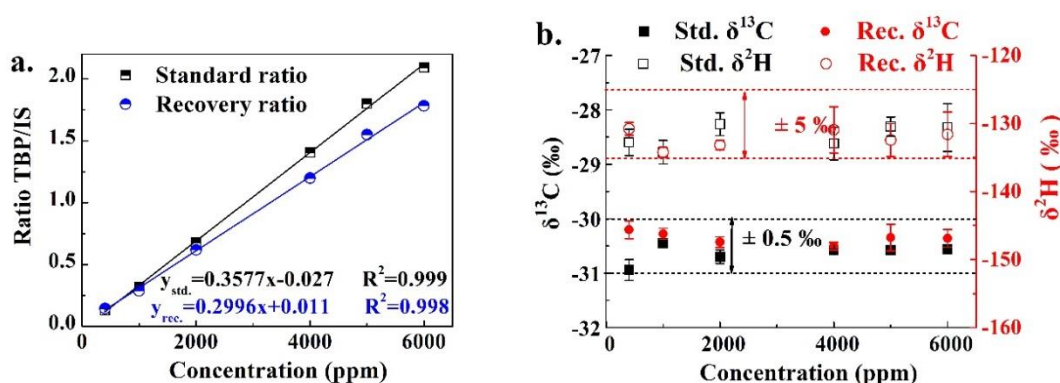


Fig. S2. Extraction recovery of TBP (a) and effects of extraction on the stable carbon and hydrogen isotope signature of TBP (b). (a) Black squares and blue circles depict the TBP concentrations of standard samples and extracted samples, respectively; (b) red circles depict isotope signatures (δ¹³C and δ²H) of TBP from extracted samples; black squares depict isotope signatures of TBP from standard samples. Error bars represent 2σ of at least 3 measurements.

4. Control experiments

Control experiments for KPS oxidation were conducted as batch experiments without the addition of KPS at pH 7, pH 9 and pH 12, respectively. Control experiments for UV/H₂O₂ oxidation were performed either without UV irradiation or without the addition of H₂O₂, respectively. Over the entire reaction time, the losses of TBP concentrations were at most 1.5 - 2.0% for the KPS control experiments at pH 7 (Fig. S3 (a)) and pH 9 (Fig. S3 (b)), and similar amounts of TBP loss were observed in the UV/H₂O₂ control experiments (Fig. S3 (d)). However, the TBP concentration decreased by about 35% within 400 h in the KPS control experiment at pH 12 due to alkaline hydrolysis of TBP (Fig. S3 c).

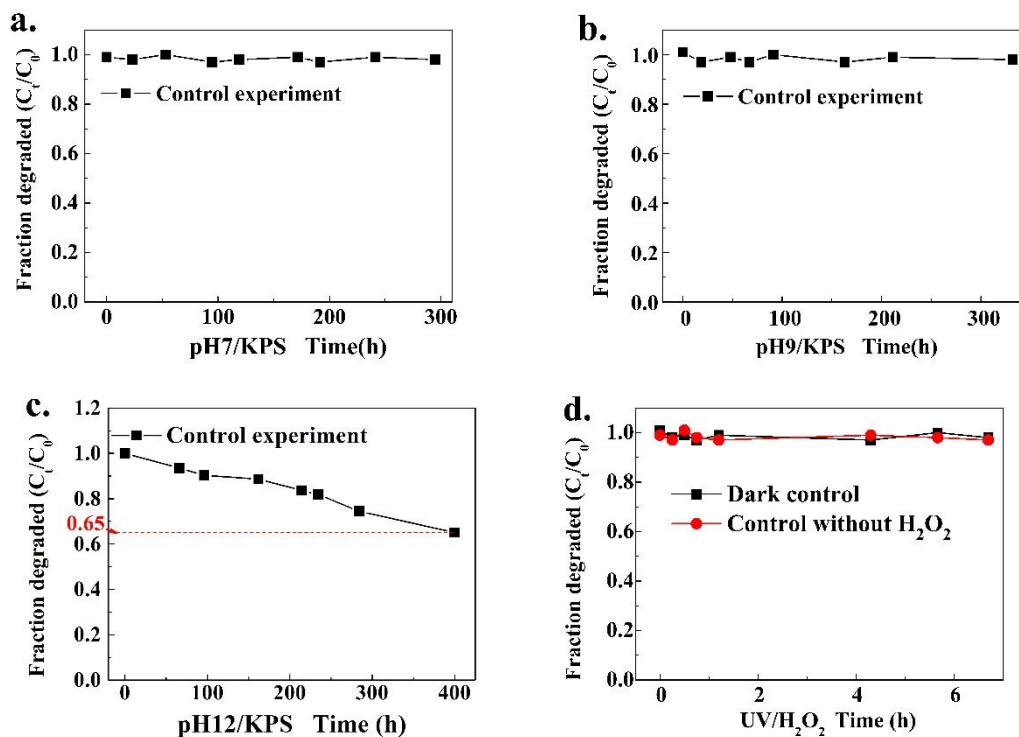


Fig. S3. Change of the TBP concentration in control experiments. (a) KPS control experiments at pH 7, (b) KPS control experiment at pH 9, (c) KPS control experiment at pH 12, (d) UV/H₂O₂ control experiments without UV irrigation (black symbols) and without the addition of H₂O₂ (red symbols).

5. Calculation of secondary radical reactions in buffer solution.

The formation of secondary radicals by reaction of $\text{SO}_4^{\cdot-}$ / $\cdot\text{OH}$ with various buffer systems was estimated to evaluate if secondary radicals could potentially affect the isotope fractionation of TBP. Secondary radicals are highly reactive species, however, generally still less reactive compared to the primary ones. Therefore, the ratios of the formation of secondary radicals have been calculated (see attached excel script). The following buffer systems have been used: $\text{KH}_2\text{PO}_4/\text{K}_2\text{HPO}_4$ buffer at pH 7, $\text{NaHCO}_3/\text{NaOH}$ buffer at pH 9 and $\text{NaH}_2\text{PO}_4/\text{NaOH}$ buffer at pH 12.

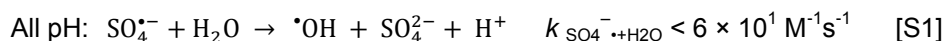
(i) The phosphate buffer system at pH 7 in UV/H₂O₂ reaction

The UV reaction with H₂O₂ forms $\cdot\text{OH}$ at pH 7 which can react with the phosphate buffer to form $\text{H}_2\text{PO}_4^{\cdot}$ or $\text{HPO}_4^{\cdot-}$ (Maruthamuthu and Neta, 1978). The reaction rate of $\cdot\text{OH}$ with TBP is estimated to be > 100 times faster than with phosphate buffer and we consider a larger predominance of the $\cdot\text{OH}$ reaction with the aliphatic side chain of TBP by H abstraction. A further secondary radical reaction of $\text{HPO}_4^{\cdot-}$ will react with H₂O₂ to form $\cdot\text{OH}$ again (Nakashima and Hayon, 1970). The reaction rate of $\text{HPO}_4^{\cdot-}$ with alcohols is estimated to be slower than with H₂O₂. Therefore, we conclude that $\cdot\text{OH}$ is only a relevant radical for TBP degradation in this buffer system (see excel script).

(ii) The phosphate buffer system at pH 7 in KPS reaction

The KPS reaction at pH 7 forms $\text{SO}_4^{\cdot-}$. Even $\text{SO}_4^{\cdot-}$ can react with water at all pH levels, however, the rate constant was very low, less than $6 \times 10^1 \text{ M}^{-1}\text{s}^{-1}$ (Eq. S1). The $\text{SO}_4^{\cdot-}$ can react with H_2PO_4^- or HPO_4^{2-} by electron transfer reaction to produce $\text{H}_2\text{PO}_4^{\cdot}$ or $\text{HPO}_4^{\cdot-}$ by the same order of reaction rates compared to the estimated rate of $\text{SO}_4^{\cdot-}$ with TBP (Maruthamuthu and Neta, 1978). The secondary reaction of $\text{HPO}_4^{\cdot-}$ with TBP (referred to $\text{HPO}_4^{\cdot-}$ reacted with *tert*-butanol and ethanol, respectively) is estimated to be calculated, and

compared with reaction by KPS (referred to the H₂O₂ reacted with HPO₄²⁻). The reaction with KPS will form SO₄^{•-}. We conclude that SO₄^{•-} is the dominant radical for reactions with TBP in this buffer system.

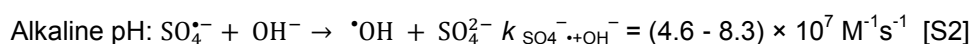


(iii) The carbonate buffer system at pH 9 in KPS reaction

The KPS reaction at pH 9 forms SO₄^{•-} and •OH (Herrmann et al., 1995; Liang and Su, 2009; Romero et al., 2010). SO₄^{•-} reacts with the HCO₃⁻ to form HCO₃[•] with a nearly 7 times higher reaction rate compared to the reaction with TBP (Huie and Clifton, 1990; Umschlag and Herrmann, 1999). The subsequent H atom abstraction reaction of the CO₃^{•-} yields an alkyl radical as in the reaction of the SO₄^{•-} with TBP.

(iv) The phosphate buffer system at pH 12 in KPS reaction

The KPS reaction at pH 12 forms almost exclusively •OH and due to that, SO₄^{•-} reacts rapidly with OH⁻ to form •OH (Eq. S2) (Herrmann et al., 1995; Liang and Su, 2009; Romero et al., 2010). Therefore, secondary reactions of SO₄^{•-} with phosphate buffer to form H₂PO₄[•] or HPO₄^{•-} are minor. The addition reaction pathway where the formed radicals (SO₄^{•-}, •OH, etc.) add to the P atom of organophosphates has been regarded to be unlikely (Abbott et al., 2010).



6. AKIE calculation

The three butyl chains of TBP can be considered identical. The C-O bond could be cleaved during hydrolysis at pH 2 and pH 7 (discussed in section 4.1 in the main text). For the calculation of AKIE_C for TBP hydrolysis, n = 12, x = 3, z = 3 were applied, resulting in 1.048 ± 0.004 at pH 2 and 1.058 ± 0.007 at pH 7, respectively. The AKIE_C at pH 9 was not calculated since two hydrolysis pathways took place simultaneously.

For the calculation of AKIE of TBP via H abstraction by •OH, we assume •OH attacks on sub-terminal carbon of the butyl chain (Fig. 1c). Therefore, n = 12, x = 3, z = 3 were used for AKIE_C calculation, resulting in 1.010 ± 0.001 (UV/H₂O₂_1), 1.007 ± 0.004 (UV/H₂O₂_2) and 1.007 ± 0.001 (UV/H₂O₂_3), respectively. AKIE_H was calculated applying n = 27, x = 6, z = 6, resulting in 1.608 ± 0.070 (UV/H₂O₂_1), 1.610 ± 0.209 (UV/H₂O₂_2) and 1.761 ± 0.418 (UV/H₂O₂_3), respectively. The AKIE_C and AKIE_H of the individual experiments were statistically identical.

SO₄^{•-} is the dominating radical species for the pH7/KPS reaction. Similar to •OH, we assume SO₄^{•-} attacks on the sub-terminal carbon of the butyl chain. The reaction of pH9/KPS proceeds by two main radicals, SO₄^{•-} and •OH, in parallel, however, via a C-H bond cleavage at the same position. Therefore, the AKIE values were calculated using Eq. (2) by applying the same parameters as described in UV/H₂O₂ experiments. AKIE_C were 1.011±0.001 and 1.010±0.001 for reaction at pH7/KPS and pH9/KPS, respectively and are statistically identical. The corresponding AKIE_H were 1.761 ± 0.167 and 2.174 ± 0.255, respectively which overlap slightly but are statistically not different taking the uncertainty into account. The AKIE values at pH12/KPS were not calculated since two degradation processes (hydrolysis and radical oxidation) took place simultaneously.

7. Analysis of transformation products of TBP via •OH oxidation

The analytical procedures for analyzing the transformation products of TBP in UV/H₂O₂ reactions were the same as described previously (Wu et al., 2017a). A Fourier-transform ion cyclotron resonance mass spectrometer (FT-ICR MS, Solarix XR 12T, Bruker Daltonics) equipped with a dynamically harmonized analyzer cell was used for the analysis of the methanolic extracts. FT-ICR MS is a mass spectrometer for determining the mass-to-charge ratio (*m/z*) of ions based on the cyclotron frequency of the ions in a fixed magnetic field. The instrument was operated with a high mass accuracy and resolution (450000 at *m/z* 200) which allowed a tentative assignment of a chemical by calculating the elementary composition of possible transformation products using the exact mass.

Solid phase extraction (SPE) using Bond Elut PPL cartridges (50 mg, Agilent) were applied to extract organic compounds from 10 mL of the reaction mixture which was taken after 4 h of reaction. The SPE extraction procedures were completed by following the manufacturer's guidelines. The transformation products were eluted with 0.5 mL methanol. The methanolic eluent was diluted 100 or 1000 times with MilliQ water/MeOH (1:1, v/v) before analysis. Samples were measured with positive and negative electrospray ionization in the direct infusion mode with a 4 MWord time domain using typical electrospray ionization (ESI) conditions.

TBP and three potential first step transformation products were identified (P1 to P3). For instance, as shown in Fig. S4, a transformation product of TBP was found in positive mode with *m/z* 281.1512 and ion formula of C₁₂H₂₆O₅P⁺, which was not present in the initial solution at time 0. All detected transformation products of TBP are listed in Table S1. The mass for P1 allows calculating a molecular formula of C₈H₁₉O₄P, suggesting that a di-*n*-butylphosphate was formed. The mass of P2 allows calculating a molecular formula of C₁₂H₂₅O₅P, suggesting that a keto-tri-butylphosphate was formed. The mass of P3 allows calculating a molecular formula of C₁₂H₂₇O₅P suggesting that a hydroxy-tri-butylphosphate was formed. The keto and hydroxyl group is probably located at the side chain in sub-terminal positions as an attack at the terminal carbon is unlikely.

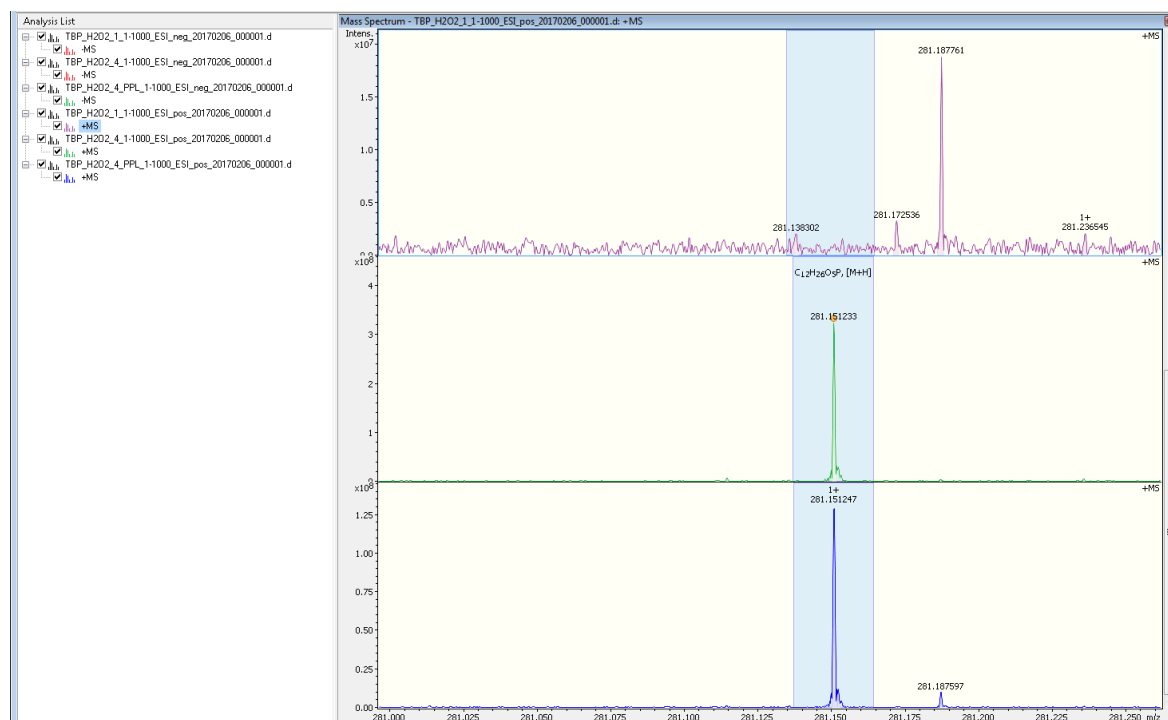
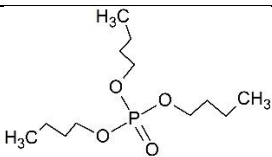
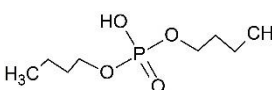
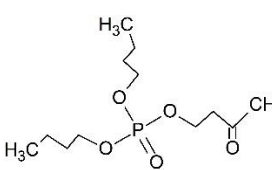
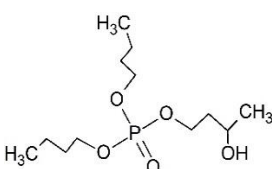


Fig. S4. Positive ionization mode: m/z 281.1512, a possible TBP product.

Table S1: List of characterized transformation products detected by FT-ICR MS.

Name	Formula	Tentative structure	Molar mass (g/mol)	m/z pos	m/z neg	Detected (pos/neg)
TBP	C ₁₂ H ₂₇ O ₄ P		266.314	267.1720 289.1539		pos(H,Na)/-
P1	C ₈ H ₁₉ O ₄ P		210.208	211.1094	209.0948	pos(H)/neg
P2	C ₁₂ H ₂₅ O ₅ P		280.298	281.1512 303.1331		pos(H,Na)/-
P3	C ₁₂ H ₂₇ O ₅ P		282.314	283.1669		pos(H,Na)/-

8. References

- Abbott, A., Sierakowski, T., Kiddle, J.J., Clark, K.K., Mezyk, S.P., 2010. Detailed Investigation of the Radical-Induced Destruction of Chemical Warfare Agent Simulants in Aqueous Solution. *The Journal of Physical Chemistry B* 114, 7681-7685.
- Herrmann, H., Reese, A., Zellner, R., 1995. Time-resolved UV/VIS diode array absorption spectroscopy of SO_x-(x=3, 4, 5) radical anions in aqueous solution. *J. Mol. Struct.* 348, 183-186.
- Huie, R.E., Clifton, C.L., 1990. Temperature dependence of the rate constants for reactions of the sulfate radical, SO₄⁻, with anions. *Journal of Physical Chemistry* 94, 8561-8567.
- Liang, C., Su, H.-W., 2009. Identification of sulfate and hydroxyl radicals in thermally activated persulfate. *Ind. Eng. Chem. Res.* 48, 5558-5562.
- Maruthamuthu, P., Neta, P., 1978. Phosphate radicals. Spectra, acid-base equilibria, and reactions with inorganic compounds. *The Journal of Physical Chemistry* 82, 710-713.
- Nakashima, M., Hayon, E., 1970. Rates of reaction of inorganic phosphate radicals in solution. *The Journal of Physical Chemistry* 74, 3290-3291.
- Renpenning, J., Kummel, S., Hitzfeld, K.L., Schimmelmann, A., Gehre, M., 2015. Compound-specific hydrogen isotope analysis of heteroatom-bearing compounds via gas chromatography-chromium-based high-temperature conversion (Cr/HTC)-isotope ratio mass spectrometry. *Anal. Chem.* 87, 9443-9450.
- Renpenning, J., Schimmelmann, A., Gehre, M., 2017. Compound-specific hydrogen isotope analysis of fluorine-, chlorine-, bromine- and iodine-bearing organics using gas chromatography–chromium-based high-temperature conversion (Cr/HTC) isotope ratio mass spectrometry. *Rapid Communications in Mass Spectrometry* 31, 1095-1102.
- Romero, A., Santos, A., Vicente, F., González, C., 2010. Diuron abatement using activated persulphate: Effect of pH, Fe(II) and oxidant dosage. *Chemical Engineering Journal* 162, 257-265.
- Sessions, A.L., 2006. Isotope-ratio detection for gas chromatography. *J. Sep. Sci.* 29, 1946-1961.
- Sherwood Lollar, B., Hirschorn, S.K., Chartrand, M.M., Lacrampe-Couloume, G., 2007. An approach for assessing total instrumental uncertainty in compound-specific carbon isotope analysis: implications for environmental remediation studies. *Anal. Chem.* 79, 3469-3475.
- Umschlag, T., Herrmann, H., 1999. The carbonate radical (HCO₃[·]/CO₃^{-·}) as a reactive intermediate in water chemistry: kinetics and modelling. *CLEAN–Soil, Air, Water* 27, 214-222.
- Wu, L., Chladkova, B., Lechtenfeld, O.J., Lian, S., Schindelka, J., Herrmann, H., Richnow, H.H., 2017a. Characterizing chemical transformation of organophosphorus compounds by ¹³C and ²H stable isotope analysis. *Sci. Total Environ.* 615, 20-28.
- Wu, L., Kummel, S., Richnow, H.H., 2017b. Validation of GC-IRMS techniques for δ¹³C and δ²H CSIA of organophosphorus compounds and their potential for studying the mode of hydrolysis in the environment. *Anal. Bioanal. Chem.* 409, 2581-2590.

Appendix 6.9.

Enantiomer and carbon isotope fractionation of α -hexachlorocyclohexane by *Sphingobium indicum* strain B90A and corresponding enzymes

Submitted manuscript: *Liu, Y.; Wu, L.; Kohli, P.; Kumar, R.; Stryhanyuk, H.; Nijenhuis, I.; Lal, R.; Richnow, H. H., Environ. Sci. Technol. 2018.*

Enantiomer and Carbon Isotope Fractionation of α -hexachlorocyclohexane by *Sphingobium indicum* Strain B90A and Corresponding Enzymes

Yaqing Liu,¹ Langping Wu,¹ Puneet Kohli,² Roshan Kumar,² Hryhoriy Stryhanyuk,¹ Ivonne Nijenhuis,¹ Rup Lal,² Hans-Hermann Richnow^{1*}

¹Department of Isotope Biogeochemistry, Helmholtz Centre for Environmental Research-UFZ, Permoserstraße 15, 04318 Leipzig, Germany

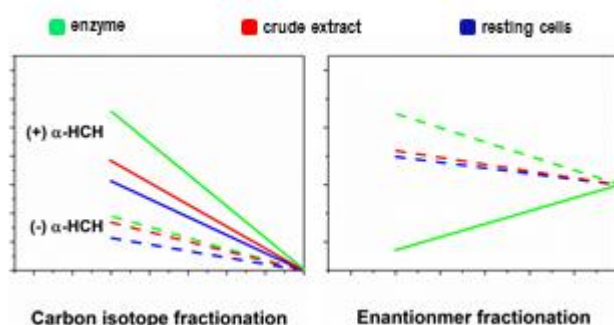
²Molecular Biology Laboratory, Department of Zoology, University of Delhi, Delhi-110007, India

*Corresponding author: Hans-Hermann Richnow

Phone: +49-3412351212; fax: +49-341451212; E-mail: hans.richnow@ufz.de

ABSTRACT

In order to understand the enantiomer specific and carbon stable isotope fractionation of α -hexachlorocyclohexane (α -HCH) during aerobic degradation, biodegradation experiments were conducted with six *Sphingobium* strains which are different in their *lin* gene inventory. Experiments were carried out with (i) resting cells and (ii) crude cell extracts of *Sphingobium indicum* strain B90A in parallel and (iii) isolated LinA1 and LinA2 proteins, to investigate the underlying mechanisms leading to carbon isotope and enantiomer fractionation of α -HCH. The isotope fractionation of individual α -HCH enantiomers, (+) α - and (-) α -HCH, along with the enantiomer fractionation were quantified to describe the degradation processes at different cell integrities. The average isotope enrichment factors obtained from parallel experiments for (+) α - and (-) α -HCH degradation were -6.3 ± 0.1 ‰ and -2.3 ± 0.03 ‰ by resting cells, -7.7 ± 0.4 ‰ and -3.4 ± 0.02 ‰ by crude extract, respectively. Purified LinA1 and LinA2 enzyme give ϵ_C of -11.1 ± 0.3 ‰ for (+) α -HCH and -3.8 ± 0.2 ‰ for (-) α -HCH, respectively. The large carbon fractionation is consistent with an E2 elimination proposed for LinA degradation mechanisms. An approximate model, we derived from the first order rate law and the definition of enantiomer ratio used in the environmental science, has been successfully applied for the evaluation of enantiomer fractionation. We also described here our consideration on the approximation conditions required for the application of the suggested model. The absolute values of enantiomer fractionation factors varied between 0.54 ± 0.14 % and 2.70 ± 0.50 % from resting cells to purified enzymes. Our study validated that enantiomer and isotope fractionations were two independent processes and those both were affected by reaction of individual enzymes and mass transport within the cell. Therefore the quantification of the fate of chiral compounds in the environment by combination of isotope and enantiomer fractionation needs to be done with caution.



TOC

INTRODUCTION

An increasing level of anthropogenic chemicals are chiral compounds which raise not only environmental concerns but also possess enantiomer-specific environmental toxicity.¹ Estimates suggest that up to one third of all anthropogenic compounds such as fungicides, herbicides, and antibiotics are chiral, of which many are produced by chemical synthesis as racemates.² The changes in enantiomer ratio have been suggested as an indicator for biodegradation of chiral compounds and have also been applied to track *in*

situ degradation at field sites.^{3,4} Similarly, the changes in stable isotope ratio of contaminants have been used to monitor biodegradation in environmental studies.⁵ Therefore, the combination of enantiomer and isotope fractionation holds immense potential for characterization and quantification of biodegradation processes.⁶ Combination of isotope fractionation and enantiomer fractionation has already been applied for the evaluation of chiral compounds in the field, for example, phenoxy acid herbicides and their metabolites.⁷

Amongst these chiral compounds, α -hexachlorocyclohexane (HCH) is one of the persistent organic pollutants posing a threat to the environment appearing world-wide as point or dispersed pollution.⁸ Its enantiomer degradation and fate under natural or field conditions should therefore be evaluated.⁹ Recently, compound specific isotope analysis (CSIA) and enantioselective stable isotope analysis (ESIA) have been proposed as tools to monitor transformation of α -HCH in a complex ground water system.¹⁰

Indeed, the application of the combined isotope and enantiomer fractionation analysis for evaluation of contaminants degradation has challenged environmental scientists for almost a decade now. Jammer et al.¹¹ provided a description of enantiomer fractionation by a quantitative structure–activity relationship model (QSAR) for enantioselective hydrolysis of 2-(phenoxy) propionate during enzymatic degradation by lipases from *Pseudomonas fluorescens*, *Pseudomonas cepacia*, and *Candida rugosa*. The authors recommend a quantification of enantiomer fractionation using the Rayleigh approach which is similar to the quantification of stable isotope fractionation. However, a theoretical foundation for models which describe the molecular mechanisms governing isotope and enantiomer fractionation processes remains lacking.

The genes responsible for HCH degradation, known as *lin* genes, are generally present in aerobic HCH degrading *Sphingomonads*. These genes were first identified and characterized in *Sphingobium japonicum* UT26¹² followed by *S. indicum* B90A¹³. The 156-amino acid long product of this gene, known as HCH dehydrochlorinase, was found localized in the periplasm.¹² The LinA enzyme performs the initial step of dehydrochlorination, converting α -HCH into α -PCCH. It has been reported that the *linA* genes are under continuous selection pressure and thus exist in several variants.¹⁴⁻¹⁸ There are two copies of *linA* genes i.e., *linA1* and *linA2* present in *S. indicum* B90A and *Pseudomonas aeruginosa* ITRC-5, whereas only *linA2* is present in *S. indicum* UT26. The *linA1* and *linA2* genes of strain B90A coded enzymes differ by 10% in their amino acid sequence, and preferentially degrade (+) α -HCH and (-) α -HCH enantiomers, respectively.¹⁹⁻²¹ Among all the strains included in the current study, the *linA* gene of strain HDIPO4 was shown as the most divergent, with 94.8 % sequence similarity to *linA1* and 92.9 % to *linA2*.²¹ So far, studies have reported the difference in the degradation potential of these *Sphingomonads* based on sequence polymorphism^{21, 22}, but there are no reports of enantiomer fractionation factors of α -HCH by using purified enzymes.

In this study, the LinA protein group was selected as a model system with two variants namely LinA1 and LinA2. In order to understand the correlation of isotope fractionation and enantiomer fractionation, a series of experiments were conducted. The initial set of experiments involved six *Sphingobium* strains (namely *Sphingobium quisquiliarum* P25, *S. lucknowense* F2, *S. chinhatense* IP26, *S. ummariense* RL3, *Sphingobium* sp. HDIPO4, *S. baderi* LLO3) to observe their efficacy for α -HCH degradation during growth. Further experiments were conducted with the objective to reduce the complexity of the degrading system, represented by resting cells, crude cell extracts and purified enzymes. Resting cells were assumed to have a stable ratio of LinA1 and LinA2 enzymes (experiment a - d). Degradation experiments by crude extract were conducted to guarantee stable concentration of Lin enzymes and to avoid the effect of cell membrane and (experiment e - h). As a further step, experiments using purified enzyme were conducted to characterize the specificity of LinA1 (experiment I - k) and LinA2 (experiment l - m) towards the α -HCH enantiomers and to portray degradation mechanisms exhibited by individual enzymes. Reaction kinetics, carbon stable isotope fractionation and enantiomer fractionation were studied as descriptors for the reaction. Isotope and enantiomer fractionation were evaluated and discussed based on the concept of rate-limitation of preceding reaction steps during uptake, membrane transport and bond cleavage. Furthermore, we discuss the implication of applying enantiomer and isotope fractionation for charactering biodegradation in field studies, based on the molecular mechanisms of isotope fractionation and enantiomer fractionation processes.

MATERIALS AND METHODS

Chemicals. α -HCH (analytical purity, 99%), hexachlorobenzene (HCB, analytical purity, 97%), imidazole (analytical purity, 99%) and ampicillin (analytical purity, 95%) were purchased from Sigma Aldrich (Germany). *n*-pentane (analytical purity, 99%) was supplied by Carl Roth, Germany. TRIS was supplied by Geyer, Germany.

Bacterial strains and Cultivation Conditions. *Sphingobium spp.* (B90A, P25, F2, IP26, RL3, HDIPO4, LLO3) and *E. coli* BL21 (AI) were maintained in the Molecular Biology Laboratory, University of Delhi, India. The information for cultivation can be found in SI.

Cell Suspension and Bacterial Crude Extract of B90A. Bacterial cells were harvested by centrifugation at $8.000 \times g$ at 4°C for 20 min when the A_{600} of cultures reached 0.5-0.6 (logarithmic phase). The cells were washed twice by sequential re-suspending and centrifugation with 0.1 M TRIS-HCl buffer at pH 7.5. The cell suspension was used in subsequent resting cell degradation experiments. For crude extract, the bacterial pellet was stored at -20°C , and crude extract was prepared with French Press (Thermo Fisher Scientific, Bremen) at 20,000 psi before using.

Enzyme Expression and Purification. Overnight grown culture was inoculated (1% v/v) in 100 mL LB media (See in SI) amended with antibiotics and incubated at 30°C with shaking at 200 rpm until the OD_{600} reached 0.5-0.6. The induced culture was then harvested by centrifugation at $8.000 \times g$ for 15 min at 4°C . Enzyme purification procedures are provided in SI section 3.

Degradation Experiments. Batch degradation experiments were conducted with 240mL bottles with 100mL medium (for growing cell degradation) or buffer (for resting cells, crude extract and enzyme degradation). The initial concentration of α -HCH was $5.5 \mu\text{M}$. Different amount of resting cells, crude extract and enzymes were used for the experiments. Bottles were sacrificed over degradation time. The detailed information of experiments, such as the concentration of enzymes and the amount that used for degradation experiments is described in SI section 2.

Analytical Methods and Data Evaluation. The concentration of HCH was analyzed by a GC equipped with a FID. The concentration of protein was quantified by NanoDrop ND-1000 Spectrophotometer from Thermo Fisher Scientific. The carbon isotope composition was analyzed by gas chromatography isotope ratio mass spectrometry (GC-IRMS), as described previously.²³ The carbon isotope fractionation of α -HCH and its enantiomers were quantified using the Rayleigh equation. A model was developed as Eq.4 for the quantification of enantiomer fractionation. The detailed information can be found in SI section 4 - 6.

RESULTS

The carbon stable isotope composition of α -HCH was analyzed during biodegradation for quantification of isotope fractionation using the Rayleigh equation (Eq. 1). Enantiomer fractionation was quantified by the model (Eq. 3). The pseudo-first-order kinetic rate constants (κ), isotope enrichment factors and enantiomer fractionation factors obtained from each set of experiments are summarized in Table 1.

Degradation by Growing Cells. Degradation experiments of α -HCH enantiomers were conducted using six *Sphingobium spp.* in minimal salt medium (MSM). Carbon isotope enrichment of α -HCH enantiomers associated with the degradation was observed in culture experiments (Fig. S1). Only the degradation of α -HCH enantiomers by strain HDIPO4 could be modeled by the pseudo-first order-kinetics with a good coefficient of determination (R^2) of 0.96/0.95 (Fig. S2). Plotting EF(-) over time (Fig. S3), the enantiomer selectivity was variable during the degradation. Each of the *Sphingomonas* species has at least two enzymes (LinA1 and LinA2) catalyzing the initial step of α -HCH enantiomers degradation. Thus, we speculated that the expression of LinA enzymes changed during growth, which might affect the degradation kinetic of individual enantiomers and therefore the enantiomer selectivity changed. The six strains also showed differences in isotope enrichment of α -HCH enantiomers (Fig. S1). This variability of enantiomer and isotope fractionation leads to a tantalizing question on mechanisms controlling both processes. Particularly for the interpretation of enantiomer and isotope patterns in the environment which is a proxy of *in situ* degradation. Therefore, to characterize the factors governing enantiomer and isotope fractionation, we conducted a series of experiments with decreasing complexity of the degrading system.

Degradation by Resting Cells. Batch experiments with different amount of resting cells from *Spingobium indicum* strain B90A were conducted based on the hypothesis that the ratio of LinA enzymes and their activities are constant over the time in the individual experiments (experiments a~d). For (+) α -HCH transformation, the degradation rates could be described by pseudo-first-order kinetics with κ^+ values between $0.06 \pm 0.01 \text{ h}^{-1}$ and $0.49 \pm 0.03 \text{ h}^{-1}$, $R^2 > 0.93$ (Fig. S6). The obtained carbon isotope enrichment factors ϵ_c^+ in the individual experiments were $-6.4 \pm 0.7 \text{ ‰}$, $-6.2 \pm 1.2 \text{ ‰}$ and $-6.1 \pm 1.1 \text{ ‰}$, which were statistically identical and thus describing isotope fractionation robustly. For (-) α -HCH transformation, no significant isotope fractionation was observed at higher κ^- values of $0.81 \pm 0.12 \text{ h}^{-1}$ and $0.76 \pm 0.09 \text{ h}^{-1}$ (Fig. S4 a, b). However, at lower rates of $\kappa^- = 0.35 \pm 0.02 \text{ h}^{-1}$ and $0.15 \pm 0.02 \text{ h}^{-1}$, significant isotope enrichment was observed with $\epsilon_c^- = -2.3 \pm 0.4 \text{ ‰}$ and $-2.3 \pm 0.3 \text{ ‰}$, respectively. This suggests that isotope fractionation was depending on the degradation rate and the uptake, transport of HCH across the cell envelope or enzyme binding which could be rate limiting and thus the higher rate constants, leading to decrease of observed carbon isotope fractionation.

However, with an increase of the κ value from $0.10 \pm 0.01 \text{ h}^{-1}$ over $0.21 \pm 0.03 \text{ h}^{-1}$ and $0.47 \pm 0.05 \text{ h}^{-1}$ to $0.61 \pm 0.06 \text{ h}^{-1}$ (Fig. S6), the enantiomer fractionation factors varied between $-1.07 \pm 0.20 \text{ ‰}$ and $-0.54 \pm 0.14 \text{ ‰}$ (Fig. 2_RC), suggesting that enantiomer fractionation was variable depending on the degradation rate.

Degradation by Crude Extract. The degradation by using different amount of cell crude extracts followed pseudo-first-order kinetics (Fig. S6 e-h). Significant isotope fractionation was observed during (+) α -HCH transformation when the κ^+ values were $0.30 \pm 0.07 \text{ h}^{-1}$ and $0.12 \pm 0.02 \text{ h}^{-1}$ (Fig. S6) and identical ϵ_c^+ were obtained with $-7.4 \pm 0.7 \text{ ‰}$ and $-8.0 \pm 1.3 \text{ ‰}$ (Fig. 1), respectively. In case of (-) α -HCH transformation, no significant isotope enrichment was observed when the corresponding κ^- values were $0.58 \pm 0.13 \text{ h}^{-1}$ and $0.45 \pm 0.06 \text{ h}^{-1}$ (Fig. S6). Significant carbon isotope enrichment of $\epsilon_c^- = -3.4 \pm 0.5 \text{ ‰}$ and $-3.4 \pm 0.6 \text{ ‰}$ were observed with lower reaction rates of $0.19 \pm 0.02 \text{ h}^{-1}$ and $0.18 \pm 0.02 \text{ h}^{-1}$, respectively. The enantiomer fractionation factors varied between $-1.35 \pm 0.13 \text{ ‰}$ and $-0.71 \pm 0.19 \text{ ‰}$ (Fig. 2_CE) with κ values between $0.11 \pm 0.02 \text{ h}^{-1}$ and $0.38 \pm 0.1 \text{ h}^{-1}$ (Fig. S6), which was similar to the resting cell degradation experiments (Table 1).

Degradation by Purified Enzymes. The enzyme experiments showed a nearly exclusive degradation of (-) α -HCH by LinA2 and of (+) α -HCH by LinA1, respectively. The degradation of α -HCH enantiomers using different amount of purified enzymes could be described by the pseudo-first-order kinetics with rate constants between $0.13 \pm 0.02 \text{ h}^{-1}$ and $0.65 \pm 0.10 \text{ h}^{-1}$ (Fig. S6). LinA1 degraded preferentially (+) α -HCH with a κ^+ of $0.28 \pm 0.02 \text{ h}^{-1}$ and $0.13 \pm 0.02 \text{ h}^{-1}$, the obtained ϵ_c^+ values were $-11.3 \pm 2.0 \text{ ‰}$ and $-10.9 \pm 1.5 \text{ ‰}$, respectively (Fig. 1). Three sets of degradation experiments were conducted with LinA2. With κ^- of $0.65 \pm 0.10 \text{ h}^{-1}$, $0.54 \pm 0.28 \text{ h}^{-1}$ and $0.27 \pm 0.05 \text{ h}^{-1}$, the isotope enrichment factors were $-3.7 \pm 0.6 \text{ ‰}$, $-4.0 \pm 1.0 \text{ ‰}$ and $-3.6 \pm 0.5 \text{ ‰}$, respectively.

The kinetic rate constants of enantiomers were used to evaluate the enantiomer fractionation (Fig. 2). For (-) α -HCH degradation by LinA2, different kinetic constants in parallel experiments (i ~k) were obtained and the enantiomer fractionation factors were statistically identical ($-2.70 \pm 0.50 \text{ ‰}$, $-2.28 \pm 0.19 \text{ ‰}$ and $-2.42 \pm 0.20 \text{ ‰}$, respectively). (+) α -HCH degradation by LinA1 resulted in the enantiomer fractionation factors of $2.13 \pm 0.52 \text{ ‰}$ and $2.37 \pm 0.48 \text{ ‰}$. In all enzyme degradation experiments, despite the variation of kinetic rate constants, the enantiomer fractionation factors were nearly identical considering the confidence intervals (Table 1).

The apparent kinetic isotope effect of carbon ($AKIE_C$) was calculated amounting to 1.035 and 1.012 for LinA1 and LinA2 respectively (Tab. S1) when assuming an E2 elimination reaction with a concerted cleavage of a C-Cl and C-H bond. The $AKIE_C$ of LinA2 has consistent order of magnitude as the quantum chemical modeling.²⁴ The $AKIE_C$ of LinA1 is higher than the value get from quantum chemical modeling but similar as the value observed in other studies which involving C-Cl bond cleavage.²⁴⁻²⁶

DISCUSSION

Quantification of Enantiomer Fractionation. Quantification of enantiomer fractionation has already been proposed using different models, mainly based on the Rayleigh model. Gasser and colleagues²⁷ proposed to apply the simplified Rayleigh equation (Eq. 1):

$$\ln\left(\frac{R_t}{R_0}\right) = \varepsilon_c \times \ln\frac{C_t}{C_0} \quad (1)$$

where $R=EF(-)/EF(+)$, EF is the enantiomer fraction, $EF(-)=C(-)/C$, $EF(+)=C(+)/C$, C is the total concentration of both enantiomers, $C(-)$ and $C(+)$ are the concentration of $(-)$ and $(+)$ enantiomers, respectively. This simplified Rayleigh equation was developed for the evaluation of isotope fractionation considering the concentration of the heavy isotope to be significantly smaller, thus, for most light elements (H, C, N and O) at natural abundance, $R_A+1 \approx 1$ ($R_A = {}^H A / {}^L A$, ${}^H A$ and ${}^L A$ are the total amounts of the heavy and light isotope of an element in compound A). However, the assumption of $R+1 \approx 1$ is not valid for the evaluation of enantiomer fractionation, as the enantiomers appear in similar initial concentration. The enantiomer fractionation was also proposed to be quantified by applying the general form of Rayleigh equation²⁸:

$$\frac{R_t}{R_0} = \left(\frac{\frac{C_t}{C_0}}{\frac{R_t+1}{R_0+1}} \right)^\varepsilon \quad (2)$$

which can be rewritten as Eq. 3.

$$\ln\left(\frac{R_t}{R_0}\right) = \varepsilon_e \times \ln\frac{C^{(+)}_t}{C^{(+)}_0} \quad (3)$$

Conventionally the Rayleigh equation for quantifying the fractionation assumes one process compiling two constant reaction rates on individual species with almost homogeneous reaction conditions and predicts the separation of both species. However, the enantiomer fractionation of α -HCH is the results of two individual degradation processes, governed by LinA1 and LinA2 as the main enzyme for $(+)$ and $(-)$ - α -HCH degradation, respectively. In this case, the Rayleigh equation is not suitable in a strict sense for quantifying enantiomer fractionation, as two independent physio-chemical processes are not necessarily correlated in a homogeneous reaction. Therefore, we developed a model for quantification of enantiomer fractionation using rate laws by characterizing the relationship between the changes of enantiomer concentrations (enantiomer ratio) and bulk α -HCH concentration over time. In this study, degradation of α -HCH followed first order or pseudo-first-order kinetics over a certain concentration range practically in resting cell as well as in degradation experiments with crude extracts or isolated enzymes (Fig. S6). The development of this model assumes the first order rate law ($C_t = C_0 \times e^{-k \times t}$) for the degradation of bulk α -HCH and can be therefore applied for the experimental data fitting the first order bulk degradation which is the same assumption as reported by Jammer²⁹. The development process of this model has been described in detail in SI section 6.

This model (Eq. 4) was applied for quantification of enantiomer fractionation of our data sets.

$$\ln\left(\frac{C^{(+)}_t}{C^{(-)}_t}\right) = \varepsilon_e \times \ln\frac{C_t}{C_0} + A \quad (4)$$

The plus and minus value of the enrichment factor indicate the preferred degradation of $(+)$ and $(-)$ - α -HCH, individually. A can be calculated by the initial concentration of enantiomers (see SI 7) and indicates the possible ordinate shift of experimental data (e.g., in Fig. 2 some slopes not going through the origin). The enantiomer fractionation factor ε_e links the changes in concentrations of individual enantiomers ($C(+)$, $C(-)$) to the changes in bulk concentration (C). Moreover, the enantiomer fractionation can be calculated from the degradation rate constants of individual enantiomers and bulk α -HCH using Eq. 5.

$$\varepsilon_e = \frac{(k^{(+)} - k^{(-)})}{k} \quad (5)$$

κ , $\kappa(-)$ and $\kappa(+)$ are the degradation rate constants of bulk α -HCH, $(-)$ - α -HCH and $(+)$ - α -HCH, respectively.

Considering the CI (95%), the enantiomer fractionation factors obtained by Eq.⁴ are identical to the ones which calculated by the corresponding κ values using Eq. 5 (Tab.1). The enantiomer fractionation quantified by Eq. 4 and Eq.5 showed a good linear correlation (Fig. 3). Empirically, both equations can be used for describing enantiomer fractionation when both enzymes have constant degradation rates and the process thus follows pseudo-first-order reaction kinetic.

Variability of Enantiomer Fractionation. Due to the high variability of enantiomer fractionation during α -HCH degradation by the six *Sphingobium* strains, enantiomer fractionation data obtained from the

growing cells of strain B90A and UT26 from our previous work²⁸ was re-evaluated by Eq. 4. For both strains, the degradation of (+) and (-) α -HCH did not follow pseudo-first-order kinetics with reliable uncertainty (Fig. S7). Similarly, the enantiomer fractionation changed over the course of degradation and the changes in concentration of bulk α -HCH and enantiomers could not be correlated by one factor (Fig. S7).

In addition, the enantiomer selectivity of *S. indicum* B90A observed in different studies also indicates the variability of enantiomer fractionation. For example, biodegradation of α -HCH by *S. indicum* B90A showed preferential degradation of the (+) α -HCH enantiomer at the beginning of the degradation²⁸. However, enantioselectivity of α -HCH was not observed with the same strain elsewhere³⁰. In the present study, the resting cells and crude extract both preferred (-) α -HCH. This indicates that different growth phases (lag phase, log phase, and stationary phase) or different cultivation conditions lead to changes in the regulation of the LinA1 and LinA2 abundance. This is in agreement with the variable enantiomer selectivity of the six *Sphingobium* strains. Potentially, different ratios of LinA1 and LinA2 may be expressed under growth conditions which change the selectivity of enantiomer degradation.

Correlation of Isotope and Enantiomer Fractionation. Isotope fractionation is determined by bond cleavage or formation in the first irreversible reaction step and can be modified due to rate limitation of preceding steps in a complex biochemical reaction^{31, 32}. The observed isotope fractionation contains information on the transition state of bond cleavage and kinetic rate limitation prior irreversible bond cleavage. The isotope fractionation follows virtually first order kinetics as it depends on the kinetics of bond cleavage in the transition state which can be quantified by the Rayleigh equation. For the degradation of HCH, LinA dehydrochlorinates the substrates most likely via an elimination mechanism (E2 reaction)³³, which is probably identical for both enantiomers³⁴. Assuming that the dehydrochlorination mechanism for both enantiomers is identical and follows E2 elimination³⁴, the rate limitation might be a result of binding within the enzyme pocket. Binding of γ and β substrates within LinA can effect transition state and reaction rates as suggested by QM/MM modeling studies³⁴. Preceding reaction steps such as transport in the cell, binding to the enzyme can modify the kinetic isotope effect (KIE) of the bond cleavage reaction³⁵. The kinetics of binding of α -HCH enantiomers to the individual enzymes might lead to rate limitation which would explain the observed different fractionation factors. However, further QM/MM modeling studies would be required to solve this question.

Enantiomer fractionation can be influenced by two factors: (i) binding of substrate to the enzyme with respect to the stereo chemical position in the enzyme pocket which can lead to different reaction ratios³⁶; (ii) the reactivity of two individual enzymes with specificity towards enantiomers as observed in the enzyme assays with LinA1 and LinA2. In this case, the enantiomer degradation should be rationalized as individual substances which are controlled by the expression and activity of individual enzymes within the machinery of the cell³⁷. The Rayleigh equation is valid for quantification of a single process, and therefore the empirical determined fractionation factor averages the two individual reactions. Empirically the obtained fractionation factors might characterize the reaction as long as the kinetic of the individual processes is constant. However if the kinetic reaction rate is changed due to individual regulation of the individual enzymes, the enantiomer fractionation process cannot be described by one factor. In growing cells experiments we observed a variability of enantiomer fractionation which leads to the hypothesis that change of reactivity of the individual enzyme systems is due to the expression of enzymes during growth. The isotope fractionation of individual enantiomers is governed by the mechanisms of bond cleavage. However, the binding within the enzyme and the transition state of bond cleavage may not be chemically identical and therefore result in different fractionation factors. As the chemical bond cleavage is probably not much different in a chemical sense, one may hypothesize that the kinetic of binding to enzymes leads to rate limitation and thus modifies the observed carbon isotope fractionation. Based on our data, we cannot evaluate the rate limitation and carbon isotope fractionation in more depth.

Effect of Mass Transport on Isotope and Enantiomer Fractionation. In order to evaluate the effect of mass transport into the cells, isotope fractionation of α -HCH during resting cells and crude extract experiments were compared. For (+) α -HCH, even with the same degradation rate, the ϵ_c^+ values obtained from resting cells and crude extract still show that mass transfer across the outer and cytoplasmic membranes may reduce the isotope enrichment, and lead to a relatively smaller isotope fractionation in resting cell experiments. Compared to resting cell and crude extract degradation of α -HCH, significant higher isotope enrichment factors were obtained in the purified enzyme (LinA1) experiments. The difference of carbon fractionation between crude extract and enzyme indicates that cell material such as vesicles or membrane remnants may affect the transport of substrate leading to lower isotope fractionation.

Interestingly, ϵ_c^- values obtained from resting cell experiments were only slightly lower than the ones from the crude extract experiments. This indicates that mass transfer into the cells does not affect the isotope fractionation of (-)- α -HCH significantly. Statistically similar values were also obtained comparing pure enzyme and crude extract experiments, indicating that mass transfer is not limited and that bond cleavage of the reaction governs the observed isotope enrichment.

Overall, the uptake and passage through the cell wall led to rate limitation reducing the carbon isotope fractionation for both enantiomers, indicating that uptake affects the isotope fractionation of individual enantiomers in a similar way. A similar effect on the reduction of carbon isotope fractionation had been observed with a non-enantiomeric substance and uptake of substrate into the cell often reduce isotope fractionation³⁸. The investigation of enantiomer and isotope fractionation of phenoxypropionic acid herbicides in aerobic biodegradation gave contrasting results as high enantiomer fractionation and minor carbon isotope fractionation were observed³⁹. Qiu and colleagues observed higher carbon isotope fractionation of (R)-DCPP in RdpA enzyme degradation compared to degradation by whole cell of the host organism *Sphingobium herbicidovorans* MH,³⁹ however the enantiomer fractionation during uptake was not studied in detail. They speculated on active transport over the cell membrane as a mechanism of enantiomer fractionation and masking of isotope fractionation. In contrast the enantiomer and isotope fractionation during α -HCH degradation is related to the reaction kinetic governed by the uptake into the cell and activity of individual enzymes (LinA and LinA2).

The mass transport into cells and in the cells have different effects on the isotope fractionation of (+)- α - and (-)- α -HCH. Significant effects will reduce the isotope enrichment and lead to smaller isotope enrichment factors. However, as enantiomer fractionation only depends on the difference of the degradation rate of (-) and (+)- α -HCH, mass transfer will only affect the enantiomer fractionation in the case that mass transfer is the rate limiting step of the reaction.

Effect of Degradation Rate on Isotope and Enantiomer Fractionation. Significant carbon isotope fractionation of (-)- α -HCH in the resting cell experiments was only observed when the κ^- were $0.35 \pm 0.02 \text{ h}^{-1}$ and $0.15 \pm 0.02 \text{ h}^{-1}$. Higher degradation rates of 0.76 ± 0.09 and $0.81 \pm 0.12 \text{ h}^{-1}$ lead to the masking of isotope fractionation as the bond cleavage is not the main rate limiting step of the reaction. The same observation was made in the crude extract experiments, which demonstrates that the isotope fractionation at higher rates does not characterize the bond cleavage as it is not the rate determining step of the reaction. When the κ^+ value of resting cell experiments fall below 0.5 h^{-1} , significant isotope enrichment can be observed and the enrichment factors of (+)- α -HCH were nearly identical in parallel experiments (Table 1). The same results were observed in the crude extract experiments. These results indicate that the degradation rate did not significantly affect the carbon isotope enrichment of (+)- α -HCH and that the bond cleavage was the main rate limiting step of the reaction.

For enantiomer fractionation, with variable rate constants of individual enantiomers, the enantiomer fractionation factors (ϵ_e) from each set of experiments also showed variability (Table 1). ϵ_e can be determined by the difference of enantiomer degradation rates ($\kappa^+ - \kappa^-$) and bulk α -HCH degradation rate (κ) using Eq. 4. The ϵ_e values indicate preferential degradation of (-)- α -HCH over (+)- α -HCH enantiomer in all resting cell and crude extract degradation experiments. The significant variability of ϵ_e indicates enantiomer fractionation depends on reaction rates governed by the activity and also the amount of each individual enzyme. Comparison of resting cell with crude extract suggests that uptake into cells reduced the enantiomer fractionation to some extent. As diffusion is identical for enantiomers, the chemical passage through the membrane should not affect the enantiomer composition. Therefore, the degradation kinetic of each enantiomer governs enantiomer fractionation. This is mechanistically not comparable to mass transfer limitation affecting isotope fractionation, as two individual substances are reacted by two individual enzymes and variability in degradation rate do not allow correlation with mass transfer limitation. If varying enantiomer fractionation over time is observed, it indicates there are multiple enzymes involved in the degradation.

ENVIRONMENTAL IMPLICATION

Our study shows that the carbon isotope fractionation of α -HCH enantiomers potentially can be used to quantify the degradation in field studies. The LinA1 and LinA2 enzymes have shown to exhibit highly selective degrading potential catalyzing the reaction of only one enantiomer almost exclusively. Therefore, the degradation can only be quantified robustly by enantiomer specific isotope analysis. The enantiomer fractionation pattern can be described by our model when both the bulk and enantiomers

degradation follow the pseudo-first-order kinetics. However, enantiomer fractionation is dependent on the expression of individual enzymes even in a pure culture. The expression of enzymes may change due to the concentration of contaminants or the physiological state of the cell. The variability of reaction conditions in soils with respect to enantiomer fractionation are currently difficult to assess.

Studies have shown that low or fluctuating levels of energy sources, high to low levels of oxygen, fluctuating and often extreme temperatures, low pH and/or high osmolality in the environment can affect the growth of microbes.⁴⁰ The physiology of cells is dependent on various abiotic and biotic factors in the environment, thereby regulating the enzymatic machinery for cellular metabolism. Thus, the enantiomer fractionation due to enzymatic degradation remains to vary for the organisms growing in field site with respect to the nutrient rich culture medium. The availability of nutrient sources affects the growth of organisms including the enzymatic activities for substrate utilization during metabolism and expression of enzymes. In the current study, highly selective LinA enzymes catalyze α -HCH enantiomer degradation by acting to provide carbon source for cellular activities²⁰. As the expression of enzymes is expected to change depending on environmental conditions, enantiomer fractionation may be variable leading to uncertainty in the quantification of biodegradation. Therefore, enantiomer fractionation may provide valuable information reflecting degradation conditions but seems to be limited value to describe a process quantitatively.

In a recent paper we used EF and isotope fractionation of individual α -HCH enantiomers for characterizing in situ degradation in complex aquifer systems in Bitterfeld Germany with changing hydrological conditions.¹⁰ We found discrepancies in calculation of the extent of biodegradation when comparing isotope and enantiomer fractionation. The mechanistic study on EF and CSIA of enantiomers show that EF fractionation is variable and depending on growth conditions. Thus, a quantitative interpretation of enantiomer fractionation needs to be taken with discretion. Attempts for using the Rayleigh equation for modeling both enantiomer and isotope fractionation⁴¹ need to be critically assessed, as the basic Rayleigh concept holds no validation for quantifying enantiomer fractionation. This study represents the first step towards developing a better understanding of isotope and enantiomer fractionation and will aid in field site evaluation.

ACKNOWLEDGEMENTS

We acknowledge the financial support from the German-Israeli Foundation for Research and Development (GIF) Grant no. I-1368-307.8/2016 ("Prediction of chiral and isotope enrichment during the transformations of halo-organic pollutants: Mechanistic and QSAR approaches"). We are grateful for the fellowship of Yaqing Liu (File No. 201301542002) and Langping Wu (File No. 201306460007) from the China Scholarship Council. Jia Liu is acknowledged for her support during set up fractionation experiments, extraction and enzyme experiments. M. Gehre, S. Kümmerl and U. Günther are acknowledged for continuous analytical support in the Isotope Laboratory of the Department of Isotope Biogeochemistry. We acknowledge the financial support of The German Academic Exchange Service (DAAD) and The Department of Science & Technology (DST) in the personal exchange program DAAD project 57035944 and DST project INT/FRG/DAAD/P-231/2013 for funding travel expenses, particularly for Puneet Kohli and Roshan Kumar.

Supporting Information Available

Additional details on strain cultivation, experiments conduction, analytic method, model development, summary of observed data.

REFERENCE

1. Ye, J.; Zhao, M.; Niu, L.; Liu, W., Enantioselective environmental toxicology of chiral pesticides. *Chem Res Toxicol* **2015**, *28*, (3), 325-38.
2. Burden, R. S.; Carter, G. A.; Clark, T.; Cooke, D. T.; Croker, S. J.; Deas, A. H.; Hedden, P.; James, C. S.; Lenton, J. R., Comparative activity of the enantiomers of triadimenol and paclobutrazol as inhibitors of fungal growth and plant sterol and gibberellin biosynthesis. *Pest Management Science* **1987**, *21*, (4), 253-267.

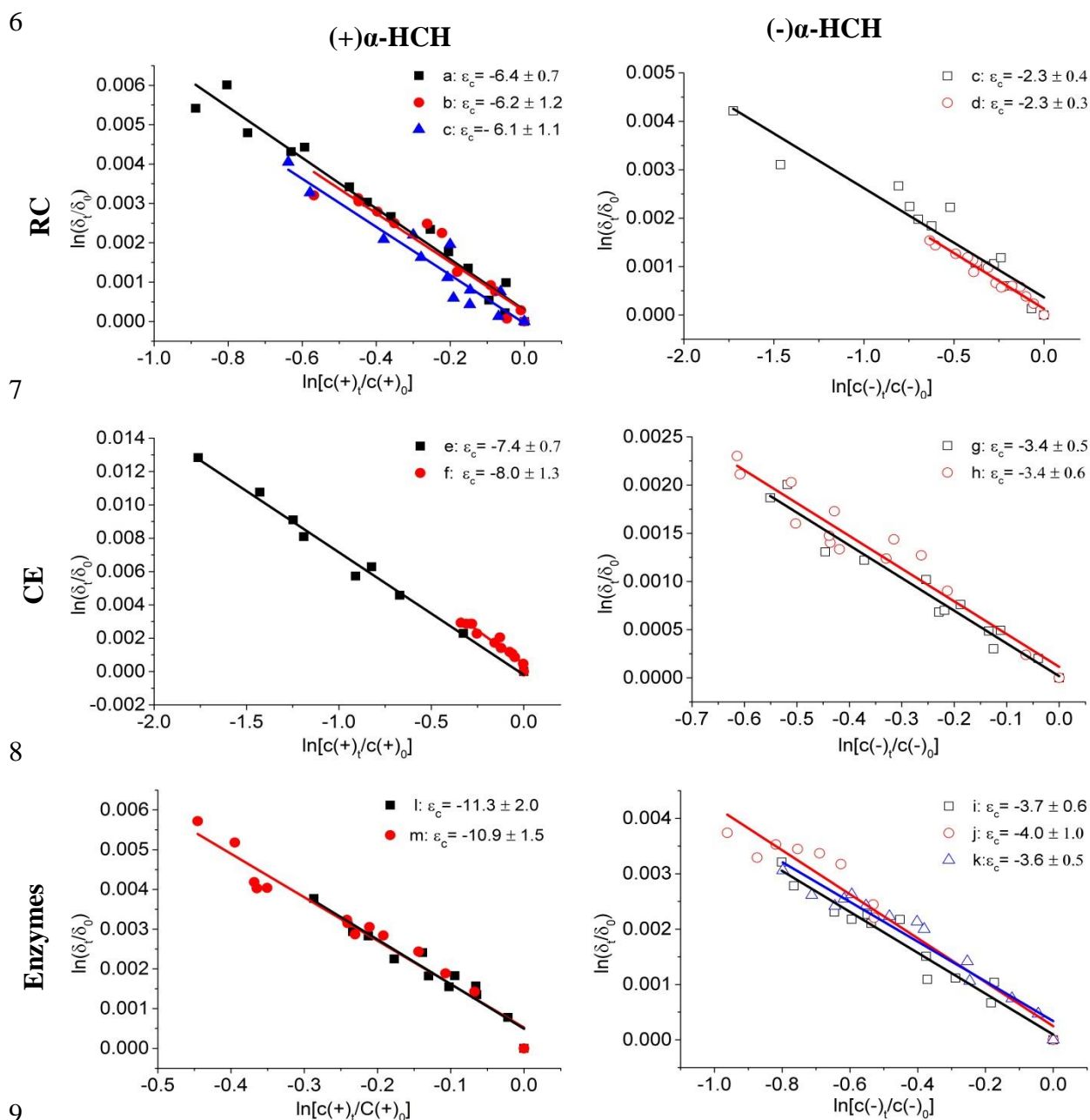
3. Muller, T. A.; Kohler, H. P., Chirality of pollutants--effects on metabolism and fate. *Appl Microbiol Biotechnol* **2004**, *64*, (3), 300-16.
4. Hashim, N.; Shafie, S.; Khan, S., Enantiomeric fraction as an indicator of pharmaceutical biotransformation during wastewater treatment and in the environment—a review. *Environmental technology* **2010**, *31*, (12), 1349-1370.
5. Vogt, C.; Dorer, C.; Musat, F.; Richnow, H.-H., Multi-element isotope fractionation concepts to characterize the biodegradation of hydrocarbons—from enzymes to the environment. *Current opinion in biotechnology* **2016**, *41*, 90-98.
6. Nijenhuis, I.; Richnow, H. H., Stable isotope fractionation concepts for characterizing biotransformation of organohalides. *Current Opinion in Biotechnology* **2016**, *41*, 108-113.
7. Milosevic, N.; Qiu, S.; Elsner, M.; Einsiedl, F.; Maier, M.; Bensch, H.; Albrechtsen, H.-J.; Bjerg, P. L., Combined isotope and enantiomer analysis to assess the fate of phenoxy acids in a heterogeneous geologic setting at an old landfill. *Water research* **2013**, *47*, (2), 637-649.
8. Ivdra, N.; Fischer, A.; Herrero-Martin, S.; Giunta, T.; Bonifacie, M.; Richnow, H.-H., Carbon, Hydrogen and Chlorine Stable Isotope Fingerprinting for Forensic Investigations of Hexachlorocyclohexanes. *Environmental Science & Technology* **2016**, *51*, (1), 446-454.
9. Lal, R.; Pandey, G.; Sharma, P.; Kumari, K.; Malhotra, S.; Pandey, R.; Raina, V.; Kohler, H. P.; Holliger, C.; Jackson, C.; Oakeshott, J. G., Biochemistry of microbial degradation of hexachlorocyclohexane and prospects for bioremediation. *Microbiology and molecular biology reviews* **2010**, *74*, (1), 58-80.
10. Liu, Y.; Bashir, S.; Stollberg, R.; Trubitsch, R.; Weiss, H.; Paschke, H.; Nijenhuis, I.; Richnow, H. H., Compound Specific and Enantioselective Stable Isotope Analysis as Tools To Monitor Transformation of Hexachlorocyclohexane (HCH) in a Complex Aquifer System. *Environ Sci Technol* **2017**.
11. Jammer, S.; Rizkov, D.; Gelman, F.; Lev, O., Quantitative structure-activity relationship correlation between molecular structure and the Rayleigh enantiomeric enrichment factor. *Environ Sci Process Impacts* **2015**, *17*, (8), 1370-6.
12. Nagata, Y.; Miyauchi, K.; Takagi, M., Complete analysis of genes and enzymes for γ -hexachlorocyclohexane degradation in *Sphingomonas paucimobilis* UT26. *Journal of industrial microbiology & biotechnology* **1999**, *23*, (4), 380-390.
13. Kumari, R.; Subudhi, S.; Suar, M.; Dhingra, G.; Raina, V.; Dogra, C.; Lal, S.; van der Meer, J. R.; Holliger, C.; Lal, R., Cloning and characterization of lin genes responsible for the degradation of hexachlorocyclohexane isomers by *Sphingomonas paucimobilis* strain B90. *Applied and environmental microbiology* **2002**, *68*, (12), 6021-6028.
14. Böltner, D.; Moreno-Morillas, S.; Ramos, J. L., 16S rDNA phylogeny and distribution of lin genes in novel hexachlorocyclohexane-degrading *Sphingomonas* strains. *Environmental Microbiology* **2005**, *7*, (9), 1329-1338.
15. Mohn, W. W.; Mertens, B.; Neufeld, J. D.; Verstraete, W.; de Lorenzo, V., Distribution and phylogeny of hexachlorocyclohexane-degrading bacteria in soils from Spain. *Environ Microbiol* **2006**, *8*, (1), 60-8.
16. Sharma, P.; Pandey, R.; Kumari, K.; Pandey, G.; Jackson, C. J.; Russell, R. J.; Oakeshott, J. G.; Lal, R., Kinetic and sequence-structure-function analysis of known LinA variants with different hexachlorocyclohexane isomers. *PLoS One* **2011**, *6*, (9), e25128.
17. Shrivastava, N.; Macwan, A. S.; Kohler, H. E.; Kumar, A., Important amino acid residues of hexachlorocyclohexane dehydrochlorinases (LinA) for enantioselective transformation of hexachlorocyclohexane isomers. *Biodegradation* **2017**, *28*, (2-3), 171-180.
18. Macwan, A. S.; Kukshal, V.; Srivastava, N.; Javed, S.; Kumar, A.; Ramachandran, R., Crystal structure of the hexachlorocyclohexane dehydrochlorinase (LinA-type2): mutational analysis, thermostability and enantioselectivity. *PLoS One* **2012**, *7*, (11), e50373.
19. Singh, A. K.; Chaudhary, P.; Macwan, A. S.; Diwedi, U. N.; Kumar, A., Selective loss of lin genes from hexachlorocyclohexane-degrading *Pseudomonas aeruginosa* ITRC-5 under different growth conditions. *Appl Microbiol Biotechnol* **2007**, *76*, (4), 895-901.
20. Suar, M.; van der Meer, J. R.; Lawlor, K.; Holliger, C.; Lal, R., Dynamics of multiple lin gene expression in *Sphingomonas paucimobilis* B90A in response to different hexachlorocyclohexane isomers. *Appl Environ Microbiol* **2004**, *70*, (11), 6650-6.
21. Verma, H.; Kumar, R.; Oldach, P.; Sangwan, N.; Khurana, J. P.; Gilbert, J. A.; Lal, R., Comparative genomic analysis of nine *Sphingobium* strains: insights into their evolution and hexachlorocyclohexane (HCH) degradation pathways. *BMC genomics* **2014**, *15*, (1), 1014.
22. Geueke, B.; Garg, N.; Ghosh, S.; Fleischmann, T.; Holliger, C.; Lal, R.; Kohler, H. P. E., Metabolomics of hexachlorocyclohexane (HCH) transformation: ratio of LinA to LinB determines metabolic fate of HCH isomers. *Environmental Microbiology* **2013**, *15*, (4), 1040-1049.

23. Badea, S. L.; Vogt, C.; Gehre, M.; Fischer, A.; Danet, A. F.; Richnow, H. H., Development of an enantiomer-specific stable carbon isotope analysis (ESIA) method for assessing the fate of alpha-hexachlorocyclo-hexane in the environment. *Rapid Commun. Mass. Sp.* **2011**, *25*, (10), 1363-1372.
24. Manna, R. N.; Dybala-Defratyka, A., Insights into the elimination mechanisms employed for the degradation of different hexachlorocyclohexane isomers using kinetic isotope effects and docking studies. *Journal of Physical Organic Chemistry* **2013**, *26*, (10), 797-804.
25. Nikolausz, M.; Nijenhuis, I.; Ziller, K.; Richnow, H. H.; Kästner, M., Stable carbon isotope fractionation during degradation of dichloromethane by methylotrophic bacteria. *Environmental Microbiology* **2006**, *8*, (1), 156-164.
26. Fletcher, K. E.; Löffler, F. E.; Richnow, H.-H.; Nijenhuis, I., Stable carbon isotope fractionation of 1, 2-dichloropropane during dichloroelimination by Dehalococcoides populations. *Environmental science & technology* **2009**, *43*, (18), 6915-6919.
27. Gasser, G.; Pankratov, I.; Elhanany, S.; Werner, P.; Gun, J.; Gelman, F.; Lev, O., Field and laboratory studies of the fate and enantiomeric enrichment of venlafaxine and O-desmethylvenlafaxine under aerobic and anaerobic conditions. *Chemosphere* **2012**, *88*, (1), 98-105.
28. Bashir, S.; Fischer, A.; Nijenhuis, I.; Richnow, H. H., Enantioselective carbon stable isotope fractionation of hexachlorocyclohexane during aerobic biodegradation by Sphingobium spp. *Environ. Sci. Technol.* **2013**, *47*, (20), 11432-11439.
29. Jammer, S.; Voloshenko, A.; Gelman, F.; Lev, O., Chiral and isotope analyses for assessing the degradation of organic contaminants in the environment: Rayleigh dependence. *Environ. Sci. Technol.* **2014**, *48*, (6), 3310-3318.
30. Suar, M.; Hauser, A.; Poiger, T.; Buser, H. R.; Müller, M. D.; Dogra, C.; Raina, V.; Holliger, C.; van der Meer, J. R.; Lal, R.; Kohler, H. P., Enantioselective transformation of alpha-hexachlorocyclohexane by the dehydrochlorinases LinA1 and LinA2 from the soil bacterium Sphingomonas paucimobilis B90A. *Appl. Environ. Microb.* **2005**, *71*, (12), 8514-8518.
31. Northrop, D. B., The expression of isotope effects on enzyme-catalyzed reactions. *Annual review of biochemistry* **1981**, *50*, (1), 103-131.
32. Swiderek, K.; Paneth, P., Binding isotope effects. *Chem Rev* **2013**, *113*, (10), 7851-79.
33. Okai, M.; Kubota, K.; Fukuda, M.; Nagata, Y.; Nagata, K.; Tanokura, M., Crystal structure of gamma-hexachlorocyclohexane Dehydrochlorinase LinA from Sphingobium japonicum UT26. *J Mol Biol* **2010**, *403*, (2), 260-9.
34. Manna, R. N.; Zinovjev, K.; Tunon, I.; Dybala-Defratyka, A., Dehydrochlorination of Hexachlorocyclohexanes Catalyzed by the LinA Dehydrohalogenase. A QM/MM Study. *J Phys Chem B* **2015**, *119*, (49), 15100-9.
35. Nijenhuis, I.; Andert, J.; Beck, K.; Kastner, M.; Diekert, G.; Richnow, H. H., Stable isotope fractionation of tetrachloroethene during reductive dechlorination by Sulfurospirillum multivorans and Desulfitobacterium sp. strain PCE-S and abiotic reactions with cyanocobalamin. *Applied and environmental microbiology* **2005**, *71*, (7), 3413-9.
36. Reetz, M. T., Laboratory evolution of stereoselective enzymes: a prolific source of catalysts for asymmetric reactions. *Angewandte Chemie International Edition* **2011**, *50*, (1), 138-174.
37. Müller, R. H.; Kleinstaub, S.; Babel, W., Physiological and genetic characteristics of two bacterial strains utilizing phenoxypropionate and phenoxyacetate herbicides. *Microbiol Res* **2001**, *156*, (2), 121-31.
38. Renpenning, J.; Rapp, I.; Nijenhuis, I., Substrate hydrophobicity and cell composition influence the extent of rate limitation and masking of isotope fractionation during microbial reductive dehalogenation of chlorinated ethenes. *Environ Sci Technol* **2015**, *49*, (7), 4293-301.
39. Qiu, S.; Gözdereliler, E.; Weyrauch, P.; Lopez, E. C. M.; Kohler, H.-P. E.; Sørensen, S. R.; Meckenstock, R. U.; Elsner, M., Small ¹³C/¹²C Fractionation Contrasts with Large Enantiomer Fractionation in Aerobic Biodegradation of Phenoxy Acids. *Environmental science & technology* **2014**, *48*, (10), 5501-5511.
40. van Elsas, J. D.; Semenov, A. V.; Costa, R.; Trevors, J. T., Survival of Escherichia coli in the environment: fundamental and public health aspects. *ISME J* **2011**, *5*, (2), 173-83.
41. Jin, B.; Rolle, M., Joint interpretation of enantiomer and stable isotope fractionation for chiral pesticides degradation. *Water Res.* **2016**, *105*, 178-186.

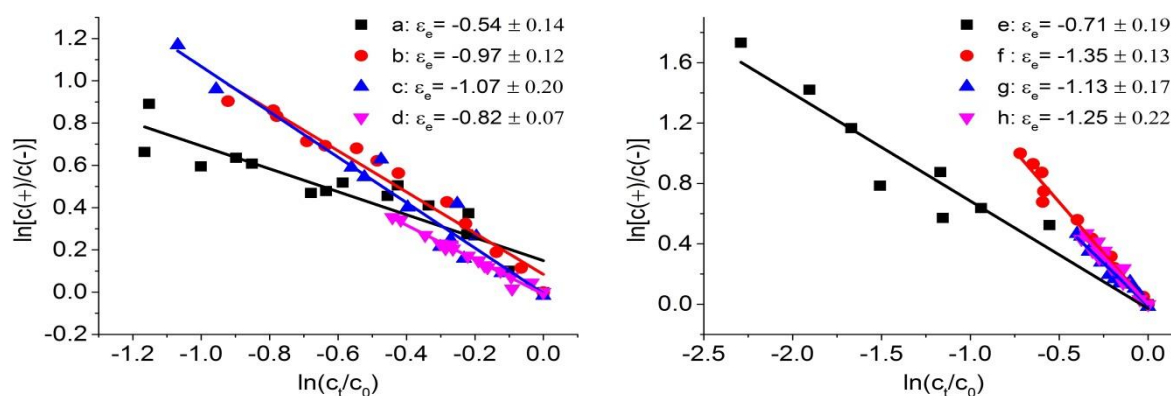
1 Table 1. Summary of carbon isotope enrichment factors (ϵ_c), enantiomer fractionation factors (ϵ_e) of (-)- α -HCH and (+)- α -HCH, and related kinetic constants (κ) in
 2 different sets of α -HCH degradation experiments by resting cell, crude extract and enzymes of strain B90A.

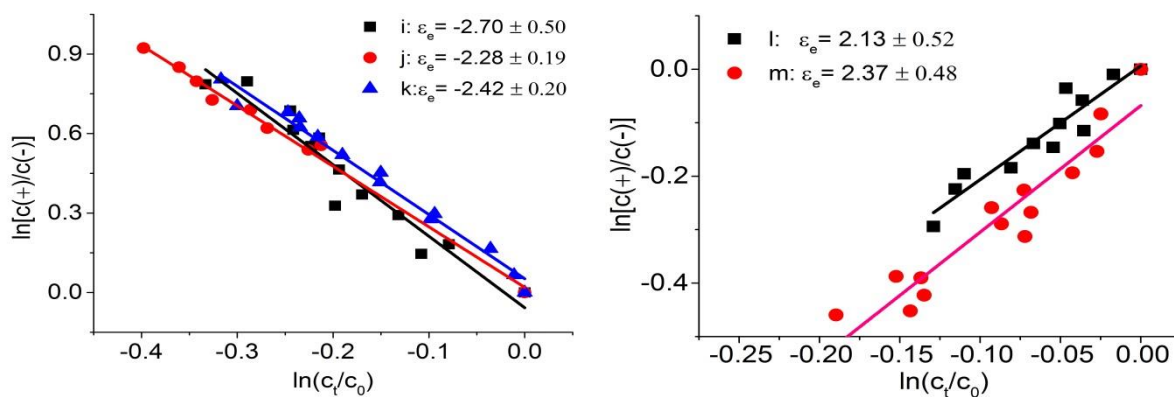
			Kinetic constant						Isotope fractionation				Enantiomer fractionation		
			bulk		(-)- α -HCH		(+)- α -HCH		(-)- α -HCH		(+)- α -HCH				
M	N	$\kappa \pm \text{CI}_{95\%}$ (h^{-1})	R^2	$\kappa \pm \text{CI}_{95\%}$ (h^{-1})	R^2	$\kappa \pm \text{CI}_{95\%}$ (h^{-1})	R^2	$\epsilon_c \pm \text{CI}_{95\%}$ (‰)	R^2	$\epsilon_c \pm \text{CI}_{95\%}$ (‰)	R^2	$\epsilon_e(\text{M})(\%)$	R^2	$\epsilon_e(\text{C})(\%)$	
Resting cell	a	15	0.61±0.06	0.98	0.81±0.12	0.95	0.49±0.03	0.99	n.s.	n.s.	-6.4±0.7	0.97	-0.54±0.14	0.84	-0.52
	b	13	0.47±0.05	0.98	0.76±0.09	0.97	0.30±0.03	0.98	n.s.	n.s.	-6.2±1.2	0.92	-0.97±0.12	0.97	-0.96
	c	12	0.21±0.03	0.96	0.35±0.02	0.99	0.12±0.02	0.96	-2.3±0.4	0.92	-6.1±1.1	0.93	-1.07±0.20	0.95	-1.11
	d	16	0.10±0.01	0.95	0.15±0.02	0.95	0.06±0.01	0.93	-2.3±0.3	0.95	n.a.	n.a.	-0.82±0.07	0.98	-0.81
	Average value									-2.3	STDV: 0.03	-6.3	STDV: 0.1		
Crude extract	e	10	0.38±0.10	0.93	0.58±0.13	0.94	0.30±0.07	0.93	n.s.	n.s.	-7.4±0.7	0.99	-0.71±0.19	0.92	-0.73
	f	13	0.24±0.04	0.94	0.45±0.06	0.96	0.12±0.02	0.91	n.s.	n.s.	-8.0±1.3	0.94	-1.35±0.13	0.98	-1.38
	g	13	0.13±0.02	0.94	0.19±0.02	0.98	0.04±0.01	0.95	-3.4±0.5	0.96	n.a.	n.a.	-1.13±0.17	0.95	-1.12
	h	14	0.11±0.02	0.91	0.18±0.04	0.91	0.05±0.01	0.91	-3.4±0.6	0.92	n.a.	n.a.	-1.25±0.22	0.93	-1.27
	Average value									-3.4	STDV: 0.02	-7.7	STDV: 0.4		
LinA2	i	13	0.23±0.06	0.87	0.65±0.10	0.95	n.a.	n.a.	-3.7±0.6	0.95	n.a.	n.a.	-2.70±0.50	0.93	-2.79
	j	9	0.23±0.11	0.76	0.54±0.28	0.74	n.a.	n.a.	-4.0±1.0	0.93	n.a.	n.a.	-2.28±0.19	0.99	-2.37
	k	14	0.11±0.02	0.90	0.27±0.05	0.91			-3.6±0.5	0.95	n.a.	n.a.	-2.42±0.20	0.98	-2.46
	Average value									-3.8	STDV: 0.2				
LinA1	l	13	0.12±0.02	0.94	n.a.	n.a.	0.28±0.02	0.98	n.a.	n.a.	-11.3±2.0	0.94	2.13±0.52	0.89	2.23
	m	14	0.05±0.01	0.91	n.a.	n.a.	0.13±0.02	0.93	n.a.	n.a.	-10.9±1.5	0.96	2.37±0.48	0.90	2.40
	Average value											-11.1	STDV: 0.3		

3 M: different sets of the experiments; N: number of samples; n.a.: not assessed since degradation was too low; n.s.: degradation observed but no significant isotope
 4 fractionation was observed, the relevant data are reported in Fig. S4); $\epsilon_e(\text{M})(\%)$: enantiomer fractionation factors by modeling using Eq. 3; $\epsilon_e(\text{C})(\%)$: enantiomer
 5 fractionation factors by calculation using Eq. 4.



10 Fig.1. Linearized Rayleigh equation plots showing the carbon isotope fractionation for the biodegradation
 11 of α-HCH enantiomers (close symbols for (+)α-HCH and open symbols for (-)α-HCH) by resting cells
 12 (RC) and crude extract (CE) of *S. indicum* strain B90A and the corresponding enzymes LinA1 and LinA2.
 13 The individual evaluation of the isotope fractionation for each individual experiment can be found in SI
 14 Fig. S5.

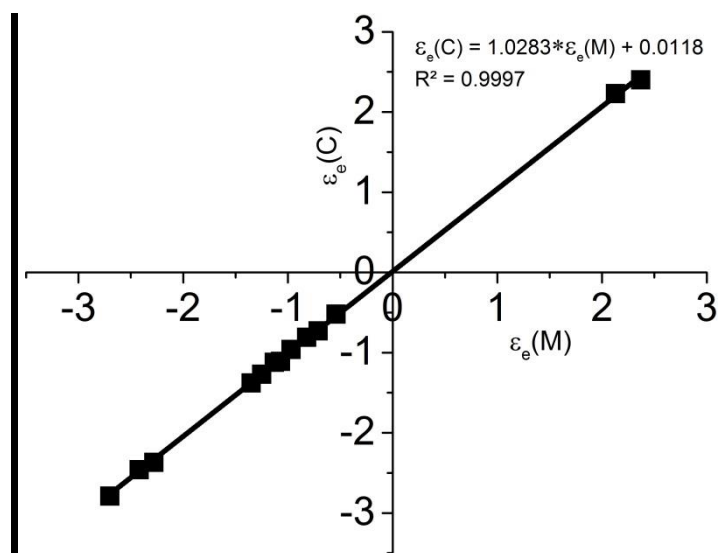




16

17 Fig.2. Linearized plots of enantiomer fractionation in the biodegradation of α -HCH: resting cells (RC);
 18 crude extract (CE); the corresponding enzyme LinA2 and LinA1. The code (a to m) refer to individual
 19 experiments of which the fractionation factors are summarized in Table 1.

20



21

22 Fig.3. Correlation of enantiomer fractionation factors derived from calculation of experimental data (ϵ_eC)
 23 and compared to modeling (ϵ_eM).

24

Supporting Information

Enantiomer and Carbon Isotope Fractionation of α -hexachlorocyclohexane by *Sphingobium indicum* Strain B90A and Corresponding Enzymes

Yaqing Liu,¹ Langping Wu,¹ Puneet Kohli,² Roshan Kumar,² Hryhoriy Stryhanyuk,¹ Ivonne Nijenhuis,¹ Rup Lal,² Hans-Hermann Richnow^{1*}

¹Department of Isotope Biogeochemistry, Helmholtz Centre for Environmental Research-UFZ, Permoserstraße 15, 04318 Leipzig, Germany

²Molecular Biology Laboratory, Department of Zoology, University of Delhi, Delhi-110007, India

*Corresponding author: Phone: +49-3412351212; fax: +49-341451212;

E-mail: hans.richnow@ufz.de

pages

7 figures

1 tables

Contents

1. Cultivation media.....	2
2. Degradation experiments	2
3. Cultivation and enzyme purification	2
4. Analytical methods	2
5. Quantification of isotope fractionation	3
6. Quantification of enantiomeric fractionation	4
7. Biodegradation of α -HCH enantiomers during growth	6
8. Biodegradation of α -HCH enantiomers in stable condition	8
9. Re-evaluation of enantiomer fractionation data from growing cells	16
References.....	17

1. Cultivation Media

Luria Bertini (LB) liquid medium: 5 g of yeast extract, 10 g of Peptone and 10 g of NaCl for 1 L of distilled water, adjust the pH to 7.0 using a NaOH (2M) solution.

Minimal salt medium (MSM): for 1 L of distilled water, 0.5 g of $(\text{NH}_4)_2\text{SO}_4$ and 0.1 g of K_2HPO_4 , 1 mL of FeSO_4 (w/w, 1%), 1 mL of $\text{Ca}(\text{NO}_3)_2$ (w/w, 1%), 10 mL of MgSO_4 (w/w, 20%), 2 mL of glucose (w/w, 50%).

2. Degradation Experiments

Batch degradation experiments with the six *Sphingobium* spp. (strain P25, F2, IP26, RL3, HDIPO4, LLO3) were performed in 240 ml bottles with 100 mL minimal salt medium (MSM), respectively. 5.5 μL of α -HCH dissolved in acetone (0.1M) was added to get an initial concentration of 5.5 μM . All the bottles were incubated at 30 °C shaking incubator (200 rpm).

All batch degradation experiments with resting cells, crude extract and purified LinA enzymes were conducted in 240 ml bottles with 100 mL Tris-buffer (0.1M, pH=7.5). 5.5 μL α -HCH in acetone (0.1 M) was spiked to get an initial concentration of 5.5 μM . All the bottles were incubated at 30 °C shaking incubator (200 rpm). Different amount (500 μL , 200 μL , 100 μL , and 50 μL) of resting cells ($2.5\text{-}3.0 \times 10^8$ cells mL^{-1}) or crude extract (from $2.5\text{-}3.0 \times 10^8$ cells mL^{-1} resting cells) were added to start the reaction, except in the abiotic controls. Three sets of degradation experiments using 10 μL , 8 μL and 5 μL of LinA2 enzyme and two sets of degradation experiment using 10 μL and 5 μL of LinA1 were conducted respectively. The concentrations of the enzymes were 70 ng μL^{-1} for LinA1 and 240 ng μL^{-1} for LinA2. The sampling and extraction were done as reported before (Bashir et al., 2013).

3. Cultivation and Enzyme Purification

LinA genes were codon optimized for expression in *Escherichia coli*. These were synthesized by Geneart AG, Regensburg Germany. Further, the so obtained synthetic genes were cloned into an shuttle vector (pDONR201) using Gateway® Technology (Invitrogen Inc.), with the help of *att* DNA recombination sequences (*attL*, *attR*, *attB* and *attP*) and enzymes such as clonase enzyme excisionase. Amplicons from this shuttle vector were then transferred to pDESTTM17 using the BP and LR reactions, as per the manufacturers' instructions (Invitrogen, CA). In addition to this to achieve proper folding of the protein in the host strain *E. coli* BL21-AITM (Invitrogen) cells were co-expressed with pGro7 chaperones as plasmids (Takara, Japan).

Initially the bacterial cells were grown in 100 ml of Luria Bertini (LB) broth with addition of ampicillin (150 $\mu\text{g mL}^{-1}$) and chloramphenicol (34 $\mu\text{g mL}^{-1}$) shaking (200rpm) at 28°C. Induction of these cells was undertaken at OD₆₀₀ around 0.5 - 0.6 by addition of L-(+)-arabinose (2 g L^{-1}). Cells were then grown overnight, followed by centrifugation to harvest the cells. The harvested culture pellet was first resuspended in equilibrium buffer containing 10 mM imidazole (pH 7.5) with 1× bug buster (Novagen, Darmstadt), followed by mild sonication. The lysate thus obtained was centrifuged and the supernatant was then used to purify the Lin protein based on poly-Histidine (6X-His) tag present in pDESTTM17 using NTA-Ni²⁺ agarose column chromatography (Qiagen, GmbH) as per the manufacturers' instructions. The protein so purified was then quantified using Nanodrop (Thermo Scientific, DE). The isolated protein was then stored in the storage buffer (pH 7.5) containing 1 mM 2-mercaptoethanol and 10% glycerol at an approximate concentration of 1 mg mL^{-1} at 4°C until use.

4. Analytical Methods

Gas chromatography - An Agilent 6890 series gas chromatograph (GC, Agilent Technologies, Palo Alto, USA) equipped with a flame ionization detector (FID) was used for measurement of bulk α -HCH concentration. Samples were separated in a HP-5 capillary column (30 m x 0.32 mm ID x 0.25 μm FD; Agilent Technologies, Palo Alto, USA) with helium as the carrier gas (flow of 2.0 mL min^{-1}). The oven temperature program started at 35°C, was held for 5 min isothermally, increased at 8 °C min^{-1} to 180 °C, then at 2 °C min^{-1} to 195 °C, and finally increased at 8 °C min^{-1} to 220 °C, where it was held for 2 min. The samples were injected in splitless mode with injection volumes of 1 μL .

Compound specific isotope ratio mass spectrometry - The stable carbon isotope ratios of bulk α -HCH and its enantiomers were analyzed by a gas chromatograph-combustion-isotope ratio mass spectrometer (GC-C-IRMS). The system consists a GC (6890, Agilent Technologies, Palo Alto, USA) coupled with Conflow III interface (Thermo Fisher Scientific, Bremen, Germany) to a MAT252 IRMS (Thermo Fisher Scientific, Bremen, Germany) as described previously¹. For CSIA of bulk α -HCH a HP-5 capillary column (30 m x 0.32 mm ID x 0.25 μ m FD; Agilent Technologies, Palo Alto, USA) was used with the temperature program used above.

A γ -DEXTM 120 chiral column (Supelco, Bellefonte, PA, USA; column length * i.d. 30m * 0.25 mm, $d_i=0.25 \mu$ m) was used for the separation of α -HCH enantiomers as described previously². Three μ L aliquots of extract were injected with a split ratio of 1:3. Samples with concentration below 1 μ M were injected with splitless mode. All samples were measured in at least three replicates and the typical uncertainty of analysis was $< \pm 0.5 \text{ ‰}$.

5. Quantification of Isotope Fractionation

The isotope composition of α -HCH was analyzed by gas chromatography isotope ratio mass spectrometry (GC-IRMS), as described previously². Quality control was done by using isotope laboratory standards of α -HCH (99%, Sigma-Aldrich Chemie GmbH, Germany) with carbon isotope ratios determined by elemental analyzer isotope ratio mass spectrometry (EA-IRMS). The carbon isotope ratios of α -HCH measured by GC-IRMS were reported in the δ notation ($\delta^{13}\text{C}$) relative to the international standard Vienna Pee Dee Belemnite (VPDB) according to eq.1³.

$$\delta^{13}\text{C}_{\text{sample}} = \frac{R_{\text{sample}}}{R_{\text{standard}}} - 1 \quad (1)$$

R_{sample} and R_{standard} are the $^{13}\text{C}/^{12}\text{C}$ ratios of the samples and VPDB, respectively. The $\delta^{13}\text{C}$ -values were reported in per mil (‰). All the samples were measured in triplicate.

Simplified Rayleigh equation in logarithmic form was used to quantify the stable carbon isotope fractionation of the biodegradation process in this study. The carbon isotope enrichment factor (ϵ_c) was determined as eq 2.

$$\ln\left(\frac{(\delta_t^{13}\text{C}+1)}{(\delta_0^{13}\text{C}+1)}\right) = \epsilon_c \ln\left(\frac{C_t}{C_0}\right) \quad (2)$$

ϵ_c were reported in per mil scale and derived from the slope of the linear regression of $\ln(C_t/C_0)$ vs $\ln[(\delta_t^{13}\text{C}+1)/(\delta_0^{13}\text{C}+1)]$. The error of ϵ_c was reported as 95% confidence interval (CI) determined by a regression curve analysis⁴.

6. Calculation of the AKIE_C of enzymes

The apparent kinetic isotope fractionation factor was calculated as previously described using Eq. 3.⁵

$$AKIE = \frac{1}{1 + \frac{nz}{x} \epsilon_c / 1000} \quad (3)$$

Where n is the number of atoms of the selected element, x is the number of reactive positions, and z is the number of indistinguishable reactive positions for intramolecular competition. We calculate the AKIE_C in order to interpret the extent of isotope fractionation and for comparison with quantum chemical calculation.

Two scenarios were considered for a dehydrochlorination reaction in order to compare the AKIE with chemical modelling. In both cases, the number of carbon (n) in HCH is 6. For the first scenario (1) we assume that all the chlorine atoms are chemically equivalent with respect to reactivity. In this case the number of reactive positions are 2 and the positions for intramolecular competition are 2 ($x=z=2$). Calculated by Eq.3, the AKIE_C for LinA1 and LinA2 are 1.072 and 1.023 (Table S1), respectively. The AKIE_C of LinA1 is higher than the Streitwieser semi-classical limit for a single C-Cl (1.057) or C-H (1.021) cleavage in the transition state. The initial step of hydrolysis is considered to be concerted bimolecular elimination

mechanism (E2 reaction) with an almost simultaneous C-Cl and C-H bond cleavage leading to the formation of a double bond.

For scenario 2 we considered a specific reaction at axial chlorine hydrogen pairs consistent with an E2 elimination reaction. Elimination at two axial H/Cl pairs of α -HCH to form pentacyclohexenes (1,3S,4s,5R,6S-PCCH for (+) α -HCH and 1,3R,4R,5S,6R-PCCH for (-) α -HCH) during dehydrochlorination support this scenario.⁶ In this case 4 carbon with axial chlorine hydrogen pairs ($x=4$) with 2 indistinguishable positions ($z=2$) may react. The AKIE of the Lin A1 (1.035) and Lin A2 (1.011) reactions are expected to be in the range of KIE of a dehydrochlorination with an E2 mechanisms (see below).

The quantum chemical modelling using 2 simplified model for enzyme reactions, the position-specific KIE_C of LinA1 (for (+) α -HCH) dehydrochlorination was 1.0168 and 1.0218 for the C-H and C-Cl bond cleavage reaction, respectively⁶ whereas the dehydrochlorination of (-) α -HCH by Lin A2, the calculated KIE_C resulting 1.0169 (C-H) and 1.0104 (C-Cl).⁶ In the quantum chemical calculation, the overall primary KIE_C in the reaction of α -HCH enantiomers by Lin A2 is smaller than by Lin A1 similar as observed in our experiments. The magnitude of the AKIE between 1.035 1.011 (AVG, Tab. S1) suggest a concerted a concerted reaction mechanism consistent with an E2 elimination reaction as the AKIE for a stepwise reaction is much above the Streitwieser Limits of a cleavage of a C-Cl (1.057) or C-H (1.021) bonds⁷.

The $AKIE_C$ of and LinA1 for (+) α -HCH is higher than the value of quantum chemical calculation for the reaction sum up to ϵ_c of -7.38 ‰ using the date of Manna and cleagues.⁶ The KIE_C of C-Cl bond cleavage which was similar as in our study was observed in the biodegradation of dichloromethane.⁸ Also the concerted dichloroelimination of 1,2 dichloroethane in biodegradation and Zn(o) reduction result in comparable $AKIE_C$ values.⁹

Table S1: calculation of AKIE value of the enzyme degradation experiments and the average values.

Enzymes	$\epsilon_c \pm CI(95\%)$ (‰)		$AKIE_C$			
	(-) α -HCH	(+) α -HCH	n=6, x=2,z=2		n=6, x=4,z=2	
LinA1		-11.3±2.0	1.073	AVG.=1.072	1.035	AVG.=1.035
		-10.9±1.5	1.070		1.034	
LinA2	-3.7±0.6		1.023	AVG.=1.023	1.011	AVG.=1.011
	-4.0±1.0		1.025		1.012	
	-3.6±0.5		1.022		1.011	

AVG. = average value

7. Quantification of Enantiomeric Fractionation

Enzymatic degradation of HCH by LinA is in a strict sense a second order kinetic reaction however most of our experimental data show that it actually follows a first order or pseudo-first-order kinetics over a certain concentration range. Only within the time range when the bulk α -HCH degradation shows a first order kinetics, the following approach can be applied. Considering that the activity of LinA follows a first order or pseudo first order kinetic reaction, the integrated first order rate law is:

$$\ln\left(\frac{C_t}{C_0}\right) = -k \times t \quad (1)$$

or

$$C_t = C_0 \times e^{-k \times t} \quad (2)$$

Where C_0 [μ M] and C_t [μ M] are the concentrations of the chiral compound at initial condition and time t , t [min] is the reaction time; k [s^{-1}] is the rate constant. For simplicity, we assign the concentrations and rate constants of the two enantiomers by the same letters, but differentiate individual enantiomers with (+) and (-)

). The experimental data on degradation kinetics for the α -HCH and the two enantiomers (+/-) α -HCH show that the reactions follow the first order kinetics (see Figure S2). Thus, the reaction kinetics of two individual enantiomers can be expressed as eq. 3:

$$C(+)_t = C(+)_0 \times e^{-k(+)\times t} \quad (3.1)$$

$$C(-)_t = C(-)_0 \times e^{-k(-)\times t} \quad (3.2)$$

The enantiomer ratio (ER) is defined as the ratio of the 2 enantiomers in a mixture and is reported as the ratio of the percent of one enantiomer in a mixture to that of the other. In this study, we redefine ER as the concentration ratio of (+) and (-) enantiomers as eq. 4:

$$ER = \frac{C(+)}{C(-)} \quad (4)$$

In order to find a relation between ER and reaction time t , Eq. 3 can be combined for the expression of the enantiomer ratio at reaction time t (ER_t):

$$ER_t = \frac{C(+)_t}{C(-)_t} = \frac{C(+)_0}{C(-)_0} \times \frac{e^{-k(+)\times t}}{e^{-k(-)\times t}} \quad (5)$$

Eq. 5 illustrates that ER_t is a function of the reaction time t and the respective first order reaction rate constant of two enantiomers. α -HCH is synthesized as a racemic mixture in equal concentration of enantiomers, therefore, assuming the initial enantiomer concentrations ($C(+)_0$ and $C(-)_0$) to be equal, the Eq.5 can be rewritten as

$$ER_t = \frac{C(+)_t}{C(-)_t} = \frac{C(+)_0 \times e^{-k(+)\times t}}{C(-)_0 \times e^{-k(-)\times t}} = \frac{C(+)_0}{C(-)_0} \times e^{(k(-)-k(+))\times t} \quad (6)$$

Taken the logarithm on both sides of the Eq.6, one can get the subtracted equation as below:

$$\ln\left(\frac{C(+)_t}{C(-)_t}\right) = \ln\frac{C(+)_0}{C(-)_0} + \ln(e^{(k(-)-k(+))\times t}) = \ln\frac{C(+)_0}{C(-)_0} + (k(-) - k(+)) \times t \quad (7)$$

Eq. 7 describes the correlation of concentrations C , rate constants k and reaction time t of the individual enantiomers. Based on reaction kinetic, one can find a correlation of kinetic parameters by the link of reaction time. The reaction time (t) can be expressed from Eq.1 as

$$t = -\frac{1}{k} \times \ln\left(\frac{C_t}{C_0}\right) \quad (8)$$

Thus, the reaction time (t) in Eq.7 can be replaced by $-\frac{1}{k} \times \ln\left(\frac{C_t}{C_0}\right)$, Eq.7 can be rewritten as

$$\ln\left(\frac{C(+)_t}{C(-)_t}\right) = \ln\frac{C(+)_0}{C(-)_0} + \frac{k(+)-k(-)}{k} \times \ln\frac{C_t}{C_0} \quad (9)$$

The $\ln\frac{C(+)_0}{C(-)_0}$ term is a constant representing an initial enantiomer ratio. The $\ln\frac{C(+)_0}{C(-)_0} = A \neq 0$ condition corresponds to a case when the values of initial enantiomer concentrations are different. This constant A has to be considered if e.g., the first experimental data were acquired when the degradation was already in progress.

$$\ln\left(\frac{C(+)_t}{C(-)_t}\right) = A + \frac{k(+)-k(-)}{k} \times \ln\frac{C_t}{C_0} \quad (10)$$

α -HCH is synthesized as a racemic mixture in equal concentration of enantiomers, therefore, assuming the initial enantiomer concentrations ($C(+)_0$ and $C(-)_0$) to be equal. In this case, $A=0$, and Eq. 10 can be rewritten as

$$\ln \left(\frac{C(+)_t}{C(-)_t} \right) = \frac{k(+)-k(-)}{k} \times \ln \frac{C_t}{C_0} \quad (11)$$

Eq. 11 describes the relation between total racemic mixture concentration (C_t and C_0) and enantiomer concentrations ($C(+)_t$ and $C(-)_t$) employing the difference in enantiomer degradation rates ($k(+)-k(-)$) normalized to the degradation rate of chiral compound (k). As $\frac{k(+)-k(-)}{k}$ is a constant, which can be defined as the enantiomeric fractionation factor ε_e :

$$\varepsilon_e = \frac{k(+)-k(-)}{k} \quad (12)$$

The enantiomer fractionation factor ε_e gets close/equal to zero when the degradation rate constants are close/equal for both enantiomers. Taking the defined enantiomer fractionation factor ε_e into account, the relation between total chiral compound concentration and two enantiomer concentrations (Eq. 11) is expressed as:

$$\ln \left(\frac{C(+)_t}{C(-)_t} \right) = \varepsilon_e \times \ln \frac{C_t}{C_0} \quad (13)$$

In the case of different values of initial enantiomer concentrations, the constant A ($A \neq 0$, Eq. 10) has to be introduced into the Eq. 13 to describe a possible ordinate shift of experimental data.

As shown in Eq. 13, ε_e is a function of racemic mixture concentration (C_t and C_0) and individual enantiomers concentrations ($C(+)_t$ and $C(-)_t$), which can be obtained by the fitting of

$$\ln \left(\frac{C(+)_t}{C(-)_t} \right) / \ln \left(\frac{C_t}{C_0} \right).$$

Based on the evaluation process above, enantiomeric fractionation factor ε_e can be calculated by numerical methods according to Eq. 12. To determine the quality of the this approach, the obtained ε_e by fitting procedure according to Eq. 13 were compared to the calculated values, and are reported in Table 1 and Figure 3 in the main text.

8. Biodegradation of α -HCH Enantiomers During Growth

Six *Sphingobium* spp. strains were cultivated and batch experiments with 5.5 μ M α -HCH in minimal salt medium (MSM). Degradation experiments were conducted for a systematic analysis of enantiomer and carbon isotope fractionation. More than 90 % degradation was observed in all experiments in a time course of less than 8 h (Fig. S1). Enrichment of isotope composition of the residual enantiomer fraction was associated with degradation in all cases.

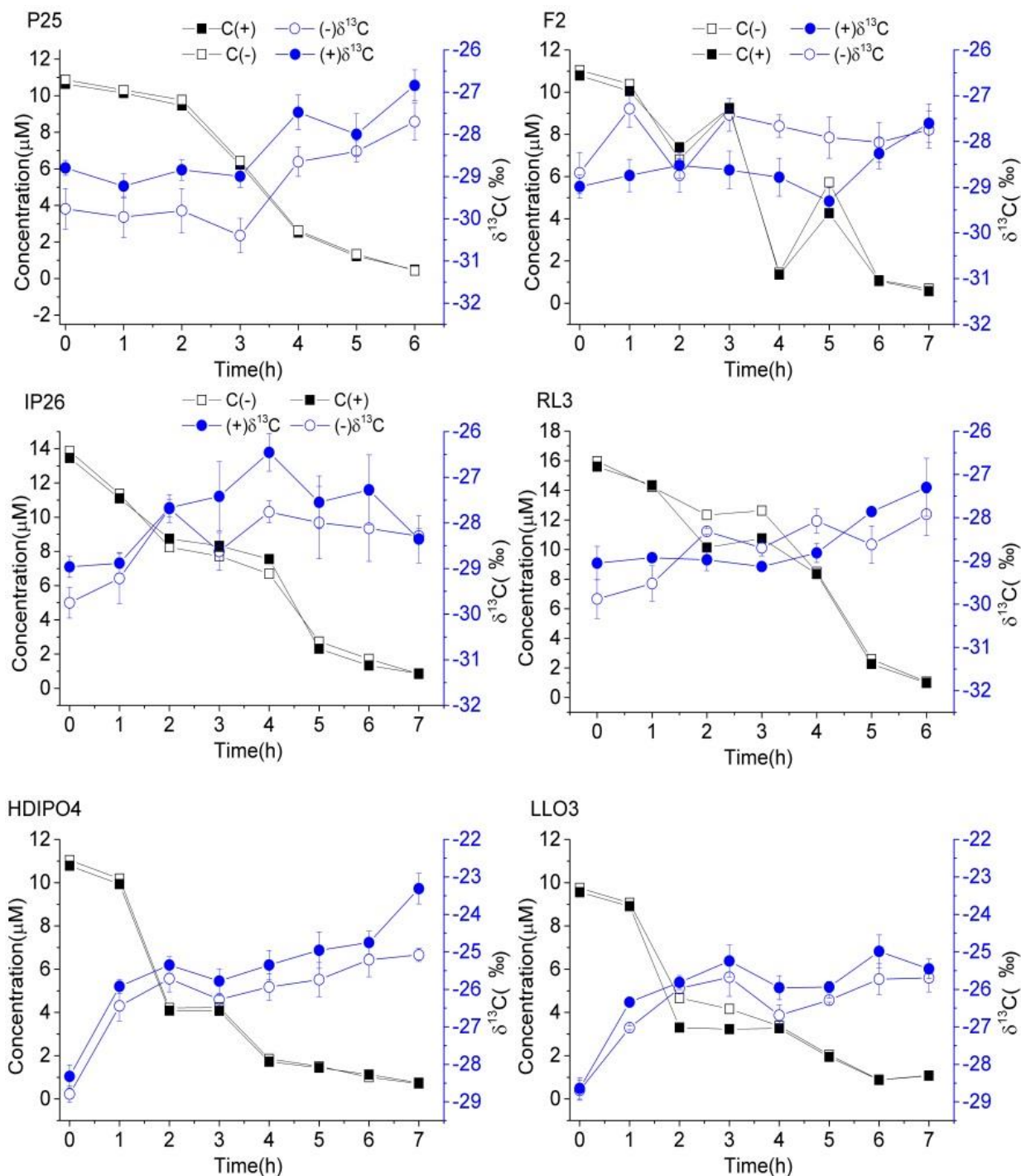


Fig. S1. Concentration (square) and carbon isotope composition (circle) of (-)- α -HCH (open symbols) and (+)- α -HCH (solid symbols) by the degradation of *Sphingobium* spp. (P25, F2, IP26, RL3, HDIPO4, LLO3).

Reaction kinetics of enantiomers were evaluated using the integrated first order rate law (Figure S2). Only the degradation of α -HCH enantiomers using strain HDIPO4 fitted the first order kinetic yielding a coefficient of determination (R^2) of 0.96/0.97. The degradation kinetics in the other experiments were variable and did not follow the pseudo first order kinetics with R^2 vary from 0.71 to 0.93, suggesting that the reaction kinetic or the mode of degradation may be changed during degradation.

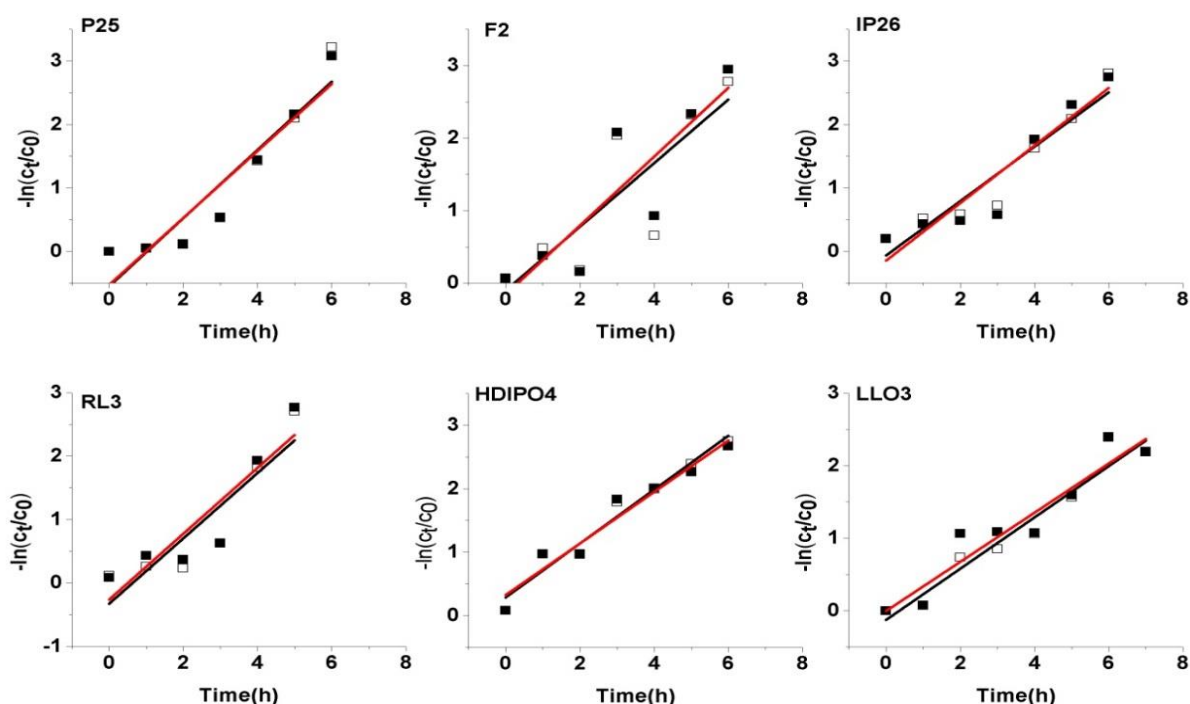


Fig. S2. Degradation kinetics of (+) α -HCH (■) and (-) α -HCH (□) by the six strains modeled by pseudo-first order kinetics.

The enantiomer selectivities of these six strains in the experiments were evaluated by plotting the EF(-) ($EF(-) = c(-)/c$, with $c(-)$ the concentration of (-) α -HCH, and C the concentration of bulk α -HCH) over time (Fig. S3). The EF(-) changed in the course of the experiments and suggested that the preferential degradation of individual α -HCH enantiomers changed over time during growth.

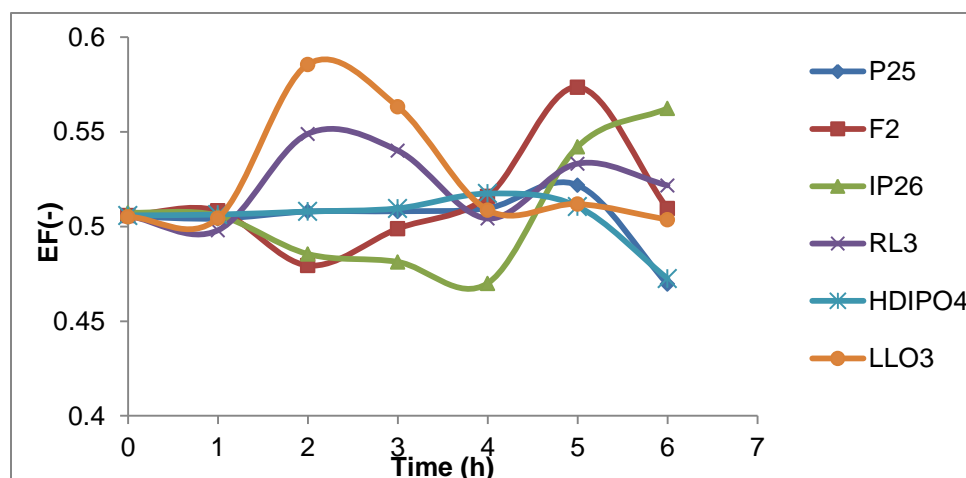
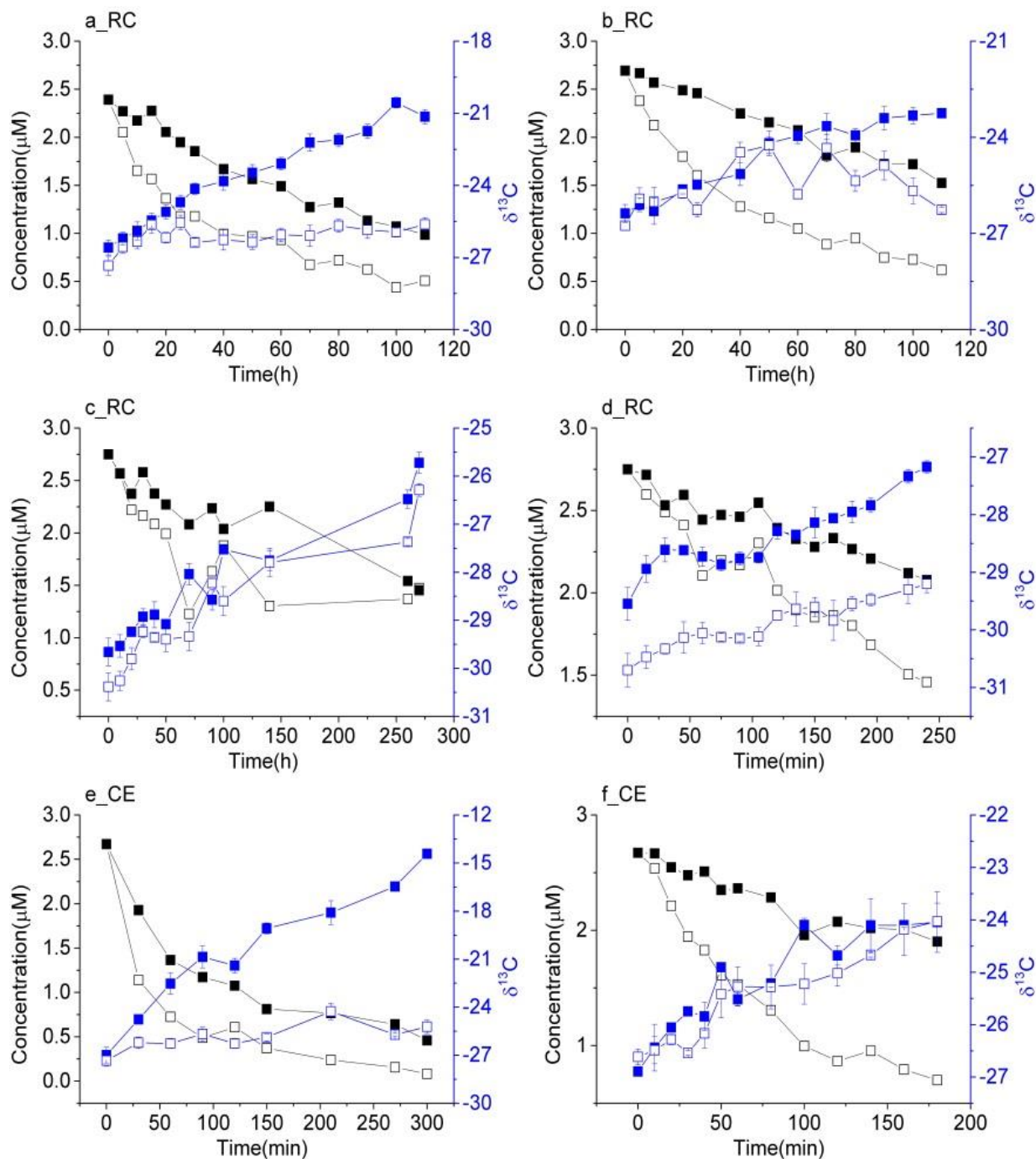


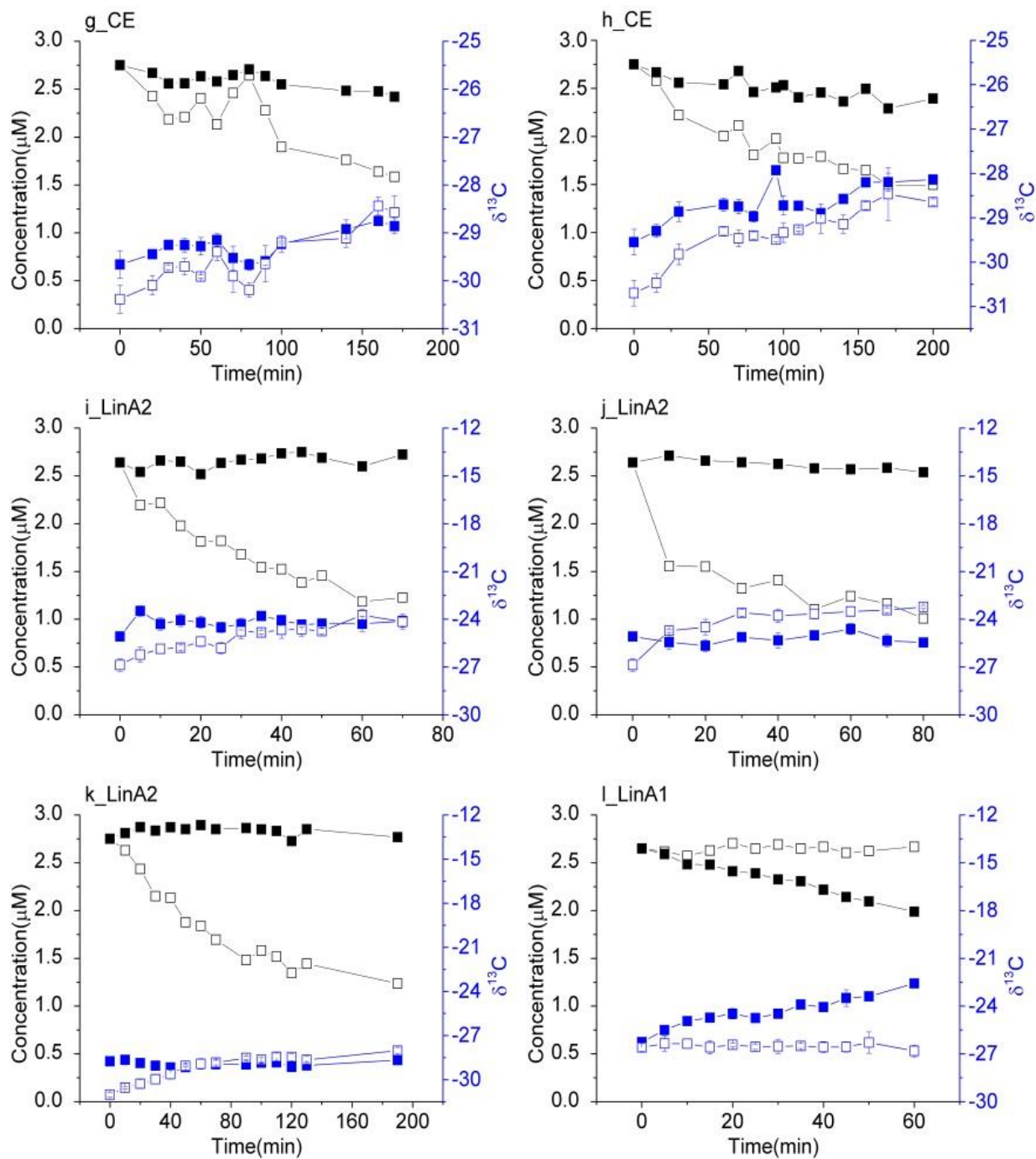
Fig. S3. Variability of EF(-) during α -HCH biodegradations during growth.

9. Biodegradation of α -HCH Enantiomers in Stable Conditions

Based on the hypothesis that the LinA proteins were relatively constant in resting cells (RC) and do not change after harvesting of grown culture, *Sphingobium indicum* B90A was selected as model strain and α -HCH degradation experiments were conducted in Tris-buffer. For comparison, α -HCH degradation experiments with crude extract (CE) of *Sphingobium indicum* B90A and purified enzymes (LinA1 and LinA2)

were also performed in Tris-buffer. All experiments were conducted at least twice to evaluate the reproducibility of the degradation.





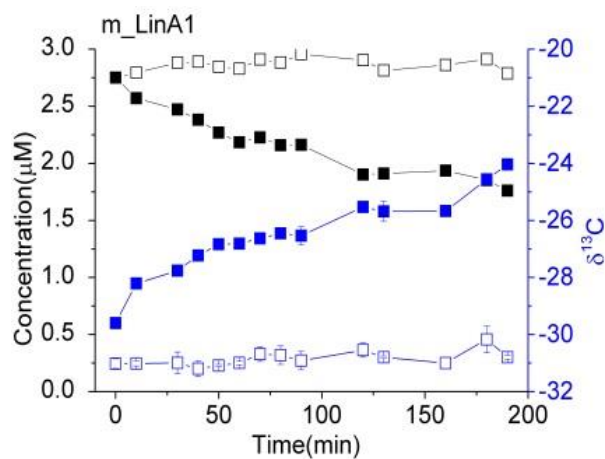
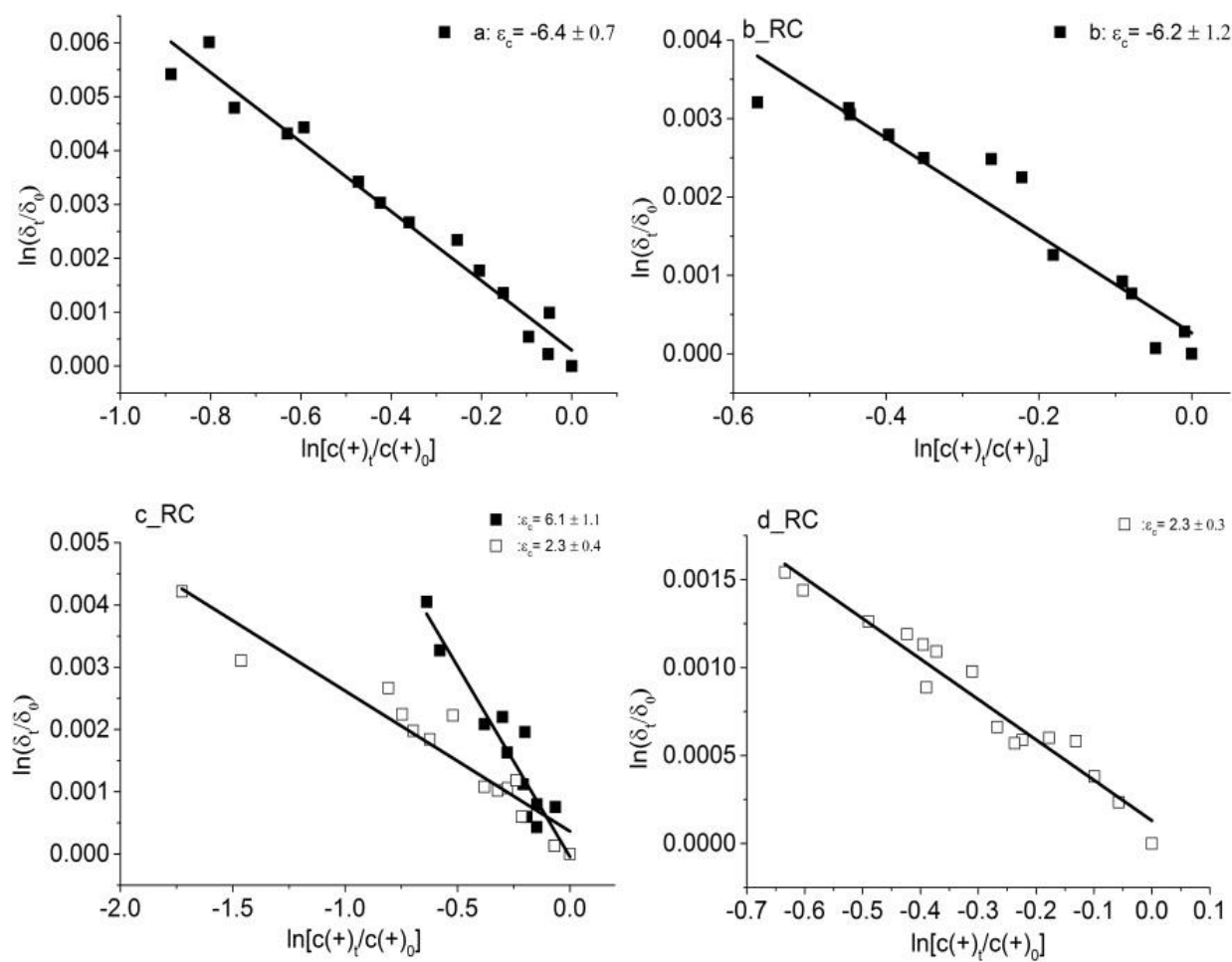
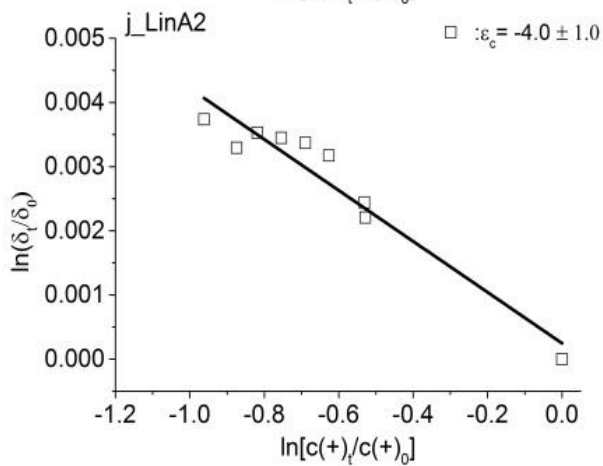
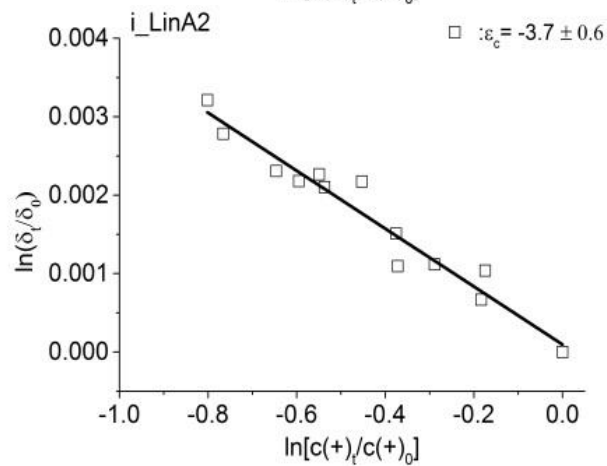
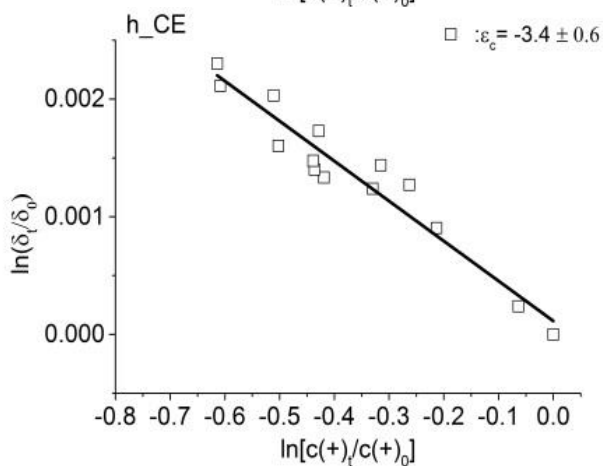
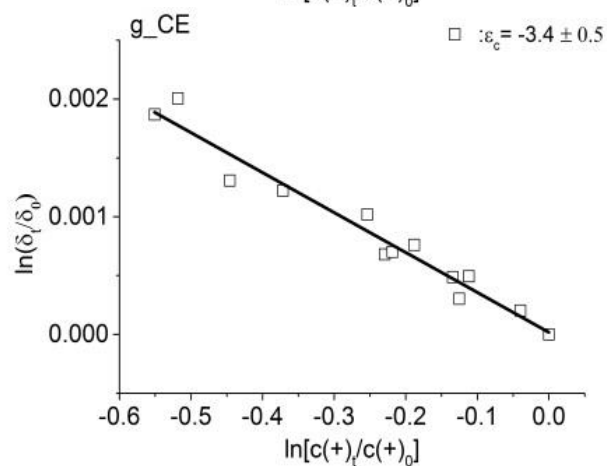
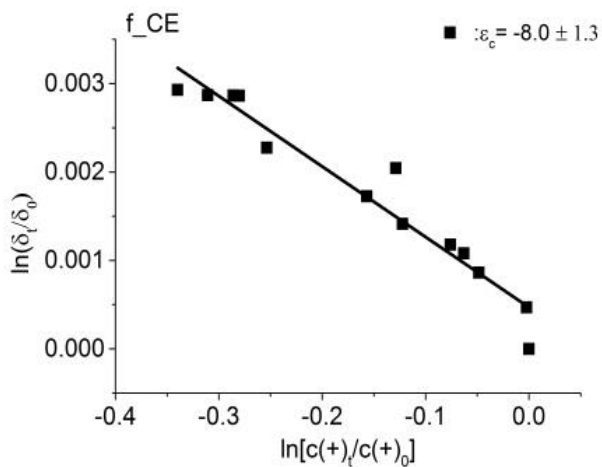
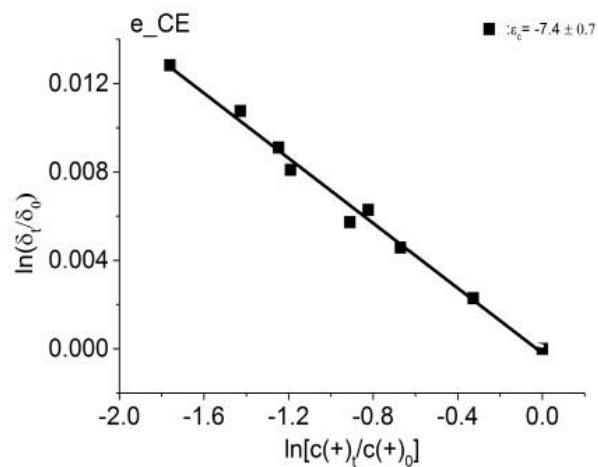


Fig. S4. The changes of concentration (black symbols) of (+)- α -HCH (solid square), (-)- α -HCH (open square) and isotope composition (blue symbols) of two individual enantiomers in degradation experiments with the resting cell (RC), crude extracts (CE) and the enzymes LinA1 and LinA2.





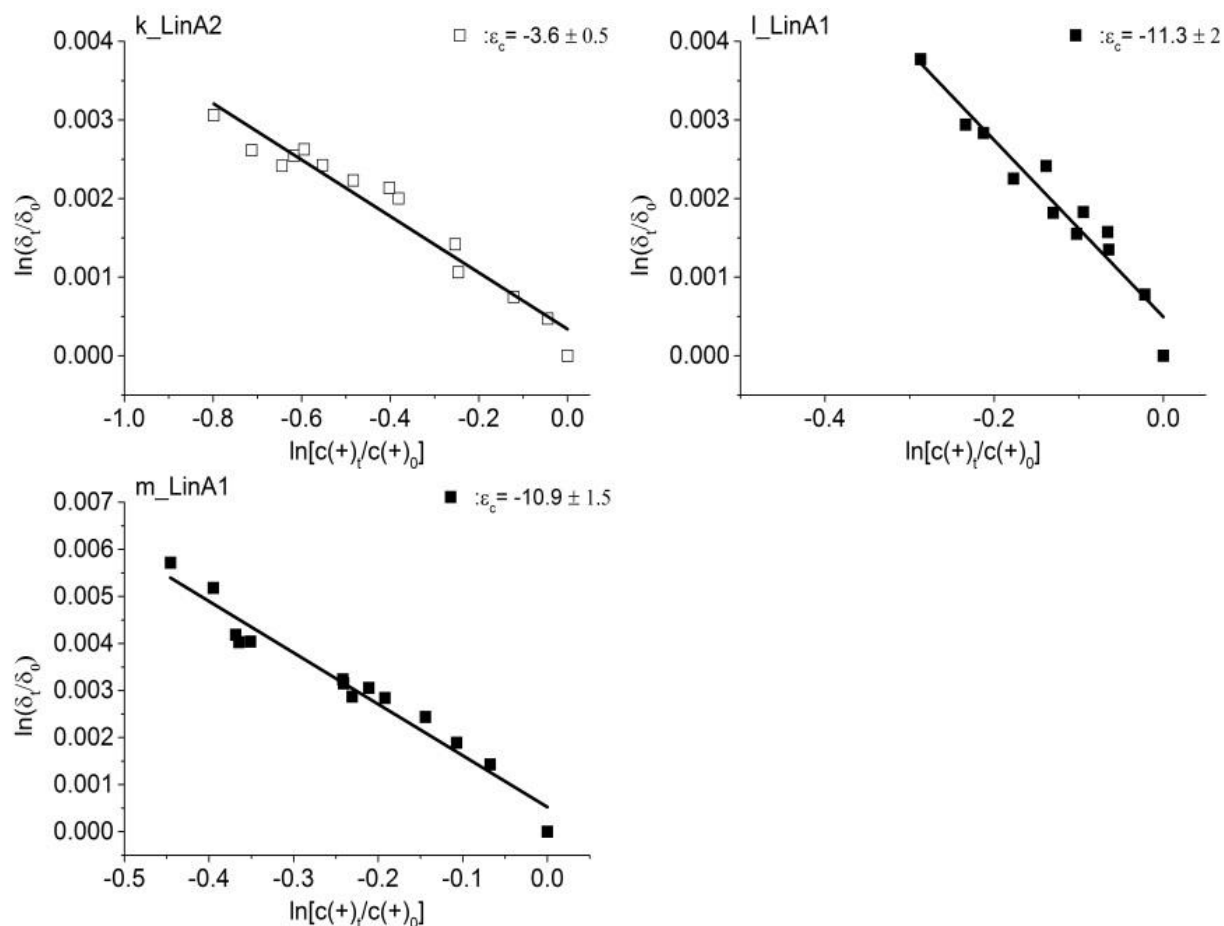


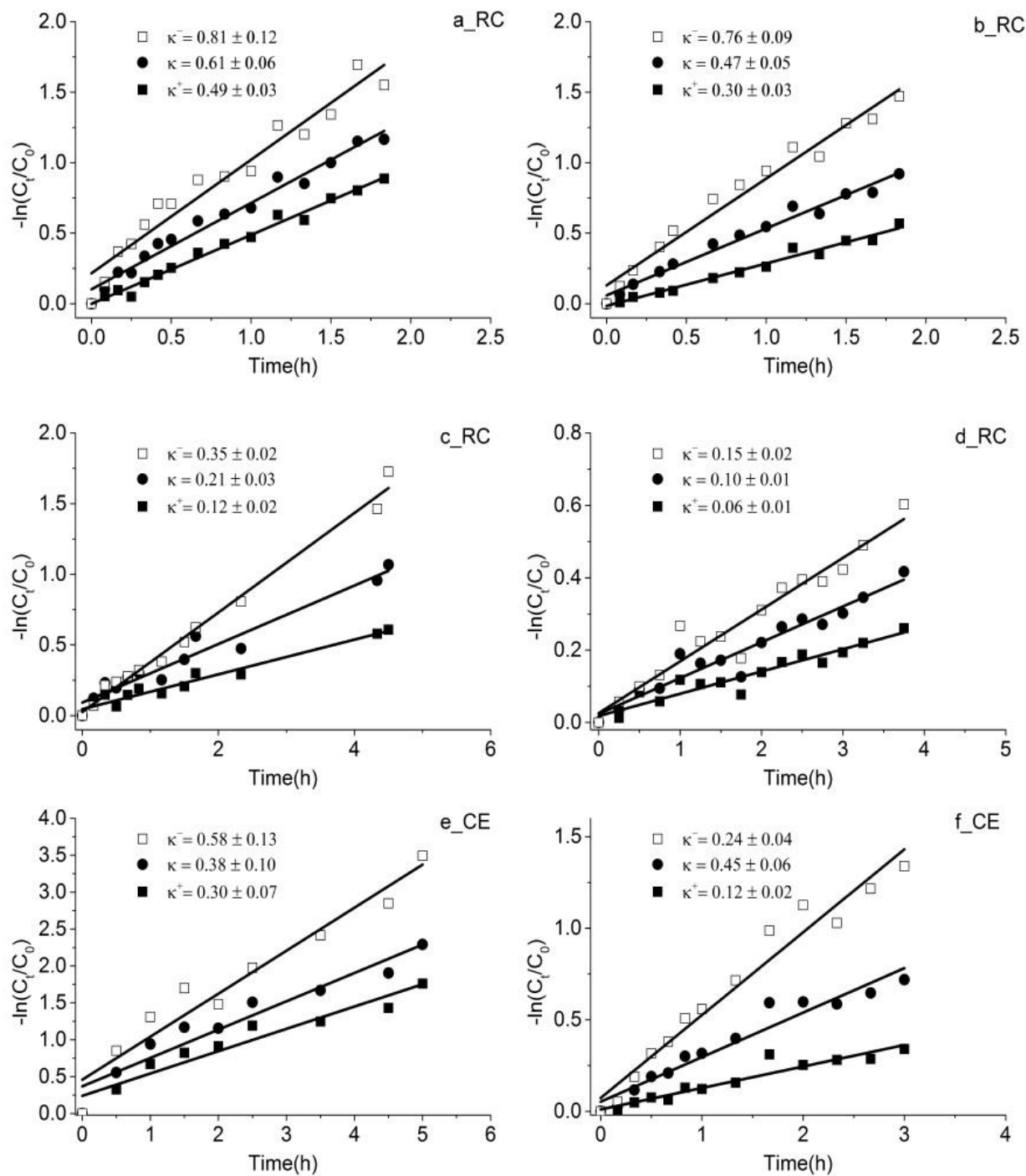
Fig.S5. Experiments for the biodegradation of α -HCH enantiomers by resting cells (RC), crude extract (CE) and the corresponding enzyme LinA1 and LinA2 of *S. indicum* strain B90A were conducted for the evaluation of carbon isotope fractionation of (+) α -HCH (■) and (-) α -HCH (□).

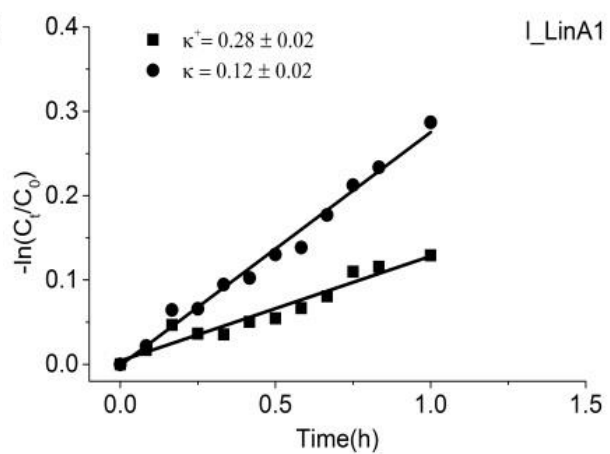
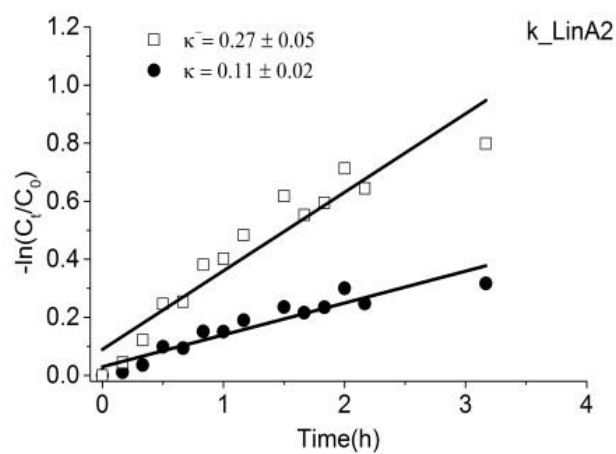
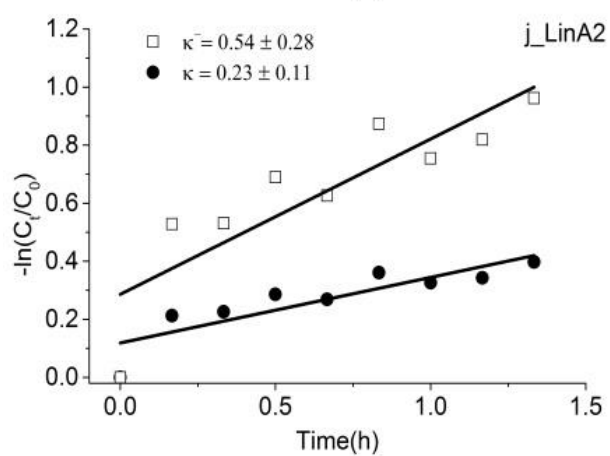
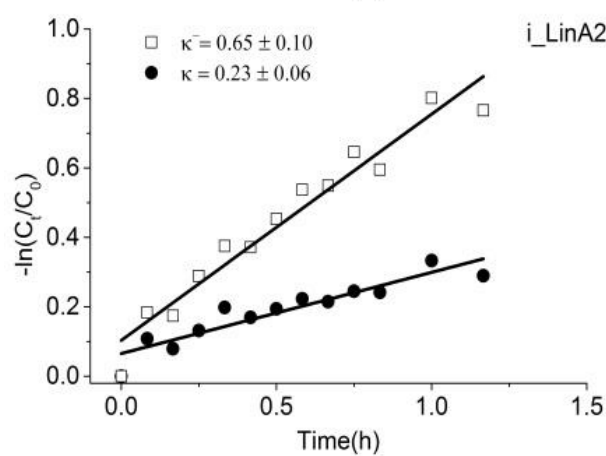
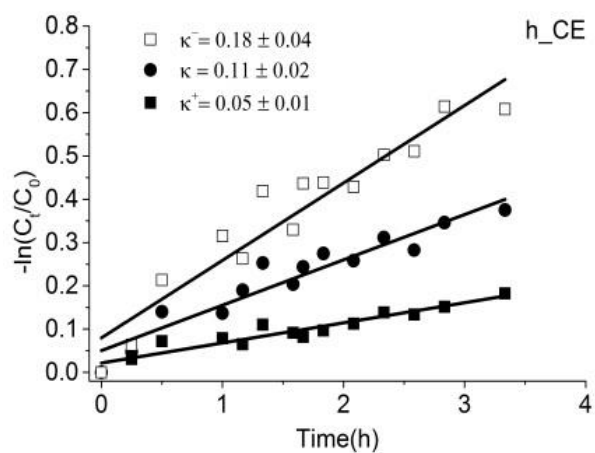
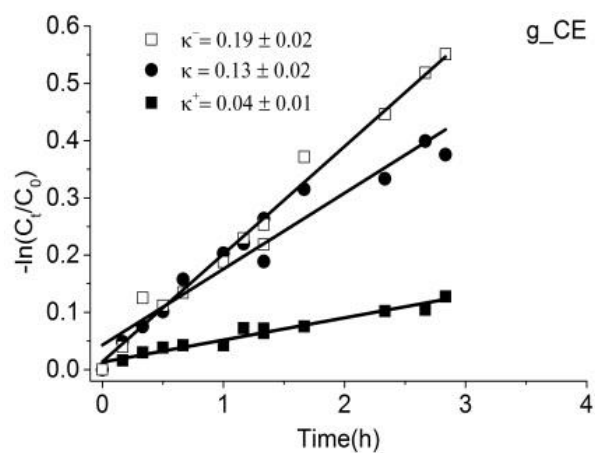
Both enantiomers were degraded in all experiments using RC and CE. However, in RC degradation experiments (Fig.S4; a, b, c, d), the isotope composition of (+) α -HCH only significantly enriched in experiment a, b and c. The degradation of (+) α -HCH in experiment d was very minor leading to around 10% degradation of the initial concentration and no significant isotope enrichment was observed. In CE degradation experiments (Fig.S4; e, f, g, h), carbon isotope enrichment factors of (+) α -HCH were obtained in experiments e and f, no significant isotope enrichment was observed in the sets g and h. In addition, carbon isotope enrichment of (-) α -HCH was observed in both RC and CE degradation experiments with relatively slower degradation, such as in experiments c, d, g and h. In contrast, in degradation experiments with faster reaction no significant isotope fractionation of (-) α -HCH could be observed (Fig. S4 a,b and e,f). Isotope enrichment of RC and CE degradation experiments was evaluated by simplified Rayleigh equation (Fig. S5 a - h).

Degradation experiments with purified enzymes were conducted for analyzing the enantiomeric specificity of the LinA proteins. In agreement with previous reports¹⁰, LinA2 catalyze preferentially (-) α -HCH whereas LinA1 catalyse (+) α -HCH degradation (Fig.S4; i-k). Both LinA proteins showed very high specificity as one enantiomer become degraded in contrast to the other enantiomer showing almost constant concentration. The degradation was accompanied with isotope enrichment whereas the isotope composition of the non-reacted enantiomer was stable. The evaluation of isotope fractionation by simplified Rayleigh equation for enzyme degradation experiments was showed in Fig. S5 (i - m).

The degradation of α -HCH enantiomers with RC, CE and purified enzymes followed the pseudo first order kinetics with R^2 vary from 0.76 to 0.98, (Fig. S6). In the RC and CE degradation experiments (Fig.S6; a - h),

the kinetic rate constants of (-)- α -HCH were higher compared to those of (+)- α -HCH, eg. 0.81 h^{-1} to 0.15 h^{-1} in RC experiments (a - d) and 0.58 h^{-1} to 0.18 h^{-1} in CE experiments (e - h). In the degradation experiments of LinA2, (-)- α -HCH was preferentially degraded with the kinetic rate constants of $0.65/0.54 \text{ h}^{-1}$ (Fig. S6; i, j). The kinetic rate constant of (+)- α -HCH degradation in LinA1 experiments was 0.28 h^{-1} (Fig. S6_k).





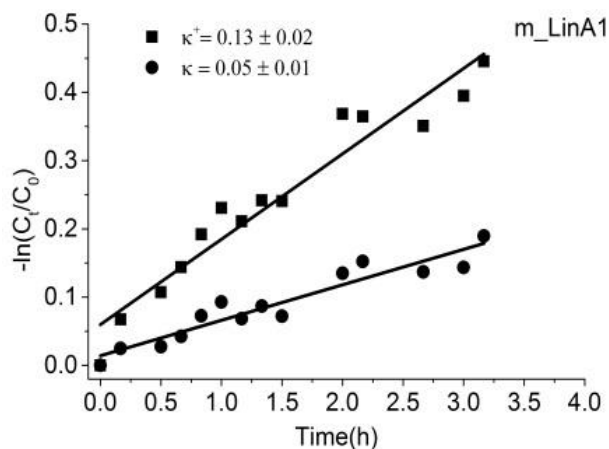


Fig. S6. The degradation kinetics of the resting cell (RC), crude extracts (CE) and enzymes (LinA1 and LinA2) degradation experiments. C, C (-) and C (+) indicates the concentration of bulk α -HCH (\bullet), (-) α -HCH (\square) and (+) α -HCH (\blacksquare), respectively.

10. Re-evaluation of Enantiomer Fractionation Data from Growing Cells

In order to compare the enantiomer fractionation of *Sphingobium indicum* B90A in growing condition, data from a previous report⁴ was re-evaluated (Fig. 6S). The enantiomer fractionation could not be described by eq. 11 as changes of enantiomeric composition and changes in concentration were not linearly correlated (Fig.S7; b1) which indicates that the mode of enantiomer fractionation changed during the reaction. Two phases can be observed with specific preferences of enantiomers, showing that the enantiomer fractionation process was governed different processes with specific preferences for enantiomers (Fig. S7; b1). Similar trends could be observed in the degradation experiments of *S. japonicum* strain UT26 (Fig S7; a2, b2).

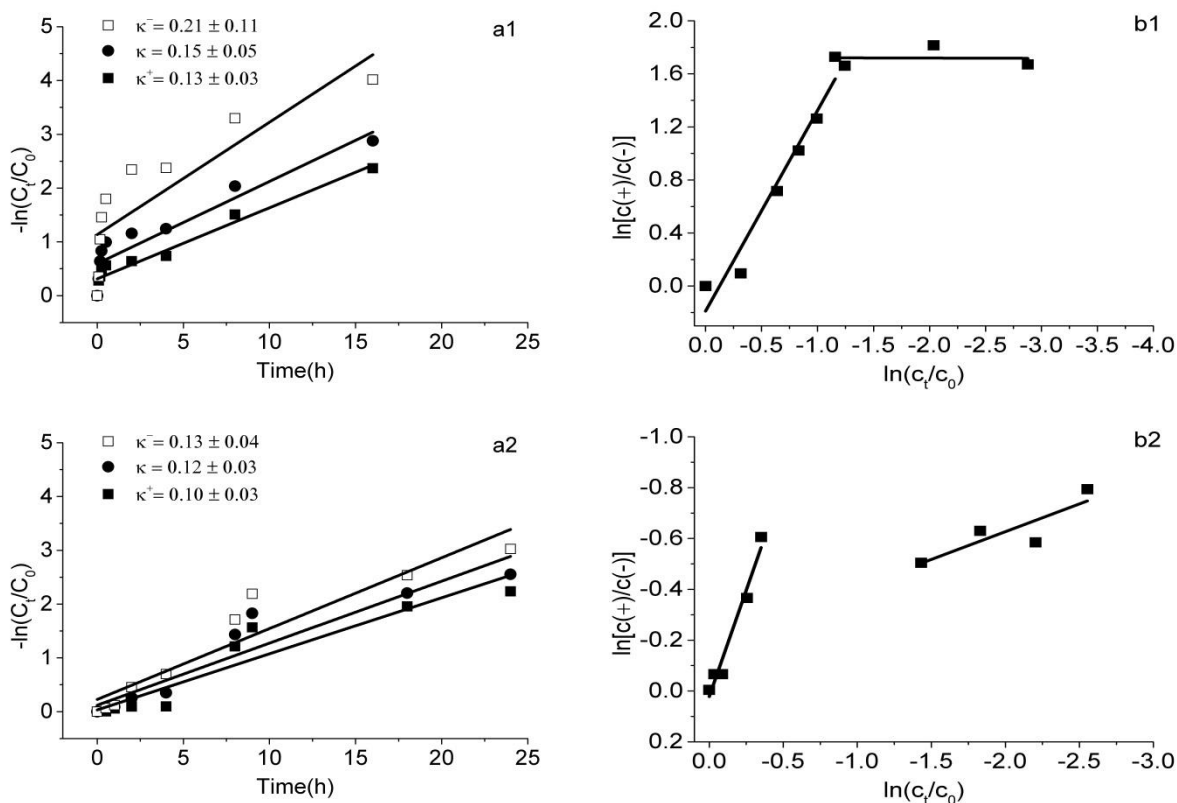


Figure S7. Biodegradation of α -HCH in growing cultures. Linearized plots showing the degradation kinetic(a) and enantiomer fractionation(b) for *S.indicum* strain B90A(1) and *S. japonicum* strain UT26(2). Data were taken from previous work ⁴.

References

1. Richnow, H. H.; Annweiler, E.; Michaelis, W.; Meckenstock, R. U., Microbial in situ degradation of aromatic hydrocarbons in a contaminated aquifer monitored by carbon isotope fractionation. *Journal of Contaminant Hydrology* **2003**, *65*, (1), 101-120.
2. Badea, S. L.; Vogt, C.; Gehre, M.; Fischer, A.; Danet, A. F.; Richnow, H. H., Development of an enantiomer-specific stable carbon isotope analysis (ESIA) method for assessing the fate of alpha-hexachlorocyclo-hexane in the environment. *Rapid Commun. Mass. Sp.* **2011**, *25*, (10), 1363-1372.
3. Coplen, T. B.; Brand, W. A.; Gehre, M.; Gröning, M.; Meijer, H. A.; Toman, B.; Verkouteren, R. M., New guidelines for δ ¹³C measurements. *Anal. Chem.* **2006**, *78*, (7), 2439-2441.
4. Bashir, S.; Fischer, A.; Nijenhuis, I.; Richnow, H. H., Enantioselective carbon stable isotope fractionation of hexachlorocyclohexane during aerobic biodegradation by *Sphingobium* spp. *Environ. Sci. Technol.* **2013**, *47*, (20), 11432-11439.
5. Elsner, M.; Zwank, L.; Hunkeler, D.; Schwarzenbach, R. P., A new concept linking observable stable isotope fractionation to transformation pathways of organic pollutants. *Environmental science & technology* **2005**, *39*, (18), 6896-6916.
6. Manna, R. N.; Dybala-Defratyka, A., Insights into the elimination mechanisms employed for the degradation of different hexachlorocyclohexane isomers using kinetic isotope effects and docking studies. *Journal of Physical Organic Chemistry* **2013**, *26*, (10), 797-804.
7. Cook, P. F., *Enzyme mechanism from isotope effects*. Crc Press: 1991.
8. Nikolausz, M.; Nijenhuis, I.; Ziller, K.; Richnow, H. H.; Kästner, M., Stable carbon isotope fractionation during degradation of dichloromethane by methylotrophic bacteria. *Environmental Microbiology* **2006**, *8*, (1), 156-164.
9. Fletcher, K. E.; Löffler, F. E.; Richnow, H.-H.; Nijenhuis, I., Stable carbon isotope fractionation of 1, 2-dichloropropane during dichloroelimination by *Dehalococcoides* populations. *Environmental science & technology* **2009**, *43*, (18), 6915-6919.
10. Suar, M.; Hauser, A.; Poiger, T.; Buser, H. R.; Muller, M. D.; Dogra, C.; Raina, V.; Holliger, C.; van der Meer, J. R.; Lal, R.; Kohler, H. P., Enantioselective transformation of alpha-hexachlorocyclohexane by the dehydrochlorinases LinA1 and LinA2 from the soil bacterium *Sphingomonas paucimobilis* B90A. *Appl. Environ. Microb.* **2005**, *71*, (12), 8514-8518.

Appendix 6.10.

Carbon and hydrogen isotope fractionation during abiotic hydrolysis and aerobic biodegradation of phthalate esters

Submitted manuscript: *Zhang, D.; Wu, L.; Yao, J.; Vogt, C.; Richnow, H. H., Environ. Sci. Technol. 2018.*

Carbon and Hydrogen Isotope Fractionation during Abiotic Hydrolysis and Aerobic Biodegradation of Phthalate Esters

Dan Zhang^{1,2}, Langping Wu², Jun Yao³, Carsten Vogt², Hans-Hermann Richnow^{2,3*}

¹School of Energy and Environmental Engineering, University of Science and Technology Beijing, Xueyuan Road No.30, Haidian District, Beijing 100083, PR China

²Department of Isotope Biogeochemistry, Helmholtz Centre for Environmental Research-UFZ, Permoserstraße 15, Leipzig 04318, Germany

³School of Water Resources and Environment, China University of Geosciences (Beijing), Xueyuan Road No.29, Haidian District, Beijing 100083, PR China

* To whom correspondence should be addressed

hans.richnow@ufz.de Tel.: +49 (0) 341 235 1212, Fax: +49 (0) 341 235 1443

ABSTRACT

This study systematically investigated the changes of carbon and hydrogen isotope signatures of three phthalate esters (PAEs) during (i) abiotic hydrolysis over the pH range of 2, 7 and 10, and (ii) aerobic biodegradation by *Rhodococcus opacus* strain DSM 43250. Significant carbon isotope fractionations were exhibited under all investigated conditions. Hydrogen isotope fractionation was observed in some experiments and is hypothesized to be a secondary hydrogen isotope effect. Dual stable isotope analysis ($\Lambda = \Delta\delta^2\text{H} / \Delta\delta^{13}\text{C}$) resulting from abiotic hydrolysis and aerobic degradation showed similar magnitudes for dimethyl phthalate (DMP) and diethyl phthalate (DEP), indicating that abiotic and enzymatically catalyzed hydrolytic processes proceed similarly. The calculated carbon apparent kinetic isotope effects (AKIE_C) for the proposed hydrolytic pathway (C-O bond cleavage) fall within an expected range of 1.03-1.09, with the exception of lower AKIE_C values for dibutyl phthalate (DBP) hydrolysis at pH 2 and aerobic biodegradation. Slightly different AKIE_C of DBP at pH 2 and pH 10 is likely related to a transition state from reactant-like to tetrahedral intermediate-like structure. Abiotic and biotic hydrolysis of PAEs demonstrate similar AKIE_C and Λ values due to the C-O bond cleavage, thus indicating the potential of dual isotope analysis to characterize hydrolytic processes of PAEs in the environment.

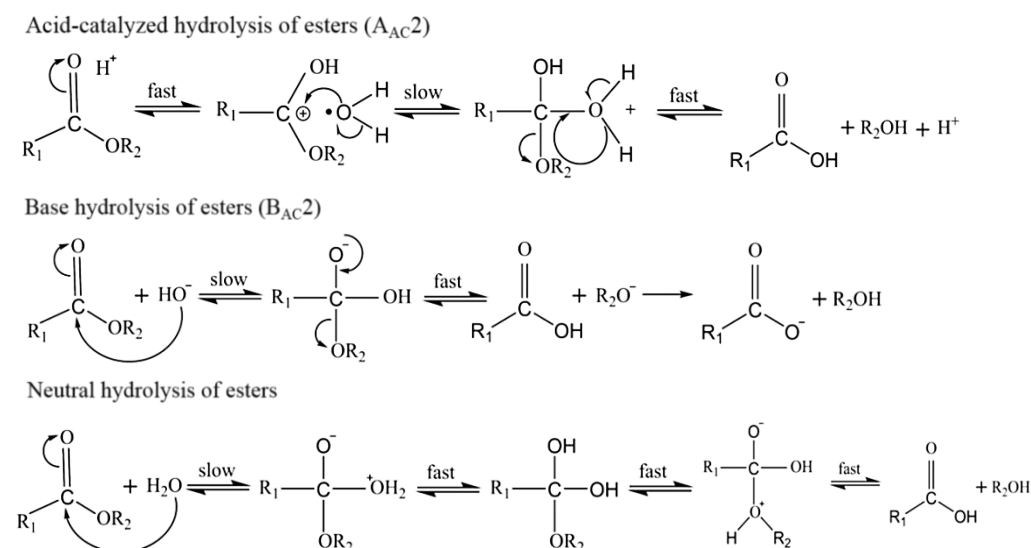
INTRODUCTION

Phthalate esters (PAEs) have drawn increasing attention due to their wide utilization as plasticizers and additives in the manufacture of plastic and personal care products. Global production of PAEs is in the order of millions of tons annually.³ PAEs can leach slowly from the products and can be transported in the environment because they are not covalently bonded to polymer chains. Therefore, PAEs have been detected in various environmental matrices, such as groundwater, rivers, lakes, soils and sediments. The majorities of PAEs are considered to end up in municipal landfills together with waste polyvinylchloride (PVC) like other compounds present in plastics. PAEs are suspected to be toxic for human beings and other organisms due to their potential carcinogenicity, teratogenicity and mutagenicity,⁸ causing particular concern about the environmental fate of PAEs.

Generally, the primary processes that could decompose PAEs in the environment are hydrolysis, photolysis and biodegradation.⁹ Among those processes, biodegradation plays an important role for PAEs removal in various environments, with the exception that PAEs are more susceptible to photooxidation by

hydroxyl radicals in the atmosphere.¹⁰ The de-esterification of phthalate diesters to phthalate monoesters is considered to be the primary biodegradation pathway under aerobic and anaerobic conditions. A well-known model organism for aerobic biodegradation of PAEs is *Rhodococcus opacus* strain DSM 43250. Even though the hydrolysis rates of PAEs are reported to be rather slow with long half-lives of more than 100 days at ambient temperature and neutral condition,¹⁰ hydrolytic process is an important chemical reaction type and hydrolysis could even become dominant abiotic process under specific environmental conditions, such as lower landfill layers due to high temperature.¹⁵ It is well noted that PAEs undergo two hydrolytic steps: they are initially converted to the corresponding monoester and one alcohol moiety via hydrolysis of the ester group, and afterwards the obtained monoester is hydrolyzed to phthalic acid and a second alcohol.¹⁰

In addition, esters hydrolysis can occur via acid-catalyzed, neutral and base hydrolysis pathways (Scheme 1). The acid-catalyzed hydrolysis of esters mainly proceeds by an $A_{AC}2$ mechanism indicating an acid-catalyzed, acyl-oxygen fission (AC) and a bimolecular reaction.¹⁸ Under acidic condition, the ester reacts with hydrogen ion and then a water molecule attacks the carbonyl carbon to produce a tetrahedral intermediate. Subsequently, the leaving group (R_2OH) quickly dissociates. Therefore, the $A_{AC}2$ mechanism is similar to a S_N2 reaction.¹⁶ The base hydrolysis takes place via a $B_{AC}2$ mechanism (B stands for base). The tetrahedral intermediate is generated via the attack of hydroxide ion on carbonyl carbon and breaks down to yield a carboxylate ion and an alcohol. At neutral condition, esters are hydrolyzed by a similar $B_{AC}2$ mechanism with a water molecule. All hydrolysis mechanisms described involve the formation of tetrahedral intermediates with slight differences.



Scheme 1. Different reaction mechanisms of ester hydrolysis.

In recent years, compound-specific stable isotope analysis (CSIA) has been well established to identify contaminant sources and monitor the extent of pollutant degradation in the environment. As the rate constant of lighter isotopologues is usually greater than that of heavier isotopologue in (bio)chemical reactions, heavier isotopes will become enriched in the residual substrate, thus leading to isotope fractionation. CSIA has the potential to provide information on reaction mechanisms and degradation pathways in contaminants decomposition due to highly reaction-specific isotope fractionation pattern.²³⁻²⁵ Previous studies provide evidence that variation of carbon and hydrogen isotope fractionation patterns has potential for characterizing different modes of hydrolysis of organophosphates. Liu and colleagues²⁸ determined the carbon isotope fractionation of dimethyl phthalate (DMP), diethyl phthalate (DEP), dibutyl phthalate (DBP) and di-*iso*-butyl phthalate (DiBP) during anaerobic biodegradation by *Bacillus* sp. SASHJ. The obtained carbon isotope enrichment factors for DMP, DEP, DBP and DiBP were $-4.6 \pm 0.4\%$, $-2.9 \pm 0.4\%$, $-0.5 \pm 0.1\%$ and $-0.8 \pm 0.1\%$, respectively. In another study, changes in carbon isotope composition of DMP and DBP during aerobic biodegradation were reported using a laboratory microcosm

system consisting of natural marine sediment.²⁹ However, quantitative analysis of carbon isotope enrichment factors was not conducted probably due to the limited numbers of the data set (n =3 or 4).

In order to investigate the potential of CSIA to characterize the hydrolysis mechanism of PAEs, we analyzed for the first time a full set of dual stable isotope analysis (C and H) for abiotic and biotic reactions. DMP, DEP and DBP were selected as model compounds to determine the carbon and hydrogen isotope fractionation during hydrolysis at acid, neutral and alkaline conditions (pH 2, 7 and 10). Kinetic studies were performed to explore the influence of pH values and chemical structure on hydrolysis rates. Furthermore, carbon and hydrogen isotope fractionation during aerobic biodegradation of DMP, DEP and DBP by *Rhodococcus opacus* strain DSM 43250 were analyzed and compared to the reported data under anoxic condition. Apparent kinetic isotope effect for primary carbon (AKIE_C) and secondary hydrogen AKIE_H were calculated to provide more information on the hydrolysis mechanism of the three PAEs.

MATERIALS AND METHODS

Hydrolysis Experiments

A list of materials and chemicals is available in the Supporting Information (SI). Hydrolysis experiments were conducted in batches at pH 2, 7 and 10, which represented typical acidic, neutral and alkaline conditions, respectively. 100 mM phosphate buffer (pH 2: KH₂PO₄ + HCl; pH 7: KH₂PO₄ + K₂HPO₄) and carbonate buffer (pH 10: Na₂CO₃ + NaHCO₃) were used to maintain the pH value throughout the whole experiment.³⁰ Two series of aqueous buffer solutions (40 mL), one spiking with 1.09 mM DMP and one spiking with 0.97 mM DEP, were prepared in glass bottles sealed with PTFE-coated rubber stoppers and aluminum crimp seals. Due to the low water solubility of DBP reportedly as 46.7 μM, initial concentration of DBP was chosen at 37 μM and batch experiments were carried out in 100 mL solution to ensure sufficient content for isotope analysis. Then the bottles were placed in an oven at a temperature of 80 °C for hydrolysis at pH 2 and 7, while hydrolysis experiments at pH 10 were conducted in a thermostatic chamber at 30 °C. Sample bottles were removed at different time intervals. 2 mL of dichloromethane (DCM) containing *ortho*-xylene (500 mg L⁻¹) as internal standard was added to the reaction solutions for extracting DMP and DEP, while 1 mL of hexane containing naphthalene (100 mg L⁻¹) as internal standard was used for the extraction of DBP. The mixture was shaken at 10 °C for at least 4 h before phase separation and then organic phase was transferred to 2 mL vial for concentration and isotope analysis.

Aerobic Biodegradation Experiments

Rhodococcus opacus DSM 43250 was purchased from the Leibniz-Institute DSMZ German Collection of Microorganisms and Cell Cultures (Braunschweig, Germany). Freeze-dried cells were initially incubated in GYM Streptomyces medium at 28 °C as suggested by the DSMZ. Modified Brunner mineral salt medium (MSM) with supplement of trace element solution SL-10 and a vitamin solution was prepared as described by Vogt and colleagues³³. The medium (pH 6.9) was used for strain cultivation and batch biodegradation experiments. MSM containing PAEs was prepared by dissolution of the corresponding PAEs into the medium separately and the initial concentrations of three PAEs were the same as those in hydrolysis experiments. Then, the obtained solutions were equilibrated overnight by gentle stirring in the dark at room temperature. Subsequently, the medium was sterilized in an autoclave at 121 °C for 20 min. Cultures were prepared for biodegradation experiments by transferring the cells into sterile medium spiked with DMP, DEP and DBP, respectively. The cultures were incubated at 28 °C in the dark using a shaking speed of 100 rpm (ISF-1-W; Kuehner, Switzerland). Cells were transferred several times into fresh medium to make sure that the cells were capable of degrading DMP, DEP and DBP as the sole carbon source, respectively.

For batch biodegradation experiments of DMP, a series of 240-mL serum bottles were prepared by dispensing 50 mL sterilized MSM containing DMP medium. Several bottles containing 50 mL sterilized MSM+DEP medium were used for DEP biodegradation experiments. The experiments for DBP aerobic biodegradation were carried out in 240-mL bottles containing 150 mL sterilized MSM+DBP medium. The microcosms were inoculated with 1 mL PAEs-pregrown cells (see above). The cultures were incubated at 28 °C in the dark shaking at 100 rpm. Abiotic control experiments of three PAEs were carried out in the

absence of inoculated microcosms. At different time intervals, 240-mL bottles were removed and sacrificed by adjusting the culture to pH 2.5 using saturated $\text{Na}_2\text{SO}_4\text{-H}_2\text{SO}_4$ solution (pH 1) to stop further degradation activity. Procedures for extraction of the residual PAEs are the same as described in hydrolysis experiments.

Concentration and Isotopic Analysis

Detailed descriptions of analytical methods and equipment are available in the SI. Briefly, concentration of PAEs residuals were measured using a gas chromatography equipped with flame ionization detector (FID). The carbon and hydrogen isotope compositions of DMP, DEP and DBP were measured using a GC coupled via a GC-Isolink interface to an isotope ratio mass spectroscopy (IRMS).

Quantification of Isotope Fractionation

Carbon and hydrogen isotope compositions of DMP, DEP and DBP were expressed in δ values, which were denoted in per mil (‰) relative to Vienna Pee Dee Belemnite (VPDB) and Vienna Standard Mean Ocean Water (VSMOW), respectively. The relationship between the extent of PAEs degradation and corresponding isotope ratio variations was evaluated according to the Rayleigh equation.³⁴

$$\ln \frac{\delta_t + 1}{\delta_0 + 1} = \varepsilon \times \ln f \quad (1)$$

where δ_t and δ_0 are the isotope ratios in the substrate at time t and zero, respectively, and f is the remaining fraction of substrate at a given time t , which stands for the ratio of substrate concentration at time t and initial concentration ($f = C_t/C_0$). The obtained slope ε is the bulk isotope enrichment factor.

The correlation of carbon and hydrogen enrichment factors obtained for a single reaction can be used diagnostically to characterize mechanisms of bond cleavage reactions.³⁵ Dual stable isotope analysis (e.g., carbon and hydrogen) can be applied to cancel possible kinetic rate limitations which affect isotope fractionation of a single element, as the kinetic rate limitations affecting the reactions prior bond cleavage (e.g. for a C-H cleavage) is almost similar for both elements.¹⁹ The relationship between the hydrogen isotopic shift ($\Delta\delta^2\text{H}$) and carbon isotopic shift ($\Delta\delta^{13}\text{C}$) during the course of one experiment is calculated by linear regression, as shown in Equation 2.¹⁹ The obtained slope (lambda value, Λ) allows differentiating the reaction mechanisms.

$$\Lambda = \frac{\Delta\delta^2\text{H}}{\Delta\delta^{13}\text{C}} \approx \frac{\varepsilon_{\text{H}}}{\varepsilon_{\text{C}}} \quad (2)$$

The obtained bulk enrichment factors (ε) are calculated by the Rayleigh equation using compound-average isotope compositions and taking into consideration of both reactive and nonreactive positions. Apparent kinetic isotope effects (AKIEs) for reactive positions are calculated using Equation 3.

$$\text{AKIE} = \frac{1}{1 + \frac{n}{x} z \cdot \varepsilon (\text{‰}) / 1000} \quad (3)$$

where ε is the obtained isotope enrichment factor, n is the number of atoms of considered element in the molecule, x is the number of reactive positions and z stands for the number of indistinguishable reactive sites.

RESULTS AND DISCUSSION

Degradation Kinetic of PAEs Hydrolysis at Different pHs

DMP, DEP and DBP containing different alkyl side chain lengths were selected to explore the influence of the chemical structure on reaction kinetics, hydrolysis mechanisms and isotope fractionation patterns. The hydrolysis experiments were conducted at pH 2, pH 7 and pH 10 to investigate the effect on hydrolysis rates. The three PAEs hydrolysis followed the pseudo-first-order kinetic reaction in all experiments ($R^2 \geq 0.977$), as shown in Table 1. Aqueous hydrolysis half-lives range from about 3 years for DMP to 22 years for DBP at pH 7 (25 °C) and acid hydrolysis rate constants were estimated to be four

orders of magnitude slower than alkaline hydrolysis.¹⁰ Additionally, the results for control experiments at 20 °C and pH = 7 (Figure S1, SI) suggested that the hydrolysis of three PAEs were both neglectable at ambient temperature. Therefore, the temperature was set at 80 °C to accelerate the degradation rate at pH 2 and pH 7. Based on the Van't Hoff equation, the reaction rate will increase by a factor of 2 to 4 for an increase of 10 °C in temperature. Compared with the rate constants of DMP in Table 1, it can be clearly seen that neutral condition are more beneficial to degradation efficiency of DMP than acid condition since the pseudo-first-order rate constant increased substantially from 0.0009 h⁻¹ at pH 2 to 0.0246 h⁻¹ at pH 7. However, the decomposition for alkaline hydrolysis at pH 10 is much faster even at ambient temperature; hence, the reaction temperature was lowered to 30 °C. Here the rate constant was 0.0965 h⁻¹ (R²=0.988), and the corresponding half-life time was calculated as 7.2 h. A further decrease of the temperature from 30 °C to 20 °C was observed to slow down the alkaline hydrolysis rate of DMP to 0.0263 h⁻¹, which is in agreement with the Van't Hoff equation. The results in Table 1 demonstrate that hydrolysis of three PAEs is both strongly pH dependent with higher rate constants at higher pHs. It can therefore be concluded that the three PAEs show alkaline hydrolysis reaction as expected, especially at higher pH values. Furthermore, the ratio of $k_{\text{pH}7}$ and $k_{\text{pH}2}$ value decreased from 26.6 (DMP), 6.7 (DEP) to 1.5 (DBP), demonstrating an increased proportion of $k_{\text{pH}2}$ along with increasing alkyl side chain length in PAEs molecules. It would be plausible that acid-catalyzed hydrolysis is likely to play a role gradually depending on the alkyl groups in PAEs.

Carbon Isotope Fractionation of PAEs during Hydrolysis and Aerobic Biodegradation

The carbon isotope compositions of three PAEs were analyzed during abiotic hydrolysis and aerobic biodegradation. The changes in C and H isotope ratios during individual reactions for DMP (Figure 1) and the isotope values of DEP and DBP (Figures S2, S3) were investigated for characterizing the degradation reactions. $\delta^{13}\text{C}$ values both showed the trend to be more positive in the remaining reactant over the course of degradation in all experiments, demonstrating that PAEs molecules containing heavy isotopes (¹³C) react slower and are left behind in the residual reactant so that a normal carbon isotope effect occurs. In addition, carbon isotope enrichment factors (ϵ_c) were evaluated by the Rayleigh equation, and 95% confidence intervals were calculated (Table 2). Highly significant fits (R² ≥ 0.93) were obtained (Figure S4). Considerable carbon isotope enrichment factors were observed in the hydrolysis processes of DMP. The values of ϵ_c at pH 2 (-3.4±0.3‰, R²=0.99) and pH 7 (-3.6±0.3‰, R²=0.99) were indistinguishable, indicating a similar reaction mechanism. According to previous kinetic results (Table 1), the k value at pH 2 is smaller than that at pH 7, which indicates no significant acid-catalyzed reaction. Therefore, neutral hydrolysis reaction is hypothesized to be dominant even at pH 2 based on carbon isotope fractionation results.

A larger ϵ_c of -4.7±0.2‰ (R²=0.99) at pH 10 was observed and attributes to alkaline hydrolysis reaction. As discussed in previous studies, even for the same type of reaction, considerable variations of isotope fractionation may occur due to the extent of bond changes in the transition state or the dependence of isotope effects on the transition state structure. As for ester hydrolysis, although C-O bond at acyl group is cleaved, three reactions of acid-catalyzed, neutral and base hydrolysis are reported to exhibit different reaction scheme steps and form tetrahedral intermediates with slight differences at rate-limiting steps (Scheme 1). Hence, it seems likely that the deviations of ϵ_c values at three pHs could be related to the subtle differences in tetrahedral intermediates during neutral and alkaline hydrolysis of DMP. The carbon isotope fractionation pattern during hydrolysis of DEP was similar to that of DMP, which agrees with the kinetic results and possibly indicates the similar dominant reaction types as DMP at three pHs. However, the ϵ_c values of DBP show a different trend with pHs compared to DMP and DEP. The obtained carbon isotope enrichment factors at pH 7 and 10 are indistinguishable and larger than hydrolysis at pH 2. A hypothesis for the difference is that the acid-catalyzed reaction plays a role during DBP hydrolysis at pH 2. In addition, the obtained ϵ_c values of the three tested PAEs at the same pH conditions decreased along with the increase of total carbon atoms in PAEs molecules (DMP>DEP>DBP), which is caused by the isotope dilution effect on the observable carbon isotope fractionation.

The aerobic biodegradation experiments were conducted with *Rhodococcus opacus* DSM 43250, which is capable of using DMP, DEP and DBP as carbon sources. The control experiments of three PAEs in the absence of microcosms (Fig. S1) indicated that the contribution of abiotic hydrolysis to biodegradation

was minor. The ϵ_C values for aerobic biodegradation of the three PAEs by *R. opacus* are reported in Table 2. The magnitude of ϵ_C for DMP ($-4.3 \pm 0.4\%$, $R^2=0.99$) and DBP ($-1.1 \pm 0.3\%$, $R^2=0.93$) agreed well with previously reported values from Liu et al.²⁸ for a *Bacillus* strain degrading DEP under anoxic condition. However, the ϵ_C value for DEP biodegradation by *R. opacus* ($-4.3 \pm 0.5\%$, $R^2=0.98$) is larger than the value reported ($-2.9 \pm 0.1\%$). The lower carbon isotope fractionation factors (ϵ_C) obtained for DEP degradation by *Bacillus* sp. SASHJ indicate that the mechanism of hydrolysis is likely a different means of catalytic hydrolysis in *Bacillus* sp. SASHJ and *R. opacus*. However, information on ^2H isotope fractionation is missing for *Bacillus* sp. SASHJ, preventing a deeper discussion on possible mechanistic differences during bond cleavage in both strains.

Hydrogen Isotope Fractionation of PAEs during Hydrolysis and Aerobic Biodegradation

Unlike the carbon isotope fractionation pattern, the measured $\delta^2\text{H}$ values of DMP did not always show an isotope enrichment trend (Figure 1). The variations of $\delta^2\text{H}$ values at pH 2 were within the analytical uncertainty ($\pm 5\%$) through the whole reaction, which was considered to be constant with no hydrogen isotope fractionation. However, $\delta^2\text{H}$ values at pH 7, pH 10 and during aerobic biodegradation by *R. opacus* showed a significant trend to be more positive, and ϵ_H values (Table 3) were calculated to be $-9 \pm 1\%$ ($R^2=0.99$), $-10 \pm 1\%$ ($R^2=0.99$) and $-20 \pm 3\%$ ($R^2=0.98$), respectively, according to the Rayleigh equation. Hydrogen isotope fractionations are considered to be caused by secondary isotope effects, because no C-H bond is broken in the rate-determining step of ester hydrolysis; hence, primary hydrogen isotope effects are not expected to occur. The extent of ^2H fractionation in all reactions was relatively low compared to primary isotope fractionation, which is in accordance with the assumed secondary hydrogen isotope effects. Almost identical hydrogen isotope fractionations of DEP at pH 7 and pH 10 are similar to those observed for DMP. The hydrogen isotope fractionation of DBP for hydrolysis at pH 10 was lower (ϵ_H value of $-6 \pm 1\%$), probably due to isotope dilution of the longer alkyl side chain. Aerobic biodegradation of DMP and DEP exhibit slightly larger ϵ_H values of $-20 \pm 3\%$ and $-14 \pm 2\%$, respectively, but it is still in a range that can be expected for secondary hydrogen isotope effects.

Apparent Kinetic Isotope Effect of PAEs

Apparent kinetic isotope effects (AKIEs) were calculated based on determined isotope enrichment factors according to Equation 3 for correcting the isotope dilution effects by nonreactive atoms in PAEs molecules and compared with literature values²⁸ (Table 2). For possible hydrolytic mechanisms under aerobic and abiotic conditions (Scheme 1), an acyl group transfer reaction of esters leads to a primary carbonyl-C kinetic isotope effect (KIE). For DMP hydrolytic reactions, ^{13}C -AKIEs were calculated using $n=10$, $x=2$ and $z=2$ because C-O bonds in two ester groups compete for reaction. Similarly, the values of x and z are both considered to be 2 and 2 for DEP and DBP, while the n value in DEP and DBP is 12 and 16, respectively. The AKIE_C values of the three PAEs in the investigated experiments are summarized in Table 2. AKIE_C values for abiotic hydrolysis at three pH values and aerobic biodegradation of DMP and DEP in this study are both within the expected typical KIE_C ranges for a $\text{S}_\text{N}2$ reaction (1.03~1.09),³⁶ which is consistent with reported AKIE_C values for anaerobic degradation of DMP and DEP by *Bacillus* sp. SASHJ.²⁸ This result shows that for hydrolytic reactions of DMP and DEP, similar AKIE_C values are obtained irrespective of abiotic, aerobic or anaerobic processes; thus, carbon isotope effects primarily indicate the type of bond cleavage (C-O).

For DBP, AKIE_C values for abiotic hydrolysis at pH 7 and 10 agree well with the typical range of 1.03-1.09, while the obtained values for hydrolysis at pH 2 (1.018) and aerobic degradation (1.018) are clearly lower than the expected range. Liu and coworkers²⁸ observed the similar phenomenon for anaerobic degradation of DBP and hypothesized that the low AKIE_C (1.008) might be caused by the masking of intrinsic isotope effects in enzyme catalyzed reactions. Another explanation is based on the findings of Marlier and O'Leary³⁸ who calculated the isotope effects of methyl benzoate hydrolyzed at acidic condition (91 °C) and at alkaline condition (25 °C). The carbonyl-C KIEs were reported to be 1.026 and 1.043 for acid-catalyzed and alkaline hydrolysis, respectively. Compared with the data in Table 2, AKIE_C values of the three PAEs hydrolyzed at pH 10 range from 1.040 to 1.054, which is in agreement with the reported carbonyl-C KIE of 1.043. Notably, the carbonyl-C KIE value of 1.026 for acid-catalyzed hydrolysis of methyl benzoate provides an indication for the lower AKIE_C value (1.018) of DBP and supports the hypothesis that acid-catalyzed reaction plays a role during DBP hydrolysis at pH 2. The

smaller magnitude of $AKIE_C$ on hydrolysis at pH 2 and aerobic biodegradation of DBP is likely related to the relatively reactant-like transition state (TS), because the isotope effect is near unity for a reactant-like TS and gradually increases when TS becomes more like the tetrahedral intermediate.³⁸

For calculating the secondary $AKIE_H$, hydrogen bonded to the adjacent carbon atom is assumed to affect the vibration of the C-O bond and hydrogen bonded to both α - and β -carbon can contribute to a secondary $AKIE_H$.³⁹ Therefore, the values of secondary $AKIE_H$ are estimated for DMP with the parameters ($n=10$, $x=6$ and $z=2$) and the corresponding values are 1.03, 1.03 and 1.07 for hydrolysis at pH 7, 10 and aerobic biodegradation, respectively (Table 3). For DEP, the secondary $AKIE_H$ values ($n=14$, $x=4$ and $z=2$) are estimated to be in the order of 1.07 (hydrolysis at pH 7), 1.07 (hydrolysis at pH 10) and 1.11 (aerobic degradation), respectively. Moreover, the calculated secondary $AKIE_H$ of DBP was found in the order 1.07 for hydrolysis at pH 10 ($n=22$, $x=4$ and $z=2$). The secondary $AKIE_H$ is assumed to be in the range of 0.95-1.05 for a S_N2 type reaction.³⁶ However, the obtained secondary $AKIE_H$ in this study ranges from 1.03 to 1.11. The latter value is above the previously observed range, which we cannot explain mechanistically.

Dual H-C Isotope Analysis of PAEs

Dual isotope plots ($\Delta\delta^2H$ versus $\Delta\delta^{13}C$) of DMP, DEP and DBP for the reactions under investigation were combined in Figure 2. Well-fitted linear regressions were obtained ($R^2 \geq 0.96$) and different slopes (Λ) were determined together with 95% confidence intervals. For DMP, hydrolysis at pH 7 and 10 lead to indistinguishable Λ values (3.0 ± 0.1 versus 2.5 ± 0.3), while the Λ value at pH 2 could not be obtained due to the absence of hydrogen isotope fractionation. In addition, a slightly larger Λ value (5.3 ± 0.4) for aerobic biodegradation was observed as a result of the higher ϵ_H value. Potential reason for this result might be slightly different reaction mechanisms of aerobic biodegradation and abiotic hydrolysis, even though hydrolytic reaction of ester bond is both assumed to occur as the initial isotope sensitive step. For DEP, except for hydrolysis at pH 2, other reactions showed the similar Λ values ranging from 1.9 ± 0.2 to 2.6 ± 0.5 , which supports the hypothesis of a similar hydrolytic mechanism. The type of reaction is considered to be acyl group transfer reaction of PAEs and primarily indicates the isotope patterns irrespective of enzymatically catalyzed or purely abiotic hydrolytic processes.

For exploring the diagnostic potential of dual H-C isotope analysis, Λ values of abiotic hydrolysis and aerobic biodegradation were compared with our previous results of chemical oxidation reactions by persulfate and OH radical oxidation (Zhang et al., 2017 submitted) (Figure 2). The carbon and hydrogen fractionation pattern of the persulfate oxidation of DMP, DEP and DBP could be clearly separated from chemical and biological hydrolysis. Acidic hydrolysis of three PAEs almost gives no 2H fractionation in any case and forms a specific pattern. The Λ value of DMP allow to distinguish biodegradation from hydrolysis, however hydrolysis at pH 7 and pH 10 exhibits similar Λ values, which overlap with OH radical oxidation (UV/H₂O₂ reaction) to some extent (2.0 ± 0.1). For DEP, the fractionation patterns of hydrolysis at pH 7 and pH 10 overlap to some extent with biodegradation and OH radical oxidation, making a separation of these reactions based on Λ value alone challenging. Persulfate and OH radical oxidation as well as hydrolysis reactions of DBP can be distinctly identified by Λ values, indicating the potential to characterize different degradation mechanisms. The low Λ values for abiotic hydrolysis and aerobic biodegradation of all three PAEs are similar due to the cleavage of a C-O bond in the rate limiting step and the PAEs with longer chain are predicted to yield not 2H isotope effect upon chemical and biological hydrolysis reactions.

ENVIRONMENTAL SIGNIFICANCE

The present study provides carbon and hydrogen isotope fractionation data in abiotic and biotic hydrolytic reactions of PAEs, which has the potential to be used as references for the further data evaluation in field studies. Both the kinetic results and carbon isotope enrichment factors support the hypothesis that the neutral hydrolysis reaction plays an important role for hydrolysis of DMP and DEP at pH 2 and pH 7. The hydrolysis rates at pH 7 and 10 give negative relationships with the side chain lengths in PAEs molecules. In addition, ϵ_C and position-specific $AKIE_C$ values demonstrate similar hydrolysis pathways irrespective of abiotic, aerobic or anaerobic processes. The exception of DBP hydrolysis at pH 2 and biodegradation is possibly caused by a reactant-like transition state and needs further study to investigate it.

Dual H-C isotope analysis has diagnostic value for characterizing mechanisms. Although the ^2H isotope fractionation is caused by a secondary isotope effects it gives a characteristic pattern for short chain phthalate. Even the hydrogen isotope fractionation is low, the secondary isotope effect still allows classification of neutral, alkaline and biological induced hydrolysis for DMP and DEP. Oxidation by sulfate and OH radical can be distinct in any case from each other. Δ values of methyl and ethyl phthalates at neutral and alkaline hydrolysis overlapped with OH radical oxidation, but with increasing length of alkyl chains, primary isotope effects of C-H bond cleavage lead to characteristic Δ values for the identification of radical reactions. This systematic investigation shows the prospects and limitation of ^2H and ^{13}C isotope fractionation analysis for diagnostically applying Δ value in laboratory and possibly in field studies. Overall, this study exhibits the potential applicability to better understand the environmental fate of PAEs at the field scale.

ASSOCIATED CONTENT

Supporting Information

Further information about materials, analytical methods, control experiments (Figure S1), changes in C and H isotope ratios of DEP (Figure S2), DBP (Figure S3) and Rayleigh isotope plots (Figure S4) is available.

ACKNOWLEDGMENTS

This work was supported by the China Scholarship Council (File No. 201506460058 for Dan Zhang, and File No. 201306460007 for Langping Wu), grants from National Science Foundation of China (41430106, 41573080, 41720104007) and International key project of Ministry of Science and Technology of China (S2016G2135). We are grateful to Stephanie Hinke for the assistance in the cultivation of cultures and Steffen Kümmel for the assistance in the Isotope Laboratory.

REFERENCES

1. Ventrice, P.; Ventrice, D.; Russo, E.; De Sarro, G., Phthalates: European regulation, chemistry, pharmacokinetic and related toxicity. *Environ. Toxicol. Pharmacol.* **2013**, *36*, (1), 88-96.
2. Sun, J. Q.; Wu, X. Q.; Gan, J., Uptake and metabolism of phthalate esters by edible plants. *Environ. Sci. Technol.* **2015**, *49*, (14), 8471-8478.
3. Julinova, M.; Slavik, R., Removal of phthalates from aqueous solution by different adsorbents: a short review. *J. Environ. Manage.* **2012**, *94*, (1), 13-24.
4. Farajzadeh, M. A.; Sorouraddin, S. M.; Afshar Mogaddam, M. R., Microextraction methods for the determination of phthalate esters in liquid samples: A review. *J. Sep. Sci.* **2015**, *38*, (14), 2470-2487.
5. Sin, J. C.; Lam, S. M.; Mohamed, A. R.; Lee, K. T., Degrading endocrine disrupting chemicals from wastewater by TiO_2 photocatalysis: A review. *Int J Photoenergy* **2012**, *2012*, 1-23.
6. Net, S.; Sempere, R.; Delmont, A.; Paluselli, A.; Ouddane, B., Occurrence, fate, behavior and ecotoxicological state of phthalates in different environmental matrices. *Environ. Sci. Technol.* **2015**, *49*, (7), 4019-4035.
7. Abdel daiem, M. M.; Rivera-Utrilla, J.; Ocampo-Perez, R.; Mendez-Diaz, J. D.; Sanchez-Polo, M., Environmental impact of phthalic acid esters and their removal from water and sediments by different technologies-a review. *J. Environ. Manage.* **2012**, *109*, 164-178.
8. Tang, W. J.; Zhang, L. S.; Fang, Y.; Zhou, Y.; Ye, B. C., Biodegradation of phthalate esters by newly isolated *Rhizobium* sp. LMB-1 and its biochemical pathway of di-n-butyl phthalate. *J. Appl. Microbiol.* **2016**, *121*, (1), 177-186.
9. Lertsirisopon, R.; Soda, S.; Sei, K.; Ike, M., Abiotic degradation of four phthalic acid esters in aqueous phase under natural sunlight irradiation. *J. Environ. Sci.* **2009**, *21*, (3), 285-290.
10. Staples, C. A.; Peterson, D. R.; Parkerton, T. F.; Adams, W. J., The environmental fate of phthalate esters: A literature review. *Chemosphere* **1997**, *35*, (4), 667-749.

11. Gao, D. W.; Wen, Z. D., Phthalate esters in the environment: A critical review of their occurrence, biodegradation, and removal during wastewater treatment processes. *Sci. Total Environ.* **2016**, *541*, 986-1001.
12. Shelton, D. R.; Boyd, S. A.; Tiedje, J. M., Anaerobic biodegradation of phthalic acid esters in sludge. *Environ. Sci. Technol.* **1984**, *18*, (2), 93-97.
13. Engelhardt, G.; Wallnöfer, P. R.; Hutzinger, O., The microbial metabolism of Di-n-Butyl phthalate and related dialkyl phthalates. *Bull. Environ. Contam. Toxicol.* **1975**, *13*, (3), 342-347.
14. Engelhardt, G.; Wallnöfer, P. R., Metabolism of di- and mono-n-butyl phthalate by soil bacteria. *Appl. Environ. Microbiol.* **1978**, *35*, (2), 243-246.
15. Huang, J. Y.; Nkrumah, P. N.; Li, Y.; Appiah-Sefah, G., Chemical behavior of phthalates under abiotic conditions in landfills. *Rev. Environ. Contam. Toxicol.* **2013**, *224*, 39-52.
16. Hilal, S. H. *Estimation of hydrolysis rate constants of carboxylic acid ester and phosphate ester compounds in aqueous systems from molecular structure by SPARC*; US Environmental Protection Agency, Office of Research and Development: 2006.
17. Schwarzenbach, R. P.; Gschwend, P. M.; Imboden, D. M., *Environmental organic chemistry*. John Wiley & Sons, Ltd.: New Jersey, 2003.
18. Day, J. N. E.; Ingold, C. K., Mechanism and kinetics of carboxylic ester hydrolysis and carboxyl esterification. *Trans. Faraday Soc.* **1941**, *37*, 686-705.
19. Elsner, M., Stable isotope fractionation to investigate natural transformation mechanisms of organic contaminants: principles, prospects and limitations. *J. Environ. Monit.* **2010**, *12*, (11), 2005-2031.
20. Elsner, M.; Imfeld, G., Compound-specific isotope analysis (CSIA) of micropollutants in the environment-current developments and future challenges. *Curr. Opin. Biotechnol.* **2016**, *41*, 60-72.
21. Vogt, C.; Dorer, C.; Musat, F.; Richnow, H. H., Multi-element isotope fractionation concepts to characterize the biodegradation of hydrocarbons-from enzymes to the environment. *Curr. Opin. Biotechnol.* **2016**, *41*, 90-98.
22. Peng, X. W.; Li, X. G.; Feng, L. J., Behavior of stable carbon isotope of phthalate acid esters during photolysis under ultraviolet irradiation. *Chemosphere* **2013**, *92*, (11), 1557-1562.
23. Zhang, N.; Bashir, S.; Qin, J.; Schindelka, J.; Fischer, A.; Nijenhuis, I.; Herrmann, H.; Wick, L. Y.; Richnow, H. H., Compound specific stable isotope analysis (CSIA) to characterize transformation mechanisms of alpha-hexachlorocyclohexane. *J. Hazard. Mater.* **2014**, *280*, 750-757.
24. Palau, J.; Shouakar-Stash, O.; Hunkeler, D., Carbon and chlorine isotope analysis to identify abiotic degradation pathways of 1,1,1-trichloroethane. *Environ. Sci. Technol.* **2014**, *48*, (24), 14400-14408.
25. Peng, X. W.; Feng, L. J.; Li, X. G., Pathway of diethyl phthalate photolysis in sea-water determined by gas chromatography-mass spectrometry and compound-specific isotope analysis. *Chemosphere* **2013**, *90*, (2), 220-226.
26. Wu, L.; Kummel, S.; Richnow, H. H., Validation of GC-IRMS techniques for delta13C and delta2H CSIA of organophosphorus compounds and their potential for studying the mode of hydrolysis in the environment. *Anal. Bioanal. Chem.* **2017**, *409*, (10), 2581-2590.
27. Wu, L.; Chladkova, B.; Lechtenfeld, O. J.; Lian, S.; Schindelka, J.; Herrmann, H.; Richnow, H. H., Characterizing chemical transformation of organophosphorus compounds by (13)C and (2)H stable isotope analysis. *Sci Total Environ* **2018**, *615*, 20-28.
28. Liu, H.; Wu, Z.; Huang, X. Y.; Yarnes, C.; Li, M. J.; Tong, L., Carbon isotopic fractionation during biodegradation of phthalate esters in anoxic condition. *Chemosphere* **2015**, *138*, 1021-1027.
29. Peng, X. W.; Li, X. G., Compound-specific isotope analysis for aerobic biodegradation of phthalate acid esters. *Talanta* **2012**, *97*, 445-449.
30. Ghauch, A.; Tuqan, A. M.; Kibbi, N., Ibuprofen removal by heated persulfate in aqueous solution: A kinetics study. *Chem. Eng. J.* **2012**, *197*, 483-492.
31. Lau, T. K.; Chu, W.; Graham, N., The degradation of endocrine disruptor di-n-butyl phthalate by UV irradiation: a photolysis and product study. *Chemosphere* **2005**, *60*, (8), 1045-1053.
32. Wolfe, N. L.; Steen, W. C.; Burns, L. A., Phthalate ester hydrolysis: Linear free energy relationships. *Chemosphere* **1980**, *9*, (7-8), 403-408.
33. Vogt, C.; Simon, D.; Alfreider, A.; Babel, W., Microbial degradation of chlorobenzene under oxygen-limited conditions leads to accumulation of 3-chlorocatechol. *Environ. Toxicol. Chem.* **2004**, *23*, (2), 265-270.
34. Aelion, C. M.; Höhener, P.; Hunkeler, D.; Aravena, R., *Environmental isotopes in biodegradation and bioremediation*. CRC Press: 2009.

35. Vogt, C.; Cyrus, E.; Herklotz, I.; Schlosser, D.; Bahr, A.; Herrmann, S.; Richnow, H.-H.; Fischer, A., Evaluation of toluene degradation pathways by Two-dimensional stable isotope fractionation. *Environ. Sci. Technol.* **2008**, *42*, (21), 7793-7800.
36. Elsner, M.; Zwank, L.; Hunkeler, D.; Schwarzenbach, R. P., A new concept linking observable stable isotope fractionation to transformation pathways of organic pollutants. *Environ. Sci. Technol.* **2005**, *39*, (18), 6896-6916.
37. Liang, X. M.; Dong, Y. R.; Kuder, T.; Krumholz, L. R.; Philp, R. P.; Butler, E. C., Distinguishing abiotic and biotic transformation of tetrachloroethylene and trichloroethylene by stable carbon isotope fractionation. *Environ. Sci. Technol.* **2007**, *41*, (20), 7094-7100.
38. Marlier, J. F.; O'Leary, M. H., Heavy-atom isotope effects on the acid-catalyzed hydrolysis of methyl benzoate. *J. Org. Chem.* **1981**, *46*, (10), 2175-2177.
39. Wolfsberg, M.; Van Hook, W. A.; Paneth, P.; Rebelo, L. P. N., Kinetic isotope effects on chemical reactions. In *Isotope Effects in the Chemical, Geological, and Bio Sciences*, Wolfsberg, M., Ed. Springer: 2009; pp 319-324.

Table 1. Hydrolysis kinetic parameters of PAEs

Experiments	DMP			DEP			DBP		
	$k (\times 10^{-4} \text{ h}^{-1})$	R^2	f	$k (\times 10^{-4} \text{ h}^{-1})$	R^2	f	$k (\times 10^{-4} \text{ h}^{-1})$	R^2	f
pH 2_80 °C	9.3	0.997	0.097	7.8	0.997	0.142	13.9	0.977	0.140
pH 7_80 °C	247.5	0.978	0.034	52.2	0.998	0.059	20.8	0.986	0.094
pH 10_30 °C	964.8	0.988	0.010	272.6	0.998	0.037	130.3	0.990	0.041
pH 10_20 °C	263.2	0.999	0.041	not analyzed			not analyzed		

Table 2. Carbon isotope enrichment factors and $AKIE_C$ of PAEs during hydrolysis and biodegradation

Experiments	DMP		DEP		DBP	
	ϵ_C (‰)	$AKIE_C$	ϵ_C (‰)	$AKIE_C$	ϵ_C (‰)	$AKIE_C$
Hydro_pH 2	-3.4±0.3	1.035	-2.6±0.4	1.033	-1.1±0.1	1.018
Hydro_pH 7	-3.6±0.3	1.037	-3.1±0.4	1.038	-2.7±0.4	1.046
Hydro_pH 10	-4.7±0.2	1.049	-4.3±0.3	1.054	-2.4±0.1	1.040
Aerobic biodegradation by <i>R. opacus</i> DSM 43250	-4.3±0.4	1.045	-4.3±0.5	1.055	-1.1±0.3	1.018
Anoxic biodegradation by <i>Bacillus</i> sp. SASHJ ^a	-4.6±0.4	1.048	-2.9±0.1	1.036	-0.5±0.1	1.008

a. The data information of anoxic biodegradation was obtained from Liu et al²⁸.

Table 3. Hydrogen isotope enrichment factors and AKIE_C of PAEs during hydrolysis and biodegradation

Experiments	DMP		DEP		DBP	
	ϵ_H (‰)	AKIE _H	ϵ_H (‰)	AKIE _H	ϵ_H (‰)	AKIE _H
Hydro_pH 2	n.d. ^a	n.d.	n.d.	n.d.	n.d.	n.d.
Hydro_pH 7	-9±1	1.03	-9±2	1.07	n.d.	n.d.
Hydro_pH 10	-10±1	1.03	-10±1	1.07	-6±1	1.07
Aerobic biodegradation by <i>R. opacus</i> DSM 43250	-20±3	1.07	-14±2	1.11	n.d.	n.d.

a. n.d. is short for “not determined”, the changes of hydrogen isotope composition were within measurement uncertainty (δ^2H : ±5‰).

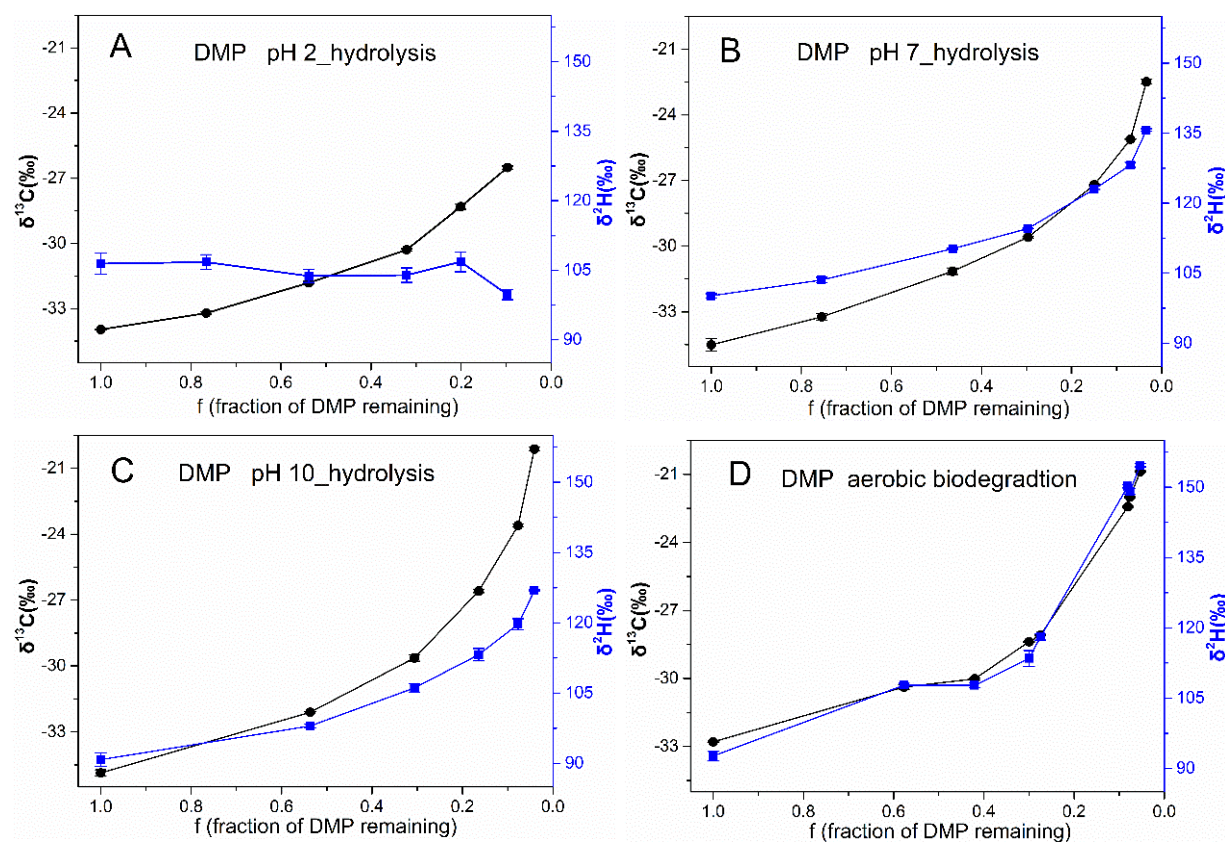


Figure 1. Isotope fractionation patterns of $\delta^{13}C$ (black circles) and δ^2H (blue squares) measured in DMP during hydrolysis at pH 2 (A), pH 7 (B), pH 10 (C) and aerobic biodegradation (D).

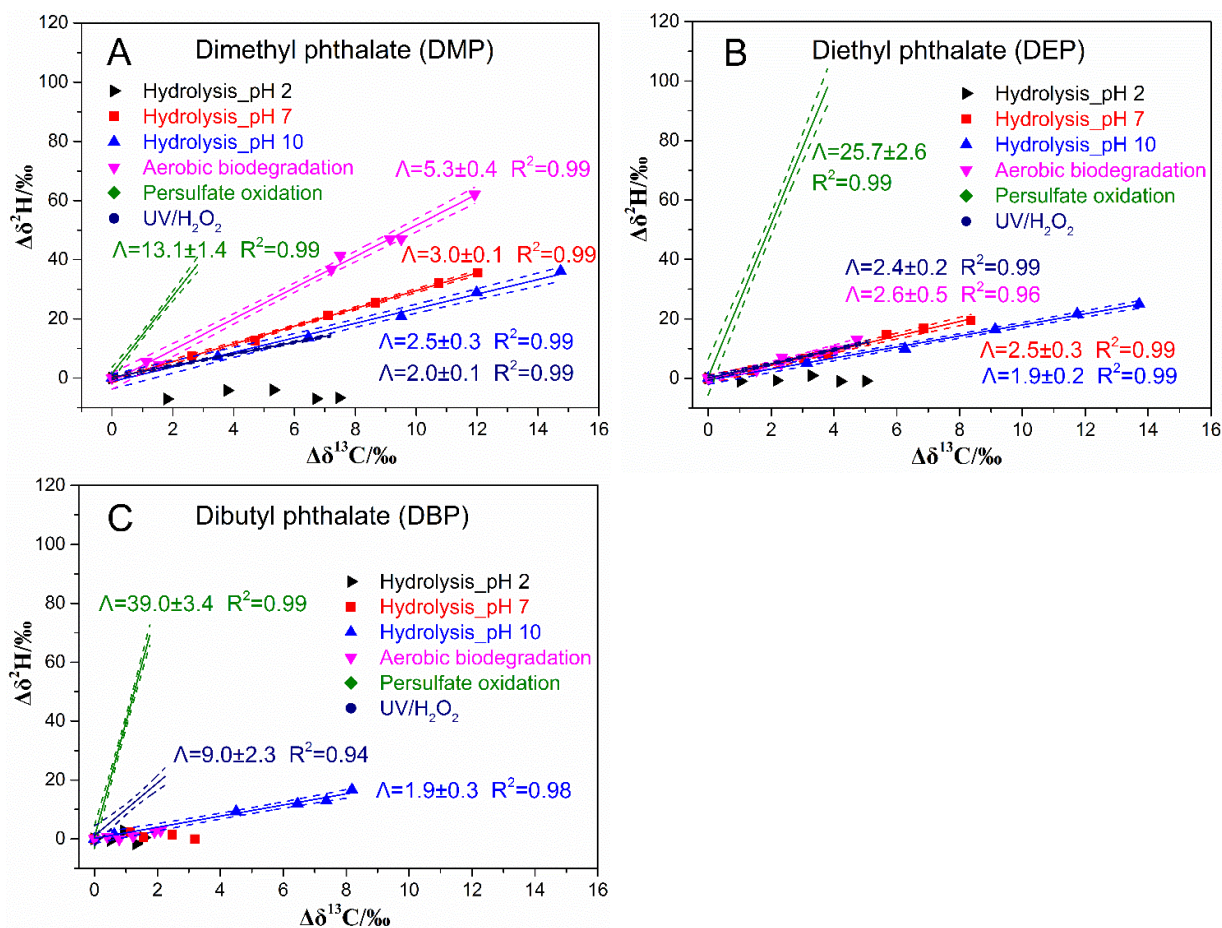
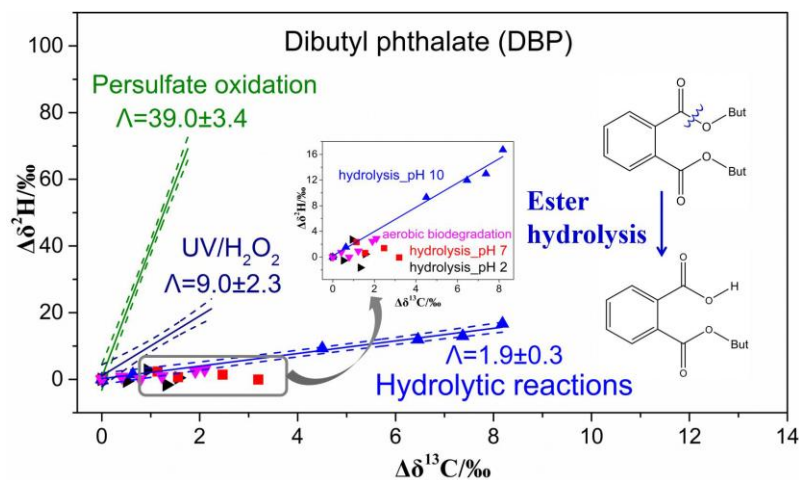


Figure 2. Dual H-C isotope plots of DMP (A), DEP (B) and DBP (C) during abiotic hydrolysis, aerobic biodegradation and chemical oxidation reactions by OH and sulfate radicals. The Λ values for persulfate and UV/ H_2O_2 oxidation were taken from Zhang and colleagues (2017, submitted).



For TOC only

Supporting Information

Carbon and Hydrogen Isotope Fractionation during Abiotic Hydrolysis and Aerobic Biodegradation of Phthalate Esters

Dan Zhang^{1,2}, Langping Wu², Jun Yao³, Carsten Vogt², Hans-Hermann Richnow^{2*}

¹School of Energy and Environmental Engineering, University of Science and Technology Beijing, Xueyuan Road No.30, Haidian District, Beijing 100083, PR China

²Department of Isotope Biogeochemistry, Helmholtz Centre for Environmental Research-UFZ, Permoserstraße 15, Leipzig 04318, Germany

³School of Water Resources and Environment, China University of Geosciences (Beijing), Xueyuan Road No.29, Haidian District, Beijing 100083, PR China

* To whom correspondence should be addressed

hans.richnow@ufz.de Tel.: +49 (0) 341 235 1212, Fax: +49 (0) 341 235 1443

5 pages

4 figures

Materials

DMP, DEP and DBP were purchased from Sinopharm Chemical Reagent Co., Ltd., (China) with 99.5% purity, and used without further purification. K_2HPO_4 , KH_2PO_4 and naphthalene were obtained from Merck (Guaranteed reagent quality, Germany). 6 M HCl solution and hexane were purchased from Carl Roth GmbH + Co. KG (Germany). Na_2CO_3 , $NaHCO_3$, *ortho*-xylene, acetonitrile and dichloromethane (DCM) were supplied by Chem solute, Th. Geyer (Germany). All other reagents for bacteria growth medium preparation were of analytic grade. Deionized water was prepared by a Milli-Q system ($>18.2 \text{ M}\Omega \text{ cm}^{-1}$, Millipore GmbH, Schwalbach/Ts. Germany) and used for preparing all experimental solutions.

Analytical Methods

Concentration measurements of PAEs residuals were performed by a gas chromatography (Agilent 7820A, USA) equipped with flame ionization detector (FID). Concentrations were determined using internal standard calibration. PAEs and internal standards were separated by a HP-5 column (30-m length, 320- μm inner diameter, 0.25- μm film thickness, Agilent, USA). The oven temperature was programmed from 60 °C (2 min) to 290 °C with a ramp of 10 °C /min and maintained at 290 °C for 2 min. Helium was used as carrier gas and the flow rate was 1.5 mL/min. The temperature of the injector was 250 °C. The injected amount of sample was 1 μL and the split ratio was 30:1.

The carbon and hydrogen isotope compositions of DMP, DEP and DBP were measured using a 6890 GC (Agilent, USA) coupled via a GC-Isolink interface to a MAT 253 isotope ratio mass

spectroscopy (IRMS, Thermo-Finnigan, Germany). The isotope analytical methods were described elsewhere.¹ The GC was equipped with a ZB-1 column (60-m length, 320- μm inner diameter, 1- μm film thickness, Phenomenex Inc., USA) to obtain good peak shapes and other parameters were set same as those in GC-FID. Carbon isotope analysis was performed in split injection mode (5:1) and the injected volume was 1 μL . Hydrogen isotope analysis was done in splitless mode. A mixture solution of DMP, DEP and DBP in hexane was used as laboratory working standard in order to monitor instrument status and quality control. Based on triplicate analyses of each sample, reproducibility of isotope values was better than typical analytical uncertainties for C and H analysis, respectively ($\delta^{13}\text{C}$ with a standard deviation $\leq 0.5\%$, $\delta^2\text{H}$ with a standard deviation $\leq 5\%$).

Control experiments

Control experiments of three PAEs for hydrolysis were conducted at 20 °C and pH = 7. The remaining fraction of DMP, DEP and DBP in Fig. S1A both showed not significant decrease in concentration within 1200 hours (50 days), which indicated that the hydrolysis process of three PAEs at ambient temperature and neutral condition was neglectable. In addition, control experiments for aerobic biodegradation were carried out under the same culture and incubation condition in the absence of inoculated microcosms. The results in Fig. S1B suggested that the contribution of abiotic hydrolysis was minor during aerobic biodegradation of DMP, DEP and DBP, because *Rhodococcus opacus* DSM 43250 was capable to degrade three PAEs in less than 100 hours.

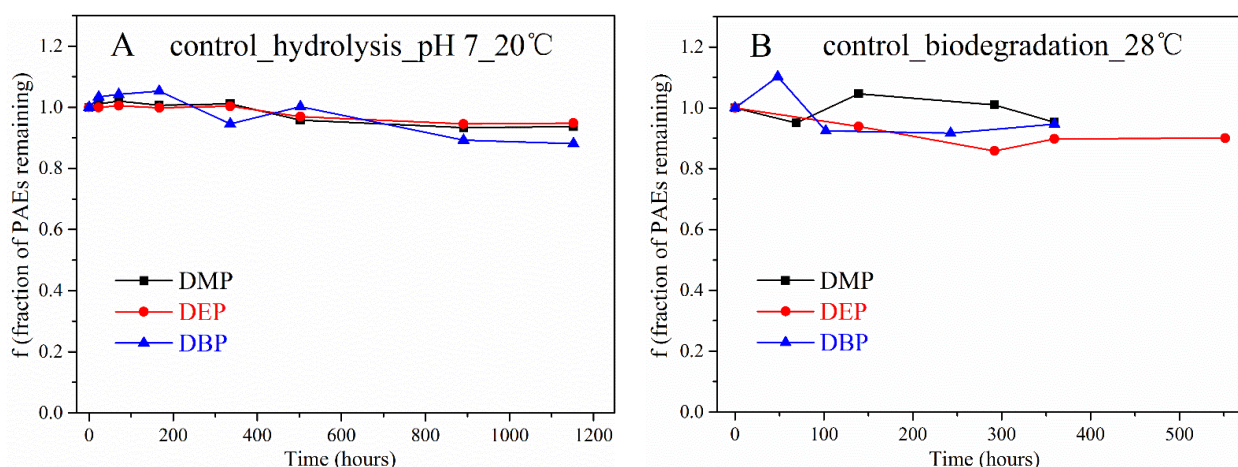


Figure S1. Remaining fraction of DMP, DEP and DBP in control experiments for hydrolysis (A) and in control experiments for aerobic biodegradation (B).

Changes in C and H Isotope Ratios of DEP and DBP in Hydrolysis and Aerobic Biodegradation

The variations of carbon and hydrogen isotope ratios along with the decomposition of DEP and DBP in the investigated experiments were shown in Figure S2 and S3, respectively. For abiotic hydrolysis at different pH values (pH 2, 7 and 10) and aerobic biodegradation, $\delta^{13}\text{C}$ values of DEP and DBP both showed a trend to be more positive during the degradation processes, which indicated a normal isotope fractionation. However, hydrogen isotope enrichment was not always observed, especially for hydrolysis at pH 2, changes in $\delta^2\text{H}$ values of three PAEs were within the analytical uncertainty ($\pm 5\%$) for $\delta^2\text{H}$ analysis, which suggested no detected hydrogen fractionation.

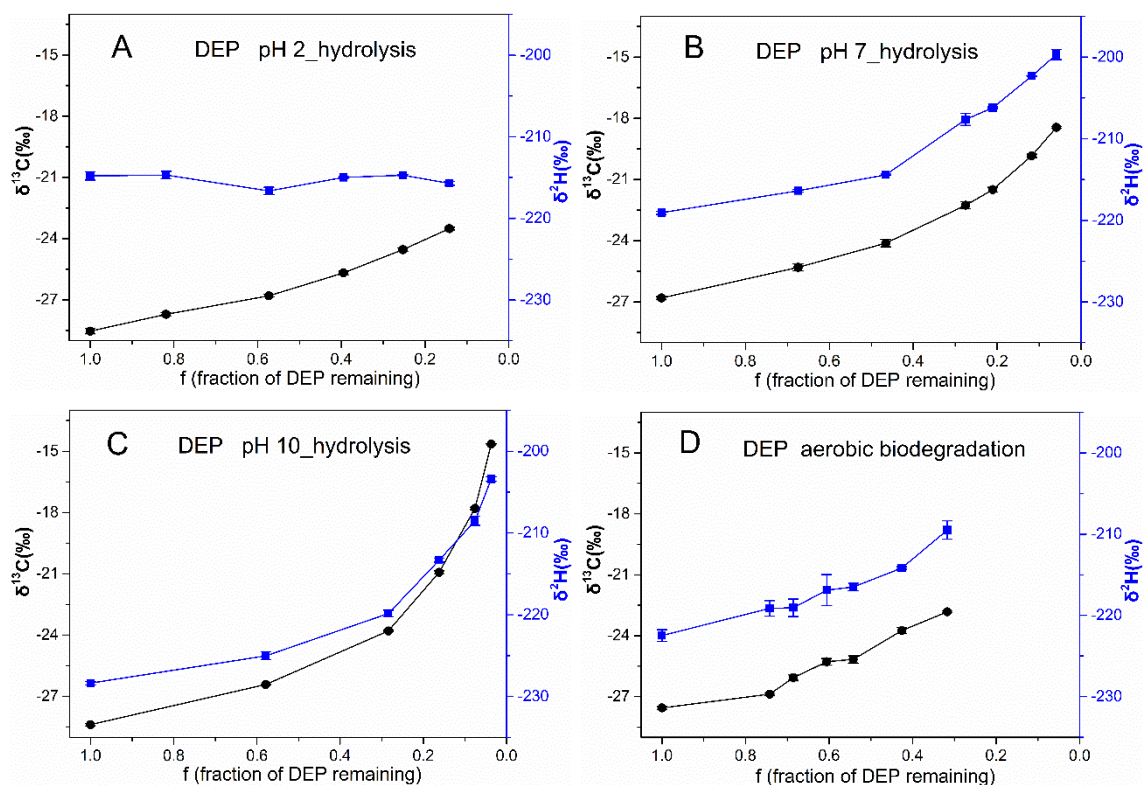


Figure S2. Isotope fractionation patterns of $\delta^{13}\text{C}$ (black circles) and $\delta^2\text{H}$ (blue squares) measured in DEP during hydrolysis at pH 2 (A), pH 7 (B), pH 10 (C) and aerobic biodegradation (D). The uncertainty of the isotope analysis is reported as standard deviation (2σ) of at least 3 individual measurement and sometime smaller than the symbol.

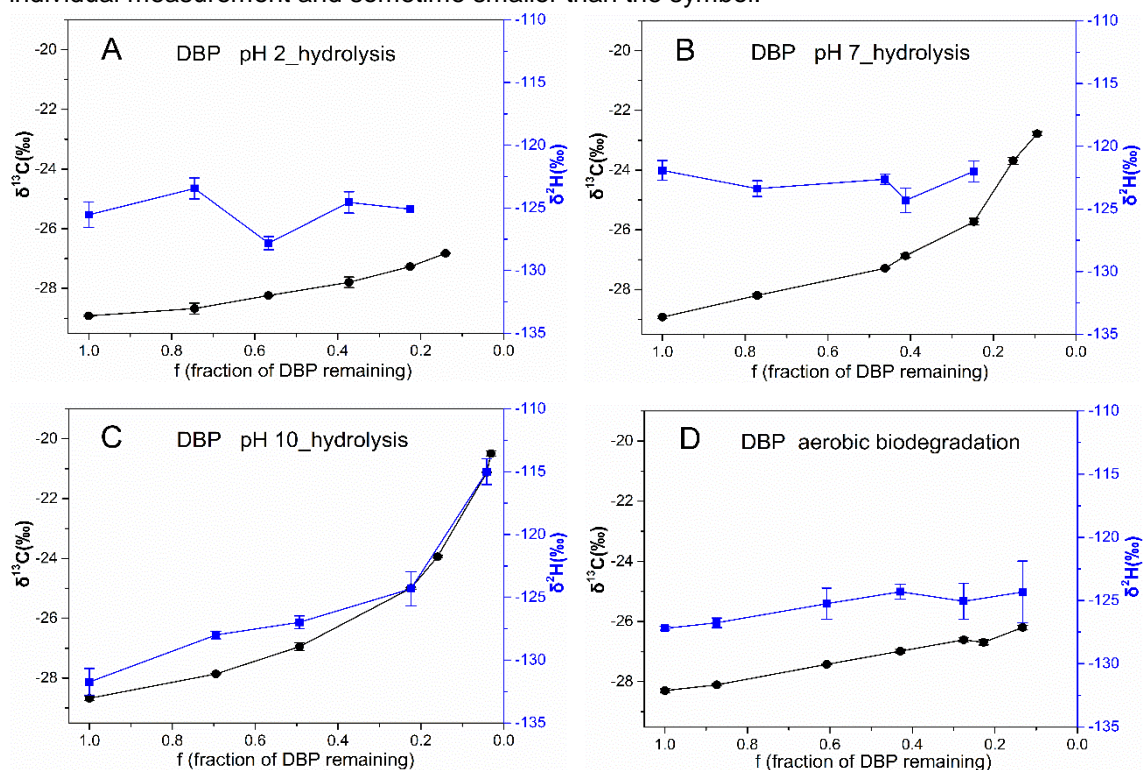


Figure S3. Isotope fractionation patterns of $\delta^{13}\text{C}$ (black circles) and $\delta^2\text{H}$ (blue squares) measured in DBP during hydrolysis at pH 2 (A), pH 7 (B), pH 10 (C) and aerobic biodegradation (D). The uncertainty of the isotope analysis is reported as standard deviation (2σ) of at least 3 individual measurement and sometime smaller than the symbol.

Rayleigh Isotope Plots

The isotope composition and the remaining fraction of PAEs described above were used to assess bulk carbon and hydrogen enrichment factors (ϵ) from the slopes of Rayleigh plots² according to Equation 1 in the main text (Figure S4). The uncertainty was reported as 95% confidence intervals.

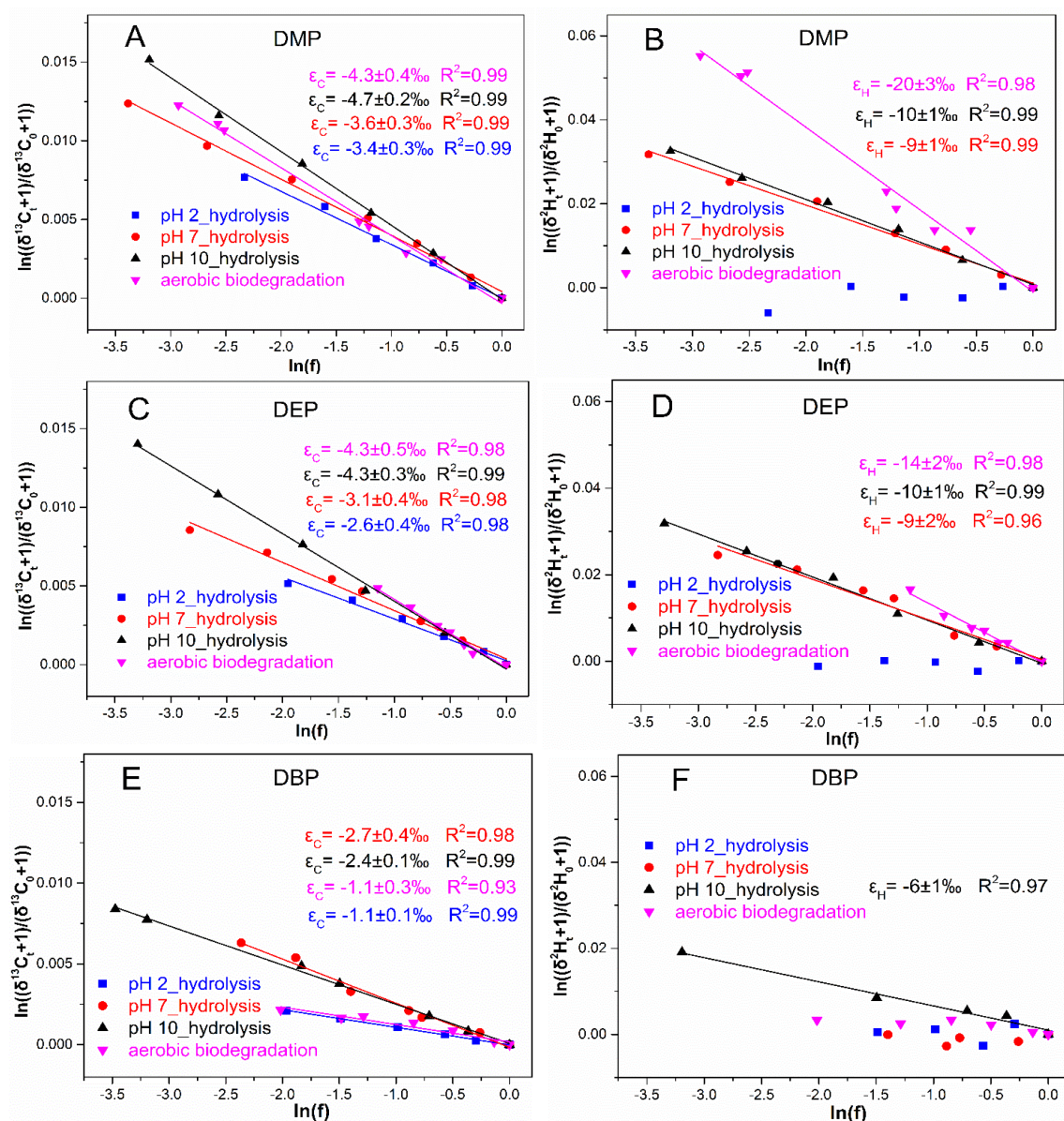


Figure S4. Logarithmic plots of carbon (left panels) and hydrogen (right panels) isotope composition during DMP (A, B), DEP (C, D) and DBP (E, F) transformation according to Rayleigh equation. Blue squares for hydrolysis at pH 2, red circles for hydrolysis at pH 7, black triangles for hydrolysis at pH 10 and magenta triangles for aerobic biodegradation.

References

- (1) Wu, L. P.; Chladkova, B.; Lechtenfeld, O. J.; Lian, S. J.; Schindelka, J.; Herrmann, H.; Richnow, H. H., Characterizing chemical transformation of organophosphorus compounds by ^{13}C and ^2H stable isotope analysis. *Sci. Total Environ.* **2018**, *615*, 20-28.
- (2) Elsner, M.; Zwank, L.; Hunkeler, D.; Schwarzenbach, R. P., A new concept linking observable stable isotope fractionation to transformation pathways of organic pollutants. *Environ. Sci. Technol.* **2005**, *39* (18), 6896-6916.

Curriculum Vitae

Personal Information

Name: Langping Wu

Current affiliation:

Helmholtz Centre for Environmental Research – UFZ

Department: Department of Isotope Biogeochemistry

Birth: 29/10/1987 Gansu, P. R. China

Email: langping.wu@ufz.de

Tel: +49 341 235 1018 (Office)

+49 17677621322 (mobile)

Address: Permoserstraße 15 / 04318 Leipzig / Germany



Current position:

Full time researcher at the Helmholtz Centre for Environmental Research – UFZ since 03/2018

Research fields:

- Developing methods and concepts for isotope fractionation analysis;
- Characterizing bond cleavage mechanisms of organic contaminants in chemical and biological reactions by multi-element compound specific isotope analysis;
- Quantification of in situ degradation using multi isotope fractionation pattern.

Education

03/2014- 09/2018	Ph.D. in Environmental Science, Eberhard Karls University of Tübingen PhD dissertation title: Characterizing transformation processes of organic contaminants by multi-element isotope analysis – developing methods and proving concepts (defensed on 18/09/2018) Supervisor: Prof. Dr. Stefan B. Haderlein; Dr. Hans H. Richnow
09/2011- 01/2014	Master of Engineering (Joint master student) in Environmental Engineering, University of Science and Technology Beijing, China University of Nova Gorica, Slovenia.

	Master thesis title: compound specific isotope analysis of organophosphorus pesticides
09/2007-06/2011	Bachelor of Engineering in Environmental Engineering, University of Science and Technology Beijing, China.

Abroad Research Experiences
(Participated/ Participating Research Projects)

01/04/2018-current	Participate the research project from the German-Israeli Foundation for Research and Development (GIF) (I-1368-307.8/2016) , Prediction of chiral and isotope enrichment during the transformations of halo-organic pollutants: Mechanistic and QSAR approaches, 01/01/2017-31/12/2019
16/02/2017-06/03/2017	Guest researcher at The Energy and Resource Institute (TERI) in India under the BMBF-DBT cooperative Science project (01DQ15006) Exploring the diversity of Organophosphorous ('OP pesticides', 'TCEP' & 'TDCPP') degrading microbes to develop a microbial biodegradation process for bioremediation of persistent OPs. 01/06/2015-31/08/2018
20/02/2016-06/04/2016	
19/02/2015-18/03/2015	Guest researcher at the University of Delhi under the Germany-India DAAD project (57035944) Assessing natural and stimulated biodegradation of the pesticide Hexachlorocyclohexane (HCH) at contaminated field sites using Compound-specific Stable Isotope Analysis (CSIA). 01/06/2013-31/05/2015
21/01/2015-06/02/2015	Guest researcher at the University Centre in Svalbard (UNIS) under the Germany-Norway DAAD project (56453656) Monitoring Sources and Sinks of Persistent Organic Pollutants (POPs) in Arctic Environments using Stable Carbon Isotope Analysis. 31/01/2013-31/12/2014

Participated International Conferences

12-17 /08/2018	Poster presentation at the The 17 th International Symposium on Microbial Ecology (ISME17), Leipzig, Germany. Title: Characterization of reactive transport processes of HCH in food webs using stable isotope fractionation concepts.
08-13 /04/2018	Oral presentation at the EGU2018, Vienna, Austria. Title: Isotope fractionation concepts for characterization of reactive transport process of HCHs in food webs.
14-18 /11/2017	Oral presentation at the the 1 st International Congress on Earth Sciences (ICES 2017), Negara Brunei Darussalam, South-East Asia. Title: Stable Isotope Fractionation Concepts to Track in situ Degradation of HCHs.
26-29 /03/2017	Poster presentation at the The 2 nd Conference on Anaerobic Biological Dehalogenation (DehaloCon II), Leipzig, Germany. Title: Stable isotope

	fractionation approach to investigate the potential of phytoremediation of HCHs from contaminated soils based on rhizosphere biodegradation and plant uptake.
21-23 /10/2016	Oral presentation at the 2016 Beijing International Environmental Technology Conference (2016IETC), Beijing, China. Title: Evaluating natural and stimulated degradation of organic pesticides at contaminated field sites using CSIA.
26-28 /10/2016	Oral presentation at the 2 nd International Workshop on Urbanization in Watersheds: Towards a Sustainable Urbanization (IWUW 2016), Xiamen, China. Title: Tracking the fate of HCHs in food webs using stable isotope fractionation concept.
20-25 /09/2015	Oral presentation at the 15 th EuCheMS International Conference on Chemistry and the Environment (ICCE2015), Leipzig, Germany. Title: Carbon and hydrogen compound-specific stable isotope analysis of organophosphorus pesticides for characterization of the degradation pathways in contaminated aquifers.
13-18 /09/2015	Oral presentation at the 42 nd International Association of Hydrogeologists Congress (AQUA2015), Rome, Italy. Title: Potential of multi isotope fingerprinting for analyzing sources and sinks of organophosphorus pesticides.
08-12 /06/2015	Poster presentation (awarded with the First Poster Prize) in the 13 th International AquaConSoil Conference (AquaConsoil 2015), Copenhagen, Denmark. Title: Evaluating in situ remediation of organophosphorus pesticides at a contaminated site using carbon and hydrogen compound specific stable isotope analysis.
27/04-02/05 /2014	Poster presentation at the European Geosciences Union General Assembly 2014 (EGU2014), Vienna, Austria. Title: An efficient thermotolerant and halophilic biosurfactant-producing bacterium isolated from Dagang oil field for MEOR application.
24-25 /04/2014	Poster presentation at the DGMK/ÖGEW-Frühjahrstagung 2014, Celle, Germany. Title: Application of MEOR by using a thermotolerant and halophilic biosurfactant producing bacterium <i>Bacillus subtilis</i> BS2 isolated from Dagang oil field.

Participated Summer School

23-27 /05/2016	Summer school on contaminated sediments: characterization and remediation. UNESCO-IHE, Delft, The Netherlands.
17-21 /08/2015	Modeling of plant uptake and application in environmental science and engineering, Technical University of Denmark, Copenhagen, Denmark.
23–28 /06/2014	10th RECETOX Summer School on Toxic Compounds in the Environment 2014, Masaryk University, Brno, Czech Republic.

Teaching & Supervision Experiences

Teaching: (16/10/2017-26/10/2017) Invited to teach a stable isotope **training course** titled on “Modern Concepts and Analytics for Compound Specific Stable Isotope Analysis of Organic Contaminants in Air, Water, Soil, and Ecosystem”.

Lecturers: Hans Richnow, Langping Wu

Teaching hours: 42 hours including lectures and lab training

Locations: China University of Geoscience Beijing (CUGB)

Co-supervision: Co-supervision of the following guest PhD, master and bachelor internship students with Dr. H.H. Richnow at the UFZ.

- **2 guest PhD students:** Jia Liu (16 months, from China), Dan Zhang (14 months, from China).
- **5 Master students:** Anke Reese (3 months, from Germany), Sonya Moses (6 months, from Germany), Barbora Chladkova (3 months, from Czech Republic), Juliane Chaud (3 months from France), Marine Desnoyers (3 months from France).
- **1 Bachelor students:** Kamile Vonzodaite (3 months, from Lithuania)

Publications

1. Liu, J.; **Wu, L.***; Kummel, S.; Yao, J.; Schaefer, T.; Herrmann, H.; Richnow, H. H., Carbon and hydrogen stable isotope analysis for characterizing the chemical degradation of tributyl phosphate. *Chemosphere* **2018**, 212, 133-142. (* Dual-first authorship)
2. **Wu, L.**; Verma, D.; Bondgaard, M.; Melvej, A.; Subudhi, S.; Vogt, C.; Richnow, H. H., Carbon and hydrogen isotope fractionation of parathion for charactering natural attenuation by hydrolysis at a contaminated site. *Water Res.* **2018**, 143, 146-154.
3. Zhang, D.; **Wu, L.**; Yao, J.; Herrmann, H.; Richnow, H. H., Carbon and hydrogen isotope fractionation of phthalate esters during degradation by sulfate and hydroxyl radicals. *Chem. Eng. J.* **2018**, 347, 111-118.
4. Passeport, E.; Zhang, N.; **Wu, L.**; Herrmann, H.; Sherwood Lollar, B.; Richnow, H.-H., Aqueous photodegradation of substituted chlorobenzenes: Kinetics, carbon isotope fractionation, and reaction mechanisms. *Water Res.* 2018, 135, 95-103.
5. Liu, W.; Duan, X.; **Wu, L.**; Masakorlac, K., Biosurfactant production by *Pseudomonas aeruginosa* SNP0614 and its effect on biodegradation of petroleum. *Appl. Biochem. Micro.* **2018**, 54, 155-162.

6. **Wu, L.**; Chladkova, B.; Lechtenfeld, O. J.; Lian, S.; Schindelka, J.; Herrmann, H.; Richnow, H. H., Characterizing chemical transformation of organophosphorus compounds by ^{13}C and ^2H stable isotope analysis. *Sci. Total. Environ.* **2018**, 615, 20-28.
7. **Wu, L.**; Kummel, S.; Richnow, H. H., Validation of GC-IRMS techniques for $\delta^{13}\text{C}$ and $\delta^2\text{H}$ CSIA of organophosphorus compounds and their potential for studying the mode of hydrolysis in the environment. *Anal. Bioanal. Chem.* **2017**, 409, (10), 2581-2590.
8. **Wu, L.**; Yao, J.; Trebse, P.; Zhang, N.; Richnow, H. H., Compound specific isotope analysis of organophosphorus pesticides. *Chemosphere* **2014**, 111, 458-463.
9. **Wu, L.**; Yao, J.; Jain, A. K.; Chandankere, R.; Duan, X.; Richnow, H. H., An efficient thermotolerant and halophilic biosurfactant-producing bacterium isolated from Dagang oil field for MEOR application. *Int.J.Curr.Microbiol.App.Sci.* **2014**, 7, (3), 586-599.

Submitted manuscripts

10. **Wu, L.**; Moses, S.; Liu, Y.; Renpenning, J.; Richnow, H. H., Development of extraction and clean-up methods for multi- element compound specific isotope analysis of hexachlorocyclohexanes for isotope forensic and food web studies. *Anal. Chem.* (re-submitted on 04/09/2018)
11. Liu, Y.; **Wu, L.**; Kohli, P.; Kumar, R.; Stryhanyuk, H.; Nijenhuis, I.; Lal, R.; Richnow, H. H., Enantiomer and carbon isotope fractionation of α -hexachlorocyclohexane by *Sphingobium indicum* strain B90A and corresponding enzymes. *Environ. Sci. Technol.* (re-submitted on 29/06/2018)
12. Zhang, D.; **Wu, L.**; Yao, J.; Vogt, C.; Richnow, H., Carbon and hydrogen isotope fractionation in abiotic hydrolysis and aerobic biodegradation of phthalate esters. *J. Hazard. Mater.* (re-submitted on 20/07/2018)